



Brunel
University
London

The Genomic Health of Human Pluripotent Stem Cells

A thesis submitted for the degree of Doctor of Philosophy

By

Marianne Patricia Henry

Division of Biosciences
College of Health and Life Sciences

May 2018

Declaration

I hereby declare that the research presented in this thesis is my own work, except where otherwise specified, and has not been submitted for any other degree.

Marianne Patricia Henry

Acknowledgements

First and foremost, I would like to thank my supervisors, Drs Jenny Boyle and Joanna Bridger, for their continuous support, suggestions and encouragement. I am extremely grateful for your guidance. I would also like to express my sincere thanks to my secondary supervisor, Dr Ross Hawkins, whose invaluable support and knowledge has been indispensable for the completion of this project.

I would like to thank the National Institute for Biological Standards and Control (NIBSC) for the funding of my PhD. Amongst the collaborations that allowed this project to succeed, I am very thankful to many members of the staff at NIBSC, including the scientists at the UK Stem Cell Bank, who have helped me during my research. I am especially thankful to Dr Jennifer Man for her training and knowledge for the handling of stem cells. In addition, I would like to thank Dr Pia Sanzone, Dr Hannah Taylor and Sophia Spyrou for their help and guidance in the labs. I would like to thank the Bioinformatics group at NIBSC, Drs Martin Fritzsche and Mark Preston for carrying out the RNA-Seq and RNA-Seq analysis, respectively, and Tom Dougall for his help with statistical analysis.

Additionally, I would also like to acknowledge Professor Wendy Bickmore and Dr Paul Perry for allowing me to use the FISH erosion scripts for my analysis, and our collaborators, Drs Lawrence Jennings and George David for their ddPCR™ advice and for sending me DNA samples. I am very grateful to Drs Temi Owoka and Sabrina Tosi, whose advice proved to be invaluable for my FISH experiments, Drs Christian Rudolph and Ian Kill for their continual moral support and enthusiasm, Lorena Ligammari for her help and constant positivity in the lab and Daniel Horton for his indispensable help in the lab.

I am very grateful to my friends, including many that I have made at my time in the labs and offices at NIBSC and Brunel, thank you for your patience, moral support and continual encouragement. I would also like to thank my Brunel PhD buddies Zoe, Hajar, Mursal, Kae and Carolina for their help and moral support, despite the many scientific discussions at odd hours! Thank you for always lifting my spirits and being hilarious.

Lastly, I would like to thank my family for all their patience, support, love and belief. Thank you to my auntie and second mother, Greta for always being able to make me laugh and only being a call away. And to Manana, the most amazing mother anyone could have, thank you for always being there for me, despite anything and everything. Thank you for listening to my science tirades and occasionally bringing me back to reality; you are forever my inspiration.

Finally, thank you to my little sister and best friend, Nicole.

Table of Contents

DECLARATION	II
ACKNOWLEDGEMENTS.....	III
TABLE OF CONTENTS	V
LIST OF FIGURES.....	IX
LIST OF TABLES.....	XII
LIST OF ABBREVIATIONS	XIII
ABSTRACT	XV
CHAPTER I: INTRODUCTION	18
1.1. GENERAL INTRODUCTION	1
1.1.1. Definition of Stem Cells	1
1.1.2. A Brief History of Stem Cells.....	2
1.1.3. Stem Cell Culture Systems.....	6
1.1.4. The Problem with Using Stem Cells	9
1.1.4.1. Ethical and Political Issues	9
1.1.4.2. Genomic Instability	10
1.1.5. Nuclear Architecture	13
1.1.6. Lamin Genes, Expression and Disruption	15
1.1.7. Genome Organisation	19
1.1.8. Mechanism of Aneuploidy Formation in Human Pluripotent Stem Cells.....	22
1.1.8.1. Mitotic Segregation Defects	22
1.1.8.2. DNA Damage	24
1.1.8.3. Bystander Effect.....	26
1.1.8.4. Nuclear Lamin Depletion	28
1.1.9. Aneuploidy Detection Methods	29
1.1.9.1. Quantitative Fluorescence Polymerase Chain Reaction	29
1.1.9.2. Multiplex Ligation-Dependent Probe Amplification	30
1.1.9.3. DNA Microarrays.....	30
1.1.9.4. Fluorescence <i>in-situ</i> Hybridisation	31
1.1.9.5. G-banding.....	31
AIMS	32
CHAPTER II: THE APPLICATION OF DROPLET DIGITAL PCR FOR SENSITIVE ANEUPLOIDY DETECTION	33
2.1 INTRODUCTION	34
2.1.1. Digital Polymerase Chain Reaction.....	34
2.2. AIMS	39
2.3 METHODS AND MATERIALS	40
2.3.1. Cell Culture and Methodology	40
2.3.2. DNA Extraction	40
2.3.3. DNA Quantification and Quality Monitoring	42
2.3.4. Karyology	42
2.3.5. DNA Fragmentation	43
2.3.5.1. Enzyme Treatment.....	43
2.3.5.2. DNA Sonication	43
2.3.6. Droplet Digital™ PCR (ddPCR™).....	46
2.2.6.1. ddPCR™ Sensitivity vs qPCR Sensitivity	49
2.3.7. Data Analysis and Bio-Informatics Tools.....	49

2.4. RESULTS.....	52
2.3.1. Titration of Female DNA into Male DNA in 6.25% Increments	56
2.3.2. Enzyme Digestion	57
2.3.2.1. Use of Different Types of Enzymes.....	57
2.3.2.2. Time needed for DNA Digestion.....	61
2.3.3. Fluorophore Signal Intensity Differences.....	63
2.3.4. Comparing Sonicated DNA with Digested DNA	66
2.3.4.1. Using DNA from collaborator labs.....	66
2.3.5. Using Reference Genes in ddPCR™.....	74
2.3.6. Detection of Chromosomal Aneuploidies using ddPCR™.....	75
2.5. DISCUSSION.....	78
2.4.1. DNA fragmentation prior to ddPCR™.....	78
2.4.2. Fluorophore Intensity Bias	80
2.4.3. DNA Sonication.....	81
CHAPTER III: UTILISING FLUORESCENCE <i>IN-SITU</i> HYBRIDISATION FOR THE CHARACTERISATION OF GENE LOCI POSITIONING IN ANEUPLOIDIES	82
3.1. INTRODUCTION	83
3.1.1. Chromatin Organisation in Interphase Nuclei.....	83
3.2. AIMS	85
3.3. METHODS AND MATERIALS	86
3.3.1. 2-D FISH	86
3.3.1.1. DNA Isolation	86
3.3.1.2. Degenerate Oligonucleotide-Primed Polymerase Chain Reaction	87
3.3.1.3. Nick Translation Labelling of Bacterial Artificial Chromosomes	89
3.3.1.4. Probe Preparation.....	90
3.3.1.5. Cell Fixation.....	91
3.3.1.6. Slide Preparation.....	91
3.3.1.7. Slide Hybridisation, Washing and Counterstaining.....	92
3.3.1.8. Image Capture.....	92
3.3.1.9. Image Analysis.....	93
3.3.1.10. Analysing Chromosome Number by Fluorescence <i>In-Situ</i> Hybridisation.....	94
3.4. RESULTS.....	95
3.4.1. Chromosome Territory Presence in Lymphoblastoid Cells	95
3.4.1. Gene Positioning in Lymphoblastoid Cells.....	97
3.5. DISCUSSION.....	103
3.5.1. Model Cell Lines.....	103
3.5.2. ALB and AMELX Positioning in Lymphoblastoids.....	104
3.5.3. Cell Morphology	106
CHAPTER IV: CORRELATION OF NUCLEAR LAMINS WITH CHROMOSOMAL ANEUPLOIDIES	108
4.1. INTRODUCTION	109
4.1.1. Nuclear Lamins	109
4.2. AIMS	110
4.3. METHODS AND MATERIALS	111
4.3.1. Immunofluorescence.....	111
4.3.2. Western Blotting	113
4.3.3. RNA Extraction and cDNA Synthesis.....	115
4.3.4. Quantitative Reverse Transcription PCR (RT-qPCR).....	117
4.4. RESULTS.....	119
4.4.1. A-Type Lamins	119
4.4.1.1. Indirect Immunofluorescence	119
4.4.1.2. Western Blotting.....	123

4.4.1.3. Reverse Transcription PCR.....	125
4.4.2. <i>B-Type Lamins</i>	127
4.4.2.1. Indirect Immunofluorescence	127
4.4.2.2. Western Blotting.....	133
4.4.2.3. Reverse Transcription PCR.....	137
4.5. DISCUSSION.....	139
CHAPTER V: THE EFFECT OF DIFFERENT MEDIA AND MATRICES ON THE GENOMIC INSTABILITY OF HUMAN PLURIPOTENT STEM CELLS.....	141
5.1. INTRODUCTION	142
5.2. AIMS	144
5.3. METHODS AND MATERIALS	145
5.2.1. <i>Cell Culture</i>	145
TeSR™2 (STEM CELL TECHNOLOGIES, UK).....	145
5.2.2. <i>Quality Control</i>	148
5.2.3. <i>Droplet Digital PCR</i>	148
5.2.4. <i>Fluorescence In-Situ Hybridisation and Image Analysis</i>	149
5.2.5. <i>Statistical Analysis</i>	149
5.4. RESULTS.....	150
5.4.1. <i>ddPCR™ of H9 Cells</i>	150
5.4.2. <i>Fluorescence In-Situ Hybridisation</i>	154
5.4.3. <i>Nuclear Morphology Analysis</i>	162
5.5. DISCUSSION.....	166
5.5.1. <i>ddPCR™ Results</i>	166
5.5.2. <i>Gene Positioning Results</i>	168
5.5.3. <i>Nuclear Morphology Analysis</i>	169
5.5.4. <i>Future Work</i>	170
CHAPTER VI: THE IMPACT OF ANEUPLOIDIES ON THE GENOMIC HEALTH OF HUMAN PLURIPOTENT STEM CELLS.....	172
6.1. INTRODUCTION	173
6.1.1. <i>The Genomic Health of Human Pluripotent Stem Cells</i>	173
6.2. AIMS	174
6.3. METHODS AND MATERIALS	175
6.3.1. <i>Cell Culture and Methodology</i>	175
6.3.2. <i>DNA/RNA Extraction</i>	176
6.3.3. <i>Droplet Digital PCR and Fluorescence In-situ Hybridisation</i>	176
6.3.4. <i>Quantitative PCR</i>	176
6.3.5. <i>Immunofluorescence and Micronuclei Counts</i>	178
6.3.6. <i>RNA-Seq</i>	179
6.3.6.1. <i>RNA-Seq Data Analysis</i>	179
6.3.6.2. <i>RNA-Seq QC</i>	179
6.4. RESULTS.....	180
6.4.1. <i>Initial ddPCR™ Runs</i>	181
6.4.2. <i>MasterShef2 and mShef2 ddPCR™ Results</i>	184
6.4.3. <i>Gene Positioning</i>	185
6.4.3.1. <i>MasterShef2 vs mShef2</i>	185
6.4.3.2. <i>The Effects of HDFs Versus Matrigel™ on Gene Positioning</i>	200
6.4.4. <i>Nuclear Morphology Analysis</i>	211
6.4.5. <i>FISH Summary</i>	220
6.4.6. <i>Micronuclei Counts</i>	226
6.4.7. <i>Indirect Immunofluorescence</i>	228
6.4.7.1. <i>A-Type Lamins</i>	229
6.4.7.2. <i>B-Type Lamins</i>	235

6.4.8. RT-qPCR for Gene Expression.....	238
6.4.9. RNA-Seq	241
6.4.10. Quality Control.....	241
6.4.11. RNA-Seq Network Analysis	241
6.5. DISCUSSION.....	250
6.5.1. ddPCR™.....	250
6.5.2. Fluorescence in-situ Hybridisation, Nuclear Morphology and Genomic Instability	251
6.5.3. RT-qPCR and Immunofluorescence.....	253
6.5.4. RNA-Seq Network Analysis in hPSCs.....	255
6.5.5. Detection of Mosaicism in Human Pluripotent Stem Cells	256
CHAPTER VII: GENERAL DISCUSSION.....	258
7.1. GENERAL DISCUSSION	259
7.1.1. Aneuploidy Detection via Droplet Digital Polymerase Chain Reaction	259
7.1.2. Aneuploidy Positioning via Fluorescence In-situ Hybridisation	261
7.1.3. Aneuploidy and Lamins	263
7.1.4. Conclusions	264
REFERENCES.....	266
APPENDIX I: KARYOLOGY	293
APPENDIX II: DATA ANALYSIS	298
NUCLEAR AREA ANALYSIS OF H9 CELLS GROWN UNDER DIFFERENT CONDITIONS.....	298
NUCLEAR CIRCULARITY OF H9 CELLS GROWN UNDER DIFFERENT CONDITIONS	299
APPENDIX III: KARYOLOGY.....	301
APPENDIX IV: DATA ANALYSIS	308
MASTERSHEF2 HDF NUCLEAR AREA	308
MASTERSHEF2 HDF NUCLEAR CIRCULARITY	309
MASTERSHEF2 MATRIGEL™ NUCLEAR AREA	310
MASTERSHEF2 MATRIGEL™ NUCLEAR CIRCULARITY	311
MSHEF2 HDF NUCLEAR AREA	312
MSHEF2 HDF NUCLEAR CIRCULARITY	313
MSHEF2 MATRIGEL™ NUCLEAR AREA.....	314
MSHEF2 MATRIGEL™ NUCLEAR CIRCULARITY.....	315
APPENDIX V: FASTQC FILES	317
APPENDIX VI: STEM CELL COLONY IMAGES.....	340
APPENDIX VII: LIST OF GENES GENERATED FROM THE RNA-SEQ ANALYSIS	357

List of Figures

CHAPTER I:

FIGURE 1.1. MULTIPLE ORIGINS OF HUMAN STEM CELLS	1
FIGURE 1.2 OVERVIEW OF STEM CELL DISCOVERY THROUGHOUT HISTORY.....	3
FIGURE 1.3. COMMON CHROMOSOME GAINS AND/OR LOSSES IN HPSCS	10
FIGURE 1.4. THE FORMATION OF LAMIN FILAMENTS.....	14
FIGURE 1.5. NUCLEAR ARCHITECTURE AND GENOME ORGANISATION IN SOMATIC VERSUS NAÏVE CELLS.....	20

CHAPTER II:

FIGURE 2.1. SCHEMATIC REPRESENTATION OF DDPCR™.....	35
FIGURE 2.2. SCHEMATIC REPRESENTATION OF THE DIFFERENT RESTRICTION DIGESTION SITES AND RESULTING FRAGMENT SIZES	44
FIGURE 2.3. QUANTASOFT 1-D PLOT OF AMELX/AMELY TEMPERATURE GRADIENT	53
FIGURE 2.4. QUANTASOFT 1-D PLOT EXAMPLE	54
FIGURE 2.5. ESTABLISHMENT OF AMELX AND AMELY IN THE DDPCR™ ASSAY	54
FIGURE 2.6. QUANTASOFT GENE RATIO EXAMPLE SCREENSHOT.....	55
FIGURE 2.7. QUANTASOFT GENE FRACTIONAL ABUNDANCE EXAMPLE SCREENSHOT	55
FIGURE 2.8. QUANTASOFT GENE FRACTIONAL ABUNDANCE SCREENSHOT.....	56
FIGURE 2.9. QUANTASOFT 2-D PLOT OF DIFFERENT ENZYME DIGESTIONS.....	58
FIGURE 2.10. SCATTER PLOT OF THE DIFFERENT ENZYMATIC TREATMENTS	60
FIGURE 2.11. QUANTASOFT 2-D PLOT OF DIFFERENT TIMES OF BSTYI DIGESTIONS	62
FIGURE 2.12. SCATTER PLOT OF DIFFERENT ENZYMATIC TREATMENT TIMES	63
FIGURE 2.13 SCATTER PLOT OF SWITCHED FLUOROPHORES	64
FIGURE 2.14. SCATTER PLOT OF DIFFERENT DNA SOURCES	65
FIGURE 2.15. SCATTER PLOT OF AMELX/AMELY RATIO IN SONICATED AND DIGESTED SAMPLES	67
FIGURE 2.16. SCATTER PLOT OF CHANNEL 1 NUMBER OF EVENTS IN SONICATED AND DIGESTED SAMPLES	68
FIGURE 2.17. SCATTER PLOT OF TOTAL NO. OF EVENTS IN SONICATED AND DIGESTED SAMPLES	69
FIGURE 2.18. QUANTASOFT 2-D PLOT OF DIFFERENT TREATMENT METHODS OF DNA.....	70
FIGURE 2.19. QUANTASOFT 2-D PLOT OF DIFFERENT TREATMENT METHODS OF DNA.....	72
FIGURE 2.20. SCATTER PLOT OF THE PERCENTAGE OF POSITIVE DROPLETS IN DDPCR™	73
FIGURE 2.21. SCATTERPLOT OF THE RATIO OF THE DIFFERENT COMBINATION OF REFERENCE GENES	74
FIGURE 2.22 AMELX DETECTION IN ANEUPLOID CELL LINES IN DDPCR™	75
FIGURE 2.23. AMELX DETECTION IN CHROMOSOME X ANEUPLOIDY IN 10% INCREMENTS SUB-POPULATIONS	76
FIGURE 2.24. SCATTERPLOT OF 2.5% TRISOMY X TITRATION IN WILD-TYPE FEMALE DNA	77
FIGURE 2.25 SCATTERPLOT OF 1% TRISOMY X TITRATION IN WILD-TYPE FEMALE DNA	77

CHAPTER III:

FIGURE 3.1. NUCLEAR POSITIONING VIA THE EROSION SCRIPT SOFTWARE IPLAB	93
FIGURE 3.2. CHROMOSOME X PRESCENCE IN INTERPHASE AND METAPHASE	96
FIGURE 3.3. AMELX AND ALB FLUORESCENCE <i>IN-SITU</i> HYBRIDISATION IMAGES OF WILD-TYPE AND ANEUPLOID LYMPHOBLASTOID CELLS	98
FIGURE 3.4. ALB POSITIONING IN WILD-TYPE AND ANEUPLOID CELL NUCLEI	99
FIGURE 3.5. AMELX POSITIONING IN WILD-TYPE AND ANEUPLOID CELL NUCLEI	100
FIGURE 3.6 CELL MORPHOLOGY ANALYSIS	102

CHAPTER IV:

FIGURE 4.1. LAMIN A AND C STAINING IN SKOV-3 CELLS.....	120
FIGURE 4.2. LAMIN A STAINING IN LYMPHOBLASTOID CELLS.....	120
FIGURE 4.3. LAMIN C STAINING IN LYMPHOBLASTOID CELLS.....	121
FIGURE 4.4. LAMIN C STAINING PATTERN ANALYSIS.....	122
FIGURE 4.5. LAMIN A AND BETA-TUBULIN WESTERN BLOT.....	123
FIGURE 4.6. LAMIN A AND BETA-TUBULIN WESTERN BLOT.....	124
FIGURE 4.7. A-TYPE LAMIN GENE EXPRESSION IN LYMPHOBLASTOID CELL LINES	126
FIGURE 4.8. LAMIN B1 RIM AND INTRANUCLEAR STAINING IN LYMPHOBLASTOID CELLS	128
FIGURE 4.9. LAMIN B1 STAINING PATTERN ANALYSIS.....	129
FIGURE 4.10. LAMIN B2 RIM STAINING IN LYMPHOBLASTOID CELLS.....	131
FIGURE 4.11. LAMIN B2 INTRANUCLEAR STAINING IN LYMPHOBLASTOID CELLS	131
FIGURE 4.12 LAMIN B2 STAINING PATTERN ANALYSIS.....	132
FIGURE 4.13. LAMIN B1 AND BETA-TUBULIN WESTERN BLOT	134
FIGURE 4.14. LAMIN B2 AND BETA-TUBULIN WESTERN BLOT	136
FIGURE 4.15. B-TYPE LAMIN GENE EXPRESSION IN LYMPHOBLASTOID CELL LINES	138

CHAPTER V:

FIGURE 5.1. MEDIA AND MATRICES COMBINATION FLOWCHART	146
FIGURE 5.2. FLOWCHART OF THE DIFFERENT H9 MEDIA AND MATRICES GROWTH CONDITIONS.....	147
FIGURE 5.3. AMELX INSTABILITY MEASUREMENT VIA DDPCR™ IN H9 CELLS GROWN IN TESR™ MEDIUM	151
FIGURE 5.4. AMELX INSTABILITY MEASUREMENT VIA DDPCR™ IN H9 CELLS GROWN IN NUTRISTEM XF/FF™ MEDIUM	152
FIGURE 5.5. AMELX INSTABILITY MEASUREMENT VIA DDPCR™ IN H9 CELLS GROWN IN ESSENTIAL 8™ MEDIUM ...	153
FIGURE 5.6. ALB POSITIONING IN TESR2™ MEDIA IN COMBINATION WITH DIFFERENT MATRICES	155
FIGURE 5.7. ALB POSITIONING IN NUTRISTEM XF/FF™ MEDIA IN COMBINATION WITH DIFFERENT MATRICES	156
FIGURE 5.8. ALB POSITIONING IN ESSENTIAL 8™ MEDIA IN COMBINATION WITH DIFFERENT MATRICES.....	157
FIGURE 5.9. AMELX POSITIONING IN ESSENTIAL 8™ MEDIA IN COMBINATION WITH DIFFERENT MATRICES	159
FIGURE 5.10. AMELX POSITIONING IN NUTRISTEM XF/FF™ MEDIA IN COMBINATION WITH DIFFERENT MATRICES	160
FIGURE 5.11. AMELX POSITIONING IN ESSENTIAL 8™ MEDIA IN COMBINATION WITH DIFFERENT MATRICES	161
FIGURE 5.12. NUCLEAR AREA OF THE DIFFERENT MEDIA AND MATRICES COMBINATIONS	163
FIGURE 5.13. NUCLEAR MORPHOLOGY ANALYSIS.....	164

CHAPTER VI:

FIGURE 6.1. SCATTER PLOT OF MRC9 AND NIBSC-5 RATIO.....	180
FIGURE 6.2. DDPCR™ RESULTS FOR HDF DETECTION IN LATE PASSAGE MSHEF2 CELLS	182
FIGURE 6.3. DDPCR™ RESULTS FOR ANEUPLOIDY DETECTION IN LATE PASSAGE MSHEF2 CELLS	183
FIGURE 6.4. DDPCR™ RESULTS FOR MASTERSHEF2 AND MSHEF2	185
FIGURE 6.5. FLUORESCENCE <i>IN-SITU</i> HYBRIDISATION RESULTS IN P3PS-P4PS	187
FIGURE 6.6. FLUORESCENCE <i>IN-SITU</i> HYBRIDISATION RESULTS IN P5PS	189
FIGURE 6.7. FLUORESCENCE <i>IN-SITU</i> HYBRIDISATION RESULTS IN P6PS	191
FIGURE 6.8. FLUORESCENCE <i>IN-SITU</i> HYBRIDISATION RESULTS IN P7PS	193
FIGURE 6.9. FLUORESCENCE <i>IN-SITU</i> HYBRIDISATION RESULTS IN P8PS	195
FIGURE 6.10. FLUORESCENCE <i>IN-SITU</i> HYBRIDISATION RESULTS IN P9PS	197
FIGURE 6.11. FLUORESCENCE <i>IN-SITU</i> HYBRIDISATION RESULTS IN P10PS	199
FIGURE 6.12. FLUORESCENCE <i>IN-SITU</i> HYBRIDISATION RESULTS IN P5PS	201
FIGURE 6.13. FLUORESCENCE <i>IN-SITU</i> HYBRIDISATION RESULTS IN P6PS	203
FIGURE 6.14. FLUORESCENCE <i>IN-SITU</i> HYBRIDISATION RESULTS IN P7PS	204
FIGURE 6.15. FLUORESCENCE <i>IN-SITU</i> HYBRIDISATION RESULTS IN P8PS	206
FIGURE 6.16. FLUORESCENCE <i>IN-SITU</i> HYBRIDISATION RESULTS IN P9PS	208
FIGURE 6.17. FLUORESCENCE <i>IN-SITU</i> HYBRIDISATION RESULTS IN P10PS	210
FIGURE 6.18. MASTERSHEF2 HDF NUCLEAR MORPHOLOGY, GENOMIC STABILITY AND GENE POSITIONING	212
FIGURE 6.19. MASTERSHEF2 MATRIGEL™ NUCLEAR MORPHOLOGY, GENOMIC STABILITY AND GENE POSITIONING	214
FIGURE 6.20. MSHEF2 HDF NUCLEAR MORPHOLOGY, GENOMIC STABILITY AND GENE POSITIONING.....	216
FIGURE 6.21. MSHEF2 MATRIGEL™ NUCLEAR MORPHOLOGY, GENOMIC STABILITY AND GENE POSITIONING	218
FIGURE 6.22. EMBRYONIC STEM CELL COLONY IMAGES	219
FIGURE 6.23. SUMMARY OF ALL FISH RESULTS IN THE EMBRYONIC STEM CELLS	221
FIGURE 6.24. MICRONUCLEUS REPRESENTATIVE IMAGE.....	226
FIGURE 6.25. NUMBER OF MICRONUCLEI IN THE HUMAN EMBRYONIC STEM CELLS	227
FIGURE 6.26. IMMUNOFLUORESCENCE STAINING OF HUMAN PLURIPOTENT STEM CELLS WITH NANOG	228
FIGURE 6.27. A-TYPE LAMIN STAINING WITHIN EMBRYONIC STEM CELL COLONIES.....	230
FIGURE 6.28. A-TYPE LAMIN STAINING OUTSIDE EMBRYONIC STEM CELL COLONIES WITHOUT NANOG STAINING	231
FIGURE 6.29. A-TYPE LAMIN STAINING OUTSIDE EMBRYONIC STEM CELL COLONIES WITH NANOG STAINING.....	232
FIGURE 6.30. A-TYPE LAMIN STAINING OUTSIDE EMBRYONIC STEM CELL COLONIES WITH LAMIN A AND C SPECKLES AND STRONG NANOG STAINING	233
FIGURE 6.31. A-TYPE LAMIN STAINING OUTSIDE EMBRYONIC STEM CELL COLONIES WITH LAMIN A AND C SPECKLES AND WEAK NANOG STAINING	234
FIGURE 6.32. B-TYPE LAMIN STAINING WITHIN EMBRYONIC STEM CELL COLONIES	236
FIGURE 6.33. B-TYPE LAMIN STAINING WITHIN EMBRYONIC STEM CELL COLONIES LACKING LAMIN B2 STAINING.	237
FIGURE 6.34. QUANTITATIVE PCR FOR PLURIPOTENCY AND LAMIN GENES.....	239
FIGURE 6.35. QUANTITATIVE PCR FOR LINEAGE-SPECIFIC GENES.....	240
FIGURE 6.36. VENN DIAGRAMS FOR TRANSCRIPTS WITH \geq LOG5FC IN THE HPSCS.....	249

List of Tables

CHAPTER II:

TABLE 2.1 CHARACTERISATION OF CELL LINES	45
TABLE 2.2. DDPCR™ REACTION MIXTURE COMPONENT CONCENTRATIONS	47
TABLE 2.3. DDPCR™ PRIMER AND PROBE DESIGN FOR AMELOGENIN X AND Y	48
TABLE 2.4 DDPCR™ THERMOCYCLER SET-UP	48
TABLE 2.5. TITRATION OF WILD-TYPE FEMALE DNA IN WILD-TYPE MALE DNA IN 6.25% INCREMENTS.....	49
TABLE 2.6. P VALUES AND SYMBOLS FOR STATISTICAL SIGNIFICANCE	51
TABLE 2.7 AVERAGE RATIO OF <i>AMELX</i> TO <i>AMELY</i>	59

CHAPTER III:

TABLE 3.1. DOP-PCR TEMPLATE AMPLIFICATION REAGENTS	87
TABLE 3.2. DOP-PCR TEMPLATE AMPLIFICATION CONDITIONS.....	88
TABLE 3.3. DOP-PCR CHROMOSOME PAINT LABELLING REAGENTS	88
TABLE 3.4. DOP-PCR CHROMOSOME PAINT LABELLING CONDITIONS.....	89
TABLE 3. 5. CONCENTRATION OF REAGENTS USED FOR THE PROBE HYBRIDISATION IN 2-D FISH	90

CHAPTER V:

TABLE 5.1. CDNA SYNTHESIS KIT COMPONENTS AND VOLUMES	116
TABLE 5.2. CDNA SYNTHESIS THERMOCYCLING CONDITIONS	116
TABLE 5.3. LAMINS A AND C PRIMER AND PROBE SEQUENCES.....	117
TABLE 5.4. LAMINS A AND C RT-QPCR THERMOCYCLING CONDITIONS.....	118
TABLE 5.5. LAMINS B1 AND B2 RT-QPCR THERMOCYCLING CONDITIONS.....	118
TABLE 5.6. MEDIA AND MATRICES USED	145
TABLE 5.7. MEDIA AND MATRICES STUDY COMBINED RESULTS	165

CHAPTER VI:

TABLE 6.1. TYPICAL C _T VALUE RANGES FOR HPSCS, DAY 7 EBS AND DAY 14 EBS	177
TABLE 6.2. MASTERSHEF2 AND MSHEF2 STUDY COMBINED RESULTS	222
TABLE 6.3. MASTERSHEF2 AND MSHEF2 STUDY COMBINED RESULTS	223
TABLE 6.4. MASTERSHEF2 AND MSHEF2 STUDY COMBINED RESULTS	224
TABLE 6.5. MASTERSHEF2 AND MSHEF2 STUDY COMBINED RESULTS	225
TABLE 6.6. NETWORK PATHWAYS ENRICHED IN MASTERSHEF2 HDF VERSUS MASTERSHEF2 MATRIGEL™ SAMPLES	242
TABLE 6.7. NETWORK PATHWAYS ENRICHED IN MSHEF2 HDF VERSUS MSHEF2 MATRIGEL™ SAMPLES.....	244
TABLE 6.8. NETWORK PATHWAYS ENRICHED IN MSHEF2 HDF VERSUS MSHEF2 MATRIGEL™ SAMPLES.....	245
TABLE 6.9. NETWORK PATHWAYS ENRICHED IN MASTERSHEF2 HDF VERSUS MASTERSHEF2 MATRIGEL™ SAMPLES	247

List of Abbreviations

3-D FISH	Three Dimensional Fluorescence <i>In-Situ</i> Hybridisation
ALB	<i>Albumin</i>
AMELX	<i>Amelogenin X</i>
AMELY	<i>Amelogenin Y</i>
BAC	Bacterial Artificial Chromosome
CNV	Copy Number Variation
DNA	Deoxyribonucleic Acid
dPCR	Digital Polymerase Chain Reaction
ddPCR	Droplet Digital Polymerase Chain Reaction
EC	Embryonic Carcinoma
ESC	Embryonic Stem Cell
ES	Embryonic Stem
<i>E. coli</i>	<i>Escherichia coli</i>
FCS	Foetal Calf Serum
FISH	Fluorescence <i>In-Situ</i> Hybridisation
GVHD	Graft-Versus-Host-Disease
HLA	Human Leukocyte Associated
HSA	Human Chromosome
ICM	Inner Cell Mass
IVF	<i>In Vitro</i> Fertilisation
KCl	Potassium Chloride
hESCs	Human Embryonic Stem Cells
hPSCs	Human Pluripotent Stem Cells
hiPSCs	Human Induced Pluripotent Stem Cells
iPS	Induced Pluripotent Stem
iPSC	Induced Pluripotent Stem Cell
LMNA	Lamin A
LMNB1	Lamin B1

<i>LMNB2</i>	Lamin B2
LJ	Lawrence Jennings, Ann & Robert H. Lurie Children's Hospital of Chicago
MPH	Marianne P. Henry
NEB	New England Biolabs
NIBSC	National Institute for Biological Standards and Control
OSKM	<i>OCT-4, SOX-2, KLF-4, C-MYC</i>
ONSL	<i>OCT-4, NANOG, SOX-2, LIN28</i>
PCR	Polymerase Chain Reaction
qPCR	Quantitative Polymerase Chain Reaction
RE	Restriction Enzyme
<i>RPP30</i>	Ribonuclease P/MRP 30kDa subunit
RT-qPCR	Quantitative Reverse Transcription Polymerase Chain Reaction
TDL	The Doctors Laboratory
UKSCB	UK Stem Cell Bank

Abstract

Human pluripotent stem cells are increasingly used for cell-based regenerative therapies worldwide, with the use of embryonic and induced pluripotent stem cells as potential treatments for a range of debilitating and chronic conditions. However, with the level of chromosomal aneuploidies the cells may generate in culture, their safety for therapeutic use could be in question. This study aimed to develop sensitive and high-throughput assays for the detection and quantification of human pluripotent stem cell aneuploidies, to assess any changes in their positioning in nuclei, as well as investigate the possible roles of lamins in the accumulation of aneuploidies.

Using Droplet Digital PCR™, we optimised the detection of aneuploid cells in a predominantly diploid background. An assay was established for the sensitive detection of up to 1% of mosaicism and was used for the monitoring of low-level chromosome copy number changes across different cell lines, conditions and passages in the human pluripotent stem cells.

In addition, fluorescence *in-situ* hybridisation was used to map genes *ALB* and *AMELX* on chromosomes 4 and X, respectively, in karyotype-stable chromosome X aneuploid lymphoblastoid cell lines. Our results demonstrated significant alternations in the gene loci positioning in the chromosome X aneuploid cell lines. Using the same established method, the positioning of *ALB* and *AMELX* was monitored, alongside the genomic instability with ddPCR™, in the different human pluripotent stem cell lines, conditions and passage. We demonstrated a highly plastic nuclear organisation in the pluripotent stem cells with many changes occurring within a single passage. Furthermore, these results were not exclusive to a single cell line or condition, regardless of the presence or absence of feeder cells and of passage number, and the flexibility of the chromatin organisation remained throughout the duration of the study. We demonstrated high levels of genomic instability with recurrent gains and losses in the *AMELX* copy number in the human embryonic stem cells during the course of our study, however no significant changes in their gene loci positioning from these abnormalities were observed.

Additionally, we observed reduced levels of lamin B2 in the aneuploid lymphoblastoid cell lines and complete loss in some hPSC samples. Our results support recent findings that suggest a link between lamin B2 loss and the formation of chromosome aneuploidies in cell culture.

In conclusion, our data demonstrates several key novel findings. Firstly, we have established a sensitive technique for the detection of up to 1% mosaicism, which to our knowledge is the most sensitive assay currently available. Secondly, we showed significant changes in the gene loci positioning between aneuploid and diploid cell lines. Thirdly, utilising our novel ddPCR™ assay, we demonstrated the karyotypical instability of hPSCs with consistent gains and/or losses of gene copy numbers in a short period of time in culture. When studying the effects of different growth conditions, we showed that the karyotypical instability was not exclusive to a single condition or a combination of conditions, and what is more, the karyotypical abnormalities detected were not observed to change the gene positioning of hPSCs significantly, with the genome organisation remaining plastic. Finally, our results support a potential association of lamin B2 loss and karyotypical instability. We conclude that more sensitive and robust techniques need to be readily used by clinicians for the screening of potential therapeutic hPSCs.

Chapter I: Introduction

1.1. General Introduction

1.1.1. Definition of Stem Cells

Stem cells are unspecialised cells that can give rise to a range of different cell types through self-renewal. Adult stem cells are unspecialised cells that can be found throughout the body in various niches, such as the small intestine, colon or bone marrow (Barker *et al.*, 2007; Héroult *et al.*, 2017). Embryonic stem cells (ESCs) are derived from the cells of the inner cell mass (ICM) in an early preimplantation embryo or blastocyst and can differentiate to form all three germ cell layers – the ectoderm, the endoderm and the mesoderm (Figure 1.1). Such cells are known as pluripotent cells, since they give rise to every cell type of the body, but not the extra-embryonic membrane or placental tissue. Induced pluripotent stem cells (iPSCs) are pluripotent cells made from the reprogramming of differentiated (usually adult) cells and can likewise give rise to a range of different cell types (Takahashi *et al.*, 2007).

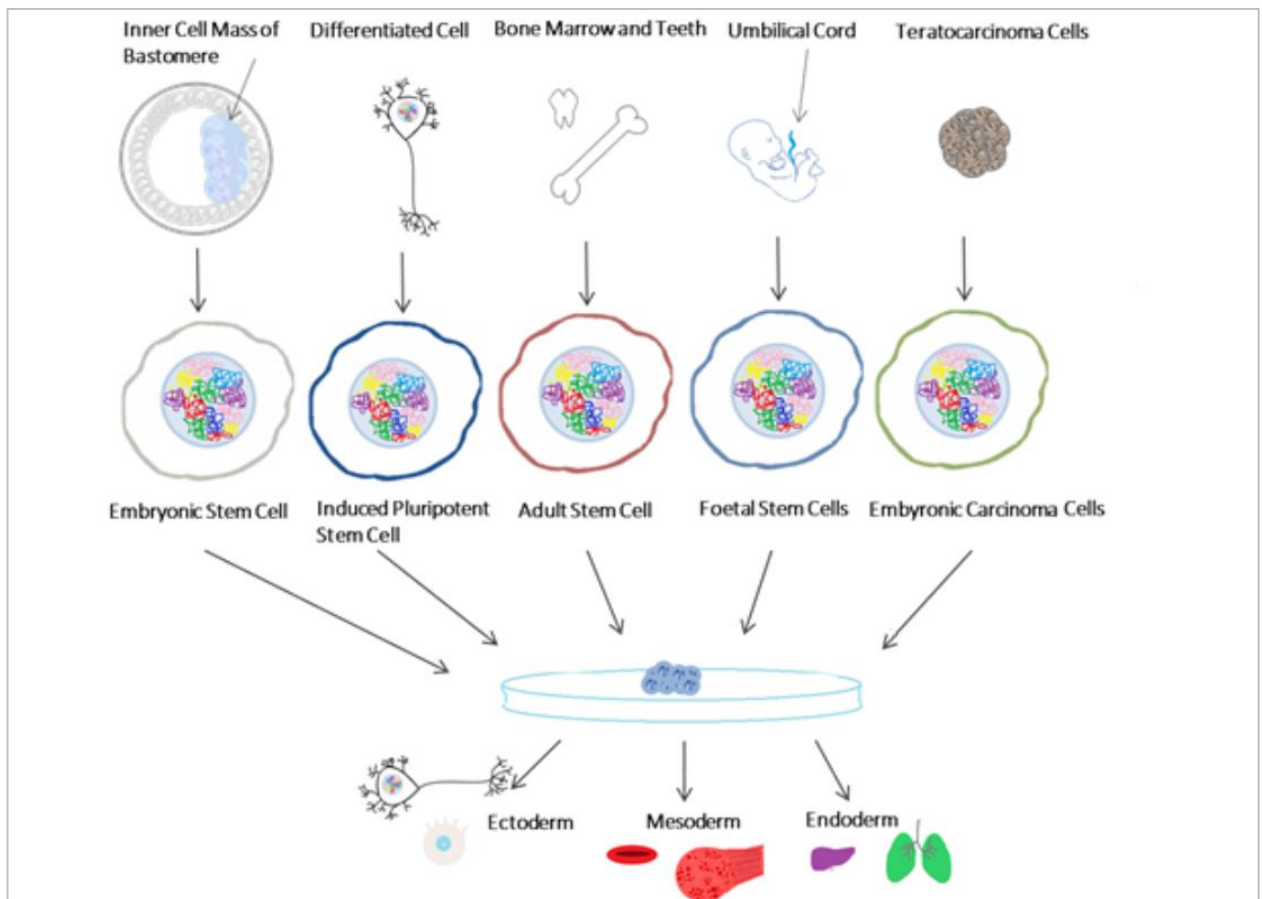


Figure 1.1. Multiple Origins of Human Stem Cells

Pluripotent stem cells may be derived from several sources and have the ability to differentiate into any cell type, with high therapeutic potential.

1.1.2. A Brief History of Stem Cells

The term “stem cells” can be traced back to the late nineteenth century, when a number of notable scientists were working on theories to explain the role stem cells played in the human body and evolutionarily where they came from (Timeline shown in Figure 1.2). Amongst them was Ernest Haeckel, a German biology professor. Haeckel believed that unicellular organisms or protozoa gave rise to multicellular organisms and he referred to these cells as “Stammzellen”. He believed that the “Stammzellen” formed the evolutionary basis of all plants and animals (all cells “stemming” from one source) and compared this theory to the development of an embryo from a single cell to complex multicellular organism. Ultimately, in 1877 he proposed that the fertilised egg cell is the origin of all cells in the body (reviewed in Maehle, 2011).

Around the same time August Weismann worked on the theory of the continuity of the “germ plasm”, which involved the belief that the nucleus carried hereditary characteristics of the cells. Weissman had an assistant Valentin Haecker, who in 1892 published a paper stating stem cells as the common precursor of all other cells. The researchers were interested in the “nuclear substance” carrying hereditary information and described the distribution and doubling of chromosomes during cell division. Weissman proposed that stem cells passed on only a part of the nuclear chromatin to somatic cells (chromatin diminution), thus leading to cell differentiation (reviewed in Maehle, 2011).

In 1909, a Russian scientist Alexander Maksimov declared at the Berlin Haematological Society the presence of haematopoietic stem cells or “polyblasts” and that all cells were derived from one common precursor cell. Interestingly, Maksimov also mentioned “Stammzellen” in the paper he published with this theory (reviewed in Maehle, 2011).

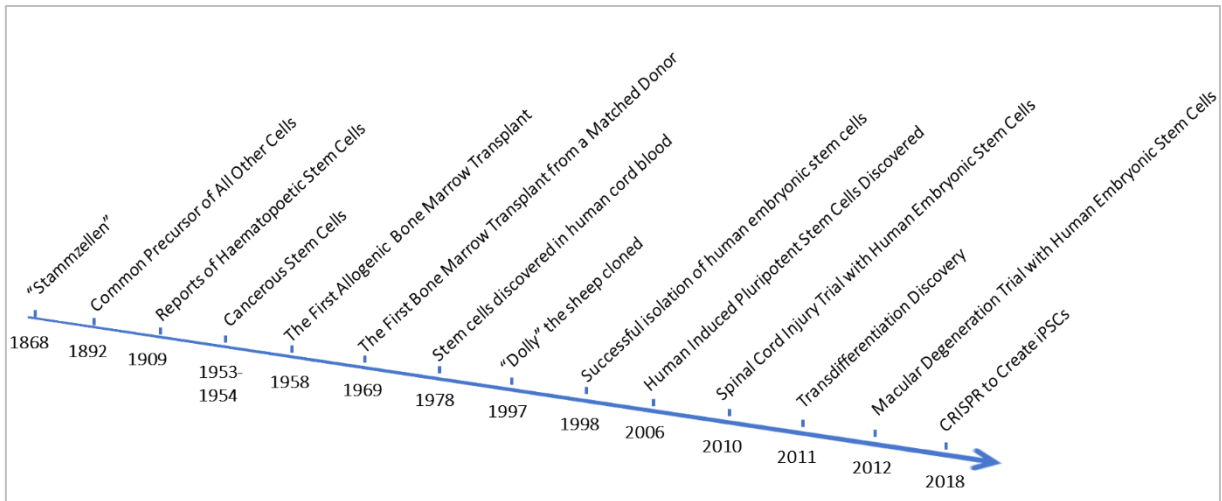


Figure 1.2 Overview of Stem Cell Discovery Throughout History

Almost fifty years later Frank J. Dixon and Robert A. Moore, together with Leroy Stevens and Clarence Cook Little found that 96.5% of testicular tumours had a germinal cell origin (Dixon and Moore, 1953) and in 1% of mice, spontaneous testicular teratoma was “undifferentiated, rapidly dividing embryonic-type cells” (Stevens and Little, 1954). This indicated that stem cells had a potential to develop into a cancer that could form into different types of tissues.

Throughout the twentieth century, the concept of stem cells gradually became more and more accepted. A significant number of studies were being performed with the injection of bone marrow stem cells into irradiated mice to successfully treat the destroyed bone marrow in the mice. Finally, in 1958 Georges Mathe injected human bone marrow from healthy donors into four patients suffering from radiation damage. What was remarkable about this incident was that despite the lack of donor-to-recipient matching at the time, all of the patients survived. This was because of the surge of healthy cells from the donors that helped the patients overcome their illness, rather than the cells being accepted by the donors. Although subsequently the patients did reject the cells, none suffered from graft-versus-host disease (GVHD), where the recipient’s immune system attacks the donor’s cells. Unfortunately, four years later when treating a leukaemia patient, the results were not as successful, and the patients died of encephalitis, probably due to a severe immune response to the foreign tissue (MATHE *et al.*, 1959). Despite the unsuccessful outcome

in Mathe's later patient, this did prompt research to match tissue types between the donors and recipients and by 1969, E. Donnall Thomas could successfully treat leukaemia via a matched sibling bone marrow transplantation. Eight years later, an unrelated donor was used, and the national registry of bone marrow was formed (Thomas and Ferrebee, 1962). This was a ground-breaking development that allowed the treatment of many diseases that were previously thought fatal.

However, it was only in 1998 when John Gearhart and James Thomson both reported the successful isolation and on-going culture of human embryonic stem cells from aborted embryos (Shamblott *et al.*, 1998) and *in vitro* fertilised embryos (Thomson *et al.*, 1998), respectively. While this phenomenon was a huge breakthrough for researchers interested in the potential of embryonic stem cells to cure a wide range of difference diseases, some argued that their use was ethically immoral and had a "dark side", due to potential negative outcome from their risk of tumour formation (Kraft, 2011). By 2006, Shinya Yamanaka had discovered a way to reprogramme differentiated cells into naïve cells and referred to them as induced pluripotent stem cells (iPSCs) (Takahashi and Yamanaka, 2006). This discovery was revolutionary to the field, as it removed the ethical concerns associated with the use of human embryonic stem cells by avoiding embryo destruction, and also lessened the risk of GVHD if the cells were to ever be used as treatment options, as the patient's own cells could potentially be reprogrammed for therapeutic use.

Stem cell research in the twenty-first century had not only a colossal impact on the molecular research associated with stem cell therapies, but also on the therapies themselves. In 2010, the first trial using human embryonic stem cells was conducted on patients suffering from spinal cord injuries (Lebkowski, 2011) and in 2012 -age-associated macular degeneration, a disease causing blindness (*ClinicalTrials.gov*, 2012). Throughout the clinical trials, advancements in the reprogramming of cells, specifically transdifferentiation was developed by Marius Wernig's group (Wernig *et al.*, 2008; Vierbuchen *et al.*, 2010). This is where one somatic cell can be transformed into another one by bypassing a step for the reprogramming into iPSCs. Similarly, more recently CRISPR-Cas9 has been implemented for chromatin modifications to generate pluripotency (Kim, Kang and Ju, 2017). Considering that embryonic stem cells

were only successfully isolated twenty years ago, these recent studies are a huge leap forward in the stem cell world and hold great promise for the development of future therapies. With such immense therapeutic potential, stem cells could be used for tissue engineering of whole organs, negating the lack of present organ donors and permitting the development of personalised medicine (Badylak, Taylor and Uygun, 2011). Due to their pluripotent properties the stem cell-based treatment of many diseases, such as age-related macular degeneration (AMD) (Song *et al.*, 2015), spinal cord injuries (SCI) (Deshpande *et al.*, 2006) and Parkinson's disease (Bjorklund *et al.*, 2002; Takagi *et al.*, 2005; Grealish *et al.*, 2014; Barker *et al.*, 2016) may soon be permitted.

1.1.3. Stem Cell Culture Systems

For the cells to be used in the clinic, their culture in the laboratory must be carefully documented and moreover, regulated. Human pluripotent stem cells are widely regarded as difficult to culture, due to their frequent spontaneous differentiation, user-to-user and/or culture condition-dependent growth i.e. media composition and dissociation methods, as well as their extreme sensitivity to other environmental factors, such as CO₂, O₂ and toxin levels (Mohyeldin, Garzón-Muvdi and Quiñones-Hinojosa, 2010; Burgess, Agathocleous and Morrison, 2014; Chen *et al.*, 2014; Ito and Suda, 2014).

Originally, inactivated mouse embryonic fibroblasts (MEFs), bovine serum albumin (BSA), glutamine, amino acids and growth factors were used as the feeder layer and supplements during the derivation of the first mouse embryonic stem cells (mESCs) (Evans and Kaufman, 1981) and human embryonic stem cells (hESCs) (Reubinoff *et al.*, 2000; Zhang *et al.*, 2006). Unfortunately, due the animal derivatives used in the original cell culturing methods, today this would not be acceptable for the expansion of potential therapies in humans. For example, the animal derivatives carry risk of contamination by mouse retroviruses, transmissible spongiform encephalopathies, or can express immunogenic non-human proteins (Martin *et al.*, 2005; Wang *et al.*, 2011). All components must fall within stringent regulations of Good Manufacturing Practice (GMP) and cell lines must be classified as European Union Tissues and Cells Directive (EUTCD) clinical grade lines; with the use of chemically-defined and xeno-free reagents. Nevertheless, MEFs have been used extensively in the culture of stem cells, due to their secretion of growth factors that help support and maintain them; these include fibroblast growth factors (FGFs), activin A and transforming growth factor beta (TGF- β) (Unger *et al.*, 2008; Yoon *et al.*, 2010). Alternative media and matrices must be used that are chemically-defined, xeno-free and comply with current regulations and standards, as well as maintain pluripotency. With the development of commercial human serum, and later serum-free media, the opportunity to generate clinical grade embryonic cell lines for therapeutic application has greatly improved (Inzunza *et al.*, 2005; Skottman and Hovatta, 2006).

Another issue that requires addressing is the standardisation of the media and/or matrices used in embryonic cell culturing systems. Considering only the use of human feeders a variety of different sources have proven effective in the maintenance of “stemness” i.e. differentiation potential and pluripotency, including foetal muscle (Richards *et al.*, 2002), foetal skin (Richards *et al.*, 2003), adult fallopian tube epithelial cells, foreskin fibroblasts (Hovatta *et al.*, 2003), adult marrow cells (Cheng *et al.*, 2003), and adult endometrial cells (Lee *et al.*, 2005), many of which have shown to be as capable as MEFs (Eiselleova *et al.*, 2008) and can additionally successfully support induced pluripotent stem cells (iPSCs) (Unger *et al.*, 2009) without altering their gene expression (Stephenson and Braude, 2010).

A frequently used basement membrane for the growth of pluripotent stem cells is the soluble basement membrane extract from Engelbreth-Holm-Swarm mouse tumour, known as matrigel (Kibbey, 1994). Matrigel is a feeder-free matrix and forms a continuous sheet of extra-cellular matrix for the cells, whilst maintaining them in their native state over prolonged periods of time (Ludwig *et al.*, 2006). This demonstrates the successful use of xeno-free conditions with synthetic matrices for cell culture conditions and promotes its use in the future (Klim *et al.*, 2010). Despite the success of using synthetic biomaterials, the cost of reagents tends to be too high for most laboratories and compels the ongoing use of MEFs as the gold standard basement feeder layer for the growth of research-grade hPSCs (Khadun, 2013).

Other culture conditions, such as the passaging method, can also have a major impact on the quality of cells cultured. Originally, hESC lines were manually cut passage-to-passage by the selection of colonies (Thomson *et al.*, 1998; Reubinoff *et al.*, 2000). This method is very labour-intensive and user-dependent. Newer methods, such as enzymatic passaging allow much faster cell culture procedures to occur by the uniform production of stem cell colonies in larger quantities (Ellerström *et al.*, 2007). Although this method would be much more practical for large-scale expansion for potential therapeutic use, the issue of more spontaneous differentiation occurring using this method has been raised (Draper *et al.*, 2004; Hasegawa *et al.*, 2006; Khadun, 2013), and more importantly, the use of enzymes, such as trypsin and accutase, for passaging has found more selective pressure for an increased level of chromosome aberrations

accumulating in the hPSCs (Brimble *et al.*, 2004; Buzzard *et al.*, 2004; Draper *et al.*, 2004; Schwartz *et al.*, 2011; Garitaonandia *et al.*, 2015). This has led to the drive to find more suitable enzymes for the large-scale production of hPSCs, but unfortunately has also increased the number of different enzymes available to scientists and decreased the level of uniformity in the stem cell community.

Furthermore, newer methods for the bulk production of hPSCs have been used increasingly in recent years. These methods include the use of support matrices in bioreactors, also known as microcarrier suspension cultures (Oh *et al.*, 2009; Gupta *et al.*, 2016), bioreactors (Kehoe *et al.*, 2010; Abraham *et al.*, 2017) and likewise CRISPR-Cas9 for disease modelling using hESCs and iPSCs (Budde *et al.*, 2017; Jacobs *et al.*, 2017; Kim, Kang and Ju, 2017). The development of such methods increases the potential of treatment for a wide range of different diseases and has given rise to a large number of research-grade cell lines, including cell lines carrying mutations for neurofibrillin (Hewitson *et al.*, 2016) and cystic fibrosis (Miere *et al.*, 2016).

With large scale automation becoming a widely accepted next step for downstream processes, the characterisation of these cells is vital. Newer methods need to be developed for the sensitive characterisation of hPSCs intended for therapeutic use.

1.1.4. The Problem with Using Stem Cells

1.1.4.1. Ethical and Political Issues

There are many ethical and political issues surrounding the use of human embryonic stem cells for research. The main problem associated with their use is the derivation of pluripotent stem cell lines from embryos, which causes the destruction of embryos (Lo and Parham, 2009). For this reason, the use of hESCs in potential therapies has been both limited and controversial. Previously, some countries, such as France, Germany and Australia have had stringent laws in place that either discourage or completely ban hESC research (Holm, 2006; Levine, 2008; Elstner *et al.*, 2009) with Ireland notably banning the use of embryos for research completely (*EuroStemCell*, 2018)

Similarly, in 2001 the Bush administration in the USA stopped federal funding for embryonic stem cell work that left the USA underperforming in hESC research (Seelye, 2001). However, in light of the Obama administration, in 2009, new regulations allowed research with previously derived stem cell lines to be considered for federal funding (Holm, 2006; Dhar and Hsi-En Ho, 2009; Nasaw, 2009). In addition, James Thomson's (Servick, 2014; Fikes, 2015; Jensen, 2015) patents on the derivation of hESCs has slowed down industrial development of hESC use. Although these patents are only valid in the USA, this combined with federal funding problems has delayed researchers globally in the development of hESC therapies.

In the UK, a Steering Committee was established in 2002 to oversee the activities within the UK Stem Cell Bank (UKSCB) and any research involved with established hESCs (*Medical Research Council*, 2018). The committee functions to make sure all proposed research uses cells ethically sourced with appropriate donor consent.

1.1.4.2. Genomic Instability

Both ESCs and iPSCs often accumulate whole chromosome gains and/or losses, also known as aneuploidies. These chromosomal abnormalities typically include chromosomes 8, 12, 17, 20 and X, as shown in Figure 1.3 (Draper *et al.*, 2004; Maitra *et al.*, 2005; Baker *et al.*, 2007; Taapken *et al.*, 2011) and are often recurrent after prolonged culturing (Amps *et al.*, 2011).

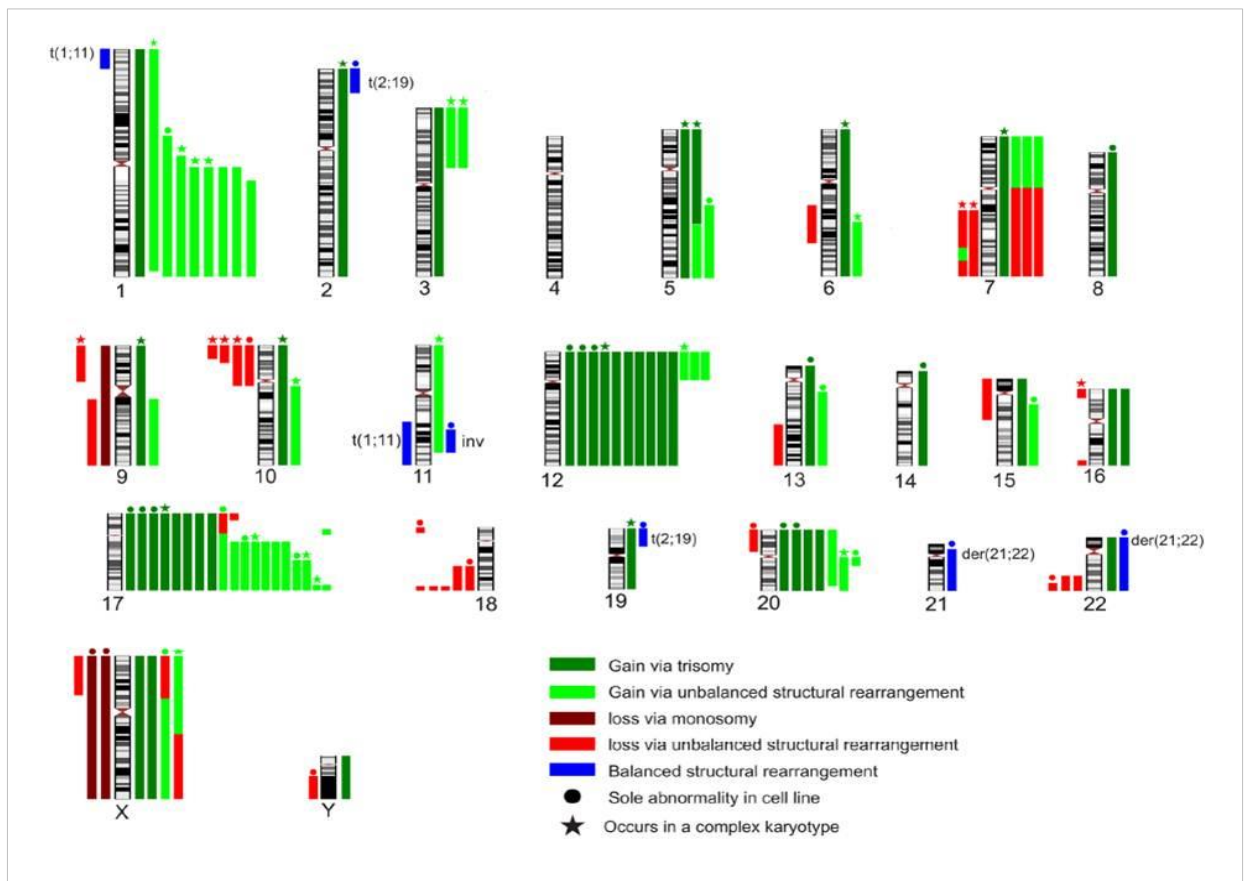


Figure 1.3. Common Chromosome Gains and/or Losses in hPSCs

Ideogram demonstrating the common gains and/or losses found in human pluripotent stem cells (Amps *et al.*, 2011). 125 human embryonic stem cells and 11 induced pluripotent stem cells from most major ethnic groups were analysed across 28 different laboratories worldwide using both cytological and sequence-based karyotyping techniques.

This is unlike in live human births, where the most common aneuploidies are the chromosomes containing fewer genes i.e. human chromosomes 13, 18 and 21 (Caine *et al.*, 2005), and in spontaneous abortions, where the common aneuploidies include human chromosomes 4, 7, 13, 15, 16, 21 and 22 (Fritz *et al.*,

2001) (Table 1. 1). Seemingly the aneuploidies accumulating in the hiPSCs in culture are not viable for life and are strikingly similar to the aneuploidies that are found in human embryonal carcinoma cells (hECC), with respect to the types of karyotypic changes observed (Summersgill *et al.*, 2001; Reuter, 2005; Harrison, Baker and Andrews, 2007) and in gene expression profiles (Sperger *et al.*, 2003), suggesting a tumorigenic potential. Furthermore, stem cells with these recurrent gains/losses display growth advantage in culture (Peterson and Loring, 2014), signifying that these chromosomes contain critical genes needed for cell growth, pluripotency and possibly tumorigenesis. This poses a serious threat to the therapeutic use of ESCs and/or iPSCs, as the effects of using genomically unstable stem cells in patients is unknown (Brimble *et al.*, 2004; Draper *et al.*, 2004; Peterson and Loring, 2014).

Cell Type	Chromosomal Abnormalities
Embryonic Stem Cells	1, 12, 17, 20, X
Induced Pluripotent Stem Cells	1, 9, 12, 20, X
Human Embryonal Carcinoma Cells	1, 12, 17, 20, X
Live Births	13, 18, 21, X, Y
Abortions	4, 7, 13, 15, 16, 21 and 22

Table 1. 1 Chromosomal Aneuploidies in Specific Cell Types or in Live Births and Abortions

The table shows in specific chromosome gains and/or losses that occur most commonly in the different cell types and in live births and abortions (Fritz *et al.*, 2001; Summersgill *et al.*, 2001; Caine, *et al.*, 2005; Reuter, 2005; Harrison, *et al.*, 2007).

Currently, it is unknown what effects these aneuploidies may have if cells containing them are administered to human patients. It has been proposed that the possibility of a malignant transformation of the cells and then unregulated proliferation could limit their use for future therapies (Herberts, Kwa and Hermsen, 2011). An issue that is particularly important to address is the risk of transplanting hPSCs into individuals

without being able to control their self-renewal capacity (Kanemura *et al.*, 2014). It has already been demonstrated when using murine mesenchymal stem cells (MSCs) that aneuploidy from prolonged cell culture can lead to malignant transformation *in vivo* (Miura *et al.*, 2006). This could, in turn, lead to devastating consequences if patients were injected with unstable differentiated cells derived from hPSCs. Tumour development from non-host origin has been reported after the injection of karyotypically normal neural stem cells into an ataxia telangiectasia patient (Amariglio *et al.*, 2009), however many details of the procedure had not been disclosed and it was thought that an extensive enough characterisation of the transplanted cells did not occur (Baker, 2009). Additionally the DNA integrity of iPSCs potentially used for patients is of concern (Yang *et al.*, 2008; Bai *et al.*, 2013). This is due to the reprogramming methods used for iPSC, particularly the use of the oncogene, *C-MYC*, where the chances of insertional mutagenesis and the inhibition of proto-oncogenes could lead to malignant transformation (Bai *et al.*, 2013); Furthermore, it has been reported that somatic cells with pre-existing chromosomal mutations limited the reprogramming of the cells to iPSCs (Yang *et al.*, 2008).

1.1.5. Nuclear Architecture

The nucleus is the organelle that protects the genetic material of the cell, as well as regulate several different functions, including DNA replication and repair, gene expression and apoptosis. Because of the range of different functions, the nucleus is organised in a highly-ordered way with a number of different compartments, such as the nucleolus, genome and nuclear envelope, which contains many different proteins that make up the nuclear architecture. Nuclear structure maintains the integrity and genomic health of nuclei and allows them to function efficiently. Disruption to any of these nuclear components has been associated with many different diseases or nucleopathies (Gruenbaum *et al.*, 2003; Bridger *et al.*, 2014).

The eukaryotic cell nucleus is separated from the cytoplasm by a complex barrier, known as the nuclear envelope, which is made up from a number of different parts, including the nuclear membrane, the nuclear lamina and finally, the nuclear pore complexes. The nuclear membrane is a double-layered membrane, where the outer membrane is a continuation of the endoplasmic reticulum, whereas the inner membrane faces the interior of the nuclei. The nuclear membrane contains a collection of over sixty-seven integral membrane proteins (IMPs), such as emerin, lamin B receptor, MAN1, nesprins, barrier to autoinegration factor (BAF) and SUN proteins (Schirmer *et al.*, 2003). These proteins, in turn, help tether the nuclear lamina to the nuclear envelope and support the interaction of IMPS, chromatin-binding proteins and chromatin or DNA to each other (Bridger and Bickmore, 1998; Gruenbaum *et al.*, 2003; Zastrow, Vlcek and Wilson, 2004; Bridger *et al.*, 2007).

The inner nuclear membrane has a role in the maintenance of nuclear morphology (Bridger *et al.*, 2007) and is scattered with multiple nuclear pore complexes, which allow the selective movement of molecules in and out of the nucleus (Goldberg, 2004). The nuclear membrane also has functions in the regulation of gene expression in different tissues and in chromatin organisation (Dechat *et al.*, 2008). The nuclear lamina is a meshwork of type V intermediate filament proteins or “nuclear lamins” (Fisher, Chaudhary and Blobel,

1986; Gerace and Burke, 1988). The lamins contain an α -helical rod domain with a globular N-terminal head at one end and a C-terminal tail domain on the other (Strelkov *et al.*, 2004); this shape helps the lamins form polymers that arrange the lamin meshwork (Figure 1.4). For lamins to form a layer between chromatin and the inner membrane of the nuclear envelope, a basic structure is assembled using the lamin monomers. The lamins, first, dimerise via their α -helical rod domain (Strelkov *et al.*, 2004; Dechat *et al.*, 2010; Dittmer and Misteli, 2011) and then, with these dimers form head-to-tail interactions with multiple other dimers (Strelkov *et al.*, 2004; Herrmann *et al.*, 2009).

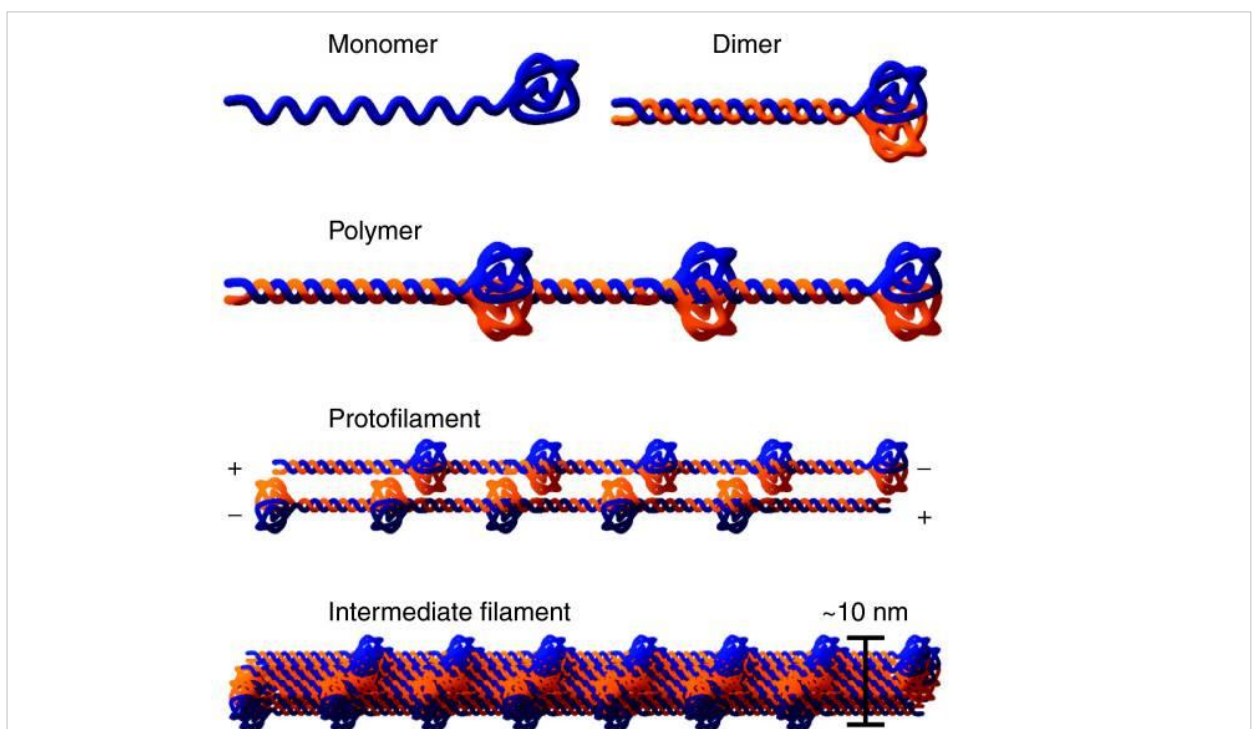


Figure 1.4. The Formation of Lamin Filaments

Cartoon representation of two parallel lamin monomers that can dimerise through coiled-coil interactions in their rod domains. The dimers then form head-to-tail interactions to assemble polymers, which further associate side-by-side with other polymers to form lamin filaments (Dittmer and Misteli, 2011; Gruenbaum, *et al.*, 2003).

1.1.6. Lamin Genes, Expression and Disruption

Humans have three lamin genes, *LMNA*, *LMNB1* and *LMNB2*, which code for seven different lamin proteins. *LMNA* encodes the A-type lamins, lamin A, A Δ 10, C and C2 (Fisher, Chaudhary and Blobel, 1986; McKeon, Kirschner and Caput, 1986; Lin and Worman, 1993; Furukawa, Inagaki and Hotta, 1994; Machiels *et al.*, 1996). Lamins A and C are alternate splicing forms of the *LMNA* gene with the former having ninety-eight additional amino acids (Berrios and Fihser, 1986) and the latter, six unique amino acids at its C-terminal end (Fisher, Chaudhary and Blobel, 1986; McKeon, Kirschner and Caput, 1986). Lamin A Δ 10 is identical to Lamin A, however it has exon 10 completely spliced out (Machiels *et al.*, 1996; Broers *et al.*, 2006), and Lamin C2 is a form of lamin A that lacks in the head and coil regions of lamin A and is found only in germ line cells (Furukawa, Inagaki and Hotta, 1994; Peter and Stick, 2012). Lamin B1 is a product of the *LMNB1* gene, whereas lamins B2 and B3 are splice variants of *LMNB2* (Pollard *et al.*, 1990; Biamonti *et al.*, 1992; Stuurman, Sasse and Fisher, 1996).

A-type lamin expression is developmentally regulated, therefore changes with differentiation (Lehner *et al.*, 1987; Rober *et al.*, 1989; Riemer *et al.*, 1995). Lamin A Δ 10 is expressed in very low levels in all cell types, whereas lamins A and C are expressed in both early and late embryos (Schatten *et al.*, 1985; Stewart and Burke, 1987; Houliston *et al.*, 1988; Foster *et al.*, 2007; Malhas *et al.*, 2007), however not in blastocytes (Schatten *et al.*, 1985; Stewart and Burke, 1987). B-type lamins, however, are expressed in most somatic cells in both adults and embryos (Vergnes *et al.*, 2004). Lamin C2 is expressed in the testis and during meiosis (Furukawa, Inagaki and Hotta, 1994; Alsheimer and Benavente, 1996), whereas lamin B3 is expressed only in sperm cells and oocytes (Furukawa, Inagaki and Hotta, 1994).

All of the lamin precursor mRNAs, except lamin C, contain a CaaX motif at the C-terminal end that allows farnesylation to occur via the enzyme farnesyltransferase. Lamin C does not undergo any post-translational modifications. Following this, both A-type and B-type lamins have been observed both at the nuclear periphery and as foci in the nucleoplasm. The distribution of lamin proteins in the nucleus can differ with

the cell cycle. For example, during the early G₁ phase A-type lamins appear as foci, however with the S-phase the lamin foci disappear (Bridger *et al.*, 1993).

In human and mouse ES cells, the presence of lamins B1 and B2 was observed, an essential part of all cell types, however lamin A/C was absent in the nuclear periphery of ES cells (Constantinescu *et al.*, 2006) (Constantinescu *et al.*, 2006) and has been observed to completely disappear with successful reprogramming of iPSCs (Mattout, Biran and Meshorer, 2011). In addition, lamin A/C was found to accumulate with the downregulation of *OCT4*, a hallmark of cells differentiating (Constantinescu *et al.*, 2006) The absence of lamins A/C has been suggested to contribute to the ESC genome plasticity compared to the more rigid state of somatic cell chromatin (Meshorer and Misteli, 2006). Lamins A/C associate with the nuclear envelope, heterochromatin and histones. As heterochromatin is often found at the nuclear periphery and can associate with lamins A/C, it is possible that with differentiation the accumulation of lamins A/C causes more association with chromatin and therefore more binding with lamin-associated proteins. This complex interaction of chromatin and the "nuclear wall", comprised of lamins and lamin-associated proteins, may compromise how "rigid" the chromatin within differentiated cell nuclei is. Moreover, in ESC nuclei because there is less of this interaction, the chromatin would be less restricted in movement (Meshorer and Misteli, 2006; Meshorer *et al.*, 2006; Morris, Kelly, Chotalia and Pombo, 2010). Furthermore, increase in lamin A has been linked to higher stability against nuclear rupture and increase in nuclear "stiffness". Such findings suggest that cell types with low levels of lamin A are more prone to nuclear stress and therefore more likely to have disruptions in chromosome territory arrangements (Swift, et al., 2014).

Lamin A directly regulates the binding of lamina-associated domains (LADs), associating the nuclear membrane to heterochromatic regions of the nucleus. This implies a role of lamin A in epigenetic regulation. Physical regulation of LADs is linked to tissue stiffness in different cell types. Additionally, lamin A knockdown affects the SRF pathway that promotes expression of abundant actin-myosin cytoskeletal components involved in the differentiation of cells (Swift and Discher, 2014). The SRF pathway is partially

regulated by nuclear actin (Olson and Nordheim, 2010; Baarlink, Wang and Grosse, 2013), which binds to lamin A (Simon, Zastrow and Wilson, 2010) and other proteins associated with lamin A, such as emerin (Simon, Zastrow and Wilson, 2010). This would suggest a functional role of lamin A in the indirect regulation of the differentiation of cells via an inhibitory effect on nuclear actin and myosins.

A-type lamins have been observed to associate with chromatin histone, DNA replication sites and RNA splicing speckles (Muralikrishna *et al.*, 2001; Zastrow, Vlcek and Wilson, 2004; Broers *et al.*, 2006). In addition, A-type lamins binds to nuclear proteins, such as emerin, lamina-associated protein 1 (LAP1), lamina-associated protein 2 (LAP2), lamin B receptor (LBR), nesprins, MAN1 and telomeres (Worman *et al.*, 1988; Shoeman and Traub, 1990; Dechat *et al.*, 2000; Sakaki *et al.*, 2001; Mansharamani and Wilson, 2005). Although it has not been clearly identified whether A-type and B-type lamins interact with each other, it has been suggested that B-type lamins are important for the structural organisation and maintenance of A-type lamins within interphase nuclei (Shimi *et al.*, 2008). As lamins are involved a number of functions within cells, potential mutation or disruption to the lamin protein expression could lead to the misregulation of many different activities and thus, also contribute or causes disease.

The abnormal expression of A-type lamins has been associated with increased tumour progression in diseases, such as small cell lung cancer, testicular germ cell tumours, Hodgkin's disease, skin cancers and in leukaemia (Kaufmann *et al.*, 1991; Kaufmann, 1992; Machiels *et al.*, 1997; Oguchi *et al.*, 2002; Burke and Stewart, 2006). Mutations in exon 11 of the *LMNA* gene can cause the most common form of Hutchinson-Gilford Progeria Syndrome (HGPS), a disease causing premature aging, disrupted heterochromatin formation, increased apoptosis and abnormally-shaped nuclei (De Sandre-Giovannoli *et al.*, 2003; Bridger and Kill, 2004; Scaffidi and Misteli, 2005; Capell and Collins, 2006).

Conversely, B-type lamin expression is thought to be essential for survival *in-vivo* (Vergnes *et al.*, 2004), although a study had found that in ESCs it is not required for the maintenance of pluripotency and self-renewal (Kim *et al.*, 2011). B-type lamins' differential expression has been linked to nuclear rotation, mitotic spindle defects (Tsai *et al.*, 2006), gene silencing (Peric-Hupkes and van Steensel, 2010) and senescence

(Shimi *et al.*, 2011). More recently Lamin B2 disruption has been linked to aneuploidy formation and changes to chromatin organisation (Ranade *et al.*, 2017).

Nuclear lamin disruption has often been linked to abnormal nuclear morphology and genomic instability. In breast cancer cells, A-type lamins are often lost completely or may be expressed heterogeneously with many cells experiencing mitotic arrest, enlarged nuclei and chromosome aneuploidies, such as chromosome X gains (Capo-chichi *et al.*, 2011). Ovarian cancer cell lines had shown similar results with lamin A/C loss leading to aneuploidy; these cells shown increased p53 and p21 protein levels, however the authors were not able to conclude whether the aneuploid cells with loss in both A-type lamins and p53 would permit cell survival (Capo-chichi *et al.*, 2011).

1.1.7. Genome Organisation

Chromosomes are organised into discrete compartments, known as chromosome territories (Cremer and Cremer, 2001) within interphase nuclei and are conserved throughout different species (Marshall *et al.*, 1996; Bridger and Bickmore, 1998; Parada and Misteli, 2002; Tanabe *et al.*, 2002; Foster, Griffin and Bridger, 2012). This organisation is influenced by the chromosome gene density and the guanine-cytosine (GC) content (Dietzel *et al.*, 1998; Visser and Aten, 1999; Bridger *et al.*, 2000; Boyle *et al.*, 2001; Cremer and Cremer, 2001; Federico *et al.*, 2006; Meaburn and Misteli, 2007), transcription (Volpi *et al.*, 2000; Mahy *et al.*, 2002; Mahy, Perry and Bickmore, 2002), differentiation (Cremer and Cremer, 2001; Parada, McQueen and Misteli, 2004; Wiblin *et al.*, 2005; Meshorer and Misteli, 2006; Szczerbal, Foster and Bridger, 2009; Fraser, Ferrai, *et al.*, 2015) and, in addition, can be altered due to disease (Cremer *et al.*, 2003; Meaburn *et al.*, 2007; Mehta *et al.*, 2011), upon infection (Knight *et al.*, 2011; Arican-Goktas *et al.*, 2014), and serum removal (Mehta *et al.*, 2010). In addition, the organisation of specific genes can change with gene expression, with genes able to loop out from their chromosome territories (Volpi *et al.*, 2000; Christova *et al.*, 2007).

Conversely, mESC nuclear architecture and positioning of the chromosomal territories is suggested to have a certain flexibility in specific location (Meshorer and Misteli, 2006), presumably in order to allow global gene activity to function whilst remaining pluripotent and maintaining self-renewal capacity. This has been supported by findings of an accumulation of heterochromatin concomitantly with differentiation (Francastel *et al.*, 2000), which implies that chromosome location is at least partially controlled through epigenetic regulation of chromatin modelling. Indeed, as shown in Figure 1.5, differentiation-dependent chromatin modifications occur in cells with an increase in silenced chromatin markers and a decrease in active chromatin markers (Keohane *et al.*, 1996; Lee, Hart and Skalnik, 2004; Meshorer *et al.*, 2006), suggesting ESC chromatin to be more open or plastic (Lee, Hart and Skalnik, 2004; Meshorer and Misteli, 2006).

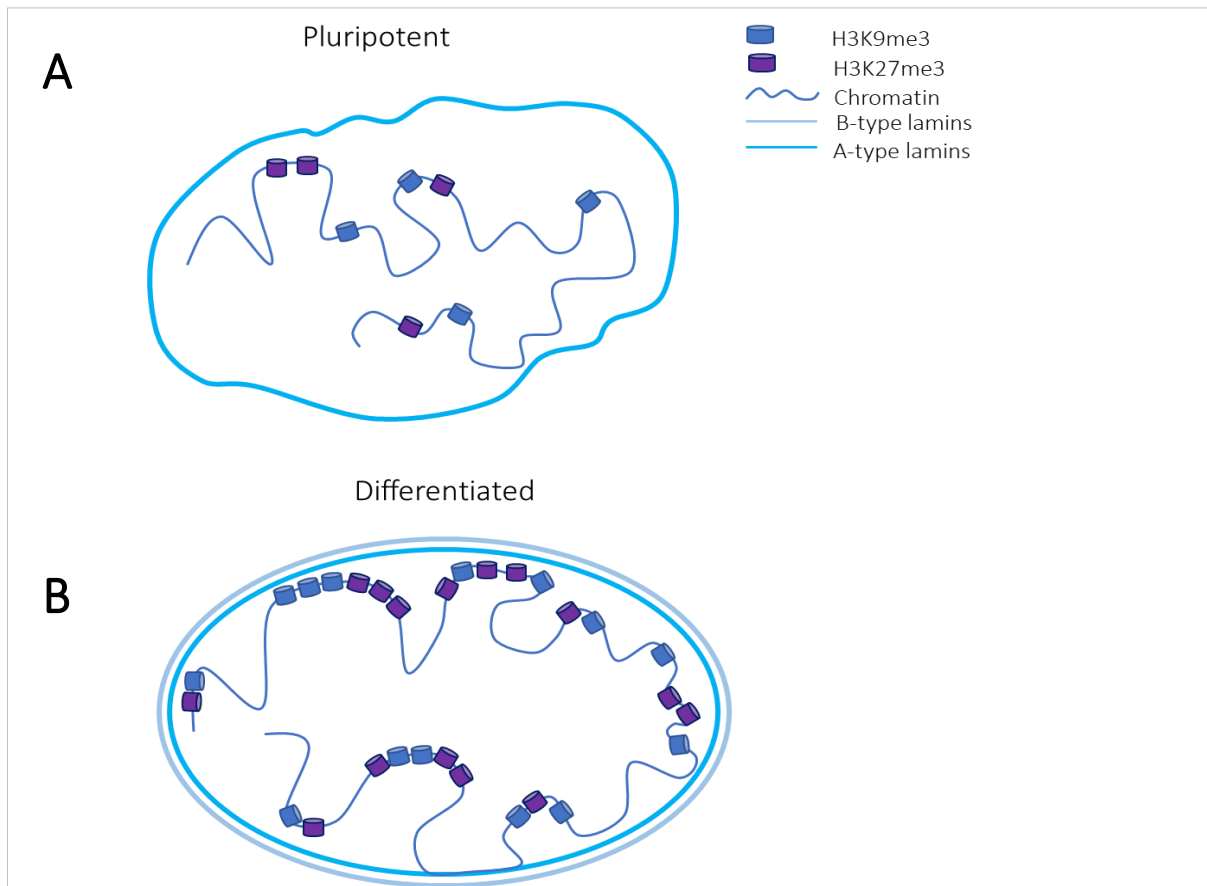


Figure 1.5. Nuclear Architecture and Genome Organisation in Somatic Versus Naïve Cells

The inner blue circle represents A type lamins, whereas the outer circle represents B type lamins. Histone modification markers associated with silenced chromatin, such as H3K9me3 and H3K29me3 are shown as purple and blue cylinders throughout the chromatin. The pluripotent cell in A depicts the lack of these histone markers in comparison to the differentiated cell shown in B. The image was created as a modification to previous studies (Meshorer and Misteli, 2006).

However, a gene-density radial distribution of chromosome territories has also been observed in hESCs (Wiblin *et al.*, 2005; Bártoová *et al.*, 2008) and in human blastomeres (Finch *et al.*, 2008), although gene-rich chromosomes 17 and 19 were positioned more centrally in granulocytes when compared to ESC (Bártoová *et al.*, 2001). Despite this, after differentiation, chromosome 17 positioning in pluripotent and somatic cells was the observed to be similar (Wiblin *et al.*, 2005; Bártoová *et al.*, 2008). However, a variation in centromere positioning (Wiblin *et al.*, 2005; Bártoová *et al.*, 2008) and in the pluripotency gene, *NANOG* (Wiblin *et al.*, 2005) was observed. In normal somatic cells centromeres are mostly, but not exclusively, found nearer to the nuclear periphery (Shelby *et al.*, 1996) or around the nucleoli (Bridger *et al.*, 1998; Carvalho *et al.*, 2001; Weierich *et al.*, 2003; Gilchrist *et al.*, 2004), although changes to their spatial arrangement may relate to

the stage of cell cycle and gene expression (Ferguson, Ward and Manueiidis, 1992; Weimer *et al.*, 1992; Hulsapas *et al.*, 1994; Janevski, Park and De Boni, 1995). Unlike somatic cells ES centromere clusters are usually positioned towards the nuclear interior, however after differentiation the centromeres arrange themselves towards the nuclear periphery (Bártová *et al.*, 2008; Butler *et al.*, 2009) or around the nucleoli (Bártová *et al.*, 2008). Similar centromere arrangements have been demonstrated in human B and T lymphocytes (Skalníková *et al.*, 2000). This rearrangement may be due to heterochromatic regions containing more inactive genes and therefore being anchored to the nuclear periphery.

Embryo genome activation (EGA) occurs during embryonic development at a time when maternal transcripts and proteins are being degraded and embryonic transcripts start synthesis. This period in development is known as the maternal-to-embryonic transition (MET) is initiated at different times dependent on species (Braude, Bolton and Moore, 1988; Sirard, 2012). In humans this occurs at the four-to-eight-cell stage (Braude, et al., 1988). As development proceeds, different genes become activated at specific time points and chromatin can rearrange itself to aid this process (Graf *et al.*, 2014). In bovine cells, the gene-dense *Bos taurus* autosome (BTA) 19 and gene-poor BTA 20 chromosome territories positions change after EGA. Prior to EGA a peripheral, radial distribution of both chromosomes was present (Graf *et al.*, 2014). However, post-EGA the organisation of chromosome territories shifted to a more gene-density-related radial distribution (Koehler, et al., 2009). This suggests that EGA could also affect hESC chromosome territory positioning. Additionally, a factor that may contribute to the different chromatin organisation patterns is the different transcription patterns between ESC and somatic cells. This is supported by the findings from Koehler, 2009, where ESCs splicing factors were distributed through the nuclei and after differentiation became more concentrated into distinct areas and is consistent with data suggesting that hESC nuclei are more plastic than somatic cells (Koehler *et al.*, 2009).

1.1.8. Mechanism of Aneuploidy Formation in Human Pluripotent Stem Cells

To maintain genomic integrity, it is essential that with each cell division the distribution of DNA in each daughter cell is equal. Unfortunately, how exactly aneuploidies come about in human pluripotent stem cells is still unknown. I discuss several different mechanisms that could lead to the formation of the gain or loss of whole chromosomes and discuss the genomic abnormalities that could contribute to aneuploidy formation.

1.1.8.1. Mitotic Segregation Defects

Telomeres are repetitive nucleotide sequences found at the end of chromosomes to prevent chromosome end-to-end fusions that can result in chromosome instability (CI). In hESCs, the telomerase enzyme is active to maintain the length of telomeres length and in iPSCs, telomerase is re-activated after reprogramming and the process of telomere lengthening begins (Marion et al., 2009; Takahashi et al., 2007; Takahashi and Yamanaka, 2006). Anaphase bridges or chromatin bridges occur when two end-to-end fused chromosomes are being pulled apart by opposing mitotic spindle fibres, attached by the kinetochores during anaphase and a chromatin bridge still links the two daughter cells. Although the formation of anaphase bridges does occur in healthy cells (Baumann *et al.*, 2007; Chan, North and Hickson, 2007), it is strongly associated with the erosion of telomeres (Tusell *et al.*, 2010), as end-to-end fusions of chromosomes causes breakage-fusion-bridge (BRB) cycles, resulting in CI (DePinho, 2000; Gisselsson *et al.*, 2001; Hackett, Feldser and Greider, 2001).

Normally, telomeres shorten as a result of each cell division and in stem cells telomerase is active to ensure the maintenance of telomere length, however, telomerase activity has been implicated in tumorigenesis (Shay and Wright, 2010). Telomeric sequences are associated with a group of proteins- TRF1, TRF2, RAP1, POT1, TIN1, and TIN2, collectively known as the shelterin complex (Liu *et al.*, 2004). The disruption of these proteins can cause fragile sites, contributing to DNA replication defects (Sfeir *et al.*, 2009), anaphase bridges (Bunch *et al.*, 2005; Nera *et al.*, 2015) , fusions (Pardo and Marcand, 2005) and the activation of DNA damage responses (Palm and de Lange, 2008). A recent study has shown that overexpression of telomeric

protein TRF1 in mouse embryonic stem cells can cause anaphase bridges to form (Lisaingo, Uringa and Lansdorp, 2014), and thus highlights the importance of telomere protection via telomeric proteins in embryonic stem cells.

On occasion, not all parts of the chromatid sisters are resolved together, due to segregation issues from the lack of a kinetochore attachment to the mitotic spindle and one daughter cell can end up with the other daughter cell's chromosome, resulting in an aneuploidy in both new cells. How the mitotic spindles assemble in hPSCs is relatively unknown, however spindle defects, such as asymmetric orientation, have been linked with carcinogenesis in *Drosophila* (Caussinus and Gonzalez, 2005; Castellanos, Dominguez and Gonzalez, 2008) and in gut epithelial stem cells (Quyn *et al.*, 2010). A balance of symmetric or asymmetric cell divisions are necessary for normal development and tissue homeostasis, however abnormal proliferation can occur and the cells may become tumorigenic (Noatynska, Gotta and Meraldi, 2012).

Alternatively, lagging chromosomes from the mitotic spindle detachment or the bipolar orientation of chromatids (Cimini *et al.*, 2002) could instead form a separate compartment of chromatin from the nucleus. Acentric and acentromeric, whole or fragment chromosomes can become micronuclei (Cimini, Tanzarella and Degrossi, 1999; Minissi *et al.*, 1999; Norppa and Falck, 2003) or double-minute (DM) chromatin, where small fragments of amplified genes occur extra-chromosomally during tumorigenesis (Haaf and Schmid, 1988; Itoh and Shimizu, 1998). Although nuclear contents may be lost in this manner, they can also be engulfed or taken back into the nucleus that lost them (Minissi *et al.*, 1999). Micronuclei or DMs can appear as a result of replicative stress and sometimes still remain transcriptionally active, albeit reduced (Hoffelder *et al.*, 2004; Utani, Kawamoto and Shimizu, 2007), with occasional nuclear lamin expression (Tanaka and Shimizu, 2000), that coincides with upregulated transcription (Utani, Kawamoto and Shimizu, 2007). Interestingly, the micronuclei that did form a nuclear lamina were also able to start DNA replication (Tanaka and Shimizu, 2000), implicating a function of lamins in DNA replication. It is currently unknown how exactly micronuclei can contribute to the overall phenotype of the cell, especially due to their lack of nuclear trafficking and reduced transcription (Hoffelder *et al.*, 2004), but the reduction of amplified genes found in

micronuclei increased the radiation sensitivity of cancer cells (Sanchez, Barrett and Schoenlein, 1998; Schoenlein *et al.*, 2003). Cells with micronuclei often underwent abnormal mitosis and had elevated levels of apoptosis (Utani *et al.*, 2010). In mouse embryonic stem cells, an increase in micronuclei formation and apoptosis was observed with the downregulation of the pluripotency marker *Oct4* (Zhao *et al.*, 2014), suggesting that compromised cell culture techniques could, in fact, directly affect the genomic instability of stem cells. Since stem cells have an increased rate of proliferation for the maintenance of their self-renewal capacity (White and Dalton, 2005; Neganova and Lako, 2008), this could be a factor contributing to their genomic instability via the formation of micronuclei (Stopper *et al.*, 2003). For example differentiation of embryonic stem cell to neural progenitor cells causes nearly a two-fold increase in micronuclei formation and an increase in CI (Sartore *et al.*, 2011).

1.1.8.2. DNA Damage

As double-stranded breaks (DSBs) are considered the first causative damage associated with chromosome abnormalities, which can further lead to formation of tumours (Pandita and Richardson, 2009), the chromosomal instability of hPSCs are of high concern. Despite elevated rates of apoptosis and hypersensitivity to apoptosis in ESCs (Dravid *et al.*, 2005; Lin *et al.*, 2005; Nagaria *et al.*, 2016), the apoptosis inhibitor protein, survivin, often associated with polyploidy development (Li *et al.*, 1999) and increased expression in cancerous cells (Altieri, 2003), is also expressed in high levels in ESCs (Mull, et al., 2014). This suggests that apoptosis alone is not enough to stop the accumulation of aneuploidies in hPSCs. However, it is well known that during development, blastocysts must go through many cell divisions very quickly, suggesting that perhaps the cells have to compromise on their DNA proof-reading machinery in order to achieve this. This is supported by the shortened G₁ phase of ESCs (Becker et al., 2006; Ghule, et al., 2008), exposing them to higher replicative errors. Furthermore, studies in hESC p53-p21 pathways have shown that during stress stimuli, the cell cycle regulator, p21, mRNA is upregulated in hESCs, however no p21 protein is detected (Dolezalova, et al., 2012). During DNA damage in ESCs, p53 binds directly to *NANOG*'s promoter, suppressing it and promoting ESC differentiation (Bradner, 2010). If the p53 levels are reduced,

the levels of spontaneous differentiations are also reduced. (Qin, et al., 2007). It seems that in hiPSCs DNA damage does not give rise to single-stranded DNA regions, with the cells, thus not activating checkpoints and not permitting DNA repair to occur (Desmarais *et al.*, 2012), despite there being elevated gene expression levels of DNA repair genes (Momcilovic *et al.*, 2010).

Furthermore, hiPSCs have been found to be deficient in intra-S checkpoints and also in G₂/M decatenation or chromatin dis-entanglement preventing delayed entry of inappropriately condensed chromosomes into mitosis and permitting the formation of anaphase bridges (reviewed in Lamm, et al., 2016). Topoisomerase II allows the chromatin decatenation to occur in G₂ to delay mitosis and to allow smooth sister chromatid segregation (Uemura *et al.*, 1987; Holm, Stearns and Botstein, 1989). When the decatenation checkpoint is disrupted entangled chromosomes segregate and can form aneuploidies (Gorbsky, 1994; Andoh and Ishida, 1998). Chromosome decatenation deficiency has been reported in mouse ESCs and human multipotent progenitor cells, however improved decatenation was observed with cell differentiation (Damelin *et al.*, 2005). The reason behind such entanglement of ESC chromatin may be due to the lack of higher chromatin organisation in nuclei. ESC nuclei lack chromatin silencing markers, such as H3K9, H3K27. Open chromatin in hPSCs with the dispersed presence of the DNA damage marker, gamma-H2AX (γ -H2AX) in hESCs (Meshorer *et al.*, 2006), suggests a more exposed, and therefore more vulnerable chromatin. The plasticity of the chromatin state may be one of the reasons for the increased genomic instability of hPSCs when grown *in vitro*. This is, however, debatable as no additional protection of heterochromatin in comparison to euchromatin has been observed from the reactive oxygen species (ROS) induction of double-stranded breaks (DSBs) (Woodbine *et al.*, 2011), since lower levels of Ataxia-telangiectasia mutated kinase (ATM) phosphorylation in iPSCs have been previously reported in cells treated with low levels of radiation, alongside hypersensitivity to apoptosis (Nagaraja *et al.*, 2016). The exact role of ATM in DNA damage is still unknown, but it has been suggested to be preferentially required in the DNA damage repair of heterochromatin (Goodarzi *et al.*, 2008). As hPSCs lack the presence of heterochromatin (Francastel *et al.*, 2000; Meshorer and Misteli, 2006), the reduced levels of ATM phosphorylation (Nagaraja *et al.*, 2016) would suggest to not have a significant effect on the genomic integrity of the cell. However, ATM-deficient

iPSCs were less efficient in reprogramming and influenced the appearance of genomic variation (Marión *et al.*, 2009; Kinoshita *et al.*, 2011; Lu *et al.*, 2016).

It should be highlighted that ATM phosphorylates a number of proteins, related to apoptosis, cell cycle checkpoints and DNA repair (Lee and Paull, 2007), therefore its potentially reduced role in hPSCs should be carefully considered. Similarly, Artemis, an endonuclease associated with non-homologous end-joining (NHEJ) is required for the maintenance of genomic stability (Woodbine *et al.*, 2011), but its absence from cells did not impair myeloid differentiation, reprogramming or show significant of genomic instability (Felgentreff *et al.*, 2014).

Human pluripotent stem cells are known to accumulate gains and/or losses of whole chromosomes (Draper *et al.*, 2004; Maitra *et al.*, 2005; Baker *et al.*, 2007; Taapken *et al.*, 2011), often showing signs of growth advantage (Enver *et al.*, 2005; Baker *et al.*, 2007), making them similar to cancerous cells (Baker *et al.*, 2007). This cultural adaptation can occur, due to specific gene amplifications and a candidate driver mutation suggested in hPSCs is found in *BCL2L1*, located on chromosome 20. *BCL2L1* is associated with anti-apoptotic properties (Boise *et al.*, 1993; Amps *et al.*, 2011; Avery *et al.*, 2013; Na *et al.*, 2014), which is a hallmark of cancer (Herszfeld *et al.*, 2006; Yang *et al.*, 2008; Avery *et al.*, 2013). The knock-down of *BCL2L1* did diminish the growth advantage effect (Avery *et al.*, 2013). Other candidate genes suggested include genes found on chromosome 12, such as pluripotency –related genes *NANOG*, *DPPA3* and *GDF3*, oncogene *KRAS* and cell cycle regulator *CCND2* (Na *et al.*, 2014), on chromosome 17, such as *BIRC5(SURVIVIN)* (Na *et al.*, 2014), which is associated with ploidy development (Li *et al.*, 1999). Another candidate mutation could be with the oncogene *PTEN*, which is found on chromosome 10, associated with many different cancers (Jemal *et al.*, 2004; Takei *et al.*, 2008).

1.1.8.3. Bystander Effect

Another possible mechanism of the process of aneuploidy accumulation is not well understood. Cells could accumulate an aneuploidy and then via a bystander effect the aneuploidies start accumulating in neighbouring cells. Such mechanisms have been observed with radiation-treated cells causing cell

senescence in neighbouring cells (Nelson *et al.*, 2012), increased sister chromatid exchange (Nagasawa and Little, 1992; Deshpande *et al.*, 1996), increased *p53* expression (Hickman *et al.*, 1994; Azzam *et al.*, 1998), and most importantly chromosomal instability (Lorimore *et al.*, 1998; Sawant *et al.*, 2001). This instability is probably observed due to the reactive oxygen species (ROS) produced from the radiation (Yamamori *et al.*, 2012) causing DNA damage to occur (Yermilov *et al.*, 1996; Balasubramanian, Pogozelski and Tullius, 1998).

A similar effect has been observed with *Enterococcus faecalis*, an intestinal bacterium, where the production of ROS molecules can induce CI in human cells with defects in mismatch repair (Huycke *et al.*, 2001; Huycke, Abrams and Moore, 2002; Wang *et al.*, 2008). Although this theory needs to be investigated further, it is well established that ROS and nitrogen species from both radiation and metabolism can cause oxidative stress that can lead to DNA damage and senescence in cells (Lindahl, 1993; Suh *et al.*, 1999; Geiszt *et al.*, 2000). Moreover, it may be the case with hPSCs that if one event triggers an aneuploidy to occur, a bystander effect could then cause neighbouring cells to also acquire aneuploidies. Alternatively, this may be due to stem cells often being grown on a layer of inactivated feeders; the feeders would be under stress and could potentially cause a stressful environment to the stem cells. Mitomycin C (MMC) is used to treat the feeder cells that hESCs are grown on. This treatment can affect the neighbouring stem cells and potentially cause or promote the generation of aneuploidies in culture. This is supported by the increased levels of micronuclei observed (Asur, Thomas and Tucker, 2009), alongside increased homologous recombination (Rugo *et al.*, 2005) and changes in the expression of mitogen-activated protein kinase (MAPK) target genes (Asur *et al.*, 2010).

It has been previously proposed that the increased age of cells and the amount of ROS are linked (Finkel and Holbrook, 2000). As human pluripotent stem cells are metabolically very active and can be maintained in cultures for long periods of time, the increased age and the fast metabolism required in these cells could also be an aspect that factors in the genomic instability often observed. In contrast, it has been reported that both high levels and low levels of ROS can impair the reprogramming ability of cells into iPSCs (Zhou

et al., 2016) and elevated levels can impair their differentiation ability as well (Rönn *et al.*, 2017). These studies suggest that optimal levels of ROS may be required for the cells to grow stably in culture.

1.1.8.4. Nuclear Lamin Depletion

LMNA mutations cause impaired differentiation of adult stem cells (Gotzmann and Foisner, 2006; Pekovic and Hutchison, 2008; Scaffidi and Misteli, 2008), altered signalling pathways in mesenchymal stem cells (MSCs; Espada *et al.*, 2008; Meshorer and Gruenbaum, 2008; Scaffidi and Misteli, 2008; Hernandez *et al.*, 2010) and MSC death (Halaschek-Wiener and Brooks-Wilson, 2007; Meshorer and Gruenbaum, 2008; Prokocimer *et al.*, 2009).

In contrast, Lamin B1 and B2 knock-out does not affect the differentiation of blastocysts, but does affect organogenesis in mice (Coffinier *et al.*, 2010; Kim *et al.*, 2011) and mitotic spindle orientation and formation (Tsai *et al.*, 2006; Ma *et al.*, 2009; Kim *et al.*, 2011). This suggests that B-type lamins would have a functional role in making sure chromosomes are efficiently segregated during mitosis. This correlates with findings of Lamin B2 depletion being associated with aneuploidy formation, prolonged mitosis and formation of anaphase bridges (Kuga *et al.*, 2014; Ranade *et al.*, 2017).

1.1.9. Aneuploidy Detection Methods

For human pluripotent stem cells to become a common available therapy, scientists must be able to screen the cells intended for therapeutic use. One of the criteria for this screen is the ability to sensitively and accurately assess their karyotype. Currently, G-banding is a common technique used by clinical cytogenetics for the prenatal diagnosis of aneuploidies and structural rearrangements in foetuses and many different assays are currently on the market for aneuploidy detection. However, each platform, whether cytological or sequence-based, has its advantages and disadvantages with regards to sensitivity, resolution, turnover time, cost and staff requirement.

1.1.9.1. Quantitative Fluorescence Polymerase Chain Reaction

Quantitative fluorescence polymerase chain reaction (QF-PCR) is a technique that utilises multiple short tandem repeats (STRs) of the common aneuploidies, such as trisomy 13, 18 and 21 and sex chromosome aneuploidies to amplify the regions of interest. The method allows the multiplexing of different fluorescence intensities produced from the PCR, resulting in a fast method for chromosome copy number detection. The method can use different samples of origin, such as amniotic fluid, chorionic villus, foetal blood, postnatal blood and foetal tissue and had been demonstrated to be 99.2% accurate for whole chromosome aneuploidy (Cirigliano *et al.*, 2004; Ogilvie *et al.*, 2005) and 20-30% mosaicism detection (Donaghue *et al.*, 2005). QF-PCR has been reported to be a much cheaper and faster alternative to other assays and many laboratories have now replaced traditional fluorescence *in-situ* hybridisation with QF-PCR (Shaffer, 2007). Unfortunately, like many assays the limitation of QF-PCR is the inability to detect balanced chromosomal translocations.

1.1.9.2. Multiplex Ligation-Dependent Probe Amplification

Multiplex Ligation-Dependent Probe Amplification (MLPA) is an assay designed to detect gene dosage abnormalities by utilising up to 45 different DNA sequences. Rather than amplify the nucleic acids in the sample, the technique amplifies the probes that are added to the sample; the amplification depends on the presence of specific sequences in the sample. The probe intensities are quantified and the whole experiment typically takes 2-3 days (Sellner and Taylor, 2004; Shaffer, 2007). Like QF-PCR, MLPA cannot detect structural aberrations.

1.1.9.3. DNA Microarrays

DNA microarrays use a panel of DNA sequences that compare the copy number of each area of interest to a control; this, then calculates the gene copy number of the sample (Shaffer, 2007). The advantage of DNA microarray is the ability to construct the target molecules, although most commonly the pre-designed, commercially- available Agilent microarray platforms for Array Comparative Genomic Hybridisation (aCGH) are used. The technique can detect DNA dosage imbalances, such as aneuploidies, deletions and duplications with a high resolution, dependent on the target of interest and is a much faster approach than methods, such as FISH, due to the high-throughput data produced. Typically, DNA microarrays can only detect 10-25% of mosaicism (Lu et al., 2007; Manning et al., 2010; Novik et al., 2014; WiCell, 2017; Xiang et al., 2008).

Similarly, another commonly used kit, albeit with less DNA targets, bacterial artificial chromosomes-on-beads (BoBs™) is a novel easy to use method for the detection of aneuploidies utilising sequences attached to beads from bacterial artificial chromosomes (Choy *et al.*, 2014). The limit of all the microarray assays, however, is the inability to detect chromosomal rearrangements. In addition, for the detection of low level aneuploidies approximately 25% of cells must be aneuploid (Novik *et al.*, 2014).

1.1.9.4. Fluorescence *in-situ* Hybridisation

Fluorescence *in-situ* Hybridisation (FISH) is a technique that uses target-specific probes that are fluorescently labelled for the copy number identification of whole chromosomes or genes (Bridger and Volpi, 2010). FISH can be used in cells that are in both metaphase and interphase and be multiplexed i.e. multicolour FISH (mFISH) or spectral karyotyping (SKY FISH) to look at the whole genome karyotype. The limitation of FISH is that it is labour-intensive and has a lower resolution in comparison to novel methods that utilise hundreds or thousands of target molecules, however unlike those methods FISH can detect structural rearrangements of the genome and mosaicism (Hultén, Dhanjal and Pertl, 2003).

1.1.9.5. G-banding

An older method and one that is still used as the gold standard in clinics today is traditional karyotyping by G-banding. G-banding uses the staining of dark and light bands in metaphase spreads to distinguish between the different chromosomes (Hultén, Dhanjal and Pertl, 2003). Unfortunately, despite its common use in clinics, this method is highly labour-intensive and time-consuming, due to the difficulty in sample analysis; trained cytogenetics are required. In addition, a small number of metaphase spreads are usually analysed, which does not pose a problem during the presence of whole population chromosomal gains and losses, however for mosaicism it may not be an appropriate method of analysis, as it is not an accurate representation of the whole cell population in the sample. G-banding has been estimated to detect 5-10 % of mosaicism in cell culture (Baker, et al., 2007).

To summarise, currently there are a limited number of methods that are regularly used for the monitoring of genomic instability of human pluripotent stem cells. However, current methods are either labour-intensive, require specialist training or expensive, as well as not sensitive for the detection of low-level mosaicism that is common occurrence in hPSCs. New methods need to be developed and optimised for the detection of genomic instability in cells intended for therapeutic use.

Aims

The aim of this project is to develop a rapid and sensitive assay for the detection of chromosomal aneuploidies utilising ddPCR™. To characterise the impact of chromosomal abnormalities in the nuclei, fluorescence *in-situ* hybridisation will be used to map and compare the gene loci positioning in diploid and aneuploid nuclei of karyotypically stable lymphoblastoid cell lines.

Lamin pattern analysis, as well as gene and protein expression levels will be monitored in the diploid and aneuploid nuclei of the karyotypically stable lymphoblastoid cell lines. Lamins A, C, B1 and B2 levels will be assessed and compared in the different cell lines to detect any significant differences.

In addition, human pluripotent stem cells will be used to monitor the genomic stability, to map gene loci positioning in the nuclei to assess the significance of different media and matrices, as well as the effect of passage number. Pluripotency and lamin gene expression levels will be measured to observe any deviations with the different cell culture conditions. Finally, RNA-Seq will be used to investigate the global gene expression changes and the different up- and down-regulated pathways in the different cell lines and conditions.

Chapter II: The Application of Droplet Digital PCR for Sensitive Aneuploidy Detection

2.1 Introduction

2.1.1. Digital Polymerase Chain Reaction

Digital polymerase chain reaction (dPCR) is a sensitive assay for the absolute quantification of target nucleic acids in a sample (Vogelstein and Kinzler, 1999). Digital PCR works by the separation of a sample into a large number of partitions and in principle, each partition would contain either one or zero copies of the target molecule allowing the increased sensitivity in the detection of the target molecule. In droplet digital PCR (BioRad ddPCR™), after the sample partitioning with all necessary PCR components, such as primers, probe(s), and mastermix, PCR is performed in the optimal conditions for each specific amplicon and the amplicons are either hybridised with fluorescent TaqMan™ probes or labelled by the incorporation of a DNA-binding dye, EvaGreen®, to allow the detection of specific sequences. The droplets are then individually passed through a fluorescence detector in a ddPCR™ droplet reader and scored as either positive or negative for each fluorescence channel. For the TaqMan™ method two different fluorophores can be used to tag the probes, allowing a duplex reaction (Figure 2.1). However, to increase the number of detectable targets in a PCR reaction, Taqman™ probes can be manipulated in different concentrations to label more than two different target molecules; this allows researchers to multiplex for more than 2 targets. Using Poisson statistics, ddPCR™ is then able to determine the initial concentration of the input sample. For example, the human diploid genome is typically 6.6pg and thus for a 40ng genomic DNA (gDNA) input, approximately 6060.6 diploid genomes or 12,121.2 gene copies are found in a 20µl reaction volume (assuming 2 gene copies/genome). This, in turn, would mean that for a wild-type sample, two copies of genes in 40ng of a 20µl reaction, the expected concentration output from ddPCR™ is 606.6 gene copies/µl, whereas for one copy of a gene, 303.3 copies/µl would be expected. If the 20µl reaction was partitioned into 20,000 droplets, the gene copies per droplet (CPD) is calculated as (12,121.2 gene copies/20,000 droplets) 0.606 CPD. However, in reality, the random partitioning of ddPCR™ leads to the uneven distribution of gene copies and the droplet occupancy is not uniform with some droplets containing more than one gene copy, alongside those with either zero or one copies. To solve this problem in the absolute

quantification of target molecules, Poisson statistics are used. Poisson statistics utilises the number of negative droplets and makes a correction for droplets that contain more than or less than 1 target copy. As a result, the absolute quantification of the original amount of target genes is possible.

Even when the number of copies per droplet is equal to 1 gene copy, the fraction of positive droplets (p) is still 0.606. For this reason, loading too much DNA, or in some cases where the abundance of the target is too high, prevents accurate ddPCR™ calculations. For the BioRad ddPCR™, 0.00005-5CPD is recommended.

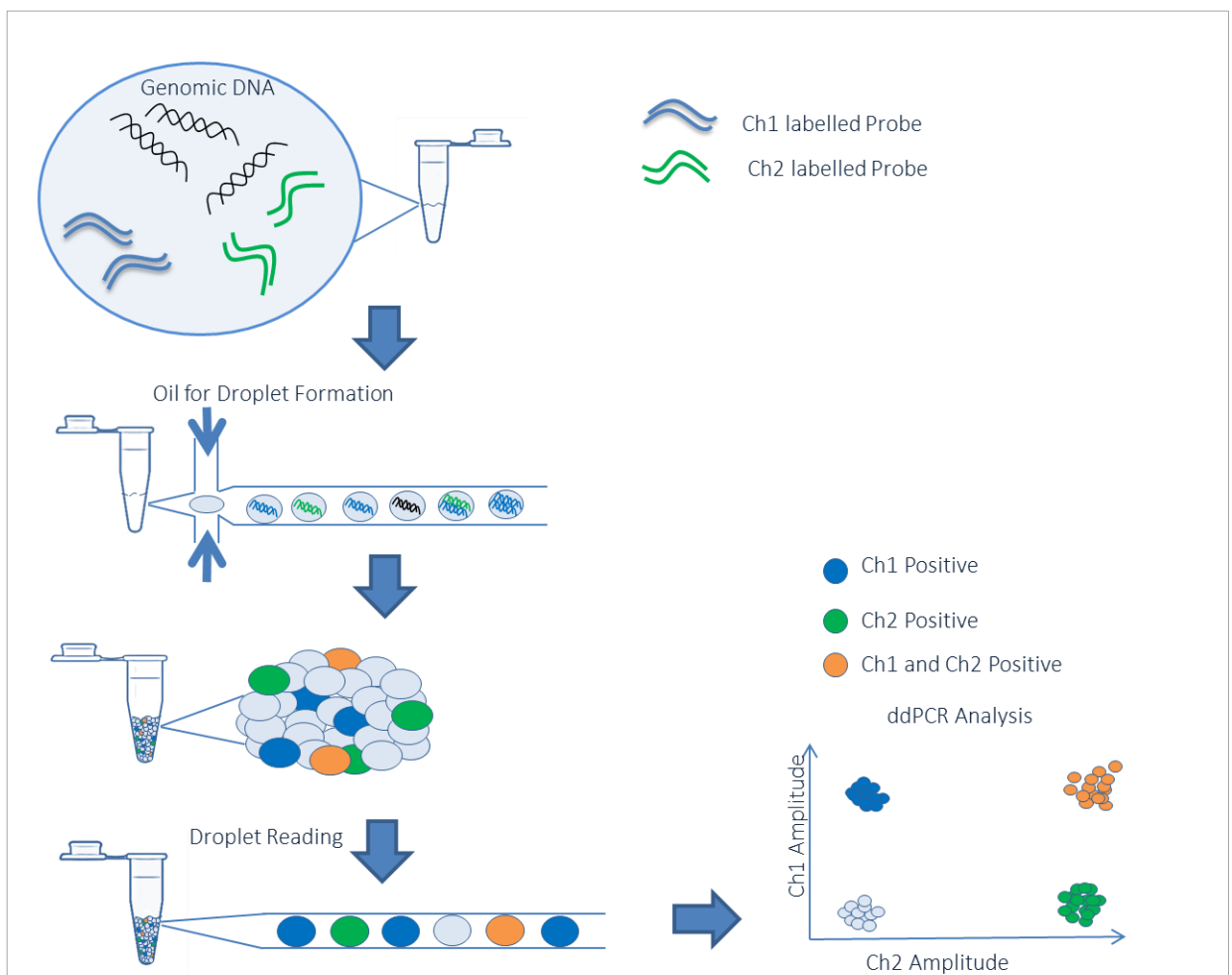


Figure 2.1. Schematic Representation of ddPCR™

The formation of droplets, the enrichment of target molecules following thermocycling conditions, droplet reading, and finally, ddPCR™ analysis (BioRad, 2018).

The sensitivity of dPCR™ is up to 0.001% of mutation detection, this puts dPCR sensitivity to 1000 times higher than quantitative PCR, qPCR; (Hindson *et al.*, 2011). It is also more accurate at low template copy number measurement (Hindson *et al.*, 2011), does not require external standard optimisation between laboratories or standard curves generated relative to reference samples (Bhat *et al.*, 2010), has reduced sensitivity to PCR inhibitors (Dingle *et al.*, 2013) and the quantification is absolute. Unlike qPCR, dPCR does not measure target presence via cycle threshold, but through end-point quantification (Strain *et al.*, 2013), therefore making it a much more suitable assay for the detection of rare mutations.

A number of mutation detection assays have been developed by measuring the fluorescence intensity of a mutant sequence in parallel with a wild-type sequence (Pohl and Shih, 2004). dPCR can be used to detect mutations, copy number variations in specific genes with amplifications or deletions and quantify specific nucleic acid sequences (Miotke *et al.*, 2014), however it is unable to detect balanced translocations.

With the purpose of being able to readily identify chromosomal aneuploidies in ESC culture, it was necessary to develop and optimise a sensitive molecular technique. dPCR is a novel technique that due to its ability to provide absolute quantification of a sample may be able to deliver accurate results for the detection of aneuploidies. The advantage of dPCR is its ability to detect a rare DNA sequence or mutant gene in a large background of wildtype DNA, or alternatively, the ability to detect small changes in the gene copy numbers. However, for this to occur a “normal” or stable/control gene needs to be used in conjunction with the mutant gene (or the gene being quantified) to see whether their relationship changes compared with normal cells or tissues. Firstly, the normal tissue or cells need to be monitored and their ratio described (Hindson *et al.*, 2011; Heredia *et al.*, 2013). This could allow the development of a more sensitive method for the detection of stem cell aneuploidies in culture.

The detection of rare events, such as single nucleotide polymorphisms (SNPs), opens up the opportunity to allow clinicians fast and sensitive diagnosis of many diseases. For example, most tumours, including small ones, have a common characteristic of allelic instability (AI), which has been found very early during colorectal neoplasia (Pohl and Shih, 2004). The earlier the detection of such diseases occurs, the better the outcome of treated patients. Similarly, this could perhaps occur in stem cells, where instead of spontaneous

accumulation or loss of chromosomes in culture, stem cells *in vitro* always have some degree of genomic instability, but it was not possible to detect it due to the absence of high sensitivity detection assays.

Since the development of personalised medicine for treating patients with specific drugs for their disease/disorder type, the need for sensitive high-throughput tests to monitor mutation levels in the patient has become increasingly necessary. For example, in the treatment of leukaemia patients with Imatinib, *BCR-ABL* mutation levels are regularly monitored (Zagaria *et al.*, 2015). Routine screening in colorectal and non-small-cell lung cancer patients is now performed for *EGFR*, *PIK3CA* and *KRAS* with the choice of chemotherapeutic drug dependent on the test outcome (Eberhard, Giaccone and Johnson, 2008; Normanno *et al.*, 2009; van Eijk *et al.*, 2011). So far a number of assays have been developed to detect gene mutations, such as *BRAF* (Reid *et al.*, 2014), *BAT26* (Traverso *et al.*, 2002), and *EGFR* (Zhu *et al.*, 2015) for a range of different diseases.

Digital PCR suggests encouraging new alternatives to many current invasive diagnostic methods, including the ability to analyse foetal DNA in the mother's blood and DNA from apoptosing or necrosing tumour cells in circulating blood (Hindson *et al.*, 2011; Reid *et al.*, 2014). Although dPCR sounds like an ideal monitoring assay for patients that require sensitive screenings for common cancer-associated genomic variants, the disadvantage of dPCR is that it would require a very large sample size from cell-free DNA (cfDNA). This is because you would need 50000 gene copies to reach a 99% probability that the sample will contain at least 1 mutant copy (1 SNP in 10000 wild-type sequences). In a healthy individual there are approximately 1000 copies per milliliter (mL) of cell-free DNA in the plasma. For it to be possible to find 1 SNP in 1000 wild-type sequences (or in 50000 gene copies) it would require 50mL of patient blood (Huggett, Cowen and Foy, 2014), possibly an impractical method for clinical use. However, the potential of dPCR remains, as its applications for the monitoring of donor DNA in recipient patients for organ/tissue transplants. Shotgun Next Generation Sequencing (NGS) has already been performed to try and predict cellular rejection of the graft by observing the amount of donor specific DNA in the patients receiving heart transplants (Snyder *et al.*, 2011), an area where dPCR may be more suitable. Similarly, trisomies in circulating foetal DNA in

maternal blood or specific SNPs that affect drug metabolism can be detected by dPCR and used by clinicians (Ouahchi, Lindeman and Lee, 2006; Wang, McLeod and Weinshilboum, 2011).

As chromosome abnormalities, such as trisomies, account for a significant number of miscarriages and stillbirths (reviewed in Fan *et al.*, 2009) and current diagnostic methods, including karyotyping cells derived from the chorionic villus and/or amniotic fluid take 1-2 weeks, this prompts the need for more rapid, sensitive, diagnostic methods. ddPCR™ has already been applied in the detection of aneuploidies from chorionic villi or amniotic fluid samples. A dPCR screening for common aneuploidies, specifically for trisomies 13 (Patau Syndrome), 18 (Edwards Syndrome), 21 (Down Syndrome), X and Y aneuploidies (XXY (Klinefelter Syndrome), XYY, and X0 (Turner Syndrome) was performed (Fan and Quake, 2007; Lo *et al.*, 2007; Fan *et al.*, 2009) and chromosome 1 was chosen as a reference target, due to its lack of aneuploidy in ongoing pregnancies. This particular study, however had used traditional karyotyping to find chromosome 1 as a stable chromosome, which is not likely to be sensitive enough (Lathi, Westphal and Milki, 2008).

ddPCR™ is a much more powerful tool for the detection of chromosome aneuploidies because of the speed results can be obtained (within approximately six hours) compared with other current techniques. It does not require trained cytogeneticists, unlike for the analysis of FISH cell karyotypes, and is not as labour-intensive (Hultén, Dhanjal and Pertl, 2003; Dudarewicz *et al.*, 2005). Additionally the sensitivity of the ddPCR™ is much higher compared with current methods used for aneuploidy detection, such as array-based comparative genomic hybridisation (aCGH), traditional karyotyping, FISH and qPCR (Baker *et al.*, 2007).

2.2. Aims

The aim of this chapter was to investigate the sensitivity of the ddPCR™ platform in the detection of aneuploidies in a background of wild-type DNA. The study was designed to optimise the ddPCR™ system via different DNA treatment methods, assessing different fluorophore intensities and finally the limit of detection for aneuploidies.

2.3 Methods and Materials

2.3.1. Cell Culture and Methodology

Eight human cell lines were used: four diploid lymphoblastoid cell lines (two male and two female) and three aneuploid lymphoblastoid cell lines (Table 2.1). Lymphoblastoid cells were cultured in RPMI-1640 medium (Sigma, UK) supplemented with 10% (v/v) Foetal Calf Serum (FCS; Sigma) and 5% (v/v) L-glutamine (Sigma) in a 5% CO₂ atmosphere at 37°C. Medium was changed approximately every four days and the cells were split once a week. To freeze the lymphoblastoid cells for different cell banks, a freezing solution was made comprised of 10% Di-Methyl Sulfoxide (DMSO; Sigma-Aldrich) and 20% FCS in RPMI-1640 (Sigma). Cells were counted using a manual haemocytometer, pelleted and then the freezing solution was used to re-suspend 5 million cells in 1mL in each cryo-vial. The cryo-vials were then placed in a “Mr Frosty” freezing container (ThermoFisher Scientific, UK) with iso-propanol and transferred to a -80°C freezer for 1-2 days before storage in liquid nitrogen.

Additionally, all cell culture samples were routinely tested for *Mycoplasma* (testing performed by Julia Sung, NIBSC) and sterility testing of cell cultures using tryptone soya broth, thioglycolate medium and sabouraud dextrose broth was carefully monitored for any contamination (testing was performed by the Microbiology Service Laboratory, NIBSC).

2.3.2. DNA Extraction

The lymphoblastoid cell lines were grown in large quantities to create single DNA stocks. Cells were cultured to approximately 70% confluency, harvested, washed in PBS and a cell count performed to produce cell pellets of a minimum of $2-5 \times 10^6$ cells that were stored at -80°C. Pellets were then thawed in a 37°C waterbath and vortexed briefly to resuspend the cells in the residual supernatant. 10ml of Cell Lysis Solution (Qiagen, UK) was added to the cell pellet and dispersed by pipetting. This was followed by the addition of 50µl RNase A Solution (Qiagen) and mixing by inverting the tube. The pellet was then incubated at 37°C for 30 minutes. Next, 3.5ml Protein Precipitation Solution (Qiagen) was added, the tube was vortexed vigorously and the sample was then centrifuged at 2500 x g for 10min. The supernatant containing the DNA

was decanted into a new tube containing 10ml 100% iso-propanol (Sigma) and gently inverted. The sample was centrifuged again at 2000 x *g* for 3min to form a pellet, the supernatant discarded, and the tube drained on a clean absorbent tissue. This was followed by the addition of 10ml 70% (v/v) ethanol (Sigma) and tube inversion to wash the DNA pellet. The sample was centrifuged again at 2000 x *g* for 1min, the ethanol was removed carefully and the tube was inverted and placed on a clean absorbent tissue to allow the pellet to air-dry for up to 6h. DNA Hydration Solution (Qiagen) was added to the tube and then the tubes were placed on a low speed blood wheel overnight at room temperature (RT) to allow good mixing of the DNA and DNA Hydration Solution. DNA at 1000µg/µl or more was stored at 4°C, whereas lower concentrations of DNA were stored at -20°C.

For DNA extraction from blood samples from MCWES01 and MCWES02 donors, a Blood and Cell Culture Mini Kit (Qiagen) was used; the blood was from normal healthy donors. To start the QIAGEN Genomic-tip 20/G was equilibrated with 1ml Buffer QBR and allowed to flow through the column by gravity. The blood samples were vortexed, thoroughly applied to the column and once more allowed to flow through by gravity. The column was washed three times with 1ml Buffer QC and then eluted with 1ml Buffer QF. Buffer QF, 1ml, was added a second time to the column to collect a maximum yield of DNA from the blood samples. 1.4ml of RT iso-propanol was then added to the eluted DNA, the tube was inverted and then centrifuged at 5,000 x *g* for a minimum of 15min at 4°C. The supernatant was carefully removed, and the pellet allowed to air-dry for 5-10min. The DNA was then re-suspended in TE, usually 30µl, and then allowed to mix overnight on a blood wheel and subsequently stored at -20°C.

2.3.3. DNA Quantification and Quality Monitoring

For DNA quantification a Qubit 2.0 Fluorometer (Thermo Fisher Scientific, UK) was used, a Nanodrop ND-1000 (Thermo Fisher Scientific) was used to check the purity of the sample, and a TapeStation bioanalyser (Agilent Technologies, UK) or agarose gel was used to determine the DNA integrity. The Qubit was chosen for the DNA quantification, due to increasing amount of literature suggesting the Qubit is a more accurate DNA quantification instrument than the Nanodrop, as the latter overestimates the amount of DNA present in a sample (O'Neill *et al.*, 2011; Sironen, Uimari and Vilkki, 2011; Simbolo *et al.*, 2013).

For agarose gel electrophoresis, 1-2% (m/v) agar was dissolved completely in TAE (40 mM Tris at pH 7.6, 20 mM acetic acid and 1 mM EDTA) buffer by heating. The mixture was allowed to cool, 1:10000 SybrSafe® (ThermoFisher Scientific) was added, the mixture was poured into a gel tank and allowed to set. TAE buffer was then added to the gel tank, the samples were added to the gel wells and were resolved at 100V until the DNA fragments were separated. The gels were visualised with a transilluminator under ultraviolet light.

2.3.4. Karyology

Lymphoblastoid cultures were grown until approximately 60-70% confluency. Fresh media was added and the cells in the flask were sent for karyotyping (The Doctors Laboratory, UK). FCWES01, FCWES02, MCWES01 and MCWES02 were sent at passages 14, 11, 13 and 11, respectively.

2.3.5. DNA Fragmentation

In order to improve the droplet segregation and distribution on the 2-D plot of the ddPCR™, DNA was fragmented using different treatments. This would potentially improve the efficiency of the assay by making sure the ddPCR™ experiment was working optimally.

2.3.5.1. Enzyme Treatment

Restriction enzyme digestion was considered in order to break down any clumps in the chromatin that may hinder the formation of droplets for ddPCR™ and furthermore prevent the binding of primers and probe to our gene of interest.

For enzymatic treatment of DNA before ddPCR™, restriction enzymes EcoRI, BstYI and BtgI (NEB, UK) were used with the CutSmart Buffer (NEB) for varying amounts of time. The mixtures were incubated at each enzyme's optimal temperature according to the manufacturer's guidelines. The size of the DNA fragments produced by the BstYI and BstGI digestion are shown in Table 2.2.

For pre-digested DNA i.e. DNA digestion before use in ddPCR™, typically, 1000µg of DNA was digested with 5 Units (U) of enzyme in a total volume of 50µl. For "in-tube digestion" of the DNA, x0.25 units (U) of BstYI was used with x0.025 of the CutSmart Buffer in the ddPCR™ mix, which included the primers, probes and mastermix. To check the efficiency of the restriction enzyme digestion, the DNA was initially run on a 1% (g/v) agarose gel

2.3.5.2. DNA Sonication

DNA was sonicated for varying periods of times and at different amplitudes using the Branson 450D sonicator (BRANDSON Ultrasonics Corporation, USA). Sonication fragments DNA randomly, as unlike in restriction enzyme digestion, sonication does not target specific DNA sequences and therefore, there will be a great distribution of fragment sizes. The sonication, however, also allows droplets in the ddPCR™ to form more readily around the DNA fragments.

The DNA samples were then resolved on an agarose gel to visualise the fragments produced from the sonication. For this both the ProMega-Markers® Lambda Ladder (Promega) and the GelPilot 500Bp Ladder (Qiagen) were used. Additionally, to quantify the DNA fragments a TapeStation (Agilent Technologies, UK) was used with either a Genomic DNA Analysis ScreenTape and, correspondingly, the Genomic DNA Reagents, or the High Sensitivity DNA ScreenTape with the High Sensitivity DNA Reagents.

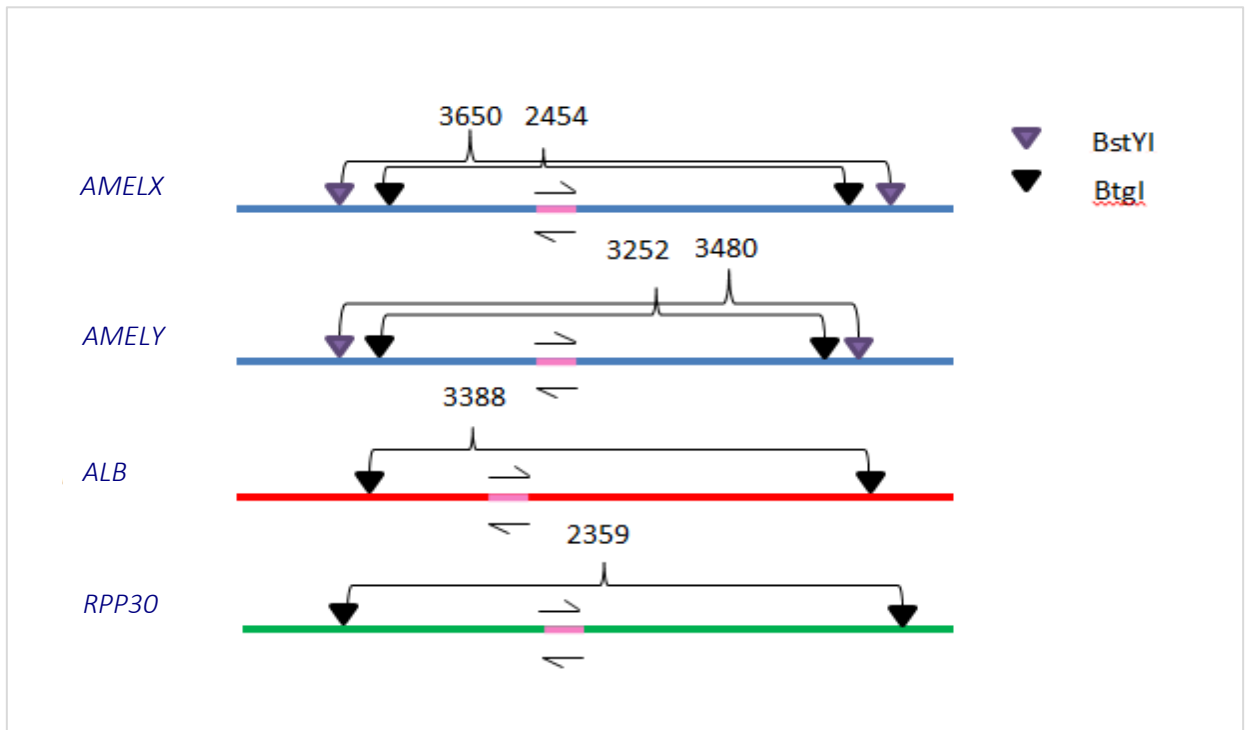


Figure 2.2. Schematic Representation of the Different restriction digestion Sites and resulting Fragment Sizes

The different gene restriction sites and the fragments produced from the digestion with *BstYI* (purple) and *BtgI* (black) enzymes are shown for the four genes analysed in this study. All of the DNA fragments for genes *AMELX* (blue), *AMELY* (blue), *ALB* (red) and *RPP30* (green) were 2000-4000bps long; the amplicons for these genes were within these fragments shown in pink with the flanking arrow symbols.

Table 2.1 Characterisation of cell lines.

The table describes the different cell lines used in this chapter, their genotypes and origin. The wild-type cell lines were provided by NIBSC, whereas the aneuploid cell lines were commercially available from ECACC (European Collection of Cell Cultures).

Cell line	Species	Age at Sampling	Origin	Karyotype	Source
FCWES01	Human	Unknown	Female lymphoblastoid cell line	46,XX[8]/46,XXad(12)(q24.3)[2](performed by TDL; see Appendix I)	NIBSC
FCWES02	Human	Unknown	Female lymphoblastoid cell line	46, XX (Performed by TDL; see Appendix I)	NIBSC
MCWES01	Human	Unknown	Male lymphoblastoid cell line	46,XY,?inv(6)q25.2q25.3)(Carried out by TDL; see Appendix I)	NIBSC
MCWES02	Human	Unknown	Male lymphoblastoid cell line	46, XY (Performed by TDL; see Appendix I)	NIBSC
DD0567	Human	1 Year and 11 Months	Female lymphoblastoid cell line	47,XXX,t(8;10)(q22.1;24.1)de novo (provided by ECACC)	ECACC
DD0710	Human	19 Years and 10 Months	Male lymphoblastoid cell line. Patient diagnosed with Klinefelter Syndrome	47,XXY (Provided by ECACC)	ECACC
DD1473	Human	18 Years and 17 Months	Female lymphoblastoid cell line. Patient diagnosed with developmental delay	48,XXXX (Provided by ECACC)	ECACC

2.3.6. Droplet Digital™ PCR (ddPCR™)

The QX200 ddPCR™ system (BioRad, UK) was used for the ddPCR™ experiments according to the manufacturer's guidelines. ddPCR™ can be used to monitor copy number variation (CNV) by selecting two genes from specific chromosomes segments and then observing the ratio between these two genes.

All primers were HPLC-purified and "lab-ready" (Integrated Device Technology, USA), whereas probes were ordered from Thermo Fisher Scientific, with ddPCR™ Supermix for Probes or ddPCR™ Supermix for Probes (no UTPs) used as the master mix (BioRad). The exact concentration of reagents used in each ddPCR™ experiment is shown in Table 2.2 and the sequence of the primers and probes for *AMELX*, *AMELY* and *ALB* are shown in Table 2.3. The probes used are TaqMan® MGB (minor groove binder) probes incorporating a 5' reporter and a 3' non-fluorescent quencher (NFQ). The *AMELX* and *AMELY* primer and probe sequences, as well as the PCR conditions, were established by our collaborators at the Anne and Robert H. Lurie Children's Hospital of Chicago and Northwestern University Feinberg School of Medicine, Chicago (George *et al.*, 2013). During this study, this group (Lawrence Jennings *et al.*) had kindly sent us a sonicated sample of male DNA and their primers and probes to test on our ddPCR™ machine.

Firstly, a 20µl reaction mixture was added to each well in the droplet cartridge (reaction mixture details are shown in Table 2.2), followed by 70µl ddPCR™ droplet generator oil. A gasket was then used to seal the cartridge, which was placed in the droplet generator (BioRad). Once in the droplet generator the PCR mix, and oil are drawn to form approximately 20,000 droplets suspended in emulsion. This emulsion was transferred into a 96-well PCR plate (BioRad) and sealed with foil in a thermal plate sealer (BioRad). Latterly the manual generation of droplets was replaced with the QX200 AutoDG, an automated droplet generator which automatically places the droplets into a 96-well plate. This required an increase in reaction mixture from 20µl to 22µl. The sealed plates are then placed in a thermocycler (BioRad), and PCR performed according to Table 2.4, with the total volume set at 35µl and the lid

temperature at 105°C. After the PCR amplification, the plate was transferred to a droplet reader (BioRad), which scanned each droplet and measured each droplet's fluorescence to classify it as positive or negative accordingly.

Additionally, the housekeeping gene Albumin (*ALB*) was selected as the reference gene in our duplex assay, due to being on a "stable chromosome" in hESCs i.e. Chromosome 4. In hPSCs, aberrations of all chromosomes, except chromosome 4 has been reported (Amps *et al.*, 2011); the area of the gene that was amplified in the PCR was not found listed as a "micro-instability" in the Supplementary Data from the International Stem Cell Initiative, 2011. *RPP30* or ribonuclease P/MRP 30kDa subunit, a BioRad recommended reference gene, located on chromosome 10, was also tested as a potential candidate reference/control gene. The primer/probe mix was ordered from BioRad.

Before use all primers and probes for each gene and genes in combination with each other in duplex reactions were tested on a temperature gradient to make sure there was a clear discrepancy between a positive and a negative signal. For *AMELX* and *AMELY*, this was performed at 55-65°C by Dr Jennifer Boyle (NIBSC). For all other genes and their combinations, this was performed at 55-62°C. For all duplex reactions 59°C was selected as the temperature for DNA annealing and elongation.

Table 2.2. ddPCR™ Reaction Mixture Component Concentrations

Reagent	Concentration/Amount
DNA	40ng
Forward (F) Primer	900µM
Reverse (R) Primer	900µM
Probe	250µM
Master Mix (MM)	2X

Table 2.3. ddPCR™ Primer and Probe Design for Amelogenin X and Y

<i>AMELX/Y</i> Forward Primer	CCCTGGGCTCTGTAAAGAATAGTG
<i>AMELX/Y</i> Reverse Primer	CAGGCTTGAGGCCAACCAT
<i>AMELX</i> Probe	ATCCCAGATGTTTCTCAA
<i>AMELY</i> Probe	CATCCCAAATAAAGTGGTT
<i>ALB</i> Forward Primer	GCTGTCATCTCTTGTGGGCTGT
<i>ALB</i> Reverse Primer	AAACTCATGGGAGCTGCTGGTT
<i>ALB</i> Probe	CCTGTCATGCCACACAAATCTCTCC

Table 2.4 ddPCR™ Thermocycler Set-up

	Temperature (°C)	Time (Minutes)	Process
Step 1	95	10	DNA Denaturation
Step 2	95	0.2	DNA Denaturation
Step 3	59	1	Annealing and DNA amplification
No Extension			
Go to Step 2 X 39			
Step 4	98	10	Enzyme denaturation and droplet hardening
Step 5	12	Infinite	Hold

2.2.6.1. ddPCR™ Sensitivity vs qPCR Sensitivity

To determine the sensitivity of the ddPCR™, several ddPCR™ experiments were performed. Firstly, female DNA, FCWES02, was titrated into male DNA, MCWES02, in 6.25% increments (Table 2.5) by the addition of two extra X chromosomes (female DNA) to the XY (male DNA). The sample started with a normal male sample i.e. 50% X chromosome/*AMELX* and the female DNA (100% X chromosome/*AMELX*) was titrated in 6.25% increments for the range of titrated samples to finally reach a fully diploid 100% female.

Table 2.5. Titration of Wild-type Female DNA in Wild-Type Male DNA in 6.25% Increments

Sample	% of gDNA		Volume of gDNA (µl)	
	Total X	Total Y	Female DNA	Male DNA
1	50	50	0	100
2	56.25	43.75	12.5	87.5
3	62.5	37.5	25	75
4	68.75	31.25	37.5	62.5
5	75	25	50	50
6	81.25	18.75	62.5	37.5
7	87.5	12.5	75	25
8	93.75	6.25	87.5	12.5
9	100	0	100	0

2.3.7. Data Analysis and Bio-Informatics Tools

NEBCutter Tool (NEB) was used to determine restriction enzyme cutting sites and fragment sizes.

All ddPCR™ data were extrapolated from the Quantasoft software Version 1.7.4.0917 (BioRad); the thresholds for the ddPCR™ plots were set manually. Additionally, the ddPCR™ 2-D plots show the raw data of the positive and negative droplets, however the ratio and fractional abundances shown in the Quantasoft software are values derived from Poisson corrections. The qPCR data was extrapolated

using the MxPro – Mx3000P software Version 4.00 (Agilent Technologies). For statistical analysis GraphPad Prism 5.0 was used.

For the statistical analysis of significance from a single sample, assuming the data was of normal distribution, a one sample t-test was used. For the statistical analysis of significance from two samples, a two-sample t-test was used. If the aim was to find whether one sample was greater than the other, then a one-tailed t-test was performed. If the aim was to find whether any significant difference was observed between two samples, then a two-tailed t-test was performed, but the type of two-tailed t-test was dependent on whether the two samples had equal or unequal variances. To see whether the difference between the variances of two samples was significantly different, a two-tailed F-test was performed. The greater value of the standard variation from one sample is divided by the smaller value of the standard variation from the other sample to get an F value. Using the degrees of freedom, the F critical value from an F-table is then compared to the calculated F value. If the F value is greater than the F critical value, then the variances of the two samples are significantly different; the t-test would have to be adjusted accordingly.

To test whether there is a significant difference between more than two groups a one-way analysis of variance (ANOVA) was performed. To look at which groups specifically showed statistical significance between each other a follow-up Tukey's Multiple Comparison Test was used. Both tests assume a normal distribution of the data analysed.

If the data was from two groups that tested samples analysed with two different methods, then a paired t-test was used, assuming the data had normal distribution. A symbol, such as an asterisk (*) was assigned to depict statistical significance on a graph between two samples; Table 2.6 shows each symbol according to the P values for t-tests and ANOVAs.

Table 2.6. P Values and Symbols for Statistical Significance

P value	Wording	Summary
< 0.001	Extremely significant	***
0.001 to 0.01	Very significant	**
0.01 to 0.05	Significant	*
≥ 0.05	Not significant	ns

Additionally, linear regression was used to analyse whether a line indeed fit the data; Significance of F, residual plots and R^2 values were also derived.

2.4. Results

To investigate the sensitive detection of aneuploidies in a background of wild-type DNA, the model cell lines, lymphoblastoid cells were used for the optimisation. In a normal male diploid genome, there is one copy of chromosome X and one copy of chromosome Y, therefore one copy of *AMELX* and one copy of *AMELY*. When using primers and probes against these two genes a 50:50 ratio should theoretically exist, and we can see this in several different ways on the BioRad ddPCR™.

Firstly, a temperature gradient experiment of 55-65°C was performed to observe the quality of droplet segregation in the ddPCR™ (Figure 2.3) and to be confident that the signals' fluorescence is well-separated from the background fluorescence. The data shows that for *AMELX* and *AMELY* that the ideal droplet segregation was approximately 56-60°C; 59°C was selected as the optimal temperature, which coincided with our collaborator's optimal temperature (George *et al.*, 2013).

The QuantaSoft software allows us to view the data in a 1D (Figure 2.4) or 2D plot (Figure 2.5), where the blue or green scatters signify droplets positive for one particular gene target, whereas the orange scatter signifies droplets in the sample that were positive for both genes. The grey scatter displays the negative droplets (Figure 2.5).

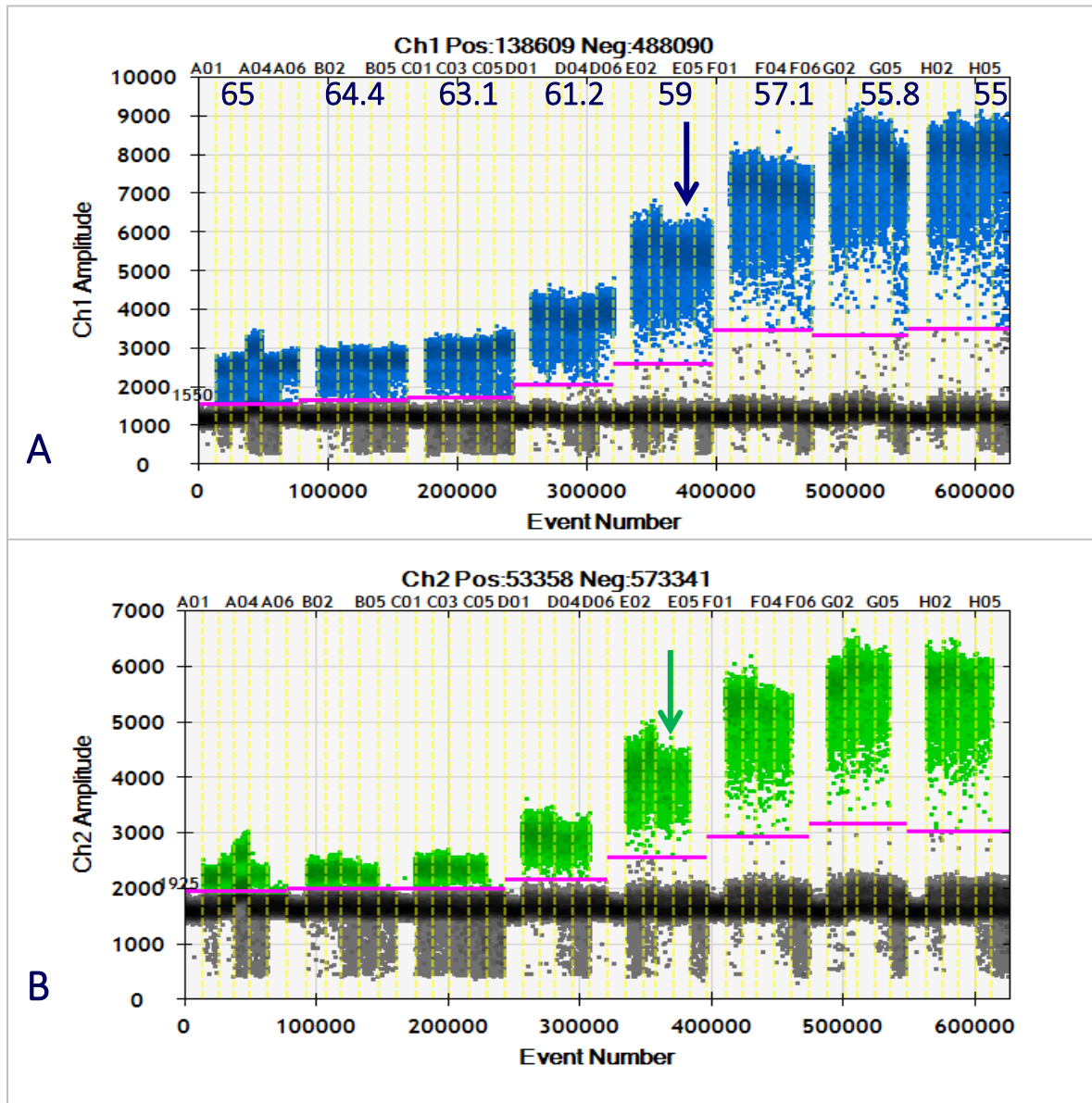


Figure 2.3. Quantasoft 1-D Plot of AMELX/AMELY Temperature Gradient

A temperature gradient from 55°C to 65°C for *AMELX*, shown in blue (A) and *AMELY*, shown in green (B), the negative droplets are shown in black. The arrows highlight 59°C on the Quantasoft 1-D plot. The pink line shows the manual threshold calling for the separation of positive and negative droplets.

m

the two channels or genes (Figure 2.6). The extrapolated data can then be converted as the fractional abundance of each gene. Fractional abundance for FAM or VIC is calculated by dividing the concentration of Channel1/Channel2 by the sum of concentration of Channel 1 and Channel 2, this is then multiplied by 100 (Figure 2.7).

To ensure the data derived are accurate, a 1-D plot may also be used; this demonstrates appropriate droplet segregation from the background fluorescence and avoids false negative or positives (Figure 2.4).

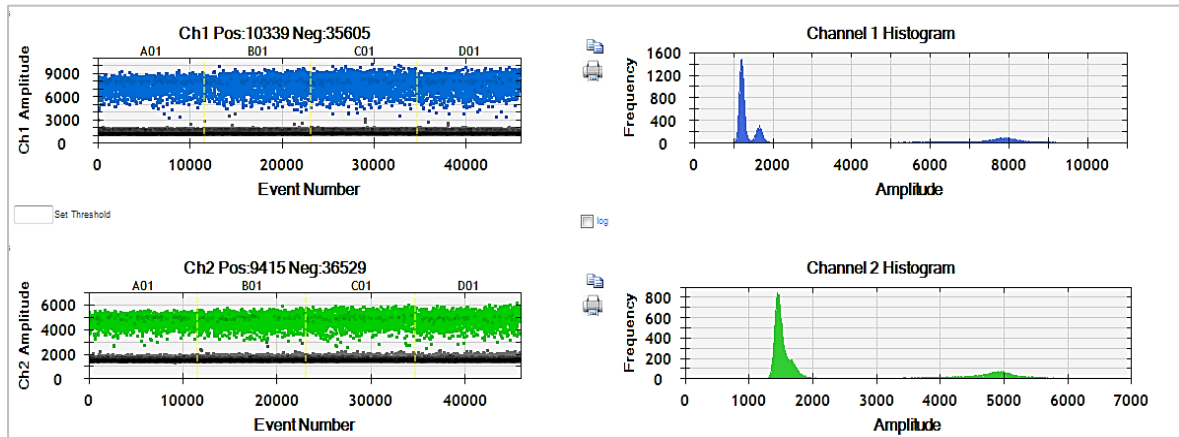


Figure 2.4. Quantasoft 1-D Plot Example

A screenshot of the 1-D plot from the BioRad Quantasoft software. The DNA that was run was not treated with any enzymes or sonication. *AMELX* is labelled on FAM (Channel 1), whereas *AMELY* on VIC (Channel 2); the FAM and VIC signal are shown separately compared to the background fluorescence, the black line underneath the blue and green signals and the peaks for each of the signal's fluorescence. The small peaks on the right are the positive droplets, whereas the left peaks are the negative droplets. The two left peaks in FAM signify potential bleed-through from the VIC channel. The plot represents four replicates of a male sample. All thresholds were called manually.

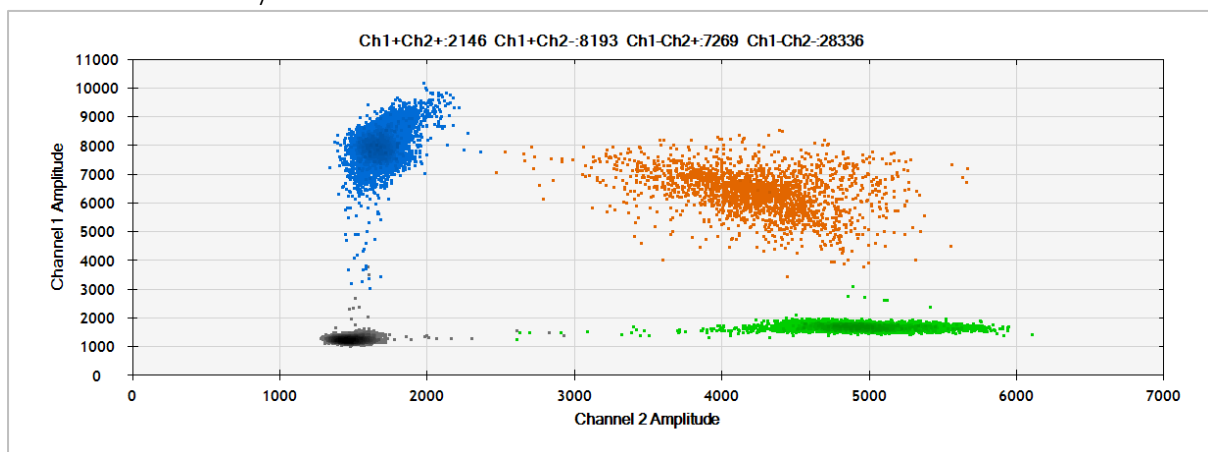


Figure 2.5. Establishment of *AMELX* and *AMELY* in the ddPCR™ Assay

A screenshot of the 2D plot from the BioRad Quantasoft software. The DNA that was run was not treated with any enzymes or sonication. *AMELX* was labelled with FAM, whereas *AMELY* with VIC; the plot represents four replicates of a male sample, MCWES02. The black points on the plot represent negative droplets, the blue points are positive droplets on the FAM channel, the green – VIC channel and the orange points represent droplets that are positive for both the FAM and VIC channels.

Method I

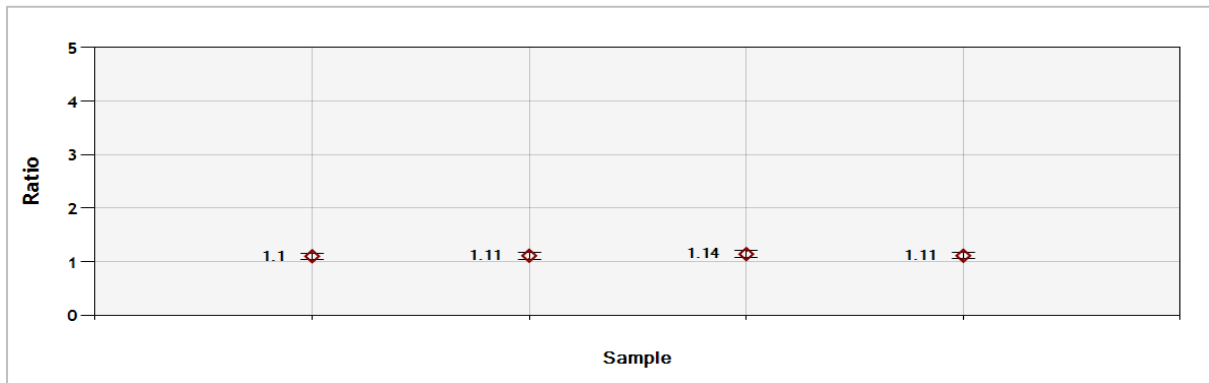


Figure 2.6. Quantasoft Gene Ratio Example Screenshot

The Quantasoft software graph depicts the ratio of the positive droplets between two channels in a sample. The example above shows the ratio of *AMELX* to *AMELY* in four wells of the ddPCR™ run. *AMELX* was in the FAM channel and *AMELY* was in the VIC channel. Male sample, MCWES02 was used; the expected values were 1.

Method II

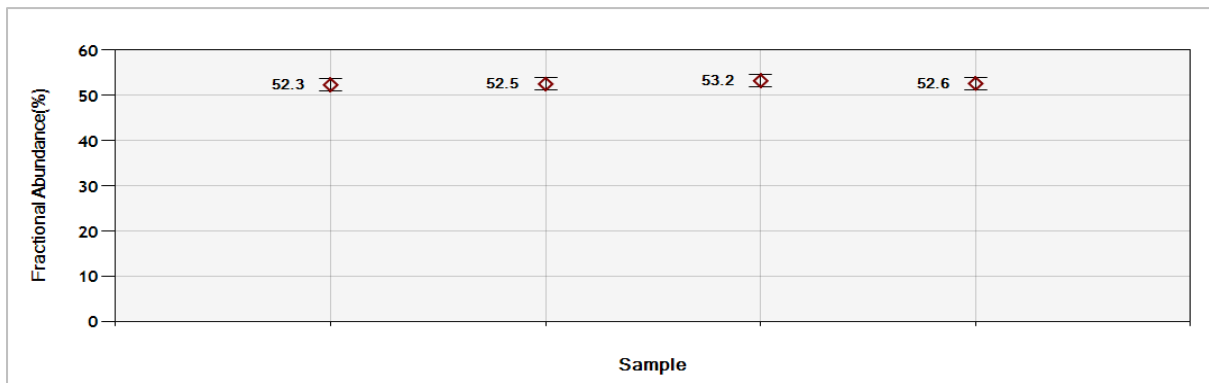


Figure 2.7. Quantasoft Gene Fractional Abundance Example Screenshot

The Quantasoft software graph depicts the fractional abundance of the positive droplets between two channels in a sample. The example above shows the fractional abundance of *AMELX* to *AMELY* in four wells of the ddPCR™ run. *AMELX* was in the FAM channel and *AMELY* was in the VIC channel. Male sample, MCWES02 was used; the expected values were 50.

2.3.1. Titration of Female DNA into Male DNA in 6.25% Increments

To test the linearity of the ddPCR™ machine the change in fractional abundance was monitored (Figure 2.8). We observed a statistically significant difference between all of the different samples from Figure 2.8; a one-way ANOVA and Turkey's Multiple Comparison Test were used. The R^2 value was 0.999 showing a strong linear regression.

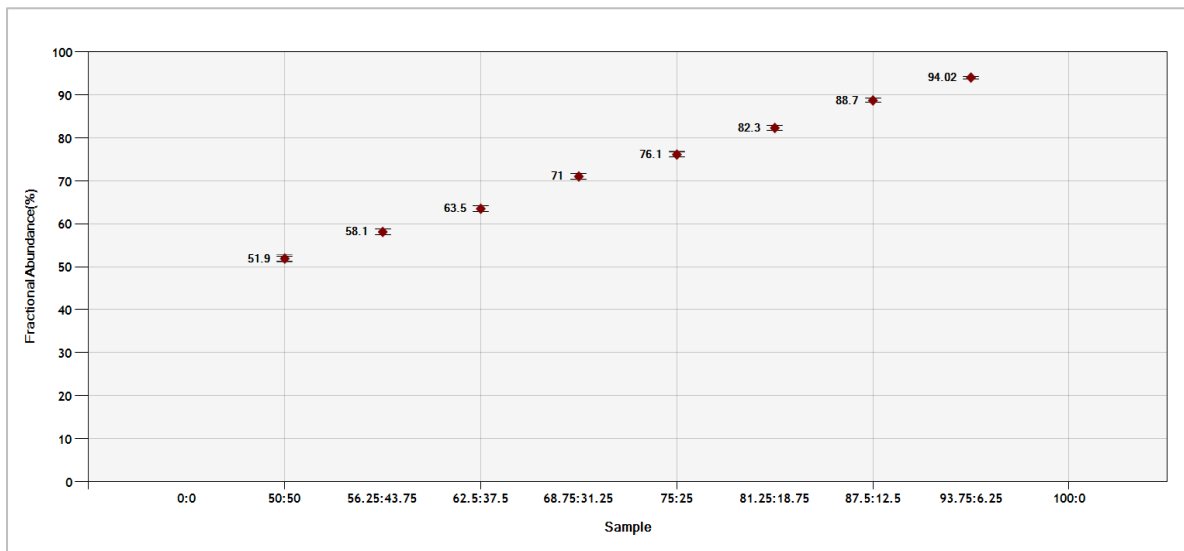


Figure 2.8. Quantasoft Gene Fractional Abundance Screenshot

The Quantasoft software graph depicts the fractional abundance of the positive droplets between two channels in a sample. The example above shows the fractional abundance of *AMELX* to *AMELY* in four wells of the ddPCR run. *AMELX* was in the FAM channel and *AMELY* was in the VIC channel. A significant difference between each of the different samples was observed using an ANOVA and Tukey's Multiple Comparison Test. The R^2 value was calculated as 0.999.

2.3.2. Enzyme Digestion

2.3.2.1. Use of Different Types of Enzymes

As mentioned before the results obtained from the ddPCR™ can be shown in 2-D plots (Figure 2.5). In an attempt to try and cluster droplets more closely together in the quadrant of the 2-D plot, the ddPCR™ DNA was digested with BstYI and EcoRI enzymes before being added to the ddPCR™ mix. Both BstYI and EcoRI enzymes produced similar fragments sizes on AMELX and AMELY (fragment sizes were determined using the NEBCutter tool (Figure 2.2). Difference in ratio and in droplet numbers produced between the control (undigested DNA) and digested DNA from MCWES02 with either EcoRI or BstYI would be observed. For these four replicates were used and then merged to produce a single average result.

In Panel A, the double-positive droplets are scattered quite randomly without a specific central cluster of droplets making it difficult to distinguish between a negative and positive droplet. This becomes especially difficult when the double-positive droplets start “merging” or overlapping with the single-positive droplets. In Panel B, the same male DNA was used for analysis on the ddPCR™, however it was first treated with an enzyme EcoRI. This resulted in the droplets being much more clustered together closely and created a more distinct difference between positive and negative droplets. Similarly, Panel C shows that by digesting a DNA sample first before adding it to the ddPCR™ mixture can improve the look of the 2-D plot by stopping the spreading of the droplets across the plot without substantially changing the ratios.

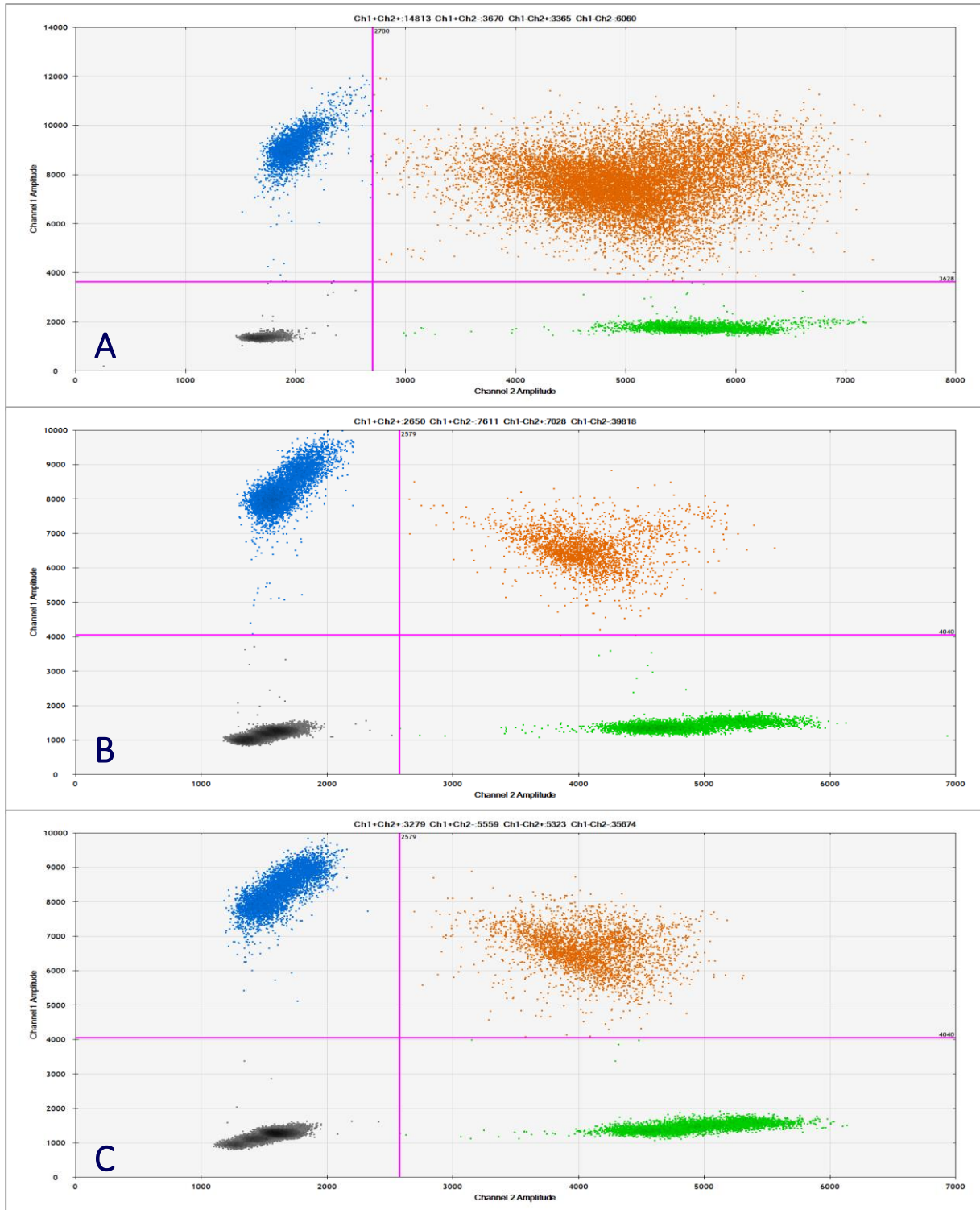


Figure 2.9. Quantasoft 2-D plot of Different Enzyme Digestions

Male DNA from MCWES02 cells were run on the ddPCR™ in triplicates. In panel A the DNA was undigested, in panel B the DNA was digested with EcoRI for 1hr and in panel C the DNA was digested with BstYI for 1hr. *AMELX* is labelled with FAM and *AMELY* – in VIC. Results were obtained from the Quantasoft software. The black points on the plot represent negative droplets, the blue points are positive droplets on the FAM channel, the green- VIC channel and the orange points represent droplets that are positive for both the FAM and VIC channels. The results show four replicates.

To see whether there was a substantial difference between the ratios or the fractional abundance of each gene in a sample when a sample was treated in different ways, a scatter plot was created, and statistical tests were performed (Figure 2.9). From Table 2.7, we see the average ratios of *AMELX* to *AMELY* and a One-Way ANOVA and Tukey's Multiple Comparisons Test was performed, no significant difference was observed ($p = 0.5696$). Although the digestion did not show any significant difference in the ratio of *AMELX* to *AMELY* (Figure 2.10), we can see that the digestion had improved the droplet segregation allowing the user to call positive and negative droplets more readily. This allowed the thresholds to be more easily. Additionally, the different enzymes did not show any significant difference to each other on the 2D plots (Figure 2.9 Panel B and C).

Table 2.7 Average Ratio of *AMELX* to *AMELY*

DNA was treated with different enzymes and then run on the ddPCR™. The average ratio of *AMELX* to *AMELY* is shown below from quadruplicates. One-Way ANOVA and Tukey's Multiple Comparisons Test was performed to measure any potential significant differences between the control and digested samples.

Sample	Control	EcoRI Digestion	BstYI Digestion
Average Ratio of <i>AMELX</i> to <i>AMELY</i>	1.031	1.067	1.03

Using ddPCR™, we found there were two ways to digest the DNA. This included adding the enzyme and buffer mix directly with the PCR mix or by pre-digesting the DNA and then adding it to the PCR mixture. No significant difference was found in the two methods using a One-Way ANOVA ($p = 0.0622$) and Tukey's Multiple Comparisons Test, however when adding the enzyme and buffer mixture directly into the PCR tube it was more difficult to control the time of the DNA digestion. Salt concentration inhibitions can cause this lack of control of too many units of enzyme in the in-tube digestions. For this reason, all further experiments with digested DNA used the "pre-digested DNA" method.

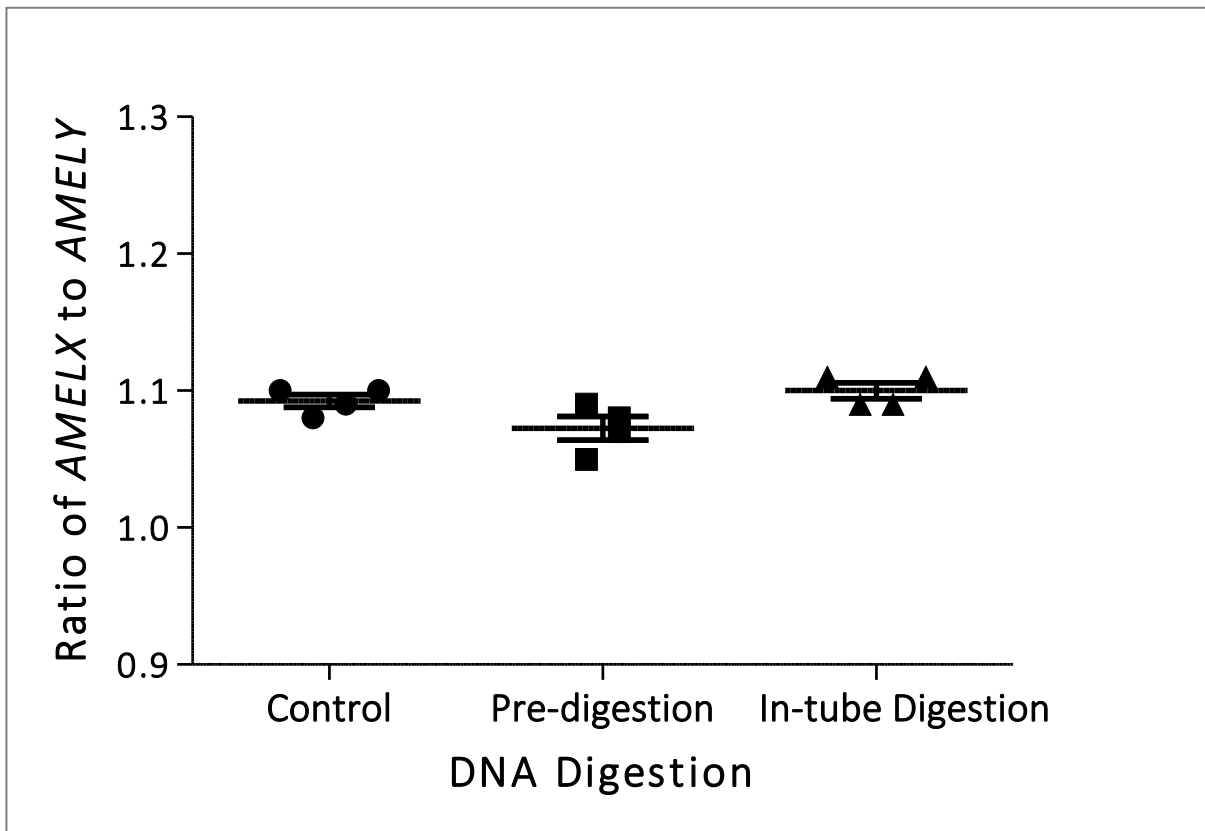


Figure 2.10. Scatter Plot of the Different Enzymatic Treatments

DNA was treated with BstYI in different ways. The pre-digested sample was first digested, whereas the in-tube digestion included added the enzyme directly into the PCR mix before running it on the ddPCR™. The control was undigested DNA. The fractional abundance of *AMELX* to *AMELY* was obtained from the Quantasoft software for four replicates and was plotted on GraphPad Prism. One-Way ANOVA and Tukey's Multiple Comparisons Test was performed to measure any potential significant differences between the control and digested samples.

2.3.2.2. Time needed for DNA Digestion

After BstYI was selected as a standard enzyme for the digestion of *AMELX* and *AMELY* due to its capacity to segregate droplets well on the 2-D plot, the amount of time needed for the digestion was monitored. From Figure 2.11, it is clear that digestion improves the droplet segregation by making the droplets “more positive” and also clustering them closer together. These results were obtained after allowing the DNA to digest for one hour, however in an aim to improve the speed and efficiency of the assay, the amount of time for digestion was altered to see how this would affect the results.

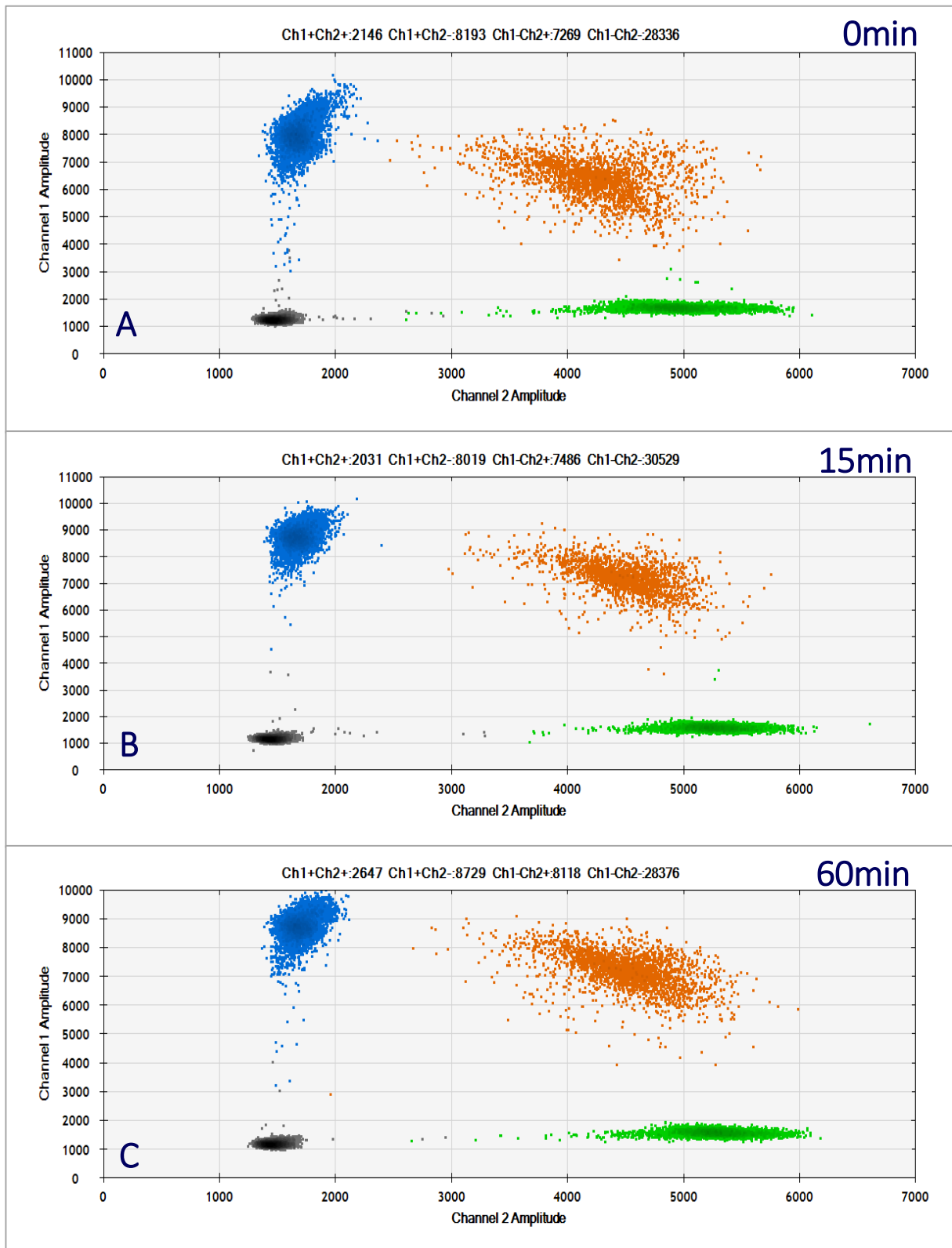


Figure 2.11. Quantasoft 2-D plot of Different Times of BstYI Digestions

Male DNA from MCWES02 cells were run on the ddPCR™ in triplicates. In panel A the DNA was undigested, in panel B the DNA was digested with BstYI for 15min and in panel C the DNA was digested with BstYI for 1h. *AMELX* is labelled with FAM and *AMELY* – in VIC. Results were obtained from the Quantasoft software. The black points on the plot represent negative droplets, the blue points are positive droplets on the FAM channel, the green- VIC channel and the orange points represent droplets that are positive for both the FAM and VIC channels. The results are shown in triplicate.

Figure 2.11 shows that by pre-digesting the DNA for 15min the droplet segregation does improve the 2-D plot and that there is no significant difference in digesting the DNA for 15 min or for 1 h. A One-Way ANOVA and Tukey's Multiple Comparisons Test was used Figure 2.12.

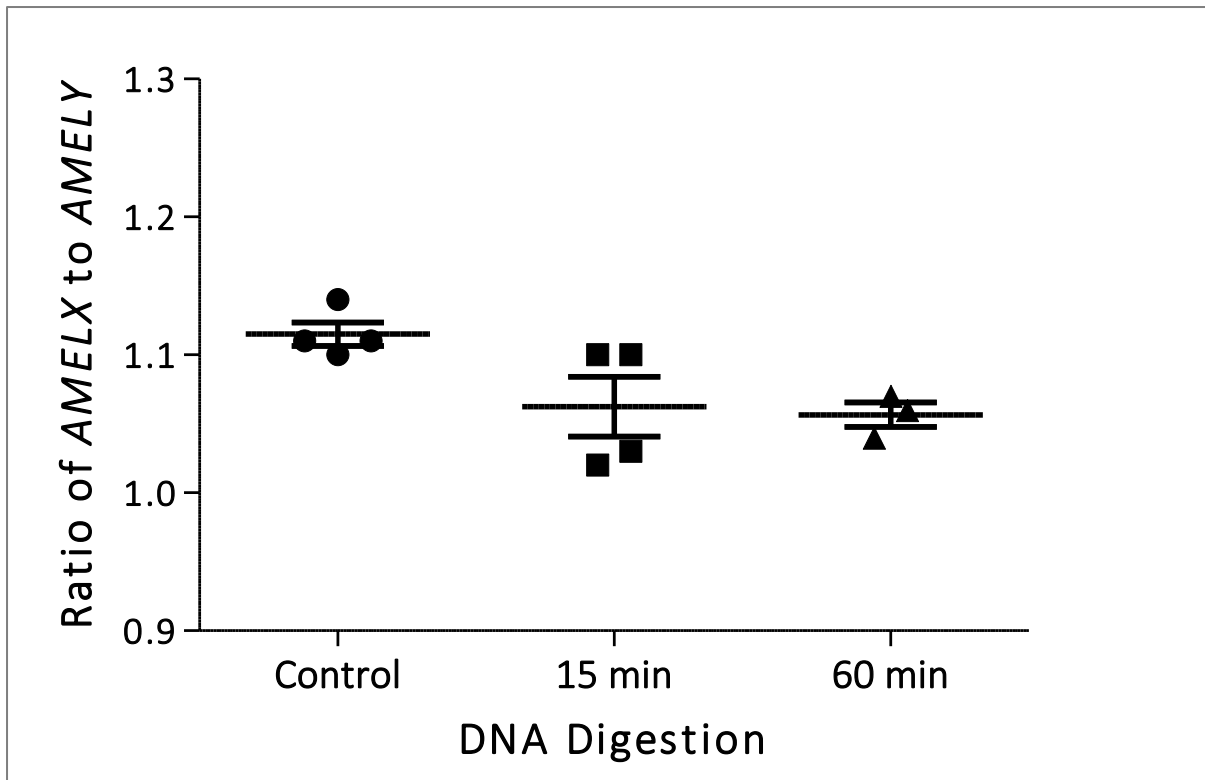


Figure 2.12. Scatter Plot of Different Enzymatic Treatment Times

DNA was treated with BstYI in different ways. One sample was digested for 15min, the other for 1h. The control was undigested DNA. The fractional abundance of *AMELX* to *AMELY* was obtained from the Qantasoft software and was plotted on GraphPad Prism.

2.3.3. Fluorophore Signal Intensity Differences

After performing a number of experiments it was observed the Channel 1 (FAM) signal, that was usually used to label *AMELX*, was constantly higher compared to the Channel 2 (VIC) signal or *AMELY* (Figure 2.6, Figure 2.10, Figure 2.12). To explore this “heightened” amount of Channel 1, two separate assessments were used. In the first instance, the labelling of the fluorophores was switched, where *AMELX* would be labelled in VIC and *AMELY*- FAM. Secondly, we extracted DNA directly from the MCWES02 donor’s blood and tested it on the ddPCR™ to see if there was a cell culture artefact; the

blood was extracted in two separate lots to ensure accuracy (Figure 2.14). Figure 2.13 shows that there is a significant difference (One-Way ANOVA and Tukey's Multiple Comparison Test) between the labelling of *AMELX* with FAM or VIC. However, when the DNA was extracted from two different vials of blood and cell culture, there was no significant difference in the ratios of *AMELX* to *AMELY* (Figure 2.14).

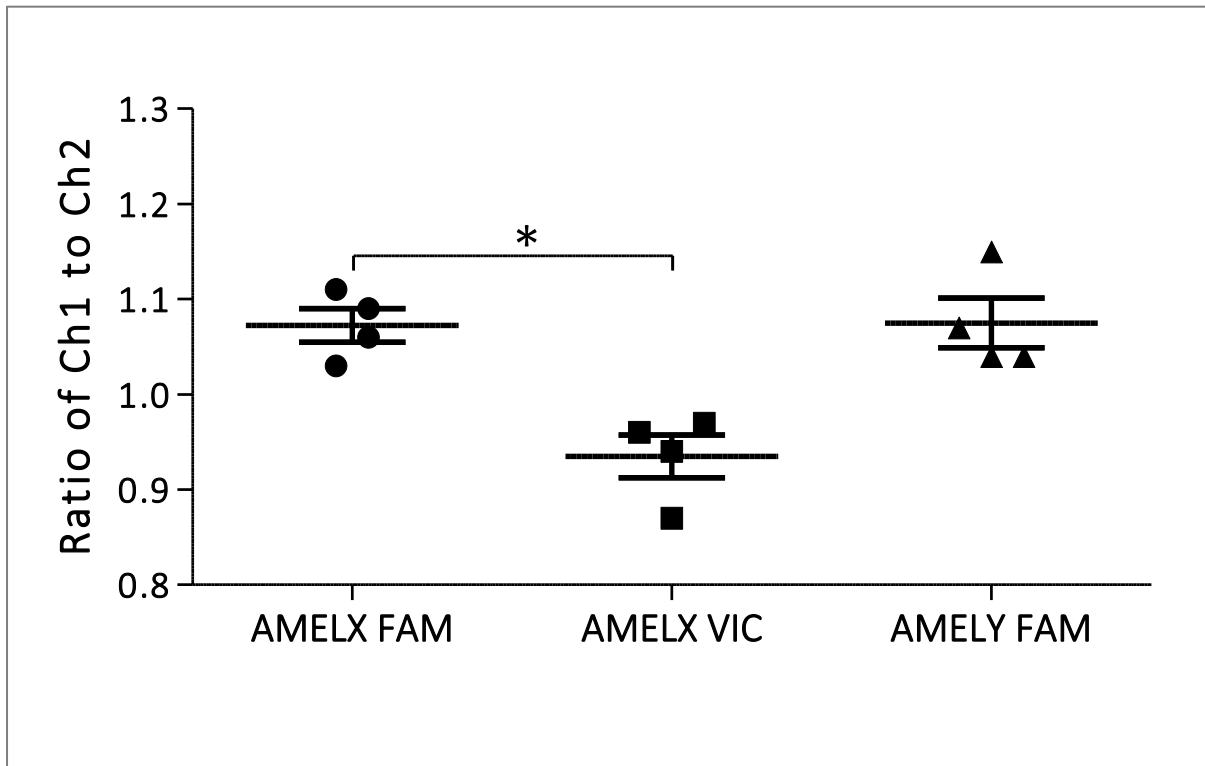


Figure 2.13 Scatter Plot of Switched Fluorophores

The ratio of *AMELX* to *AMELY* was obtained from the Quantasoft software and was plotted on GraphPad Prism. AMELX FAM shows when *AMELX* was labelled with FAM, AMELX VIC – *AMELX* labelled with VIC and AMELY FAM, where *AMELY* was labelled with FAM. A One-Way ANOVA and Tukey's Multiple Comparison Test was performed. The asterisk (*) symbolises statistically significant differences between two groups.

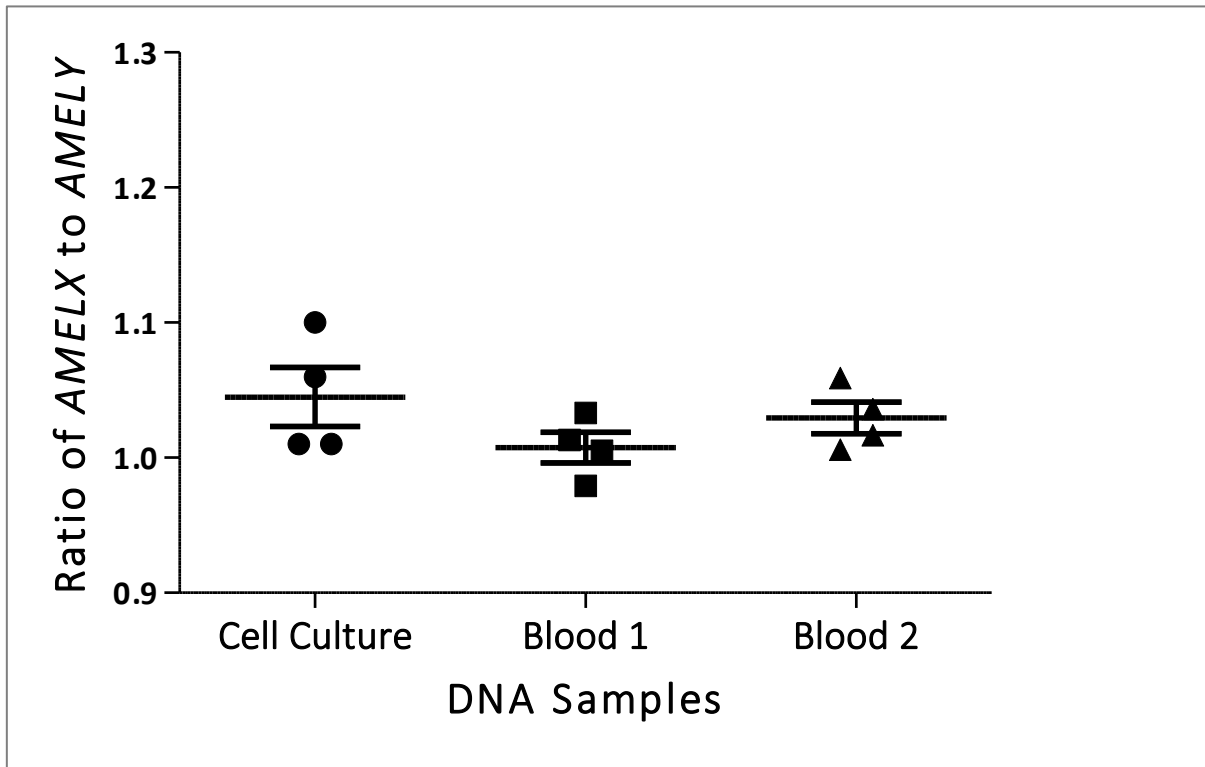


Figure 2.14. Scatter Plot of Different DNA Sources

DNA was extracted from two different sources- cell culture and blood. The blood was extracted from separate blood vials – 1 and 2. Both samples were from the same male donor, MCWES02 and taken on the same instance. The ratio of *AMELX* to *AMELY* was obtained from the Quantasoft software and was plotted on GraphPad Prism. A One-Way ANOVA and Tukey's Multiple Comparison Test was performed. No significant difference was observed.

2.3.4. Comparing Sonicated DNA with Digested DNA

2.3.4.1. Using DNA from collaborator labs

As we had derived our original ddPCR™ set-up from our collaborator Lawrence Jennings (from Ann & Robert H. Lurie Children's Hospital of Chicago and Northwestern University Feinberg School of Medicine), we wanted to make sure our results were comparable. To do this the Jennings group had kindly sent us a wild-type male DNA sample and their primers and probes to run on our machine. The DNA is sonicated in their lab, whereas their primers and probes were exactly the same sequence as ours (George *et al.*, 2013).

From the results it could be observed that the sonicated DNA produced a closer ratio to 1 (Figure 2.15), whether using the primers and probes from the Jennings group (Reagents 2) or ours (Reagents 1) compared to our digested DNA. Additionally, the sonicated DNA produced a higher concentration of *AMELX* and *AMELY* due to producing more positive droplets (Figure 2.16), regardless of the total number of droplets (Figure 2.17). This indicated that the differences in results are solely due to the sonicated DNA and not the primers and probes.

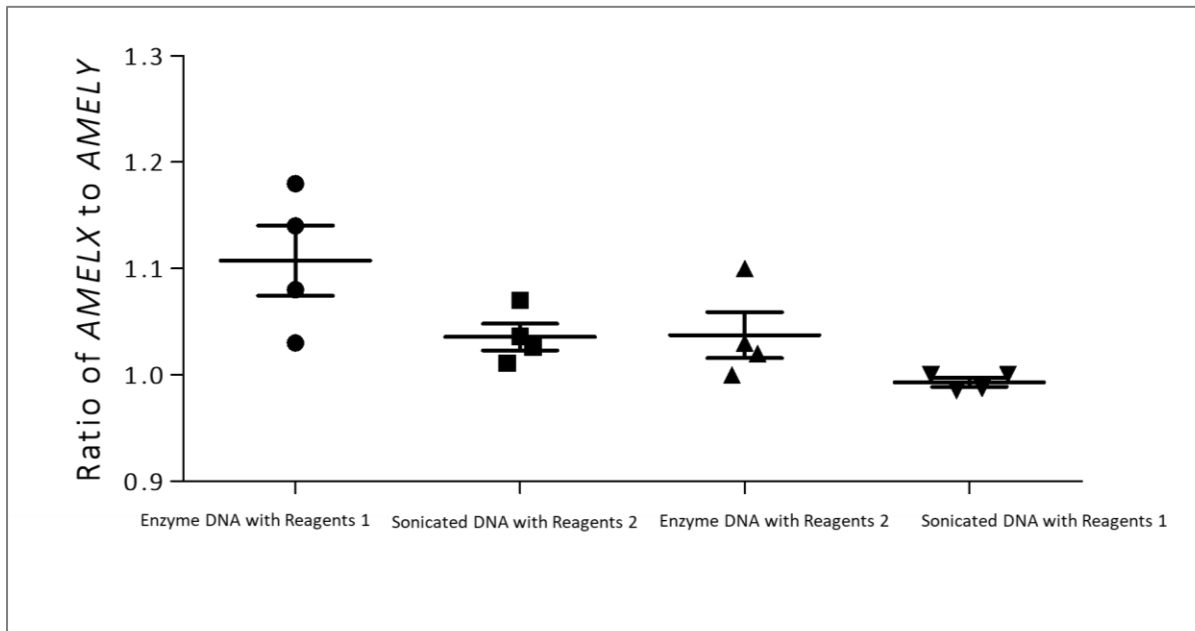


Figure 2.15. Scatter Plot of *AMELX/AMELY* Ratio in Sonicated and Digested Samples

The graph shows the ratio of *AMELX* to *AMELY* for our and our collaborators' samples. Our DNA sample was DNA enzymatically digested, whereas our collaborator's sample was sonicated. "Reagents 1" refers to our in-house primers and probes, whereas "Reagents 2" refers to our collaborator's in-house primers and probes. The ratio of *AMELX* to *AMELY* was obtained from the Qantasoft software and was plotted on GraphPad Prism. Four replicates were used. No significant difference was observed.

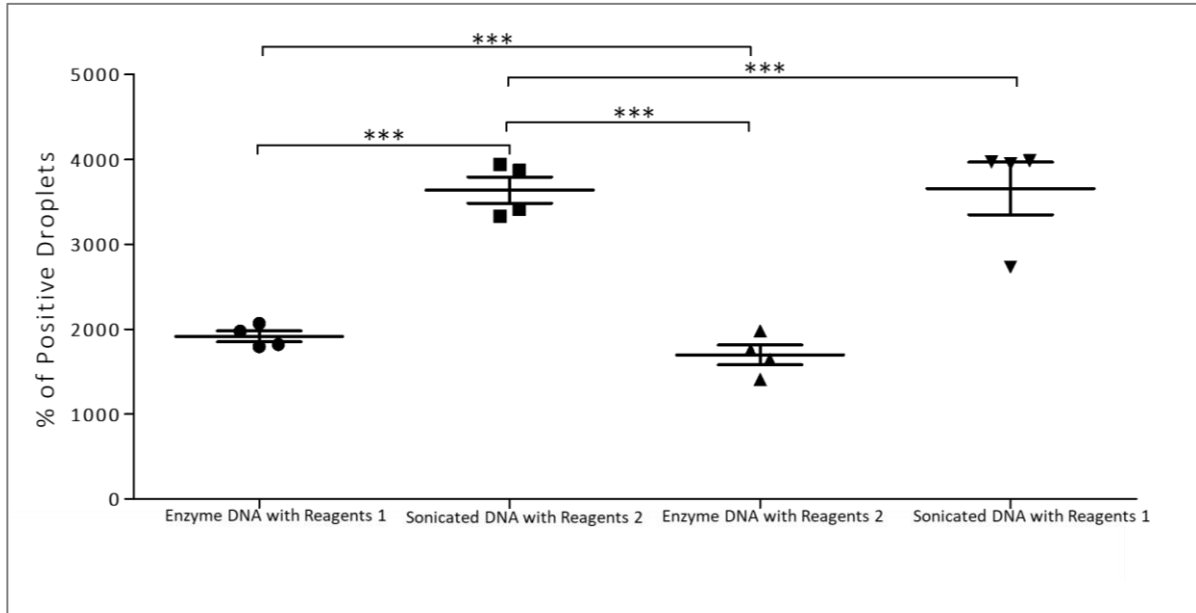


Figure 2.16. Scatter Plot of Channel 1 Number of Events in Sonicated and Digested Samples

The graph shows the number of events for *AMELX* in Ch1 (FAM) for our and our collaborator's samples. Our DNA was enzymatically digested, whereas our collaborator's sample was sonicated. "Reagents 1" refers to our in-house primers and probes, whereas "Reagents 2" refers to our collaborator's in-house primers and probes. The number of events of *AMELX* was obtained from the Quantasoft software and was plotted on GraphPad Prism. Four replicates were used. No significant difference was observed.

Additionally, it was observed that although sonicated DNA produced a higher number of positive droplets, it also caused the 2D plot to look "messier" by scattering the droplets across the plot (Figure 2.18 Panel B). Fewer droplets showed distinct area of clustering compared to using restriction enzyme-digested DNA (Panel A). This was again seen when switching the primers and probes (Panels C and D).

Extremely significant differences were observed in the all of the different samples (Figure 2.16). Although the number of positive droplets were different, the total number of droplets were not (Figure 2.17).

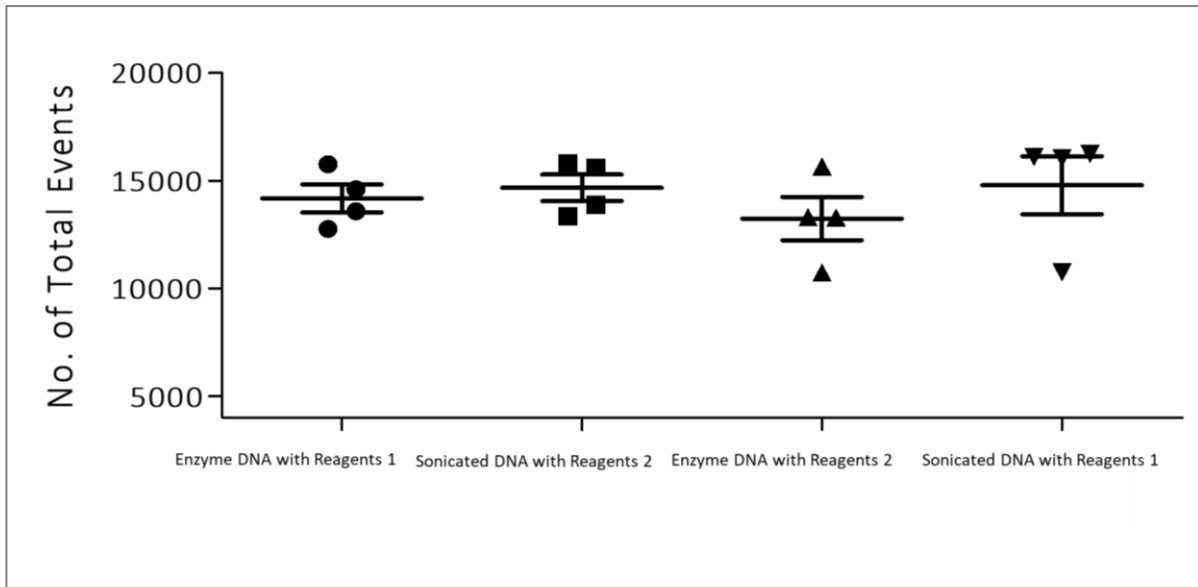


Figure 2.17. Scatter Plot of Total No. of Events in Sonicated and Digested Samples

The graph shows the total number of events for *AMELX* and *AMELY* for our and our collaborator's samples. Our DNA enzymatically digested, whereas our collaborator's sample was sonicated. "Reagents 1" refers to our in-house primers and probes, whereas "Reagents 2" refers to our collaborator's in-house primers and probes. Number of events of *AMELX* was obtained from the Qantasoft software and was plotted on GraphPad Prism. Four replicates were used. No significant difference was observed.

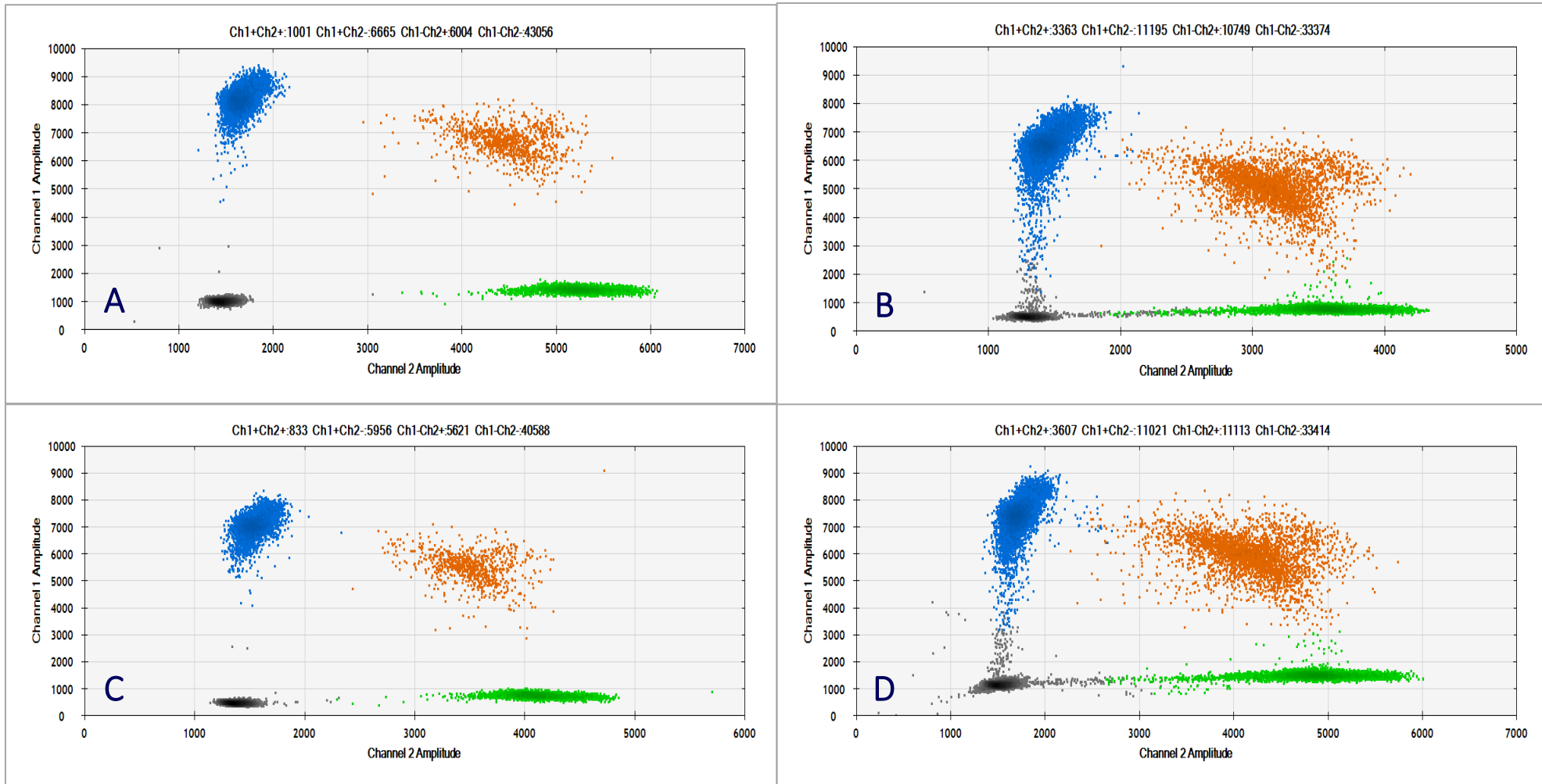


Figure 2.18. Quantasoft 2-D plot of Different Treatment Methods of DNA

Male DNA from MCWES02 cells were run on the ddPCR™ in quadruplicates. In panel A our wild-type male, digested DNA is shown in combination with our in-house primers and probes, in panel B our collaborator's sonicated DNA with their primers and probes, in panel C- our digested DNA in combination with our collaborator's primers and probes and in panel D- our collaborator's sonicated DNA with our in-house primers and probes. *AMELX* is labelled with FAM and *AMELY* – VIC. Results were obtained from the Quantasoft software. The black points on the plot represent negative droplets, the blue points are positive droplets on the FAM channel, the green-VIC channel and the orange points represent droplets that are positive for both the FAM and VIC channels. The results are shown in triplicate.

Figure 2.19 shows the sonication of MCWES01 at 200ng/μl in a 100μl total volume for 10s at amplitude of 20% (Amplitude 2 on the Branson 450 D). This condition was chosen, due to the ease of replicability of fragment sizes, consistent fragmentation of the DNA and lastly, the increased number of positive droplets we see in Figure 2.19 and Figure 2.20. Previously, we had tested a 10% amplitude on the DNA, however no noticeable effect had been observed. Different concentrations of DNA were also tested, where lower concentrations were very difficult to observe on the gel and higher concentrations did not fragment easily. Similarly, when sonicating the DNA for short periods of time, the DNA did not fragment efficiently and for longer periods of time it was difficult to observe on the gel. From Figure 2.19, we observe the segregation of the droplets much closer following the digestion, whereas after sonication the appearance of “rain” increased. On average, a significantly increased percentage of positive droplets were observed with both the digestion and sonication; a 1.6% and 3.4% increase, respectively (Figure 2.20).

As proof of concept dictated, it was easier and more reliable to sonicate the control DNA, rather than digest it with different enzymes, dependent on the amplicon size and location in the human genome. We, therefore, decided that within each ddPCR™ experiment, the same stock of sonicated DNA would be used as a positive control. This would eliminate any possible differences in the comparison of control DNA to the DNA being tested in the experiment.

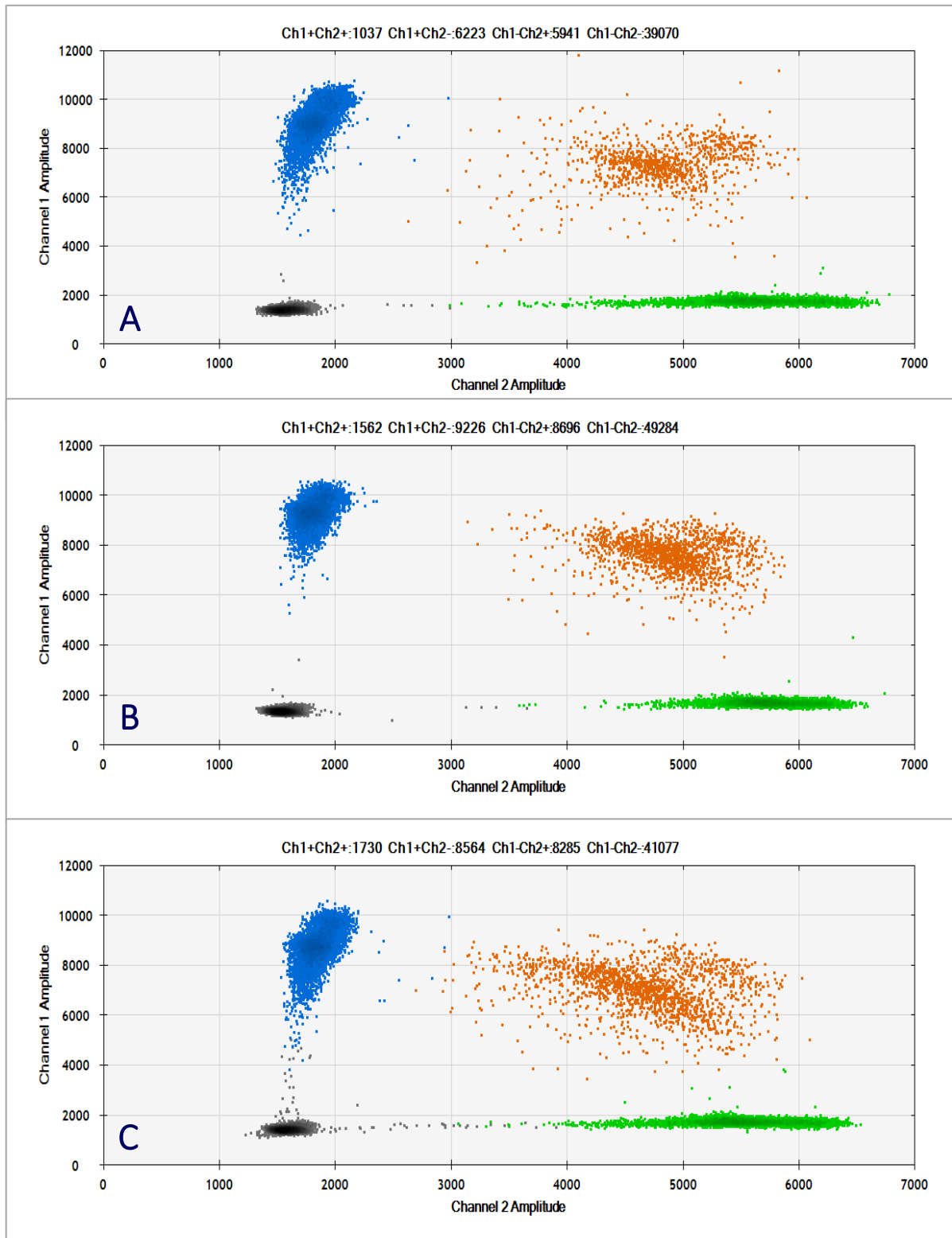


Figure 2.19. Quantasoft 2-D plot of Different Treatment Methods of DNA

Male DNA from MCWES01 cells were run on the ddPCR™ in quadruplicates. In panel A, our wild-type male is untreated, in panel B, the DNA is digested with BstYI, in panel C, the DNA is sonicated for 10s at amplitude 2. *AMELX* is labelled with FAM and *AMELY* – VIC. Results were obtained from the Quantasoft software. The black points on the plot represent negative droplets, the blue points are positive droplets on the FAM channel, the green- VIC channel and the orange points represent droplets that are positive for both the FAM and VIC channels. The results are shown in triplicate.

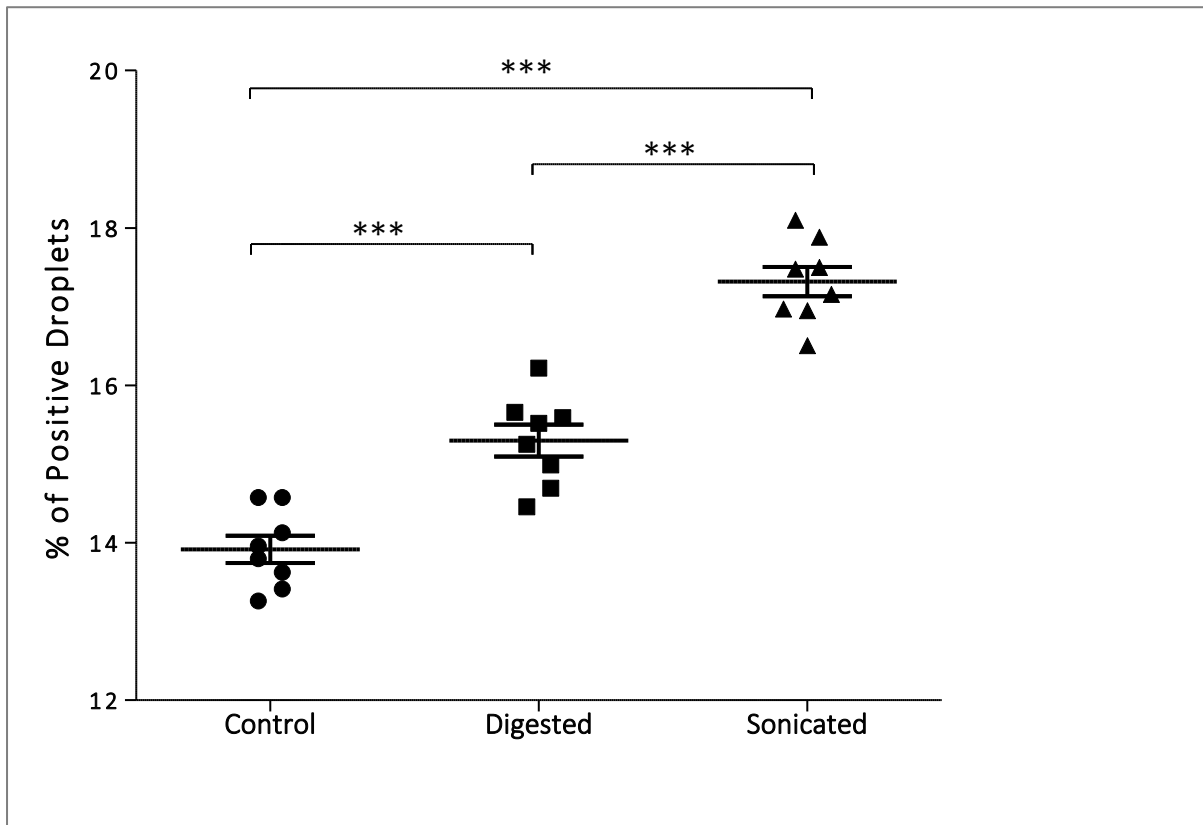


Figure 2.20. Scatter Plot of the Percentage of Positive Droplets in ddPCR™

The graph shows the percentage of positive droplets in comparison to the total number of droplets generated in the ddPCR™ experiment. The control DNA was the untreated, wild-type MCWES01, the digested DNA was the MCWES01 digested with BstYI and the sonicated DNA was MCWES01 sonicated for 10s on amplitude 2 at 200ng/μl in a 100μl volume. Results were obtained from the Quantasoft software, where *AMELX* was labelled with FAM and *AMELY* – VIC. One-Way ANOVA was calculated with Tukey's Multiple Comparison Test; significant differences are shown with asterisk(s).

2.3.5. Using Reference Genes in ddPCR™

Previously, we had always used our ddPCR™ set-up template from the Jennings lab, however from BioRad's guidelines for ddPCR™ it was recommended we use a stable reference gene for copy number variation. In an attempt to reference our gene of interest to a stable gene, a literature search for stable gene in human pluripotent stem cells was performed. Due to the huge amount of genomic instability present in the hPSCs, all apart from one chromosome commonly accumulate as aneuploidies in recurrent gains and /or losses; chromosome 4 was reported as a stable chromosome in hPSCs, despite the structural variants that were observed (Amps *et al.*, 2011). In a female sample, where there are two copies of our gene of interest i.e. *AMELX* and two copies of the housekeeping genes *ALB* and /or *RPP30*, we expect a ratio of 1:1. Additionally, as a control, we also tested *RPP30* labelled on FAM and VIC together to make sure none of the positive droplets were positive for a single Ch1. If the results showed any droplets positive for the blue (Ch1/FAM) or green (Ch2/VIC) channels, then this would signify that the probes were not binding to the target DNA sequences equally.

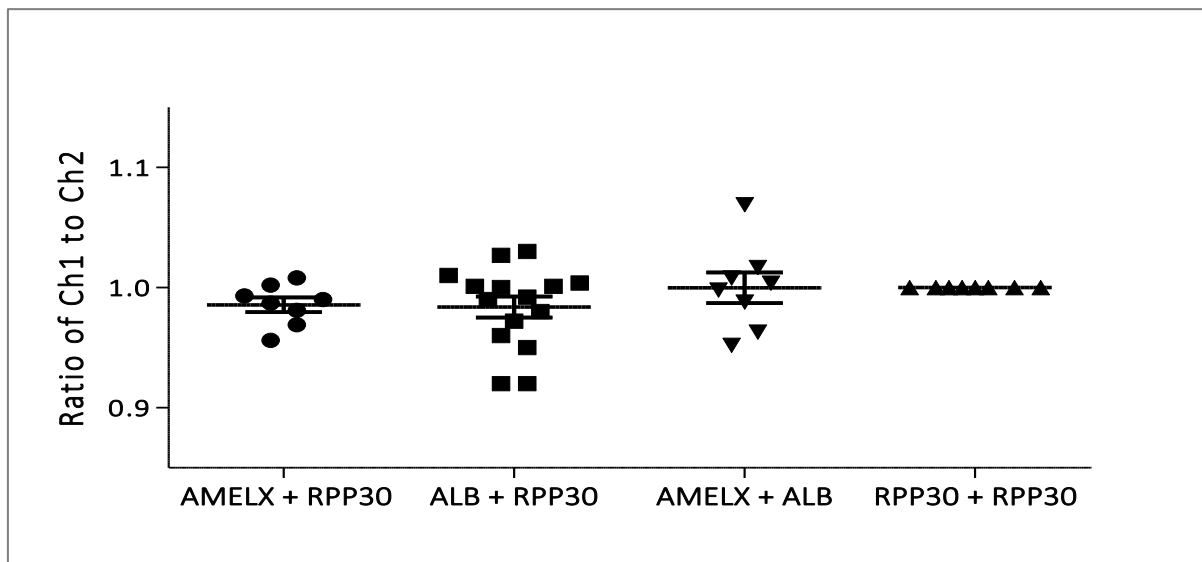


Figure 2.21. Scatterplot of the Ratio of the Different Combination of Reference Genes

The graph shows the ratio of different combination of genes using wild-type female DNA from FCWES01. The data was obtained from the Quantasoft software and was plotted on GraphPad Prism. One-Way ANOVA was calculated with Tukey's Multiple Comparison Test; significant difference was not observed between any of the samples analysed.

From Figure 2.21, it is clear that by using a reference gene in ddPCR™, the resulted values are highly close to the expected results, where the ratio of *RPP30* (labelled with FAM) to *RPP30* (labelled with VIC) was exactly 1 for all of the replicates.

2.3.6. Detection of Chromosomal Aneuploidies using ddPCR™

Using ddPCR™, three aneuploidy lymphoblastoid cell lines (Table 2.1) were analysed to observe the ratio change between genes *AMELX* and *ALB* (Figure 2.22) when whole cell populations contain aneuploidy chromosomes. With each additional chromosome X, approximately a 0.5 increase was detected.

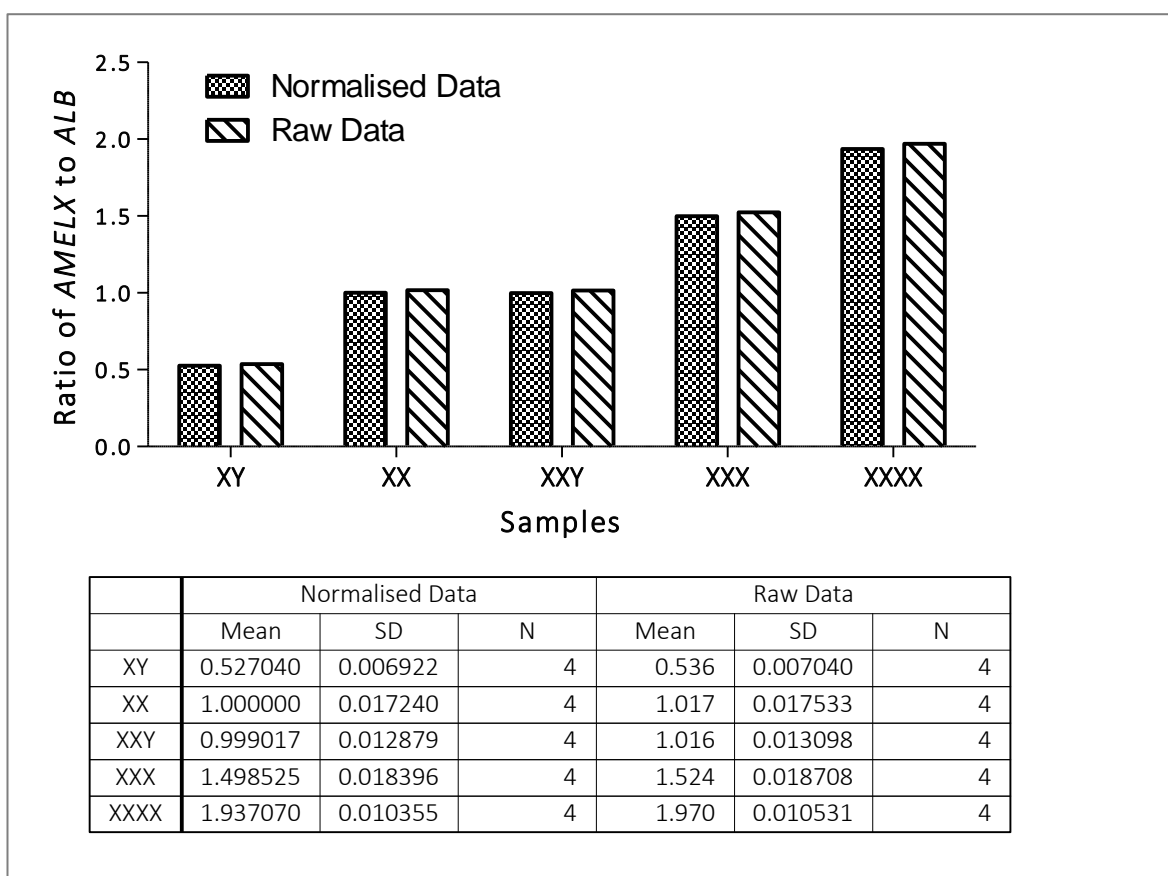


Figure 2.22 *AMELX* Detection in Aneuploid Cell Lines in ddPCR™

AMELX detection in chromosome X aneuploidy cell lines by ddPCR™ is shown. An increasing ratio of *AMELX* to *ALB* for different samples was observed. Approximately a 0.5 increase with each additional X. Standard error of mean is shown. Cell lines MCWES01 (XY), FCWES02 (XX), DD0567 (XXX), DD1473 (XXXX) and DD0710 (XXY) were used. The raw data, normalised data and expected results are shown, the “Normalised Data” was adjusted to the diploid XX karyotype.

In order to observe how sub-populations of aneuploidies in cell culture look on the ddPCR™ machine, a 10% increment titration of XXX (Cell line DD0567) in a background of XX (Cell line FCWES02) experiment was designed. Figure 2.22 shows a steady increase in ratio of *AMELX* to *ALB*.

In addition, a similar titration was performed with the addition of 2.5% of XXX (DD0567) into XX female DNA (FCWES02) to observe the ratio change of *AMELX* to *ALB*. Figure 2.24 shows the possibility of detecting a 2.5% of aneuploid cells in a background of wild-type DNA, whereas Figure 2.25 shows the ability of the assay to detect p to 1% aneuploidy in a background of diploid cells.

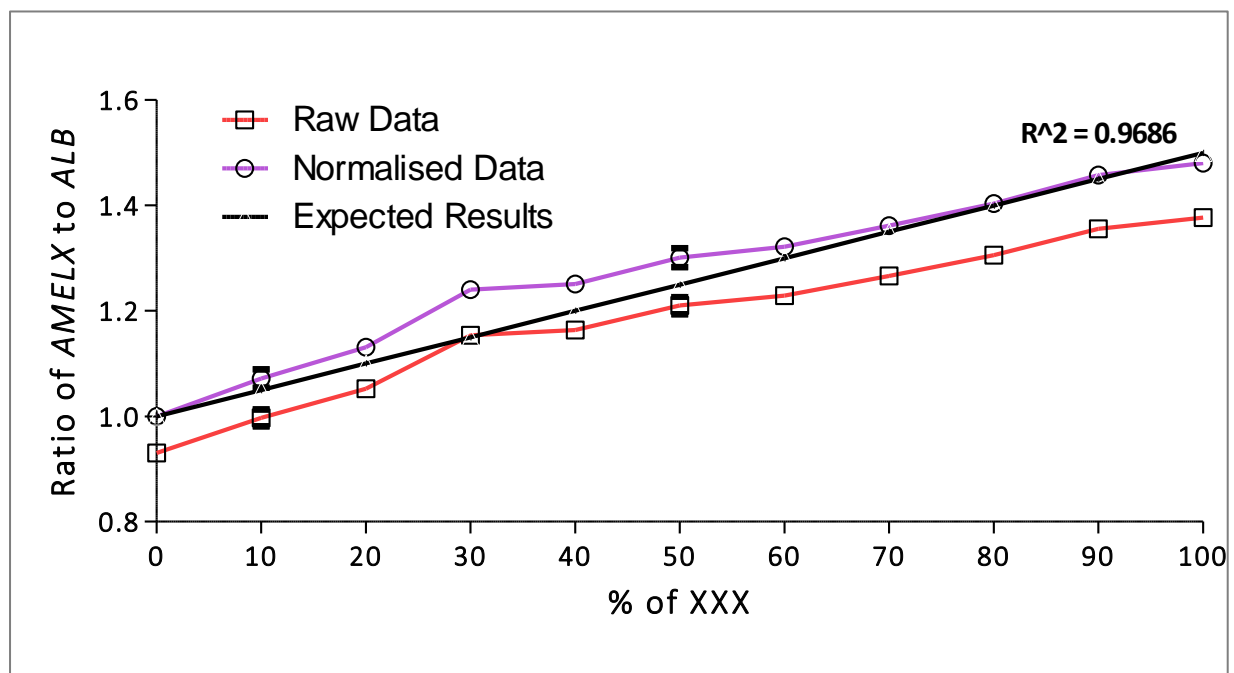


Figure 2.23. *AMELX* Detection in Chromosome X Aneuploidy in 10% Increments Sub-populations *AMELX* detection in the titration of trisomy X (DD0567) in wild-type female DNA (FCWES02) in 10% increments by ddPCR™. Increasing ratio of *AMELX* to *ALB* for different titrations is shown. Approximately a 0.05 increase (equivalent to an additional 10% *AMELX* target in the sample) with each additional 10% trisomy X titration was observed. Standard error of mean and the R^2 value are shown. The raw data (red), normalised data (purple) and expected results (black) were plotted; eight replicates were used.

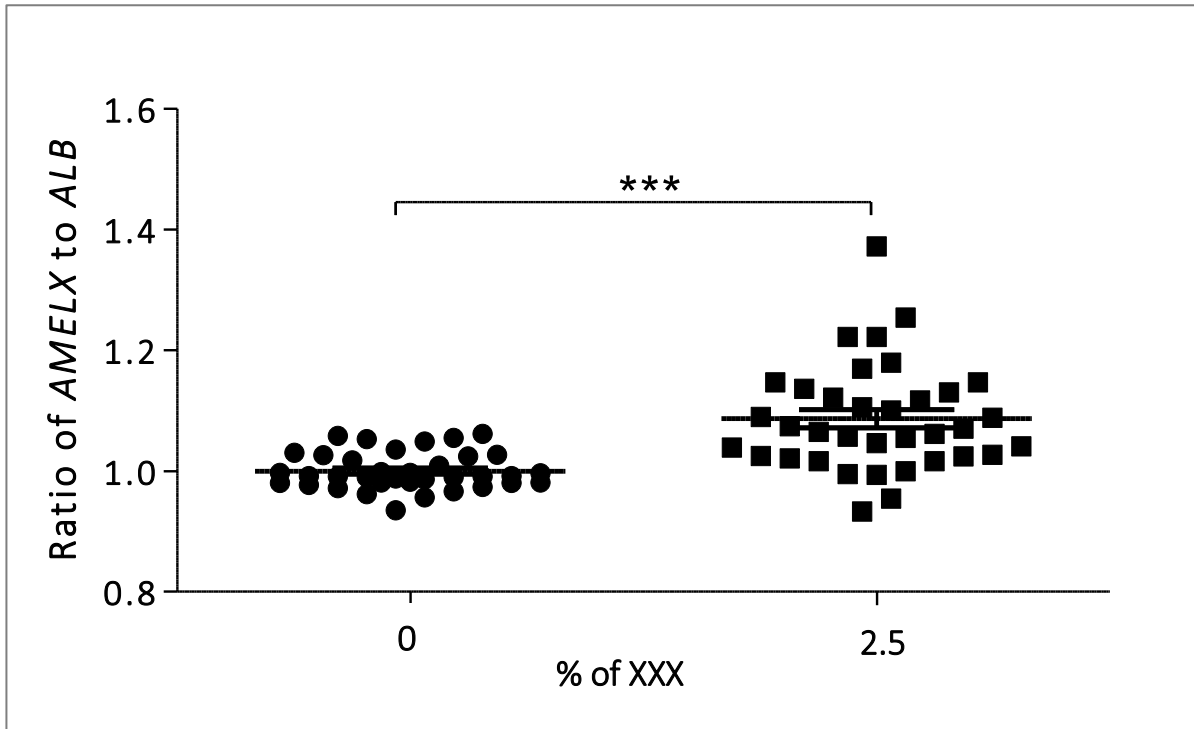


Figure 2.24. Scatterplot of 2.5% Trisomy X Titration in Wild-Type Female DNA

AMELX detection in the 2.5% titration of trisomy X (DD0567) in wild-type female DNA (FCWES02) by ddPCR™ is shown. Two-tailed t-test was calculated; significant difference is shown with asterisks. An F-test was used to calculate the significantly different variances between the two samples.

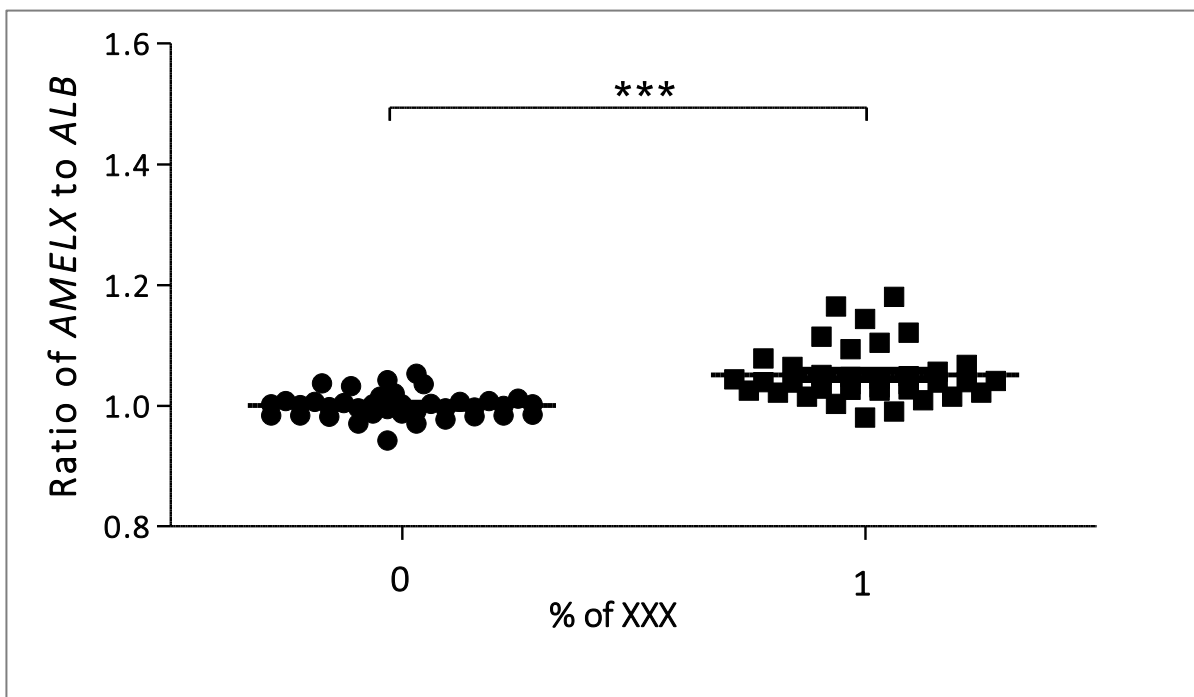


Figure 2.25 Scatterplot of 1% Trisomy X Titration in Wild-Type Female DNA

AMELX detection in the 1% titration of trisomy X (DD0567) in wild-type female DNA (FCWES02) by ddPCR™ is shown. Two-tailed t-test was calculated; significant difference is shown with asterisks. An F-test was used to calculate the significantly different variances between the two samples.

2.5. Discussion

Droplet Digital Polymerase Reaction (ddPCR™) is a powerful tool, which can be utilised for the detection of rare events and copy number variation (CNV) (Pohl and Shih, 2004; Miotke *et al.*, 2014). ddPCR™ has a reported sensitivity of detecting 1 SNP in a background of 10000 wild-type sequences (Huggett, Cowen and Foy, 2014) and has already been developed for the detection of a number of aneuploidies (Fan *et al.*, 2009). Studies have shown that human pluripotent stem cells are susceptible to a number of aneuploidies (Baker *et al.*, 2007) and the aneuploidies have been associated with prolonged growth in cell culture (Amps *et al.*, 2011). Our aim in this study was to optimise and develop ddPCR™ as a quick, sensitive and consistent method for the detection of aneuploidies in human pluripotent stem cells. Our optimisation process included using model cell lines to mimic the accumulation of aneuploidies in the hPSC culture. In order to improve the sensitivity of the ddPCR™, the DNA was treated in different ways and the sensitivity of each method was carefully monitored.

2.4.1. DNA fragmentation prior to ddPCR™

From the digestion results, we observed clearer and more distinct droplet segregation on the 2-D plot of our samples (Figure 2.9 and Figure 2.11). We suggest that the digested DNA produces fragments, allowing the formation of more droplets for ddPCR™ and consequently permits primers to bind to the specific DNA sequences more readily. This would then encourage the amplification of the target gene and the fluorescence frequency of the probe to increase. These observations are in line with current BioRad guidelines and the research of McMahon, *et al.*, 2017 (McMahon *et al.*, 2017) .

The enzymatic digestion method is a quick and easy way of eliminating highly viscous DNA to enable its use in a PCR mix and has been used frequently by others (Hindson *et al.*, 2011; Strain *et al.*, 2013; Dong *et al.*, 2014). Whilst enzymatic digestion is a common way of treating the DNA and is recommended by BioRad it does have its disadvantages. These include the possibility of the buffer in the digestion mix to

interact with the PCR mix (Yukl *et al.*, 2014) , as well as reduced ddPCR™ target copies, due to the enzyme digesting the DNA sequence that required amplification (Shehata *et al.*, 2017).

Other methods, such as shredding or sonicating the DNA has also been proposed for the improvement of ddPCR™ results (Vitomirov *et al.*, 2017). For the shredding of DNA, a QIASHredder (Qiagen) is recommended; the method is said to reduce the chance of any enzymatic buffer interactions with the PCR mix and have <1% chance of breakage within the amplicon sequence (Yukl *et al.*, 2014). However, with both of these methods there is a risk of damaging the DNA integrity and therefore, losing your target gene sequence. Unlike the enzyme treatments, the sonication or shredding of DNA is random, so the risk of targeting your sample is higher. Nevertheless, the sonication or shredding of DNA eliminates the need to look for enzymes that do not cut in your amplicon sequence. This may prove difficult when designing experiments with multiple sequences being amplified (multiplexing). Additionally, a disadvantage of using enzymatic digestion is that the digested fragment sizes are not uniform. This problem may be reduced, however, with the use of a g-TUBE™ (Covaris, UK), which produced fragments of uniform size and is now incorporated for the pre-treatment of DNA prior to nanopore sequencing (Oxford NanoPore Technologies, UK) (Laver *et al.*, 2015; Eckert *et al.*, 2018). But as with every method of DNA fragmentation, the use of the g-TUBE™ may be limited in the absolute quantification of nucleic acids. Unlike in sequencing, where reads can be aligned, the amplicons have to be fully-amplified for the probe to fluoresce and therefore be read.

Despite all of the different enzymatic treatments that we had tested on our DNA samples, none of them had any effect of the ratio of the two target genes, highlighting that none of the conditions affected the absolute quantification of gene copy numbers. Thus, a stock sample of sonicated DNA was created, as to avoid any inconsistencies in the sample fragmentation and used with each ddPCR™ run as a control.

2.4.2. Fluorophore Intensity Bias

How well a fluorophore emits light is dependent on a number of factors, including the molar extinction coefficient- the ability of dyes to absorb light, the quantum yield – the ability to convert absorbed light into emission, photostability – the ability to undergo repeated excitations and dye environment – pH, temperature and solvent. From our results, we observed that the FAM signal intensity, that was usually labelling the *AMELX* gene, was always higher in comparison to the VIC signal intensity, usually labelling *AMELY* (Figure 2.10, Figure 2.12). This could be explained by the fact that possibly one fluorophore may have a stronger signal compared to the other due to a higher fluorescent intensity produced. Many commercial companies usually recommend labelling low copy number gene targets with FAM, due to its strong fluorescence signal, whereas lower signal fluorophores could be used for more abundant gene targets (Houck, 2015; Integrated DNA Technologies, 2015). FAM has been shown to be a stronger probe than VIC, due to its stronger relative signal height (Brabetz and Weber, 2014).

Due to the possible bias from the FAM signal, it was decided that *AMELX* and *AMELY* probes were to be switched around so *AMELX* would now be labeled with VIC and *AMELY* with FAM. After switching the probes around an equal “over-read” was observed on the *AMELY* gene as it was before on *AMELX* (Figure 2.13). This originally pointed back to the idea that the FAM signal may still be over-read by the BioRad ddPCR™ machine (independent of the bound-target). However, when running the *RPP30* control in both fluorophore channels (Figure 2.21), all of the droplets contained target copies positive for both channels. This demonstrated that the fluorophores are equally strong at binding to the target sequences.

Alternatively, another factor contributing to this “over-expression” or “over-reading” of *AMELX* may be due to the DNA analysed being from cell pellet extractions. It has been known that chromosome Y is a small chromosome that often gets lost in culture and therefore it may explain the excess amount of FAM signal (Pierre and Hoagland, 1972). For this reason, wild-type male blood DNA samples were run on the ddPCR™ to see whether the amount of *AMELX* and *AMELY* would balance. Interestingly, the

fractional abundance of *AMELX* did decrease in the blood samples (Figure 2.14), in comparison to the cell culture samples (Figure 2.13), however all except one of the values were higher than 1. The results point to the theory that Y chromosome loss in cell culture probably does occur and is probably less evident in blood, but this theory does not explain why the VIC signal is rarely seen to be over 1. In order to adjust for this, all of the samples were run with a normal diploid cell line and later normalised to it.

2.4.3. DNA Sonication

Although sonication is not a recommended DNA treated method by BioRad's manufacturer's guidelines, it is nevertheless a treatment method that some groups use before ddPCR™ (George *et al.*, 2013; Vitomirov *et al.*, 2017). Additionally, when Formalin-Fixed, Paraffin-Embedded (FFPE) tissue, degraded DNA samples or cell-free DNA (cfDNA) is used, BioRad does not recommend enzymatic treatment since the DNA is already fragmented. From our results we have observed increased droplet numbers with sonication, albeit increased "rain" in our ddPCR™ 2-D plots. The increased readings in the ddPCR™ were in line with the work of Shehata *et al.*, 2017. Increased rain has also been reported previously and software has been designed in an attempt to make calls whether a droplet belongs to one population or the other (Jones *et al.*, 2014).

Additionally, by running a control cell line with each run we are able to make sure the results in each ddPCR™ run is consistent, due to the possibility of normalising our data. This consistency allows us to directly compare results between different ddPCR™ runs.

In conclusion, we have successfully established a sensitive ddPCR™ assay for the detection of low copy number chromosomal aneuploidies in a diploid background of DNA. To our knowledge, the method is the most sensitive assay currently available at the detection limit of up to 1% aneuploidy detection.

Chapter III: Utilising Fluorescence *In-Situ*
Hybridisation for the Characterisation of
Gene Loci Positioning in Aneuploidies

3.1. Introduction

3.1.1. Chromatin Organisation in Interphase Nuclei

In humans, wild-type nuclei contain forty-six chromosomes arranged into discrete non-randomly positioned chromosome territories. However, in some cases, an abnormal number of chromosomes are present in nuclei and are known as aneuploidies. Although aneuploidies represent 35% of spontaneous abortions (Hassold and Hunt, 2001), due to their copy number variation in genes (O'Connor, 2008), some aneuploidies persist and are viable for life. The gene density distribution of chromosomes within nuclei suggests a biological significance; changes to this evolutionarily conserved arrangement proposes a disruption to the normal function of the nucleus (Boyle *et al.*, 2001; Petrova *et al.*, 2007; Meaburn *et al.*, 2009, 2016; Leshner *et al.*, 2016). Conflicting evidence of chromosome positioning between aneuploid and diploid cells has been reported. Cremer *et al.*, 2003 had found a general radial positioning of HSA1 and 19 maintained, but with marked differences in the chromosome territory positioning between tumour and wild-type cells in cell lines with both mosaic and stably abnormal karyotypes. Similarly, human pluripotent stem cells displayed significant differences in chromosome positioning between aneuploid and diploid cells (Wiblin *et al.*, 2005; Shete *et al.*, 2014). In chromosome X aneuploidies, Petrova *et al.*, 2007 demonstrated a relocation of chromosome territories in comparison to wild-type nuclei; a shift in the active X (X_a) and chromosome 1 of XXXXY cells towards the nuclear periphery in comparison to their wild-type male XY (Petrova *et al.*, 2007). On the other hand, Sengupta *et al.*, 2007 concluded that artificially introduced chromosomes did not induce a global chromosome relocation, however each study had looked at different approaches to illustrate the genome positioning in the cells, which may contribute to the different in opinion (Sengupta *et al.*, 2007). More recently, studies with 3-D FISH and Hi-C have shown that homologous chromosomes are far apart from each other and do not interact frequently (Heride *et al.*, 2010; Selvaraj *et al.*, 2013; Fraser, Williamson, *et al.*, 2015). Although genome-wide approaches provide large datasets to understand the chromatin interactions in multiple sites and in whole cells populations, fluorescence

imaging methods provide single-cell level information to understand chromatin positioning using computational methods for position analysis (Ollion *et al.*, 2015). In addition, chromosome rearrangement detected by FISH can be tissue-specific in diseases and aid in diagnostics and prognosis (Meaburn *et al.*, 2016).

3.2. Aims

The aim of this part of the project was to use fluorescence *in-situ* hybridisation gene loci positioning to evaluate the impact of aneuploidies in the aneuploid nuclei. We utilised chromosome X aneuploidies to model the possible differences in gene loci positioning. Two genes were selected to compare the gene loci positioning in wild-type versus aneuploid nuclei. The housekeeping gene, “stable” in human pluripotent stem cells, *ALB* and a gene found on chromosome X, *AMELX*, were employed as probes.

Additionally, the study was designed to observe the general morphology of the cell nuclei and whether there were any differences between wild-type and aneuploid cell nuclei. The objective was to determine whether the additional chromosomes in the aneuploid cell lines caused a change in the size or shape of the nuclei. We used the FISH images generated in Fiji (ImageJ) to analyse nuclear area and shape.

3.3. Methods and Materials

3.3.1. 2-D FISH

3.3.1.1. DNA Isolation

Bacterial Artificial Chromosomes (BACs) with specific gene sequences can be tagged with fluorescent labels and used as probes for fluorescence *in-situ* hybridisation (FISH). Two BACs (ThermoFisher Scientific), Clone ID RP11.580P21 and RP11.121K9 for *ALB* and *AMELX*, respectively were used. The BACs were in DH11 *Escherichia coli* (*E. coli*) and were grown on Luria Broth (LB) agar (1% NaCl, 1% Tryptone, 0.5% Yeast Extract, 1.5% Agar) with 12.5µg/µl chloramphenicol (Sigma). Following this, a small number of cells were scraped off the agar plate and inoculated in LB supplemented with chloramphenicol and placed on an agitator/shaker overnight at 37°C. To make low temperature stocks of BACs the bacterial culture was mixed with 50% of glycerol in cryovials, frozen and stored at -80°C.

To isolate the BACs, an alkaline lysis method was used; the protocol was provided by Dr Temi Owoka from Dr Sabrina Tosi's lab (Brunel University London). For 50ml of bacterial culture, the cells were spun down at 2500 x *g* for 10min and the supernatant removed. The pellet was then resuspended in 3ml of an ice-cold resuspension buffer (50mM Glucose, 25mM TrisCl (pH 8.0), 10mM EDTA (pH 8.0), 100µg/ml RNase A) and incubated on ice for 5min, followed by the addition of 6ml of lysis buffer (0.2M NaOH, 1% SDS). The mixture was inverted and incubated for 5min. Finally, 4.5ml of neutralisation buffer (3M Potassium Acetate (pH 4.8)) was added, the tube inverted and incubated on ice for 5min, followed by a centrifugation at 21 500 x *g* for 10min at 4°C. The supernatant was transferred to a clean tube and re-centrifuged until the supernatant was clear. The supernatant was removed once again, and an equal amount of iso-propanol was added. The tube was inverted and centrifuged at 21 500 x *g* for 30min at RT. The supernatant was discarded, and the pellet was washed with ice-cold 70% ethanol, followed by a centrifugation at 21 500 x *g* for 5min at RT. The supernatant was removed, and the pellet allowed to air-dry for 15min. The pellet was then resuspended in an appropriate volume of nuclease-free water. The DNA was quantified by running an agarose gel and a Nanodrop 100 was used to look at any possible

RNA or protein contamination. To confirm that the BACs were truly the sequences we required, qPCR was performed on the Stratagene MX3000 qPCR machine, according to the same conditions, primers and probes as mentioned in Chapter II (Section 2.3.6).

3.3.1.2. Degenerate Oligonucleotide-Primed Polymerase Chain Reaction

Degenerate Oligonucleotide-Primed Polymerase Chain Reaction (DOP-PCR) was performed for whole chromosome FISH. The template chromosome paints were a kind gift from Michael Bittner and amplified for each use (Table 3.1) in a thermocycler under specific conditions (Table 3.2).

For the labelling of the template chromosome paints either biotin or digoxigenin was used in the amounts described in Table 3.3. The thermocycling conditions are shown in Table 3.4. After this step the chromosome paints were precipitated (Section 3.3.1.4. Probe Hybridisation and Preparation).

Table 3.1. DOP-PCR Template Amplification Reagents

Reagent	Amount (μ l)
5 x DOP-PCR Buffer (Sigma-Aldrich)	10
dACGTP (2mM) (Promega)	5
dTTP (2mM) (Promega)	5
DOP Primers (20 μ M)	5
Taq Polymerase (1U/ μ l) (KAPA Biosystems, USA)	1
Water	23
Template Chromosome Paint DNA	1

Table 3.2. DOP-PCR Template Amplification Conditions

	Temperature (°C)	Time (Minutes)	Process
Step 1	95	3	DNA Denaturation
Step 2	98	0.3	DNA Denaturation
Step 3	62	1	Annealing
Step 4	72	0.2	DNA amplification
Go to Step 2 X 31			
Step 4	72	5	Final Step
Step 5	4	Infinite	Hold

Table 3.3. DOP-PCR Chromosome Paint Labelling Reagents

Reagent	Amount (µl)
5 x DOP-PCR Buffer (Sigma-Aldrich)	10
dACGTP (2mM) (Promega)	5
dTTP (2mM) (Promega)	2
DOP Primers (20µM)	5
Biotin-16-dUTP/Dig-11-dUTP (Roche)	10
Taq Polymerase (1U/µl) (KAPA Biosystems, USA)	1
Water	23
Template Chromosome Paint DNA	5

Table 3.4. DOP-PCR Chromosome Paint Labelling Conditions

	Temperature (°C)	Time (Minutes)	Process
Step 1	95	3	DNA Denaturation
Step 2	98	0.3	DNA Denaturation
Step 3	62	1	Annealing
Step 4	72	0.2	DNA amplification
Go to Step 2 X 34			
Step 4	72	5	Final Step
Step 5	4	Infinite	Hold

To make sure the genes labelled with digoxigenin (DIG) or biotin were approximately 200-500bps long, a 2% agarose gel with X25000 SybrSafe (ThermoFisher, UK) was prepared and run to 100V for separation. 2µl of the DIG-labelled mixture (~100ng) and 5µl of the biotin-labelled mixture (~100ng) were usually prepared with x 12 loading buffer from the PeqGOLD DNA Sizer XIII (VWR Peqlab, UK).

3.3.1.3. Nick Translation Labelling of Bacterial Artificial Chromosomes

After the DNA extraction nick translation was performed to label the BACs with either biotin, Biotin-16-dUTP (ThermoFisher Scientific) or digoxigenin (DIG), digoxigenin-11-dUTP (Roche). *AMELX* was labelled with DIG, whereas *ALB* was labelled with biotin nucleotides. Both nick translations were performed using the Nick Translation Labelling Kit (ThermoFisher Scientific). This was followed by a centrifugation using a MicroSpin Column (GE Healthcare, UK) to separate any unlabelled sequences from the labelled nucleotides.

3.3.1.4. Probe Preparation

Both the biotin-labelled probe (*ALB*) and DIG-labelled probe (*AMELX*) were precipitated using 200ng of probe, 1µg of Cot-1 DNA (Roche), 1µg of Herring Sperm (ThermoFisher Scientific) with 1/10th of Sodium Acetate and X2 100% ice-cold ethanol (Table 3.1). The mixture was then incubated at -80°C for at least 30min.

Table 3. 5. Concentration of reagents used for the probe hybridisation in 2-D FISH

Component	Concentration/Amount
DNA Probe	0.2-0.4µg
Cot-1 DNA	7µg
Salmon/Herring Sperm DNA	3µg
3M Sodium Acetate	1/10 th Volume of Total of Probe, Cot-1 DNA and Salmon/Herring Sperm DNA
100% Ethanol	X2 of Total Volume

After the incubation, the probes were centrifuged at 16 000 x *g* for 30min at 4°C. After the centrifugation, the supernatant was removed, and the pellet produced was washed with 400µl of ice-cold 70% ethanol. The mixture was centrifuged again at 16 000 x *g* for 30min at 4°C and the supernatant removed. The pellet was then dried at 37°C on a hot block until it became transparent. 12µl of hybridisation buffer/mix (50% formamide, 10% dextran sulphate, 2X SSC and 1% Tween 20) was added to the dried pellet and it was allowed to dissolve at 37°C for 10 - 120min or left overnight at RT. The mixture was denatured at 75°C for 10min and allowed to re-anneal at 37°C for 10-120min.

3.2.1.5. Cell Fixation

Cells were grown to approximately 70% confluency and centrifuged at 250 x *g* for 5min and the supernatant removed. The pellet was resuspended in freshly prepared 0.075M potassium chloride (KCl) for each sample, the solution was added slowly drop-by-drop whilst agitating the cells. Approximately 5-7ml of KCl was used. Cells were then incubated at room temperature for exactly 15min. After the incubation, the cells were centrifuged at 120 x *g* for 5min, the supernatant was removed.

Afterwards, the cell pellet was re-suspended in freshly prepared ice-cold fixative solution (methanol: acetic acid 3:1 v/v) agitating the cells and slowly adding the fixative. Again approximately 5-7ml of the fixative was used. The newly re-suspended cells were incubated for 1h at -20°C.

After the incubation, the tubes were centrifuged at 120 x *g* for 5min. Then drop-by-drop freshly prepared ice-cold fixative was added to the pellet for re-suspension. These cells were then dropped onto damp SuperFrost slides (ThermoFisher Scientific) and visualised using a phase contrast Olympus CK2 inverted microscope to determine whether the cell density and quality was appropriate for use i.e. the loss of cytoplasm. The samples were stored at -20 °C in the fixative indefinitely.

3.3.1.6. Slide Preparation

After dropping the fixed cells onto the slides, the slides were aged for either two days at RT or baked at 70 °C for 1h. The slides were allowed to cool down after which they were dehydrated via 70%, 90% and 100% ethanol washes, 5min each. Slides were dried on a warm plate and placed into a 70°C oven for 5min. The slides were then placed in Denaturing Solution (70% Formamide and 2XSSC (pH 7.0)) at 70°C for 2 min and then placed in ice-cold 70% ethanol for 5min. Following this, they were placed in 90% and then 100% ethanol, for 5min each. Slides were dried on the warm plate again before 10µl of the prepared probe (3.3.1.4. Probe Preparation) was placed on each slide, a 22 X 22 coverslip was applied on top and secured in place with rubber cement. The slides were left in a humidified chamber for two days.

3.3.1.7. Slide Hybridisation, Washing and Counterstaining

After the hybridisation, the rubber cement was removed from the coverslips and the slides were first washed three times in Wash Buffer 1 (50% Formamide and 2XSSC (pH 7.0)) for 5min at 45°C, followed by another three 5min washes in Wash Buffer 2 (0.1XSSC (pH 7.0)) which was pre-warmed to 60°C and then transferred to a 45°C waterbath once the slides were immersed. The slides were then placed in a room temperature 4XSSC solution for 10min.

100µl of 4% Bovine Serum Albumin (BSA) in 4XSSC was added to each slide for blocking and covered with a 22 X 50 coverslip for 10min at RT. Coverslips were removed and 100µl of streptavidin-conjugated cyanine 3 (Cy3) (1:30 dilution (ThermoFisher Scientific)) in 1% BSA and 4XSSC was added to each biotin-labelled slide. For DIG-labelled slides, anti-DIG mouse antibody FITC (Jackson Laboratories, USA) was re-suspended in 350µl and then a 1:100 dilution was used with 1% BSA and 4XSSC. 100µl of this solution was then applied onto each DIG-labelled slide. 22 X 50 coverslips were applied to the slides and incubated at 37°C for 30min, away from the light. The slides were washed three times in Wash Buffer 3 (0.1% Tween 20 in 4XSSC) at 42°C for 5min. The slides were then quickly washed with deionized distilled water before counterstaining with 1.5µg/ml Vectashield 4', 6-Diamidino-2-Phenyindole (DAPI) (Vector Laboratories, UK). 22 X 40 coverslips were applied to the slides.

3.3.1.8. Image Capture

Using the Olympus BX41 or Leica DM 4000 immunofluorescence microscope at X100 magnification with immersion oil, nuclei were visualised. The value of the fixed time exposure on the microscope was manual. To visualise the signals from the slides either "SmartCapture 3.0" (Digital Scientific, UK) for the Olympus microscope or "LAS AF" (Leica, UK) was used. Approximately one-hundred images of the nuclei with signals were taken for each slide.

3.3.1.9. Image Analysis

To quantify the position of whole chromosomes or genes within the interphase nuclei, an erosion script analysis programme was run in IPLAB (Croft *et al.*, 1999; Clements *et al.*, 2016). The images were uploaded into the software and the programme divided each nucleus into 5 Shells of equal area. The 1st Shell is the peripheral shell of the nucleus, where the 5th – internal (Figure 3.1). The software considers the intensity of the DAPI signal or DNA concentration by the pixel intensity of each image, alongside the intensity of the chromosome or gene signals.

For each shell, the intensity of the probe's signal was normalised; the percentage of the probe signal was divided by the percentage of the DAPI signal in each individual shell. The average probe:DAPI values were calculated for each shell and graphed with the standard error of the mean (SEM).

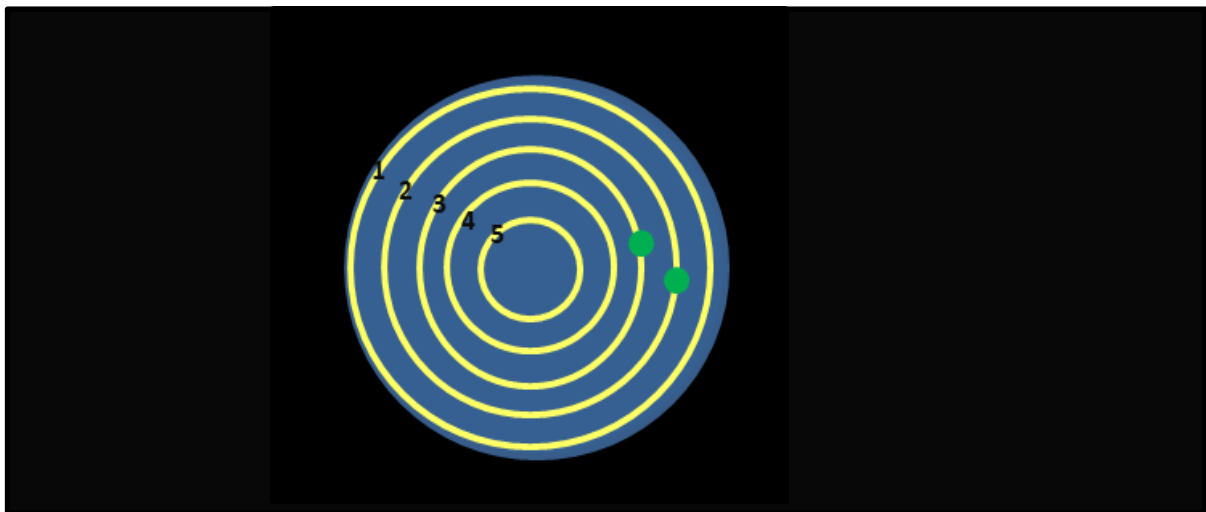


Figure 3.1. Nuclear Positioning via the Erosion Script software IPLAB

A cartoon image is displayed with the yellow concentric circles surrounding the blue nucleus. The 1st shell or concentric circle is the most peripheral, whereas the 5th – the most internal. The genes being positioned are shown in green.

Misshapen nuclei have been associated with a range of different diseases, including premature ageing (Taimen *et al.*, 2009), Pelger–Huët anomaly, a blood laminopathy causing a differentiation defects in the white blood cells (Hoffmann *et al.*, 2002) and cancers, such as cervical and small-cell lung carcinoma (Zink, Fische and Nickerson, 2004). In order to analyse the morphology of the nuclei, the

software Fiji (ImageJ) was used. A Macro was used to batch analyse the nuclei for cell area, circularity, aspect ratio and roundness. The circularity calculation formula is $4\pi\left(\frac{area}{perimeter^2}\right)$; a perfect circle has the value of 1. The aspect ratio calculation formula is $\frac{major\ axis}{minor\ axis}$; a perfect circle as the value of 1. The roundness calculation formula

is $\frac{4 \times area}{\pi \times (major\ axis)^2}$; roundness is the inverse of aspect ratio. Up to 200 cell nuclei were analysed for these calculations.

3.3.1.10. Analysing Chromosome Number by Fluorescence *In-Situ* Hybridisation

To block cells in metaphase, 05µg/mL of KaryoMAX Colcemid Solution (ThermoFisher Scientific) was added to the cell culture and incubated overnight at 37°C. Following this the cells were fixed as per Section 3.2.1.5.

3.4. Results

3.4.1. Chromosome Territory Presence in Lymphoblastoid Cells

Fluorescence *in-situ* hybridisation (FISH) was performed with whole chromosome paints on all of the lymphoblastoid cell lines shown in Figure 3.2. The results were consistent with the karyotyping (shown in Appendix I) for chromosome X. Approximately 30 metaphase spreads were examined; the results confirmed the wild-type cell lines, MCWES01 and FCWES02, contained one and two X chromosomes, respectively. Additionally, the results established DD0710, DD0567, and DD1473 to contain two, three and four X chromosomes, respectively.

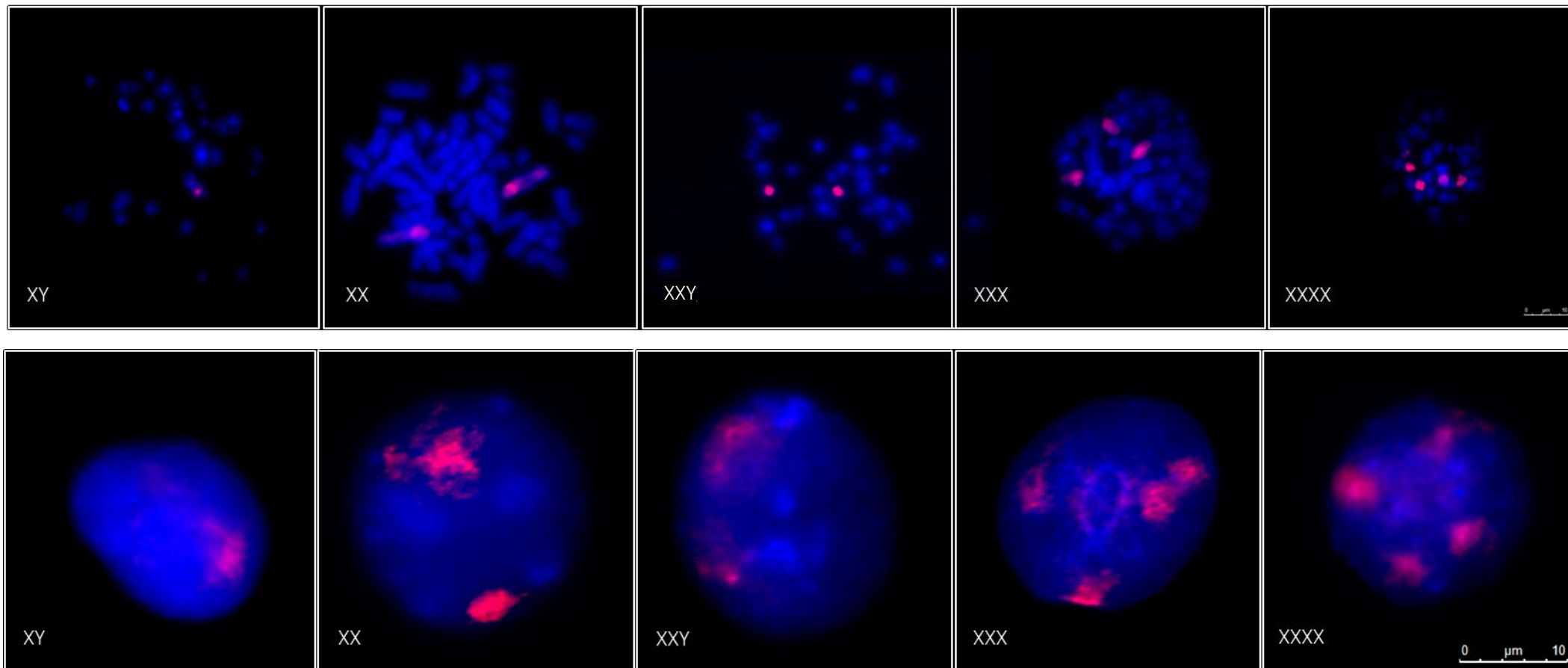


Figure 3.2. Chromosome X Presence in Interphase and Metaphase

The different panels show examples of fluorescence *in-situ* hybridisation images in both wild-type and aneuploid lymphoblastoid cell lines. The top row shows the cells in interphase, where the lower row shows cells in metaphase after colcemid treatment. The cell lines used are MCWES01 (XY), FCWES02 (XX), DD0710 (XXY), DD0567 (XXX) and DD1473 (XXXX). The scale bars are shown. Whole chromosome paints for chromosome X were used.

3.4.1. Gene Positioning in Lymphoblastoid Cells

Fluorescence *in-situ* hybridisation was performed using *ALB* and *AMELX* gene probes on the lymphoblastoid cell lines to compare their positioning in the nuclei dependent on their aneuploidy.

Figure 3.3 shows a panel of both *AMELX* and *ALB* gene signals in wild-type and aneuploidy cell lines.

For *ALB* positioning (chromosome 4), the cells displayed consistent results across all of the cell lines, except for two incidences, both in Shell 2. The significant difference was between FCWES02 (XX) and DD1473 (XXXX), and DD0567 (XXX) and DD1473 (XXXX) for Shell 2 (Figure 3.4). The samples were all compared to each other using one-way analysis of variance (ANOVA) and Tukey's Multiple Comparison Test. For all of the lymphoblastoid samples, a peripheral positioning of *ALB* was observed.

On the other hand, for *AMELX* positioning, a significant difference was shown in Shell 1 between cell lines MCWES01 (XY) and DD0710 (XXY), MCWES01 (XY) and DD0567 (XXX), and MCWES01 (XY) and DD1473 (XXXX) (Figure 3.5). For these statistical difference calculations, a Tukey's Multiple Comparison Test was used. For samples MCWES01 (XY), FCWES02 (XX) and DD0567 (XXX) a peripheral positioning of *AMELX* was observed, however DD0710 (XXY) and DD1473 (XXXX) had shown a reduced localisation to the nuclear edge and displayed a more intermediate nuclear positioning of *AMELX*.

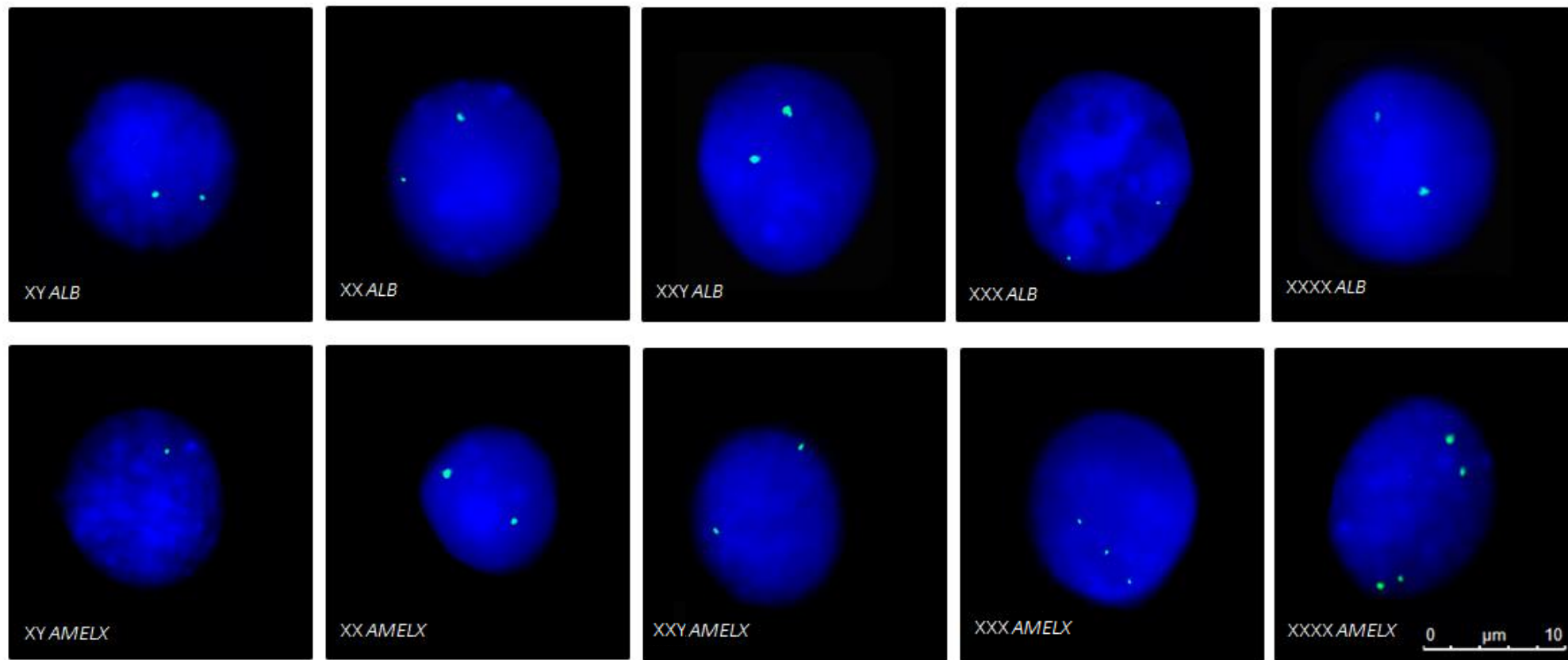


Figure 3.3. AMELX and ALB Fluorescence *In-Situ* Hybridisation Images of Wild-Type and Aneuploid Lymphoblastoid Cells

The different panels show examples of fluorescence *in-situ* hybridisation nuclei in both wild-type and aneuploid lymphoblastoid cell lines. The cell lines used are MCWES01 (XY), FCWES02 (XX), DD0710 (XXY), DD0567 (XXX) and DD1473 (XXXX). The scale bar is shown.

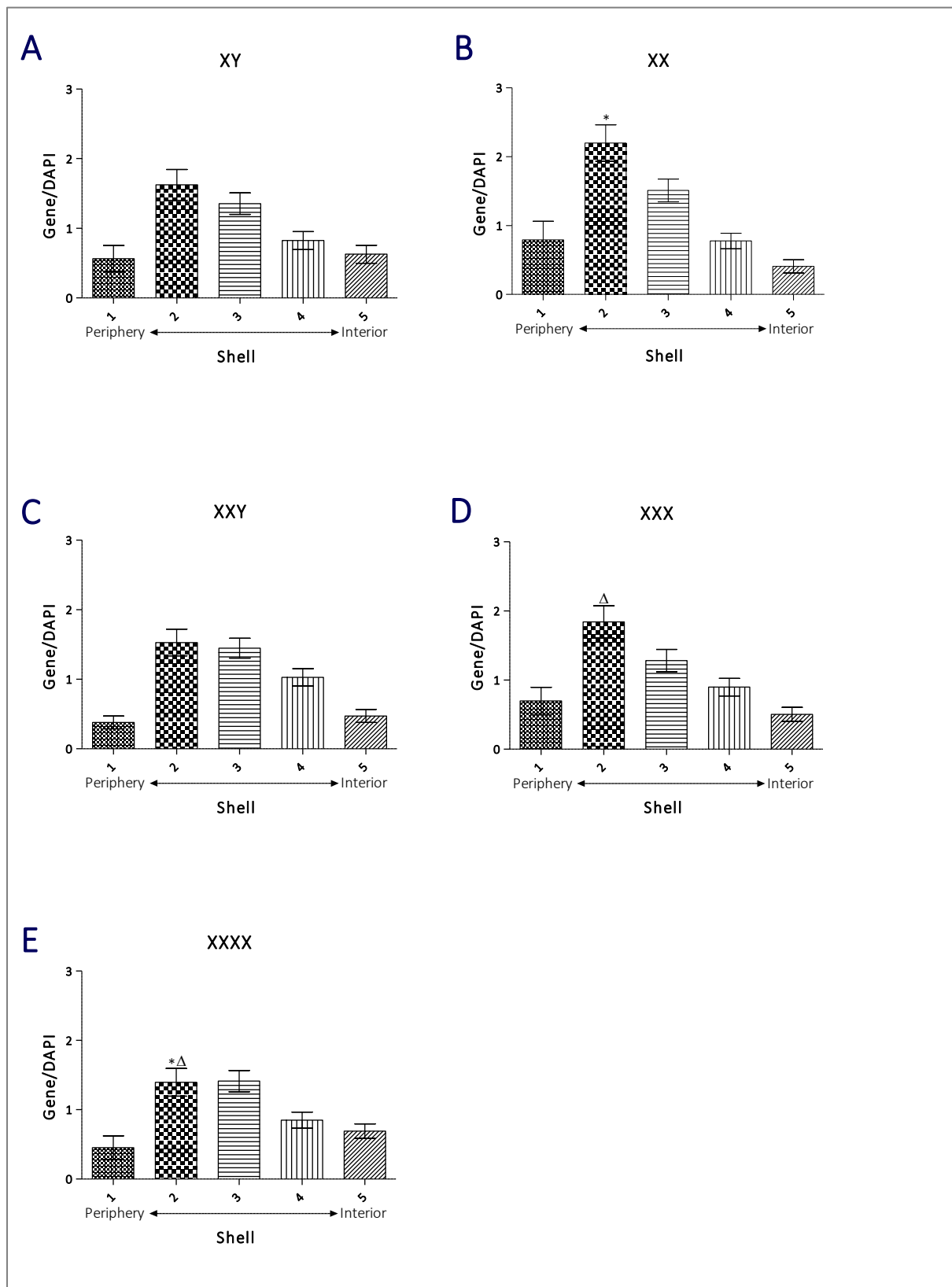


Figure 3.4. *ALB* Positioning in Wild-Type and Aneuploid Cell Nuclei

Different aneuploid cell lines' *ALB* positioning is shown in approximately 100 nuclei using the Erosion Script on the IPLAB software. Panel A shows MCWES01 (XY), B – FCWES02 (XX), C – DD0710 (XXY), D – DD0567 (XXX) and E – DD1473 (XXXX). The symbols (* and Δ) represent significant difference from Tukey's Multiple Comparison Test; standard error of mean is shown as the error bars.

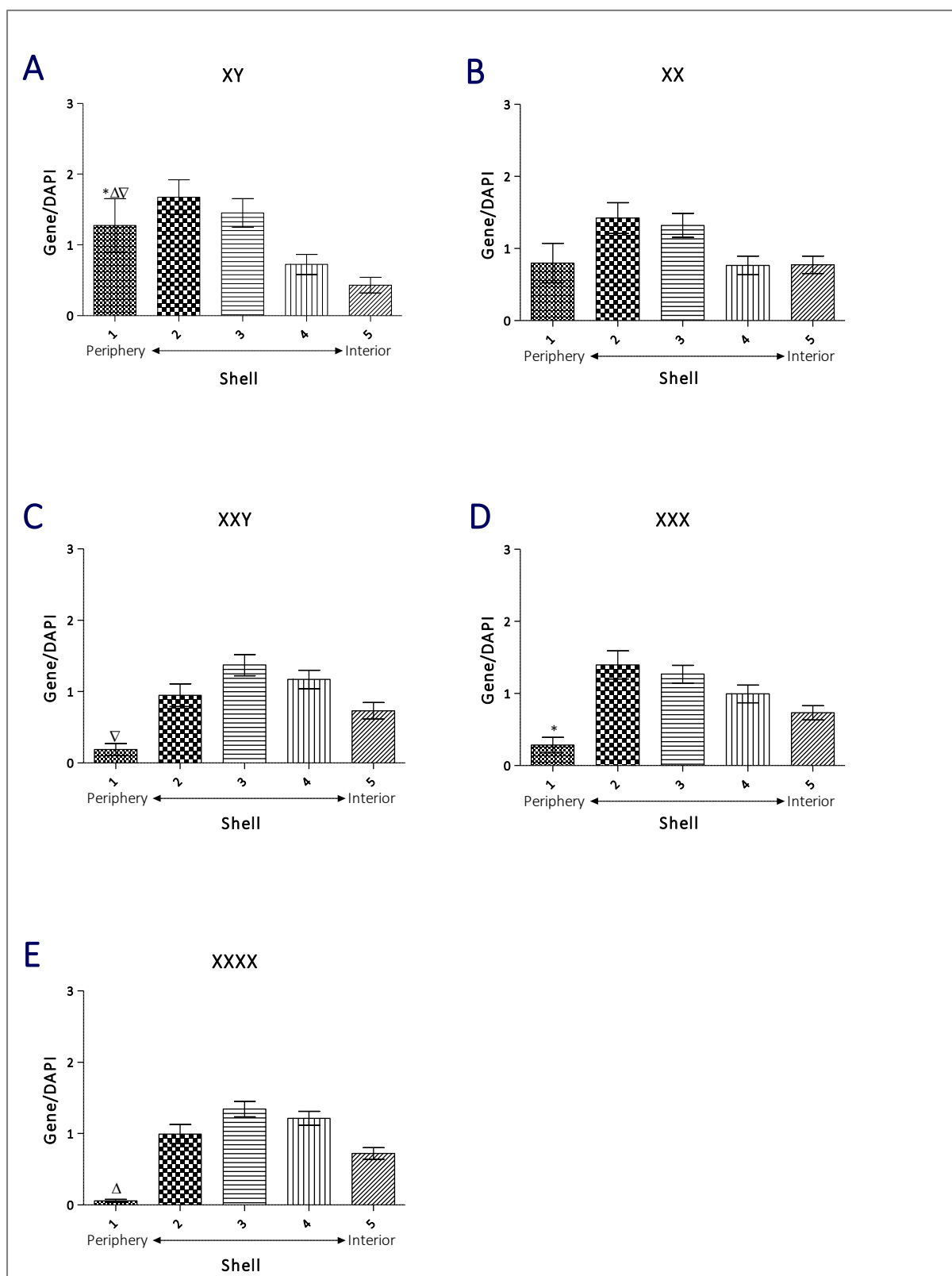


Figure 3.5. AMELX Positioning in Wild-Type and Aneuploid Cell Nuclei

Different aneuploid cell lines' *ALB* positioning is shown in approximately 100 nuclei using the Erosion Script on the IPLAB software. Panel A shows MCWES01 (XY), B – FCWES02 (XX), C – DD0710 (XXY), D – DD0567 (XXX) and E – DD1473 (XXXX). The symbols (*, ∇ and Δ) represent significant difference from Tukey's Multiple Comparison Test; standard error of mean is shown as the error bars.

Additionally, to compare the effect of aneuploidies, if any, on the nuclei, the nuclear morphology, specifically the circularity, was analysed with Fiji (ImageJ; Figure 3.6). A significant difference in nuclear size was observed between the wild-type male and female cell lines, as well as between the wild-type and abnormal cell lines nuclear size. However, no significant difference was observed between the aneuploid cell lines. It seems like the aneuploid cell lines are all smaller in size, despite the extra chromosomes in their nuclei. In order to observe the characteristic shape of the nuclei, the cell circularity, aspect ratio and roundness were analysed. All three of the categories' results for the nuclear shape were consistent, where significant differences were observed between the wild-type male and wild-type female cell lines, and between the wild-type male and DD0567 (XXX).

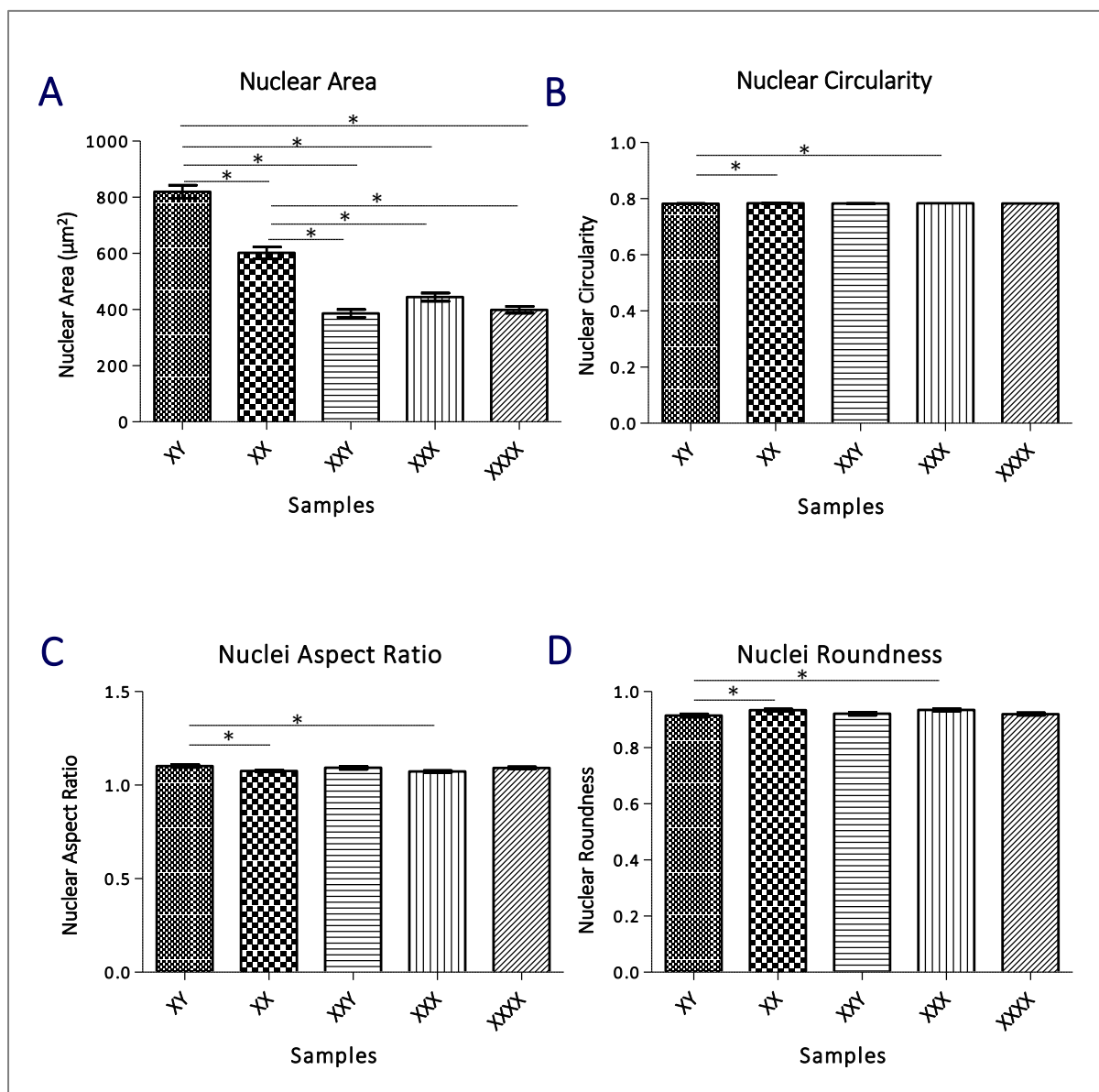


Figure 3.6 Cell Morphology Analysis

Images from fluorescence *in-situ* hybridisation were analysed with a macro in Fiji (Image J); up to 200 nuclei were analysed. Nuclear area (A), nuclear circularity (B), aspect ratio (C) and roundness (D) were all parameters that were measured; SEM is shown. The asterisk (*) represents significant difference from Tukey's Multiple Comparison Test.

3.5. Discussion

3.5.1. Model Cell Lines

Lymphoblastoid cell lines have demonstrated gene-density dependent (Boyle *et al.*, 2001; Tanabe *et al.*, 2002) intrinsic organisation patterns between different wild-type EBV-immortalised cells lines with differential chromatin arrangement dependent on their proliferative state (Ollion *et al.*, 2015). Unlike fibroblasts, lymphoblastoid cells have shown no modifications to chromosome territory arrangements in cell lines containing emerin or A-type lamin mutations (Meaburn *et al.*, 2005). In addition, lymphoblastoid cells are a good model for studying chromosome and gene positioning, as they are easy to obtain and grow. For our study, lymphoblastoid cells were derived from different donors, however the use of the same cell type makes them a good model for comparison between different karyotypes. Previously, different cell types have been used for comparison to make conclusions about the chromatin positioning alterations in aneuploidies (Cremer *et al.*, 2003). The same paper had demonstrated differential positioning in different cells types (Cremer *et al.*, 2003), therefore this comparison may not be the most suitable. Other studies have demonstrated, radial chromosome positioning to be conserved throughout species and cell types (Marshall *et al.*, 1996; Bridger and Bickmore, 1998; Kuroda *et al.*, 2004; Foster, Griffin and Bridger, 2012), however elusive differences do exist with differentiation (Wiblin *et al.*, 2005; Meshorer and Misteli, 2006; Szczerbal, Foster and Bridger, 2009; Fraser, Ferrai, *et al.*, 2015). Therefore, for our study it is essential to use cell types from the same origin when comparing karyotypic effect on chromatin positioning within nuclei.

3.5.2. *ALB* and *AMELX* Positioning in Lymphoblastoids

This chapter has explored the gene positioning of *ALB* and *AMELX*, located on chromosomes 4 and X, respectively. The study was assessing the impact, if any, of the aneuploidies for chromosome X on the gene positioning in lymphoblastoid cells. Despite the low somatic mutation rate of EBV-transformed lymphocytes (Mohyuddin *et al.*, 2004), we, firstly, had to assess whether the cells were truly aneuploid for chromosome X by performing 2-D FISH on the whole chromosome X. Our data were comparable to that of the Doctor's Laboratory, which had performed the G-banding analysis of our cell lines (Appendix I). The confirmed data from both the metaphase cells and nuclei allowed us to carry on with our study of the effects of aneuploidies on the cell nuclei and the gene loci positioning.

The 2D analysis assessed the positioning of gene loci and revealed that *ALB* had a peripheral position in the nuclei in all of the cell lines, regardless of the number of chromosome X's. There was a slight difference in the Gene/DAPI intensity in Shell 2 between FCWES02 (XX) and DD0567(XXX), and FCWES02 (XX) and DD1473 (XXXX), but generally all of the cell lines showed a peripheral positioning of *ALB*, which has been consistent with previous studies for chromosome 4 (Boyle *et al.*, 2001). One possible explanation for these differences in *ALB* positioning could be the difference in the gene transcription. *ALB* expression can be gender-specific (Li *et al.*, 2014) and sex hormones have been suggested as a possible cause for this preferential expression (Sugamori, Brennehan and Grant, 2011).

On the other hand, *AMELX* positioning showed more obvious differences between the cell lines. Wild-type cell lines MCWES01 (XY) and FCWES02 (XX), and aneuploid cell line DD0567 (XXX) positioned *AMELX* towards the nuclear periphery, whereas DD0710 (XXY) and DD1473 (XXXX) positioned *AMELX* more intermediately. No significant difference was observed between the wild-type cell lines, as expected, however all of the aneuploid cell lines showed a significant difference in the Gene/DAPI intensity at the periphery (Shell 1) with reference to the wild-type male, but not the female. This may be due to the larger amount of extra chromosome X's between the male and aneuploid cell lines in comparison to the female. This difference in gene positioning with X chromosome aneuploidies has

been observed in previous studies (Petrova *et al.*, 2007; Shete *et al.*, 2014), where their data have shown that X chromosome aneuploidy does not necessarily only affect the positioning of chromosome X, but also globally across different territories. In contrast to the data of Petrova *et al.*, 2007, where additional chromosome X's in the nuclei caused an increased attraction to the nuclear periphery, our data had shown a loss of association with the nuclear edge in DD0710 (XXY) and DD1473 (XXXX), but not in DD0567 (XXX).

For both of the genes, the data have been consistent with previous studies performed on the same chromosome territories on which *ALB* and *AMELX* genes are located with the conserved spatial organisation, despite the varied karyotypes (Bolzer *et al.*, 2005). Although a conserved radial positioning was identified in our study in all of the cells, independent of aneuploidies, subtle differences have been identified in the aneuploid cell lines in comparison to the wild-type. Consistent with our results, the artificial addition of chromosomes 7, 18 and 19 in the nuclei did not change the overall positioning of those chromosomes (Sengupta *et al.*, 2007), however shifts in the chromatin organisation have been described with the addition of aneuploidies (Cremer *et al.*, 2003; Wiblin *et al.*, 2005; Sengupta *et al.*, 2007; Shete *et al.*, 2014). This coupled with the positioning of chromosome 4 and X being very similar to previous work from our lab (Mehta, *et al.*, unpublished; Bikkul, *et al.*, Manuscript in Preparation) and other labs (Kozubek *et al.*, 2002; Cremer *et al.*, 2003), suggests that although the general organisation remains the same, additional chromosomes do cause changes to the genome organisation. Recent studies have highlighted that homologous chromosome are located far apart from each other (Heride *et al.*, 2010; Selvaraj *et al.*, 2013; Fraser, Williamson, *et al.*, 2015); it can be speculated that the nuclear space may be more adaptable to additional chromosomes and therefore, maintain the radial distribution of chromosome territories in the different karyotypes.

Aneuploid nuclei have often displayed a very significant change in their gene expression profiling (Upender *et al.*, 2004; Grade *et al.*, 2006), especially an increase in transcripts for the specific chromosome that was gained (Upender *et al.*, 2004) and also in the protein expression levels

(Habermann *et al.*, 2007; Torres, Williams and Amon, 2008). How the aneuploidies in the cell lines from our study affect the overall gene expression in the cell is unknown. Further investigation is required; however, a good example would be to combine the work of Sengupta *et al.* and Habermann, *et al.*, to model chromosome aneuploidies transfer and then measure the protein expression levels (Habermann *et al.*, 2007; Sengupta *et al.*, 2007). The transcriptional changes observed in aneuploidies (Uppender *et al.*, 2004; Grade *et al.*, 2006) and work performed in the prognostic potential of chromosome positioning in cancer (Leshner *et al.*, 2016; Meaburn *et al.*, 2016) highlights the significance that chromatin modifications could potentially have on the normal functioning of the nucleus. Further investigation is required to study the implication of aneuploidies on chromatin organisation and thereby, transcription.

3.5.3. Cell Morphology

Cell morphology analyses were performed to study the possible differences between the wild-type and aneuploid lymphoblastoid cell lines. From our analyses, we have observed a significantly reduced cell area in the aneuploid cell nuclei in comparison to the wild-type lymphoblastoid cell lines. A potential factor that could impact the nuclear size is the source of the material. The aneuploid cell lines were from donor with genetic disorders; patients living with disorders caused from aneuploidies often experience health problems, including increased immunological disorders with increased X chromosome dose (Keller *et al.*, 2013; Liu *et al.*, 2016; Schatorjé *et al.*, 2016); these included Klinefelter's and Turner's Syndromes (Kurosawa, Kimura and Sagawa, 1991; Jørgensen *et al.*, 2010; Aksglaede *et al.*, 2013). Additionally, reports have shown a possible link between aneuploidies and immunodeficiency (Schwanitz and Zerres, 1987; Kurtyka *et al.*, 1988; Ram and Chinen, 2011; Jiang *et al.*, 2013; Schatorjé *et al.*, 2016), however a precise mechanism is yet to be found (Keller *et al.*, 2013; Schatorjé *et al.*, 2016).

In addition, the inactive and active chromosome X territories have been reported to be different in shape with the inactive X (X_i) observed to be more compact (Falk *et al.*, 2002). This is due to the *XIST*

transcript that inactivates the X chromosome and causes heterochromatin formation, the resulting chromosome is then known as a Barr body (Brown *et al.*, 1991). We propose that with the additional chromosomes that require X chromosome inactivation (XCI), more heterochromatin is formed via epigenetic modification creating a more compact genome and therefore, suggesting a possible explanation to the smaller aneuploid nuclei we observed. The increased production of *XIST* has been observed in X chromosome aneuploidies (Ji *et al.*, 2015) and heterochromatin spreading has been reported previously (Talbert and Henikoff, 2006; Honda *et al.*, 2010; Wang *et al.*, 2014). For this reason, we propose the possibility of heterochromatin spreading from the aneuploid X chromosomes to the rest of the genome creating more compact nuclei overall.

With regards to the data from the cell morphology analysis, we found a significant difference between the wild-type male and female cell lines and between the wild-type male and trisomy X cell lines. Cell morphology has often been used as an indicator for prognosis (Mitmaker, Begin and Gordon, 1991) and for blastomere selection (Agerholm *et al.*, 2008). Despite this, no conclusive evidence has been given whether the cell's circularity is a direct indicator of aneuploidy. In line with our findings, previous studies had observed no correlation of nuclear size or shape to aneuploidies (Cremer *et al.*, 2003; Agerholm *et al.*, 2008). Further studies into this topic are required for conclusive evidence.

Chapter IV: Correlation of Nuclear Lamins with Chromosomal Aneuploidies

4.1. Introduction

4.1.1. Nuclear Lamins

The aberrant expression and localisation of nuclear lamins is commonly featured in different cancers (Broers *et al.*, 1993; Moss *et al.*, 1999; Venables *et al.*, 2001; Willis *et al.*, 2008; Capo-chichi *et al.*, 2011; Wazir *et al.*, 2013) and studies have suggested abnormal expression to be associated with poorer patient outcomes caused from increased metastasis and cell proliferation (Venables *et al.*, 2001; Davidson *et al.*, 2014). In addition, lamin disruption can also cause chromatin mislocalisation and changes in morphology of interphase nuclei (Malhas *et al.*, 2007; Meaburn *et al.*, 2007; Mewborn *et al.*, 2010; Mehta *et al.*, 2011; Solovei *et al.*, 2013; Ranade *et al.*, 2017), highlighting the role of lamin proteins in chromatin organisation and nuclear morphology.

Lamins have been associated with the conservation of genomic stability (Vergnes *et al.*, 2004; Kuga *et al.*, 2014; Ranade *et al.*, 2017). Although the complete knockout of B-type lamins causes lethality, the knockdown did permit aneuploidies in mice and cancerous cells (Vergnes *et al.*, 2004; Ranade *et al.*, 2017), but not in keratinocytes (Yang *et al.*, 2011). However, Ranade, *et al.*, 2017 had demonstrated that in colorectal adenocarcinoma cells lamin A/C and B2 knockdown can cause transcriptional deregulation of specific chromosomes and lamin B2 knockdown to induce the formation of aneuploidies with changes in the chromosome territory positioning (Ranade *et al.*, 2017). These studies suggest a link between B-type lamin depletion and genomic instability.

4.2. Aims

The aim of this study was to compare the lamin gene and protein expression levels between karyotypically normal and aneuploid cell lines. We were interested in assessing the distribution of the different staining patterns observed in nuclei. Our study was designed to quantify the total protein expression levels of each lamin protein via Western blotting and gene expression levels via RT-qPCR.

4.3. Methods and Materials

4.3.1. Immunofluorescence

Lymphoblastoid cells were grown in RPMI-1640 medium (Sigma-Aldrich, UK) supplemented with 10% Foetal Calf Serum (FCS) (Sigma-Aldrich, UK) and 5% L-Glutamine (Sigma-Aldrich, UK) in a 5% CO₂ atmosphere at 37°C. These cells were then centrifuged at 1500 x *g* and re-suspended in ice-cold methanol: acetone (1:1), and then dropped onto poly-L-lysine slides (Sigma-Aldrich, UK). The slides were washed three times for five minutes each time with agitation in 1xPBS and then the primary antibody was applied with 1% BSA in PBS (v/v). These slides were incubated in a humidified chamber for thirty minutes at 37°C or at room temperature for one hour. After this incubation, the slides were washed another three times in PBS with agitation for five minutes each time. The secondary antibody was applied diluted in 1% BSA in PBS and left for thirty minutes at 37°C or at room temperature for one hour in a humidified chamber. The slides were washed another three times on the shaker in PBS and finally washed in distilled water. A drop of VECTASHIELD Antifade Mounting Medium with DAPI (Vectorlabs, USA) was applied the slide and a 22 x 40 mm coverslip was placed on top and sealed.

For the mouse lamin A antibody (Abcam, UK) a dilution of 1:100 was used, for rabbit lamin C (ThermoFisher, UK) – 1:200, for rabbit Lamin B1 – 1:500 and mouse Lamin B2 – 1:400. For the secondary antibodies a donkey anti-rabbit labelled with Cy3 (Merck MiliPore, UK) was used at a 1:500 dilution and goat anti-mouse labelled with FITC (Abcam, UK) – 1:1000.

Ovarian cancer cells from the SKOV-3 cell line were stained for the A-type lamins as a positive control to confirm that the lamin A antibody was viable. The cells were grown by Aakila Sammy (Brunel University London) in the same media and conditions as the lymphoblastoid cells, however as the cells were adherent, the cells were first grown on coverslips and then subjected to indirect immunofluorescence.

Slides were analysed using the x100 lens with emersion oil on the Olympus BX41 and Leica DM4000 fluorescent microscopes. The slides were scored for different distributions for each cell line and each protein stained. When a specific pattern of staining was observed, cells were scored until at least 200 of them displayed that specific pattern. All of the types of patterns observed were then converted to percentages for analysis. This was performed for a minimum of three times for each cell line.

4.3.2. Western Blotting

In order to quantify the amount of lamin proteins in the different cell lines, two million viable cells were counted using a manual haemocytometer (LabTech, UK). The cells were centrifuged at 500 x *g*, and the pellet washed two times with ice-cold PBS. The cell pellets were then re-suspended in 100µl of 3x Sample Buffer (SB) (100mM Tris-HCL (pH6.8), 4% SDS, 0.2% bromophenol blue, 20% glycerol, 0.2 % β-mercaptoethanol) via vortexing after being boiled at 100°C for at least fifteen minutes. 10µl of this solution, equivalent to 2 X 10⁵ cells, was loaded into each well of 10% MiniPROTEAN® TGXTM precast polyacrylamide gels (Bio-Rad, UK) with TGS Running Buffer (BioRad, UK). Gels were run, at a constant voltage of 80-150V until the Precision Plus Protein Dual Colour Standard marker (BioRad, UK) exited the gel. The proteins in the gel were then transferred onto nitrocellulose membranes (Amersham Biosciences, UK) in transfer buffer (50 mM Tris, 380 mM glycine, 20% methanol (v/v)) on ice for one hour at 400mA. To check if the transfer was successful Ponceau S (Sigma-Aldrich, UK) staining was used. After the transfer, the membrane was washed three times for five minutes each on a shaker in Blot Rinse Buffer (BRB; 0.01M Tris, 0.15M NaCl, 0.001M of EDTA, 0.1% Tween 20, pH7.4). The nitrocellulose membrane was then blocked with 4% (w/v) dried skimmed milk (Marvel) in the BRB for at least one hour. After the blocking, the membrane was washed another three times with the BRB. The primary antibodies were diluted in 1% (w/v) dried skimmed milk in BRB and then placed onto the membrane overnight at 4°C on a shaker. The following morning the membrane was washed again in BRB another three times and the secondary antibody with 1% (w/v) dried skimmed milk in BRB was added for one hour at room temperature on a shaker.

The primary antibodies from the immunofluorescence study were used; anti-lamin A was used at a dilution of 1:500, anti-lamin C – 1:100, anti-lamin B1 – 1:1000, anti-lamin B2 – 1:1000. Additionally, mouse and rabbit α-Tubulin antibodies (Abcam, UK) were used as controls in each membrane at a 1:7000 dilution. Secondary antibodies goat anti-mouse IRDye 680RD (LI-COR, UK) and donkey anti-rabbit IRDye 800CW (LI-COR, UK) were used at a 1:5000 dilution. The membranes were then visualised

using the Odyssey Imaging System (LI-COR, UK); bands in the 680RD range were visualised as red and in 800CW – as green.

4.3.3. RNA Extraction and cDNA Synthesis

The cells were grown in the conditions described in Chapter II (Section 2.3.1.). Invitrogen™ RNAlater™ Stabilization Solution was used to re-suspend the cells that were pelleted following cell culture, the solution was then incubated at 4°C overnight and then transferred to -80°C for long-term storage.

The re-suspended cells were first thawed on ice and the RNA extraction was performed using the Maxwell® RSC simplyRNA Cells Kit (Promega) and Maxwell® RSC Instrument (Promega). The solution of cells was centrifuged at 300 x *g* for 5min, followed by a wash in ice-cold 1XPBS and then centrifuged at 300 x *g* for another 5min. The supernatant was removed and 200µl of 1-Thioglycerol/Homogenization Solution was added, and the cells were vortexed until the pellet dispersed. Next, 200µl of Lysis Buffer was added, followed by vortexing and the 400µl of lysate was transferred to the first well on the Maxwell RSC Cartridge. DNase I solution of 5µl was added to the fourth well, a Plunger was placed into the eighth well and 50µl of nuclease-free water was added to the elution tubes. The cartridges were then loaded onto the instrument and RNA was automatically extracted. For quantification and qualification of RNA, the QIAxpert (Qiagen) was used. To make sure the RNA was of high quality- RNA Integrity Number, RIN, value of at least 8- the RNA samples were run on the Agilent TapeStation Bioanalyser, as described in Chapter II (Section 2.3.5).

For cDNA synthesis, the High-Capacity cDNA Reverse Transcription Kit (ThermoFisher Scientific) was used with 200ng of RNA. First, a reverse transcription (RT) master mix (Table 5.1) was made with RNase Inhibitor on ice. Next, 10µl of the 2 X RT master mix was pipetted into each well of a 96-well reaction plate or individual tube with 200ng of RNA sample in a maximum volume of 10µl; if necessary the volume was supplemented with nuclease-free water. The solution was mixed and centrifuged to eliminate any air bubbles and then loaded onto a thermocycler using the conditions described in Table 5.2.

Table 5.1. cDNA Synthesis Kit Components and Volumes

The High-Capacity cDNA Reverse Transcription Kit components and volumes are shown below.

Component	Volume (μ l)
10 X RT Buffer	2.0
25 X dNTP Mix (100mM)	0.8
10 X RT Random Primers	2.0
MultiScribe™ Reverse Transcriptase	1.0
RNase Inhibitor	1.0
Nuclease-free Water	3.2

Table 5.2. cDNA Synthesis Thermocycling Conditions

The High-Capacity cDNA Reverse Transcription Kit thermocycling conditions are shown below.

	Step 1	Step 2	Step 3	Step 4
Temperature ($^{\circ}$ C)	25	37	85	4
Time (min)	10	120	5	Hold

4.3.4. Quantitative Reverse Transcription PCR (RT-qPCR)

Quantitative reverse Transcription PCR (RT-qPCR) was performed for lamins A, C, B1 and B2 to measure the levels of gene expression in diploid cell lines FCWES02 and MCWES01, and in aneuploid cell lines DD0567, DD0710 and DD1473. The gene expression was measured relative to the ratio of *GAPDH* expression via duplex assays for each reaction; all of the work was performed in triplicate.

For lamins A and C gene expression analysis, the protocol was established by (Rodriguez *et al.*, 2009). The sequences are shown in Table 5.3. The primers were custom-ordered from IDT, whereas the probes were custom-ordered as Taqman® MGBNFQ from ThermoFisher. For the RT-qPCR reaction mix, a total of 20µl was used per well; 300nM forward primer, 900nM reverse primer, and 200nM of the MGB probe were used. The thermocycling conditions are shown in Table 5.4. The Stratagene RT-qPCR machine was used (Agilent Technologies). TaqMan® Gene Expression Master Mix was used at x2 concentration.

Table 5.3. Lamins A and C Primer and Probe Sequences

The primer and probe sequences from Rodriguez, *et al.*, 2009 are shown below. Both probes were labelled with FAM.

	Lamin A	Lamin C
Forward Primer	5'-TCTTCTGCCTCCAGTGTCACG-3'	5'-CAACTCCACTGGGAAGAAGTG-3'
Reverse Primer	5'-AGTTCTGGGGGCTCTGGGT-3'	5'-CGGCGGCTACCACTCAC-3'
Probe	5'-ACTCGCAGCTACCG-3'	5'-ATGCGCAAGCTGGTG-3'

Table 5.4. Lamins A and C RT-qPCR Thermocycling Conditions

The RT-qPCR thermocycling conditions for the gene expression analysis of lamins A and C. The conditions were established by Rodriguez, *et al.*, 2009.

	Step 1	Step 2	Step 3	Step 4
Temperature (°C)	50	95	95	60
Time (min)	2	10	0.25	0.75
No. of Cycles	1	1	50	

For the gene expression analysis of Lamin B1 (*LMNB1*) and B2 (*LMNB2*), as well as the reference gene, *GAPDH*, custom-made mixes of primers and probes were ordered from ThermoFisher Scientific. For *GAPDH* on VIC, the Assay ID was Hs02758991_g1, for *LMNB1* on FAM – Hs01059210_m1 and *LMNB2* on FAM - Hs00383326_m1. Each of the primer and probe mixes from ThermoFisher Scientific contained 900nM of primers and 250nM of probe; 1µl was used per reaction. TaqMan® Gene Expression Master Mix was used x2. Thermocycling conditions for the ready-made assays are shown in Table 5.5.

Table 5.5. Lamins B1 and B2 RT-qPCR Thermocycling Conditions

The RT-qPCR thermocycling conditions for the gene expression analysis of lamins B1 and B2.

	Step 1	Step 2	Step 3	Step 4
Temperature (°C)	50	95	95	60
Time (min)	2	10	0.25	1
No. of Cycles	1	1	40	

4.4. Results

4.4.1. A-Type Lamins

4.4.1.1. Indirect Immunofluorescence

Indirect immunofluorescence was performed for the whole panel of lymphoblastoid cell lines. As a positive control the lamin A and lamin C antibodies were used in an ovarian cell line SKOV-3 (Figure 4.1) to confirm that the antibodies were viable. For A-type lamins, absence of lamin A staining in the cell nuclei of all of the cell lines tested was observed (Figure 4.2). Both lamins A and C positively stained the SKOV-3 cells and confirmed that the lamin A and lamin C antibodies were working in our hands. The SKOV-3 nuclei showed peripheral staining for both A-type lamins with large internal foci within the nucleoli. As no staining of lamin A was observed in any of the lymphoblastoid cell lines, we did not quantify this further. On the other hand, for lamin C staining in the lymphoblastoid cells lines, internal foci within the nuclei were observed, as well as negative staining (Figure 4.2). The lamin C foci tended to be randomly dispersed across the nuclei, but occasionally clustered towards the nuclear periphery. Such examples of the internal foci are shown in Figure 4.3.

In order to quantify the different lamin C patterns observed from the immunofluorescence, a pattern analysis of staining within the nuclei was performed for lamin C. The results had shown that the majority of the cell lines had stained for a pattern of internal foci within the nuclei with the wild-type female cell line, FCWES01 expressing the highest amount, 96%. In contrast, the aneuploid cell line DD0710 expressed the lowest amount at 78% (Figure 4.4). The only other category of staining detected for lamin C staining analysis was negative staining.

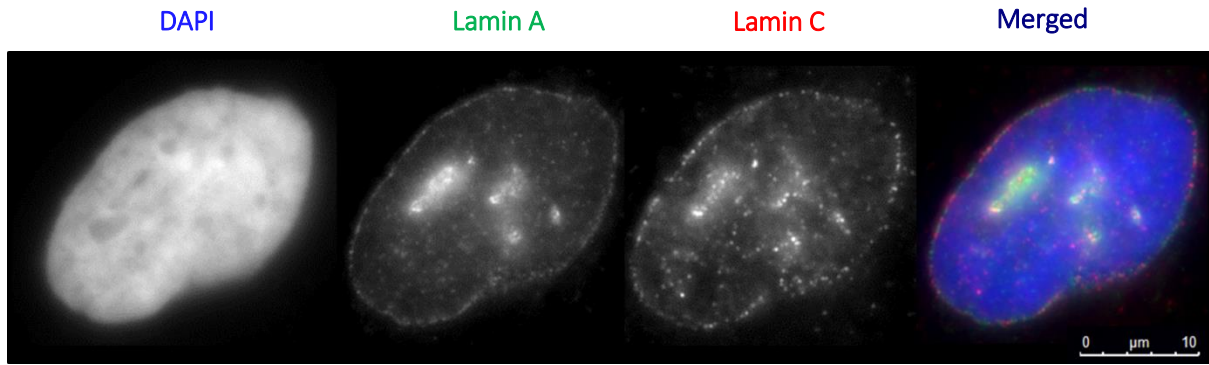


Figure 4.1. Lamin A and C Staining in SKOV-3 Cells

Staining for the nucleus in the DAPI channel, Lamin A in the FITC channel and Lamin C in the Cy3 channel are shown in grayscale and then merged together with DAPI in blue, Lamin A in green and Lamin C in red. The scale bar is shown.

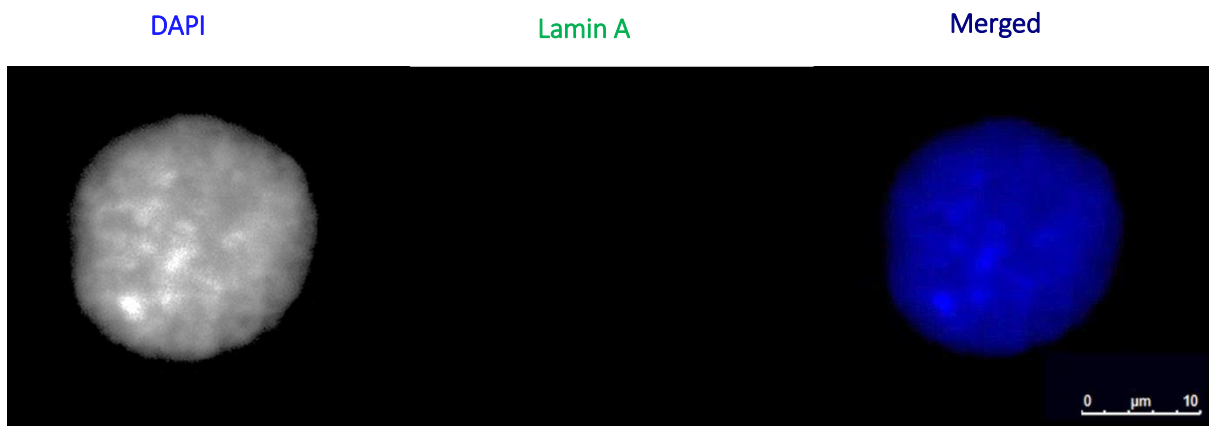


Figure 4.2. Lamin A Staining in Lymphoblastoid Cells

Staining for the nucleus in the DAPI channel and Lamin A in the FITC channel are shown in grayscale and then merged together with DAPI in blue and Lamin A in green. The scale bar is shown.

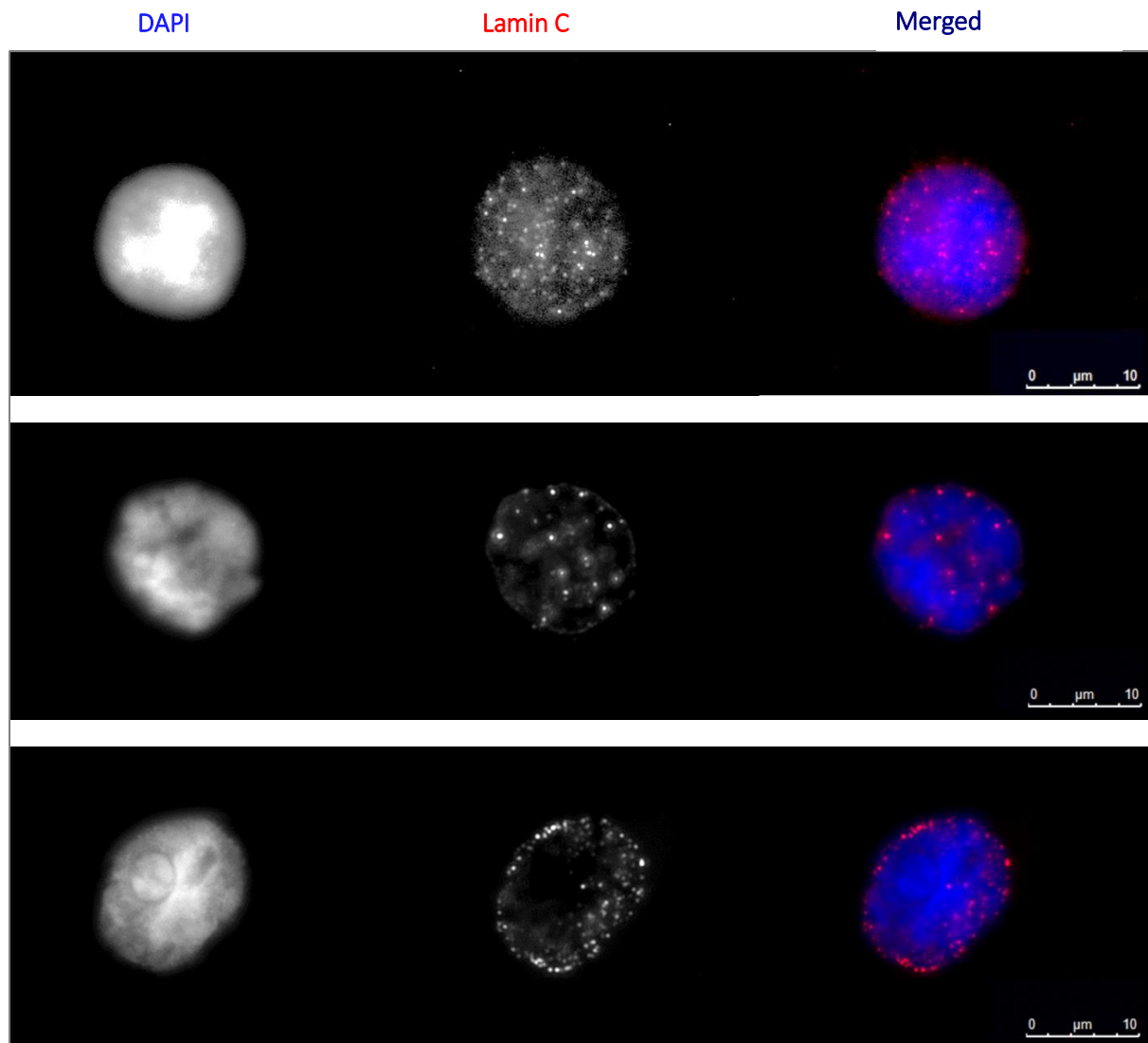


Figure 4.3. Lamin C Staining in Lymphoblastoid Cells

Staining for the nucleus in the DAPI channel and Lamin C in the Cy3 channel are shown in grayscale and then merged together with DAPI in blue and Lamin C in red. The scale bar is shown. Lamin C staining showed internal foci dispersed throughout the nuclei. Each of these staining patterns shown above were identified and classified as internal foci.

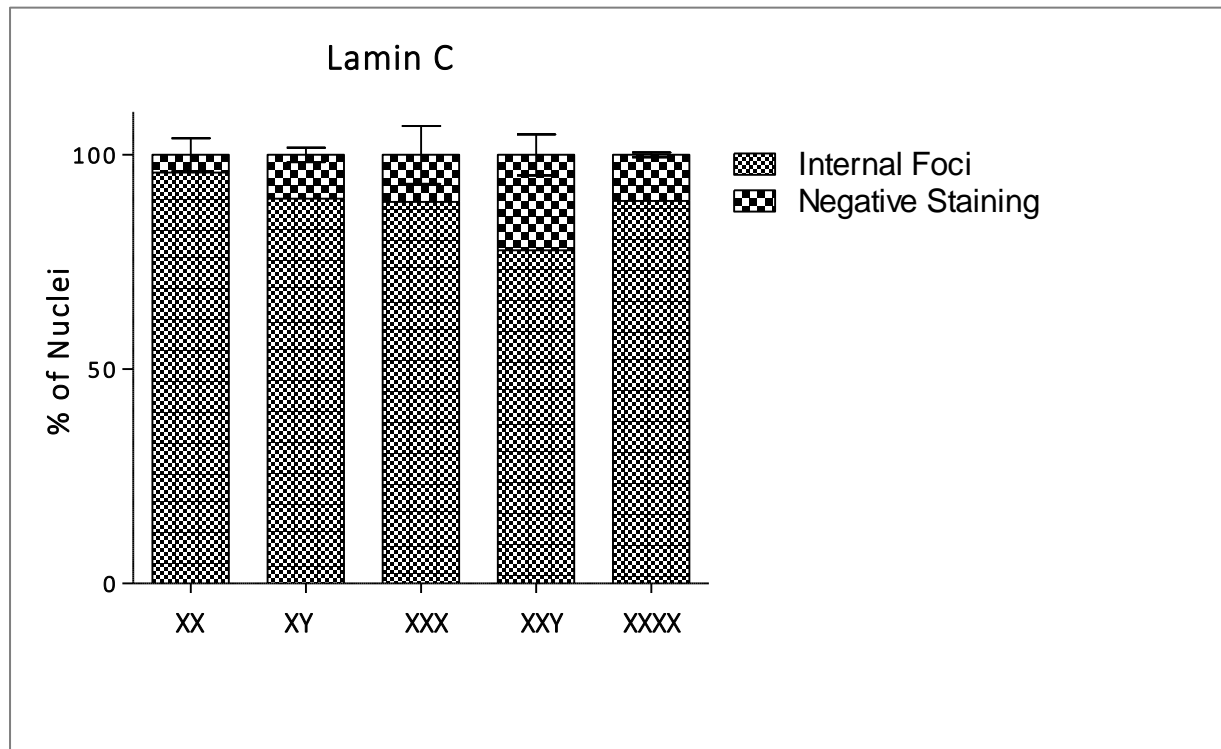


Figure 4.4. Lamin C Staining Pattern Analysis

The cell nuclei were stained for Lamin C and their staining patterns analysed. Two staining patterns for Lamin C were identified, negative staining and internal foci. The percentage of nuclei for each staining pattern type is shown. Cell lines FCWES02, MCWES01, DD0567, DD0710 and DD1473 with karyotypes XX, XY, XXX, XXY and XXXX, respectively, were analysed. Standard error of mean for the internal foci is shown.

4.4.1.2. Western Blotting

Western Blotting was performed for all of the lymphoblastoid cell lines, FCWES01, FCWES02, MCWES01, MCWES02, DD0567, DD0710, DD1473 and for the control primary human dermal fibroblast cell line NB1, for A-type lamins, A and C separately, as well as β -tubulin as the reference gene. Their expression levels were monitored and compared alongside NB1 cells that were used as a positive control.

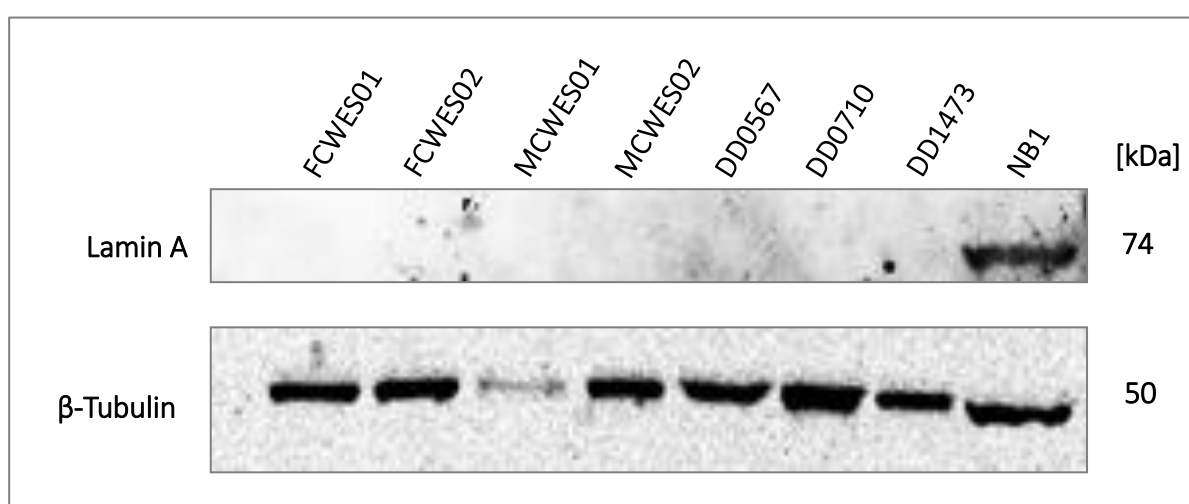


Figure 4.5. Lamin A and Beta-Tubulin Western Blot

Lymphoblastoid cell lines FCWES01, FCWES02, MCWES01, MCWES02, DD0567, DD0710, DD1473 and fibroblast NB1s were analysed. All of them were negative for Lamin A, except the positive control NB1 for Lamin A that was observed at 74kDa. The positive control (β -Tubulin) was observed at approximately 50kDa in the 800CW channel.

No lamin A was observed in any of the lymphoblastoid cell lines by Western blotting; the NB1 cell were positive for lamin A at 74kDa and all of the cell lines expressed the reference gene, β -tubulin at 50kDa (Figure 4.5). A minimum of three independent Western blots were performed.

Similarly, western blotting was performed for all of the lymphoblastoid cell lines for lamin C and β -tubulin. Their expression levels were monitored and compared alongside NB1 cells that were used as the positive control. Similar to the lamin A results (Figure 4.5), the lymphoblastoid cell lines did not express lamin C, unlike the NB1 cells used as the positive control (Figure 4.6). The lamin C protein showed at approximately 65kDa. All of the cell lines expressed the reference gene, β -tubulin in the region of 50kDa. A minimum of three independent western blots were performed.

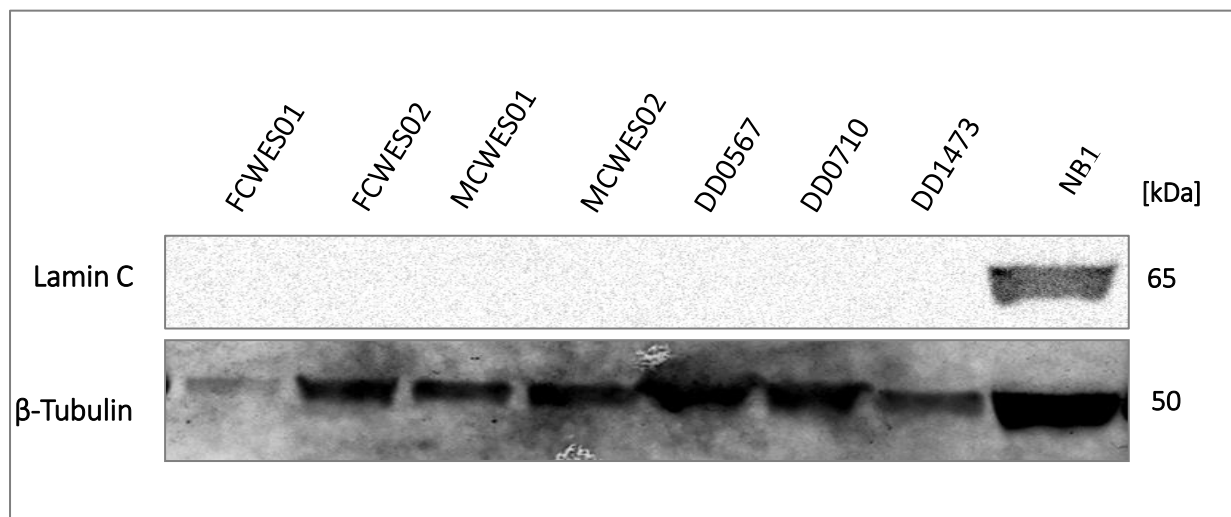


Figure 4.6. Lamin A and Beta-Tubulin Western Blot

Lymphoblastoid cell lines FCWES01, FCWES02, MCWES01, MCWES02, DD0567, DD0710, DD1473 and fibroblast NB1s were analysed. All of them were negative for Lamin A, except the positive control NB1 for Lamin A that was observed at 65kDa. The positive control (β -Tubulin) was observed at approximately 50kDa in the 800CW channel.

4.4.1.3. Reverse Transcription PCR

For lamin A, an extremely significant difference in the gene expression was observed (Figure 4.7A; $p < 0.0001$). The wild-type female cell line, FCWES02, showed extremely significant difference to the male wild-type cell line, MCWES01 and very significant difference to the aneuploid cell lines, DD0567 and DD0710. MCWES01 had also shown extremely significant difference to all of the aneuploid cell lines. Additionally, aneuploid cell line, DD1473, had shown very significant difference to the remaining aneuploid cell lines, DD0567 and DD0710.

For lamin C, an extremely significant difference in the gene expression was observed (Figure 4.7B; $p < 0.0001$). The wild-type female cell line, FCWES02, showed extremely significant difference to the male wild-type cell line, MCWES01 and very significant difference to the aneuploid cell line, DD1473. In addition, the male wild-type cell line, MCWES01 had demonstrated extremely significant difference to all of the aneuploid cell lines. Between the aneuploid cell lines, DD1473 displayed extremely and very significant difference to both DD0567 and DD0710.

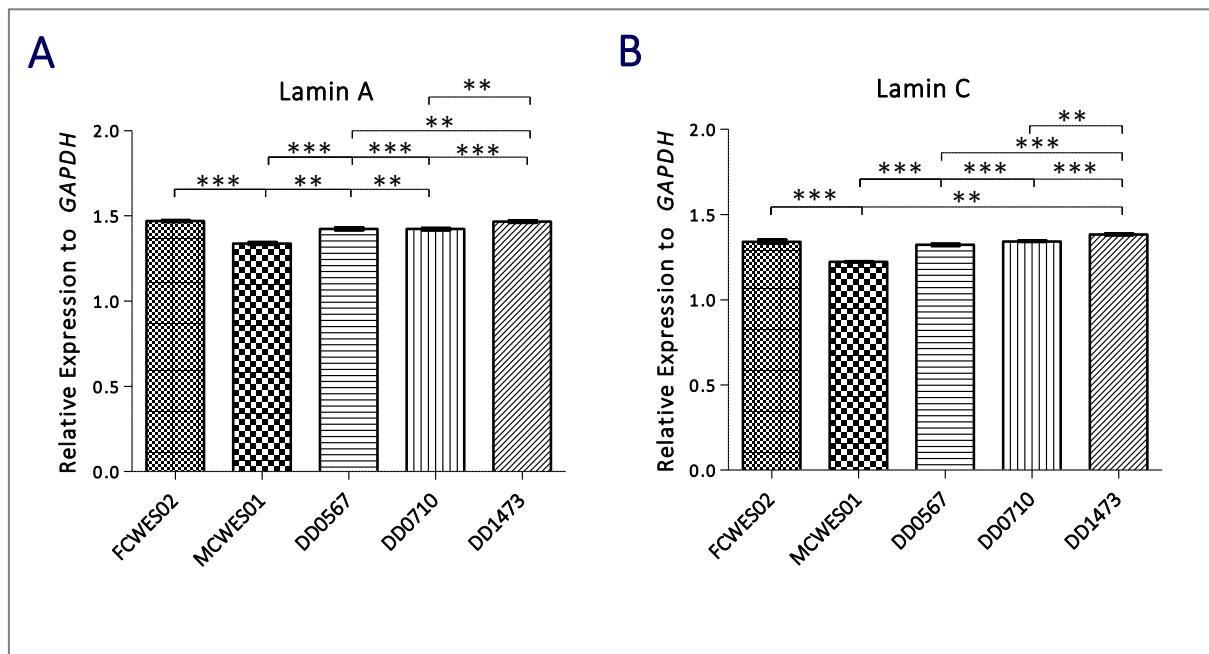


Figure 4.7. A-Type Lamin Gene Expression in Lymphoblastoid Cell Lines

A-type lamin gene expression was measured via RT-qPCR in a duplex reaction with *GAPDH* as the reference gene. The relative gene expression to *GAPDH* were plotted for each cell line and a one-way analysis of variance (ANOVA) and Tukey's Multiple Comparison Test was performed between each sample; the significant differences between samples are shown in asterisks. The gene expression of lamin A (A) and lamin C (B) are shown. Wild-type lymphoblastoid female and male cells lines, FCWES02 and MCWES01 are shown, respectively, alongside aneuploid lymphoblastoid cell lines, DD0567, DD0710 and DD1473. * $p < 0.05$, ** $p < 0.01$, *** $p < 0.001$.

4.4.2. B-Type Lamins

4.4.2.1. Indirect Immunofluorescence

For B-type lamins, lamin B1 and B2 were stained via immunofluorescence and the distribution analysis was performed for all of the cell lines. The results demonstrated that most of the nuclei, regardless of the cell line, expressed lamin B1 protein staining as a rim around individual nuclei. An example of this is shown in Figure 4.8. In addition, the wild-type female cell line, FCWES02 and the aneuploid cell line, DD1473 expressed the highest amounts of rim staining around the nuclei, both close to 99%. In contrast, the wild-type male, MCWES01 expressed the lowest amount of lamin B1 rim staining at 80% (Figure 4.9). Another type of staining pattern observed in the lymphoblastoid cells for the intranuclear staining, the lamin B1 staining was also observed within the nuclei (Figure 4.8). The highest amount was observed in the wild-type male cell line, MCWES01 with nearly 20%, whereas the lowest was observed in the aneuploid cell line DD1473 with less than 1% intranuclear staining. A one-way analysis of variance was carried out for all of the cell lines and the lamin B1 staining distribution that was observed; $p < 0.0001$ demonstrating extreme statistical significance between the samples for both rim and intranuclear staining in the cell lines.

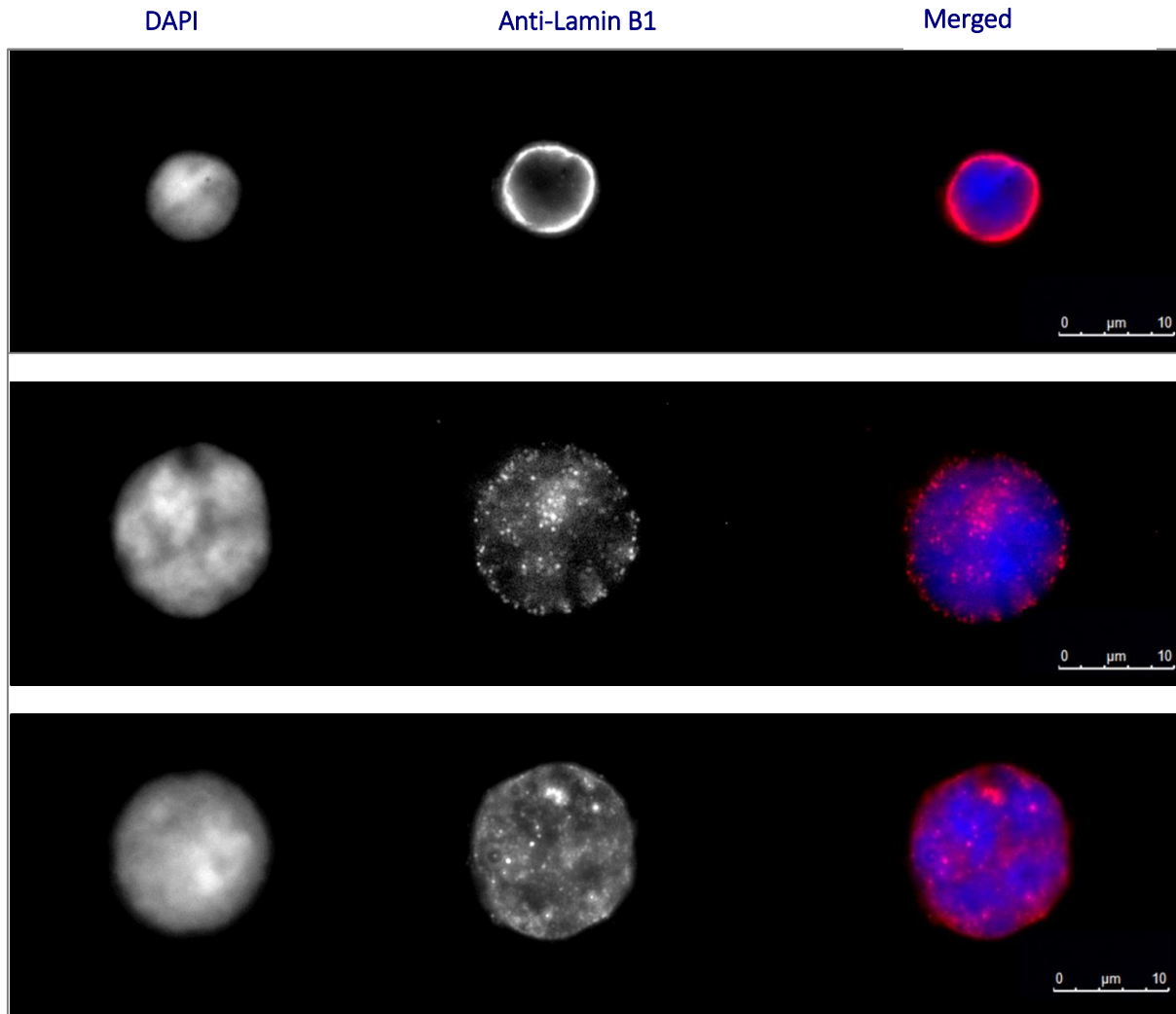


Figure 4.8. Lamin B1 Rim and Intranuclear Staining in Lymphoblastoid Cells

Staining for the nucleus in the DAPI channel and Lamin B1 in the Cy3 channel are shown in grayscale and then merged together with DAPI in blue and Lamin B1 in red. The scale bar is shown. Lamin B1 staining showed as a rim in A and as intranuclear staining in the nuclei with either dots dispersed throughout the nuclei with a homogenous staining in B and C.

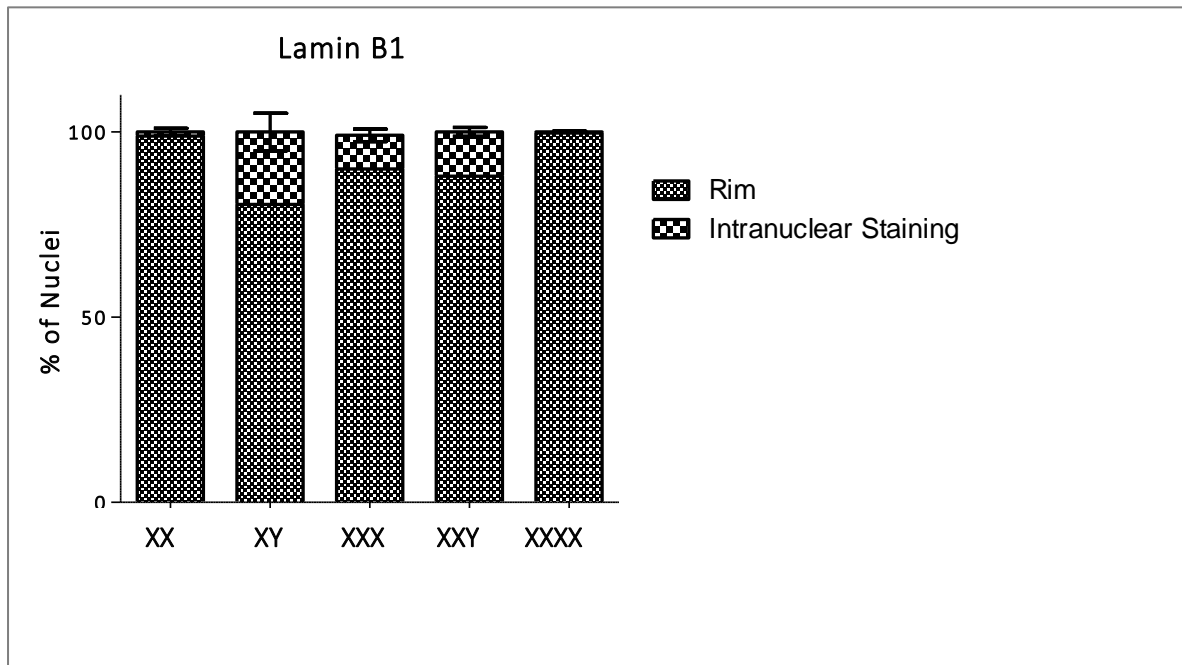


Figure 4.9. Lamin B1 Staining Pattern Analysis

Indirect immunofluorescence was performed for Lamin B1 in the whole panel of lymphoblastoid cell lines and their distribution was analysed. Two staining patterns for Lamin B1 were identified as a rim around the periphery of the nucleus and intranuclear staining referring to dispersed dots and homogenous staining of the nuclei. The percentage of nuclei for each staining pattern type is shown with standard error of mean error bars. Cell lines FCWES02, MCWES01, DD0567, DD0710 and DD1473 with karyotypes XX, XY, XXX, XXY and XXXX, respectively, were analysed. A one-way analysis of variance was calculated for the rim and intranuclear staining patterns across the different cell lines; $p < 0.0001$ signifying extreme statistical significance for the rim staining and intranuclear staining.

For lamin B2 staining, the results had demonstrated that most of the samples, except DD0567, expressed lamin B2 protein staining as a rim around the nuclei, as previously observed for the lamin B1 staining. Examples of such staining patterns are shown in Figure 4.10. A percentage of the cells demonstrated intranuclear staining, similar to the intranuclear staining observed in lamin B1 (Figure 4.11).

To quantify the lamin B2 staining results, a pattern analysis within the nuclei was performed. The results displayed that all of the cell lines had mostly stained for a rim around the periphery of the nucleus with the aneuploid cell line, DD1473 expressing the highest amount, 89%, whereas the aneuploid cell line, DD0567, the lowest amount of 8% (Figure 4.12). In addition, the lamin B2 staining in the nuclei was also observed within the nuclei, as per Figure 4.11. The highest amount was observed in the aneuploid line, DD0567 with nearly 92%, whereas the lowest was observed in the aneuploid cell line DD1473 with 11% intranuclear staining. A one-way analysis of variance was carried out for all of the cell lines and the lamin B2 staining distribution that was observed; $p < 0.0001$ demonstrating extreme statistical significance between the samples for both rim and intranuclear staining in the cell lines.

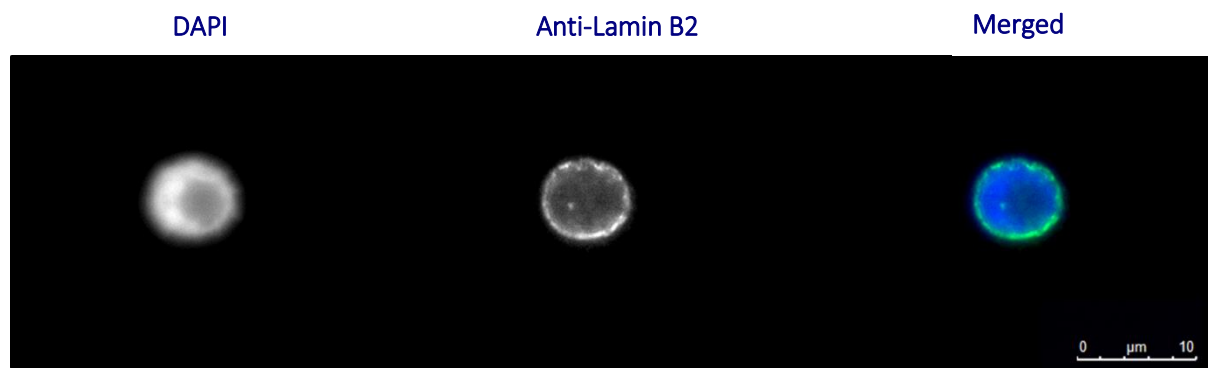


Figure 4.10. Lamin B2 Rim Staining in Lymphoblastoid Cells

Staining for the nucleus in the DAPI channel and Lamin B2 in the FITC channel are shown in grayscale and then merged together with DAPI in blue and Lamin B2 in green. The scale bar is shown. Lamin B2 staining showed rim staining around the periphery of the nuclei. Each of these staining patterns shown above were identified and classified as rim staining.

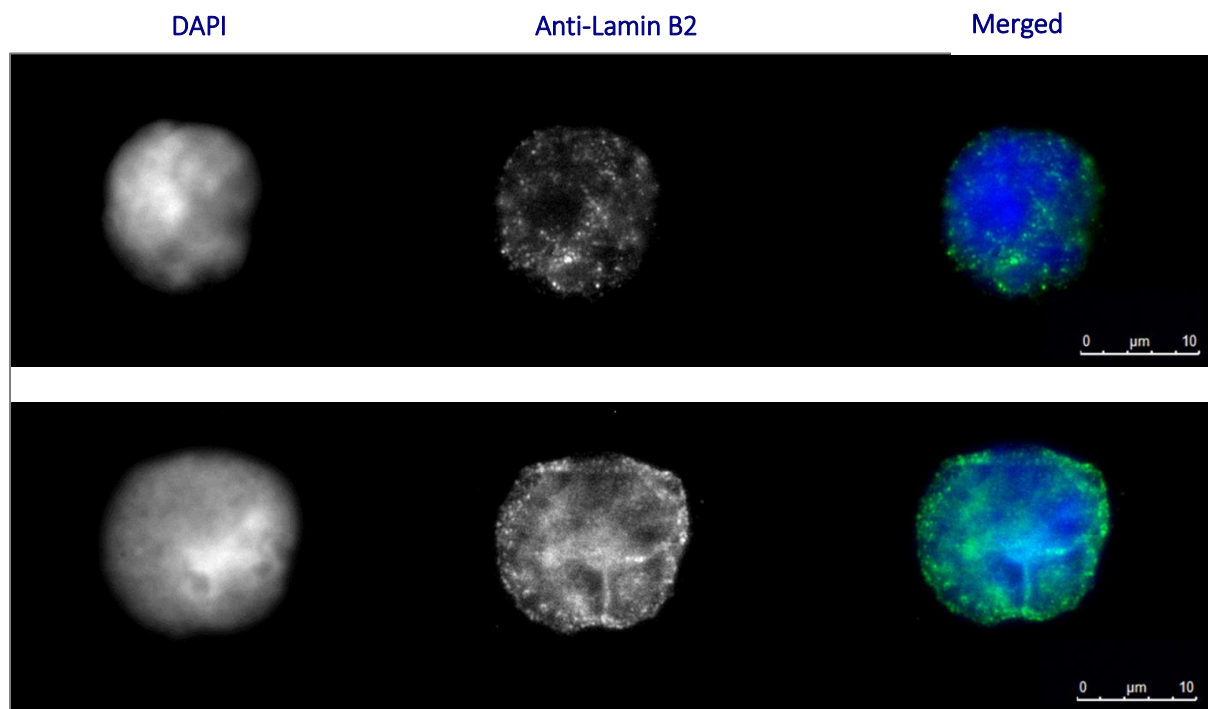


Figure 4.11. Lamin B2 Intranuclear Staining in Lymphoblastoid Cells

Staining for the nucleus in the DAPI channel and Lamin B2 in the FITC channel are shown in grayscale and then merged together with DAPI in blue and Lamin B2 in green. The scale bar is shown. Lamin B2 staining showed an intranuclear staining in the nuclei with either dots dispersed throughout the nuclei with a homogenous staining. Each of these staining patterns shown above were identified and classified as intranuclear staining.

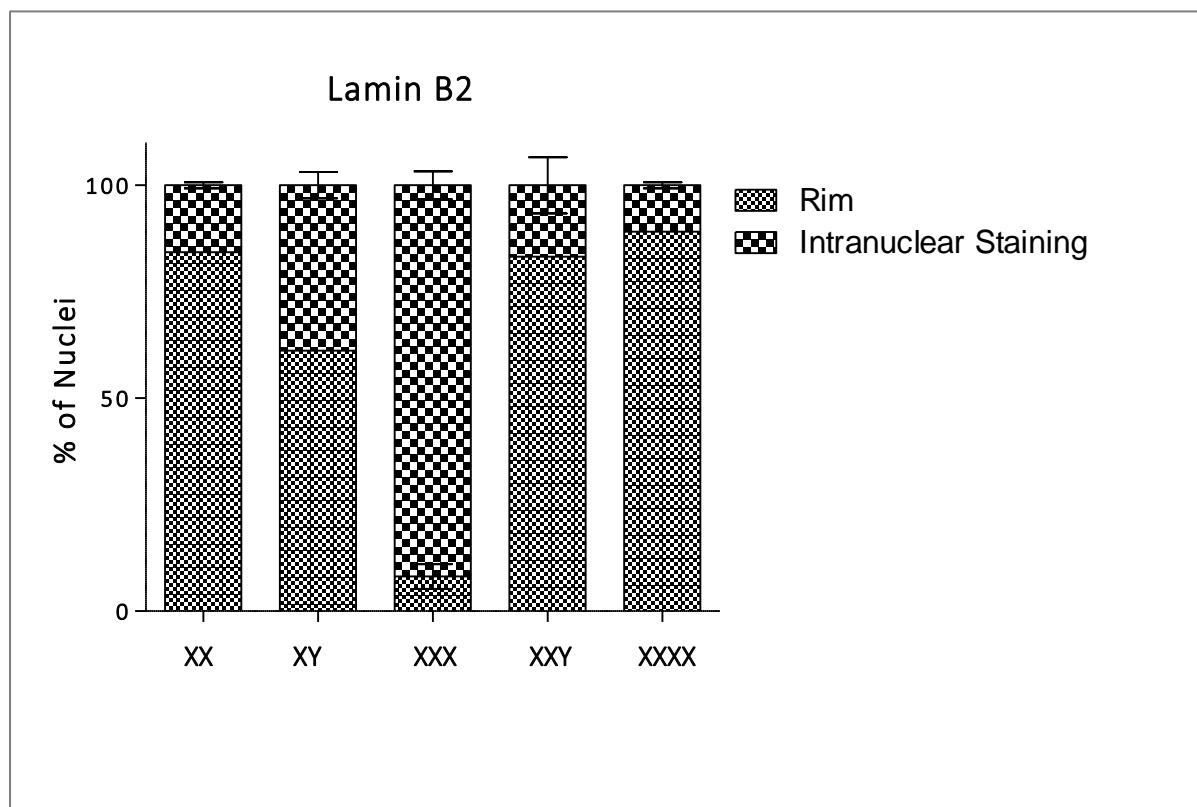


Figure 4.12 Lamin B2 Staining Pattern Analysis

The cell nuclei were stained for Lamin B2 and their staining patterns analysed. Two staining patterns for Lamin B2 were identified as a rim around the periphery of the nucleus and intranuclear staining referring to dispersed dots and homogenous staining of the nuclei. The percentage of nuclei for each staining pattern type is shown with standard error of mean as error bars. Cell lines FCWES02, MCWES01, DD0567, DD0710 and DD1473 with karyotypes XX, XY, XXX, XXY and XXXX, respectively, were analysed. A one-way analysis of variance was calculated for the rim and intranuclear staining patterns across the different cells lines; $p < 0.0001$ signifying extreme statistical significance for the rim staining and intranuclear staining.

4.4.2.2. Western Blotting

For B-type lamins, western blotting was performed out on the lymphoblastoid cells for lamins B1 and B2, alongside β -Tubulin, as the reference gene. An example western blot of lamin B1 and β -tubulin is shown in and the ratio of the mean gray intensities of lamin B1 to β -tubulin was plotted (Figure 4.13 B). No significant difference was observed from a One-way analysis of variance (ANOVA; $P= 0.7087$) and Tukey's Multiple Comparison Test in the different lymphoblastoid cell lines for Lamin B1 protein expression from the Western Blots. Images were analysed via Fiji/ImageJ in a minimum of three by monitoring the mean gray intensities of the bands in reference to the positive control, β -tubulin.

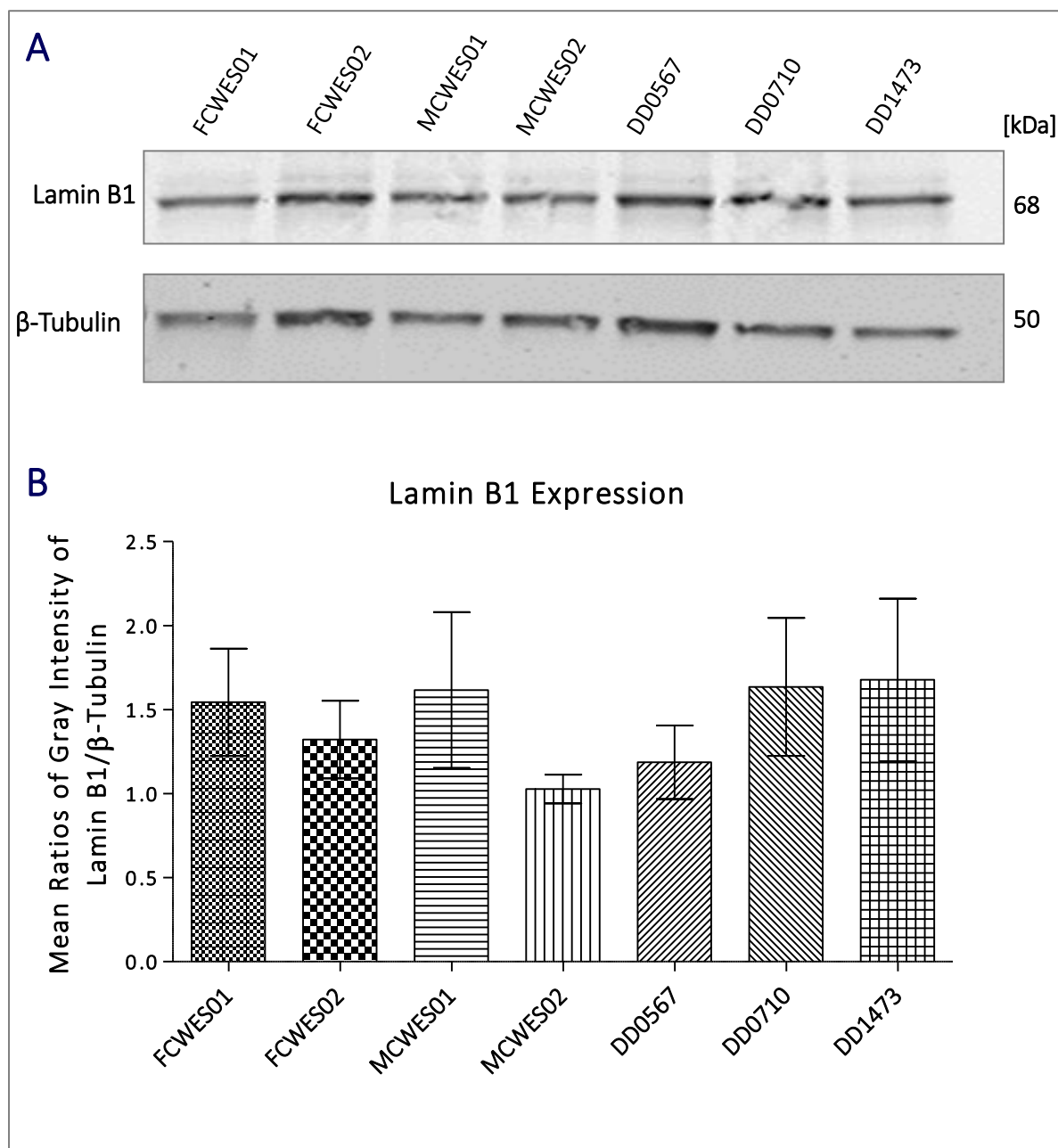


Figure 4.13. Lamin B1 and Beta-Tubulin Western Blot

Lymphoblastoid cell lines FCWES01, FCWES02, MCWES01, MCWES02, DD0567, DD0710, DD1473 were positive for Lamin B1 at approximately 68kDa and for the positive control, β -tubulin at approximately 50kDa (A).

The ratio of the mean gray intensities of lamin B1 to β -tubulin were plotted (B). The standard error of mean was used as the error bars. A minimum of three blots were analysed. No significant difference was observed between the different samples using a One-way analysis of variance (ANOVA; $p=0.7087$) and Tukey's Multiple Comparison Test.

Similarly, lamin B2 western blots were performed with the lymphoblastoid cells and with β -tubulin as the reference gene and the ratio of the mean gray intensities of lamin B2 to β -tubulin were plotted (Figure 4.14). No significant difference was observed from a One-way ANOVA ($p= 0.7944$) and Tukey's Multiple Comparison Test in the different lymphoblastoid cell lines for Lamin B2 protein expression. Images were analysed via Fiji/ImageJ in a minimum of three by monitoring the mean gray intensities of the bands in reference to the positive control, β -tubulin.

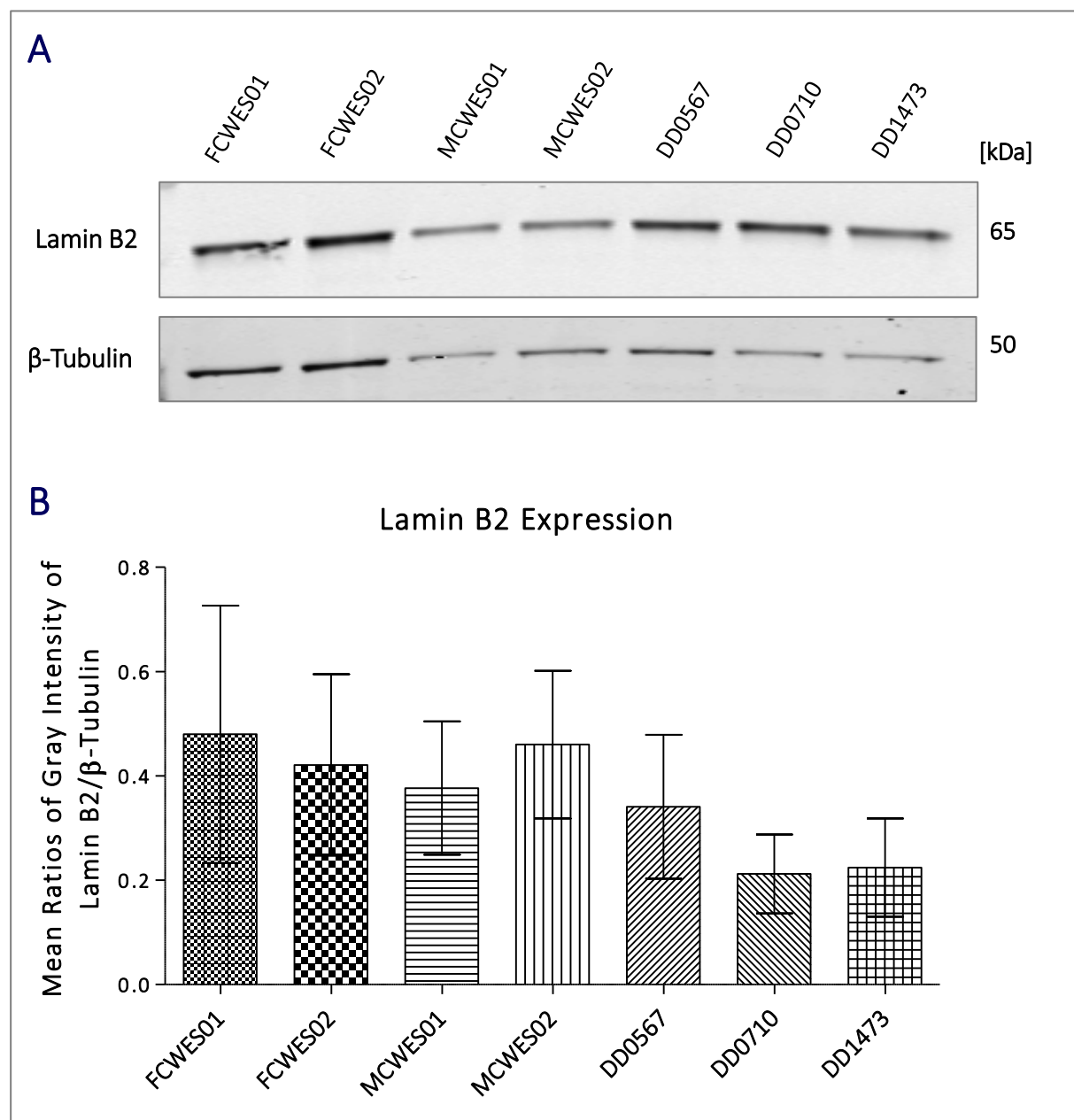


Figure 4.14. Lamin B2 and Beta-Tubulin Western Blot

Lymphoblastoid cell lines FCWES01, FCWES02, MCWES01, MCWES02, DD0567, DD0710, DD1473 were positive for Lamin B2 at approximately 65kDa and for the positive control (β -Tubulin) was observed at approximately 50kDa (A).

The ratio of the mean gray intensities of lamin B2 to β -tubulin were plotted (B). The standard error of mean was used as the error bars. A minimum of three blots were analysed. No significant difference was observed between the different samples using a One-way analysis of variance (ANOVA; $p=0.7944$) and Tukey's Multiple Comparison Test.

4.4.2.3. Reverse Transcription PCR

To measure the gene expression of the B-type lamins, RT-qPCR was performed on all of the lymphoblastoid cell lines; relative expression to *GAPDH* was measured. A One-way ANOVA and Tukey's Multiple Comparison Test was performed between all of the cell lines for each gene.

Interestingly, lamin B1 gene expression did not show any significant difference between any of the samples analysed (ANOVA $p=0.2234$; Figure 4.15 C). In contrast, for lamin B2 gene expression the wild-type female cell line, FCWES02 had shown significant difference to the aneuploid cell line, DD0170 and very significant difference to aneuploid cell line DD1473 (ANOVA $p=0.0045$; Figure 4.15 D).

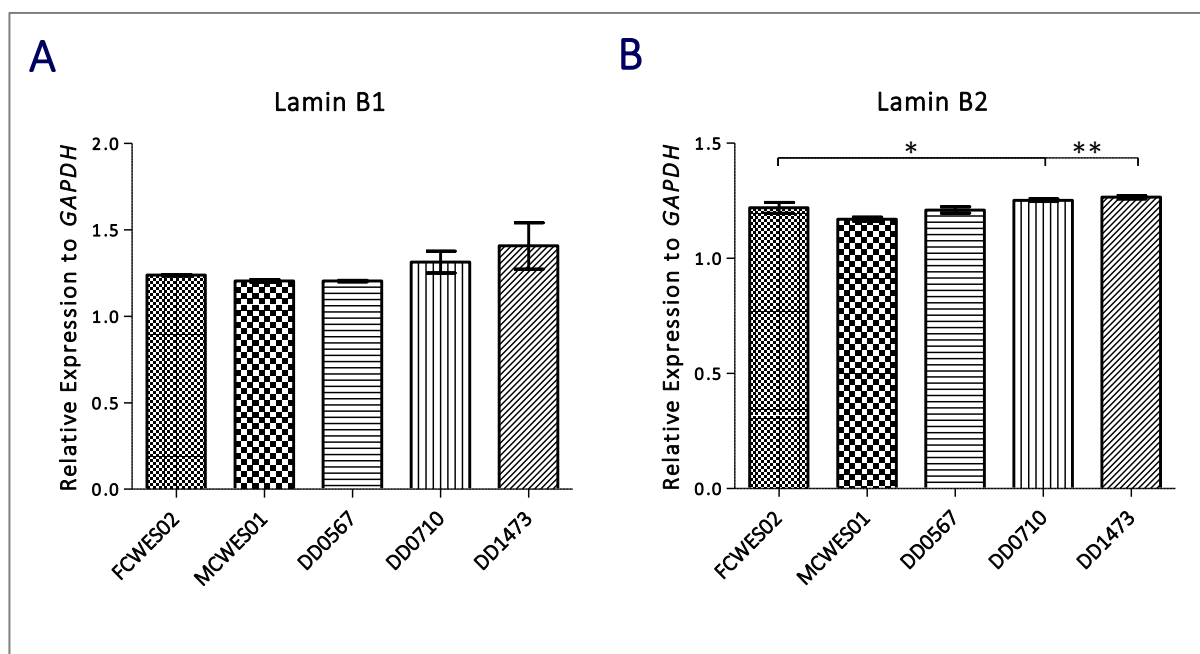


Figure 4.15. B-Type Lamin Gene Expression in Lymphoblastoid Cell Lines

B-type lamin gene expression was measured via RT-qPCR in a duplex reaction with *GAPDH* as the reference gene. The relative gene expression to *GAPDH* were plotted for each cell line and a one-way analysis of variance (ANOVA) and Tukey's Multiple Comparison Test was performed between each sample; the significant differences between samples are shown in asterisks; * for statistically significant different ($p < 0.05$) and ** for very statistically significant different ($p < 0.01$). The gene expression of lamin B1 (A) and lamin B2 (B) are shown. Wild-type lymphoblastoid female and male cells lines, FCWES02 and MCWES01 are shown, respectively, alongside aneuploid lymphoblastoid cell lines, DD0567, DD0710 and DD1473.

4.5. Discussion

The inner nuclear membrane has a role in the maintenance of nuclear morphology (Bridger *et al.*, 2007) and also has functions in the regulation of gene expression in different tissues and in chromatin organisation (Dechat *et al.*, 2008). Our results have been consistent with previously studies that observed the lack of A-type lamins in lymphoblastoid cell lines. However, unlike our result, this study did observe small amounts of lamins A and C (Reichart *et al.*, 2004). Although, we did not observe any A-type lamins using western blotting for protein detection, we did see some small amounts of staining using immunofluorescence. One possible explanation of this could be the antibodies used in this study. Most studies have not used antibodies for both lamins A and C separately, but instead stain for lamin A/C. As lamin A and C differ only by the last 98 amino acids, antibodies to distinguish the two target the ends of these proteins. For this reason, it is possible that during the protein preparation for western blotting the ends of these proteins denature so that the antibody cannot bind and therefore detect them on the western blots. Further work would be required using different antibodies to establish whether the antibody used in this study did not detect small amounts of protein in the cell nuclei. Alternatively, another technique, such as enzyme-linked immunosorbent assay (ELISA) could confirm the presence or absence of lamin protein and more sensitively quantify them in these cell lines.

Furthermore, our IF data demonstrated significantly increased levels of negative lamin C staining in the aneuploid cell lines. As very few research groups stain for both A-type lamins, it is difficult to compare our data with other findings. Previously, one group had identified that the absence of lamin A can cause lamin C intranuclear speckles to aggregative throughout the nucleus and suggested that lamin A is required for the nuclear envelope localisation of lamin C (Pugh *et al.*, 1997; Vaughan *et al.*, 2001). Similarly, not much is known about the state of lamin proteins in aneuploid cell types, the reduced percentage of lamin C internal foci may be a possible indicator of the difference in chromosome copy number, however further work is required to reach a conclusion.

Interestingly, although no significant difference was observed in B-type lamin protein expression between the wild-type and aneuploid cells, B2 protein expression was lower in the aneuploid cell lines. In addition, using RT-qPCR we confirmed a significant difference between the wild-type female cell line and the aneuploid cell lines DD0710 and DD1473 with karyotypes XXX and XXXX, respectively, suggesting a link between the two. In addition, DD0567 with XXY karyotype expressed the least rim-like patterns of lamin B2. Previously, a study had observed reduced lamin B2 to cause the accumulation of aneuploidies in the cell nuclei (Ranade *et al.*, 2017). Further research into this with more cell lines with known aneuploidies and using B2 depletion techniques, such as siRNA, is required to establish this link between aneuploidies and lamin B2 reduction.

Chapter V: The Effect of Different Media and Matrices on the Genomic Instability of Human Pluripotent Stem Cells

5.1. Introduction

As mentioned in Chapter I, currently no method or media for the growth of human pluripotent stem cells has been standardised. Human embryonic stem cells and induced pluripotent stem cells are commonly grown on a layer of human dermal fibroblasts as feeder cells or on a soluble basement membrane, such as Matrigel™. Although the latter is a good xeno-free alternative to feeders (Ludwig *et al.*, 2006), it has not been readily used by researchers, partly due to the high cost of feeder-free basement membranes (Khadun, 2013).

Similarly, the passage number of stem cells needs to be monitored more closely, along with the method of culture, including whether the cells are manually or enzymatically passaged. This would help during the characterisation of these cells, as certain methods may allow faster cell culture, but may also have disadvantages, such as the faster accumulation of chromosome aneuploidies in culture (Brimble *et al.*, 2004; Buzzard *et al.*, 2004; Draper *et al.*, 2004; Schwartz *et al.*, 2011; Garitaonandia *et al.*, 2015).

With emerging practises for the upscaling of hPSCs, novel methods are required to monitor and standardise the use and production of cellular materials intended for therapeutic use. Despite the increasing availability of novel techniques to increase the yield and/or quality of cells, the quality control for these cells remains unchanged; karyology, flow cytometry, differentiation potential and gene expression studies typically make up the characterisation of hPSCs. More sensitive and high-throughput methods need to be developed to understand how the novel techniques may affect the potential end-products. For example, despite the advancement in the large-scale production of human pluripotent stem cells, the low resolution and insensitive karyotyping method, G-banding, still remains the gold standard for karyology. Similarly, the use of methods, such as qPCR for observing gene expression of “pluripotent” genes remains a widely-used method for stem cell characterisation, despite the need for standard curves for accurate quantification. Newer techniques are required to sensitively characterise hPSCs, as well as be practical to be used widely across different laboratories. High-throughput methods are required to screen hPSC that can accurately determine the cells’ pluripotency and genomic stability.

Although newer methods, such as the NanoString Technologies™ Human Karyotype Panel, a microarray-based technique for aneuploidy detection, BioRad's Droplet Digital PCR™ for absolute quantification of nucleic acids and BioMark™ Fluidigm®, a high-throughput PCR system, are being developed, these methods need to be better integrated into the stem cell community. Firstly, these newer methods are semi-automated, reducing the risk of both contamination and human error, as well as utilise microfluidic technology for the use of small sample volumes to multiplex their assays.

5.2. Aims

The aims of this study were to evaluate the genomic health of the human pluripotent stem cells provided by our collaborators using minimum sample quantities. The UKSCB performed an evaluation on the effect of different media and matrices combinations on viability, genomic stability, differentiation potential and pluripotency marker expression. Whilst the UKSCB's usual method of determining genomic stability is via G-banding, we aimed to assess whether ddPCR™ using *AMELX* as a model for aneuploidy detection could provide a more sensitive method to evaluate the genomic stability and FISH to characterise the genome organisation of *AMELX* and *ALB* within these cells. In addition, we investigated whether specific media and matrices combinations have a particular negative or positive effect on the genomic instability of the hPSCs and their genome organisation in interphase nuclei.

5.3. Methods and Materials

All cell culture work was performed by Jennifer Man and Craig Nowell (UKSCB). Cell pellets were provided for ddPCR™, whereas FISH sample were collected and fixed as per Chapter III by me.

5.2.1. Cell Culture

After thawing from a cryopreserved vial, the H9 human embryonic stem cells, also known as WA09 (WiCell, USA), originally derived at the University of Wisconsin by Dr James Thomson (Thomson *et al.*, 1998), were first stabilised for approximately five passages on inactivated human dermal fibroblasts (HDFs; used internally at the UKSCB), after which they were transferred to different media and matrix combinations. On thawing, the H9 cells were labelled as P0; every subsequent passage was labelled as P_nPS (passage, number of passages and post-seed).

The H9 cells were grown in 6-well plates and 12 different media-matrix combinations were tested (Table 5.6). During each passage, samples were collected for analyses, including flow cytometry, G-banding, embryoid body (EB) formation and qPCR. Figure 5.1 shows how the cells were scaled up for the UKSCB use.

Table 5.6. Media and Matrices Used

Medium	Matrix
Essential 8™ Medium (ThermoFisher Scientific)	Matrigel (Corning)
NutriStem XF/FF Culture Medium for Human iPS and ES Cells (Stemgent, USA)	Laminin 511 (BioLamina, Sweden)
TeSR™2 (Stem Cell Technologies, UK)	Laminin 521 (BioLamina, Sweden)
	Vitronectin XF™ (Stem Cell Technologies, UK)

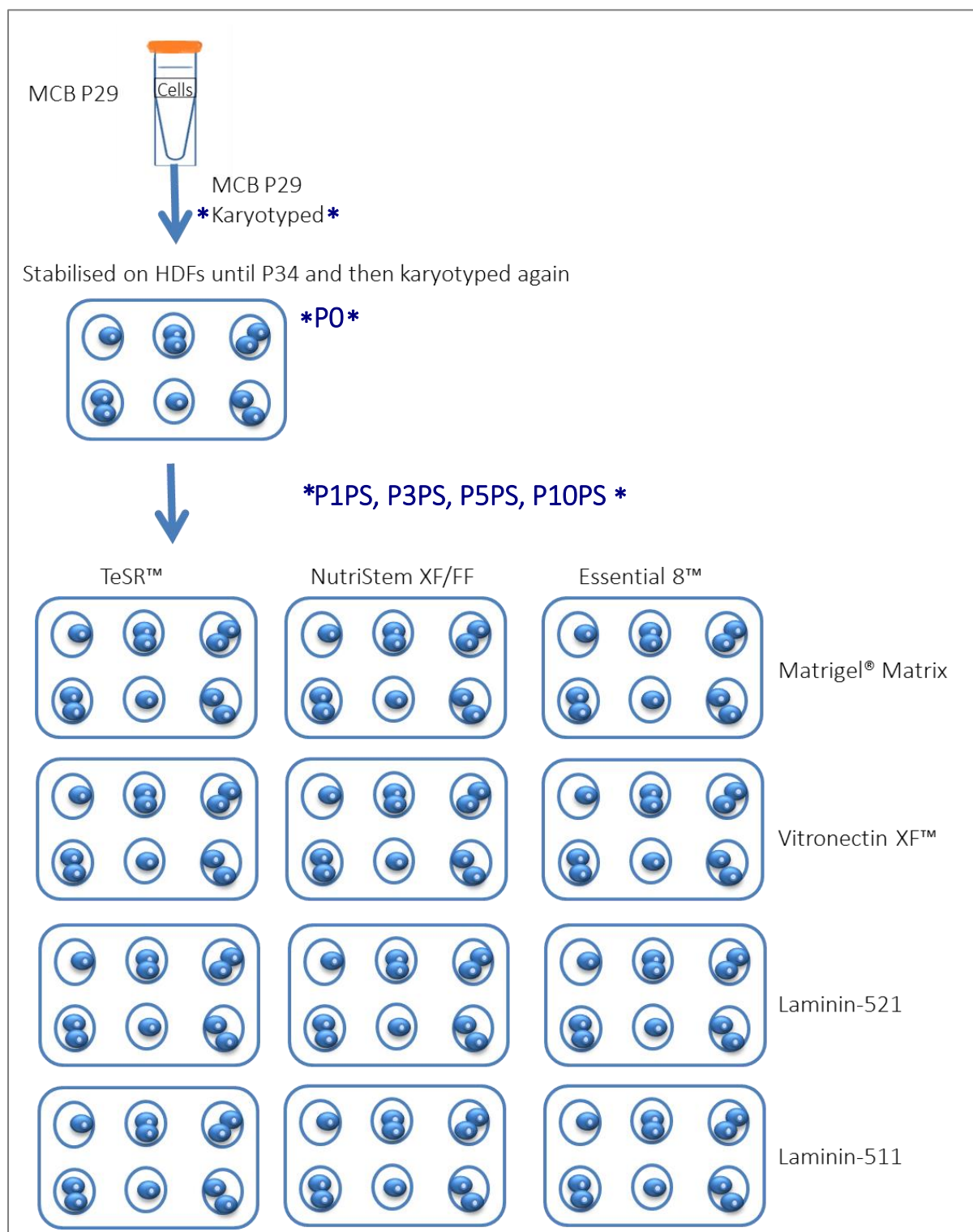


Figure 5.1. Media and Matrices Combination Flowchart

The image above shows the experimental workflow of the project. The H9 cells were thawed from the mastercell bank (MCB) at passage 29 (P29) and sent for karyotyping. The cells were then allowed to stabilise on inactivated human dermal fibroblasts until P34, where they were sent for karyotyping again and re-labelled as P0. The cells were then passaged onto different media and matrices combinations i.e. TeSR™, NutriStem XF/FF and Essential 8™ media in combination with Matrigel®, Vitronectin XF™, Laminin-521 and Laminin-511 matrices. At passages 1, 3, 5 and 10 in each combination, the cells were sent for karyotyping.

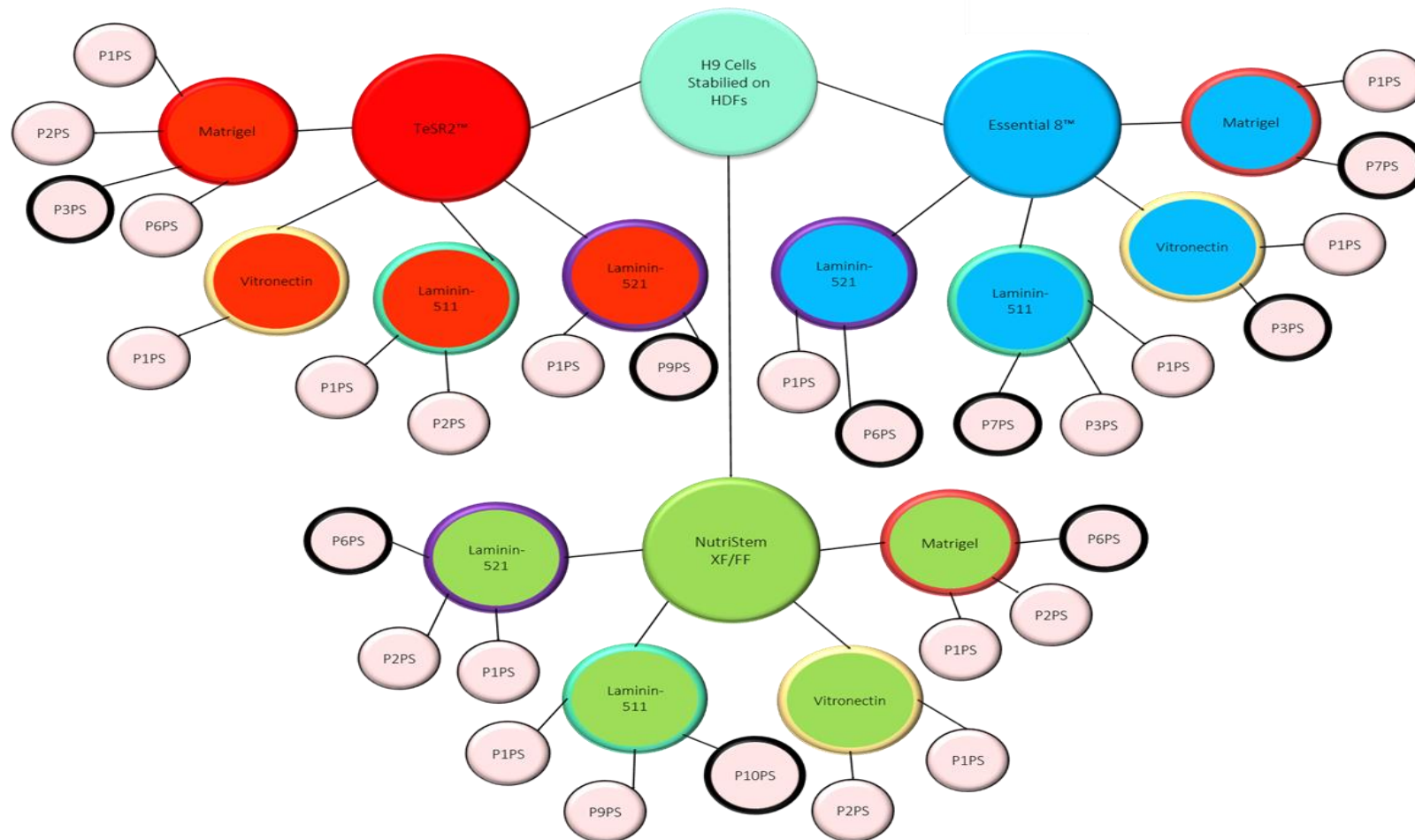


Figure 5.2. Flowchart of the Different H9 Media and Matrices Growth Conditions

The flowchart shows how the H9 cells were initially grown on human dermal fibroblasts (HDFs) for stabilisation, followed by the individual media and matrices combinations used in the study. The red circles show the samples grown in TeSR2™ medium, the blue – Essential 8™ medium and the green – NutriStem XF/FF medium, whereas the different coloured outlines signify the different matrices. The red outlined circles indicate the use of Matrigel®, the yellow – Vitronectin XF™, the turquoise – Laminin-511 and purple – Laminin 521. The samples used in the ddPCR™ are shown as passage number post-seed (PnPS) in pink circles; the black outlined samples are the ones that were also used for both ddPCR™ and for fluorescence *in-situ* hybridisation (FISH) experiments.

5.2.2. Quality Control

For quality control monitoring of the cells, the UKSCB test hPSCs for a number of different factors, including qPCR for stem cell markers, flow cytometry for pluripotency cell surface markers, karyology via G-banding, differentiation efficiency via embryoid body (EB) formation (tested for differentiation markers on qPCR) and viability (tested on the NucleoCounter, NC-100™ (Chemometec, Denmark)). These assays were performed by Drs Man and Nowell.

The H9 cells were karyotyped by G-banding at the Sheffield Diagnostic Genetics Service (Sheffield Children's NHS Foundation Trust, UK); the master cell bank of H9 cells were karyotyped after thawing (P29), immediately before passaging (P34 or pre-seed) onto the different media and matrice conditions and also P1PS, P3PS, P5PS and P10PS (Figure 5.1).

5.2.3. Droplet Digital PCR

DNA was extracted as per Section 2.2.2. using the GenElute DNA Extraction Kit. The DNA quantification and quality monitoring were performed as per Section 2.2.3. For the ddPCR™, the concentration of primers and probes were used as per Section 2.2.6, using AMELX and ALB. The DNA was neither enzymatically treated nor sonicated, due to the small amount provided by the UKSCB. The AutoDG was used for all of the experiments. Wild-type female samples, FCWES01 and FCWES02, and sonicated FCWES01 were used as the positive controls. All of the data in this study were normalised to the average of these controls as per Chapter II.

As the design of the experiment originally did not include ddPCR™, there were not always enough samples at each passage for ddPCR™ to be performed. Figure 5.2 shows which samples were used for ddPCR™; all of the pink circles are the samples used in ddPCR™.

5.2.4. Fluorescence *In-Situ* Hybridisation and Image Analysis

All of the fluorescence *in-situ* hybridisation (FISH) work and the associated image analysis for the cell morphology was performed as per Section 3.3.1. using *AMELX* and *ALB* fluorescent probes for a minimum of 100 nuclei for FISH and 200 for morphology analyses.

As the design of the experiment originally did not include FISH, there was not always enough sample at each passage for our FISH experiments. Figure 5.2 shows pink circles with black outlines which were the samples used for both FISH and ddPCR™.

5.2.5. Statistical Analysis

The same criterion as Chapter II was applied throughout this chapter for the statistical analysis of samples.

5.4. Results

Human embryonic stem cells from H9 were originally derived in 1998 and karyotyped at passage 2 to 9; the results showed a normal 46, XX karyotype (Thomson *et al.*, 1998). The H9 cells used in this study were sent for karyotyping by G-banding at passage 29 (P29) when they were first thawed onto feeder cells and then again at P34. Both passages showed normal 46, XX karyotypes (personal correspondence, J. Man, UKSCB). A further 48 samples were sent for G-banding at P1PS, P3PS, P5PS and P10PS in each media and matrix condition, although for unknown reasons results for only 38 of the samples were provided. All 38 samples demonstrated a diploid female karyotype of 46, XX in all 20-30 of the metaphase cells, except in 1 sample, where a gain of whole chromosome 12 (47, XX +12) was observed at P1PS in TeSR2™ Laminin-521 (personal correspondence, J. Man, UKSCB). However, this was observed only in one of thirty metaphase spreads examined and was not present in the later passages i.e. P3PS, P5PS and P10PS.

5.4.1. ddPCR™ of H9 Cells

The H9 cells were then assessed for an alteration in the ratio of *AMELX* to *ALB* by ddPCR™ as an indicator of X chromosome aneuploidy. In order to stratify the data analysis, the samples were grouped into three categories, according to the medium in which they were cultured; TeSR™, NutriStem XF/FF and Essential 8™ (Figure 5.3, Figure 5.4 and Figure 5.5).

Figure 5.3 shows that the TeSR™ combinations for H9 cells had no significant difference between the samples provided by the UKSCB and the diploid female control used (As per Chapter II) for the number of *AMELX* copies. No effect was observed over time or in the different matrices used in combination with TeSR2™.

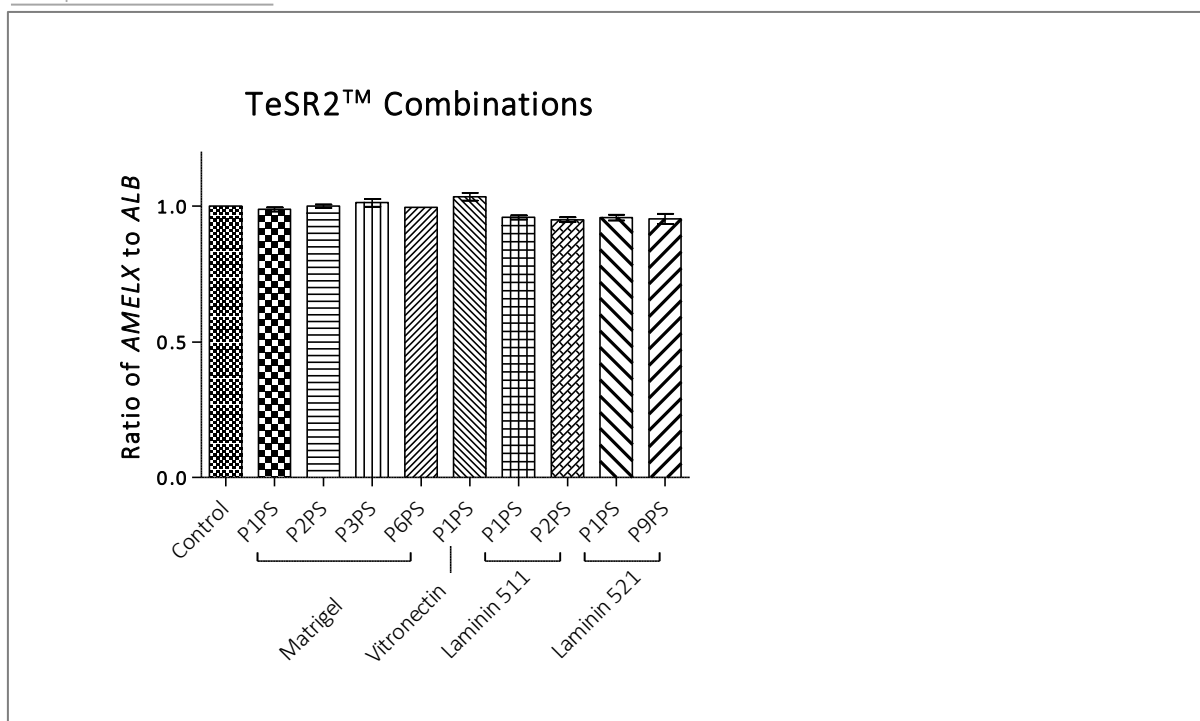


Figure 5.3. Relative AMELX Copy Number Measurement via ddPCR™ in H9 Cells Grown in TeSR™ Medium

ddPCR™ results for the ratio of AMELX to ALB is shown for each sample. H9 cells were grown in TeSR™ medium with different matrices – Matrigel®, Vitronectin XF™, Laminin-521 and Laminin-511 across different passages labelled as P followed by the number of the passage and PS (post-seed of P34) in the format P_nPS.

A two-tailed t-test and F-test were performed for each sample to the control, the average of the wild-type female lymphoblastoid cell lines, FCWES01 and FCWES02. Both control and the samples were analysed in triplicates, the standard error of mean is shown for error bars. No significant difference was observed in any of the samples analysed.

In Figure 5.4, 10 of 11 of the NutriStem XF/FF™ combinations for H9 cells showed a significant difference between the control and the individual sample; a two-tailed t-test and F-test were used. Figure 5.4 shows the level of significance between each sample. The only combination that showed no statistically significant difference from the control was NutriStem XF/FF™Laminin-511 at P1PS, which at the later passages of P9PS and P10PS had displayed a reduction in the AMELX copy number to 82.7% and 78.77%, respectively (derived from the ratio of AMELX to ALB). Similar reductions in the copy number of AMELX were observed in the Matrigel® and Laminin-521 combinations to approximately 60% and 90%, respectively. Conversely, the Vitronectin XF™ combination had shown an increase of AMELX in approximately 5% across one passage.

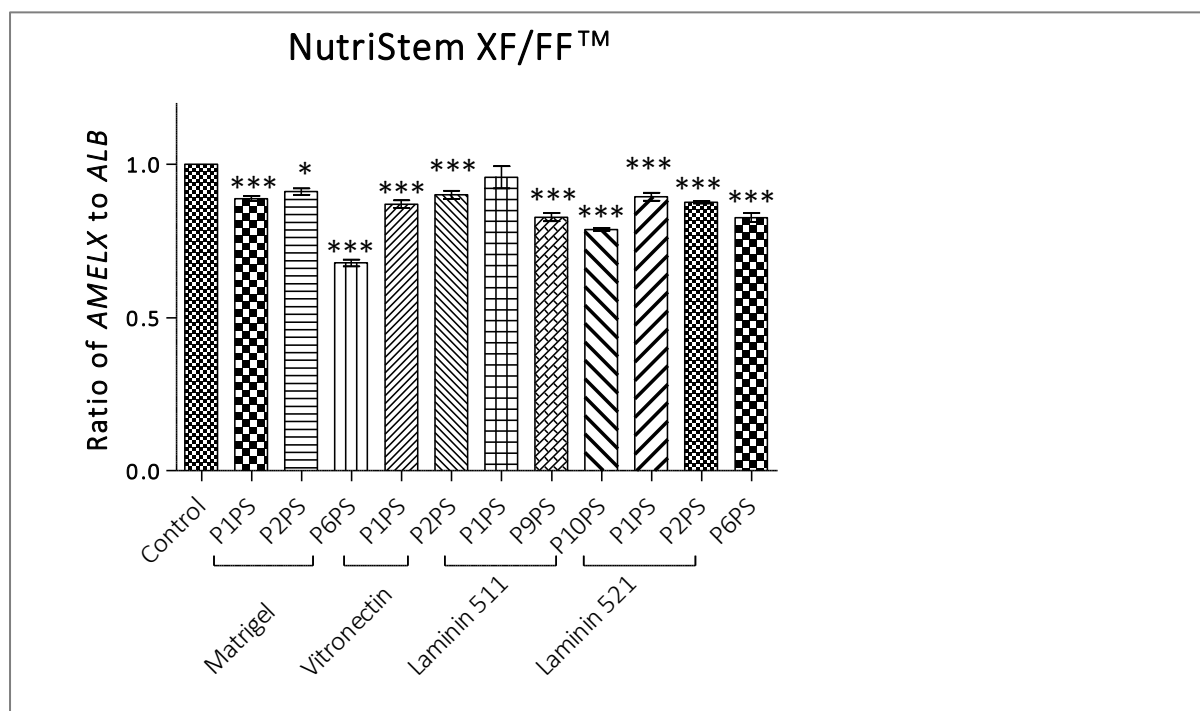


Figure 5.4. Relative AMELX Copy Number Measurement via ddPCR™ in H9 Cells Grown in NutriStem XF/FF™ Medium

ddPCR™ results for the ratio of AMELX to ALB is shown for each sample. H9 cells were grown in NutriStem XF/FF™ medium with different matrices – Matrigel®, Vitronectin XF™, Laminin-521 and Laminin-511 across different passages labelled as P followed by the number of the passage and PS (post-seed of P34) in the format P_nPS.

A two-tailed t-test and F-test were performed for each sample to the control, the average of the wild-type female lymphoblastoid cell lines. Both control and the samples were analysed in triplicates, the standard error of mean is shown for error bars. Significant difference between the control and sample is shown as * when p<0.05, ** when p<0.01 and *** when p<0.001.

In Figure 5.5, seven of nine Essential 8™ combinations for H9 cells showed a significant difference between the control and the individual sample; a two-tailed t-test and F-test were used. Figure 5.5 shows the level of significance between each sample. The only combination that showed no statistical significance to the control was Essential 8™ Matrigel® at P7PS and Laminin-511 at P7PS. Interestingly, unlike the NutriStem XF/FF™ samples, the AMELX copy number have shown a gradual increase across passages in all of the matrices combinations. Although the increase in AMELX copy number, it did range from 1-5% approximately.

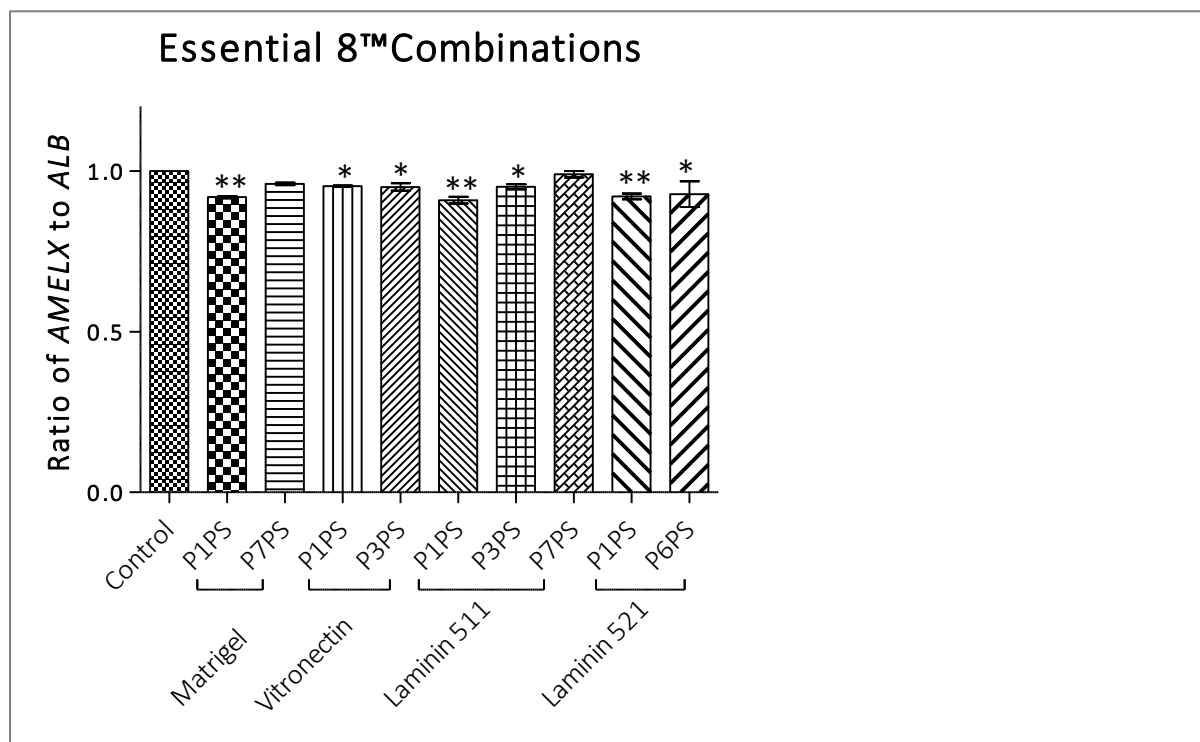


Figure 5.5. Relative AMELX Copy Number Measurement via ddPCR™ in H9 Cells Grown in Essential 8™ Medium

ddPCR™ results for the ratio of AMELX to ALB is shown for each sample. H9 cells were grown in Essential 8™ medium with different matrices – Matrigel®, Vitronectin XF™, Laminin-521 and Laminin-511 across different passages labelled as P followed by the number of the passage and PS (post-seed of P34) in the format P_nPS.

A two-tailed t-test and F-test were performed for each sample to the control, the average of the wild-type female lymphoblastoid cell lines. Both control and the samples were analysed in triplicates, the standard error of mean is shown for error bars. Significant difference between the control and sample is shown as * when $p < 0.05$, ** when $p < 0.01$ and *** when $p < 0.001$.

5.4.2. Fluorescence *In-Situ* Hybridisation

FISH was performed on the different media and matrix combinations on H9 cells provided by Drs Jennifer Man and Craig Nowell from the UKSCB. A one-way analysis of variance (ANOVA) and Tukey's Multiple Comparison Test were used to compare the samples to each other. For the *ALB* positioning, only two samples showed a significant difference between each other. This was observed between Shell 5 of NutriStem XF/FF™ Laminin-511 P10PS (Figure 5.7 Panel B) and Essential 8™ Laminin-521 P6PS (Figure 5.8 Panel D). The *ALB* positioning in all of the samples generally maintained a peripheral positioning in the cell nuclei, with the exception of NutriStem XF/FF™ Laminin-511 P10PS (Figure 5.7 Panel B), where there seemed to be a more central positioning for *ALB* and Essential 8™ Vitronectin XF™P3PS (Figure 5.8 Panel B) displays a more intermediate positioning of *ALB* in the nuclei of the cells.

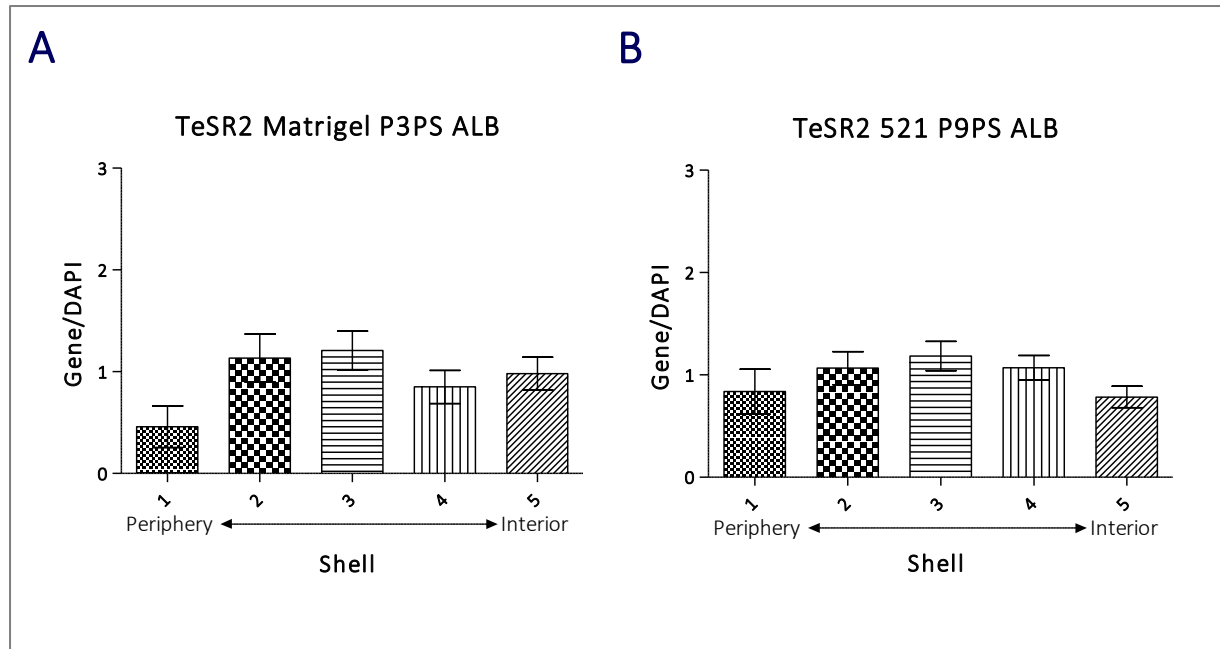


Figure 5.6. ALB Positioning in TeSR2™ Media in Combination with Different Matrices

Cell line H9 was grown under different combinations of TeSR2™ medium and Matrigel® (A) and Laminin-521 (B) matrices at passages 3 and 9, respectively. ALB positioning is shown in approximately 100 nuclei using the Erosion Script on the IPLAB software. Neither of the samples had shown any significant difference to the other samples in the one-way analysis of variance (ANOVA) and from the Tukey's Multiple Comparison Test; standard error of mean is shown as the error bars.

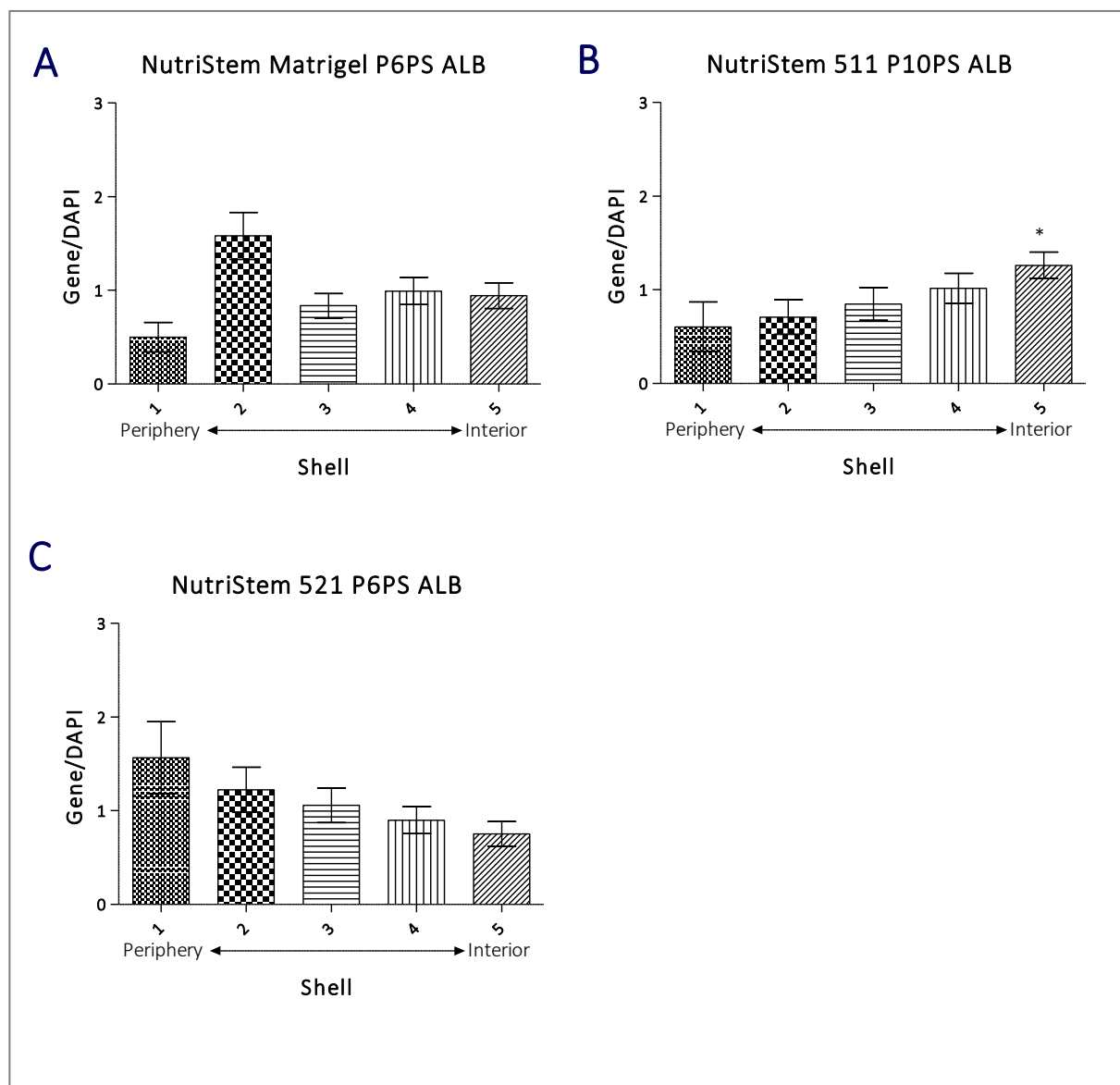


Figure 5.7. ALB Positioning in NutriStem XF/FF™ Media in Combination with Different Matrices

Cell line H9 was grown under different combinations of NutriStem XF/FF™ medium with Matrigel® at P6PS (A), Laminin-511 at P10PS (B) and Laminin-521 at P6PS (C). ALB positioning is shown in approximately 100 nuclei using the Erosion Script on the IPLAB software. The asterisk (*) in B represents a significant difference to Essential 8™ Laminin-521 at P6PS (Figure 5.8 Panel D) in Shell 5 using one-way analysis of variance (ANOVA) and Tukey's Multiple Comparison Test; standard error of mean is shown as error bars.

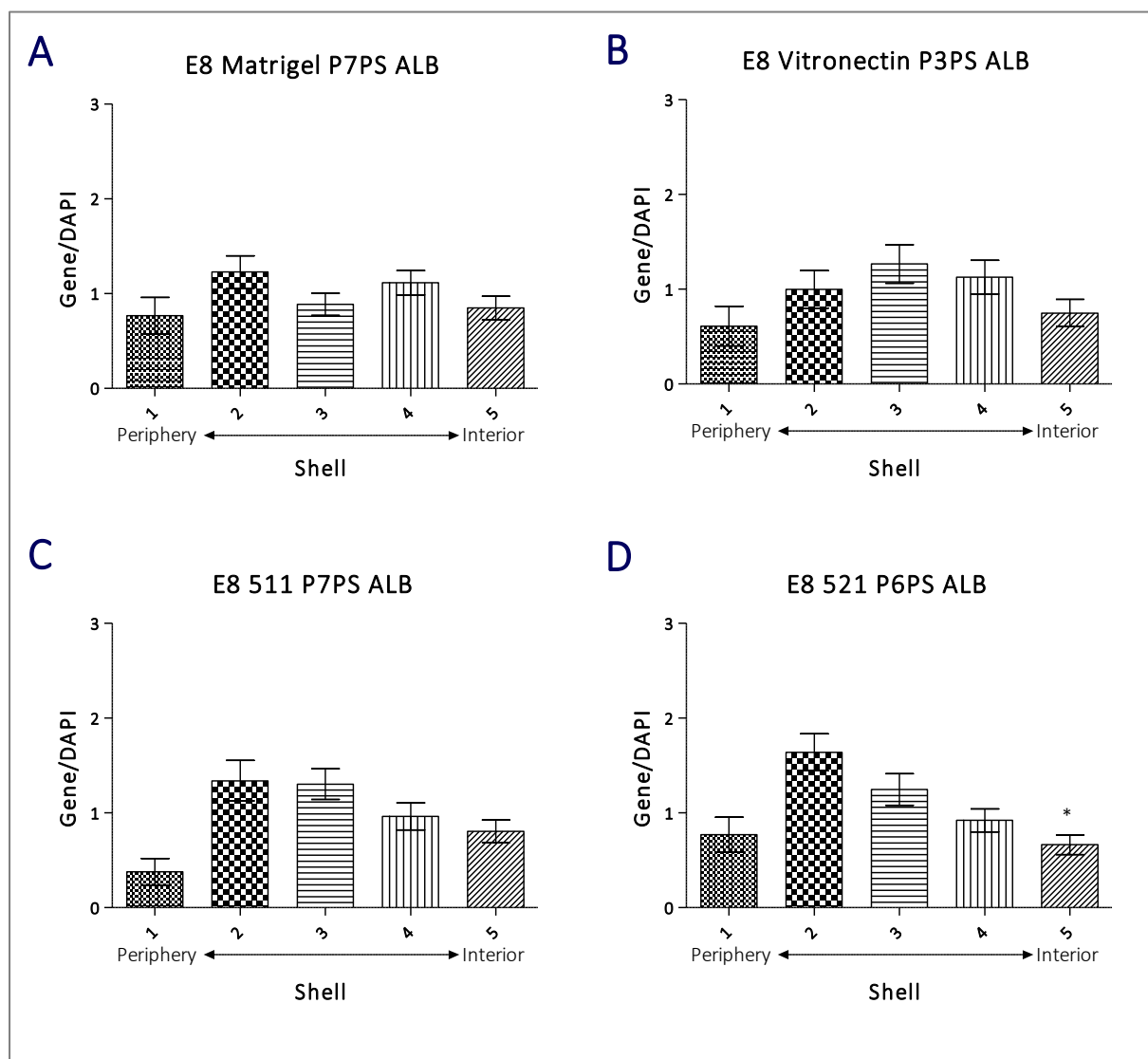


Figure 5.8. ALB Positioning in Essential 8™ Media in Combination with Different Matrices

Cell line H9 was grown under different combinations of Essential 8™ medium with Matrigel® at P7PS (A), Vitronectin XF™ (B) at P3PS, Laminin-511 (C) at P7PS and Laminin-521 at P6PS (D). ALB positioning is shown in approximately 100 nuclei using the Erosion Script on the IPLAB software. The asterisk (*) represents a significant difference to NutriStem XF/XX Laminin-511 at P10PS (Figure 5.7 Panel D) from the one-way analysis of variance (ANOVA) and Tukey's Multiple Comparison Test; standard error of mean is shown as the error bars.

For the *AMELX* positioning more differences in the gene positioning were observed in comparison to *ALB*, especially for Shell 5, the innermost shell of the nucleus. The sample that had shown the most significant difference to all of the other samples is Essential 8™ Laminin-521 P6PS (Figure 5.11 Panel D), where for Shells 1 and 2 were significantly different to Essential 8™ Laminin-511 P7PS (Figure 5.11 Panel C) and for Shell 5, it was again significantly different to Essential 8™ Laminin-511 P7PS (Figure 5.11 Panel C), and in addition to all of the NutriStem samples i.e. NutriStem XF™ Matrigel® P6PS (Figure 5.10 Panel A), NutriStem XF™ Laminin-511 P10PS (Figure 5.10 Panel B), NutriStem XF™ Laminin-521 P6PS (Figure 5.10 Panel C) and also to Essential 8™ Matrigel® P7PS (Figure 5.11 Panel A).

Additionally, Essential 8™ Laminin-511 P7PS (Figure 5.11 Panel C) had shown a central positioning, whereas TeSR2™ Matrigel P3PS (Figure 5.9 Panel A) and NutriStem XF/FF™ Matrigel® P6PS (Figure 5.10 Panel A) had a more intermediate positioning for *AMELX*. Interestingly, both *ALB* and *AMELX* in TeSR2™ Matrigel P3PS (Figure 5.6 Panel A and Figure 5.9 Panel A, respectively) samples had shown this intermediate positioning.

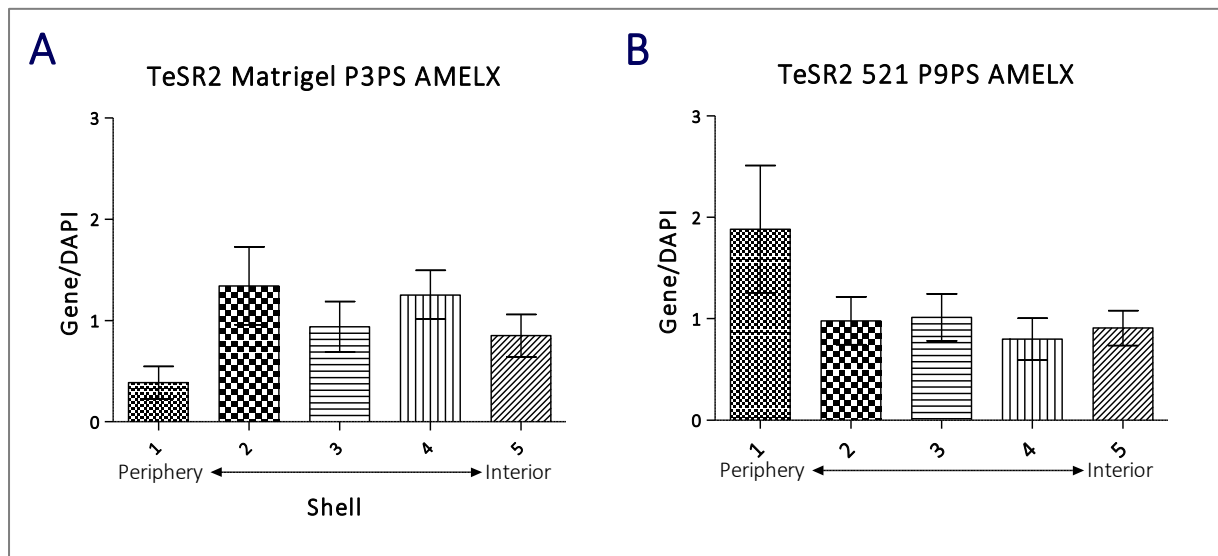


Figure 5.9. *AMELX* Positioning in Essential 8™ Media in Combination with Different Matrices

Cell line H9 was grown under different combinations of Essential 8™ medium with Matrigel® at P3PS (A) and Laminin-521 at P9PS (B). *AMELX* positioning is shown in approximately 100 nuclei using the Erosion Script on the IPLAB software. Neither of the samples had shown any significant difference to the other samples in the one-way analysis of variance (ANOVA) and from the Tukey's Multiple Comparison Test; standard error of mean is shown as the error bars.

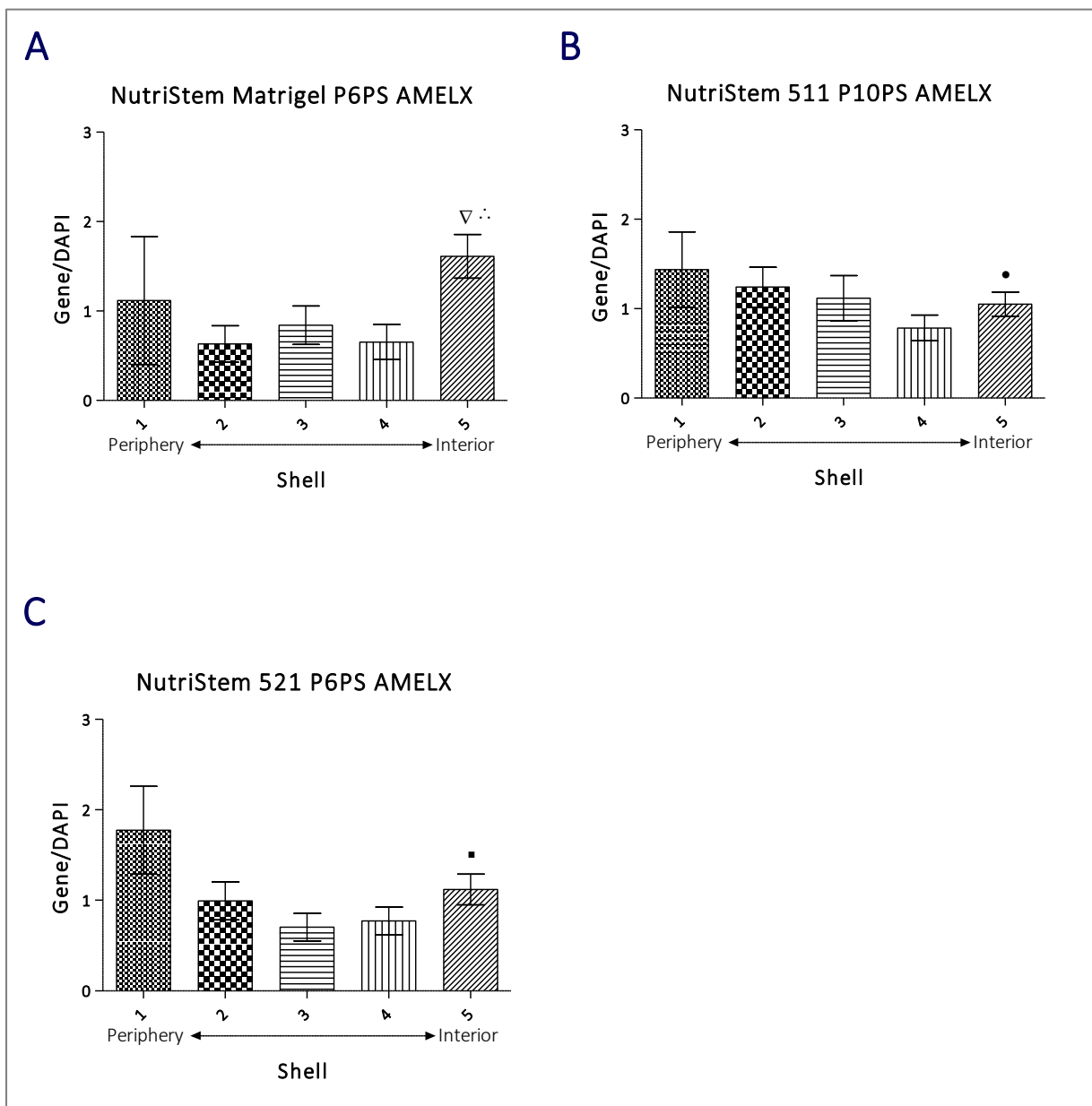


Figure 5.10. AMELX Positioning in NutriStem XF/FF™ Media in Combination with Different Matrices
 Cell line H9 was grown under different combinations of NutriStem XF/FF™ medium with Matrigel® at P6PS (A), Laminin-511 at P10PS (B) and Laminin-521 at P6PS (C). AMELX positioning is shown in approximately 100 nuclei using the Erosion Script on the IPLAB software. The symbols ▽ and ▣ on NutriStem XF™ Matrigel® (A) at P6PS represents a significant difference to Essential 8™ Vitronectin XF™ at P3PS (Figure 5.11 Panel B) and Essential 8™ Laminin-521 at P6PS (Figure 5.11 Panel D), respectively, in Shell 5, whereas the dot symbol (•) in NutriStem XF™ Laminin-511 at P10PS (B) and the square symbol (▣) in NutriStem XF™ Laminin-521 at P6PS (C) represents a significant difference to Essential 8™ Laminin-521 at P6PS (Figure 5.11 Panel D) from the one-way analysis of variance (ANOVA) and Tukey's Multiple Comparison Test; standard error of mean is shown as the error bars.

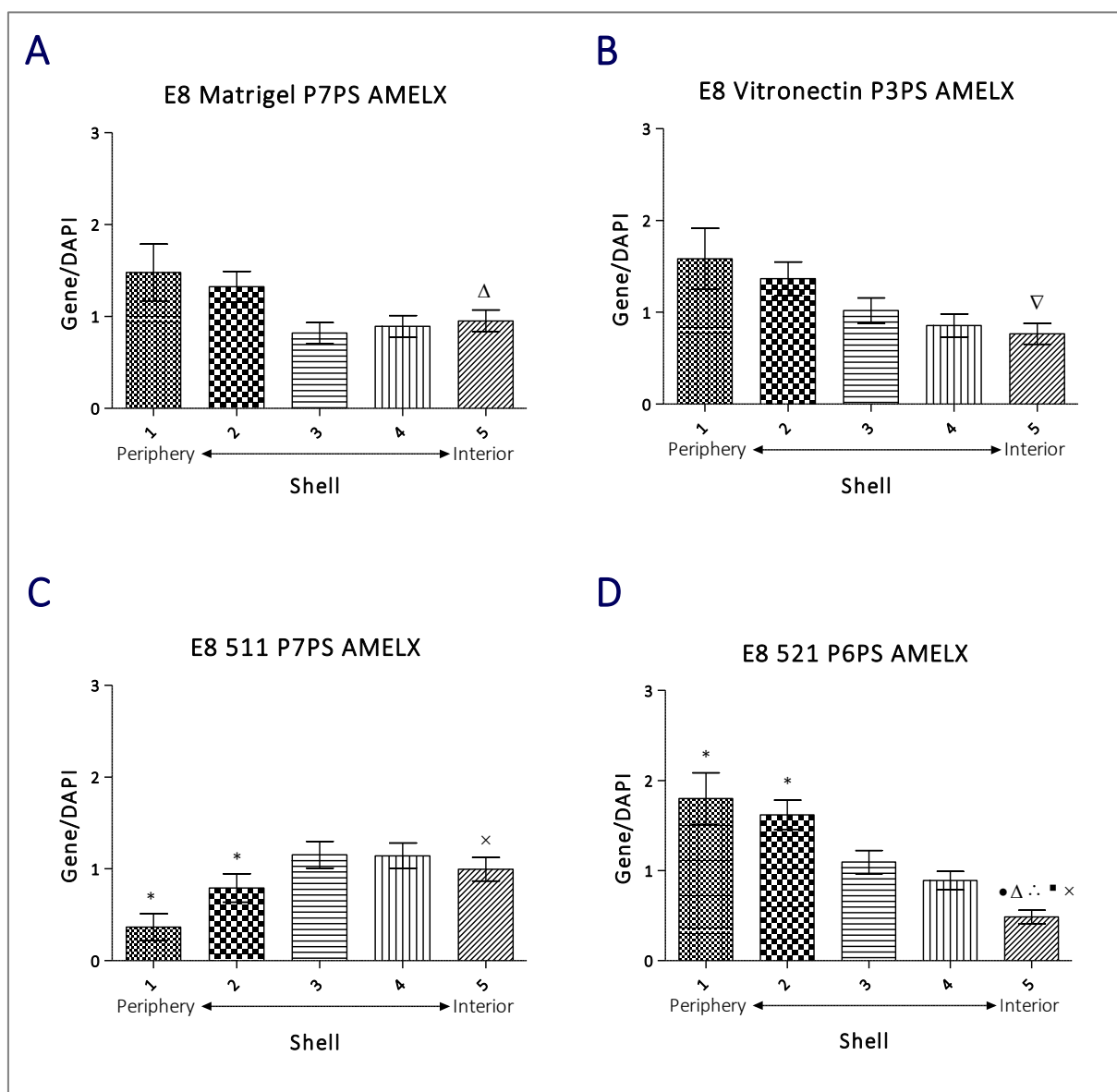


Figure 5.11. AMELX Positioning in Essential 8™ Media in Combination with Different Matrices

Cell line H9 was grown under different combinations of Essential 8™ medium with Matrigel® at P7PS (A), Vitronectin XF™ at P3PS (B), Laminin-511 P7PS (C) and Laminin-521 at P6PS (D). AMELX positioning is shown in approximately 100 nuclei using the Erosion Script on the IPLAB software. The symbols Δ and X on Essential 8™ Matrigel® at P7PS (A) and Essential 8™ at P7PS (C), respectively, represent statistical significance to Essential 8™ Laminin-521 at P6PS (D) on Shell 5. The ∇ symbol on Essential 8™ Vitronectin XF™ at P3PS (B) represents a significant difference to NutriStem XF/FF™ Matrigel® at P6PS (Figure 5.10 Panel A) in Shell 5 and the asterisk symbols (*) on Essential 8™ Laminin-511 at P7PS (C) represent a significant different to Essential 8™ Laminin-521 at P6PS (D) in Shells 1 and 2. The symbols ■, •, ∇ and X represent significant difference of Essential 8™ Laminin-521 at P6PS (D) to NutriStem XF/FF™ Matrigel® at P6PS (Figure 5.10 Panel A), NutriStem XF/FF™ Laminin-511 at P10PS (Figure 5.10 Panel B), NutriStem XF/FF™ Laminin-521 (Figure 5.10 Panel C), respectively, in Shell 5. For all of the statistically significant different calculations a one-way analysis of variance (ANOVA) and Tukey's Multiple Comparison Test was performed; standard error of mean is shown as the error bars.

5.4.3. Nuclear Morphology Analysis

In addition to the gene positioning, the morphology of the nuclei from the different conditions were also analysed via Fiji (ImageJ; Figure 5.12). Using One-way analysis of variances (ANOVA) and Tukey's Multiple Comparison Test, significant difference was found in the nuclear area between all of the individual matrices samples in each category i.e. different matrix combination of cells grown in TeSR2™, NutriStem XF™ and Essential 8™. Details of the statistical significance between each of the samples is shown in Appendix II.

Despite the same cell line H9 being used this study, the morphology of the nuclei varied greatly, dependent on the conditions. This suggests that the media and matrices composition have a huge impact on the cells. The results had shown that the two TeSR2™ conditions, TeSR2™ Matrigel P3PS and TeSR2™ Laminin-521 P9PS, one out of four of the Essential 8™ conditions - Essential 8™ Vitronectin P3PS and one out of three conditions for the NutriStem XF/FF conditions – NutriStem XF/FF Laminin-511 P10PS had shown the least statistically significant difference from the rest of the samples. In all three of the aforementioned cases, the samples showed no significant difference (N.S.) to three or more different medium-matrix combinations.

On the other hand, the samples that showed the most significant difference to the rest of the media and matrice study samples were the Essential 8™ conditions - Essential 8™ Matrigel P7PS and Essential 8™ Laminin-511 P7PS and the NutriStem XF/FF Matrigel P6PS. From the Tukey's Multiple Comparison Test those particular samples had shown statistical significance to all of the other samples, albeit one.

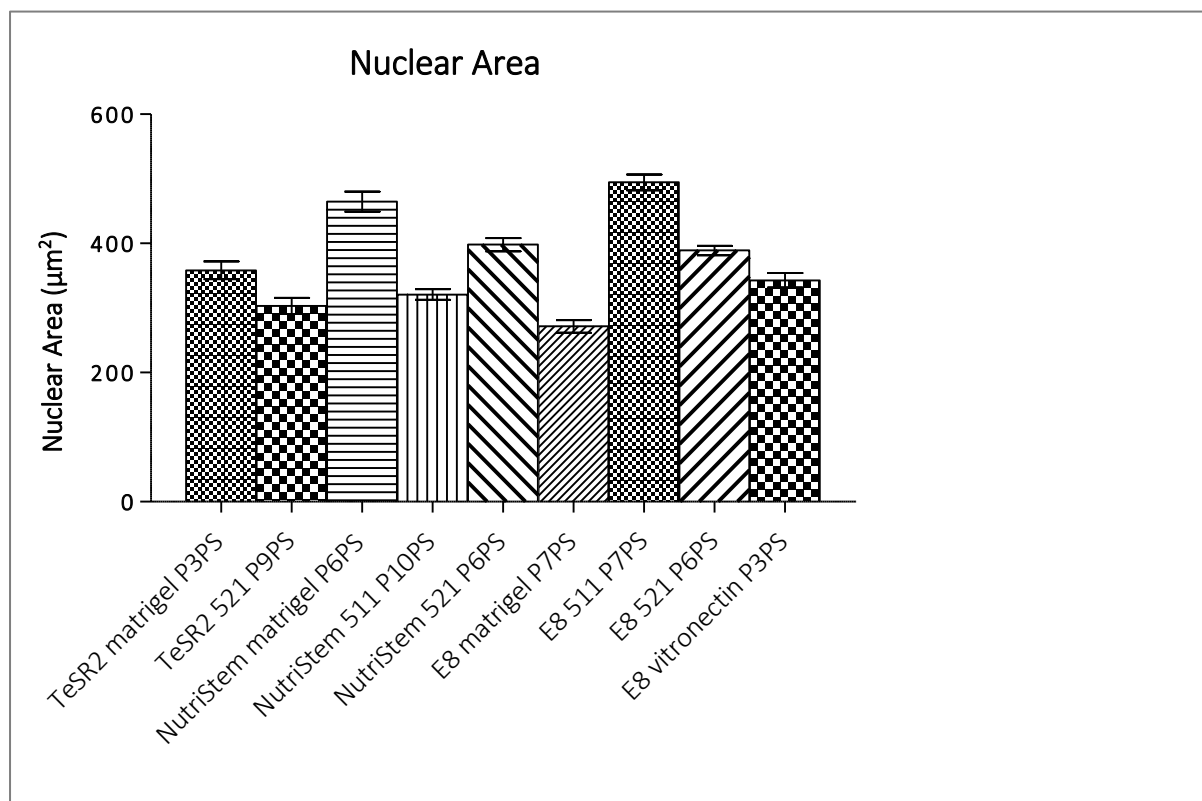


Figure 5.12. Nuclear Area of the Different Media and Matrices Combinations

Images from fluorescence *in-situ* hybridisation were analysed in Fiji (Image J); up to 200 nuclei were analysed. Nuclear area is shown in μm^2 ; standard error of mean is shown as error bars. Tukey's Multiple Comparison Test was carried out between the samples and the p values are shown in Appendix II.

Additionally, the nuclear circularity was calculated on Fiji (ImageJ) to determine the shape of the nuclei had changed in the different media and matrices conditions (Figure 5.13).

Similar to the nuclear area statistical analysis (Figure 5.12), all of the samples in the same category (TeSR2™, NutriStem XF/FF™ and Essential 8™) had shown significant difference between each other (Figure 5.13). Details of the statistical significance between each of the samples is shown in Appendix II.

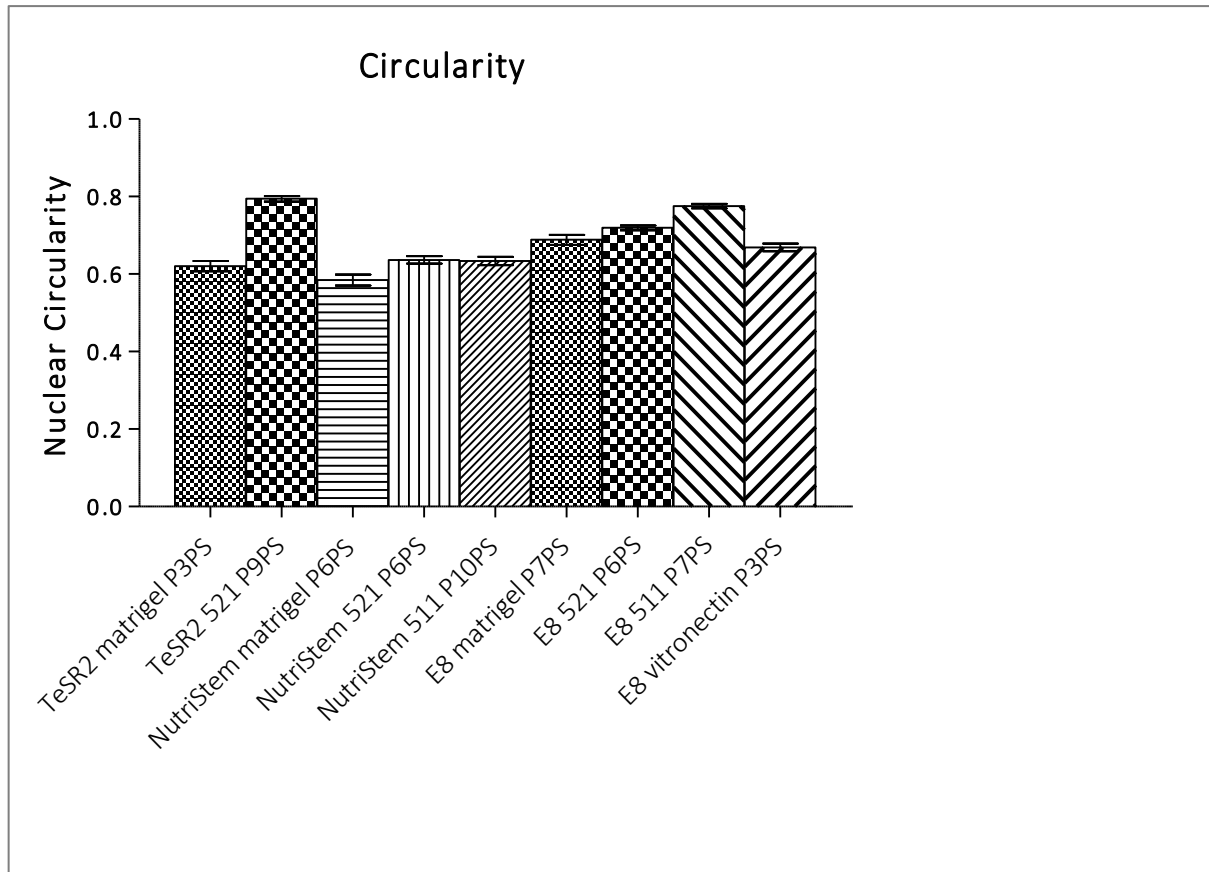


Figure 5.13. Nuclear Morphology Analysis

Images from fluorescence *in-situ* hybridisation were analysed in Fiji (Image J) for nuclear circularity; up to 200 nuclei were analysed. Standard error of mean was used for the error bars.

Table 5.7. Media and Matrices Study Combined Results

The table shows all of the results from this study, including the ddPCR™ *AMELX* to *ALB* ratios, the FISH gene positioning data, nuclei area and nuclei circularity. The asterisks (*) identify the H9 samples that were significantly different in *AMELX* to *ALB* ratio to the control sample.

Sample	ddPCR™ <i>AMELX</i> / <i>ALB</i> Ratio	<i>AMELX</i> Positioning	<i>ALB</i> Positioning	Nuclei Area (µm ²)	Nuclei Circularity
TeSR2™ Matrigel P3PS	1.01 (N.S.)	Intermediate	Intermediate	358.5	0.62
TeSR2™ Laminin-521 P9PS	0.95 (N.S.)	Peripheral	Intermediate	303.3	0.79
NutriStem XF/FF Matrigel P6PS	0.87 (***)	Central and Peripheral (Sig. Diff. in Shell 5)	Peripheral	464.7	0.58
NutriStem XF/FF Laminin-511 P10PS	0.79 (***)	Peripheral	Central (Sig. Diff. in Shell 5)	320.9	0.63
NutriStem XF/FF Laminin-521 P6PS	0.83 (***)	Central and Peripheral (Sig. Diff. in Shell 5)	Peripheral	398.1	0.64
Essential 8™ Matrigel P7PS	0.96 (N.S.)	Peripheral (Sig. Diff. in Shell 1)	Intermediate	271.7	0.68
Essential 8™ Vitronectin P3PS	0.95 (*)	Peripheral (Sig. Diff. in Shell 5)	Intermediate	343.0	0.67
Essential 8™ Laminin-511 P7PS	0.99 (N.S.)	Intermediate (Sig. Diff. in Shell 1, 2 and 5)	Peripheral	494.7	0.78
Essential 8™ Laminin-521 P6PS	0.93 (*)	Peripheral (Sig. Diff. in Shell 1, 2 and 5)	Peripheral (Sig. Diff. in Shell 5)	389.1	0.72

5.5. Discussion

To assess human pluripotent stem cells intended for therapeutic use, the cells must fall into specific criteria to warrant their safety, including demonstrating a normal diploid karyotype of 46 chromosomes. Although human pluripotent stem cells have widely been reported to accumulate and/or lose whole chromosomes (Draper *et al.*, 2004; Baker *et al.*, 2007; Amps *et al.*, 2011; Avery *et al.*, 2013), the exact mechanism of how this occurs is yet to be explained. Suggestions have been made that poor cell culture techniques may be to blame (Kim *et al.*, 2012) and more recently the quality of the preserved material has been suggested to be dictated by the individual cell's size, morphology and the preservation medium (Stacey *et al.*, 2017). In this study, we focused on the effects of the combinations of different matrices and media on cell size, morphology, gene positioning and karyology in hESC line H9.

5.5.1. ddPCR™ Results

In our study, the ddPCR™ results have suggested that a small amount of the X chromosome instability occurs in the H9 cells as indicated by *AMELX* copy number changes, dependent on culture conditions i.e. the media and/or matrix used. Despite the genomic instability that we had observed with ddPCR™, the G-banding data from the UKSCB did not show any significant number of chromosomal gains or losses for the cells that were analysed by Sheffield Genetics Service. Although human pluripotent stem cells are known to be highly unstable with frequent recurrent aneuploidies for chromosomes 12, 17, 20 and X (Brimble *et al.*, 2004; Baker *et al.*, 2007; Amps *et al.*, 2011), the karyology results for H9 had not suggested such an occurrence. This demonstrates that ddPCR™ is a much more sensitive method for the detection of small copy number variations.

From Figure 5.3, we can see that the TeSR2™ had shown the most stability with regards to the different matrices and also over time. Due to the lack of data for the later passages, we cannot be certain whether TeSR2™ combinations with Vitronectin XF™ and Laminin-511 would also have been as stable

as Matrigel® and Laminin-521. However, we can hypothesise from the rest of our results that the TeSR2™ medium generates the most genomically stable hPSCs. On the other hand, the use of NutriStem XF/FF™ medium demonstrated the most abnormalities on the H9 cells, regardless of the matrix used. Even at P1PS, three out of four of the different matrices already had significant differences in comparison to the control. And for the one sample that was not significantly different (NutriStem XF/FF™ Laminin-511) at P1PS, in the later passages i.e. P9Ps and P10PS, showed significant difference to the control.

In addition, the NutriStem XF/FF™ medium combinations, always exhibited a reduced copy number of *AMELX* (corresponding to chromosome X in our study), was observed over time. This was particularly apparent in Figure 5.4, where the NutriStem XF/FF Matrigel® combination had reduced very sharply to approximately 68% *AMELX* copy numbers, which may be attributed to the loss of a normal diploid genome and emergence of a monoploid X population. Similarly, the NutriStem XF/FF™ combination with Laminin-511 and -521 had seen this reduced amount of *AMELX*. These results suggest that the NutriStem XF/FF™ medium may not be a suitable choice to maintain a normal diploid karyotype.

Furthermore, a reduced amount of *AMELX* in reference to *ALB* was also observed in most of the Essential 8™ matrices combinations. However, there was not a sudden drop in *AMELX*, as seen in the NutriStem XF/FF™ combinations, in the later passages. Our results have found that TeSR2™ is the most stable medium to use for the growth of hPSCs in combinations with most of the matrices for the maintenance of genomic stability in the cells.

It is important to point out, that genomic instability does not equate to the maintenance of pluripotency in hPSCs. The UKSCB fluorescent-activated cell sorting (FACS) data highlighted that the TeSR2™ medium was, in fact, the worst medium for the maintenance of pluripotency markers, *NANOG* and *OCT4* expression. However, with the exception of TeSR2™ Vitronectin XF™, which demonstrated 0% positive *NANOG* and *OCT4* expression, all of the TeSR2™ samples showed an improvement in the *NANOG* and *OCT4* expression over time in cell culture. Comparing the early passage TeSR2™ samples to the later

passage samples, a consistent increase in the pluripotency marker expression from an average of 10% to 80% was observed. On the other hand, the NutriStem XF/FF™ combinations that demonstrated the most genomic instability on the ddPCR™ results, showed the highest pluripotency marker expression. Similarly, the NutriStem XF/FF™ and Essential 8™ Laminin-511 or -521 combinations had shown the best differentiation potential when looking at qPCR gene expression for lineage specific genes after EB formation (personal correspondence with J. Man). These data suggest that although the cells grown in TeSR2™ medium display genomic stability, the medium does not maintain their pluripotent characteristics. Tosca *et al.*, had found that small copy number variations detected by aCGH in the hPSC culture did not affect the differentiation capabilities of the hPSCs (Tosca *et al.*, 2015), however Fazeli *et al.*, had found altered patterns of differentiation in abnormal cells karyotyped by G-banding (Fazeli *et al.*, 2011). This suggests that although small copy number variations may not affect the differentiation of hPSCs, larger abnormalities may significantly disrupt both gene expression and differentiation of these cells.

5.5.2. Gene Positioning Results

From previous studies in our lab (Mehta, *et al.*, 2010; Bikkul, *et al.*, Manuscript in Preparation), other labs (Kozubek *et al.*, 2002; Cremer *et al.*, 2003) and Chapter III, we know that both the chromosomes that have *AMELX* and *ALB* have a peripheral positioning in the nucleus. This seemed to have been maintained for some of the growth conditions, but interestingly not for all of them, despite the cells being from one source.

From our FISH data, we have observed the most atypical positioning of *AMELX* and *ALB* in the NutriStem XF/FF™ and Essential 8™ medium combinations. For the *ALB* positioning, all of the different media and matrice combinations demonstrated a general peripheral or intermediate positioning for the gene, except NutriStem XF/FF™ Laminin-511 at P10PS, which showed a central positioning of the gene. Previous studies have shown that transcription and differentiation can affect the genome positioning of genes (Volpi *et al.*, 2000; Mahy, Perry and Bickmore, 2002; Wiblin *et al.*, 2005) and in both human

and mouse ESCs, *ALB* gene expression can vary according to the growth factors that supplement the medium (Shirahashi *et al.*, 2004; Davidson *et al.*, 2014). This may be a possible explanation as to why the positioning of *ALB* varies in the different growth conditions, despite the stability of the gene copy number.

On the other hand, *AMELX* positioning demonstrated much more varied results, in comparison to *ALB*. For NutriStem XF/FF™ Matrigel® at P6PS and NutriStem XF/FF™ Laminin-511 at P10PS a central and peripheral positioning was observed, where both Shells 1 and 5 displayed increased amount of signal in comparison to the background. This suggests that in the case of a normal diploid genome, where two chromosomes or gene copies are present, that one chromosome is in the periphery, whereas the other is localised more centrally in the nuclei. From the ddPCR™ results we know that for both of these conditions, the samples displayed a loss in *AMELX* copy number of approximately 15-20%. One possible explanation of this is that with the loss of chromosome X in a small number of the cell population, the monosomy X nuclei have a more central positioning, whereas the diploid X chromosomes maintain the peripheral positioning. This could be why we observe the central and peripheral positioning in those particular samples.

5.5.3. Nuclear Morphology Analysis

With regards to the effects individual media and matrix combinations can have on the nuclear circularity and nuclear area, to our knowledge no study has looked this before. Previously, studies for the effects of different feeder cells on the colony shape of hPSC have shown differences whether MEFs or HDFs were used; HDF grown cells had shown elongated colonies (Amit *et al.*, 2003; Khadun, 2013). It is unknown how the nuclear circularity of hPSCs, could affect their characteristics. Our data demonstrated that the NutriStem XF/FF™ medium, the medium with the most abnormalities and positioning disruption, had the least circular nuclei (Average of 0.62), whereas the TeSR2™ and Essential 8™ media - the most circular (Average of 0.71 for both categories). This suggests that perhaps with more genomic instability, the cells are less round in shape. It is difficult to speculate whether this is a direct effect of

the genomic instability in these cells or whether the cells are simply shaped in that way. However, the fact that the cells with the highest circularity (0.79) were grown in the TeSR2™ Laminin-521 condition, one of the worst conditions for the maintenance of pluripotent markers (personal correspondence with J. Man), suggests that it may be differentiation or cell type-specific. Despite some studies using nuclear shape as a prognostic discriminant (Mitmaker, Begin and Gordon, 1991), further studies into the different circularity of hPSCs is required to understand this.

5.5.4. Future Work

Despite the efforts of many researchers no perfect marker, gene or cell surface marker, has been identified to characterise the pluripotency of the cell and its ability to differentiate into all three lineages. Further investigation with chemically-defined culture conditions is required to investigate the effects of different media and matrices on human pluripotent stem cells.

Of all three media used in combinations with different matrices over time, TeSR2™ had demonstrated the most karyotypic stability for the cells, whereas NutriStem XF/FF - the least.

From personal correspondence with Dr Jennifer Man, we know that the TeSR2™ Matrigel® combination did not work well in terms of its *NANOG* and *OCT4* expression (by flow cytometry), whereas the NutriStem XF/FF and Essential 8™ Laminin-511 or -521 worked very well with over 80% of the cells being positive for both markers. Additionally, Drs Nowell and Man's data has also shown good differentiation potential of the cells from NutriStem XF/FF and Essential 8™ Laminin-511 or -521 combinations when looking at qPCR gene expression for lineage specific genes after EB formation. This suggests that despite the normal ratio of *AMELX* to *ALB* that we observed on the ddPCR™ of the TeSR2™ combinations, the cells are in reality not stem cells anymore and perhaps the gene positioning change from FISH data is an indicator of this change. The UKSCB had suggested that the NutriStem XF/FF™ and Essential 8™ Laminin-511 or -521 combinations could be investigated further to be used as a potential stable feeder-free expansion method. Laminin-511 and -521 matrices are becoming more popular due

to their reliability of maintained of hPSCs (Hongisto *et al.*, 2012, 2017; Albalushi *et al.*, 2017). From our data we found the NutriStem XF/FF™ combinations to be potentially the most genomically unstable, however whether these aberrations are too small to cause any phenotypic affect is unknown (Barber, 2005; Khadun, 2013). In addition, hPSCs are known for their genomic instability in culture (Brimble *et al.*, 2004; Maitra *et al.*, 2005; Amps *et al.*, 2011) and perhaps that is a characteristic that is normal for them, therefore a higher level of aneuploidies in hPSCs in comparison to somatic cells may be normal. Unfortunately, smaller aberrations found by cytogeneticists during G-banding are not always reported (Barber, 2005), as they are a frequent occurrence in the general human cell population and do not have an apparent phenotype (Khadun, 2013). Therefore, it is possible that these smaller aberrations normally would be regarded as insignificant and are reported more in stem cell culture documentation. More guidance for cytogeneticists is required for the appropriate standardisation of reporting of karyotypic abnormalities. And in addition, it is still vital, for researchers to understand the presence and effect of low-level aneuploidies in cell intended for therapeutic use. Further investigation into these different media and matrices combinations and their effects on the cells is required.

In addition, the media that were used for this study are not chemically-defined, so whether a specific growth factor or molecule in the medium or a combination of those factors with the matrix is good or bad for the cell culture, it is not possible to establish a straightforward answer without further information. Additionally, metabolomics analysis of the exchange media can be analysed to make sure none of the growth conditions used limit the cells due to either substrate loss or toxic accumulation. The metabolites in the media have an essential role in the regulation of stem cell fate (Ito and Suda, 2014; Vernardis *et al.*, 2017), epigenetic landscape, reprogramming (Kida *et al.*, 2015), (Sperber *et al.*, 2015) and differentiation (Bhute *et al.*, 2017). Such analysis can not only help understand specific molecules responsible for the maintenance of pluripotency, but can also promote the integration of new technology for the mass expansion of hPSCs (Silva *et al.*, 2015).

Chapter VI: The Impact of Aneuploidies on the Genomic Health of Human Pluripotent Stem Cells

6.1. Introduction

6.1.1. The Genomic Health of Human Pluripotent Stem Cells

In recent years, human pluripotent stem cells have been widely used in research laboratories and many advances have been made for their use in the clinic. However, the safety of the therapeutic use of hPSC is still debated, mainly due to the lack of understanding of their genomic health. As described before in Chapter I and V, human embryonic stem cell (hESCs) and induced pluripotent stem cells (iPSCs) are a good source of hPSC material, however they are prone to genomic instability, often with specific whole chromosome gains and losses. In addition, as the telomerase enzyme is active in these cells it is currently unknown how the cells' self-renewal capabilities can be controlled during clinical use. These characteristics, coupled with the lack of standard methods of culture for hPSCs, the lack of consistent assays for their characterisation and the lack of sensitive methods to detect potential aneuploidies in the culture, has contributed to the slow development of hPSCs as therapeutics.

Currently, very few studies have observed the chromatin organisation of both hESCs and iPSCs (Wiblin *et al.*, 2005; Bártová *et al.*, 2008). Although studies have demonstrated the general epigenetic profile of these cell types, they mainly describe histone modifications and methylation profiles in comparison to somatic cell types (Branco and Pombo, 2006; Meshorer *et al.*, 2006). These studies have been the basis of researchers suggesting the plasticity of the hPSC genome and it has been that speculated that it is because of this particular quality that hPSCs can differentiate into a wide range of different cell types.

To our knowledge, no study has observed interphase gene positioning, nuclear morphology and gene expression in hPSCs grown for extended periods under different growth conditions.

6.2. Aims

The aim of this chapter was to investigate the genomic health of the different sub-populations of the hESC cell line Shef2. The study was designed to grow the two cell sub-types over time in different conditions and monitor them using the different optimised technologies; ddPCR™, qPCR, FISH and IF, as well as RNA-Seq to monitor the global gene expression changes in the two cell lines. Our aim was to look at the different pathways up- and/or down-regulated between cell lines, different cell culture conditions, and the effect of time in culture.

6.3. Methods and Materials

6.3.1. Cell Culture and Methodology

The cell culture for the cell lines used in this study was performed by Drs Jennifer Man and Yvonne Pang. Human embryonic stem cell line, Shef2, was grown from two separate vials, one early passage at P19 and one later at P23. Although both vials were from the same original cell line, the early passage was from a master cell bank, referred to as masterShef2, and was banked as a clinical grade cell line, whereas the later was a research cell line, referred to as mShef2. For this study, both sub-cultures are referred to as separate cell lines, despite their shared origin.

The masterShef2 and mShef2 cell lines were grown in NutriStem XF/FF™ Culture Medium for Human iPS and ES Cells (STEMGENT, USA) and stabilised on human dermal fibroblasts (HDFs) as the feeder basement layer for four passages post-thaw, similar to Chapter V. Following this, each cell line was then divided into two; one continued to be cultured on the feeder cells, whereas the other was grown in non-feeder conditions, on Matrigel®. The Matrigel® basement layer was diluted in DMEM/F-12 with 15mM HEPES (STEMCELL Technologies, UK) as per manufacturer's guidelines. The NIBSC-5 iPSC line was established by the UKSCB from the MRC-9 primary human dermal fibroblasts. The cells were grown on standard 6-well plate in mTesR1 (STEMCELL Technologies) medium on a base of Matrigel®. All cell lines were enzymatically passaged using TrypLE Express Enzyme™ (ThermoFisher Scientific; as per Chapter II) and grown in 6-well plates in a 5% CO₂ atmosphere at 37°C. The medium was changed every 2-3 days and the cells passaged once a week and divided 1:6.

This study was designed similarly to Chapter V, however at each passage cells were collected for ddPCR™, FISH and IF. The cells were karyotyped at passage 5 post-seed (P5PS) by Sheffield Diagnostic Genetics Service (Sheffield Children's NHS Foundation Trust) for 30 metaphase cells. At P9PS to P11PS, qPCR and RNA-Seq was performed on the samples.

6.3.2. DNA/RNA Extraction

DNA was extracted using the GenElute DNA Extraction Kit (Sigma) as per Chapter II. For DNA quantification a Qubit 2.0 Fluorometer (Thermo Fisher Scientific, UK) was used, a Nanodrop ND-1000 (Thermo Fisher Scientific) was used to check the purity of the sample, and a TapeStation Bioanalyser or agarose gel was used to determine the DNA integrity.

For RNA extraction the Maxwell® RSC simplyRNA Cells Kit (Promega) and Maxwell® RSC Instrument (Promega) were used as per Chapter IV. For quantification and qualification of RNA, the QIAxpert (Qiagen) was used. To ensure the RNA was of high quality, an RNA Integrity Number (RIN) value of at least 8 was obtained following resolution on the TapeStation Bioanalyser (described in Chapter II).

6.3.3. Droplet Digital PCR and Fluorescence *In-situ* Hybridisation

The DNA from each passage was used for ddPCR™ analysis of genomic stability monitoring; using the AutoDG system to generate droplets. *AMELX* was labelled with FAM and *ALB* with VIC, as per Chapter II.

For gene positioning analysis, gene *AMELX* and *ALB* were labelled using nick translation and FISH was performed on each cell line at each passage. The Erosion script was run in IPlab, as per Chapter III.

6.3.4. Quantitative PCR

Quantitative PCR (qPCR) was performed on P9-P11PS for a number of pluripotency marker and lineage-specific markers; thresholds for these markers were set according to the standards previously established by the UKSCB (Table 6.1). The primers and probes were from ThermoFisher Scientific; the RT-qPCR was performed by the same conditions described in Chapter IV. Three separate wells from the 6-well plates were used as technical replicates. The same RNA samples were used for RNA-Seq analysis.

Table 6.1. Typical C_t Value Ranges for hPSCs, Day 7 EBs and Day 14 EBs

The expected C_t value ranges for the different cell types and different gene types measured by RT-qPCR. Global refers to the gene expression globally in all cell types, whereas Day 7 and Day 14 EBs refers to the pre-differentiated and differentiated embryoid body gene expression, respectively. This table was designed according to the quality control paperwork managed by the UKSCB.

Typical C _t Values Range						
Type	Gene	Assay ID	Global	hPSCs	Day 7 EBs	Day 14 EBs
Housekeeping	<i>ACTB</i>	Hs01060665_g1	15-18	15-16	16.5-17.5	17.18
	<i>GAPDH</i>	Hs02758991_g1	17-20	17-18.5	18.5-20	19-20
Self-renewal	<i>NANOG</i>	Hs04399610_g1	22-34	22-26	30.5-34	30-33
	<i>OCT4</i>	Hs04260367_gH	16-33	16.5-18.5	26-33	27-32
	<i>SOX2</i>	Hs01053049_s1	19-24	19.5-21.5	21-24	21-25
Ectoderm	<i>HES5</i>	Hs01387463_g1	20-31	30-36	20.5-25	22-27
	<i>NEUROD1</i>	Hs01922995_s1	22-36	31-36	23-30	22-29
	<i>PAX6</i>	Hs00240871_m1	20-33	26.5-33	20-27	21-29
Endoderm	<i>CXCR4</i>	Hs00607978_s1	24-33	28-33	24-24	24-27
	<i>FOXA2</i>	Hs00232764_m1	25-39	25-29	35-38	32-39
	<i>GATA6</i>	Hs00232018_m1	28-36	29-36	28-36	29-35
Mesoderm	<i>DCN</i>	Hs00754870_s1	28-39	34-39	31-36	28-34
	<i>NCAM1</i>	Hs00941830_m1	N/A	N/A	N/A	N/A
	<i>PECAM</i>	Hs00169777_m1	32-36	32-36	32-36	33-36
	<i>VIM</i>	Hs00185584_m1	17-22	18-20	18-20	17-20

6.3.5. Immunofluorescence and Micronuclei Counts

Coverslips were placed into the wells of each 6-well plate; feeders or Matrigel™ was placed on the coverslip followed by the hESCs cultures. Following one week in culture, the coverslips were washed with PBS and ice-cold methanol acetone 1:1 (v/v) was added for 5 min. The coverslips were then removed with forceps and washed for 5min three times in PBS. Immunofluorescence was performed for the lamins (A, C, B1 and B2) in conjunction with the pluripotency marker Nanog on both of the cell lines across passages P9-P11PS. Cellular distribution of lamin proteins was performed as per Chapter IV. The same dilutions as used previously for the lamin antibodies were employed in 1% (v/v) fetal calf serum (FCS) in PBS; for Nanog IF a chicken anti-Nanog from Abcam, UK was used at 1:200 (v/v) with the secondary antibody goat anti-chicken (Abcam) at 1:50 (v/v). For micronuclei scoring, 1000 cells were counted, and the number of micronuclei recorded.

6.3.6. RNA-Seq

TruSeq® Stranded mRNA RNA-Seq (Illumina, UK) was performed on the two cell lines on passages P9-11PS using the low samples (LS) protocol by Dr Martin Fritzsche (Department of Bioinformatics, NIBSC). The Illumina NextSeq 500 Sequencer was used. The same RNA samples were used to produce cDNA for the RT-qPCR described above. Three separate wells from the 6-well plates of the cell cultures were used to provide three biological replicates. This was performed for all 12 different samples, except “masterShef2 Matrigel™ P9PS”, where only one replicate was available due to the lack of cell growth at that timepoint. Dr Mark Preston (Department of Bioinformatics, NIBSC) performed the data normalisation and statistical analysis for the RNA-Seq samples.

6.3.6.1. RNA-Seq Data Analysis

The Illumina NextSeq 500 Sequencer was used to generate 75bp reads from the three biological replicates of each sample. Reads were mapped to the human reference genome GRCh37 using the TUXEDO software package. The Cuffdiff software was used to identify significant changes in transcript expression levels. Genes were filtered at the $\geq \log_5$ fold change threshold and pathways enrichment was analysed using the Cytoscape software (Shannon *et al.* 2003) with Reactome FI (Wu *et al.* 2010).

6.3.6.2. RNA-Seq QC

To ensure the RNA-Seq was producing accurate results, a QC report was produced. The quality of calls on most platforms will degrade as the run progresses, so it is common to see base calls falling into the orange area towards the end of a read. The high quality of the base call value scores are in green. See Appendix V for the raw FastQC files.

6.4. Results

The UKSCB reported that an in-house generated iPSC, known as NIBSC-5, developed pentasomal X aneuploidy at passage 10 (Appendix I). Dr Jennifer Man kindly provided us a sample from the original fibroblast cell line, MRC-9 at passage 9. The MRC-9 sample was from before it was reprogrammed to an iPSC, whereas the iPSC sample was from passage 20. A ddPCR™ experiment was performed to monitor the difference in the ratio of *AMELX* to *ALB* between the two samples. From Figure 6.1, we observe that the MRC-9 had two copies of *AMELX*, as would be expected for a female sample, whereas the NIBSC-5 was indeed aneuploid for chromosome X, but with an average ratio of 1.85, equivalent to 3.7 chromosome X copies per diploid genome.

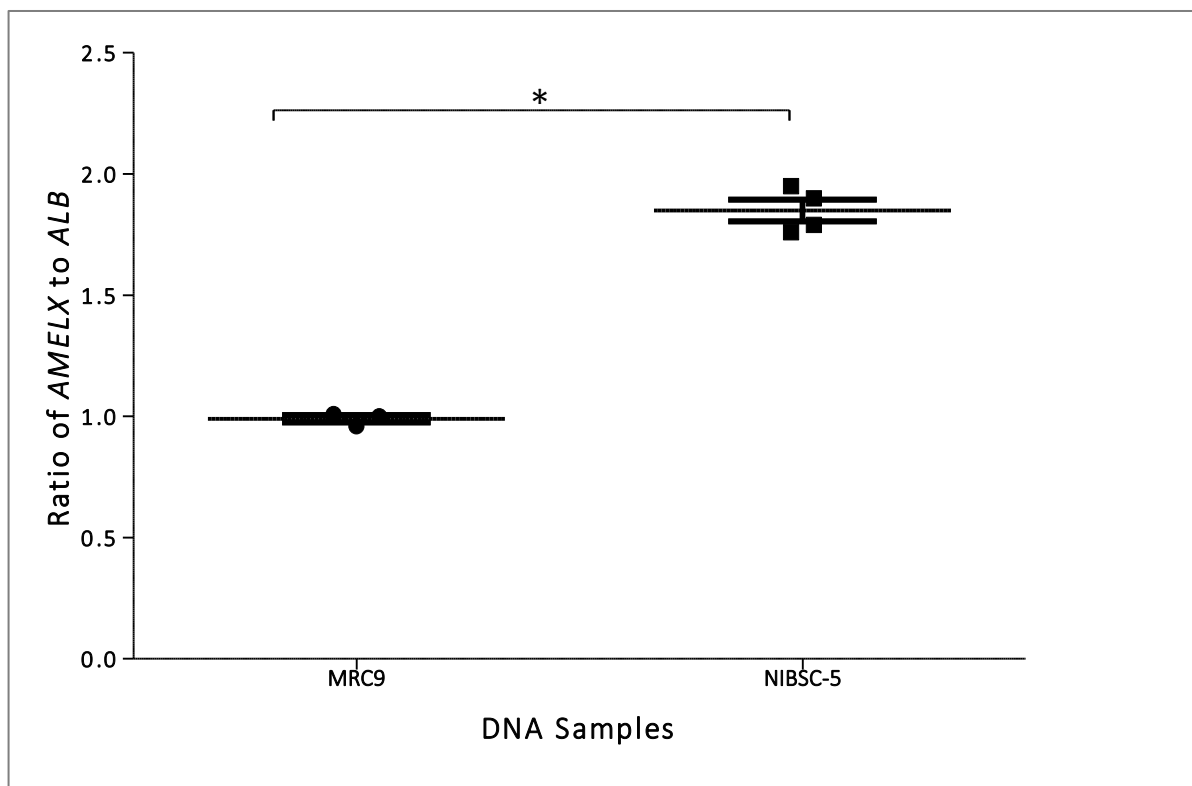


Figure 6.1. Scatter Plot of MRC9 and NIBSC-5 Ratio

The ratio of *AMELX* to *ALB* was calculated from MRC9 and NIBSC-5 cells. Data was extracted from the Quantasoft software. *AMELX* was labelled with FAM and *ALB* –VIC. Two-tailed t-test was calculated; significant difference is shown with an asterisk (*). An F-test was used to calculate the whether there was any significant difference between the variances of the two samples. The F-test showed no significant difference in variances; the t-test showed significant difference between samples.

From previously analysed results, we found that G-banding often produced inaccurate results, due to the poor resolution, therefore it may not be appropriate for the sensitive and high-throughput characterisation of hPSCs. We found in iPSC cell line NIBSC-5 pentasomal X had been reported via G-banding, however during our analysis by observing the ratio of *AMELX* to *ALB* via ddPCR™ the results were not accurate and indicative of mosaicism. For this reason, this last study was designed to grow two cell lines in parallel and using our different assays to characterise the genomic instability of hPSCs.

Embryonic stem cell line mShef2 was sent from the distribution vials for G-banding by the UK Stem Cell Bank at passage 32 and found complete monosomy for chromosome X (Appendix III). In addition, when the cell line was grown once more under different conditions NutriStem and Laminin-521™ at P28 and Essential 8™ and Laminin-511 at P28 they displayed 100% and 85% monosomy X, respectively (Appendix IV). Interestingly, when the mShef2 samples were grown on Essential 8™ and Laminin-511™ (Chapter V) for prolonged periods of time (P41), the G-banding results had shown the return of a complete diploid karyotype (46, XX; Appendix III). The clinical-grade cell line equivalent of mShef2, known here as masterShef2, displayed a normal karyotype according to personal correspondence with the UKSCB and from the records at the Human Pluripotent Stem Cell Registry, however due to the short time in culture these aberrations may not have become apparent at the time of G-banding. For this reason, we investigated the two cell lines in parallel combining all of the techniques developed in this PhD project.

6.4.1. Initial ddPCR™ Runs

Initially, to confirm that the mShef2 cell line the UKSCB was reporting as aneuploid for chromosome X was indeed fully aneuploid, a ddPCR™ run was performed to compare the ratio of *AMELX* to *ALB* (as seen in Chapter II). Late passage cells were supplied from the distribution bank vials provided by Sofia Spyrou from the UKSCB. The mShef2 cells are usually grown on HDFs, however in this case they were also grown on Matrigel™, therefore it was possible to compare the two samples side-by-side, along with the feeder cells the mShef2 cells were grown on. The HDF feeder cells have an XY karyotype,

therefore only one chromosome X would be present. Using the *AMELY* detection assay on the ddPCR™, the contribution of feeders could also be observed.

To look at how much material or how many cells the HDFs contribute to each well of the stem cells in culture, the ratio of *AMELX* to *AMELY* was observed in a ddPCR™ run with the same samples from Figure 6.3. The results confirmed that the HDFs had a ratio of 1 (Figure 6.2), as one copy of *AMELX* and one copy of *AMELY* are present, due to the XY karyotype. Additionally, the contribution of feeders in the mShef2 culture was 0.5%, whereas in the mShef2 and Matrigel™ sample, no *AMELY* was detected. Interestingly, a sample, where cells are manually picked from colonies, was provided from the UKSCB and was used to demonstrate how much carryover of HDFs occurs during the manual passage of hESC. Although not statistically significant, we observed a reduced carryover of the HDFs using manual cutting techniques; 0.3% of HDFs were detected in the ddPCR™ results.

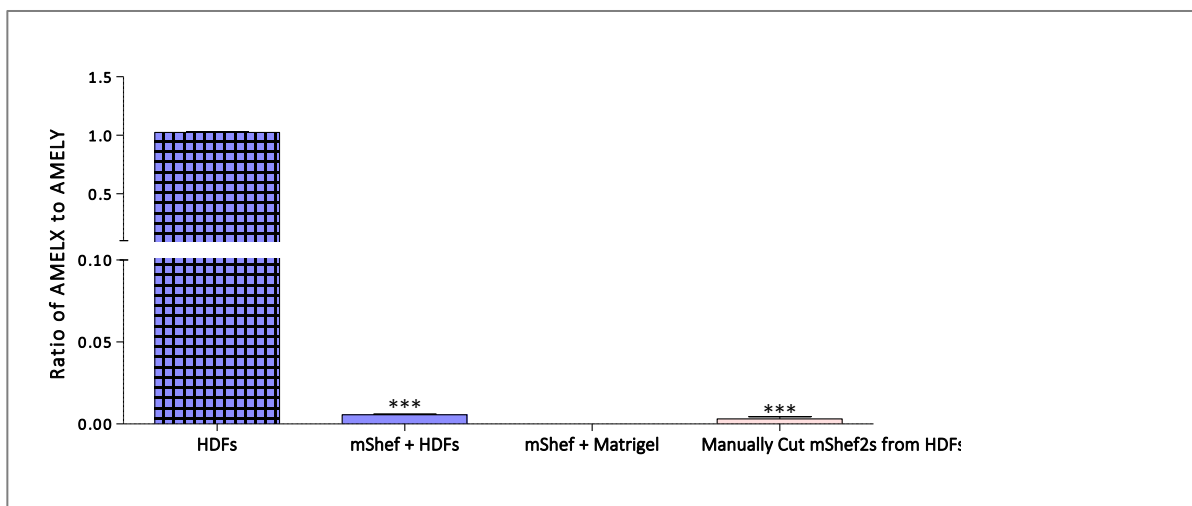


Figure 6.2. ddPCR™ Results for HDF Detection in Late Passage mShef2 Cells

ddPCR™ was performed on the HDFs, mShef2 cell line grown on both HDFs and Matrigel™ and on cells manually cut from HDFs during passage. mShef2 cells were at passage P43. The ratio of *AMELX* to *AMELY* observed in all of the samples. The asterisk symbols (***) signify the extremely statistically significant observed ($p < 0.001$) using a one-tailed t-test. No statistical analysis was performed on the mShef2 + Matrigel sample, as no HDFs were detected. The y-axis is segmented at 0.1 to highlight lower HDF values.

The ddPCR™ results demonstrated that the ratio of *AMELX* to *ALB* was 0.53 in mShef2 samples grown on both HDFs and Matrigel™ and in the HDF feeder cells and in addition, these samples were extremely statistically significant with a two-tailed t-test (Figure 6.3; $p < 0.001$). This suggests complete monosomy for chromosome X in these samples.

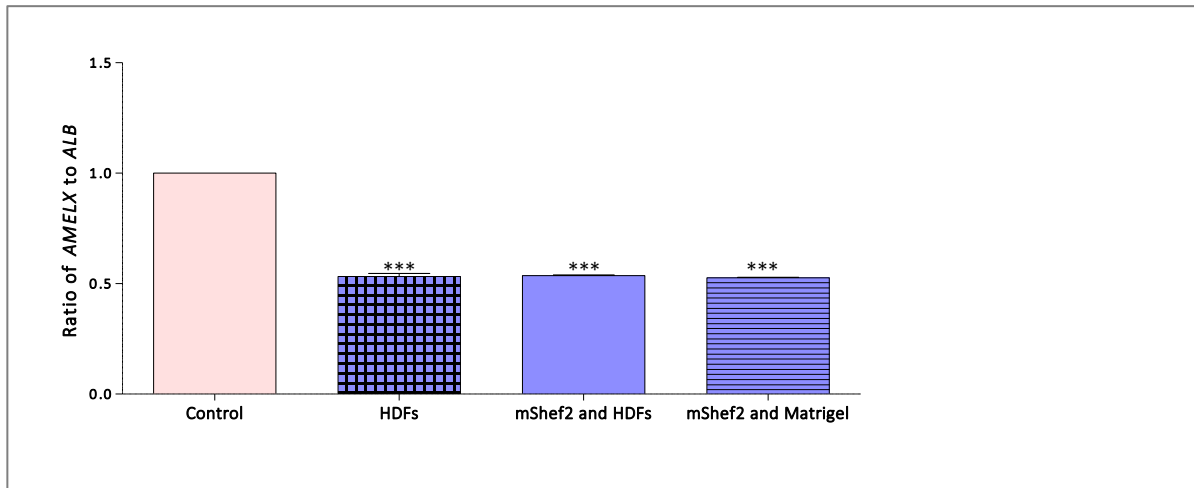


Figure 6.3. ddPCR™ Results for Aneuploidy Detection in Late Passage mShef2 Cells

ddPCR was performed on the mShef2 cell line grown on both HDFs and Matrigel™ and on the HDF cells to observe the ratio of *AMELX* to *ALB* versus the control. mShef2 cells were at passage P43, the control was the same as per Chapter II, a stock of female lymphoblastoid DNA was used. The asterisk symbols (***) signify the extremely statistically significant observed ($p < 0.001$) using a one-tailed t-test.

6.4.2. MasterShef2 and mShef2 ddPCR™ Results

The two embryonic stem cell lines masterShef2 and mShef2 were thawed at the same time and cultured in parallel to monitor the change in the genomic stability over time. The samples were referred to their passage number post-seed i.e. passage n post-seed (PnPS), n is the passage number. The first sample available for ddPCR™ was P2PS; a ddPCR™ run was performed for each following passage until P11PS; at P11PS, due to sample surplus two separate pellets of the two cell lines grown on HDFs were analysed. At P4PS, both cell lines were placed onto two different matrices, HDFs and Matrigel™, to study the effects of feeders and feeder-free conditions on genomic instability.

From Figure 6.4, we can observe the change in ratio of *AMELX* to *ALB* over time. A significant difference of ratio relative to the control was detected in the masterShef2 HDF samples at P4PS, P5PS, P6PS, P7PS and P9PS with approximately 6-60% increases in *AMELX*. Interestingly, the 58.33% increase detected at P9PS was not carried over to P10PS or P11PS. From the result, mShef2 displayed less incidence of significant difference to the control. P6PS in mShef2 HDF showed a 6.41 % decrease in *AMELX* and an 7.5% and 25.2% increase at P7PS and P11Ps in sample 1, respectively. MasterShef2 Matrigel™ showed a significant difference at P5PS, P10PS and P11PS in sample 1, where an increase of 8.14% and 6.64% was observed at P5PS and P11PS in sample 1 and a decrease of 41.29% at P10PS. For mShef2 grown on Matrigel™ at P11PS in sample 1 a 44.81% decrease was observed.

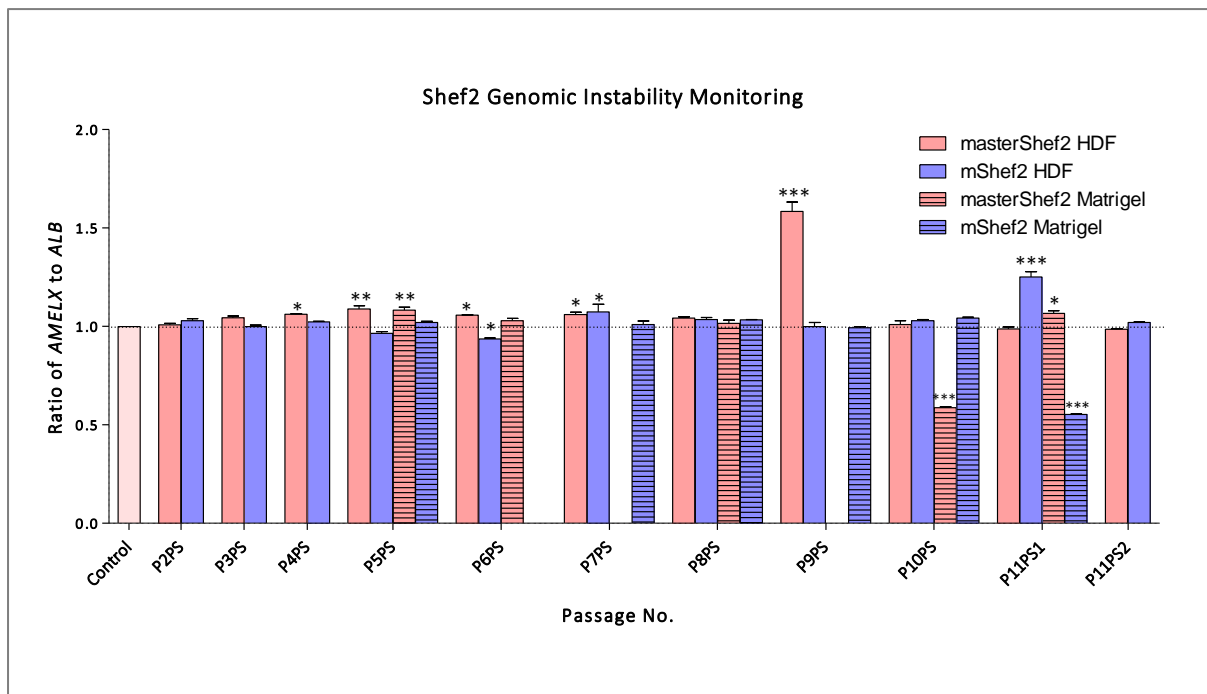


Figure 6.4. ddPCR™ Results for masterShef2 and mShef2

The two embryonic stem cell lines mastershef2 and mShef2 were grown in parallel over 11 passages. The two cell lines were grown on HDFs and Matrigel™ from P5PS. Statistical significance was calculated using a two-sample t-test and is shown using asterisks. The control was the same as per Chapter II, a stock of female lymphoblastoid DNA was used. The asterisk symbols (*, ** and ***) signify the statistically significant, very statistical significance and extremely statistical significance, respectively, using a one-tailed t-test.

6.4.3. Gene Positioning

Fluorescence *in-situ* hybridisation was performed to analyse interphase gene positioning on the two embryonic stem cells masterShef2 and mShef2 from passages P3PS to P11PS for the genes *AMELX* and *ALB*. Additionally, from P5PS the cells were grown on both HDFs and Matrigel™. In order to compare the two cell lines and the conditions accurately over time the interphase gene positioning results were divided into two parts; the first compares the two cell lines mastershef2 vs mShef2, whereas the second compares each cell line grown on HDFs and Matrigel™.

6.4.3.1. MasterShef2 vs mShef2

This study was performed to compare the two cell lines' gene positioning across each passage. From Figure 6.5, we have observed differences in positioning between samples and over time. In Figure 6.5

Panel A mastershef2 HDF had shown an interior positioning of *ALB*, whereas mShef2 HDF displayed a more intermediate positioning; a significant difference between the two samples in Shell 1 was observed. *ALB* positioning had stayed interior in P4PS in masterShef2 HDF and intermediate in mShef2 HDF (Figure 6.5 Panel C).

For *AMELX* positioning, a peripheral positioning was observed in masterShef2 HDF P3PS and a more intermediate positioning was observed in mShef2 HDF P3PS; a significant difference between the two samples in Shell 1 was observed (Figure 6.5 Panel B). For P4PS, masterShef2 HDF displayed a more bimodal distribution of *AMELX* positioning in the cell nuclei, whereas in mShef2 HDF it was more central (Figure 6.5 Panel D).

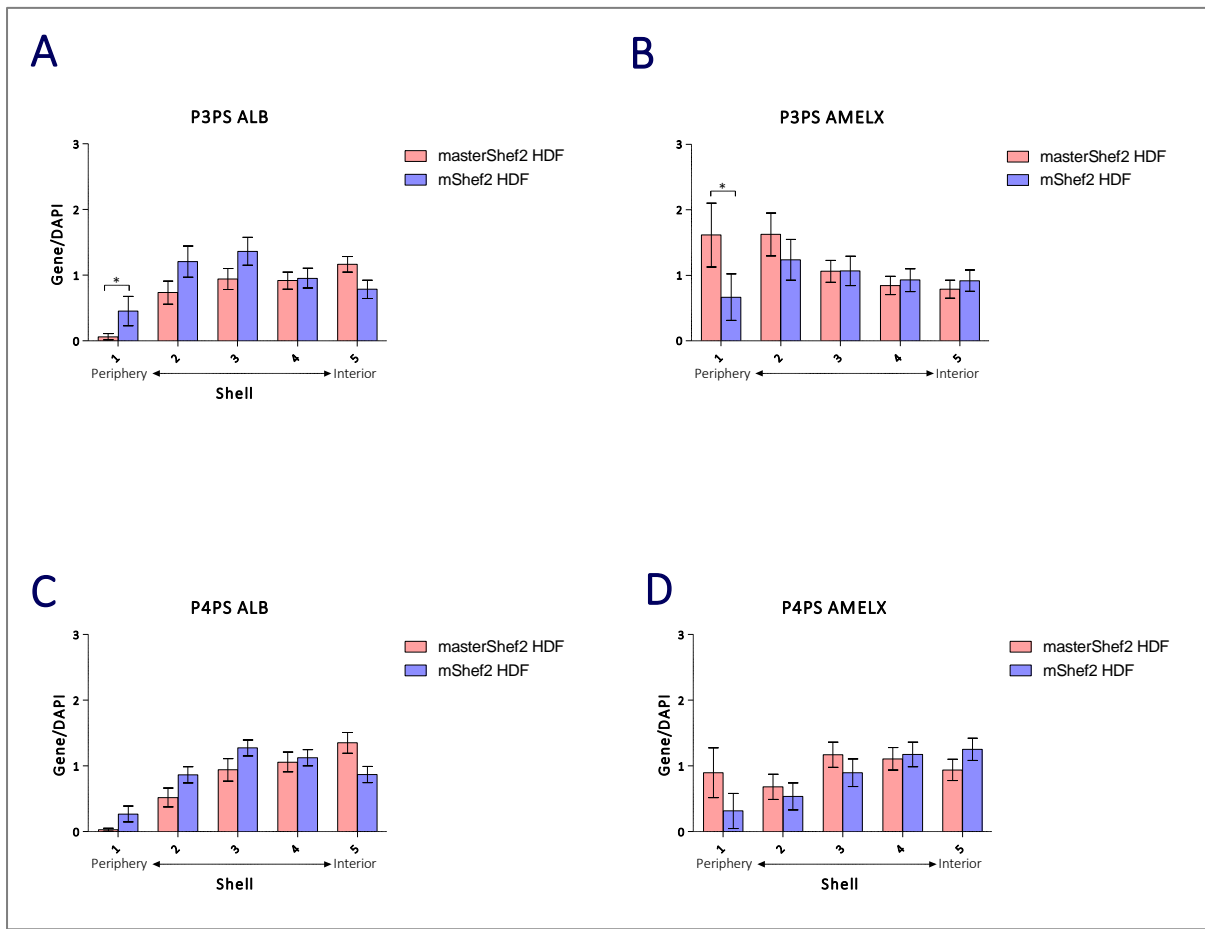


Figure 6.5. Fluorescence *in-situ* Hybridisation Results in P3PS-P4PS

FISH was performed for *ALB* and *AMELX* on masterShef2 and mShef2 grown on HDFs for P3PS and P4PS. A two-sample t-test was performed between each sample to P3PS to their corresponding shell and gene to observe any difference in positioning over time. A two-sample t-test was also performed between the two embryonic stem cell samples to observe any difference in positioning between the two cell lines. The asterisk symbol (*) signifies statistical difference observed over time, whereas an asterisk with a line above shows the statistical significance between the two samples. Standard error of mean is shown as error bars.

From the results displayed in Figure 6.6 Panel A, masterShef2 HDF shifted to a bimodal distribution of *ALB* positioning in the nuclei with a large amount of gene signal from the intermediate and interior shell; mShef2 HDF, on the other hand, shifted to an interior positioning, compared to the previous passage, where intermediate positioning of *ALB* was observed. Their counterparts grown on Matrigel™ displayed bimodal distribution toward the periphery and Shell 4 for masterShef2 and mShef2 on Matrigel™, respectively (Figure 6.6 Panel B).

For *AMELX* positioning, a bimodal peripheral positioning was observed in masterShef2 HDF P5PS and a peripheral organisation was displayed in mShef2 HDF P5PS (Figure 6.6 Panel C). For P5PS samples grown on Matrigel™, masterShef2 displayed an intermediate positioning of *AMELX*, whereas mShef2 displayed a random distribution mainly in intermediate shells of the nuclei (Figure 6.6 Panel D).

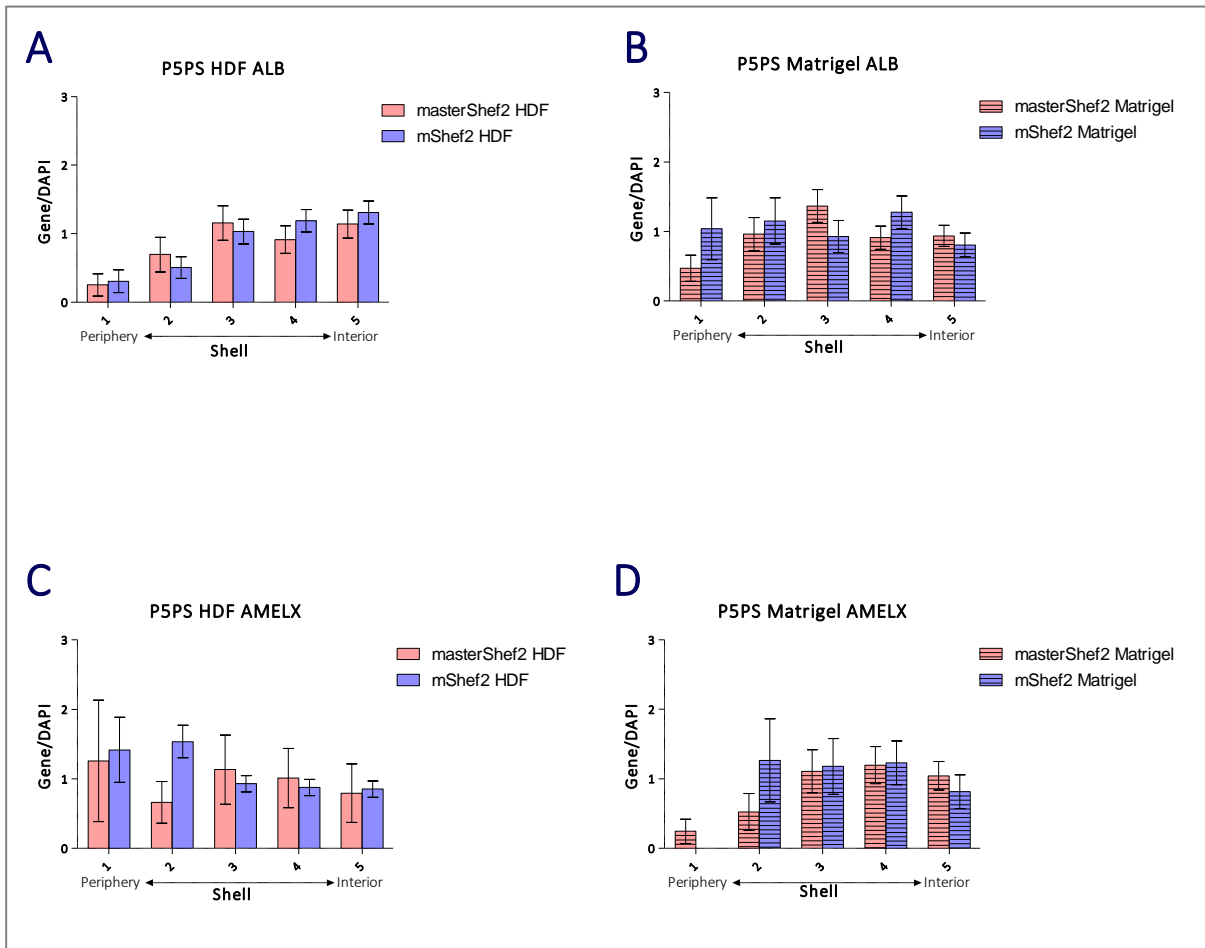


Figure 6.6. Fluorescence *in-situ* Hybridisation Results in P5PS

FISH was performed for *ALB* and *AMELX* on masterShef2 and mShef2 grown on HDFs and Matrigel™ for P5PS. A two-sample t-test was performed between each sample to P3PS to their corresponding shell and gene to observe any difference in positioning over time. A two-sample t-test was also performed between the two embryonic stem cell samples to observe any difference in positioning between the two cell lines. Standard error of mean is shown as error bars.

From the results displayed in Figure 6.7 Panel A, a peripheral positioning of *ALB* was observed in both masterShef2 and mShef2 HDF samples P6PS, however for the Matrigel™ counterparts a more intermediate positioning was observed for the two samples with significant differences observed in Shells 1, 2 and 4 (Figure 6.7 Panel B).

For *AMELX* positioning, a bimodal positioning was displayed in both masterShef2 HDF and mShef2 HDF at P6PS (Figure 6.7 Panel C). For P6PS samples grown on Matrigel™, masterShef2 displayed a bimodal distribution of *AMELX* at the periphery and in the intermediate shells of the nuclei, whereas mShef2 displayed intermediate positioning (Figure 6.7 Panel D).

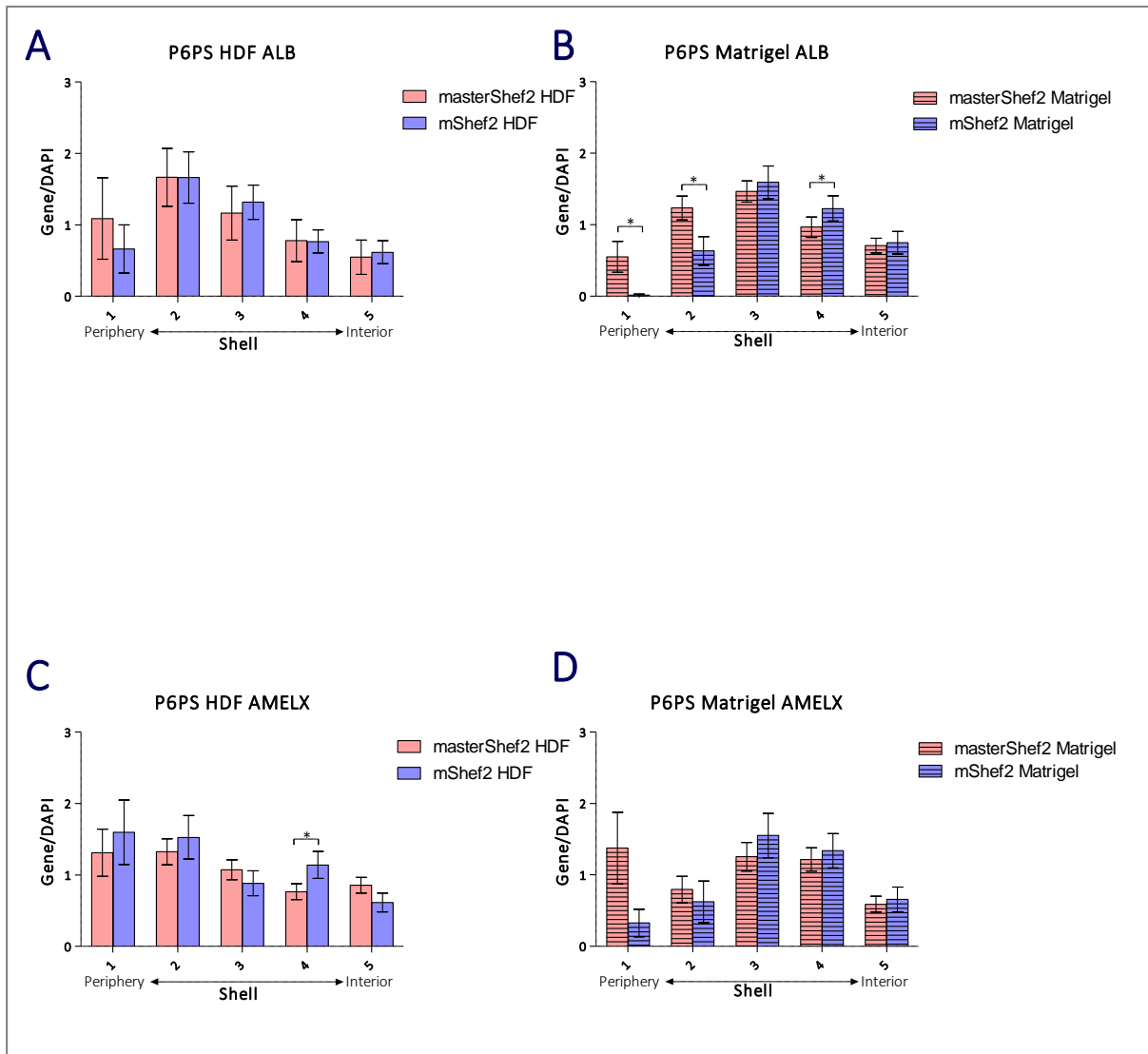


Figure 6.7. Fluorescence *in-situ* Hybridisation Results in P6PS

FISH was performed for *ALB* and *AMELX* on masterShef2 and mShef2 grown on HDFs and Matrigel™ for P6PS. A two-sample t-test was performed between each sample to P3PS to their corresponding shell and gene to observe any difference in positioning over time. A two-sample t-test was also performed between the two embryonic stem cell samples to observe any difference in positioning between the two cell lines. The asterisk symbol (*) signifies statistical difference observed over time, whereas an asterisk with a line above shows the statistical significance between the two samples. Standard error of mean is shown as error bars.

At P7PS, masterShef2 HDF displayed an intermediate positioning of *ALB*, whereas mShef2 HDF – peripheral; significant difference was observed between the two samples in Shell 2 (Figure 6.8 Panel A). Interestingly, the significant difference in Shell 2 remained between masterShef2 and mShef2 Matrigel™ samples; however, both samples displayed a more random positioning of *ALB* compared to when they were grown on HDFs (Figure 6.8 Panel B).

AMELX positioning, on the other hand, was peripheral for masterShef2 HDF and bimodal, mainly peripheral for mShef2 HDF; significant difference was observed between the two cell lines in Shell 2 (Figure 6.8 Panel C). For *AMELX* positioning in the two cell lines grown on Matrigel™, only mShef2 results were available and displayed a peripheral positioning (Figure 6.8 Panel D).

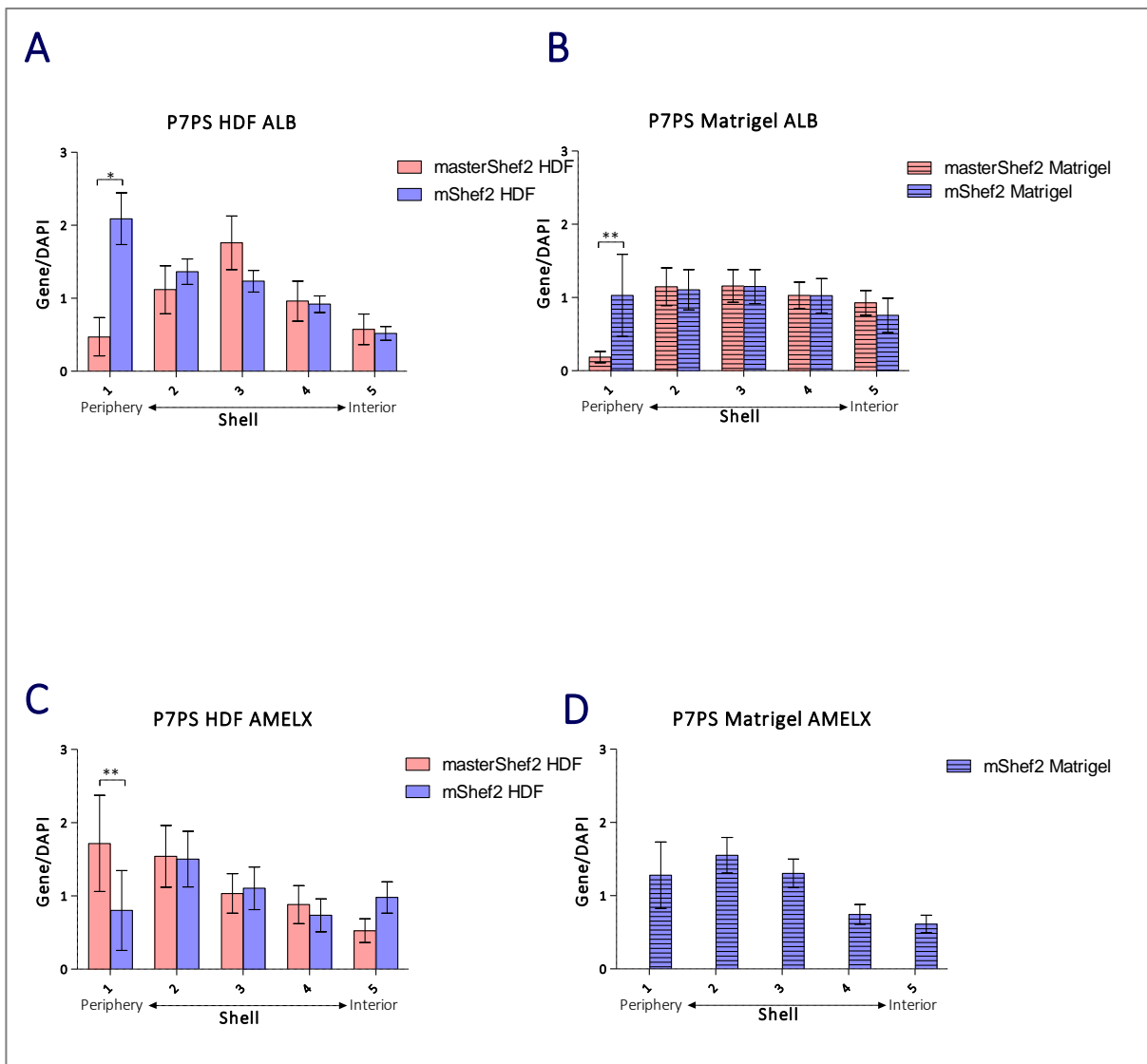


Figure 6.8. Fluorescence *in-situ* Hybridisation Results in P7PS

FISH was performed for *ALB* and *AMELX* on masterShef2 and mShef2 grown on HDFs and Matrigel™ for P7PS. A two-sample t-test was performed between each sample to P3PS to their corresponding shell and gene to observe any difference in positioning over time. A two-sample t-test was also performed between the two embryonic stem cell samples to observe any difference in positioning between the two cell lines. The asterisk symbol (*) signifies statistical difference observed over time, whereas an asterisk with a line above shows the statistical significance between the two samples. Due to lack of sample of masterShef2 Matrigel™ at P7PS, no FISH was performed (Panel D). Standard error of mean is shown as error bars.

At P8PS, *ALB* positioning was intermediate and bimodal for masterShef2 and mShef2 HDF, respectively (Figure 6.9 Panel A), whereas for Matrigel™ intermediate positioning was displayed (Figure 6.9 Panel B). For *AMELX* positioning, interior positioning was displayed in masterShef2 HDF nuclei and peripheral for mShef2 HDF nuclei; significant difference was observed between the two samples in Shells 1, 2 and 5 (Figure 6.9 Panel C). For the samples grown on Matrigel™, masterShef2 expressed interior positioning and mShef2- intermediate positioning (Figure 6.9 Panel D).

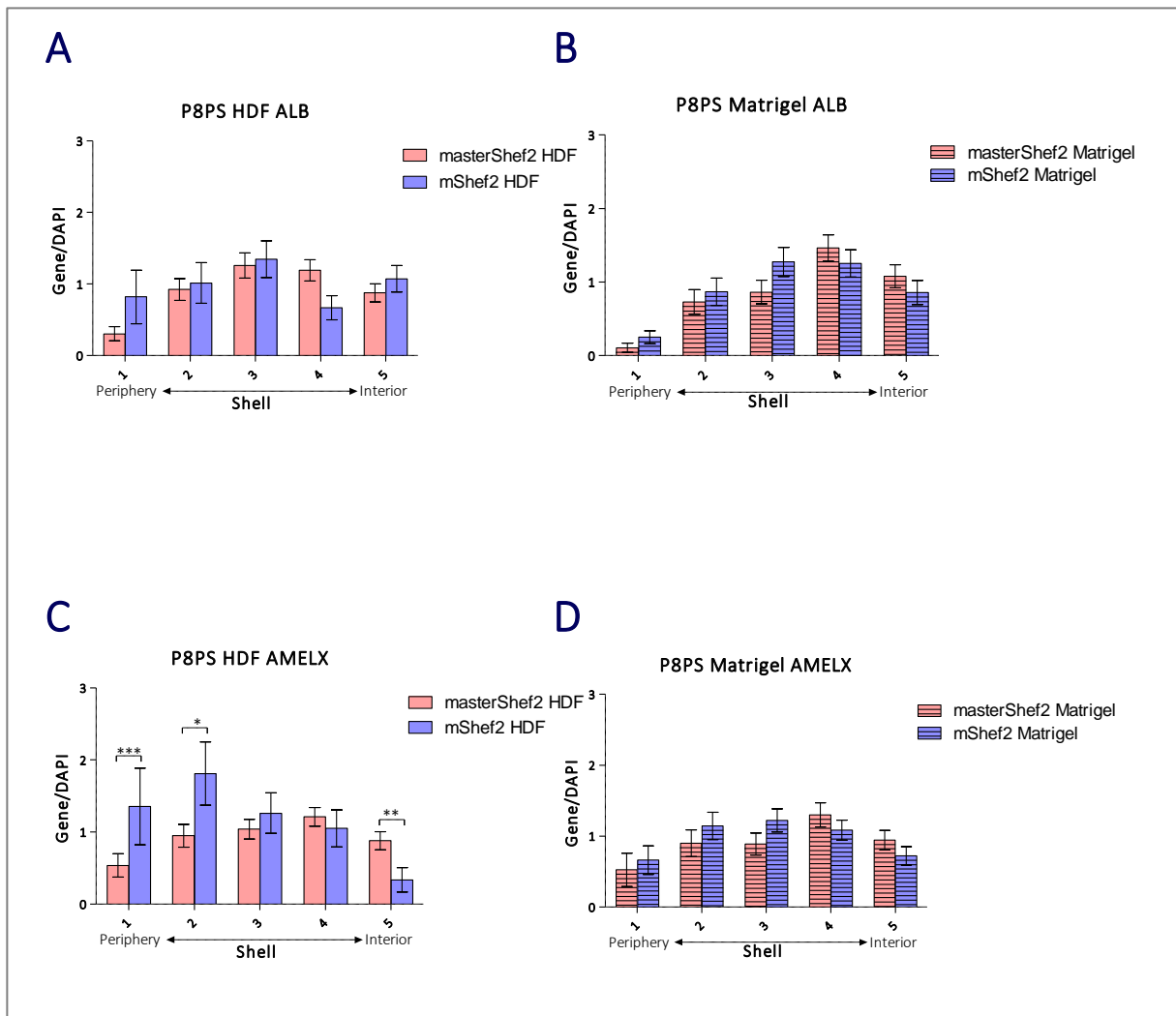


Figure 6.9. Fluorescence *in-situ* Hybridisation Results in P8PS

FISH was performed for *ALB* and *AMELX* on masterShef2 and mShef2 grown on HDFs and Matrigel™ for P8PS. A two-sample t-test was performed between each sample to P8PS to their corresponding shell and gene to observe any difference in positioning over time. A two-sample t-test was also performed between the two embryonic stem cell samples to observe any difference in positioning between the two cell lines. The asterisk symbol (*) signifies statistical difference observed over time, whereas an asterisk with a line above shows the statistical significance between the two samples. Standard error of mean is shown as error bars.

At P9PS, *ALB* positioning was bimodal and central for masterShef2 and mShef2 HDF, respectively (Figure 6.10 Panel A), whereas for Matrigel™ peripheral and intermedia positioning was displayed in masterShef2 and mShef2 samples, respectively (Figure 6.10 PanelB). For *AMELX* positioning, bimodal peripheral positioning was displayed in masterShef2 HDF nuclei and bimodal for mShef2 HDF nuclei; significant difference was observed between the two samples in Shell 1 (Figure 6.10 Panel C). For the samples grown on Matrigel™, masterShef2 and mShef2 nuclei exhibited random positioning (Figure 6.10 Panel D).

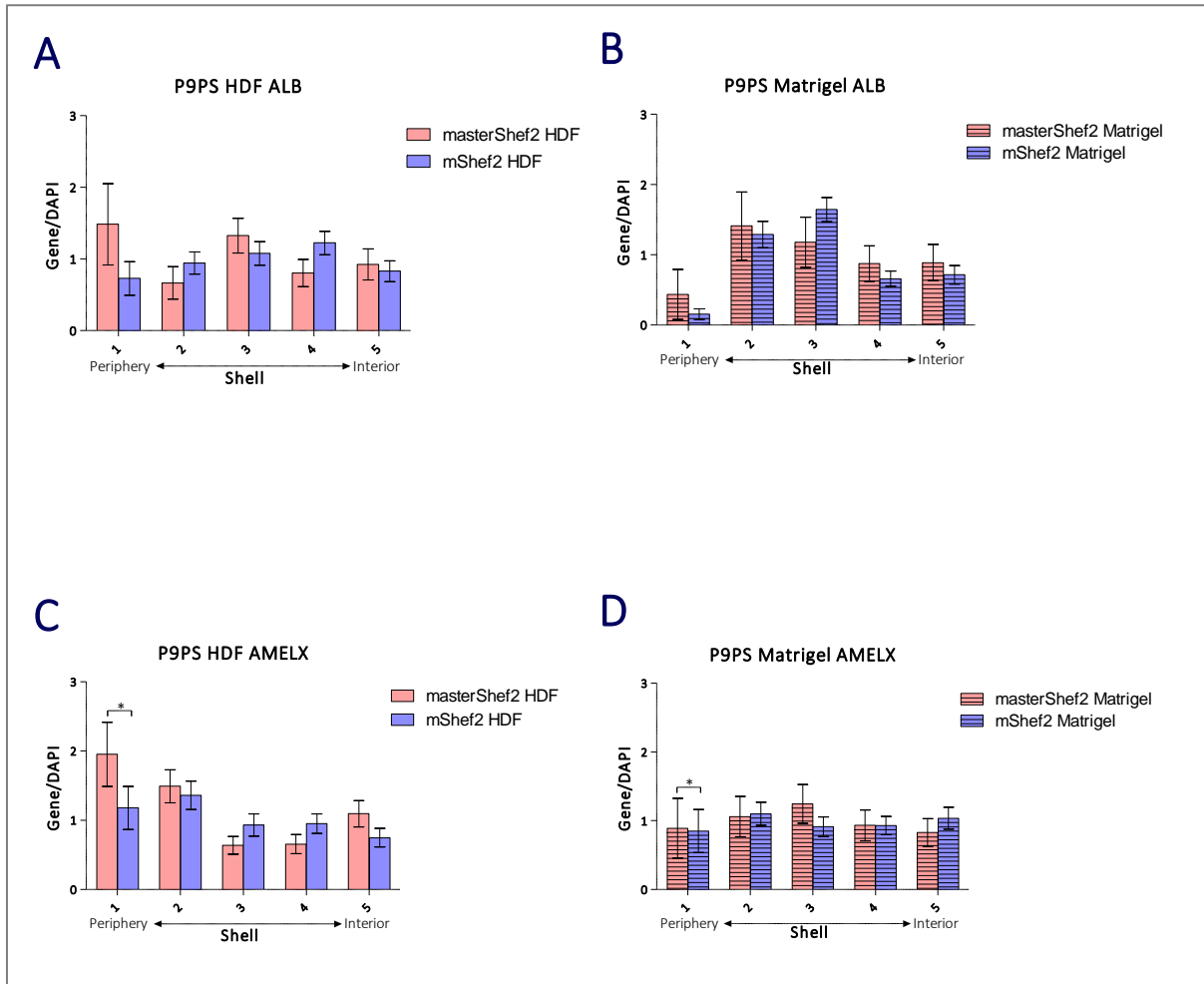


Figure 6.10. Fluorescence *in-situ* Hybridisation Results in P9PS

FISH was performed for *ALB* and *AMELX* on masterShef2 and mShef2 grown on HDFs and Matrigel™ for P9PS. A two-sample t-test was performed between each sample to P3PS to their corresponding shell and gene to observe any difference in positioning over time. A two-sample t-test was also performed between the two embryonic stem cell samples to observe any difference in positioning between the two cell lines. The asterisk symbol (*) signifies statistical difference observed over time, whereas an asterisk with a line above shows the statistical significance between the two samples. Standard error of mean is shown as error bars.

ALB positioning in masterShef2 and mShef2 HDF samples were peripheral (Figure 6.11 Panel A), whereas in the Matrigel™ condition masterShef2 was peripheral once more, however mShef2 showed a shift to a more interior positioning (Figure 6.11 Panel B). For *AMELX* positioning, masterShef2 HDF had a peripheral positioning and mShef2 HDF – bimodal (Figure 6.11 Panel C), however in the Matrigel™ condition, masterShef2 exhibited bimodal positioning, whereas mShef2 was intermediate; a very significant difference was observed between the two samples in Shell 1 (Figure 6.11 Panel D).

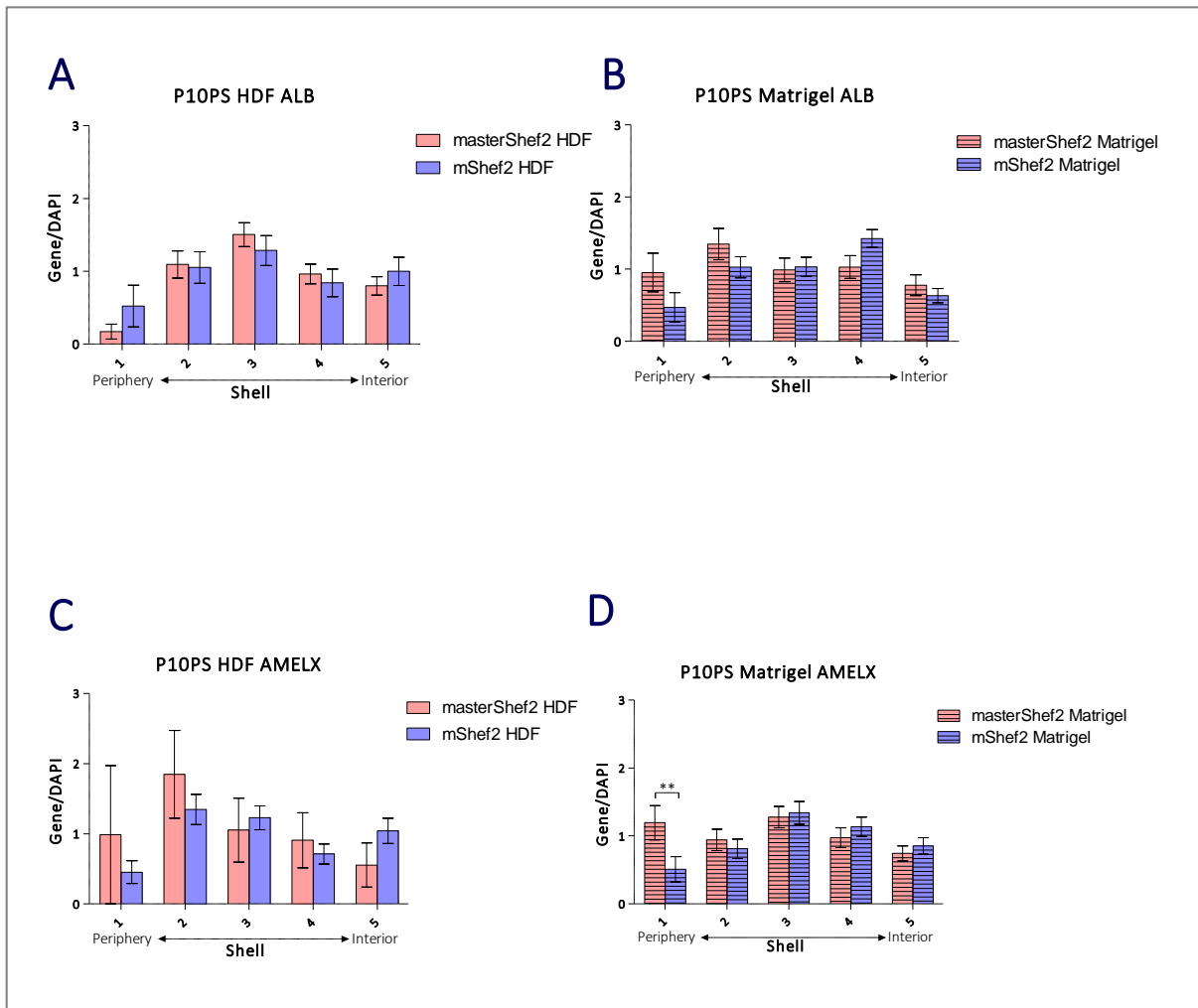


Figure 6.11. Fluorescence *in-situ* Hybridisation Results in P10PS

FISH was performed for *ALB* and *AMELX* on masterShef2 and mShef2 grown on HDFs and Matrigel™ for P10PS. A two-sample t-test was performed between each sample to P3PS to their corresponding shell and gene to observe any difference in positioning over time. A two-sample t-test was also performed between the two embryonic stem cell samples to observe any difference in positioning between the two cell lines. The asterisk symbol (*) signifies statistical difference observed over time, whereas an asterisk with a line above shows the statistical significance between the two samples. Standard error of mean is shown as error bars.

6.4.3.2. The Effects of HDFs Versus Matrigel™ on Gene Positioning

To compare the effects of different basement membranes on the gene positioning of hESCs, the two embryonic stem cell lines mastershef2 and mShef2 were plotted side-by-side with the two different conditions i.e. HDFs and Matrigel™. Statistical significance was calculated using two-sample t-tests between conditions for each cell line.

For *ALB* positioning in masterShef2 HDF and Matrigel™ bimodal intermediate and intermediate positioning was displayed, respectively, with no significant difference detected (Figure 6.12 Panel A), whereas for the mShef2 HDF and Matrigel™ conditions interior and bimodal positioning, respectively, was observed with significant differences in Shells 2 and 5 (Figure 6.12 Panel B). On the other hand, *AMELX* positioning showed bimodal peripheral and intermediate positioning in masterShef2 HDF and interior in masterShef2 Matrigel™ with significant difference detected in Shell 1 (Figure 6.12 Panel C). In mShef2, the HDF samples were peripheral, whereas in Matrigel™ it was intermediate (Figure 6.12 Panel D).

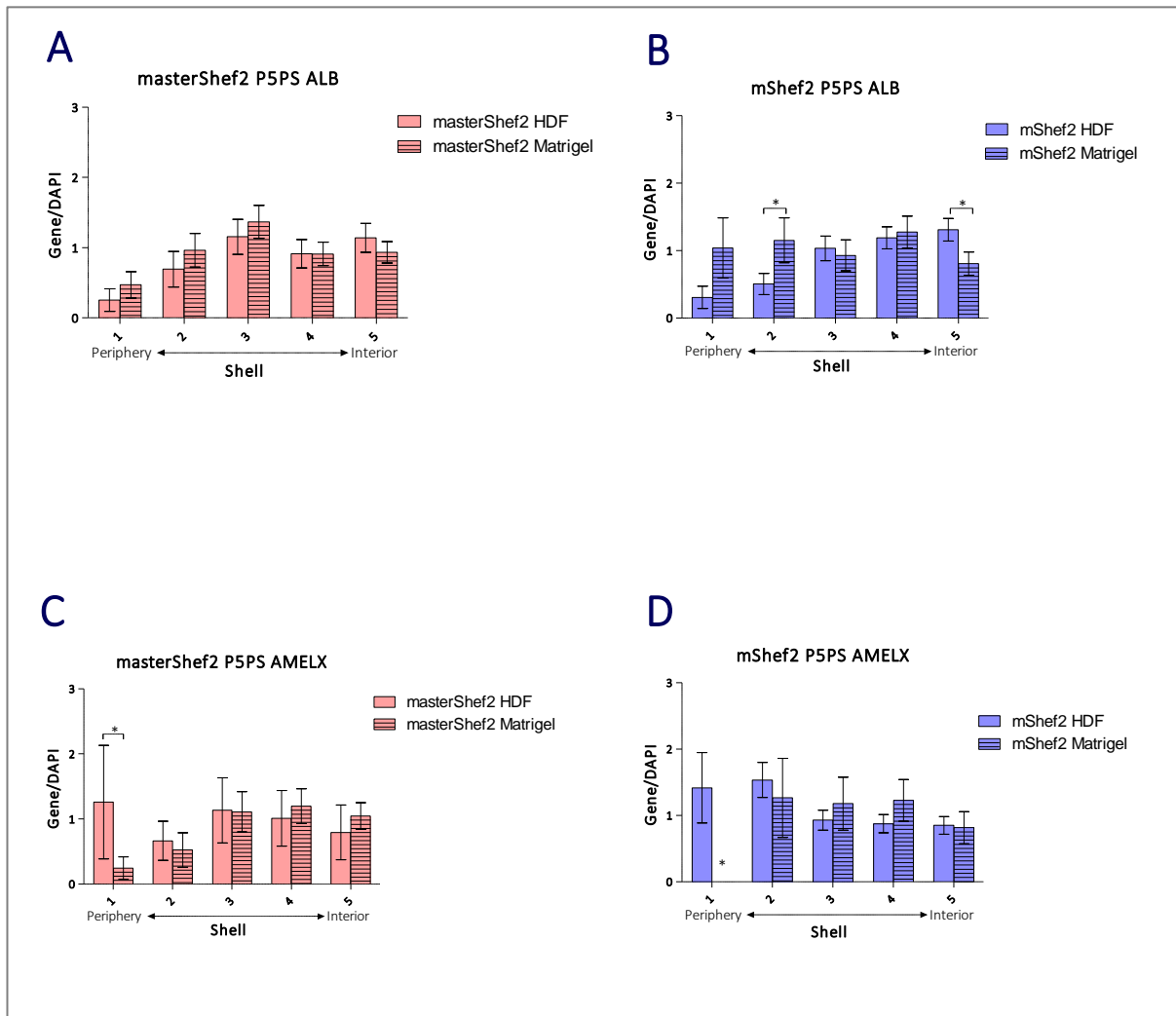


Figure 6.12. Fluorescence *in-situ* Hybridisation Results in P5PS

FISH was performed for *ALB* and *AMELX* on masterShef2 and mShef2 grown on HDFs and Matrigel™ for P5PS. A two-sample t-test was performed for each cell line between the different conditions to observe any difference between the two basement membranes. The asterisk symbol (*) signifies statistical difference observed over time, whereas an asterisk with a line above shows the statistical significance between the two conditions. Standard error of mean is shown as error bars.

For *ALB* positioning, masterShef2 HDF and Matrigel™ displayed peripheral and intermediate positioning, respectively (Figure 6.12 Panel A). Significant differences over time (compared to P3PS corresponding samples) were detected in Shell 2 and 5 for masterShef2 HDF and Shells 2, 3 and 5 for masterShef2 Matrigel. For mShef2, *ALB* positioning in the HDF conditions was peripheral and for Matrigel™ - intermediate; significant difference was observed in Shell 1 and very significant difference in Shell 2 (Figure 6.12 Panel B).

For *AMELX* positioning, peripheral and bimodal central and peripheral positioning was observed in masterShef2 HDF and Matrigel™, respectively. Additionally, a statistically significant difference was observed using a two-sample t-test between the two conditions for Shell 2 and a very statistically significant difference in Shell 4 (Figure 6.12 Panel C). In mShef2 HDF and Matrigel samples a peripheral and intermediate positioning of *AMELX* was revealed with significant difference in Shell 1 (Figure 6.12 Panel D).

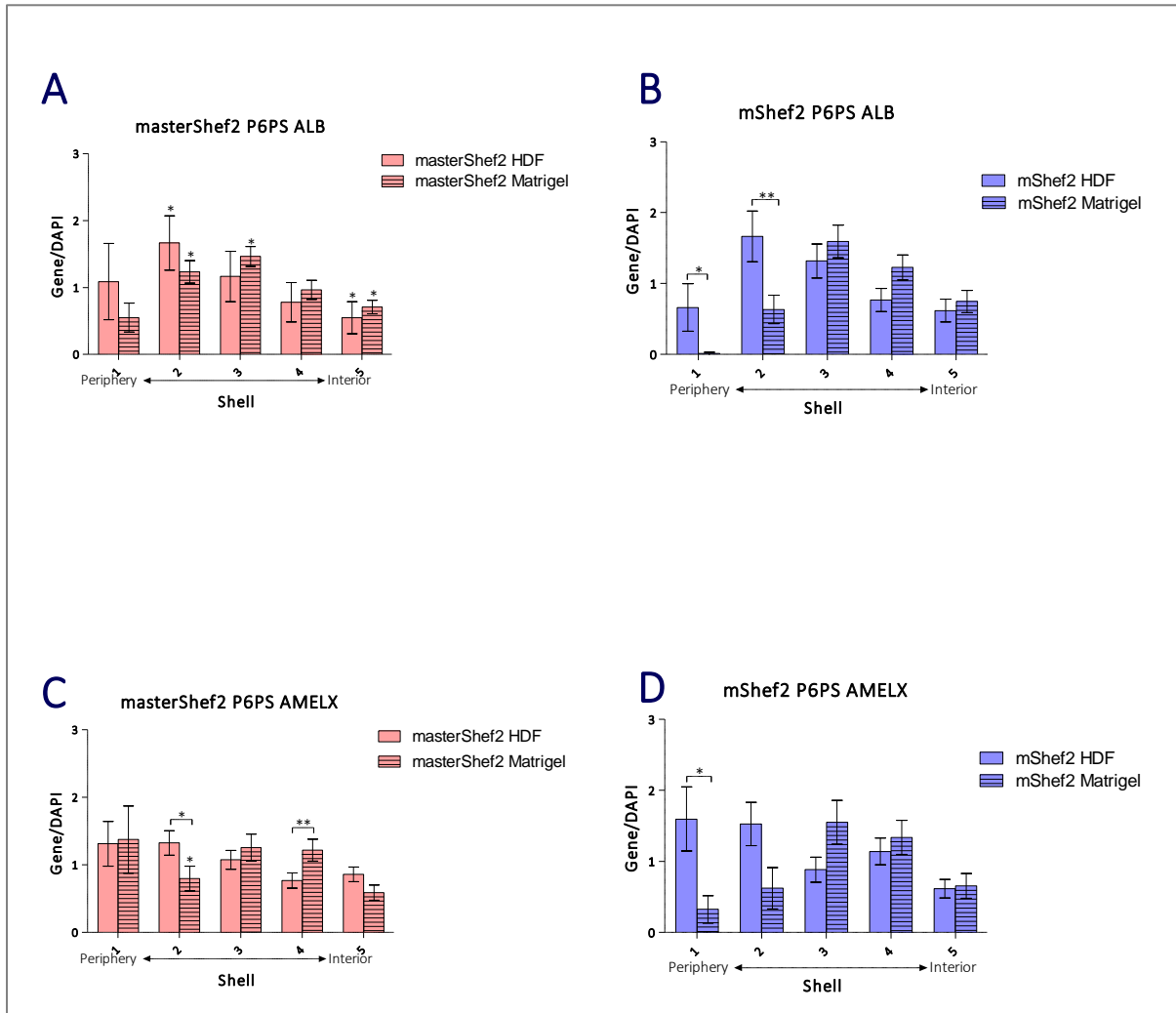


Figure 6.13. Fluorescence *in-situ* Hybridisation Results in P6PS

FISH was performed for *ALB* and *AMELX* on masterShef2 and mShef2 grown on HDFs and Matrigel™ for P6PS. A two-sample t-test was performed for each cell line between the different conditions to observe any difference between the two basement membranes. The asterisk symbol (*) signifies statistical difference observed over time, whereas an asterisk with a line above shows the statistical significance between the two conditions. Standard error of mean is shown as error bars.

In masterShef2 HDF and Matrigel™ samples at P7PS, an intermediate and bimodal central positioning of *ALB* was observed, respectively. For mastershef2 HDF significant difference over time (compared to P3PS corresponding samples) were detected in Shells 3 and 5 (Figure 6.14 Panel A). For mShef2, *ALB* positioning in the HDF condition was peripheral and for Matrigel™ - intermediate; a very significant difference was observed in Shell 1 (Figure 6.14 Panel B). For *AMELX*, masterShef2 HDF, mShef2 HDF and mShef2 Matrigel™ all displayed peripheral positioning (Figure 6.14 Panel C and D).

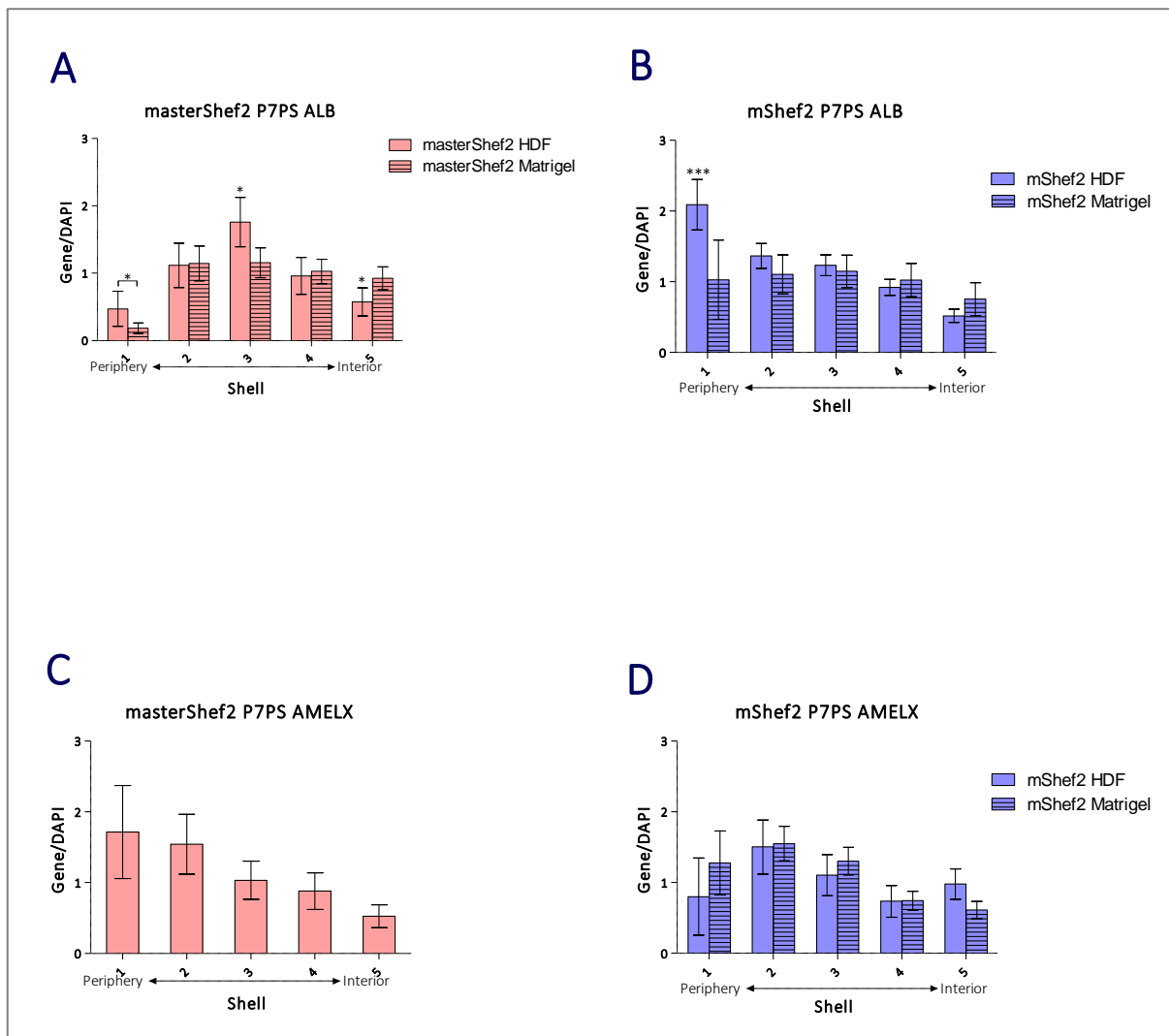


Figure 6.14. Fluorescence *in-situ* Hybridisation Results in P7PS

FISH was performed for *ALB* and *AMELX* on masterShef2 and mShef2 grown on HDFs and Matrigel™ for P7PS. A two-sample t-test was performed for each cell line between the different conditions to observe any difference between the two basement membranes. The asterisk symbol (*) signifies statistical difference observed over time, whereas an asterisk with a line above shows the statistical significance between the two conditions. Standard error of mean is shown as error bars.

In masterShef2 HDF and Matrigel™ samples at P8PS, an intermediate and central positioning of *ALB* was observed, respectively. For mastershef2 Matrigel™ significant difference over time (compared to P3PS corresponding samples) were detected in Shell 4 (Figure 6.15 Panel A). For mShef2, *ALB* positioning in the HDF condition was bimodal peripheral and central, whereas for Matrigel™ it was peripheral (Figure 6.15 Panel B). For *AMELX*, masterShef2 HDF and Matrigel™ the nuclei displayed central positioning (Figure 6.15 Panel C). Using two-sample t-tests significant difference was observed over time (compared to P3PS corresponding samples) in masterShef2 HDF in Shell 1 , whereas in masterShef2 Matrigel™ significant idfference was detected in Shells 2 and 4.

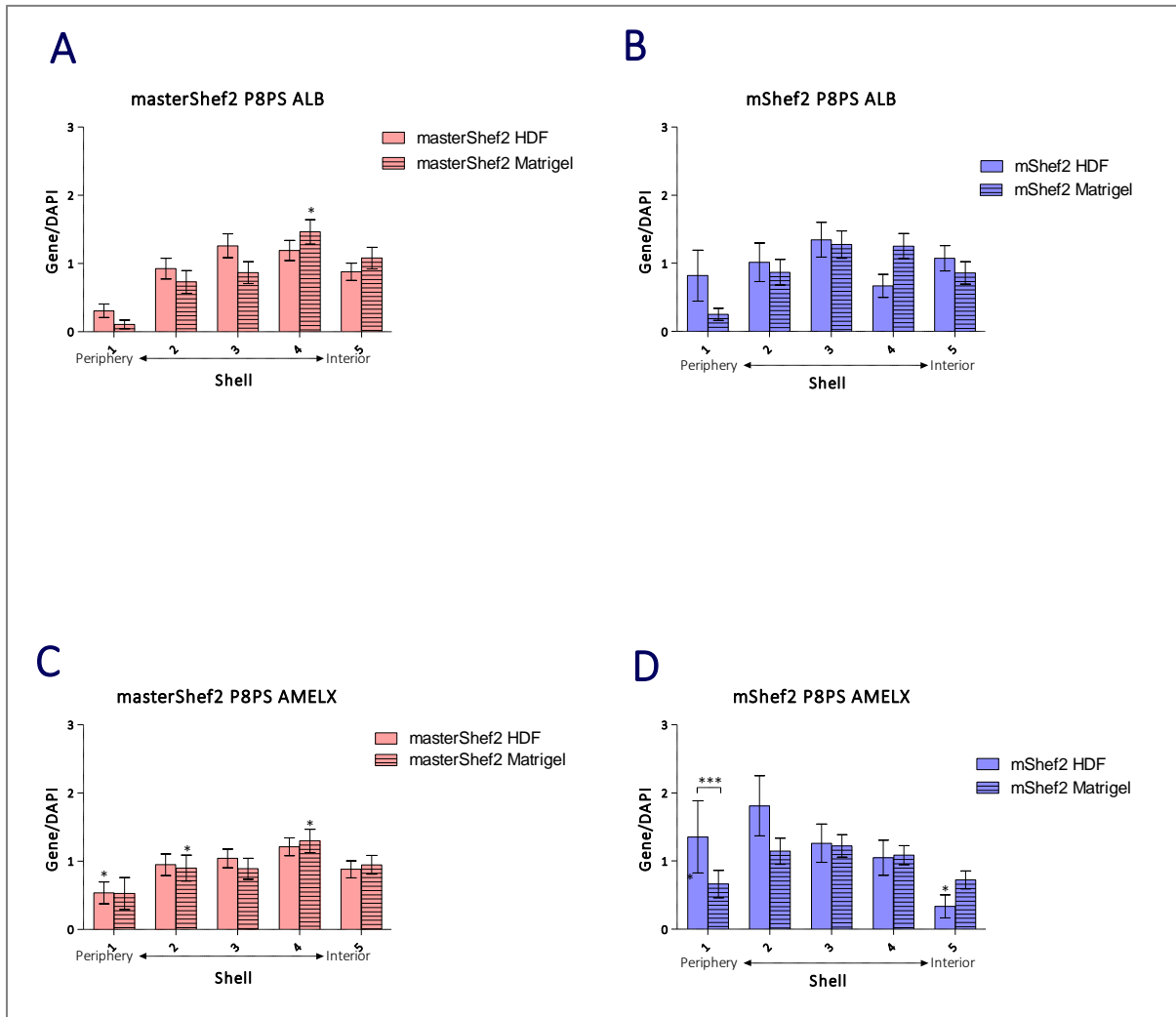


Figure 6.15. Fluorescence *in-situ* Hybridisation Results in P8PS

FISH was performed for *ALB* and *AMELX* on masterShef2 and mShef2 grown on HDFs and Matrigel™ for P8PS. A two-sample t-test was performed for each cell line between the different conditions to observe any difference between the two basement membranes. The asterisk symbol (*) signifies statistical difference observed over time, whereas an asterisk with a line above shows the statistical significance between the two conditions. Standard error of mean is shown as error bars.

For *ALB* positioning, masterShef2 HDF demonstrated bimodal peripheral and intermediate positioning with significant difference over time (compared to masterShef2 HDF P3PS) in Shell 3, whereas in masterShef2 Matrigel™ peripheral positioning was observed with significant difference in Shell 2 observed over time when compared to masterShef2 Matrigel™ P3PS (Figure 6.16 Panel A). In mShef2 HDF and Matrigel™ nuclei, intermedia positioning was observed with significant differences between the cell line grown on different basement membranes in Shells 1, 3 and 4 (Figure 6.16 Panel B).

For *AMELX* positioning, masterShef2 HDF showed bimodal peripheral and interior positioning, whereas for Matrigel™ is was intermediate; significant difference between the two conditions was observed in Shells 1 and 3 using a two-sample t-test (Figure 6.16 Panel C). Interestingly, random positioning was observed in mShef2 HDF and Matrigel™ (Figure 6.16 Panel D), significant difference was observed between the two conditions in Shell 1 (Figure 6.16 Panel D).

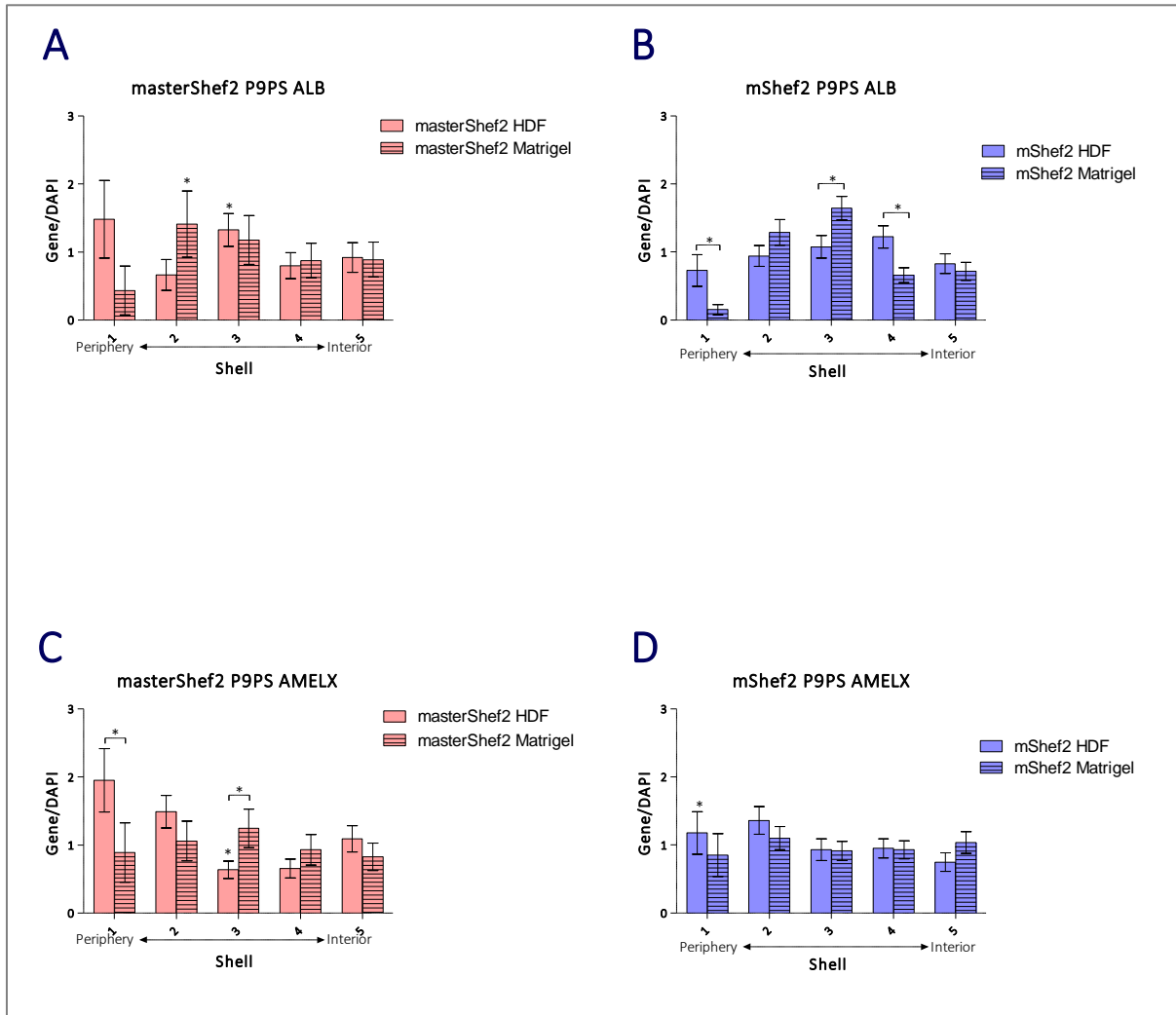


Figure 6.16. Fluorescence *in-situ* Hybridisation Results in P9PS

FISH was performed for *ALB* and *AMELX* on masterShef2 and mShef2 grown on HDFs and Matrigel™ for P9PS. A two-sample t-test was performed for each cell line between the different conditions to observe any difference between the two basement membranes. The asterisk symbol (*) signifies statistical difference observed over time, whereas an asterisk with a line above shows the statistical significance between the two conditions. Standard error of mean is shown as error bars.

In *ALB* positioning of masterShef2 HDF and Matrigel™ intermediate positioning was observed in the P10PS samples (Figure 6.17 Panel A). The masterShef2 HDF nuclei demonstrated significant differences in Shells 3 and 5 when compared to masterShef2 HDF P3PS nuclei, whereas in masterShef2 Matrigel™ this was observed in Shells 2 and 5. On the other hand, mShef2 HDF and Matrigel™ showed bimodal positioning and interior positioning, respectively (Figure 6.17 Panel B).

For *AMELX* positioning, masterShef2 HDF and masterShef2 Matrigel™ exhibited peripheral and bimodal intermediate positioning, respectively (Figure 6.17 Panel C). In comparison, mShef2 HDF and Matrigel™ nuclei showed bimodal peripheral and central positioning and intermediate positioning, respectively (Figure 6.17 Panel D).

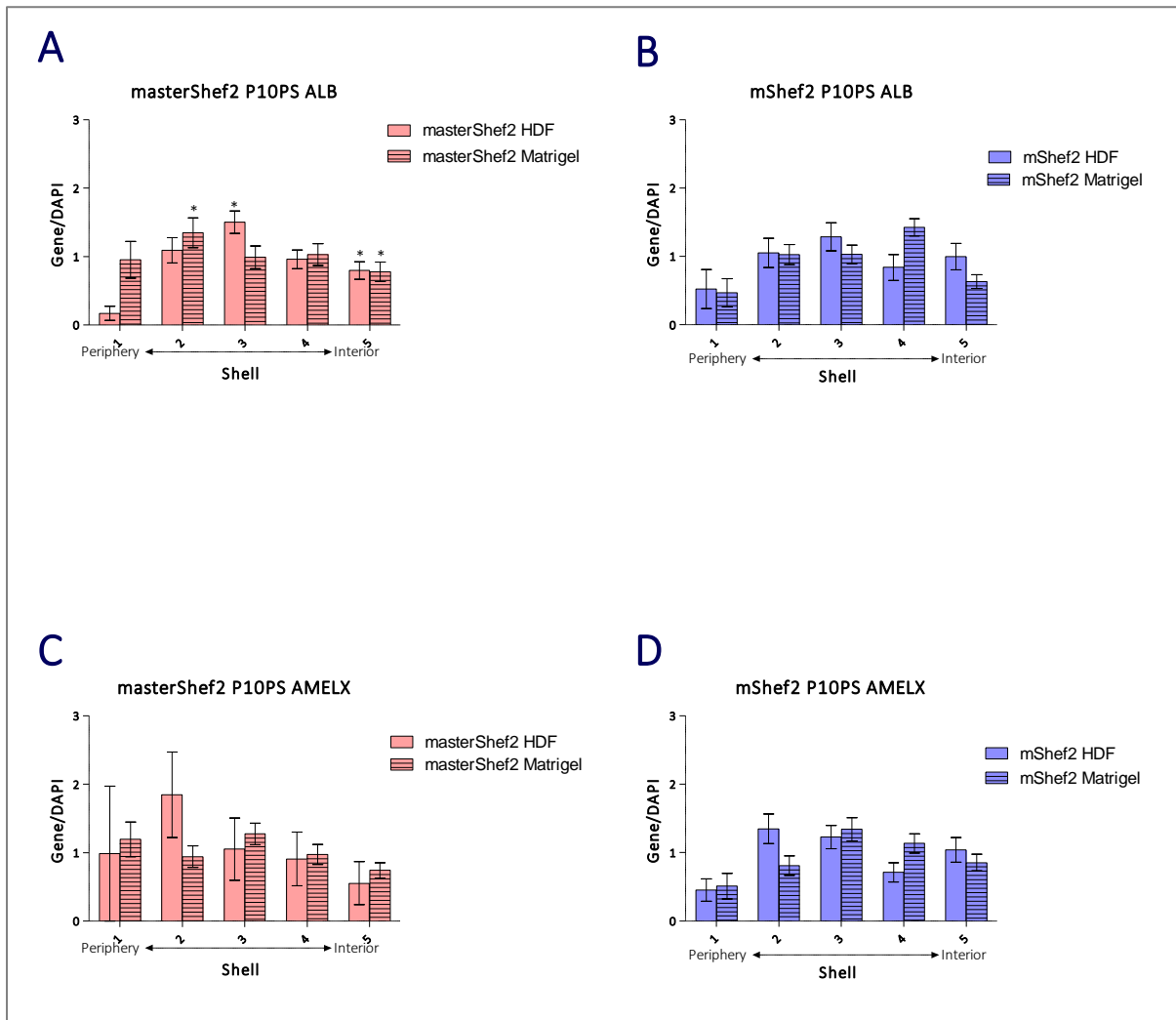


Figure 6.17. Fluorescence *in-situ* Hybridisation Results in P10PS

FISH was performed for *ALB* and *AMELX* on masterShef2 and mShef2 grown on HDFs and Matrigel™ for P10PS. A two-sample t-test was performed for each cell line between the different conditions to observe any difference between the two basement membranes. The asterisk symbol (*) signifies statistical difference observed over time, whereas an asterisk with a line above shows the statistical significance between the two conditions. Standard error of mean is shown as error bars.

6.4.4. Nuclear Morphology Analysis

Nuclear morphology was analysed using Fiji (Image J), as per Chapter II to look at the association of genomic instability, gene positioning, nuclear area and circularity. In Figure 6.18, masterShef2 HDF positioning for *ALB* (Panel A) and *AMELX* (Panel B) is shown. The average nuclear area is increasing from P4PS to P8PS, and then reduces to P10PS, whereas nuclei circularity stayed relatively stable across all of the passages. In addition, the pattern of *ALB* followed a relatively similar pattern through the passages. The *ALB* positioning graph from P3PS to P4PS stayed the same and then started changing to a more bimodal shape in P5PS. This was followed by a peripheral organisation for the next two passages. In P8PS, the shape of the graph shifted to bimodal distribution once more until P10PS, where the distribution was more intermediate.

For *AMELX* positioning (Figure 6.18 Panel B), the gene positioning fluctuated more than the *ALB* graph (Panel A). The distribution of *AMELX* started peripheral, followed by different bimodal distributions as the cells progressed over time. Interestingly, the an increase in the bimodal distribution of both *AMELX* and *ALB* was observed at P9PS when a 60% increase of *AMELX* was observed.

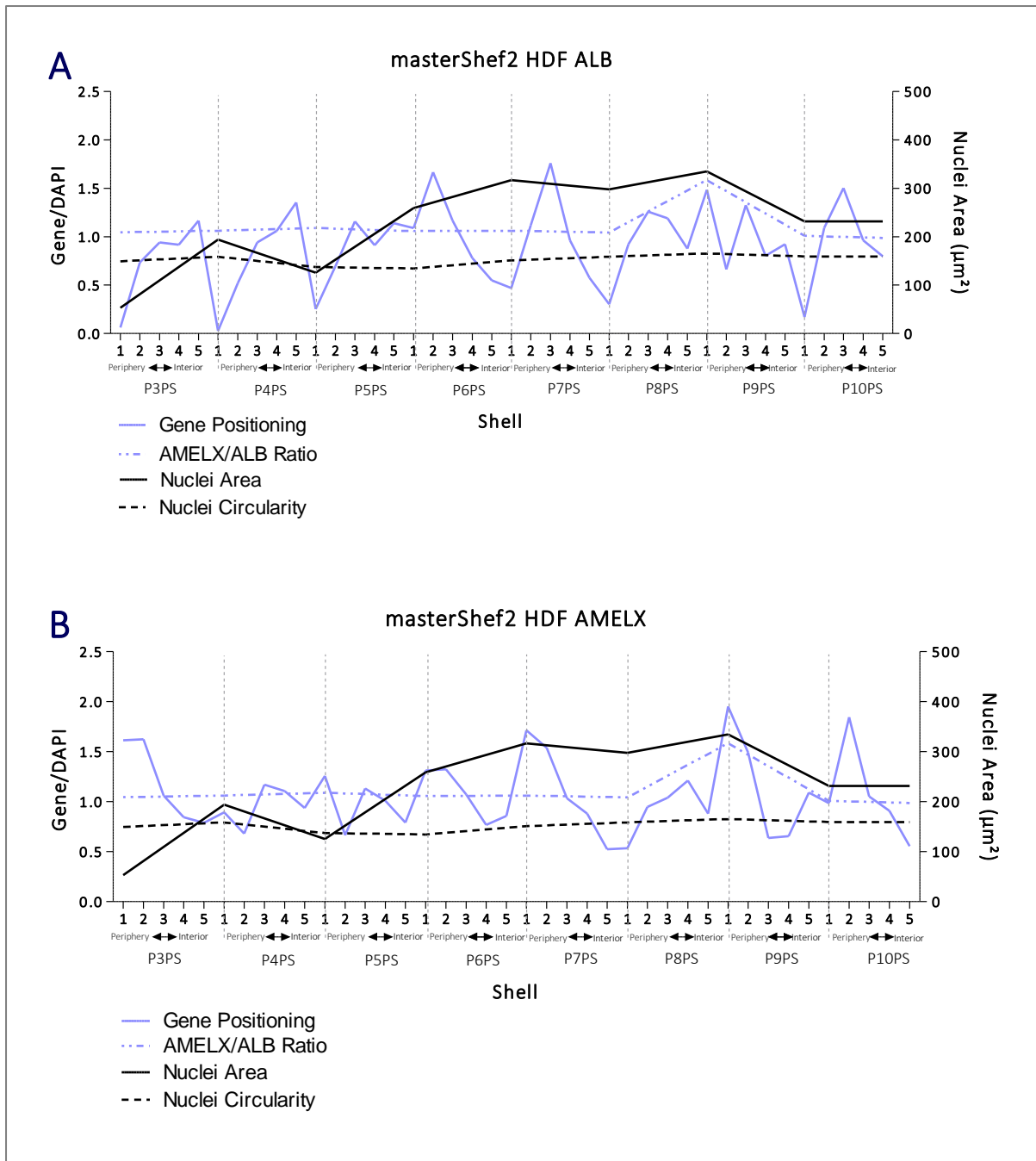


Figure 6.18. MasterShef2 HDF Nuclear Morphology, Genomic Stability and Gene Positioning

Results from all of the different assays were combined in the graphs above throughout all passages; gene positioning is shown in blue, the average nuclear area in a solid black line, average nuclear circularity in a black dashed line and the genomic instability, shown in *AMELX* to *ALB* ratio, is represented in a dashed blue line. Panel A shows the *ALB* positioning, where Panel B shows the *AMELX* positioning.

In Figure 6.19, masterShef2 Matrigel™ positioning for *ALB* (Panel A) and *AMELX* (Panel B) is shown. The nuclei area is increasing from P4PS to P5PS and from P8PS to P9PS, and reduces P5PS to P6PS and P9PS to P10PS. On the other hand the nuclei circularity increases P5PS to P7PS and is then stable throughout the rest of the study.

For *ALB* positioning (Figure 6.19 Panel A), the gene positioning distribution displayed little consistency in pattern throughout the eight passages with a mainly intermediate distribution of the *ALB* gene.

For *AMELX* positioning (Figure 6.19 Panel B), the gene positioning fluctuated more than the *ALB* graph once again. The distribution of *AMELX* included bimodal distribution, with a large amount of the nuclei demonstrating peripheral or intermediate organisation. An increase in the bimodal distribution can be observed at P10PS when a drop in 40% of *AMELX* was reported from the ddPCR™ results (Figure 6.19).

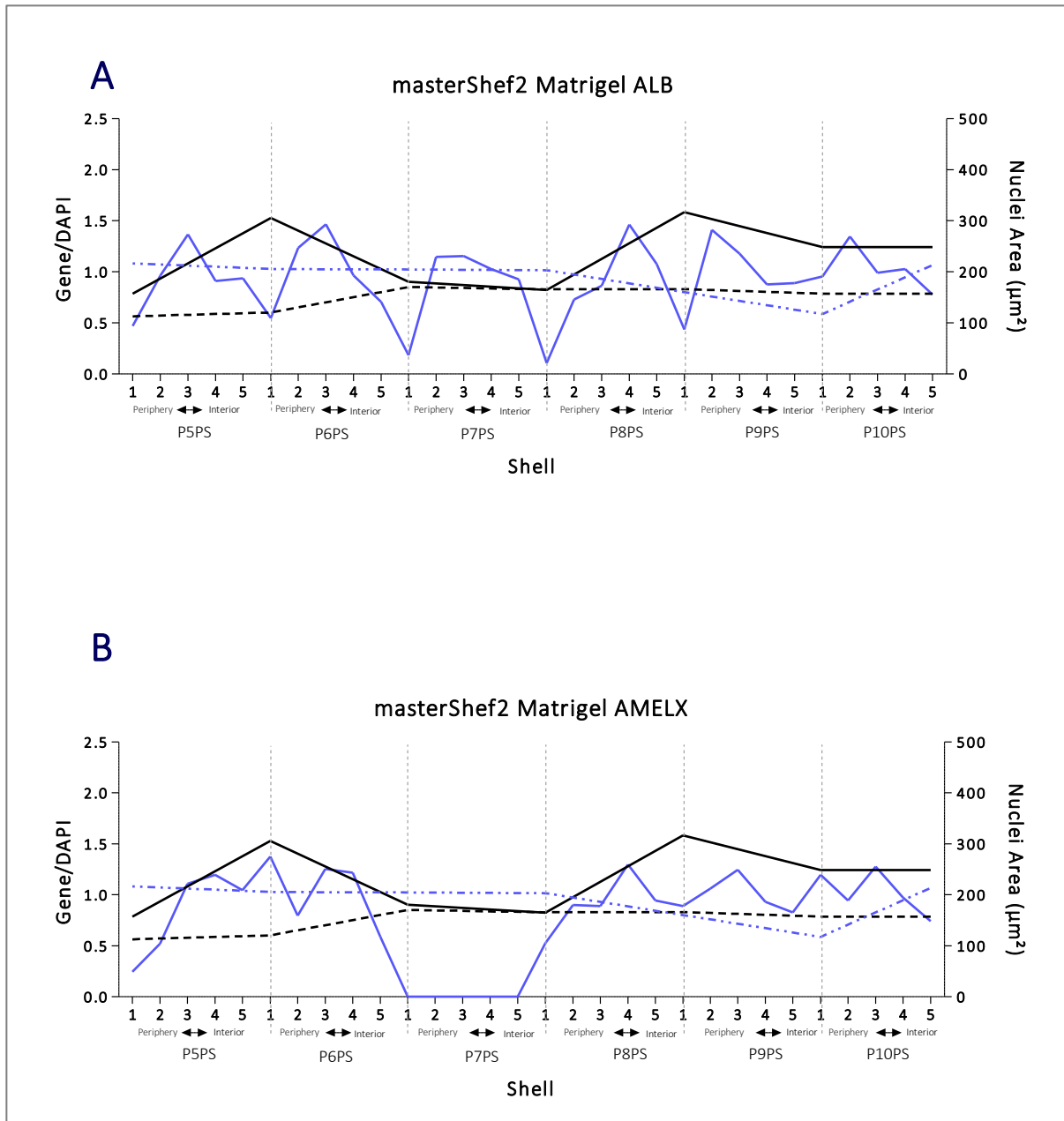


Figure 6.19. MasterShef2 Matrigel™ Nuclear Morphology, Genomic Stability and Gene Positioning Results from all of the different assay were combined in the graphs above throughout all of passages; gene positioning is shown in blue, the average nuclei area in a solid black line, average nuclei circularity in a black dashed line and the genomic instability, shown in *AMELX* to *ALB* ratio, is represented in a dashed blue line. Panel A shows the *ALB* positioning, where Panel B shows the *AMELX* positioning. No sample was available for masterShef2 Matrigel™ at P7PS.

In Figure 6.20, mShef2 HDF positioning for *ALB* (Panel A) and *AMELX* (Panel B) is shown. The nuclei area is very inconsistent throughout the different passages with a gradual increase up to P9PS and then a drop again in P10PS. On the other hand the nuclei circularity remained relatively constant.

For *ALB* positioning (Figure 6.20 Panel A), the gene positioning distribution displayed a semi-consistent pattern at the beginning of the culture, where the positioning was intermediate. However, as the culture progressed peripheral organisation and then finally bimodal distribution appeared.

The *AMELX* positioning (Figure 6.20 Panel B) too displayed altered gene positioning throughout the culture time. The nuclei originally displayed intermediate organisation of *AMELX* and then slowly progressed to internal, peripheral and finally, bimodal.

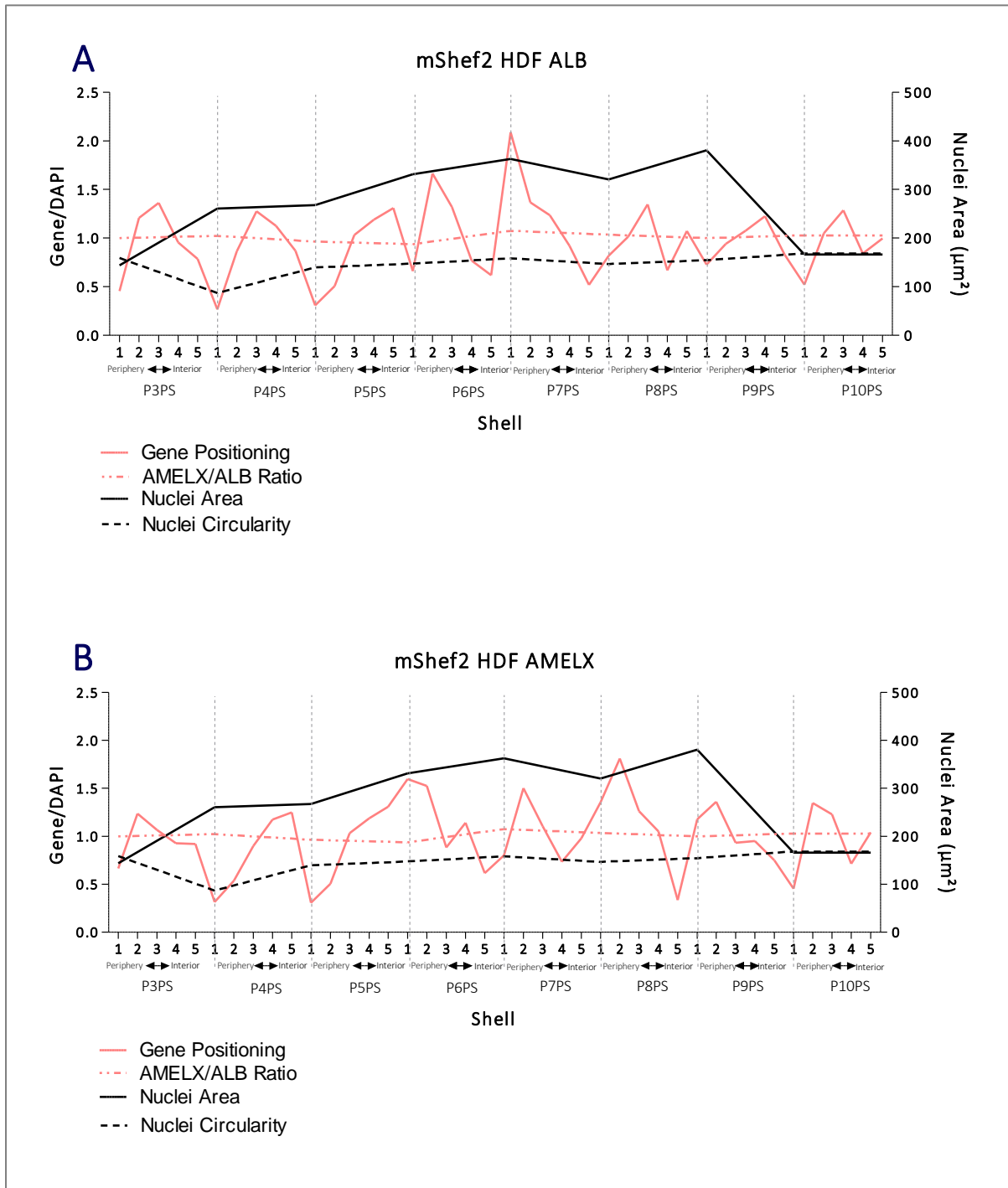


Figure 6.20. mShef2 HDF Nuclear Morphology, Genomic Stability and Gene Positioning

Results from all of the different assay were combined in the graphs above throughout all of passages; gene positioning is shown in pink, the average nuclei area in a solid black line, average nuclei circularity in a black dashed line and the genomic instability, shown in *AMELX* to *ALB* ratio, is represented in a dashed pink line. Panel A shows the *ALB* positioning, where Panel B shows the *AMELX* positioning.

In Figure 6.21 a drop in the nuclear area from P5PS to P6PS has been observed, followed by a gradual increase in nuclear size until P8PS. After this the nuclear area had once again dropped until P10PS. During this time the nuclear circularity fluctuated upto P7PS, after which it remained stable throughout the study.

The *ALB* positioning had once again displayed relative stability across the different passage with a mainly intermediate positioning in the nuclei, whereas *AMELX* positioning remained stable until P9Ps, whereafter a bimodal distribution was observed.

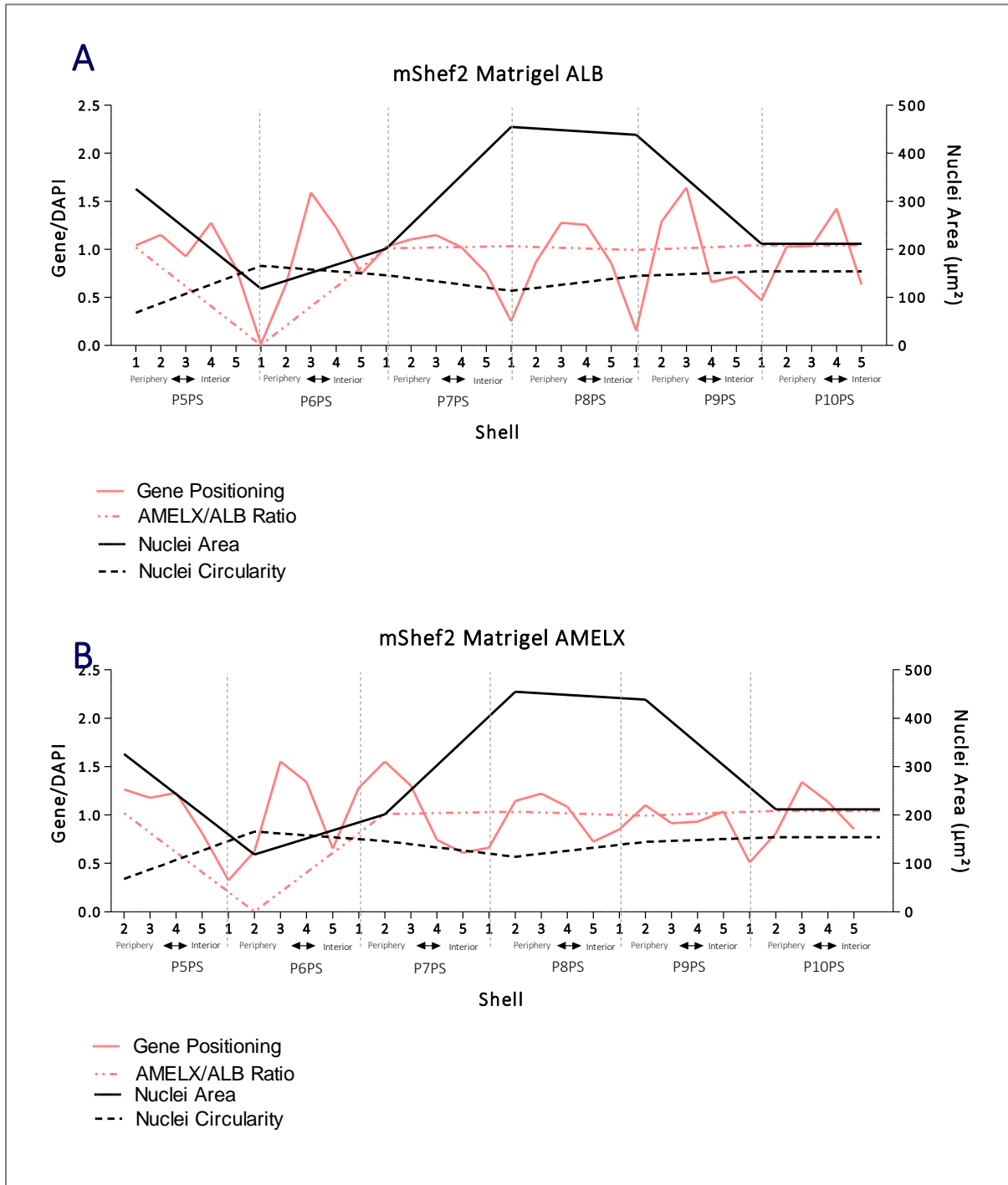


Figure 6.21. mShef2 Matrigel™ Nuclear Morphology, Genomic Stability and Gene Positioning
 Results from all of the different assay were combined in the graphs above throughout all of passages; gene positioning is shown in pink, the average nuclei area in a solid black line, average nuclei circularity in a black dashed line and the genomic instability, shown in *AMELX* to *ALB* ratio, is represented in a dashed pink line. Panel A shows the *ALB* positioning, where Panel B shows the *AMELX* positioning. No data was available for the *AMELX/ALB* ratio at P6PS.

In addition, images of the embryonic stem cell colonies were taken to observe any potential differentiation that may have occurred, as seen in Figure 6.22 Image B with the white arrow. When the cells were grown on HDFs, we could observe the feeder cells surround the hESC colonies (Figure 6.22 Image A Blue Arrow) and interestingly, when cells were grown on Matrigel™ these cells were creating a type of niche by differentiating at the edge of the colonies into cells similar to feeders in morphology (Figure 6.22 Image B Blue Arrow).

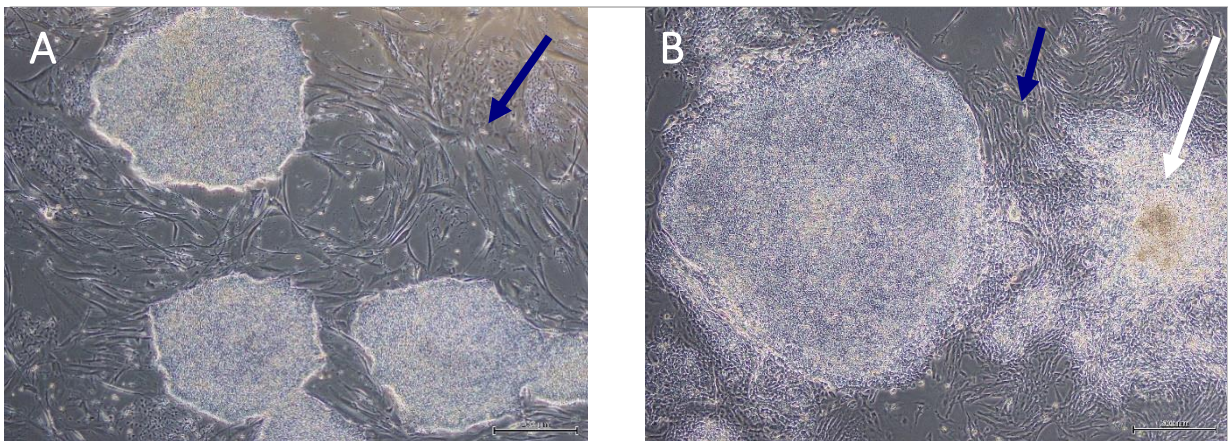


Figure 6.22. Embryonic Stem Cell Colony Images

Example images were taken during the cell culture of masterShef2 and mShef2 cell lines. Image A shows masterShef2 cell colonies surrounded by human dermal fibroblasts (HDFs), whereas Image B shows mShef2 grown on Matrigel™. Both cell lines shown in the images above are at P7PS. Scale bar is shown. The blue arrows point to the feeder cells surrounding the hESC colonies, whereas the white arrow highlights the hESC cells with poor morphology.

6.4.5. FISH Summary

To summarise the FISH results, Figure 6.23 displayed all of the *ALB* (Panel A) and *AMELX* (Panel B) results throughout the eight passages in both of the embryonic stem cell lines grown on both HDFs and Matrigel™. Between samples a very similar pattern of *ALB* distribution was observed, especially between the samples from the same cell line i.e. mShef2 HDF and mShef2 Matrigel™. On the other hand, the *AMELX* organisation in the nuclei of the different samples was more diverse, although once more, the samples from the same cell line grown on different conditions were more similar than between the two cell lines. Additionally, Table 6.2, Table 6.3, Table 6.4 and Table 6.5 list a summary of all of the ddPCR™, FISH and nuclear morphology analysis.

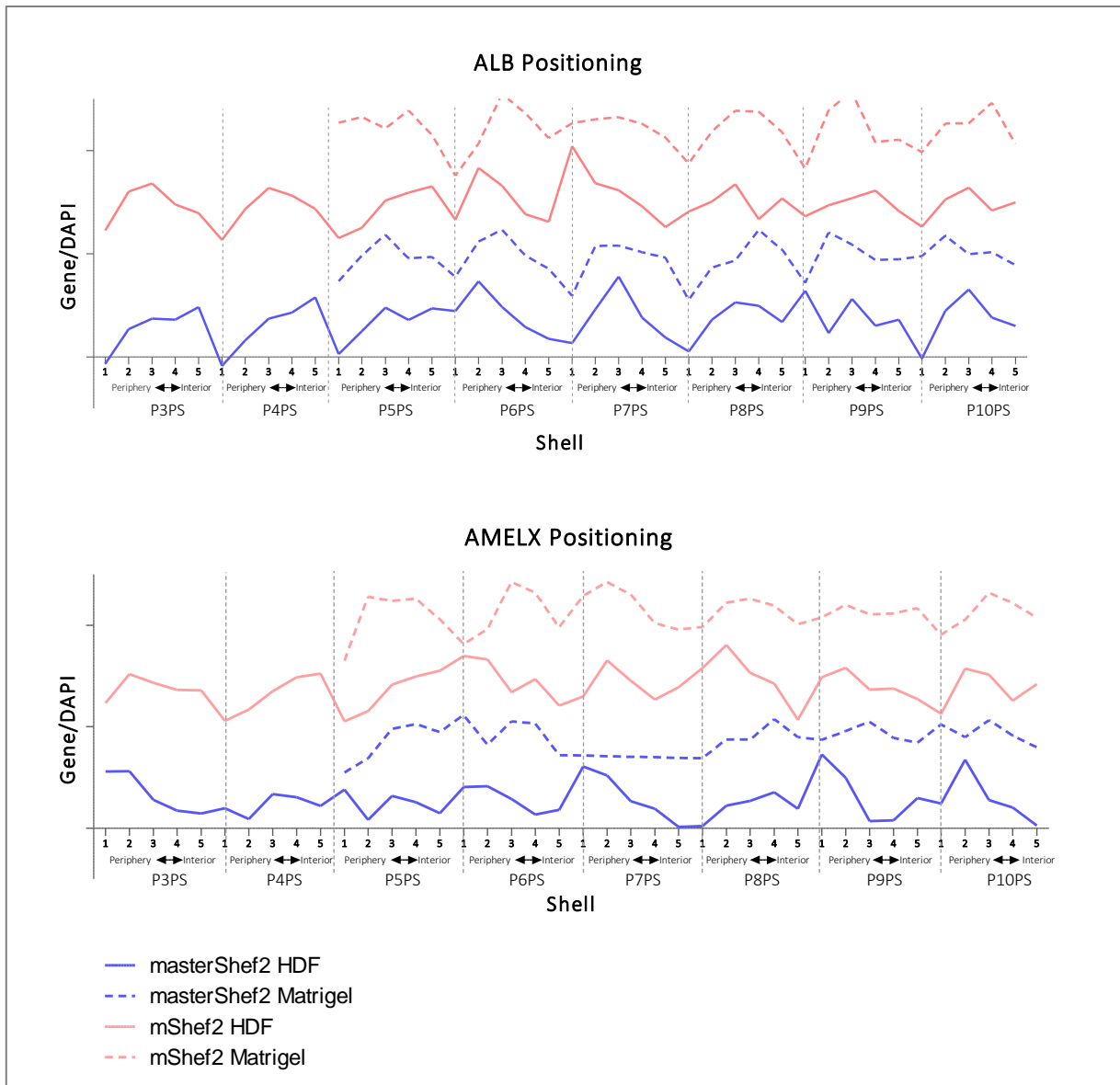


Figure 6.23. Summary of all FISH Results in the Embryonic Stem Cells

The line graph displays the masterShef2 HDF (blue solid line), masterShef2 Matrigel™ (blue jagged line) mShef2 HDF (pink solid line) and mShef2 Matrigel™ (pink jagged line) gene positioning of *ALB* and *AMELX* throughout eight passages.

Table 6.2. MasterShef2 and mShef2 Study Combined Results

The table shows all of the results from this study, including the ddPCR™ *AMELX* to *ALB* ratios, the FISH gene positioning data, nuclear area and nuclear circularity in P3PS-P5PS.

Passage	Cell Line	Condition	ddPCR™ <i>AMELX/ALB</i> Ratio	<i>AMELX</i> Positioning	<i>ALB</i> Positioning	Nuclear Area (μm^2)	Nuclear Circularity
P3PS	masterShef2	HDF	1.04	Periphery	Interior	53	0.75
	mShef2	HDF	1.00	Intermediate	Intermediate	143.9	0.8
P4PS	masterShef2	HDF	1.06	Periphery and Intermediate	Interior	194.4	0.79
	mShef2	HDF	1.02	Interior	Intermediate	260.5	0.43
P5PS	masterShef2	HDF	1.09	Periphery and Intermediate	Intermediate and Interior	125.6	0.69
	mShef2		0.96	Periphery	Interior	267.7	0.70
	masterShef2	Matrigel™	1.08	Intermediate	Periphery and Interior	157.5	0.56
	mShef2		1.02	Intermediate	Intermediate	326.1	0.34

Table 6.3. MasterShef2 and mShef2 Study Combined Results

The table shows all of the results from this study, including the ddPCR™ *AMELX* to *ALB* ratios, the FISH gene positioning data, nuclei area and nuclei circularity in P6PS-P7PS.

Passage	Cell Line	Condition	ddPCR™ <i>AMELX/ALB</i> Ratio	<i>AMELX</i> Positioning	<i>ALB</i> Positioning	Nuclei Area (μm^2)	Nuclei Circularity
P6PS	masterShef2	HDF	1.06	Periphery and Intermediate	Periphery	259	0.67
	mShef2		0.94	Periphery and Intermediate	Periphery	331.5	0.74
	masterShef2	Matrigel™	1.03	Periphery and Intermediate	Intermediate	305.4	0.60
	mShef2		-	Intermediate	Intermediate	117.9	0.83
P7PS	masterShef2	HDF	1.06	Periphery	Intermediate	317	0.75
	mShef2		1.07	Periphery and Interior	Periphery	362.7	0.79
	masterShef2	Matrigel™	-		Intermediate	180.8	0.85
	mShef2		1.01	Periphery	Random	201.5	0.73

Table 6.4. MasterShef2 and mShef2 Study Combined Results

The table shows all of the results from this study, including the ddPCR™ *AMELX* to *ALB* ratios, the FISH gene positioning data, nuclei area and nuclei circularity in P8PS-P9PS.

Passage	Cell Line	Condition	ddPCR™ <i>AMELX/ALB</i> Ratio	<i>AMELX</i> Positioning	<i>ALB</i> Positioning	Nuclei Area (μm^2)	Nuclei Circularity
P8PS	masterShef2	HDF	1.04	Intermediate	Intermediate	297.7	0.79
	mShef2		1.03	Periphery	Intermediate and Interior	320.6	0.73
	masterShef2	Matrigel™	1.02	Periphery and Interior	Intermediate	164.1	0.83
	mShef2		1.03	Intermediate	Intermediate	454.9	0.57
P9PS	masterShef2	HDF	1.59	Periphery and Interior	Periphery and Intermediate	334.7	0.83
	mShef2		1.00	Periphery and Interior	Intermediate	380.5	0.77
	masterShef2	Matrigel™	-	Random	Intermediate and Interior	316.8	0.83
	mShef2		1.00	Random	Intermediate and Interior	438.6	0.72

Table 6.5. MasterShef2 and mShef2 Study Combined Results

The table shows all of the results from this study, including the ddPCR™ *AMELX* to *ALB* ratios, the FISH gene positioning data, nuclei area and nuclei circularity in P10PS.

Passage	Cell Line	Condition	ddPCR™ <i>AMELX/ALB</i> Ratio	<i>AMELX</i> Positioning	<i>ALB</i> Positioning	Nuclei Area (μm^2)	Nuclei Circularity
P10PS	masterShef2	HDF	1.0	Periphery	Intermediate	231.7	0.8
	mShef2		1.03	Intermediate and Interior	Intermediate and Interior	166.2	0.84
	masterShef2	Matrigel™	0.59	Periphery and Intermediate	Periphery	248.7	0.79
	mShef2		1.04	Intermediate	Interior	211.9	0.77

6.4.6. Micronuclei Counts

In order to look at the level of genomic instability in the hPSCs, the number of micronuclei per 1000 nuclei was counted on the microscope for each of the two embryonic stem cells, masterShef2 and mShef2. This was performed for both of the cells grown on HDFs and on Matrigel™ from passage P9PS to P11PS. An example image is shown in Figure 6.24.

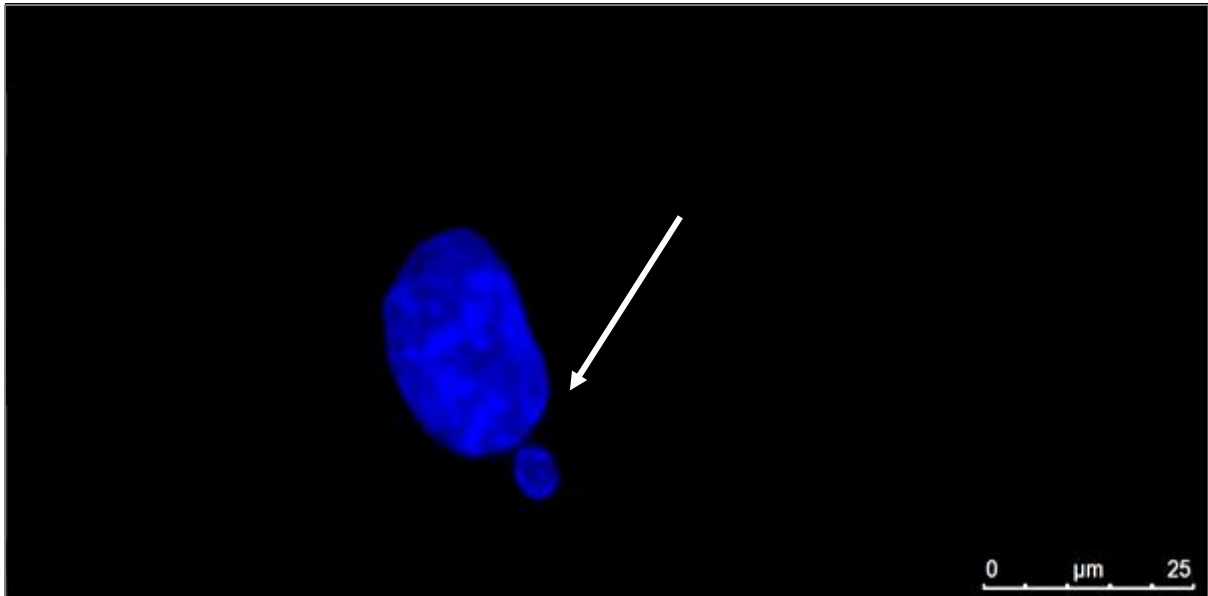


Figure 6.24. Micronucleus Representative Image

An image of a micronucleus formed out a nucleus is shown above with a white arrow. The nuclei were stained with DAPI and imaged with the Leica microscope; the scale bar is displayed.

From the micronuclei counts (Figure 6.25), varying numbers of micronuclei between samples were observed. No significant difference was observed between the samples at P9PS using a two-sample t-test. In addition, at P9PS between 5-15% of micronuclei was observed in each of the cell lines, whereas at the next passages P10PS and P11PS, reduced to approximately 1.5-6%. For masterShef2 Matrigel™ and mShef2 Matrigel™ this was statistically significant ($p=0.0208$) and statistically very significant ($p=0.0065$), respectively, in comparison to the P9PS number of micronuclei (a two-sample t-test was used). Furthermore, mShef2 HDF and mShef2 Matrigel™ displayed statistically significant number of micronuclei between each other ($p=0.0186$).

At P11PS, masterShef2 Matrigel™ micronuclei was 1.73% and was statistically significant to its counterpart at P9PS at 10.37% micronuclei per 1000 nuclei ($p= 0.0132$). MasterShef2 Matrigel™ at P11PS and mShef2 Matrigel at P11PS demonstrated statistically significant difference between each other ($p=0.0344$).

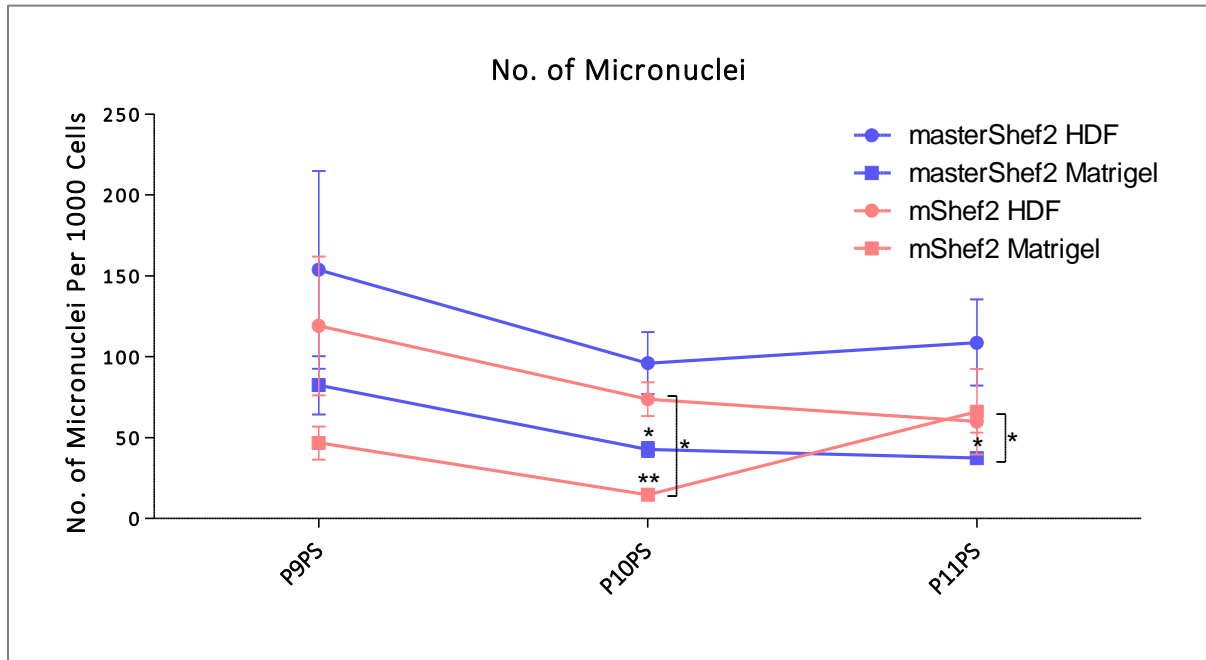


Figure 6.25. Number of Micronuclei in the Human Embryonic Stem Cells

The number of micronuclei per 1000 nuclei are displayed for each embryonic stem cell line grown on HDFs or Matrigel™ across three passages P9PS-P11PS. Standard error of mean is shown as error bars.

6.4.7. Indirect Immunofluorescence

MasterShef2 and mShef2 were grown on coverslips and indirect immunofluorescence was performed for lamin proteins in P9PS to P11PS in conjunction with the pluripotency marker, Nanog, to confirm the cells were still stem cells and that they did not differentiate. The cell nuclei stained for Nanog within the hESC colonies (Figure 6.26)

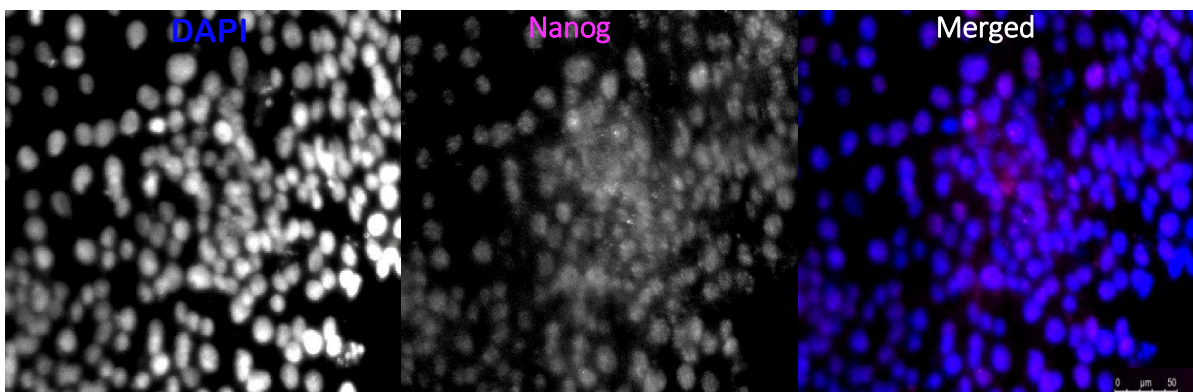


Figure 6.26. Immunofluorescence Staining of Human Pluripotent Stem Cells with Nanog

A human pluripotent stem cell colony is visualised using the Leica microscope. The cell nuclei are counterstained with DAPI in blue and Nanog protein in Magenta. A scale bar is shown.

6.4.7.1. A-Type Lamins

Due to the large number of cells growing in a single colony, the distribution of lamins were analysed dependent on whether the nuclei were within a colony or outside a colony.

Lamins A and C were not detected in the embryonic stem cells growing deep within the colonies; but Nanog expression was detected in these cells (Figure 6.27). However, when lone cells were imaged outside their colonies, both lamins A and C started appearing in low levels throughout the whole nuclei, whilst Nanog expression was reduced. Interestingly, lamin A and C staining appeared strongly in the nucleoli (Figure 6.28). In contrast, some cells outside the colonies still expressed Nanog, despite the appearance of lamin A and C expression throughout the nucleoplasm (Figure 6.29).

On the other hand, a small number of cells outside the embryonic stem cell colonies expressed lamins A and C in speckles, rather than an homogenous veil as seen in Figure 6.29, in the cell nuclei with strong Nanog staining within and outside the nuclei (Figure 6.30), however some cells did not express Nanog protein staining outside the colonies with lamin A and C speckle staining (Figure 6.31). These speckles were seen throughout both of the cell line when the nuclei was outside the main cell colonies and were more numerous for lamin C staining, than lamin A, although some speckles were still visible (Figure 6.30 and Figure 6.31).

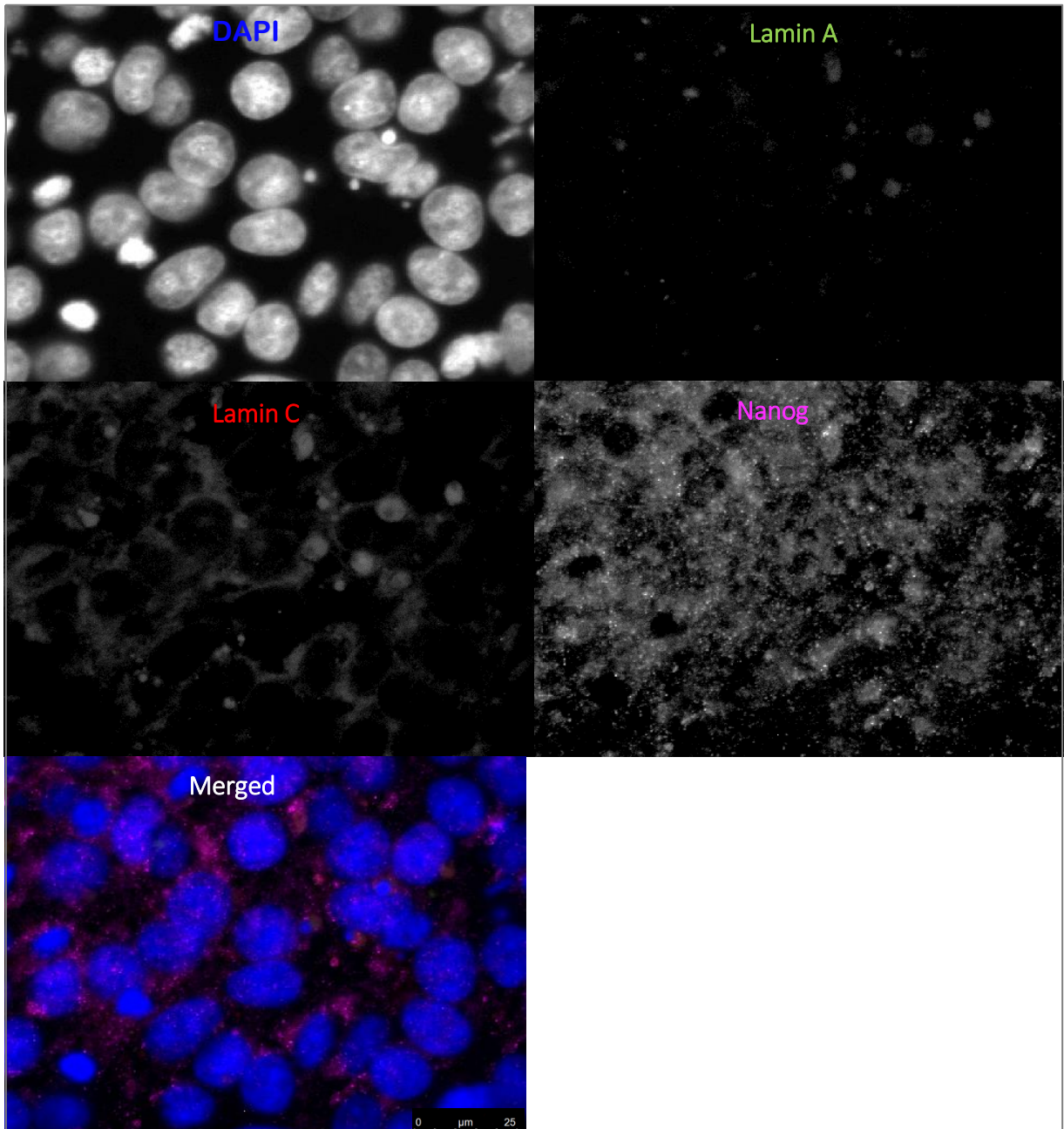


Figure 6.27. A-Type lamin Staining Within Embryonic Stem Cell Colonies

Cell nuclei were stained with DAPI in blue, lamin A in green, lamin C in red and Nanog in magenta. The scale bar is shown.

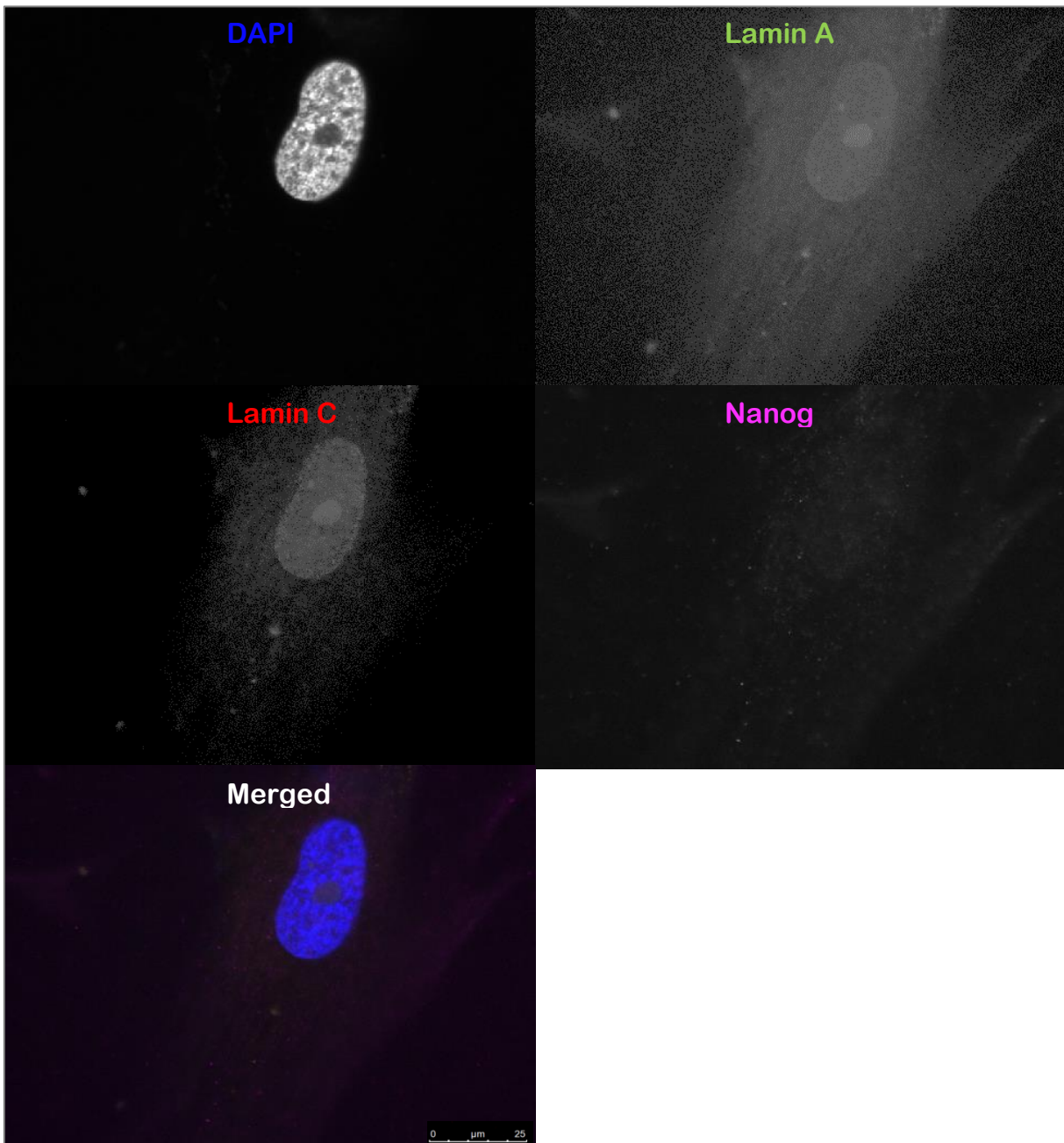


Figure 6.28. A-Type lamin Staining Outside Embryonic Stem Cell Colonies without Nanog Staining
Cell nuclei were stained with DAPI in blue, lamin A in green, lamin C in red and Nanog in magenta. The A-type lamins stained throughout the cell nucleus, whereas Nanog staining was very faint in the cell nucleus. The scale bar is shown.

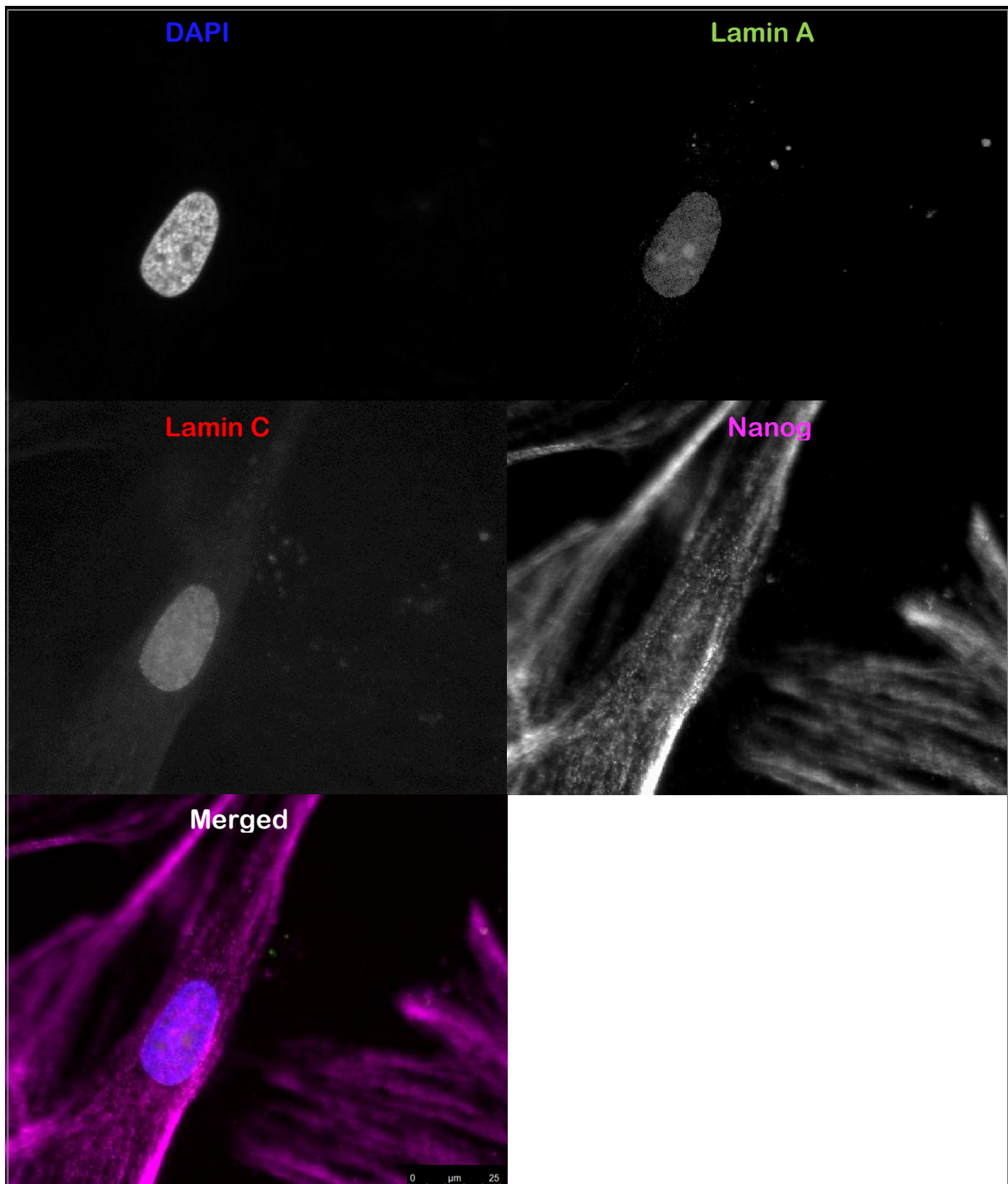


Figure 6.29. A-Type lamin Staining Outside Embryonic Stem Cell Colonies with Nanog Staining

Cell nuclei were stained with DAPI in blue, Lamin A in green, Lamin C in red and Nanog in magenta. Lamin A nuclear staining was very faintly observed, whereas lamin C staining was observed throughout the nucleus. Nanog staining was very strong within and outside the nucleus. The scale bar is shown.

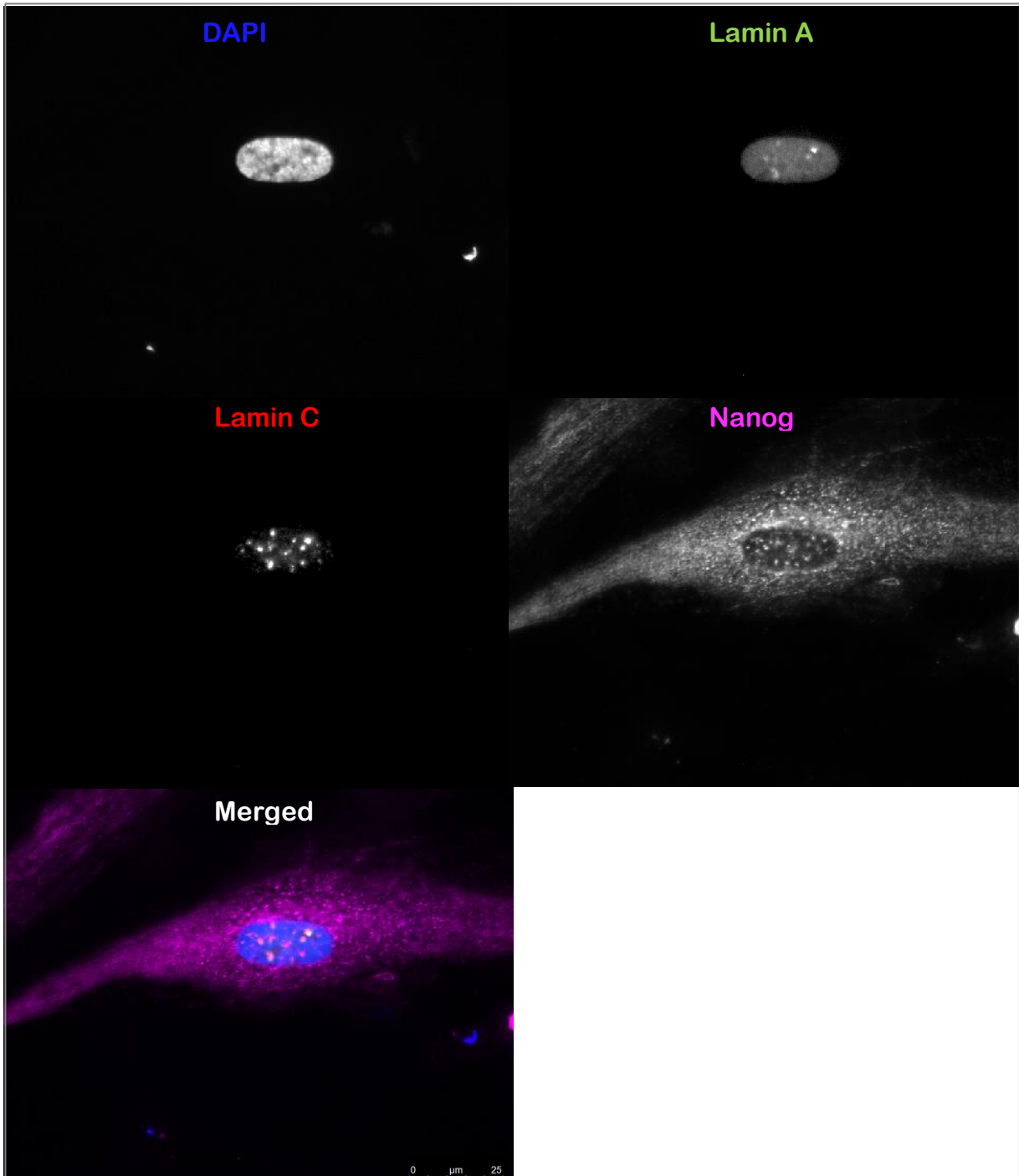


Figure 6.30. A-Type lamin Staining Outside Embryonic Stem Cell Colonies With lamin A and C Speckles and Strong Nanog Staining

Cell nuclei were stained with DAPI in blue, Lamin A in green, Lamin C in red and Nanog in magenta. Lamin A staining was observed as strong spots, along with some staining throughout the nucleus, whereas lamin C staining only displayed strong spots. Nanog staining was observed outside and inside the nucleus. The scale bar is shown.

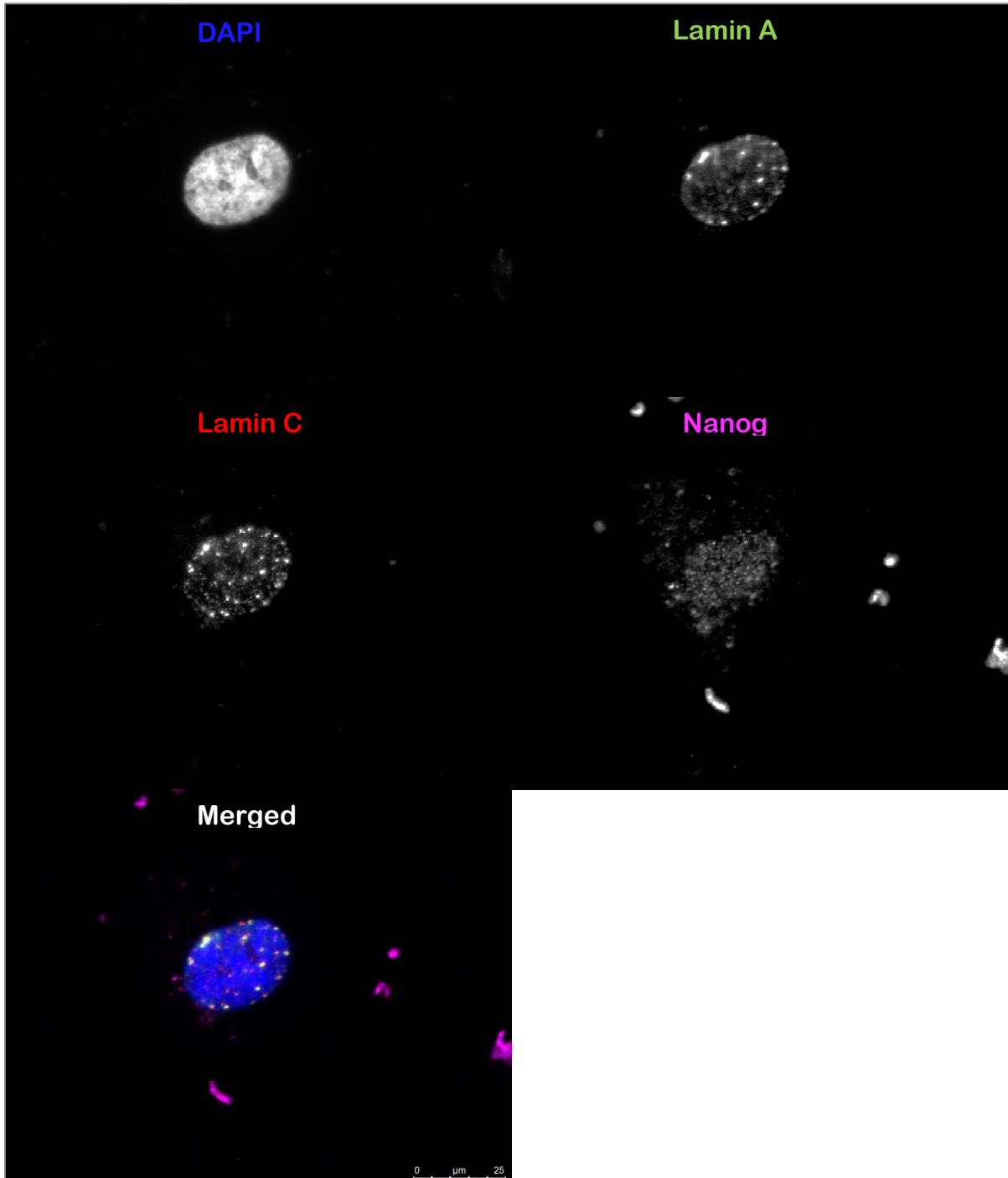


Figure 6.31. A-Type lamin Staining Outside Embryonic Stem Cell Colonies With lamin A and C Speckles and Weak Nanog Staining

Cell nuclei were stained with DAPI in blue, Lamin A in green, Lamin C in red and Nanog in magenta. A-type lamin staining was observed as strong spots throughout the nucleus, whereas Nanog stained faintly throughout the cell nucleus. The scale bar is shown.

6.4.7.2. B-Type Lamins

Similar to A-type lamins staining pattern analysis, the B-type lamin staining pattern analysis was also performed by observing the staining within and outside the embryonic stem cell colonies.

Lamins B1 and B2 were expressed as rims in the stem cell colonies with Nanog staining within the nuclei (Figure 6.32). Although most of the samples displayed this staining pattern, some samples, such as masterShef2 grown on HDF at P10PS, expressed very weak rims for Lamin B2 until eventually the rim completely disappeared at P11PS (Figure 6.33). Despite Lamin B2 staining disappearing over time, the pluripotency marker Nanog staining remained. Outside the stem cell colonies, both lamins B1 and B2 expressed speckled aggregates in the cell nuclei.

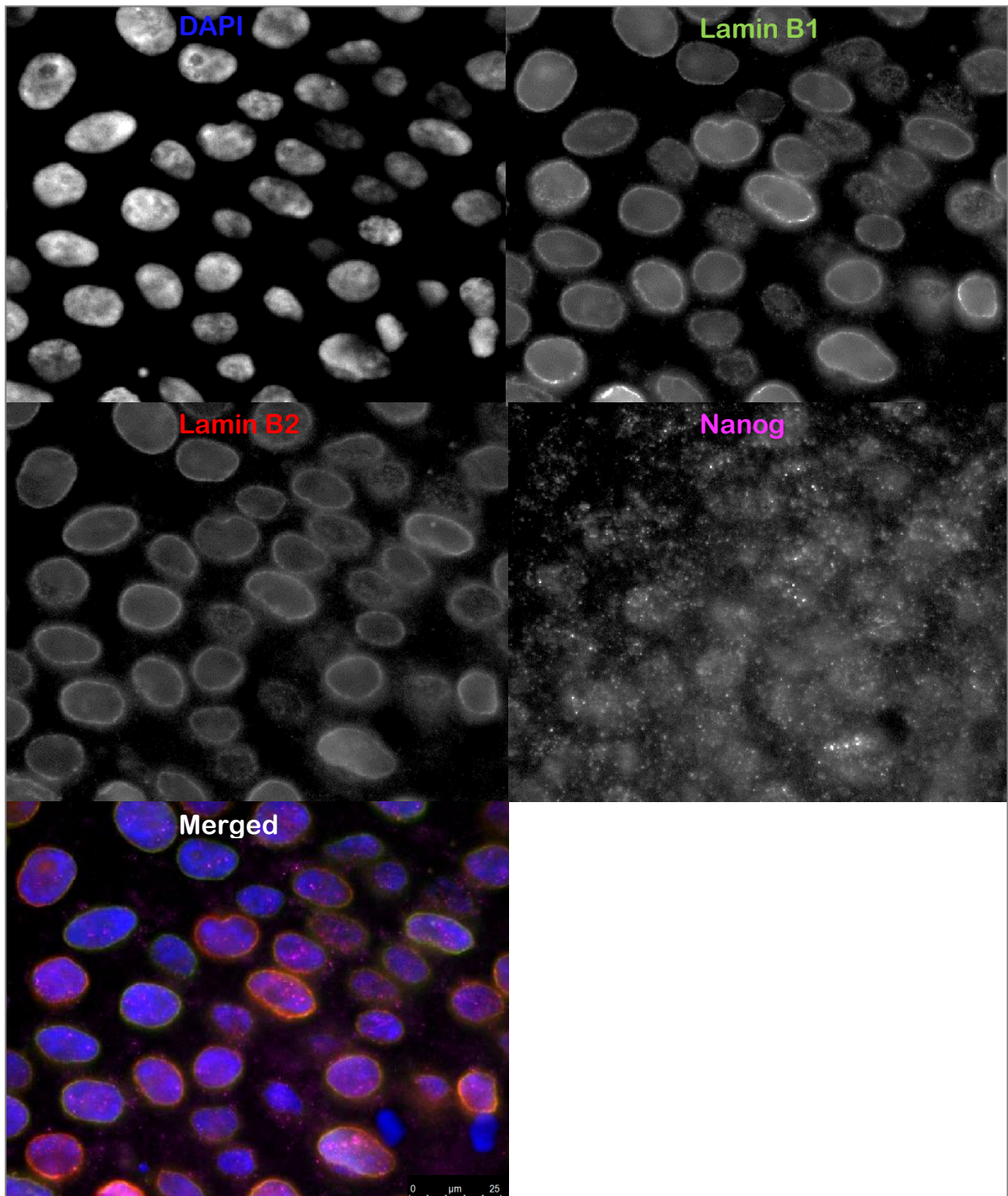


Figure 6.32. B-Type Lamin Staining Within Embryonic Stem Cell Colonies

Cell nuclei were stained with DAPI in blue, Lamin B1 in green, Lamin B2 in red and Nanog in magenta. B-type lamins were observed as rims around the cell nuclei, whereas Nanog mainly stained as speckles throughout the nucleus. The scale bar is shown.

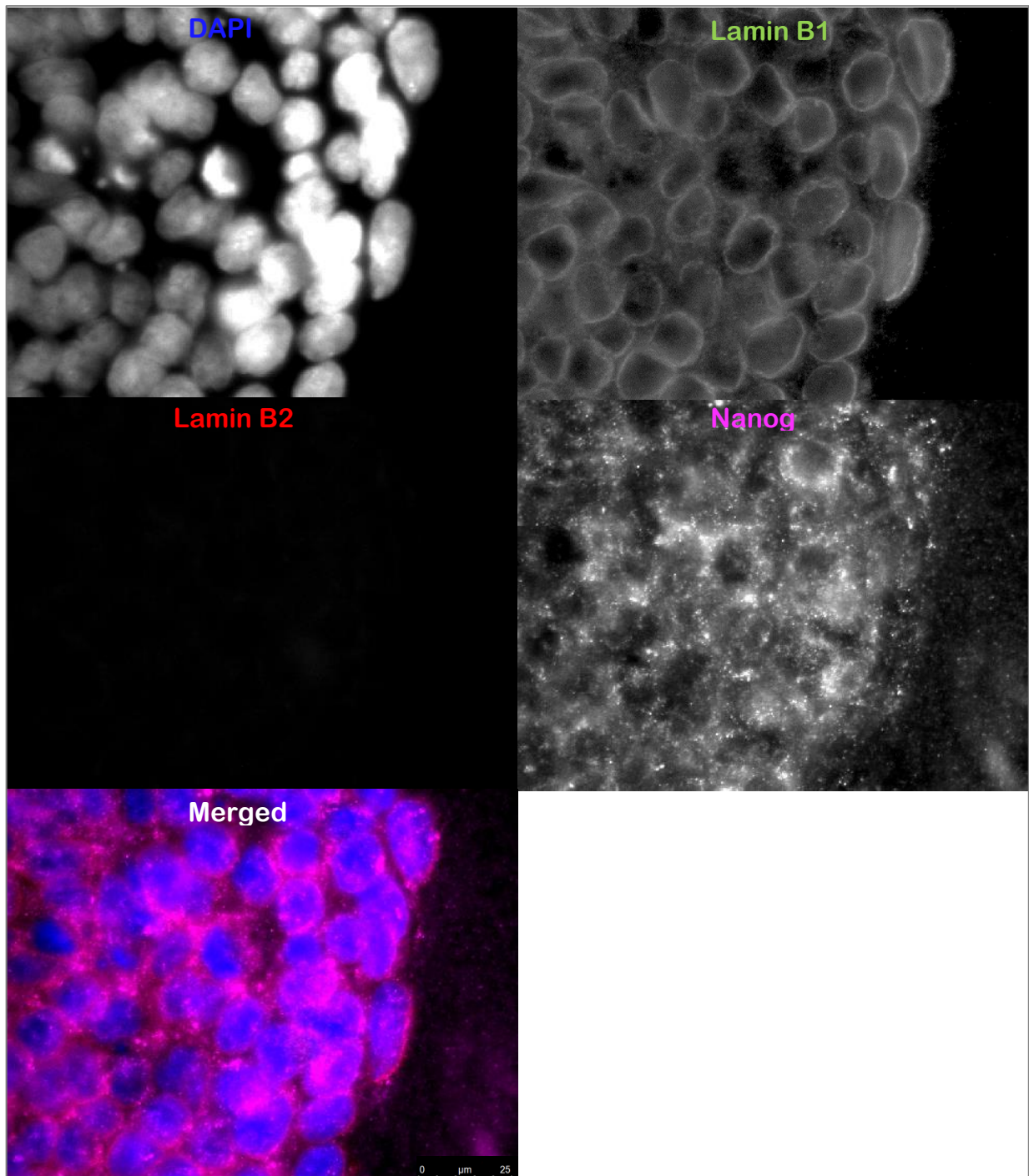


Figure 6.33. B-Type Lamin Staining Within Embryonic Stem Cell Colonies Lacking Lamin B2 Staining
Cell nuclei were stained with DAPI in blue, Lamin B1 in green, Lamin B2 in red and Nanog in magenta. Lamin B1 was observed as rims around the cell nucleus, whereas lamin B2 staining was not observed. Nanog staining was strongly observed within and outside the cell nucleus. The scale bar is shown.

6.4.8. RT-qPCR for Gene Expression

Using the RT-qPCR assay from the UKSCB, a range of different markers were analysed for gene expression changes over time and in the different cell lines. Thresholds were set in the graphs for the minimum amount of gene expression of pluripotency markers required by the cells to be categorised as hPSCs; these thresholds were set by the UKSCB. This is shown as a yellow dashed line in Figure 6.34. All of the cell lines under the different cell culture conditions passed the quality control threshold values to meet the hPSC requirement, except mShef2 HDF P11PS for *SOX2* expression.

Differentiation markers for all three of the lineages i.e. mesoderm, endoderm and ectoderm were measured by RT-qPCR. These genes are highly expressed only in differentiated cells and should not reach above a certain threshold for cells that are to still be considered as hPSCs. This threshold is shown as a red jagged line in Figure 6. 35. All of the cell lines in all of the cell culture conditions passed this quality control threshold values to be classified as hPSCs.

In addition, although no threshold values were identified for the lamin gene expression levels in hPSCs, as this was not a routine RT-qPCR at the UKSCB, all of the samples expressed similar levels of lamin genes. However, it was noted that a sharp drop was detected in masterShef2 HDF P10PS sample, consistent with the immunofluorescence data.

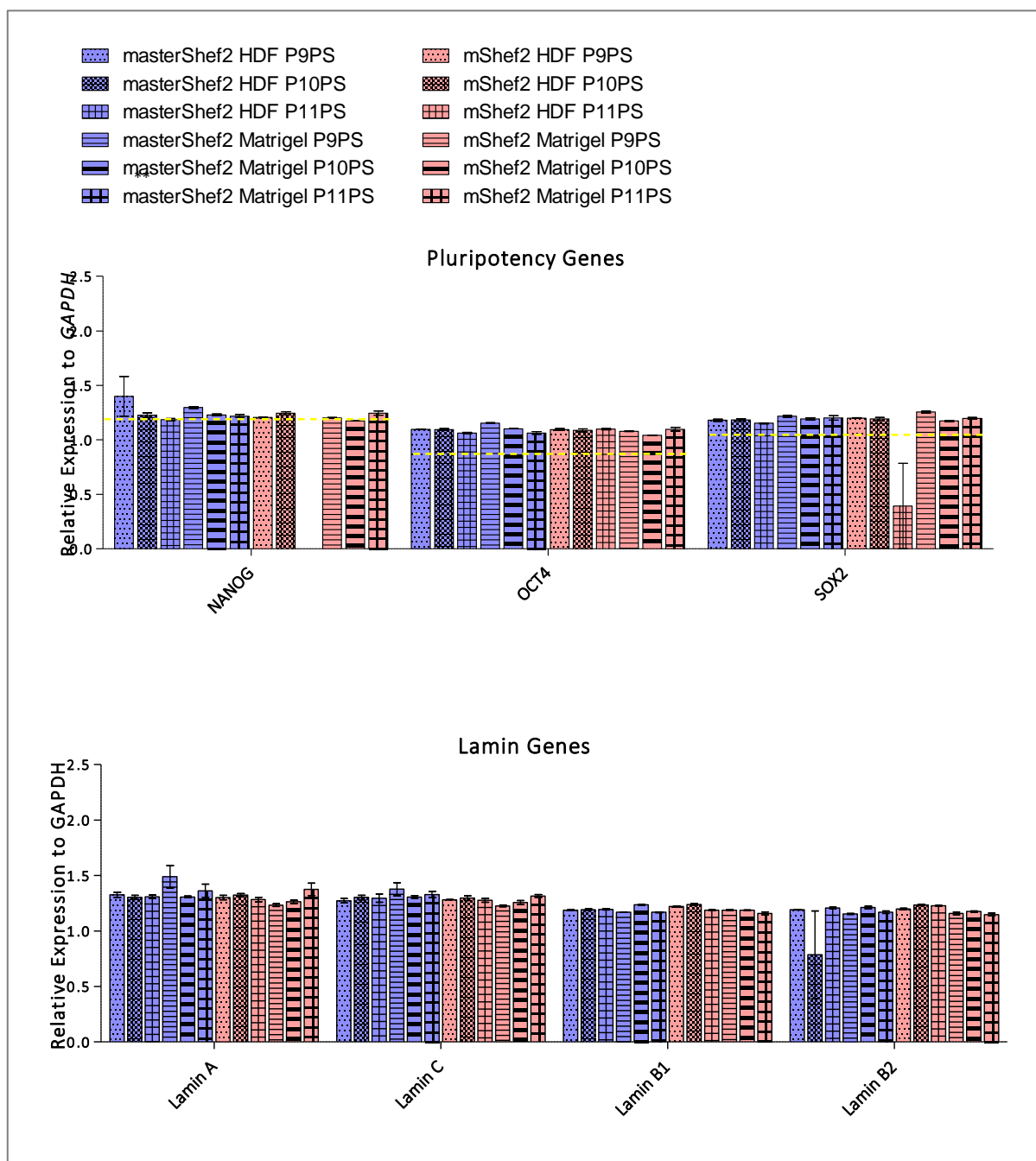


Figure 6.34. Quantitative PCR for Pluripotency and Lamin Genes

The graph shows the gene expression values, relative to *GAPDH* for pluripotency and lamin genes. Cell lines masterShef2 and mShef2 were grown on HDFs or Matrigel™. The yellow jagged lines show the minimum threshold required by the cells to be categorised as hPSCs. The error bars are the standard error of mean.

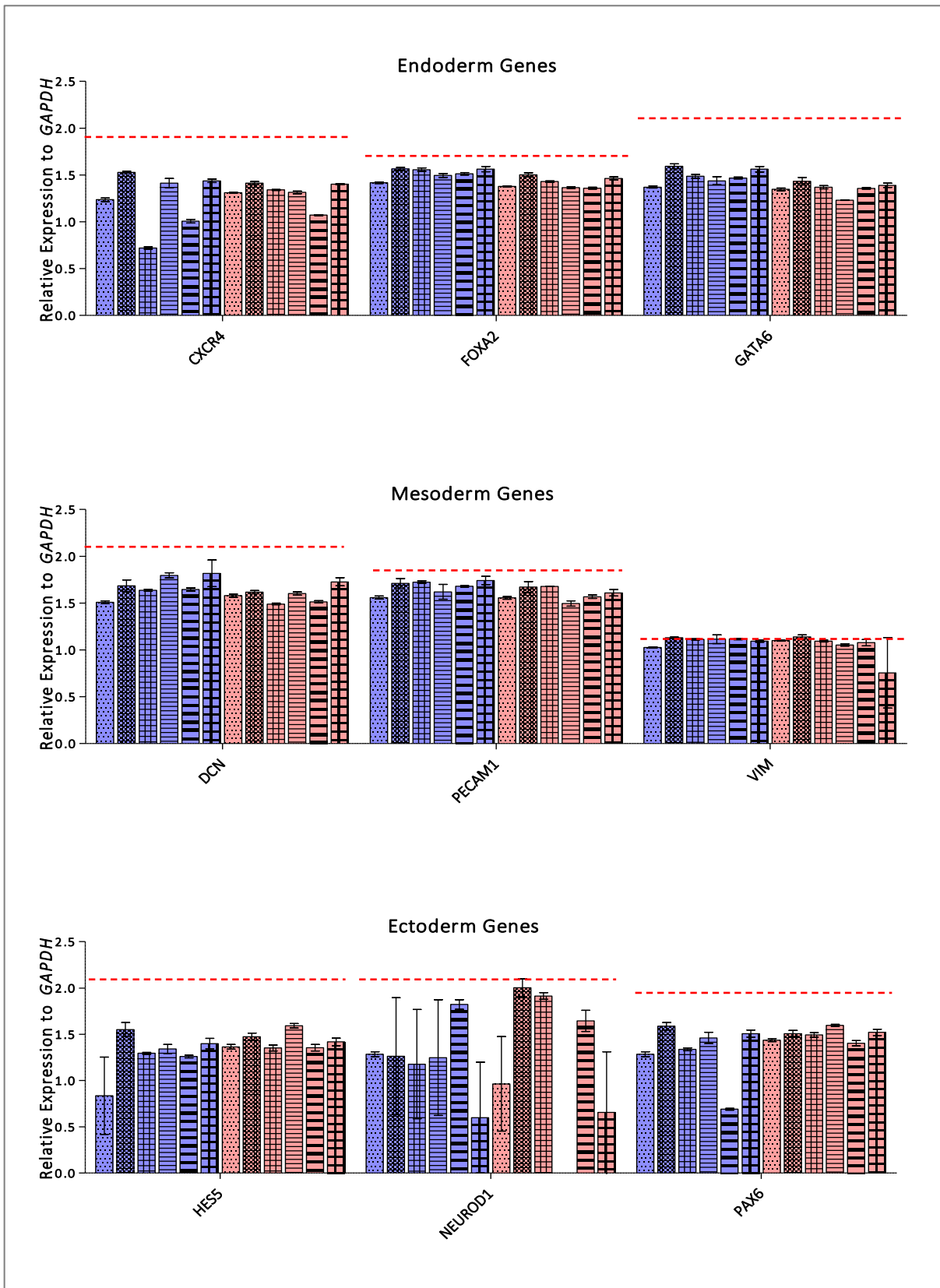


Figure 6. 35. Quantitative PCR for Lineage-specific Genes

The graph shows the gene expression values, relative to *GAPDH* for endoderm, mesoderm and ectoderm lineages. Cell lines masterShef2 and mShef2 were grown on HDFs or Matrigel™. The red jagged lines show the maximum threshold the cells are permitted to reach to be categorised as hPSCs. The error bars are the standard error of mean.

6.4.9. RNA-Seq

6.4.10. Quality Control

To assess the overall quality of the RNA-Seq run, all of the samples were analysed by quality control checks on raw sequence data coming from high throughput sequencing pipelines. The per base sequence quality determined that all of our samples were above 32, demonstrating that the run was of good quality. All of the raw FASTQC files are shown in Appendix V.

6.4.11. RNA-Seq Network Analysis

To detect which genes and pathways were differentially expressed, comparisons between RNA-Seq data sets were made by setting log 5-fold change as the threshold value. The analysis was grouped into three parts – the comparison of different cell culture conditions, the comparison of the different cell lines used in this study, and the effect of passage number on each of the cell lines in their respective growth conditions.

The comparison between masterShef HDF samples versus masterShef2 Matrigel™ revealed 167 genes with different expression (156 up-regulated; 11 down-regulated). Network analyses using Cytoscape (Shannon *et al.* 2003) with ReactomeFI (Wu *et al.* 2010) were used to classify highly interacting groups of genes (modules) and to identify the associated pathways from the RNA-Seq datasets. Cytoscape with ReactomeFI were used to identify pathways to which differentially expressed (DE) genes belong to. Comparing mastershef2 HDF samples versus mastershef2 Matrigel™ demonstrated that twenty-three pathways were significantly enriched in the dataset of 167 overexpressed genes in mastershef2 Matrigel™. Interestingly, the extracellular matrix organisation, vitamin digestion and absorption and retinoid metabolism and transport pathways were amongst these enriched pathways (Table 6.6). All of the pathways identified had a p-value and false discovery rate (FDR) <0.05. The full list of differentially expressed genes are shown in Appendix VII.

Table 6.6. Network Pathways Enriched in MasterShef2 HDF versus MasterShef2 Matrigel™ Samples

Genes were analysed based on their log5FC thresholds. The network enrichment was determined via Cytoscape analysis with ReactomeFI. The enriched pathways are shown below with the total number of genes up-regulated in response to the different growth conditions in the masterShef2 cell line. The P-value and the false discovery rate (FDR) are shown. The nodes identify specific genes/proteins from our log5FC threshold datasets that are present in the enriched networks.

	Protein from Network	P-Value	FDR	Nodes
Extracellular matrix organisation	12	7.18E-07	2.97E-04	<i>VTN, HAPLN1, FGB, FGA, FGG, PECAM1, ITGA8, COL15A1, PLG, TTR, LUM, COL3A1</i>
Vitamin digestion and absorption	3	1.90E-03	0.0247	<i>APOB, APOA1, APOA4</i>
Retinoid metabolism and transport	8	6.21E-09	7.18E-07	<i>RBP4, APOB, APOA2, APOA1, APOA4, TTR, APOC3, APOC2</i>

On the other hand, in mShef2 HDF samples versus mShef2 Matrigel™ samples 84 genes demonstrated different expression (30 up-regulated; 54 down-regulated). The upregulated genes identified twenty-three pathways that were significantly enriched in the mShef2 Matrigel™ samples (Table 6.7), whereas the down-regulated genes identified six pathways that were significantly reduced in the mShef2 Matrigel™ samples (Table 6.8). Amongst the down-regulated pathways were the WNT ligand biogenesis and trafficking, cancer and basal cell carcinoma pathways. For the up-regulated pathways the fibrinolysis pathway, plasminogen activating cascade and FOXA1 transcription factor network pathways were identified. All of the pathways identified had a p-value and FDR <0.05. The full list of differentially expressed genes are shown in Appendix VII.

Table 6.7. Network Pathways Enriched in mShef2 HDF versus mShef2 Matrigel™ Samples

Genes were analysed based on their log5FC thresholds. The network enrichment was determined via Cytoscape analysis with ReactomeFI. The enriched pathways are shown below with the total number of genes down-regulated in response to the different growth conditions in the mShef2 cell line. The P-value and the false discovery rate (FDR) are shown. The nodes identify specific genes/proteins from our log5FC threshold datasets that are present in the enriched networks.

	Protein from Network	P-Value	FDR	Nodes
WNT ligand biogenesis and trafficking	2	7.60E-04	0.0122	<i>WNT8B, WNT7B</i>
Pathways in cancer	4	2.89E-03	0.0364	<i>WNT8B, MMP1, WNT7B, PAX8</i>
Basal cell carcinoma	2	3.31E-03	0.0364	<i>WNT8B, WNT7B</i>

Table 6.8. Network Pathways Enriched in mShef2 HDF versus mShef2 Matrigel™ Samples

Genes were analysed based on their log5FC thresholds. The network enrichment was determined via Cytoscape analysis with ReactomeFI. The enriched pathways are shown below with the total number of genes upregulated in response to the different growth conditions in the mShef2 cell line. The P-value and the false discovery rate (FDR) are shown. The nodes identify specific genes/proteins from our log5FC threshold datasets that are present in the enriched networks.

	Protein from Network	P-Value	FDR	Nodes
Fibrinolysis pathway	3	8.27E-06	6.21E-04	<i>FGB, FGA, FGG</i>
Plasminogen activating cascade	2	3.35E-04	3.35E-03	<i>FGB, FGA</i>
FOXA1 transcription factor network	2	6.86E-03	0.0431	<i>C4BPB, INS</i>

In addition, cell lines masterShef2 and mShef2 were compared based on their cell culture conditions i.e. HDF or Matrigel™. Comparing mastershef2 HDF versus mShef2 HDF, 28 genes with ≥ 5 -log fold change expression (16 up-regulated; 12 down-regulated) were detected. Using the Cytoscape network analysis software no pathways were identified between these two samples.

In contrast, mastershef2 Matrigel™ versus mShef2 Matrigel™ showed differential expression of 135 genes (114 up-regulated; 21 down-regulated). Once again, the upregulated genes in the masterShef2 Matrigel™ samples identified the extracellular matrix organisation, retinoid metabolism and plasminogen activating cascade pathways amongst the enriched pathways (Table 6.9). The full list of differentially expressed genes are shown in Appendix VII.

Table 6.9. Network Pathways Enriched in MasterShef2 HDF versus MasterShef2 Matrigel™ Samples

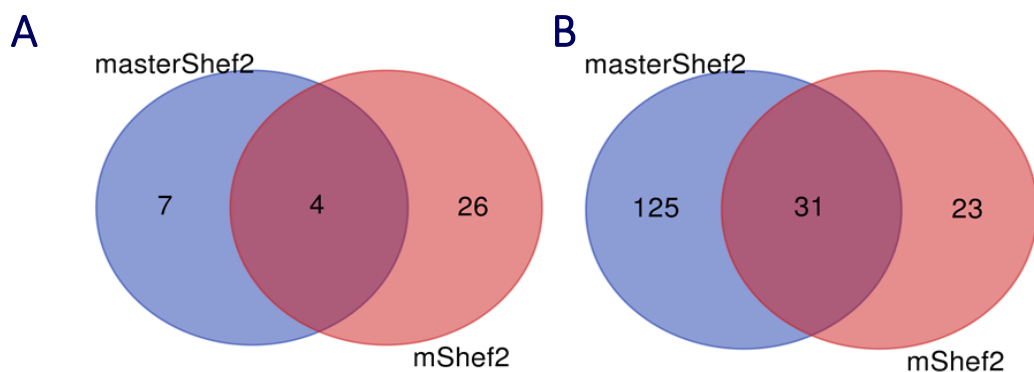
Genes were analysed based on their log5FC thresholds. The network enrichment was determined via Cytoscape analysis with ReactomeFI. The enriched pathways are shown below with the total number of genes up-regulated in response to the different growth conditions in the masterShef2 cell line. The P-value and the false discovery rate (FDR) are shown. The nodes identify specific genes/proteins from our log5FC threshold datasets that are present in the enriched networks.

	Protein from Network	P-Value	FDR	Nodes
Extracellular matrix organisation	12	7.18E-07	2.97E-04	<i>VTN, HAPLN1, FGB, FGA, FGG, PECAM1, ITGA8, COL15A1, PLG, TTR, LUM, COL3A1</i>
Plasminogen activating cascade	3	7.90E-05	1.90E-03	<i>FGB, FGA, PLG</i>
Retinoid metabolism and transport	8	6.21E-09	7.18E-07	<i>RBP4, APOB, APOA2, APOA1, APOA4, TTR, APOC3, APOC2</i>

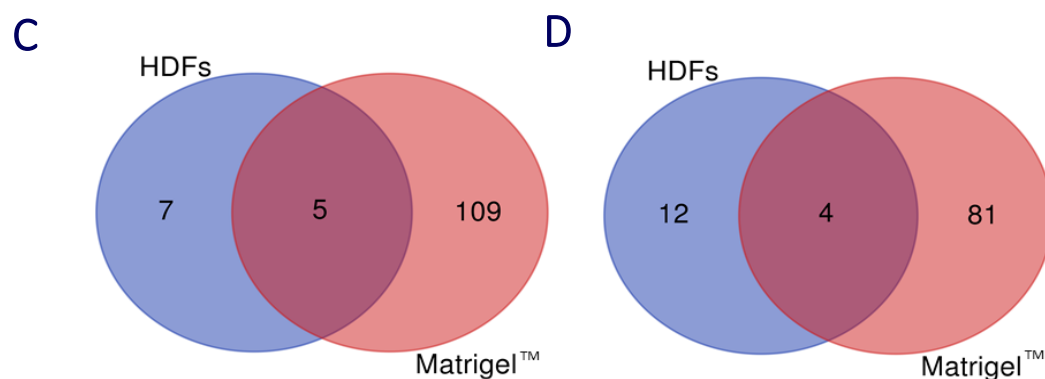
To consider the effect of the time in culture on the gene expression in human pluripotent stem cells, each of the cell lines at passage 9 post-seed were compared to their respective cell line and cell culture condition at passage 11 post-seed. For example, masterShef2 HDF at P9PS was compared to masterShef2 HDF at P11PS. This resulted in ≤ 10 genes differentially expressed between all of the different combinations and no pathway enrichment was identified.

Finally, Venn diagrams were designed to look at the overlap of genes up- and down-regulated in the different cell lines and conditions over time (Figure 6.36). All of the gene transcripts analysed at the set threshold had shown an overlap with the different cell line or condition in our study, however when observing the effect of time on the cell samples no overlap in the gene transcripts was observed (Figure 6.36 E). The list of genes for all of the different conditions in the Venn diagrams are listed in Appendix VII.

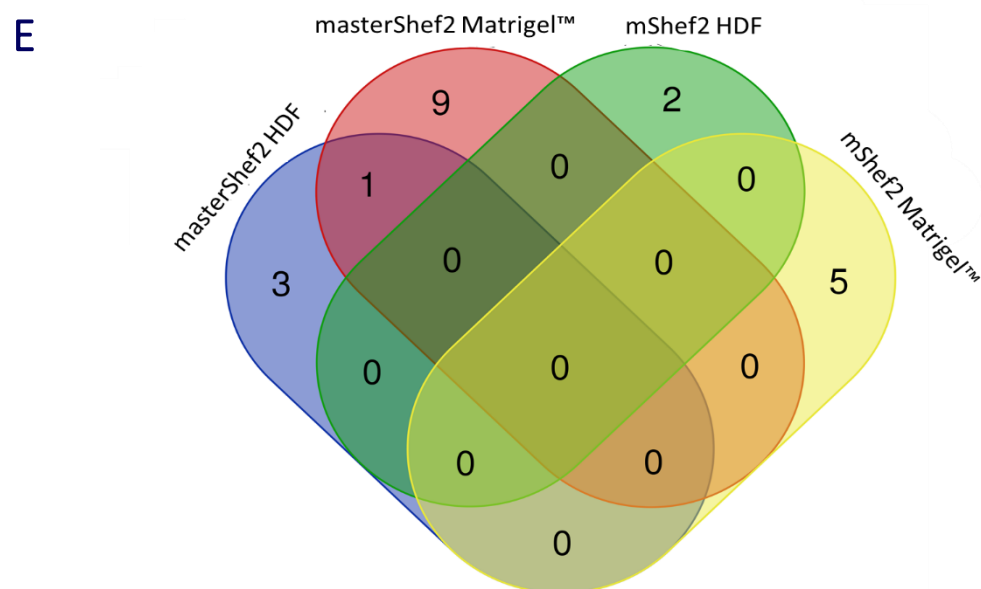
The Effects of Different Conditions on masterShef2 and mShef2 Cell Lines



The Common Effects on Different Cell Lines



The Effects of Time/Passage on Different Cell Lines in Different Conditions

Figure 6.36. Venn Diagrams for Transcripts With $\geq \text{Log}_5\text{FC}$ in the hPSCs

Venn diagrams demonstrating the number of genes up- or down-regulated in the cell lines masterShef2 and mShef2 in the different cell culture conditions i.e. HDFs or Matrigel™ are shown. A shows the number of genes downregulated in each of the cell lines masterShef2 and mShef2 and also the overlap between the groups, B - the number of genes upregulated in each of the two cell line and the overlap between the groups, C - the number of genes downregulated in the cell lines grown on HDFs or Matrigel™, D - the number of genes upregulated in the cell lines grown on HDFs or Matrigel™ and E shows the number of genes downregulated in all of the cell lines and different conditions over time. The full list of genes differentially expressed are shown in Appendix VII.

6.5. Discussion

6.5.1. ddPCR™

The ddPCR™ results from Figure 6.4 indicate the genomic instability of the hPSCs over time. Due to the small amount of DNA required to perform the ddPCR™ experiments, it has been possible to observe the ratio of *AMELX* to *ALB* for each passage in the cells and also for each of the cell culture conditions. This is the first study that has been able to observe the changes in genomic stability so sensitively. In addition, this part of the study had demonstrated the amount of genomic instability that occurs in the hPSC genomes with each passage.

Here, we have shown that although some cell populations can appear to be fully aneuploid from results provided from karyotyping via G-banding, in reality that may not be, as G-banding only looks at a very small proportion of the cell population. Our results, on the other hand, provide a capture of the whole cell population, making it a more accurate method for total cell population analyses. In addition, G-banding only looks at the presence or absence of aberrations in dividing cells from the metaphase spreads formed from the supplementation of mitosis blocking agents, such as colcemid or nocodazole. If aneuploid cells indeed have a growth advantage in culture (Maitra *et al.*, 2005; Amps *et al.*, 2011; Avery *et al.*, 2013), then presumably they are more actively dividing than the diploid cells. On one hand, if these cells were blocked in mitosis and never formed future daughter cells, then this would result in an over-representation of aneuploidies in the G-banding results and potentially give a false indication of the number of aneuploidies in the total cells population.

Interestingly, the results from this chapter have also demonstrated the diversity of the genomic stability in hPSCs and their ability to lose and regain gene copy numbers in a short period of time. For example, in Figure 6.4 we show masterShef2 HDF P9PS with a large rise in the amount of *AMELX* at P9PS, despite it being not significantly different to the control at the passage before. However, at P10PS this rise had gone back down to a level that was not significantly different to the control once again. This was not

exclusive to any particular cell line or condition, once again indicating that hPSC have the ability to gain or lose gene copy numbers very quickly. Furthermore, this discovery may also lead us to believe that perhaps when hPSCs are classified as aneuploid using G-banding, they may recover in the following passages. Additionally, findings displayed in Figure 6.4, where masterShef2 and mShef2 at P11PS DNA was extracted from two separate wells have highlighted again the genomic stability diversity in hPSCs. We hypothesise this is due to the fact that hPSC grow in colonies making them very different and therefore, separate to each other.

6.5.2. Fluorescence *in-situ* Hybridisation, Nuclear Morphology and Genomic Instability

The data described in section 6.4.3. have demonstrated the level of chromatin plasticity in the hPSC cell nuclei. Like the ddPCR results, hPSC gene loci location shifted at each passage and in many of the cell nuclei gene positioning showed bimodal positioning. For example, in masterShef2 HDF at P9PS, *AMELX* positioning seemed to be both internal and peripheral. We put forward two theories that can explain this characteristic in hPSC. One theory is that this is due to cell mosaicism in the population, where one population of cells have a diploid gene copy number, whereas the other has an aneuploid number of a particular gene or chromosome. This would result in two different gene positionings and therefore the overall image of the gene positioning would look bimodal on a graph. This theory is supported from our results in Chapter II, where a change in gene positioning of different cell lines with different karyotypes has been observed and also from another group that has been looking at gene positioning for the prognosis of different cancers (Meaburn *et al.*, 2009, 2016; Leshner *et al.*, 2016). They believe that with the appearance of different sub-types of cancer is it possible to anticipate a patient's response to treatment, dependent on the chromosome organisation. The second theory is that the hPSC chromatin is highly flexible and therefore the gene positioning can shift very easily dependent on the environment. This theory is supported by the previous studies performed on reviewing the amount of the histone modifications between somatic and naïve cells (Meshorer and Misteli, 2006; Meshorer *et al.*, 2006; Morris, Kelly, Chotalia and Pombo, 2010; Mattout, Biran and Meshorer, 2011).

From our results in section 6.4.4. we have not identified a particular predisposition in gene positioning of hPSCs, due a specific cell culture condition or passage. This has also been similarly identified in Chapter V. In addition, no correlation between nuclear circularity, area, gene positioning or genome instability has been observed in the hPSCs, suggesting that perhaps the hPSCs are indeed flexible or plastic in their genome stability, morphology and organisation.

Additionally, because of the high genomic instability presence in the hPSCs, it was no surprise that the number of micronuclei present in the hPSCs was also high. However, no correlation of the number of micronuclei at the last three passages and the genome instability as measured via indirect immunofluorescence was observed. Further analysis with more data from more passages would be required to make a definite conclusion. In addition, it is worth noting that unlike the method above, the traditional method for measuring genomic instability is by the addition of cytochalasin B and observing the number of micronuclei in binucleated cells (Sinitsky and Druzhinin, 2014).

To our knowledge, no study has yet been conducted that observed the change in gene positioning so closely for each passage and for the different conditions studied in parallel. Our results have been novel for using the different assays from our study in parallel to research the gene positioning and genomic instability in hPSCs.

6.5.3. RT-qPCR and Immunofluorescence

In order to make sure that the hPSCs we were studying were indeed still stem cell-like, RT-qPCR was performed for the commonly used pluripotency markers and lineage-specific markers. Using these markers, we have determined that the hPSCs used in this study were indeed still expressing the genes required to classify the cells as hPSCs. However, although almost all the cells had passed the threshold values set, some variation between the samples were observed. Only one sample mShef2 HDF at P11PS did not pass the minimum threshold level of *SOX2* expression, as no FISH was performed for that sample, no data are available to observe any potential changes in the gene positioning. As gene expression is an indicator of whether cells are differentiated or naïve, and therefore, their gene positioning in the nucleus, this variation could affect the gene positioning we studied. However, due to the high number of nuclei analysed in this study, it is highly unlikely that would have impacted the gene positioning. In addition, the differential protein expression is clear from the IF data, where cells outside the colonies started differentiating and expressing A-type lamins and potentially also changing in the expression with other differentiation-associated genes. This mixed population of RNA extracted from each well of the cell culture dish would explain the small variation in the RT-qPCR differentiation-associated gene expression.

When using indirect immunofluorescence to analyse the different staining patterns of lamin proteins in nuclei, A-type lamins were not present in the hPSCs that grew within the colonies in cell culture. However, cells that were further away from the colonies expressed for A-type lamins suggesting that the cells were beginning to differentiate. As Nanog staining was also performed in parallel with the lamin protein staining, we were able to observe whether the differentiation state was still naïve. Interestingly, despite Nanog staining being present in the nuclei, A-type lamins staining was also present. This suggests that A-type lamins may be a better marker for determining the differentiation state of hPSCs (Constantinescu *et al.*, 2006). In addition, although it has been previously studied that undifferentiated nuclei do not express A-type lamins, the gene expression is still present in these cells.

Furthermore, it is worth noting that the pattern expression of A-type lamin outside the hPSC colonies was different in terms of sometimes displaying a homogenous veil and sometimes displaying speckles within the nuclei. This suggests that when differentiation occurred at the edges of the colonies or outside the colonies the cells differentiated into different types of cells, therefore displayed different A-type lamin staining patterns. Often studies do not look at the A-type lamins A and C separately; here, we have demonstrated that both the staining and expression can vary despite the two proteins originating from the same gene *LMNA*.

Additionally, lamin A protein formation has been suggested to regulate chromatin protein dynamics (Melcer *et al.*, 2012) and also affect the physical plasticity of the stem cell nucleus with differentiation (Pajerowski *et al.*, 2007). This would once again support the idea of lamin A as a better differentiation marker of hPSCs and also suggest another explanation as to why the hPSC nuclei is so vulnerable to damage.

For B-type lamin analysis using IF we observed a sudden loss of lamin B2 staining in some of the samples analysed. Although this was not present in all of the biological replicates analysed i.e. the coverslips in the hPSC wells, nor in all of the biological replicates for the RT-qPCR, there was still a notable drop in lamin B2. As lamin B2 loss has recently been linked to the appearance of aneuploidies in colorectal carcinoma cells (Ranade *et al.*, 2017), it is of particular interest in hPSCs. It is worth mentioning that despite the loss of lamin B2 in these samples, Nanog protein was still strongly expressed in the hPSC samples, suggesting that lamin B2 loss does not affect the pluripotency.

We suggest that lamin B2 could be a contributor to the genomic instability well-established in hPSCs. Our results from Chapter IV support this hypothesis, as reduced levels of lamin B2 was also observed in the aneuploid cell lines in comparison to the diploid lymphoblastoid cell lines. Further research with more cell lines across more passages is required to study the effect of lamin B2 on hPSCs. One possibility could be by using new technology, such as CRISPR-Cas9 to study the effect of lamin B2 loss on hPSCs, however this may not be possible due to the importance of B-type lamins for life. In this case, siRNA could be used to knockdown the gene and monitor the effect it has on genomic instability of hPSCs.

6.5.4. RNA-Seq Network Analysis in hPSCs

When analysing the RNA-Seq data for the pathway enrichment in different cell culture conditions between the HDFs and Matrigel™, we saw an upregulation in the pathways associated with extracellular matrix organisation, vitamin digestion and absorption and retinoid metabolism and transport in the masterShef2 Matrigel™ samples. Embryonic stem cells are often grown on feeder layers, and it has been established that human dermal fibroblasts secrete growth factors (GFs), despite being mitotically inactive, that help maintain the hPSC culture (Jin, 2007; Moogk *et al.*, 2010; Abdian *et al.*, 2015). However, when ESCs are removed from feeder layers we have noticed the stem cell colonies tended to form feeder cell-like layer around them. We hypothesise this was to help maintain their niche and their stem cell-like properties in culture. This has been previously reported by other groups (Moogk *et al.*, 2010; Abdian *et al.*, 2015) and our RNA-Seq data showing the enrichment in extracellular matrix organisation in Matrigel™ samples supports this theory (Table 6.6, Table 6.8 and Table 6.9). Furthermore, the enrichment of vitamin digestion and absorption pathway is of particular interest. In recent years, vitamin C has been identified as a key regulator of stem cell biology, specifically its role in the maintenance of pluripotency, self-renewal and differentiation in the stem cell culture (D’Aniello *et al.*, 2017). The presence of vitamin C has been shown to stimulate the extracellular matrix (ECM) secretion of collagen glycosaminoglycan, and has been associated with improved somatic cell reprogramming (D’Aniello *et al.*, 2017). More importantly, has been shown to impact the epigenetic signature of hPSCs by counteracting H3K9 and H3K36 DNA methylation (Comes *et al.*, 2013; D’Aniello *et al.*, 2017), which would suggest its crucial role in the chromatin organisation of hPSCs.

The natural and synthetic analogues of retinol/vitamin A are also known as retinoids and new evidence suggests that this metabolite has a key role in the regulation of stem cell self-renewal, especially as an extracellular function (Khillan, 2014). Similarly, the fibrinolysis and plasminogen activating cascade pathway (Table 6.8) have also shown a significant role in the self-renewal of stem cells (Heissig *et al.*,

2007, 2009; Ruf, 2016). These data along with our RNA-Seq data would suggest that the pathways activated in the feeder-free Matrigel™ samples required the extra vitamins and GFs in the ECM to be able to support and maintain the cells' pluripotency, especially with the significant overlap of upregulated gene transcripts we have observed in Figure 6.36 B.

With our gene positioning data demonstrating the remarkable mobility of chromatin in the hPSCs and the upregulation of extracellular matrix organisation and vitamin digestion and absorption pathways in the feeder-free conditions, this would again support the vital role growth factors from HDF secretion or from the niche the stem cells on the feeder-free conditions themselves create play in the maintenance of pluripotency. We would theorise that this environment around the stem cells are key regulators in the plasticity of the hPSC nuclei. Further investigation in this area is required to observe the function of growth factors and vitamins on the hPSC nucleus.

6.5.5. Detection of Mosaicism in Human Pluripotent Stem Cells

From our results, we have observed that ddPCR™ is a very promising tool for the sensitive detection of aneuploidy mosaicism in human pluripotent stem cells (Figure 6.1). When comparing directly to the NIBSC -5 karyology results (Appendix III), it is clear how biased it is to only look at 20-30 metaphase spreads to determine the cells' karyotype. Although ddPCR™ cannot detect the precise number of chromosomal aneuploidies in a mosaic culture, it provides the ability to look at the whole cell population from a very small sample and detect abnormalities that appear over time. This is a very important characteristic of ddPCR™, due to its potential in terms of stem cell therapeutic use in the future and the regulatory requirements for their use. Additionally, it is unknown whether the aneuploid cells in a whole population are still actively dividing and give rise to new cells or whether they are blocked in mitosis. If these cells are blocked in mitosis, then the level of aneuploidy would not change and eventually these cells would disappear without having affected the hPSC genome. Furthermore, if the pentasomal X cells are giving rise to new cells, it is unclear whether they are dividing at a rate

different to the diploid cells in the population. Previous reports have shown hPSCs to accumulate aneuploidies that give them a growth advantage in culture (Avery *et al.*, 2013) .

It must be noted, however, that the karyology results from the NIBSC-5 cells were from passage 10, whereas the sample we tested on the ddPCR™ was from a later passage of 20. It is a possibility that some changes may have occurred between passages 10-20. Despite this all, our results would suggest lower level mosaicism in the NIBSC-5 cells rather than 75% chromosome X aneuploidy, as the karyological results had suggested.

Chapter VII: General Discussion

7.1. General Discussion

The aim of this project was to develop a sensitive and high-throughput screen for the detection of chromosome aneuploidies in human pluripotent stem cells, as well as characterise gene loci positioning in aneuploid nuclei. Human pluripotent stem cells have long been known to develop chromosomal aberrations in culture via whole chromosome gains and/or losses, particularly for chromosomes 12, 17, 20 and X (Draper *et al.*, 2004; Baker *et al.*, 2007; Harrison, Baker and Andrews, 2007; Amps *et al.*, 2011). However, no method has yet been developed to sensitively detect these aneuploidies or characterise their role in the nucleus and the hPSC population. The aim was to look at the effect of different cell culture conditions on general genomic health of hPSCs and observe potential global gene expression changes utilising pathway analysis.

7.1.1. Aneuploidy Detection via Droplet Digital Polymerase Chain Reaction

Currently, karyotyping cells via G-banding is the gold standard and a requirement for cells intended for therapeutic use. Although cost effective, the method is labour-intensive and requires trained cytogeneticists for the analysis. In addition, G-banding resolution is typically 10Mb with a sensitivity of 10% aneuploidy detection and typical turnover time of five weeks; these factors drastically discourage its use.

Several different approaches were undertaken to determine the most appropriate and sensitive method to detect the abnormalities via Droplet Digital PCR™ (ddPCR™). Initially, a model experiment was performed for genes *AMELX* and *AMELY* located on chromosome X and Y, respectively. DNA from diploid male and female lymphoblastoid cell lines was used in a titration experiment to model how the pluripotent stem cells would behave when mosaic cultures would start appearing. Our results had demonstrated the sensitive detection of up to 1% of aneuploidy in a background diploid cells.

We demonstrated improved droplet segregation in the 2D plots of the ddPCR™ software when treating the DNA with enzymes or sonicating the DNA. Although the enzymatic treatment did not affect the overall ratio of the two amplicons, sonication significantly increased the number of positive droplets in the results. We hypothesised that the fragmented DNA allows efficient binding of the primers to the DNA sequences and thus, improves their amplification. This has been consistent with previous findings using enzymes or sonication as a pre-treatment of the DNA intended for ddPCR use (Yukl *et al.*, 2014; McMahon *et al.*, 2017; Vitomirov *et al.*, 2017). In addition, we initially observed a bias in the level of fluorescent signal from the FAM channel when using the *AMELX* and *AMELY* model in the male cell lines. This proved to be a cell culture artefact in the male cells, where potentially the Y chromosome is lost (Pierre and Hoagland, 1972), resulting in a strong FAM channel. We had shown this with the use of the same male blood samples as the cell culture samples and demonstrated a closer ratio of *AMELX* and *AMELY* to one. Because of this slightly higher *AMELX* to *AMELY* ratio, the same control sample was run in each ddPCR experiment performed and was used to normalise the rest of the samples.

Most importantly, our study demonstrated the inefficiency of G-banding versus ddPCR (Chapter V). In this manner, the optimisation of the ddPCR assay set-up in Chapter I demonstrated the ability to detect 1% aneuploidy in a background of diploid DNA, a level of sensitivity that has not been reported for other methodologies. Furthermore, the sensitivity of the assay allowed the monitoring of small percentage changes in the level of *AMELX* with regards to the reference gene, *ALB* for an extended amount of time in culture. This would, therefore allow the sensitive detection of low-level aneuploidy population emergence in culture. This previously been impossible with other assays, such as G-banding, aCGH and KaryoLite BoBs™, due to both the amount of DNA required to carry out such analysis and the lack of sensitivity. Our study demonstrated the amount of genomic alteration hPSCs appear to go through with each passage, something that had not been performed before. In the future, panels around unstable areas of the genome, such as multiple locations on chromosome 12, 17, 20 and X could be set-up to monitor the genomic instability of hPSCs. Such assays have already been developed for qPCR (*STEMCELL TECHNOLOGIES*, 2018), however not for the more sensitive ddPCR™.

7.1.2. Aneuploidy Positioning via Fluorescence *In-situ* Hybridisation

The nucleus is a highly organised organelle with chromosome territories occupying specific discrete areas in the nucleus with intermingling tendencies (Volpi *et al.*, 2000; Branco and Pombo, 2006). In lymphoblastoid cell lines, results from the reference gene *ALB* (HSA4) demonstrated positioning across all aneuploid cell lines consistent with previous studies using somatic cells (Boyle *et al.*, 2001; Mehta, *et al.*, Unpublished; Bikkul, *et al.*, Manuscript in Preparation). This consistency with other studies demonstrated the robustness and accuracy of our results.

On the other hand, *AMELX* (HSAX) demonstrated more significant differences when compared between different chromosome X aneuploid lymphoblastoid cell lines. Once again, this had been previously been observed with other research groups containing different types of aneuploidies (Petrova *et al.*, 2007; Shete *et al.*, 2014). Interestingly, despite the changes in positioning a conserved radial distribution was still observed in our data, which was similar to other studies (Cremer *et al.*, 2003; Wiblin *et al.*, 2005; Sengupta *et al.*, 2007; Shete *et al.*, 2014).

Unlike the results in the lymphoblastoid cell lines, the stem cell lines showed great variation in the positioning of both *ALB* and *AMELX* genes. This was not exclusive to one particular cell culture condition (Chapter V) or passage number (Chapter VI). As previously mentioned, we suggest that this phenomenon is a particular attribute of hPSCs, where cells are still in a naïve state and have not terminally differentiated, therefore, their chromatin is highly flexible and can shift readily dependent on the transcription requirement. This is supported by the lack of heterochromatin and the amount of histone modifications in the cells (Meshorer and Misteli, 2006; Meshorer *et al.*, 2006; Morris, Kelly, Chotalia and Pombo, 2010; Mattout, Biran and Meshorer, 2011). Furthermore, our results from Chapter VI demonstrated that this flexibility remained over 10 passages in two different sub-types of the same cell line with very little variation to the global gene transcription and despite the changes in the genomic instability. Previous studies have established that aneuploid nuclei often display significant changes to

their gene expression profile (Upender *et al.*, 2004; Grade *et al.*, 2006). Our study has not identified such changes, however as our study was dealing with presumed mosaic cell cultures, rather than whole aneuploid populations, this may be the reason for the small changes in the transcript levels. Further work could incorporate the data from this study and identify the global gene expression changes in hPSCs with whole chromosome aneuploidies. Single-cell RNA-Seq could be one potential method for the design of such studies.

In addition, our study was designed with the use of media and matrices that are commercially available, however many are not chemically defined, nor xeno-free. For research to move forward in the potential clinical use of hPSCs, the effect of specific molecules needs to be more extensively studied. Our data has shown different responses of cells in the different conditions with regards to their pluripotency markers. Therefore, the cell culture conditions could have a great effect on the therapeutic potential of hPSCs.

Interestingly, unlike the lymphoblastoid cell lines that showed significant differences in both nuclear size and nuclear circularity, in hPSC no correlation was observed. This was true for the different cell lines, the cells grown in different conditions and also across different passages. One explanation for this, as supported by our qPCR and IF staining findings, could be that within each cell culture colony small populations of the hESC cells differentiate into different lineages. Thus, this mixed population of cells may potentially skew the area and circularity data. One potential suggestion for future work that cells could first be stained via IF for multiple different pluripotency markers, their pluripotency confirmed and only then images be taken for cell morphology analysis.

Furthermore, in order to better understand the genome organisation of human pluripotent stem cells, chromosome territories could be positioned for chromosome 4 and X to observe whether genes, *ALB* and *AMELX* are within or outside these territories. In addition, whether the chromosome territories are also as flexible as the gene organisation within nuclei.

7.1.3. Aneuploidy and Lamins

Lamins have long been implicated in the normal functioning of the cells and their disruption has been linked with several diseases. Our study was designed to observe the protein staining pattern and expression, as well as the gene expression of both A-type and B-type lamins. Interestingly, very little staining of A-type lamins was observed in the lymphoblastoid cell lines, however in the hESCs the staining patterns were more variable. We observed no A-type lamin staining in hESCs that were grown in the colonies, however A-type lamin faint staining appeared with further distance away from these colonies. We hypothesise that the differentiation abilities of the hESCs allow these cells to differentiate into a wide range of different cell types and results in the heterogeneous staining we observed in Chapter VI. This concept is supported by the colony differentiation we observed in culture (Images in Appendix VI) and from our varied nuclear size and shape (Chapter VI and Appendix IV). This has been consistent with previous findings that suggest A-type lamins to have a role in the regulation of chromatin dynamics (Melcer *et al.*, 2012) as well as the physical plasticity of the stem cell nucleus (Pajerowski *et al.*, 2007). In comparison to A-type lamin expression, B-type lamins demonstrated much more reduced levels in the protein expression in aneuploid lymphoblastoid cell lines versus diploid cell lines. Similarly, their staining patterns showed significant differences between the cell lines, especially in DD0567 (XXX) and their gene expression levels for lamin B2 were significantly different in DD0710 (XXY) and DD1473 (XXXX) versus the female diploid control cell line. Interestingly, in the hESCs staining patterns as rims were observed inside and outside the hESC colonies, however some samples displayed the complete loss of lamin B2 in both the gene expression and protein staining in the nucleus. This is of particular importance as recent research has demonstrated that the loss of lamin B2 is associated with the formation of aneuploidies in culture (Ranade *et al.*, 2017). In order to make a clear link between the two, further research is required. Previously, it was established that B-type lamin complete knock-out can cause embryonic lethality (Vergnes *et al.*, 2004). Therefore, we propose further research on the stable knockdown of the gene, rather than transient. Alternatively, the use of CRISPR-Cas9 could

improve research and finally, prove whether lamin B2 reduction indeed is a direct cause of aneuploidy formation in cells.

Finally, we had performed RNA-Seq on several different cell lines across different conditions alongside our different assays to monitor the global gene expression differences. Although the RNA-Seq results were consistent with previous views of HDFs being required for the production of GFs and the creation of stem cell microenvironments, very little research had demonstrated this as clearly as our data. Further analysis of our data needs to be performed to monitor the transcription levels of each chromosome across the different cell lines and conditions. This would provide us with a valuable insight into the potential changes in the transcriptomics of hESCs during genomic instability.

7.1.4. Conclusions

We have successfully established a sensitive and high-throughput method for the detection of low-level aneuploidies in a majority diploid population. The sensitivity of our ddPCR™ assay, to our knowledge, is the most sensitive to date with the detection limit of up to 1% aneuploidies in a diploid population. In addition, our study not only optimised the use of ddPCR™, but also performed multiple studies on several different hPSC lines and the cell lines grown in different conditions. The robustness of our assay can be applied to other genes for the sensitive detection of common aneuploidies and the use of a control with each run increases the consistency of the results allowing us to compare different ddPCR™ runs.

Furthermore, we have performed the first study that had used multiple platforms to monitor the effects of different cell lines, conditions and passage on the genomic health of human pluripotent stem cells. The data from our gene positioning have demonstrated the genomic plasticity of the hPSCs, alongside the appearance of genomic instability in the cells. We theorise, that it is this flexibility in genome organisation that gives hPSCs their pluripotent capabilities and makes them susceptible to genomic aberrations, thus a concern for therapeutic use in clinics.

Finally, our results demonstrate the following key findings:

- Droplet Digital PCR™ can successfully detect up to 1% of aneuploidies in a background of diploid cells
- Chromosome X aneuploidies in lymphoblastoid cell lines can cause significant alterations to nuclear organisation
- Human pluripotent stem cells demonstrate a very high level of genomic stability with the ability to lose and regain gene copy numbers in very short periods of time, however these abnormalities do not change their gene positioning significantly
- Using fluorescence *in-situ* hybridisation, we demonstrated that chromatin organisation in human pluripotent stem cells is highly flexible, regardless of the presence or absence of feeder cells and of passage number
- The association of lamin B2 loss with aneuploidy formation in human embryonic stem cells
- Pathways, associated with the creation of stem cell microenvironments and the enrichment of vitamin digestion and absorption, are upregulated in human embryonic stem cells grown in feeder-free conditions

References

References

1. Abdian, N. *et al.* (2015) 'Comparison of human dermal fibroblasts (HDFs) growth rate in culture media supplemented with or without basic fibroblast growth factor (bFGF)', *Cell and Tissue Banking*, 16(4), pp. 487–495. doi: 10.1007/s10561-015-9494-9.
2. Abraham, E. *et al.* (2017) 'Platforms for Manufacturing Allogeneic, Autologous and iPSC Cell Therapy Products: An Industry Perspective', in: Springer, Berlin, Heidelberg, pp. 1–28. doi: 10.1007/10_2017_14.
3. Agerholm, I. E. *et al.* (2008) 'Nuclei size in relation to nuclear status and aneuploidy rate for 13 chromosomes in donated four cells embryos.', *Journal of assisted reproduction and genetics*. Springer, 25(2–3), pp. 95–102. doi: 10.1007/s10815-008-9199-0.
4. Aksglaede, L. *et al.* (2013) '47,XXY Klinefelter syndrome: Clinical characteristics and age-specific recommendations for medical management', *American Journal of Medical Genetics Part C: Seminars in Medical Genetics*. Wiley Subscription Services, Inc., A Wiley Company, 163(1), pp. 55–63. doi: 10.1002/ajmg.c.31349.
5. Albalushi, H. *et al.* (2017) 'Laminin 521 stabilizes the pluripotency expression pattern of human embryonic stem cells initially derived on feeder cells'. Available at: https://gallery.mailchimp.com/904c6d30608c6bb764db7cb28/files/eeb6826d-139d-4185-822b-288ae4e8b2bd/7127042_6_.pdf?utm_source=BioLamina+StemCell+list&utm_campaign=5a2467d43f-Newsletter+Q1+2018+non-customers&utm_medium=email&utm_term=0_b5222628eb-5a2467d43f (Accessed: 4 February 2018).
6. Alsheimer, M. and Benavente, R. (1996) 'Change of Karyoskeleton during Mammalian Spermatogenesis: Expression Pattern of Nuclear Lamin C2 and Its Regulation', *Experimental Cell Research*, 228(2), pp. 181–188. doi: 10.1006/excr.1996.0315.
7. Amariglio, N. *et al.* (2009) 'Donor-derived brain tumor following neural stem cell transplantation in an ataxia telangiectasia patient', *PLoS Medicine*. Edited by A. Fischer, 6(2), pp. 0221–0231. doi: 10.1371/journal.pmed.1000029.
8. Amit, M. *et al.* (2003) 'Human Feeder Layers for Human Embryonic Stem Cells1', *Biology of Reproduction*. Oxford University Press, 68(6), pp. 2150–2156. doi: 10.1095/biolreprod.102.012583.
9. Amps, K. *et al.* (2011) 'Screening ethnically diverse human embryonic stem cells identifies a chromosome 20 minimal amplicon conferring growth advantage', *Nature biotechnology*. Centre for Stem Cell Biology, Department of Biomedical Science, The University of Sheffield, Sheffield, UK., 29(12), pp. 1132–1144. doi: 10.1038/nbt.2051 [doi].
10. Andoh, T. and Ishida, R. (1998) 'Catalytic inhibitors of DNA topoisomerase II'. Available at: http://ac.els-cdn.com/S016747819800133X/1-s2.0-S016747819800133X-main.pdf?_tid=eaa273b8-811d-11e7-9962-00000aacb35e&acdnat=1502735295_2cf5c2760908eefbb05be00f4fe94934 (Accessed: 14 August 2017).
11. Arican-Goktas, H. D. *et al.* (2014) 'Differential Spatial Repositioning of Activated Genes in Biomphalaria glabrata Snails Infected with Schistosoma mansoni', *PLoS Neglected Tropical Diseases*. Edited by M. K. Jones. Public Library of Science, 8(9), p. e3013. doi: 10.1371/journal.pntd.0003013.
12. Asur, R. *et al.* (2010) 'Bystander effects induced by chemicals and ionizing radiation: evaluation of changes in gene expression of downstream MAPK targets', *Mutagenesis*. Oxford University Press, 25(3), pp. 271–279. doi: 10.1093/mutage/geq003.
13. Asur, R. S., Thomas, R. A. and Tucker, J. D. (2009) 'Chemical induction of the bystander effect in normal human lymphoblastoid cells', *Mutation Research/Genetic Toxicology and Environmental Mutagenesis*, 676(1), pp. 11–16. doi: 10.1016/j.mrgentox.2009.02.012.
14. Avery, S. *et al.* (2013) 'BCL-XL Mediates the Strong Selective Advantage of a 20q11.21

- Amplification Commonly Found in Human Embryonic Stem Cell Cultures', *Stem Cell Reports*, 1(5), pp. 379–386. doi: 10.1016/j.stemcr.2013.10.005.
15. Azam, E. I. *et al.* (1998) 'Intercellular communication is involved in the bystander regulation of gene expression in human cells exposed to very low fluences of alpha particles.', *Radiation research*, 150(5), pp. 497–504. Available at: <http://www.ncbi.nlm.nih.gov/pubmed/9806590> (Accessed: 8 April 2017).
 16. Baarlink, C., Wang, H. and Grosse, R. (2013) 'Nuclear Actin Network Assembly by Formins Regulates the SRF Coactivator MAL', *Science*, 340(6134), pp. 864–867. doi: 10.1126/science.1235038.
 17. Badylak, S. F., Taylor, D. and Uygun, K. (2011) 'Whole-Organ Tissue Engineering: Decellularization and Recellularization of Three-Dimensional Matrix Scaffolds'. Annual Reviews. Available at: <http://www.annualreviews.org/doi/abs/10.1146/annurev-bioeng-071910-124743> (Accessed: 3 February 2016).
 18. Bai, Q. *et al.* (2013) 'Embryonic stem cells or induced pluripotent stem cells? A DNA integrity perspective.', *Current gene therapy*. InSerm, 13(2), pp. 93–8. Available at: <http://www.ncbi.nlm.nih.gov/pubmed/23317057> (Accessed: 9 July 2017).
 19. Baker, D. E. C. *et al.* (2007) 'Adaptation to culture of human embryonic stem cells and oncogenesis in vivo.', *Nature biotechnology*, 25(2), pp. 207–215. doi: 10.1038/nbt1285.
 20. Baker, M. (2009) 'Unregulated stem cell transplant causes tumours', *Nature Reports Stem Cells*. Nature Publishing Group. doi: 10.1038/stemcells.2009.32.
 21. Balasubramanian, B., Pogożelski, W. K. and Tullius, T. D. (1998) 'DNA strand breaking by the hydroxyl radical is governed by the accessible surface areas of the hydrogen atoms of the DNA backbone', *Chemistry*, 95, pp. 9738–9743. Available at: <http://www.pnas.org/content/95/17/9738.full.pdf> (Accessed: 29 August 2017).
 22. Barber, J. C. K. (2005) 'Directly transmitted unbalanced chromosome abnormalities and euchromatic variants', *Journal of Medical Genetics*, 42(8), pp. 609–629. doi: 10.1136/jmg.2004.026955.
 23. Barker, N. *et al.* (2007) 'Identification of stem cells in small intestine and colon by marker gene Lgr5', *Nature*. Nature Publishing Group, 449(7165), pp. 1003–1007. doi: 10.1038/nature06196.
 24. Barker, R. A. *et al.* (2016) 'Are Stem Cell-Based Therapies for Parkinson's Disease Ready for the Clinic in 2016?', *Journal of Parkinson's Disease*. IOS Press, 6(1), pp. 57–63. doi: 10.3233/JPD-160798.
 25. Bártová, E. *et al.* (2001) 'Higher-order chromatin structure of human granulocytes.', *Chromosoma*. Springer-Verlag, 110(5), pp. 360–70. doi: 10.1007/s004120100141.
 26. Bártová, E. *et al.* (2008) 'Epigenome and chromatin structure in human embryonic stem cells undergoing differentiation.', *Developmental dynamics : an official publication of the American Association of Anatomists*. Wiley-Liss, Inc., 237(12), pp. 3690–3702. doi: 10.1002/dvdy.21773.
 27. Baumann, C. *et al.* (2007) 'PICH, a Centromere-Associated SNF2 Family ATPase, Is Regulated by Plk1 and Required for the Spindle Checkpoint', *Cell*, 128(1), pp. 101–114. doi: 10.1016/j.cell.2006.11.041.
 28. Berrios, M. and Fihser, P. . (1986) 'A myosin heavy-chain-like polypeptide is associated with the nuclear envelope in higher eukaryotic cells. - PubMed - NCBI', *J Cell Biol.*, 103(3), pp. 711–24. Available at: <https://www.ncbi.nlm.nih.gov/m/pubmed/2943745/>.
 29. Bhat, S. *et al.* (2010) 'Comparison of Methods for Accurate Quantification of DNA Mass Concentration with Traceability to the International System of Units', *Analytical Chemistry*. American Chemical Society, 82(17), pp. 7185–7192. doi: 10.1021/ac100845m.
 30. Bhute, V. J. *et al.* (2017) 'Metabolomics Identifies Metabolic Markers of Maturation in Human Pluripotent Stem Cell-Derived Cardiomyocytes.', *Theranostics*. Ivyspring International Publisher, 7(7), pp. 2078–2091. doi: 10.7150/thno.19390.
 31. Biamonti, G. *et al.* (1992) 'The gene for a novel human lamin maps at a highly transcribed locus of chromosome 19 which replicates at the onset of S-phase.', *Molecular and cellular biology*, 12(8),

- pp. 3499–506. Available at: <http://www.ncbi.nlm.nih.gov/pubmed/1630457> (Accessed: 9 February 2018).
32. Bjorklund, L. M. *et al.* (2002) 'Embryonic stem cells develop into functional dopaminergic neurons after transplantation in a Parkinson rat model.', *Proceedings of the National Academy of Sciences of the United States of America*, 99(4), pp. 2344–9. doi: 10.1073/pnas.022438099.
 33. Boise, L. H. *et al.* (1993) 'bcl-x, a bcl-2-related gene that functions as a dominant regulator of apoptotic cell death.', *Cell*, 74(4), pp. 597–608. Available at: <http://www.ncbi.nlm.nih.gov/pubmed/8358789> (Accessed: 4 April 2017).
 34. Bolzer, A. *et al.* (2005) 'Three-dimensional maps of all chromosomes in human male fibroblast nuclei and prometaphase rosettes', *PLoS Biology*. Public Library of Science, 3(5), pp. 0826–0842. doi: 10.1371/journal.pbio.0030157.
 35. Boyle, S. *et al.* (2001) 'The spatial organization of human chromosomes within the nuclei of normal and emerin-mutant cells.', *Human molecular genetics*, 10(3), pp. 211–219. doi: 10.1093/hmg/10.3.211.
 36. Brabetz, W. and Weber, C. (2014) 'Novel combination of fluorescent dyes for the detection of nucleic acids'.
 37. Branco, M. R. and Pombo, A. (2006) 'Intermingling of Chromosome Territories in Interphase Suggests Role in Translocations and Transcription-Dependent Associations', *PLoS Biology*. Edited by P. Becker. Public Library of Science, 4(5), p. e138. doi: 10.1371/journal.pbio.0040138.
 38. Braude, P., Bolton, V. and Moore, S. (1988) 'Human gene expression first occurs between the four- and eight-cell stages of preimplantation development', *Nature*, 332(6163), pp. 459–461. doi: 10.1038/332459a0.
 39. Bridger, J. M. *et al.* (1993) 'Internal lamin structures within G1 nuclei of human dermal fibroblasts', *Journal of Cell Science*, 104(2). Available at: <http://jcs.biologists.org/content/104/2/297.long> (Accessed: 14 August 2017).
 40. Bridger, J. M. *et al.* (2000) 'Re-modelling of nuclear architecture in quiescent and senescent human fibroblasts', *Current Biology*, 10(3), pp. 149–152. doi: 10.1016/S0960-9822(00)00312-2.
 41. Bridger, J. M. *et al.* (2007) 'The nuclear lamina', *FEBS Journal*. Blackwell Publishing Ltd, 274(6), pp. 1354–1361. doi: 10.1111/j.1742-4658.2007.05694.x.
 42. Bridger, J. M. *et al.* (2014) 'The Non-random Repositioning of Whole Chromosomes and Individual Gene Loci in Interphase Nuclei and Its Relevance in Disease, Infection, Aging, and Cancer', in *Advances in experimental medicine and biology*, pp. 263–279. doi: 10.1007/978-1-4899-8032-8_12.
 43. Bridger, J. M. and Bickmore, W. a. (1998) 'Putting the genome on the map', *Trends in Genetics*, 14(98), pp. 403–409. doi: 10.1016/S0168-9525(98)01572-8.
 44. Bridger, J. M. and Kill, I. R. (2004) 'Aging of Hutchinson–Gilford progeria syndrome fibroblasts is characterised by hyperproliferation and increased apoptosis', *Experimental Gerontology*, 39(5), pp. 717–724. doi: 10.1016/j.exger.2004.02.002.
 45. Bridger, J. M. and Volpi, E. V. (2010) *Fluorescence in situ Hybridization (FISH): Protocols and Applications (Methods in Molecular Biology)*. 2010th edn. Edited by J. M. Bridger and K. Morris. Springer Protocols.
 46. Brimble, S. N. *et al.* (2004) 'Karyotypic stability, genotyping, differentiation, feeder-free maintenance, and gene expression sampling in three human embryonic stem cell lines derived prior to August 9, 2001', *Stem cells and development*. BresaGen, Inc., Athens, GA 30605, USA., 13(6), pp. 585–597. doi: 10.1089/scd.2004.13.585 [doi].
 47. Broers, J. L. *et al.* (1993) 'Nuclear A-type lamins are differentially expressed in human lung cancer subtypes.', *The American journal of pathology*. American Society for Investigative Pathology, 143(1), pp. 211–20. Available at: <http://www.ncbi.nlm.nih.gov/pubmed/8391215> (Accessed: 3 March 2018).
 48. Broers, J. L. V. *et al.* (2006) 'Nuclear Lamins: Laminopathies and Their Role in Premature Ageing', *Physiological Reviews*, 86(3), pp. 967–1008. doi: 10.1152/physrev.00047.2005.

49. Brown, C. J. *et al.* (1991) 'A gene from the region of the human X inactivation centre is expressed exclusively from the inactive X chromosome', *Nature*, 349(6304), pp. 38–44. doi: 10.1038/349038a0.
50. Budde, J. P. *et al.* (2017) 'Precision genome-editing with CRISPR/Cas9 in human induced pluripotent stem cells', *bioRxiv*. Cold Spring Harbor Laboratory, p. 187377. doi: 10.1101/187377.
51. Bunch, J. T. *et al.* (2005) 'Distinct requirements for Pot1 in limiting telomere length and maintaining chromosome stability.', *Molecular and cellular biology*. American Society for Microbiology, 25(13), pp. 5567–78. doi: 10.1128/MCB.25.13.5567-5578.2005.
52. Burgess, R. J., Agathocleous, M. and Morrison, S. J. (2014) 'Metabolic regulation of stem cell function.', *Journal of internal medicine*. NIH Public Access, 276(1), pp. 12–24. doi: 10.1111/joim.12247.
53. Burke, B. and Stewart, C. L. (2006) 'The Laminopathies: The Functional Architecture of the Nucleus and Its Contribution to Disease', *Annual Review of Genomics and Human Genetics*, 7(1), pp. 369–405. doi: 10.1146/annurev.genom.7.080505.115732.
54. Butler, J. T. *et al.* (2009) 'Changing nuclear landscape and unique PML structures during early epigenetic transitions of human embryonic stem cells', *Journal of Cellular Biochemistry*, 107(4), pp. 609–621. doi: 10.1002/jcb.22183.
55. Buzzard, J. J. *et al.* (2004) 'Karyotype of human ES cells during extended culture', *Nature Biotechnology*. Nature Publishing Group, 22(4), pp. 381–382. doi: 10.1038/nbt0404-381.
56. Caine, A. *et al.* (2005) 'Prenatal detection of Down's syndrome by rapid aneuploidy testing for chromosomes 13, 18, and 21 by FISH or PCR without a full karyotype: A cytogenetic risk assessment', *Lancet*, 366(9480), pp. 123–128. doi: 10.1016/S0140-6736(05)66790-6.
57. Capell, B. C. and Collins, F. S. (2006) 'Human laminopathies: nuclei gone genetically awry', *Nature Reviews Genetics*, 7(12), pp. 940–952. doi: 10.1038/nrg1906.
58. Capo-chichi, C. D. *et al.* (2011) 'Nuclear envelope structural defects cause chromosomal numerical instability and aneuploidy in ovarian cancer', *BMC Medicine*. BioMed Central, 9(1), p. 28. doi: 10.1186/1741-7015-9-28.
59. Castellanos, E., Dominguez, P. and Gonzalez, C. (2008) 'Centrosome Dysfunction in Drosophila Neural Stem Cells Causes Tumors that Are Not Due to Genome Instability', *Current Biology*, 18(16), pp. 1209–1214. doi: 10.1016/j.cub.2008.07.029.
60. Caussinus, E. and Gonzalez, C. (2005) 'Induction of tumor growth by altered stem-cell asymmetric division in Drosophila melanogaster', *Nature Genetics*, 37(10), pp. 1125–1129. doi: 10.1038/ng1632.
61. Chan, K.-L., North, P. S. and Hickson, I. D. (2007) 'BLM is required for faithful chromosome segregation and its localization defines a class of ultrafine anaphase bridges', *The EMBO Journal*, 26(14), pp. 3397–3409. doi: 10.1038/sj.emboj.7601777.
62. Chen, K. G. *et al.* (2014) 'Human pluripotent stem cell culture: considerations for maintenance, expansion, and therapeutics.', *Cell stem cell*. NIH Public Access, 14(1), pp. 13–26. doi: 10.1016/j.stem.2013.12.005.
63. Cheng, L. *et al.* (2003) 'Human Adult Marrow Cells Support Prolonged Expansion of Human Embryonic Stem Cells in Culture', *Stem Cells*, 21(2), pp. 131–142. doi: 10.1634/stemcells.21-2-131.
64. Choy, R. K. W. *et al.* (2014) 'BACs-on-beads: a new robust and rapid detection method for prenatal diagnosis', *Expert Review of Molecular Diagnostics*, 14(3), pp. 273–280. doi: 10.1586/14737159.2014.899468.
65. Christova, R. *et al.* (2007) 'P-STAT1 mediates higher-order chromatin remodelling of the human MHC in response to IFN', *Journal of Cell Science*, 120(18), pp. 3262–3270. doi: 10.1242/jcs.012328.
66. Cimini, D. *et al.* (2002) 'Merotelic kinetochore orientation versus chromosome mono-orientation in the origin of lagging chromosomes in human primary cells.', *Journal of cell science*, 115(Pt 3), pp. 507–15. Available at: <http://www.ncbi.nlm.nih.gov/pubmed/11861758> (Accessed: 3 April

- 2017).
67. Cimini, D., Tanzarella, C. and Degrassi, F. (1999) 'Differences in malsegregation rates obtained by scoring ana-telophases or binucleate cells.', *Mutagenesis*, 14(6), pp. 563–8. Available at: <http://www.ncbi.nlm.nih.gov/pubmed/10567031> (Accessed: 3 April 2017).
 68. Cirigliano, V. *et al.* (2004) 'Rapid prenatal diagnosis of common chromosome aneuploidies by QF-PCR. Assessment on 18000 consecutive clinical samples', *MHR: Basic science of reproductive medicine*, 10(11), pp. 839–846. doi: 10.1093/molehr/gah108.
 69. Clements, C. S. *et al.* (2016) 'Visualizing the Spatial Relationship of the Genome with the Nuclear Envelope Using Fluorescence In Situ Hybridization', in: Humana Press, New York, NY, pp. 387–406. doi: 10.1007/978-1-4939-3530-7_24.
 70. *ClinicalTrials.gov* (2012) *A Study Of Implantation Of Retinal Pigment Epithelium In Subjects With Acute Wet Age Related Macular Degeneration*. Available at: <https://clinicaltrials.gov/ct2/show/study/NCT01691261> (Accessed: 19 May 2018).
 71. Coffinier, C. *et al.* (2010) 'Abnormal development of the cerebral cortex and cerebellum in the setting of lamin B2 deficiency', *Proceedings of the National Academy of Sciences*, 107(11), pp. 5076–5081. doi: 10.1073/pnas.0908790107.
 72. Comes, S. *et al.* (2013) 'L-Proline Induces a Mesenchymal-like Invasive Program in Embryonic Stem Cells by Remodeling H3K9 and H3K36 Methylation', *Stem Cell Reports*, 1(4), pp. 307–321. doi: 10.1016/j.stemcr.2013.09.001.
 73. Constantinescu, D. *et al.* (2006) 'Lamin A/C expression is a marker of mouse and human embryonic stem cell differentiation.', *Stem cells*. Wiley-Blackwell, 24(1), pp. 177–185. doi: 10.1634/stemcells.2004-0159.
 74. Cremer, M. *et al.* (2003) 'Inheritance of gene density–related higher order chromatin arrangements in normal and tumor cell nuclei', *The Journal of Cell Biology*, 162(5), pp. 809–820. doi: 10.1083/jcb.200304096.
 75. Cremer, T. and Cremer, C. (2001) 'Chromosome territories, nuclear architecture and gene regulation in mammalian cells', *Nature Reviews Genetics*, 2, pp. 292–301. Available at: <http://www.ncbi.nlm.nih.gov/pubmed/11283701>.
 76. Croft, J. a. *et al.* (1999) 'Differences in the localization and morphology of chromosomes in the human nucleus', *The Journal of cell biology*, 145(6), pp. 1119–31. doi: 10.1083/jcb.145.6.1119.
 77. D'Aniello, C. *et al.* (2017) 'Vitamin C in Stem Cell Biology: Impact on Extracellular Matrix Homeostasis and Epigenetics.', *Stem cells international*. Hindawi Limited, 2017, p. 8936156. doi: 10.1155/2017/8936156.
 78. Damelin, M. *et al.* (2005) 'Decatenation checkpoint deficiency in stem and progenitor cells', *Cancer Cell*. Cell Press, 8(6), pp. 479–484. Available at: <https://www.sciencedirect.com/science/article/pii/S1535610805003612?via%3Dihub> (Accessed: 14 August 2017).
 79. Davidson, P. M. *et al.* (2014) 'Nuclear deformability constitutes a rate-limiting step during cell migration in 3-D environments.', *Cellular and molecular bioengineering*. NIH Public Access, 7(3), pp. 293–306. doi: 10.1007/s12195-014-0342-y.
 80. Dechat, T. *et al.* (2000) 'Lamina-associated polypeptide 2alpha binds intranuclear A-type lamins.', *Journal of cell science*, 113 Pt 19, pp. 3473–84. Available at: <http://www.ncbi.nlm.nih.gov/pubmed/10984438> (Accessed: 22 May 2018).
 81. Dechat, T. *et al.* (2008) 'Nuclear lamins: major factors in the structural organization and function of the nucleus and chromatin.', *Genes & development*. Cold Spring Harbor Laboratory Press, 22(7), pp. 832–53. doi: 10.1101/gad.1652708.
 82. Dechat, T. *et al.* (2010) 'Nuclear Lamins', *Cold Spring Harbor Perspectives in Biology*, 2(11), pp. a000547–a000547. doi: 10.1101/cshperspect.a000547.
 83. DePinho, R. A. (2000) 'The age of cancer.', *Nature*, 408(6809), pp. 248–254. doi: 10.1038/35041694.
 84. Deshpande, A. *et al.* (1996) 'Alpha-particle-induced sister chromatid exchange in normal human

- lung fibroblasts: evidence for an extranuclear target.', *Radiation research*, 145(3), pp. 260–7. Available at: <http://www.ncbi.nlm.nih.gov/pubmed/8927692> (Accessed: 8 April 2017).
85. Deshpande, D. M. *et al.* (2006) 'Recovery from paralysis in adult rats using embryonic stem cells.', *Annals of neurology*. John Wiley and Sons Inc., 60(1), pp. 32–44. doi: 10.1002/ana.20901.
 86. Desmarais, J. A. *et al.* (2012) 'Human Embryonic Stem Cells Fail to Activate CHK1 and Commit to Apoptosis in Response to DNA Replication Stress', *STEM CELLS*, 30(7), pp. 1385–1393. doi: 10.1002/stem.1117.
 87. Dhar, D. and Hsi-En Ho, J. (2009) 'Stem cell research policies around the world.', *The Yale journal of biology and medicine*. Yale Journal of Biology and Medicine, 82(3), pp. 113–5. Available at: <http://www.ncbi.nlm.nih.gov/pubmed/19774124> (Accessed: 4 May 2018).
 88. Dietzel, S. *et al.* (1998) 'Separate and variably shaped chromosome arm domains are disclosed by chromosome arm painting in human cell nuclei', *Chromosome Research*, 6(1), pp. 25–33. doi: 10.1023/A:1009262223693.
 89. Dingle, T. C. *et al.* (2013) 'Tolerance of droplet-digital PCR vs real-time quantitative PCR to inhibitory substances.', *Clinical chemistry*. Clinical Chemistry, 59(11), pp. 1670–2. doi: 10.1373/clinchem.2013.211045.
 90. Dittmer, T. A. and Misteli, T. (2011) 'The lamin protein family', *Genome Biology*, 12(5), p. 222. doi: 10.1186/gb-2011-12-5-222.
 91. Dixon, F. J. and Moore, R. A. (1953) 'Testicular tumors; a clinicopathological study', *Cancer*. Not Available, 6(3), pp. 427–454.
 92. Donaghue, C. *et al.* (2005) 'Detection of mosaicism for primary trisomies in prenatal samples by QF-PCR and karyotype analysis', *Prenatal Diagnosis*, 25(1), pp. 65–72. doi: 10.1002/pd.1086.
 93. Dong, L. *et al.* (2014) 'Evaluation of droplet digital PCR for characterizing plasmid reference material used for quantifying ammonia oxidizers and denitrifiers.', *Analytical and bioanalytical chemistry*. Springer, 406(6), pp. 1701–12. doi: 10.1007/s00216-013-7546-1.
 94. Draper, J. S. *et al.* (2004) 'Recurrent gain of chromosomes 17q and 12 in cultured human embryonic stem cells', *Nature biotechnology*. Department of Biomedical Science, University of Sheffield, Western Bank, Sheffield S10 2TN, UK., 22(1), pp. 53–54. doi: 10.1038/nbt922 [doi].
 95. Dravid, G. *et al.* (2005) 'Defining the Role of Wnt/ β -Catenin Signaling in the Survival, Proliferation, and Self-Renewal of Human Embryonic Stem Cells', *Stem Cells*. Wiley-Blackwell, 23(10), pp. 1489–1501. doi: 10.1634/stemcells.2005-0034.
 96. Dudarewicz, L. *et al.* (2005) 'Molecular methods for rapid detection of aneuploidy', *J Appl Genet.*, 46(2), pp. 207–215. Available at: <http://www.ncbi.nlm.nih.gov/pubmed/15876689>.
 97. Eberhard, D. a, Giaccone, G. and Johnson, B. E. (2008) 'Biomarkers of response to epidermal growth factor receptor inhibitors in Non-Small-Cell Lung Cancer Working Group: standardization for use in the clinical trial setting.', *Journal of clinical oncology : official journal of the American Society of Clinical Oncology*, 26(6), pp. 983–994. doi: 10.1200/JCO.2007.12.9858.
 98. Eckert, S. E. *et al.* (2018) 'Enrichment by hybridisation of long DNA fragments for Nanopore sequencing'. doi: 10.1099/mgen.0.000087.
 99. van Eijk, R. *et al.* (2011) 'Rapid KRAS, EGFR, BRAF and PIK3CA mutation analysis of fine needle aspirates from non-small-cell lung cancer using allele-specific qPCR', *PLoS ONE*, 6(3). doi: 10.1371/journal.pone.0017791.
 100. Eiselleova, L. *et al.* (2008) 'Comparative study of mouse and human feeder cells for human embryonic stem cells', *The International Journal of Developmental Biology*, 52(4), pp. 353–363. doi: 10.1387/ijdb.082590le.
 101. Ellerström, C. *et al.* (2007) 'Facilitated Expansion of Human Embryonic Stem Cells by Single-Cell Enzymatic Dissociation', *Stem Cells*. John Wiley & Sons, Ltd., 25(7), pp. 1690–1696. doi: 10.1634/stemcells.2006-0607.
 102. Elstner, A. *et al.* (2009) 'The changing landscape of European and international regulation on embryonic stem cell research', *Stem Cell Research*. Elsevier, 2(2), pp. 101–107. doi: 10.1016/J.SCR.2008.10.003.

103. Enver, T. *et al.* (2005) 'Cellular differentiation hierarchies in normal and culture-adapted human embryonic stem cells', *Human Molecular Genetics*. Oxford University Press, 14(21), pp. 3129–3140. doi: 10.1093/hmg/ddi345.
104. Espada, J. *et al.* (2008) 'Nuclear envelope defects cause stem cell dysfunction in premature-aging mice', *The Journal of Cell Biology*, 181(1), pp. 27–35. doi: 10.1083/jcb.200801096.
105. EuroStemCell (2018) *Regulation of stem cell research in Ireland*. Available at: <https://www.eurostemcell.org/regulation-stem-cell-research-ireland> (Accessed: 4 May 2018).
106. Evans, M. J. and Kaufman, M. H. (1981) 'Establishment in culture of pluripotential cells from mouse embryos.', *Nature*, pp. 154–156. doi: 10.1038/292154a0.
107. Falk, M. *et al.* (2002) 'Topography of genetic elements of X-chromosome relative to the cell nucleus and to the chromosome X territory determined for human lymphocytes', *Gene*. Elsevier, 292(1–2), pp. 13–24. doi: 10.1016/S0378-1119(02)00667-4.
108. Fan, H. C. *et al.* (2009) 'Microfluidic digital PCR enables rapid prenatal diagnosis of fetal aneuploidy', *American Journal of Obstetrics and Gynecology*. Elsevier Inc., 200(5), p. 543.e1–543.e7. doi: 10.1016/j.ajog.2009.03.002.
109. Fan, H. C. and Quake, S. R. (2007) 'Detection of Aneuploidy with Digital Polymerase Chain Reaction', *Analytical Chemistry*, 79(19), pp. 7576–7579. doi: 10.1021/ac0709394.
110. Fazeli, A. *et al.* (2011) 'Altered patterns of differentiation in karyotypically abnormal human embryonic stem cells', *The International Journal of Developmental Biology*, 55(2), pp. 175–180. doi: 10.1387/ijdb.103177af.
111. Federico, C. *et al.* (2006) 'Gene-rich and gene-poor chromosomal regions have different locations in the interphase nuclei of cold-blooded vertebrates', *Chromosoma*, 115(2), pp. 123–128. doi: 10.1007/s00412-005-0039-z.
112. Felgentreff, K. *et al.* (2014) 'Differential role of nonhomologous end joining factors in the generation, DNA damage response, and myeloid differentiation of human induced pluripotent stem cells.', *Proceedings of the National Academy of Sciences of the United States of America*. National Academy of Sciences, 111(24), pp. 8889–94. doi: 10.1073/pnas.1323649111.
113. Ferguson, M., Ward, D. C. and Manueiidis, L. (1992) 'Cell cycle dependent chromosomal movement in pre-mitotic human T-lymphocyte nuclei', *Chromosoma*, 101, pp. 557–565. Available at: http://download.springer.com/static/pdf/767/art%253A10.1007%252FBF00660315.pdf?originUrl=http%3A%2F%2Flink.springer.com%2Farticle%2F10.1007%2FBF00660315&token2=exp=1493756771~acl=%2Fstatic%2Fpdf%2F767%2Fart%25253A10.1007%25252FBF00660315.pdf%3ForiginUrl%3Dhttp%253A%252F%252Flink.springer.com%252Farticle%252F10.1007%252FBF00660315*~hmac=c0ba3da2c5fcce27986721a499780f8b419f549f601a4a5d9d4d05dfcf63cb60 (Accessed: 2 May 2017).
114. Fikes, B. J. (2015) *The Sunday Diego Union-Tribune, Supreme Court rejects stem cell patent case involving San Diego researcher - The San Diego Union-Tribune*. Available at: <http://www.sandiegouniontribune.com/business/biotech/sdut-supreme-court-rejects-warf-patent-case-2015feb24-story.html> (Accessed: 5 May 2018).
115. Finch, K. A. *et al.* (2008) 'Nuclear organisation in totipotent human nuclei and its relationship to chromosomal abnormality.', *Journal of cell science*, 121(Pt 5), pp. 655–63. doi: 10.1242/jcs.025205.
116. Finkel, T. and Holbrook, N. J. (2000) 'Oxidants, oxidative stress and the biology of ageing', *Nature*. Nature Publishing Group, 408(6809), pp. 239–247. doi: 10.1038/35041687.
117. Fisher, D. Z., Chaudhary, N. and Blobel, G. (1986) 'cDNA sequencing of nuclear lamins A and C reveals primary and secondary structural homology to intermediate filament proteins.', *Proceedings of the National Academy of Sciences of the United States of America*. National Academy of Sciences, 83(17), pp. 6450–4. Available at: <http://www.ncbi.nlm.nih.gov/pubmed/3462705> (Accessed: 9 February 2018).
118. Foster, H. A. *et al.* (2007) 'Lamins A and C are present in the nuclei of early porcine embryos,

- with lamin A being distributed in large intranuclear foci', *Chromosome Research*. Springer Netherlands, 15(2), pp. 163–174. doi: 10.1007/s10577-006-1088-8.
119. Foster, H. A., Griffin, D. K. and Bridger, J. M. (2012) 'Interphase chromosome positioning in in vitro porcine cells and ex vivo porcine tissues', *BMC Cell Biology*. BioMed Central, 13(1), p. 30. doi: 10.1186/1471-2121-13-30.
 120. Francastel, C. *et al.* (2000) 'Nuclear compartmentalization and gene activity.', *Nature reviews. Molecular cell biology*. Macmillan Magazines Ltd., 1(2), pp. 137–43. doi: 10.1038/35040083.
 121. Fraser, J., Williamson, I., *et al.* (2015) 'An Overview of Genome Organization and How We Got There: from FISH to Hi-C.', *Microbiology and molecular biology reviews : MMBR*. American Society for Microbiology (ASM), 79(3), pp. 347–72. doi: 10.1128/MMBR.00006-15.
 122. Fraser, J., Ferrai, C., *et al.* (2015) 'Hierarchical folding and reorganization of chromosomes are linked to transcriptional changes in cellular differentiation.', *Molecular systems biology*. European Molecular Biology Organization, 11(12), p. 852. doi: 10.15252/MSB.20156492.
 123. Fritz, B. *et al.* (2001) 'Cytogenetic analyses of culture failures by comparative genomic hybridisation (CGH)-Re-evaluation of chromosome aberration rates in early spontaneous abortions.', *European journal of human genetics : EJHG*, 9(7), pp. 539–47. doi: 10.1038/sj.ejhg.5200669.
 124. Furukawa, K., Inagaki, H. and Hotta, Y. (1994) 'Identification and Cloning of an mRNA Coding for a Germ Cell-Specific A-Type Lamin in Mice', *Experimental Cell Research*, 212(2), pp. 426–430. doi: 10.1006/excr.1994.1164.
 125. Garitaonandia, I. *et al.* (2015) 'Increased Risk of Genetic and Epigenetic Instability in Human Embryonic Stem Cells Associated with Specific Culture Conditions', *PLOS ONE*. Edited by T.-Y. Roh. Public Library of Science, 10(2), p. e0118307. doi: 10.1371/journal.pone.0118307.
 126. Geiszt, M. *et al.* (2000) 'Identification of renox, an NAD(P)H oxidase in kidney.', *Proceedings of the National Academy of Sciences of the United States of America*. National Academy of Sciences, 97(14), pp. 8010–4. doi: 10.1073/pnas.130135897.
 127. George, D. *et al.* (2013) 'Detection and quantification of chimerism by droplet digital PCR', *Journal of Chimerism*, pp. 102–108. doi: 10.1016/j.jmoldx.2013.10.007.
 128. Gerace, L. and Burke, B. (1988) 'Functional Organization of the Nuclear Envelope', *Annual Review of Cell Biology*, 4(1), pp. 335–374. doi: 10.1146/annurev.cb.04.110188.002003.
 129. Gisselsson, D. *et al.* (2001) 'Telomere dysfunction triggers extensive DNA fragmentation and evolution of complex chromosome abnormalities in human malignant tumors.', *Proceedings of the National Academy of Sciences of the United States of America*. National Academy of Sciences, 98(22), pp. 12683–8. doi: 10.1073/pnas.211357798.
 130. Goodarzi, A. A. *et al.* (2008) 'ATM Signaling Facilitates Repair of DNA Double-Strand Breaks Associated with Heterochromatin', *Molecular Cell*, 31(2), pp. 167–177. doi: 10.1016/j.molcel.2008.05.017.
 131. Gorbsky, G. J. (1994) 'Cell cycle progression and chromosome segregation in mammalian cells cultured in the presence of the topoisomerase II inhibitors ICRF-187 [(+)-1,2-bis(3,5-dioxopiperazinyl-1-yl)propane; ADR-529] and ICRF-159 (Razoxane).', *Cancer research*, 54(4), pp. 1042–8. Available at: <http://www.ncbi.nlm.nih.gov/pubmed/8313360> (Accessed: 14 August 2017).
 132. Gotzmann, J. and Foisner, R. (2006) 'A-type lamin complexes and regenerative potential: a step towards understanding laminopathic diseases?', *Histochemistry and Cell Biology*, 125(1–2), pp. 33–41. doi: 10.1007/s00418-005-0050-8.
 133. Grade, M. *et al.* (2006) 'Aneuploidy-Dependent Massive Deregulation of the Cellular Transcriptome and Apparent Divergence of the Wnt/ β -catenin Signaling Pathway in Human Rectal Carcinomas', *Cancer Research*, 66(1), pp. 267–282. doi: 10.1158/0008-5472.CAN-05-2533.
 134. Graf, A. *et al.* (2014) 'Fine mapping of genome activation in bovine embryos by RNA sequencing.', *Proceedings of the National Academy of Sciences of the United States of America*. National Academy of Sciences, 111(11), pp. 4139–44. doi: 10.1073/pnas.1321569111.

135. Grealish, S. *et al.* (2014) 'Human ESC-Derived Dopamine Neurons Show Similar Preclinical Efficacy and Potency to Fetal Neurons when Grafted in a Rat Model of Parkinson's Disease', *Cell Stem Cell*, 15(5), pp. 653–665. doi: 10.1016/j.stem.2014.09.017.
136. Gruenbaum, Y. *et al.* (2003) 'The nuclear lamina and its functions in the nucleus'. Academic Press, 226, pp. 1–62. doi: 10.1016/S0074-7696(03)01001-5.
137. Gupta, P. *et al.* (2016) 'Optimization of agitation speed in spinner flask for microcarrier structural integrity and expansion of induced pluripotent stem cells', *Cytotechnology*, 68(1), pp. 45–59. doi: 10.1007/s10616-014-9750-z.
138. Haaf, T. and Schmid, M. (1988) 'Analysis of Double Minutes and Double Minute-Like Chromatin in Human and Murine Tumor Cells Using Antikinetochores Antibodies', *Cancer Genetics and Cytogenetics*. Available at: http://ac.els-cdn.com/0165460888900945/1-s2.0-0165460888900945-main.pdf?_tid=52e79852-80b2-11e7-9962-00000aacb35e&acdnat=1502689084_245f671fc0173d935f89ea942a27355e (Accessed: 14 August 2017).
139. Habermann, J. K. *et al.* (2007) 'Stage-specific alterations of the genome, transcriptome, and proteome during colorectal carcinogenesis', *Genes, Chromosomes and Cancer*. Wiley Subscription Services, Inc., A Wiley Company, 46(1), pp. 10–26. doi: 10.1002/gcc.20382.
140. Hackett, J. A., Feldser, D. M. and Greider, C. W. (2001) 'Telomere dysfunction increases mutation rate and genomic instability.', *Cell*, 106(3), pp. 275–86. Available at: <http://www.ncbi.nlm.nih.gov/pubmed/11509177> (Accessed: 1 April 2017).
141. Halaschek-Wiener, J. and Brooks-Wilson, A. (2007) 'Progeria of stem cells: stem cell exhaustion in Hutchinson-Gilford progeria syndrome.', *The journals of gerontology. Series A, Biological sciences and medical sciences*, 62(1), pp. 3–8. Available at: <http://www.ncbi.nlm.nih.gov/pubmed/17301031> (Accessed: 9 April 2017).
142. Harrison, N. J., Baker, D. and Andrews, P. W. (2007) 'Culture adaptation of embryonic stem cells echoes germ cell malignancy.', *International journal of andrology*, 30(4), p. 275–81; discussion 281. doi: 10.1111/j.1365-2605.2007.00762.x.
143. Hasegawa, K. *et al.* (2006) 'A Method for the Selection of Human Embryonic Stem Cell Sublines with High Replating Efficiency After Single-Cell Dissociation', *Stem Cells*. John Wiley & Sons, Ltd., 24(12), pp. 2649–2660. doi: 10.1634/stemcells.2005-0657.
144. Hassold, T. and Hunt, P. (2001) 'To err (meiotically) is human: the genesis of human aneuploidy', *Nature Reviews Genetics*. Nature Publishing Group, 2(4), pp. 280–291. doi: 10.1038/35066065.
145. Heissig, B. *et al.* (2007) 'The Plasminogen Fibrinolytic Pathway Is Required for Hematopoietic Regeneration', *Cell Stem Cell*, 1(6), pp. 658–670. doi: 10.1016/j.stem.2007.10.012.
146. Heissig, B. *et al.* (2009) 'Contribution of the fibrinolytic pathway to hematopoietic regeneration', *Journal of Cellular Physiology*. Wiley-Blackwell, 221(3), pp. 521–525. doi: 10.1002/jcp.21897.
147. Hérault, A. *et al.* (2017) 'Myeloid progenitor cluster formation drives emergency and leukaemic myelopoiesis', *Nature*. Nature Research. doi: 10.1038/nature21693.
148. Herberts, C. A., Kwa, M. S. G. and Hermsen, H. P. H. (2011) 'Risk factors in the development of stem cell therapy.', *Journal of translational medicine*, 9, p. 29. doi: 10.1186/1479-5876-9-29.
149. Heredia, N. J. *et al.* (2013) 'Droplet Digital??? PCR quantitation of HER2 expression in FFPE breast cancer samples', *Methods*. Elsevier Inc., 59(1), pp. 183–186. doi: 10.1016/j.ymeth.2012.09.012.
150. Heride, C. *et al.* (2010) 'Distance between homologous chromosomes results from chromosome positioning constraints', *Journal of Cell Science*, 123(23), pp. 4063–4075. doi: 10.1242/jcs.066498.
151. Hernandez, L. *et al.* (2010) 'Functional Coupling between the Extracellular Matrix and Nuclear Lamina by Wnt Signaling in Progeria', *Developmental Cell*, 19(3), pp. 413–425. doi: 10.1016/j.devcel.2010.08.013.

152. Herrmann, H. *et al.* (2009) 'Intermediate filaments: primary determinants of cell architecture and plasticity', *Journal of Clinical Investigation*, 119(7), pp. 1772–1783. doi: 10.1172/JCI38214.
153. Herszfeld, D. *et al.* (2006) 'CD30 is a survival factor and a biomarker for transformed human pluripotent stem cells', *Nature Biotechnology*. Nature Publishing Group, 24(3), pp. 351–357. doi: 10.1038/nbt1197.
154. Hewitson, H. *et al.* (2016) 'Generation of KCL024 research grade human embryonic stem cell line carrying a mutation in NF1 gene.', *Stem cell research*. Elsevier, 16(2), pp. 243–5. doi: 10.1016/j.scr.2016.01.010.
155. Hickman, A. W. *et al.* (1994) 'Alpha-particle-induced p53 protein expression in a rat lung epithelial cell strain.', *Cancer research*, 54(22), pp. 5797–800. Available at: <http://www.ncbi.nlm.nih.gov/pubmed/7954402> (Accessed: 8 April 2017).
156. Hindson, B. J. *et al.* (2011) 'High-throughput droplet digital PCR system for absolute quantitation of DNA copy number', *Analytical Chemistry*, 83(22), pp. 8604–8610. doi: 10.1021/ac202028g.
157. Hoffelder, D. *et al.* (2004) 'Resolution of anaphase bridges in cancer cells', *Chromosoma*. Springer-Verlag, 112(8), pp. 389–397. doi: 10.1007/s00412-004-0284-6.
158. Hoffmann, K. *et al.* (2002) 'Mutations in the gene encoding the lamin B receptor produce an altered nuclear morphology in granulocytes (Pelger–Huët anomaly)', *Nature Genetics*. Nature Publishing Group, 31(4), pp. 410–414. doi: 10.1038/ng925.
159. Holm, C., Stearns, T. and Botstein, D. (1989) 'DNA topoisomerase II must act at mitosis to prevent nondisjunction and chromosome breakage.', *Molecular and cellular biology*, 9(1), pp. 159–68. Available at: <http://www.ncbi.nlm.nih.gov/pubmed/2538717> (Accessed: 14 August 2017).
160. Holm, S. (2006) 'Are countries that ban human embryonic stem cell research hypocritical?', *Regenerative Medicine*. Future Medicine Ltd London, UK, 1(3), pp. 357–359. doi: 10.2217/17460751.1.3.357.
161. Honda, S. *et al.* (2010) 'The DMM complex prevents spreading of DNA methylation from transposons to nearby genes in *Neurospora crassa*', *Genes & Development*, 24(5), pp. 443–454. doi: 10.1101/gad.1893210.
162. Hongisto, H. *et al.* (2012) 'Laminin-511 expression is associated with the functionality of feeder cells in human embryonic stem cell culture', *Stem Cell Research*, 8(1), pp. 97–108. doi: 10.1016/j.scr.2011.08.005.
163. Hongisto, H. *et al.* (2017) 'Xeno- and feeder-free differentiation of human pluripotent stem cells to two distinct ocular epithelial cell types using simple modifications of one method', *Stem Cell Research & Therapy*, 8(1), p. 291. doi: 10.1186/s13287-017-0738-4.
164. Houck, M. M. (2015) *Forensic Biology*. Elsevier.
165. Houlston, E. *et al.* (1988) 'Expression of nuclear lamins during mouse preimplantation development.', *Development (Cambridge, England)*, 102(2), pp. 271–8. Available at: <http://www.ncbi.nlm.nih.gov/pubmed/3046911> (Accessed: 9 February 2018).
166. Hovatta, O. *et al.* (2003) 'A culture system using human foreskin fibroblasts as feeder cells allows production of human embryonic stem cells', *Human Reproduction*. Oxford University Press, 18(7), pp. 1404–1409. doi: 10.1093/humrep/deg290.
167. Huggett, J. F., Cowen, S. and Foy, C. a. (2014) 'Considerations for Digital PCR as an Accurate Molecular Diagnostic Tool', *Clinical Chemistry*, 61(1), pp. 79–88. doi: 10.1373/clinchem.2014.221366.
168. Hulspas, R. *et al.* (1994) 'The nuclear position of pericentromeric DNA of chromosome 11 appears to be random in G 0 and non-random in G 1 human lymphocytes', *Chromosoma*, 103, pp. 286–292. Available at: <http://download.springer.com/static/pdf/998/art%253A10.1007%252FBF00352253.pdf?originUrl=http%3A%2F%2Flink.springer.com%2Farticle%2F10.1007%2FBF00352253&token2=exp=1493757020~acl=%2Fstatic%2Fpdf%2F998%2Fart%25253A10.1007%25252FBF00352253.pdf%3ForiginUr>

1%3Dhttp%253A%252F%252Flink.springer.com%252Farticle%252F10.1007%252FBF00352253*~h mac=6c9e6d26fa741a987b5aa3d867f435a1be30ecb176b4fa1ac683495b3518d461 (Accessed: 2 May 2017).

169. Hultén, M. a., Dhanjal, S. and Pertl, B. (2003) 'Rapid and simple prenatal diagnosis of common chromosome disorders: Advantages and disadvantages of the molecular methods FISH and QF-PCR', *Reproduction*, 126(3), pp. 279–297. doi: 10.1530/reprod/126.3.279.
170. Huycke, M. M. *et al.* (2001) 'Extracellular superoxide production by *Enterococcus faecalis* requires demethylmenaquinone and is attenuated by functional terminal quinol oxidases.', *Molecular microbiology*, 42(3), pp. 729–40. Available at: <http://www.ncbi.nlm.nih.gov/pubmed/11722738> (Accessed: 5 April 2017).
171. Huycke, M. M., Abrams, V. and Moore, D. R. (2002) 'Enterococcus faecalis produces extracellular superoxide and hydrogen peroxide that damages colonic epithelial cell DNA', *Carcinogenesis*. Oxford University Press, 23(3), pp. 529–536. doi: 10.1093/carcin/23.3.529.
172. Integrated DNA Technologies (2015) *qPCR Probes—selecting the best reporter dye and quencher*. Available at: <http://www.idtdna.com/pages/decoded/decoded-articles/pipet-tips/decoded/2015/04/07/qpcr-probes-selecting-the-best-reporter-dye-and-quencher> (Accessed: 23 December 2017).
173. Inzunza, J. *et al.* (2005) 'Derivation of Human Embryonic Stem Cell Lines in Serum Replacement Medium Using Postnatal Human Fibroblasts as Feeder Cells', *Stem Cells*, 23(4), pp. 544–549. doi: 10.1634/stemcells.2004-0201.
174. Ito, K. and Suda, T. (2014) 'Metabolic requirements for the maintenance of self-renewing stem cells', *Nature Reviews Molecular Cell Biology*, 15(4), pp. 243–256. doi: 10.1038/nrm3772.
175. Itoh, N. and Shimizu, N. (1998) 'DNA replication-dependent intranuclear relocation of double minute chromatin.', *Journal of cell science*, 111 (Pt 22), pp. 3275–85. Available at: <http://www.ncbi.nlm.nih.gov/pubmed/9788870> (Accessed: 14 August 2017).
176. Jacobs, E. Z. *et al.* (2017) 'CRISPR/Cas9-mediated genome editing in naïve human embryonic stem cells', *Scientific Reports*. Nature Publishing Group, 7(1), p. 16650. doi: 10.1038/s41598-017-16932-y.
177. Janevski, J., Park, P. C. and De Boni, U. (1995) 'Organization of Centromeric Domains in Hepatocyte Nuclei: Rearrangement Associated with De Novo Activation of the Vitellogenin Gene Family in *Xenopus laevis*', *Experimental Cell Research*, 217(2), pp. 227–239. doi: 10.1006/excr.1995.1082.
178. Jemal, A. *et al.* (2004) 'Cancer statistics, 2004.', *CA: a cancer journal for clinicians*, 54(1), pp. 8–29. Available at: <http://www.ncbi.nlm.nih.gov/pubmed/14974761> (Accessed: 15 August 2017).
179. Jensen, D. (2015) *California Stem Cell Report, California's Consumer Watchdog Loses U.S. Supreme Court Challenge to WARF Stem Cell Patents*. Available at: <https://californiastemcellreport.blogspot.co.uk/2015/02/californias-consumer-watchdog-loses-us.html> (Accessed: 5 May 2018).
180. Ji, B. *et al.* (2015) 'Over-expression of XIST, the Master Gene for X Chromosome Inactivation, in Females With Major Affective Disorders.', *EBioMedicine*. Elsevier, 2(8), pp. 909–18. doi: 10.1016/j.ebiom.2015.06.012.
181. Jiang, J. *et al.* (2013) 'Translating dosage compensation to trisomy 21.', *Nature*. NIH Public Access, 500(7462), pp. 296–300. doi: 10.1038/nature12394.
182. Jin, Y. (2007) 'Human embryonic stem cells create their own niche', *Cell Research*. Nature Publishing Group, 17(9), pp. 744–745. doi: 10.1038/cr.2007.76.
183. Jones, M. *et al.* (2014) 'Low copy target detection by Droplet Digital PCR through application of a novel open access bioinformatic pipeline, "definetherain"', *Journal of Virological Methods*. Elsevier B.V., 202, pp. 46–53. doi: 10.1016/j.jviromet.2014.02.020.
184. Jørgensen, K. T. *et al.* (2010) 'Autoimmune diseases in women with Turner's Syndrome', *Arthritis & Rheumatism*. Wiley Subscription Services, Inc., A Wiley Company, 62(3), pp. 658–666. doi: 10.1002/art.27270.

185. Kanemura, H. *et al.* (2014) 'Tumorigenicity studies of induced pluripotent stem cell (iPSC)-derived retinal pigment epithelium (RPE) for the treatment of age-related macular degeneration.', *PloS one*. Public Library of Science, 9(1), p. e85336. doi: 10.1371/journal.pone.0085336.
186. Kaufmann, S. H. *et al.* (1991) 'Differential expression of nuclear envelope lamins A and C in human lung cancer cell lines.', *Cancer research*, 51(2), pp. 581–6. Available at: <http://www.ncbi.nlm.nih.gov/pubmed/1985776> (Accessed: 22 May 2018).
187. Kaufmann, S. H. (1992) 'Expression of nuclear envelope lamins A and C in human myeloid leukemias.', *Cancer research*, 52(10), pp. 2847–53. Available at: <http://www.ncbi.nlm.nih.gov/pubmed/1581898> (Accessed: 22 May 2018).
188. Kehoe, D. E. *et al.* (2010) 'Scalable Stirred-Suspension Bioreactor Culture of Human Pluripotent Stem Cells', *Tissue Engineering Part A*, 16(2), pp. 405–421. doi: 10.1089/ten.tea.2009.0454.
189. Keller, M. D. *et al.* (2013) 'Immunodeficiency in patients with 49,XXXXY chromosomal variation.', *American journal of medical genetics. Part C, Seminars in medical genetics*. NIH Public Access, 163C(1), pp. 50–4. doi: 10.1002/ajmg.c.31348.
190. Keohane, A. A. M. *et al.* (1996) 'X-Inactivation and histone H4 acetylation in embryonic stem cells.', *Developmental biology*, 180(2), pp. 618–30. doi: 10.1006/dbio.1996.0333.
191. Khadun, S. (2013) *The support of undifferentiated human embryonic stem cell lines by different matrices*. University of Herfordshire.
192. Khillan, J. S. (2014) 'Vitamin A/retinol and maintenance of pluripotency of stem cells.', *Nutrients*. Multidisciplinary Digital Publishing Institute (MDPI), 6(3), pp. 1209–22. doi: 10.3390/nu6031209.
193. Kibbey, M. C. (1994) 'Maintenance of the EHS sarcoma and Matrigel preparation', *Journal of Tissue Culture Methods*. Kluwer Academic Publishers, 16(3–4), pp. 227–230. doi: 10.1007/BF01540656.
194. Kida, Y. S. *et al.* (2015) 'ERRs Mediate a Metabolic Switch Required for Somatic Cell Reprogramming to Pluripotency', *Cell Stem Cell*, 16(5), pp. 547–555. doi: 10.1016/j.stem.2015.03.001.
195. Kim, E. J., Kang, K. H. and Ju, J. H. (2017) 'CRISPR-Cas9: a promising tool for gene editing on induced pluripotent stem cells.', *The Korean journal of internal medicine*. Korean Association of Internal Medicine, 32(1), pp. 42–61. doi: 10.3904/kjim.2016.198.
196. Kim, Y.-E. *et al.* (2012) 'Chromosomal Modification in Human Embryonic Stem Cells Cultured in a Feeder-Free Condition after Single Cell Dissociation using Accutase.', *Development & reproduction*. Korean Society of Developmental Biology, 16(4), pp. 353–61. doi: 10.12717/DR.2012.16.4.353.
197. Kim, Y. *et al.* (2011) 'Mouse B-type lamins are required for proper organogenesis but not by embryonic stem cells.', *Science (New York, N.Y.)*, 334(6063), pp. 1706–10. doi: 10.1126/science.1211222.
198. Kinoshita, T. *et al.* (2011) 'Ataxia-telangiectasia mutated (ATM) deficiency decreases reprogramming efficiency and leads to genomic instability in iPS cells', *Biochemical and Biophysical Research Communications*, 407(2), pp. 321–326. doi: 10.1016/j.bbrc.2011.03.013.
199. Klim, J. R. *et al.* (2010) 'A defined glycosaminoglycan-binding substratum for human pluripotent stem cells', *Nature Methods*. Nature Publishing Group, 7(12), pp. 989–994. doi: 10.1038/nmeth.1532.
200. Knight, M. *et al.* (2011) 'Non-random organization of the *Biomphalaria glabrata* genome in interphase Bge cells and the spatial repositioning of activated genes in cells co-cultured with *Schistosoma mansoni*', *International Journal for Parasitology*, 41(1), pp. 61–70. doi: 10.1016/j.ijpara.2010.07.015.
201. Koehler, D. *et al.* (2009) 'Changes of higher order chromatin arrangements during major genome activation in bovine preimplantation embryos'. doi: 10.1016/j.yexcr.2009.02.016.
202. Kozubek, S. *et al.* (2002) '3D Structure of the human genome: order in randomness',

- Chromosoma*. Springer-Verlag, 111(5), pp. 321–331. doi: 10.1007/s00412-002-0210-8.
203. Kuga, T. *et al.* (2014) 'Lamin B2 prevents chromosome instability by ensuring proper mitotic chromosome segregation', *Oncogenesis*. Nature Publishing Group, 3(3). doi: 10.1038/oncsis.2014.6.
 204. Kuroda, M. *et al.* (2004) 'Alteration of chromosome positioning during adipocyte differentiation', *Journal of Cell Science*, 117(24). Available at: <http://jcs.biologists.org/content/117/24/5897.long> (Accessed: 13 July 2017).
 205. Kurosawa, S., Kimura, O. and Sagawa, A. (1991) 'Systemic lupus erythematosus in a patient with the 47, XXX karyotype', *Arthritis & Rheumatism*. John Wiley & Sons, Inc., 34(3), pp. 371–372. doi: 10.1002/art.1780340317.
 206. Kurtyka, Z. E. *et al.* (1988) 'Trisomy 8 Mosaicism Syndrome', *Clinical Pediatrics*, 27(11), pp. 557–564. doi: 10.1177/000992288802701109.
 207. Lathi, R. B., Westphal, L. M. and Milki, A. a. (2008) 'Aneuploidy in the miscarriages of infertile women and the potential benefit of preimplantation genetic diagnosis', *Fertility and Sterility*, 89(2), pp. 353–357. doi: 10.1016/j.fertnstert.2007.02.040.
 208. Laver, T. *et al.* (2015) 'Assessing the performance of the Oxford Nanopore Technologies MinION', *Biomolecular Detection and Quantification*. Elsevier, 3, pp. 1–8. doi: 10.1016/J.BDQ.2015.02.001.
 209. Lebkowski, J. (2011) 'GRNOPC1: the world's first embryonic stem cell-derived therapy', *Regenerative Medicine*, 6(6s), pp. 11–13. doi: 10.2217/rme.11.77.
 210. Lee, J.-H., Hart, S. R. L. and Skalnik, D. G. (2004) 'Histone deacetylase activity is required for embryonic stem cell differentiation.', *Genesis (New York, N.Y. : 2000)*, 38(1), pp. 32–8. doi: 10.1002/gene.10250.
 211. Lee, J.-H. and Paull, T. T. (2007) 'Activation and regulation of ATM kinase activity in response to DNA double-strand breaks', *Oncogene*. Nature Publishing Group, 26(56), pp. 7741–7748. doi: 10.1038/sj.onc.1210872.
 212. Lee, J. E. J. B. *et al.* (2005) 'Establishment and Maintenance of Human Embryonic Stem Cell Lines on Human Feeder Cells Derived from Uterine Endometrium under Serum-Free Condition¹', *Biology of Reproduction*. Oxford University Press, 72(1), pp. 42–49. doi: 10.1095/biolreprod.104.033480.
 213. Lehner, C. F. *et al.* (1987) 'Differential expression of nuclear lamin protei... - Xenbase Paper', *J Cell Biol.*, 105(1), pp. 577–87. Available at: <http://www.xenbase.org/literature/article.do?method=display&articleId=28080> (Accessed: 9 February 2018).
 214. Leshner, M. *et al.* (2016) 'Locus-specific gene repositioning in prostate cancer', *Molecular Biology of the Cell*, 27(2), pp. 236–246. doi: 10.1091/mbc.E15-05-0280.
 215. Levine, A. D. (2008) 'Identifying Under- and Overperforming Countries in Research Related to Human Embryonic Stem Cells', *Cell Stem Cell*. Cell Press, 2(6), pp. 521–524. doi: 10.1016/J.STEM.2008.05.008.
 216. Li, F. *et al.* (1999) 'Pleiotropic cell-division defects and apoptosis induced by interference with survivin function.', *Nature cell biology*, 1(8), pp. 461–6. Available at: <http://www.ncbi.nlm.nih.gov/pubmed/10587640> (Accessed: 15 August 2017).
 217. Li, Q. *et al.* (2014) 'A promoter that drives gene expression preferentially in male transgenic rats.', *Transgenic research*. NIH Public Access, 23(2), pp. 341–9. doi: 10.1007/s11248-013-9773-9.
 218. Lin, F. and Worman, H. J. (1993) 'Structural organization of the human gene encoding nuclear lamin A and nuclear lamin C.', *The Journal of biological chemistry*, 268(22), pp. 16321–6. Available at: <http://www.ncbi.nlm.nih.gov/pubmed/8344919> (Accessed: 9 February 2018).
 219. Lin, T. *et al.* (2005) 'p53 induces differentiation of mouse embryonic stem cells by suppressing Nanog expression', *Nature Cell Biology*, 7(2), pp. 165–171. doi: 10.1038/ncb1211.
 220. Lindahl, T. (1993) 'Instability and decay of the primary structure of DNA', *Nature*, 362(6422), pp. 709–715. doi: 10.1038/362709a0.

221. Lisaingo, K., Uringa, E.-J. and Lansdorp, P. M. (2014) 'Resolution of telomere associations by TRF1 cleavage in mouse embryonic stem cells.', *Molecular biology of the cell*. American Society for Cell Biology, 25(13), pp. 1958–68. doi: 10.1091/mbc.E13-10-0564.
222. Liu, D. *et al.* (2004) 'Telosome, a Mammalian Telomere-associated Complex Formed by Multiple Telomeric Proteins', *Journal of Biological Chemistry*, 279(49), pp. 51338–51342. doi: 10.1074/jbc.M409293200.
223. Liu, K. *et al.* (2016) 'X Chromosome Dose and Sex Bias in Autoimmune Diseases: Increased Prevalence of 47,XXX in Systemic Lupus Erythematosus and Sjögren's Syndrome.', *Arthritis & rheumatology (Hoboken, N.J.)*. NIH Public Access, 68(5), pp. 1290–1300. doi: 10.1002/art.39560.
224. Lo, B. and Parham, L. (2009) 'Ethical issues in stem cell research.', *Endocrine reviews*. The Endocrine Society, 30(3), pp. 204–13. doi: 10.1210/er.2008-0031.
225. Lo, Y. M. D. *et al.* (2007) 'Digital PCR for the molecular detection of fetal chromosomal aneuploidy.', *Proceedings of the National Academy of Sciences of the United States of America*. National Academy of Sciences, 104(32), pp. 13116–13121. doi: 10.1073/pnas.0705765104.
226. Lorimore, S. A. *et al.* (1998) 'Chromosomal instability in the descendants of unirradiated surviving cells after alpha-particle irradiation.', *Proceedings of the National Academy of Sciences of the United States of America*, 95(10), pp. 5730–3. Available at: <http://www.ncbi.nlm.nih.gov/pubmed/9576952> (Accessed: 8 April 2017).
227. Lu, J. *et al.* (2016) 'Influence of ATM -Mediated DNA Damage Response on Genomic Variation in Human Induced Pluripotent Stem Cells', *Stem Cells and Development*, 25(9), pp. 740–747. doi: 10.1089/scd.2015.0393.
228. Ludwig, T. E. *et al.* (2006) 'Derivation of human embryonic stem cells in defined conditions', *Nature Biotechnology*. Nature Publishing Group, 24(2), pp. 185–187. doi: 10.1038/nbt1177.
229. Ma, L. *et al.* (2009) 'Requirement for Nudel and dynein for assembly of the lamin B spindle matrix', *Nature Cell Biology*, 11(3), pp. 247–256. doi: 10.1038/ncb1832.
230. Machiels, B. M. *et al.* (1996) 'An alternative splicing product of the lamin A/C gene lacks exon 10.', *The Journal of biological chemistry*, 271(16), pp. 9249–53. Available at: <http://www.ncbi.nlm.nih.gov/pubmed/8621584> (Accessed: 9 February 2018).
231. Machiels, B. M. *et al.* (1997) 'NUCLEAR LAMIN EXPRESSION IN NORMAL TESTIS AND TESTICULAR GERM CELL TUMOURS OF ADOLESCENTS AND ADULTS', *The Journal of Pathology*, 182(2), pp. 197–204. doi: 10.1002/(SICI)1096-9896(199706)182:2<197::AID-PATH823>3.0.CO;2-P.
232. Mahy, N. L. *et al.* (2002) 'Spatial organization of active and inactive genes and noncoding DNA within chromosome territories.', *The Journal of cell biology*. The Rockefeller University Press, 157(4), pp. 579–89. doi: 10.1083/jcb.200111071.
233. Mahy, N. L., Perry, P. E. and Bickmore, W. A. (2002) 'Gene density and transcription influence the localization of chromatin outside of chromosome territories detectable by FISH.', *The Journal of cell biology*, 159(5), pp. 753–63. doi: 10.1083/jcb.200207115.
234. Maitra, A. *et al.* (2005) 'Genomic alterations in cultured human embryonic stem cells.', *Nature genetics*. Nature Publishing Group, 37(10), pp. 1099–1103. doi: 10.1038/ng1631.
235. Malhas, A. *et al.* (2007) 'Defects in lamin B1 expression or processing affect interphase chromosome position and gene expression', *The Journal of Cell Biology*, 176(5), pp. 593–603. doi: 10.1083/jcb.200607054.
236. Mansharamani, M. and Wilson, K. L. (2005) 'Direct Binding of Nuclear Membrane Protein MAN1 to Emerin *in Vitro* and Two Modes of Binding to Barrier-to-Autointegration Factor', *Journal of Biological Chemistry*, 280(14), pp. 13863–13870. doi: 10.1074/jbc.M413020200.
237. Marión, R. M. *et al.* (2009) 'A p53-mediated DNA damage response limits reprogramming to ensure iPS cell genomic integrity', *Nature*. Nature Publishing Group, 460(7259), pp. 1149–1153. doi: 10.1038/nature08287.
238. Marshall, W. F. *et al.* (1996) 'Specific interactions of chromatin with the nuclear envelope: positional determination within the nucleus in *Drosophila melanogaster*.', *Molecular biology of the cell*, 7(5), pp. 825–842.

239. Martin, M. J. *et al.* (2005) 'Human embryonic stem cells express an immunogenic nonhuman sialic acid', *Nature Medicine*, 11(2), pp. 228–232. doi: 10.1038/nm1181.
240. Mattout, A., Biran, A. and Meshorer, E. (2011) 'Global epigenetic changes during somatic cell reprogramming to iPS cells', *Journal of Molecular Cell Biology*. Oxford University Press, 3(6), pp. 341–350. doi: 10.1093/jmcb/mjr028.
241. McKeon, F. D., Kirschner, M. W. and Caput, D. (1986) 'Homologies in both primary and secondary structure between nuclear envelope and intermediate filament proteins', *Nature*, 319(6053), pp. 463–468. doi: 10.1038/319463a0.
242. McMahon, T. C. *et al.* (2017) 'Multiplexed Single Intact Cell Droplet Digital PCR (MuSIC ddPCR) Method for Specific Detection of Enterohemorrhagic E. coli (EHEC) in Food Enrichment Cultures', *Frontiers in Microbiology*. Frontiers, 8, p. 332. doi: 10.3389/fmicb.2017.00332.
243. Meaburn, K. J. *et al.* (2005) 'Chromosome positioning is largely unaffected in lymphoblastoid cell lines containing emerlin or A-type lamin mutations', *Biochemical Society Transactions*, 33(6), p. 1438. doi: 10.1042/BST20051438.
244. Meaburn, K. J. *et al.* (2007) 'Primary laminopathy fibroblasts display altered genome organization and apoptosis', *Aging Cell*. Blackwell Publishing Ltd, 6(2), pp. 139–153. doi: 10.1111/j.1474-9726.2007.00270.x.
245. Meaburn, K. J. *et al.* (2009) 'Disease-specific gene repositioning in breast cancer', *The Journal of Cell Biology*, 187(6), pp. 801–812. doi: 10.1083/jcb.200909127.
246. Meaburn, K. J. *et al.* (2016) 'Tissue-of-origin-specific gene repositioning in breast and prostate cancer', *Histochemistry and Cell Biology*, 145(4), pp. 433–446. doi: 10.1007/s00418-015-1401-8.
247. Meaburn, K. J. and Misteli, T. (2007) 'Cell biology: chromosome territories.', *Nature*, 445(January). doi: 10.1038/445379a.
248. Medical Research Council (2018) *UK Stem Cell Bank steering committee - Research - Medical Research Council*. Available at: <https://mrc.ukri.org/research/policies-and-guidance-for-researchers/uk-stem-cell-bank-steering-committee/> (Accessed: 5 May 2018).
249. Mehta, I. S. *et al.* (2010) 'Rapid chromosome territory relocation by nuclear motor activity in response to serum removal in primary human fibroblasts.', *Genome biology*, 11(1), p. R5. doi: 10.1186/gb-2010-11-1-r5.
250. Mehta, I. S. *et al.* (2011) 'Farnesyltransferase inhibitor treatment restores chromosome territory positions and active chromosome dynamics in Hutchinson-Gilford progeria syndrome cells.', *Genome biology*, 12(8), p. R74. doi: 10.1186/gb-2011-12-8-r74.
251. Melcer, S. *et al.* (2012) 'Histone modifications and lamin A regulate chromatin protein dynamics in early embryonic stem cell differentiation', *Nature Communications*. Nature Publishing Group, 3(1), p. 910. doi: 10.1038/ncomms1915.
252. Meshorer, E. *et al.* (2006) 'Hyperdynamic plasticity of chromatin proteins in pluripotent embryonic stem cells.', *Developmental cell*, 10(1), pp. 105–16. doi: 10.1016/j.devcel.2005.10.017.
253. Meshorer, E. and Gruenbaum, Y. (2008) 'Gone with the Wnt/Notch: stem cells in laminopathies, progeria, and aging', *The Journal of Cell Biology*, 181(1), pp. 9–13. doi: 10.1083/jcb.200802155.
254. Meshorer, E. and Misteli, T. (2006) 'Chromatin in pluripotent embryonic stem cells and differentiation', *Nat Rev Mol Cell Biol*. Nature Publishing Group, 7(7), pp. 540–546. doi: 10.1038/nrm1938.
255. Mewborn, S. K. *et al.* (2010) 'Altered Chromosomal Positioning, Compaction, and Gene Expression with a Lamin A/C Gene Mutation', *PLoS ONE*. Edited by B. A. Sullivan, 5(12), p. e14342. doi: 10.1371/journal.pone.0014342.
256. Miere, C. *et al.* (2016) 'Generation of KCL021 research grade human embryonic stem cell line carrying a Δ F508 mutation in the CFTR gene.', *Stem cell research*. Elsevier, 16(1), pp. 177–9. doi: 10.1016/j.scr.2015.12.042.
257. Minissi, S. *et al.* (1999) 'Effect of cytochalasin B on the induction of chromosome missegregation by colchicine at low concentrations in human lymphocytes.', *Mutagenesis*, 14(1),

- pp. 43–9. Available at: <http://www.ncbi.nlm.nih.gov/pubmed/10474820> (Accessed: 3 April 2017).
258. Miotke, L. *et al.* (2014) 'High sensitivity detection and quantitation of DNA copy number and single nucleotide variants with single color droplet digital PCR', *Analytical Chemistry*, 86(5), pp. 2618–2624. doi: 10.1021/ac403843j.
 259. Mitmaker, B., Begin, L. R. and Gordon, P. H. (1991) 'Nuclear shape as a prognostic discriminant in colorectal carcinoma', *Diseases of the Colon & Rectum*. Springer-Verlag, 34(3), pp. 249–259. doi: 10.1007/BF02090165.
 260. Miura, M. *et al.* (2006) 'Accumulated chromosomal instability in murine bone marrow mesenchymal stem cells leads to malignant transformation.', *Stem cells (Dayton, Ohio)*, 24(4), pp. 1095–103. doi: 10.1634/stemcells.2005-0403.
 261. Mohyeldin, A., Garzón-Muvdi, T. and Quiñones-Hinojosa, A. (2010) 'Oxygen in Stem Cell Biology: A Critical Component of the Stem Cell Niche', *Cell Stem Cell*. Cell Press, 7(2), pp. 150–161. doi: 10.1016/J.STEM.2010.07.007.
 262. Mohyuddin, A. *et al.* (2004) 'Genetic instability in EBV-transformed lymphoblastoid cell lines', *Biochimica et Biophysica Acta (BBA) - General Subjects*. Elsevier, 1670(1), pp. 81–83. doi: 10.1016/J.BBAGEN.2003.10.014.
 263. Momcilovic, O. *et al.* (2010) 'DNA Damage Responses in Human Induced Pluripotent Stem Cells and Embryonic Stem Cells', *PLoS ONE*. Edited by M. C. Capogrossi, 5(10), p. e13410. doi: 10.1371/journal.pone.0013410.
 264. Moogk, D. *et al.* (2010) 'Human ESC Colony Formation Is Dependent on Interplay Between Self-Renewing hESCs and Unique Precursors Responsible for Niche Generation Key terms', *Cytometry. Part A : the journal of the International Society for Advancement of Cytometry*. doi: 10.1002/cyto.a.20878.
 265. Morris, Kelly, J., Chotalia, M. and Pombo, A. (2010) 'Nuclear Architecture in Stem Cells', *Advances in Experimental Medicine and Biology*, 695(December), pp. 1–222. doi: 10.1007/978-1-4419-7037-4.
 266. Moss, S. F. *et al.* (1999) 'Decreased and aberrant nuclear lamin expression in gastrointestinal tract neoplasms.', *Gut*. BMJ Publishing Group, 45(5), pp. 723–9. doi: 10.1136/GUT.45.5.723.
 267. Muralikrishna, B. *et al.* (2001) 'Distinct changes in intranuclear lamin A/C organization during myoblast differentiation.', *Journal of cell science*, 114(Pt 22), pp. 4001–11. Available at: <http://www.ncbi.nlm.nih.gov/pubmed/11739632> (Accessed: 22 May 2018).
 268. Na, J. *et al.* (2014) 'Aneuploidy in pluripotent stem cells and implications for cancerous transformation.', *Protein & cell*. Springer, 5(8), pp. 569–79. doi: 10.1007/s13238-014-0073-9.
 269. Nagaria, P. K. *et al.* (2016) 'High-Fidelity Reprogrammed Human iPSCs Have a High Efficacy of DNA Repair and Resemble hESCs in Their MYC Transcriptional Signature', *Stem Cells International*. Hindawi, 2016, pp. 1–14. doi: 10.1155/2016/3826249.
 270. Nagasawa, H. and Little, J. B. (1992) 'Induction of sister chromatid exchanges by extremely low doses of alpha-particles.', *Cancer research*, 52(22), pp. 6394–6. Available at: <http://www.ncbi.nlm.nih.gov/pubmed/1423287> (Accessed: 8 April 2017).
 271. Nasaw, D. (2009) 'The Guardian', *Obama overturns Bush policy on stem cell research*. Available at: <https://www.theguardian.com/world/2009/mar/09/obama-administration-stem-cell-funding> (Accessed: 19 May 2018).
 272. Neganova, I. and Lako, M. (2008) 'G1 to S phase cell cycle transition in somatic and embryonic stem cells', *Journal of Anatomy*, 213(1), pp. 30–44. doi: 10.1111/j.1469-7580.2008.00931.x.
 273. Nelson, G. *et al.* (2012) 'A senescent cell bystander effect: senescence-induced senescence.', *Aging cell*, 11(2), pp. 345–9. doi: 10.1111/j.1474-9726.2012.00795.x.
 274. Nera, B. *et al.* (2015) 'Elevated levels of TRF2 induce telomeric ultrafine anaphase bridges and rapid telomere deletions', *Nature Communications*, 6, p. 10132. doi: 10.1038/ncomms10132.
 275. Noatynska, A., Gotta, M. and Meraldi, P. (2012) 'Mitotic spindle (DIS)orientation and DISease: Cause or consequence?', *The Journal of Cell Biology*, 199(7). Available at: <http://jcb.rupress.org/content/199/7/1025#F1> (Accessed: 4 April 2017).

276. Normanno, N. *et al.* (2009) 'Implications for KRAS status and EGFR-targeted therapies in metastatic CRC.', *Nature reviews. Clinical oncology*. Nature Publishing Group, 6(9), pp. 519–527. doi: 10.1038/nrclinonc.2009.111.
277. Norppa, H. and Falck, G. C.-M. (2003) 'What do human micronuclei contain?', *Mutagenesis*, 18(3), pp. 221–33. Available at: <http://www.ncbi.nlm.nih.gov/pubmed/12714687> (Accessed: 3 April 2017).
278. Novik, V. *et al.* (2014) 'The accuracy of chromosomal microarray testing for identification of embryonic mosaicism in human blastocysts.', *Molecular cytogenetics*. BioMed Central, 7(1), p. 18. doi: 10.1186/1755-8166-7-18.
279. O'Connor, C. (2008) 'Chromosomal Abnormalities: Aneuploidies', *Nature Education*, 1 (1):172. Available at: <https://www.nature.com/scitable/topicpage/chromosomal-abnormalities-aneuploidies-290> (Accessed: 9 July 2017).
280. O'Neill, M. *et al.* (2011) 'Comparison of the TLDA with the Nanodrop and the reference Qubit system', *Journal of Physics: Conference Series*, 307, p. 012047. doi: 10.1088/1742-6596/307/1/012047.
281. Ogilvie, C. M. *et al.* (2005) 'Rapid Prenatal Diagnosis of Aneuploidy Using Quantitative Fluorescence-PCR (QF-PCR)', *Journal of Histochemistry & Cytochemistry*, 53(3), pp. 285–288. doi: 10.1369/jhc.4B6409.2005.
282. Oguchi, M. *et al.* (2002) 'Expression of lamins depends on epidermal differentiation and transformation.', *The British journal of dermatology*, 147(5), pp. 853–8. Available at: <http://www.ncbi.nlm.nih.gov/pubmed/12410693> (Accessed: 22 May 2018).
283. Oh, S. K. W. *et al.* (2009) 'Long-term microcarrier suspension cultures of human embryonic stem cells', *Stem Cell Research*. Elsevier, 2(3), pp. 219–230. doi: 10.1016/J.SCR.2009.02.005.
284. Ollion, J. *et al.* (2015) 'Proliferation-dependent positioning of individual centromeres in the interphase nucleus of human lymphoblastoid cell lines.', *Molecular biology of the cell*. American Society for Cell Biology, 26(13), pp. 2550–60. doi: 10.1091/mbc.E14-05-1002.
285. Olson, E. N. and Nordheim, A. (2010) 'Linking actin dynamics and gene transcription to drive cellular motile functions.', *Nature reviews. Molecular cell biology*, 11(5), pp. 353–65. Available at: <http://www.ncbi.nlm.nih.gov/pubmed/20414257> (Accessed: 13 May 2018).
286. Ouahchi, K., Lindeman, N. and Lee, C. (2006) 'Copy number variants and pharmacogenomics.', *Pharmacogenomics*, 7(1), pp. 25–29. doi: 10.2217/14622416.7.1.25.
287. Pajerowski, J. D. *et al.* (2007) 'Physical plasticity of the nucleus in stem cell differentiation', *Proceedings of the National Academy of Sciences*, 104(40), pp. 15619–15624. Available at: <http://www.pnas.org/content/pnas/104/40/15619.full.pdf> (Accessed: 9 April 2018).
288. Palm, W. and de Lange, T. (2008) 'How Shelterin Protects Mammalian Telomeres', *Annual Review of Genetics*, 42(1), pp. 301–334. doi: 10.1146/annurev.genet.41.110306.130350.
289. Pandita, T. K. and Richardson, C. (2009) 'Chromatin remodeling finds its place in the DNA double-strand break response', *Nucleic Acids Research*, 37(5), pp. 1363–1377. doi: 10.1093/nar/gkn1071.
290. Parada, L. a. and Misteli, T. (2002) 'Chromosome positioning in the interphase nucleus', *Trends in Cell Biology*, 12(9), pp. 425–432. doi: 10.1016/S0962-8924(02)02351-6.
291. Parada, L. a, McQueen, P. G. and Misteli, T. (2004) 'Tissue-specific spatial organization of genomes.', *Genome biology*. BioMed Central, 5(7), p. R44. doi: 10.1186/gb-2004-5-7-r44.
292. Pardo, B. and Marcand, S. (2005) 'Rap1 prevents telomere fusions by nonhomologous end joining.', *The EMBO journal*. European Molecular Biology Organization, 24(17), pp. 3117–27. doi: 10.1038/sj.emboj.7600778.
293. Pekovic, V. and Hutchison, C. J. (2008) 'Adult stem cell maintenance and tissue regeneration in the ageing context: the role for A-type lamins as intrinsic modulators of ageing in adult stem cells and their niches', *Journal of Anatomy*, 213(1), pp. 5–25. doi: 10.1111/j.1469-7580.2008.00928.x.
294. Peric-Hupkes, D. and van Steensel, B. (2010) 'Role of the Nuclear Lamina in Genome

- Organization and Gene Expression', *Cold Spring Harbor Symposia on Quantitative Biology*, 75(0), pp. 517–524. doi: 10.1101/sqb.2010.75.014.
295. Peter, A. and Stick, R. (2012) 'Evolution of the lamin protein family What introns can tell', *Nucleus*, 3(1), pp. 44–59. doi: 10.4161/nucl.3.1.18927.
296. Peterson, S. E. and Loring, J. F. (2014) 'Genomic instability in pluripotent stem cells: implications for clinical applications.', *The Journal of biological chemistry*. American Society for Biochemistry and Molecular Biology, 289(8), pp. 4578–84. doi: 10.1074/jbc.R113.516419.
297. Petrova, N. V *et al.* (2007) 'Changes in chromosome positioning may contribute to the development of diseases related to X-chromosome aneuploidy', *Journal of Cellular Physiology*. Wiley Subscription Services, Inc., A Wiley Company, 213(1), pp. 278–283. doi: 10.1002/jcp.21118.
298. Pierre, R. V and Hoagland, H. C. (1972) 'Age-associated aneuploidy: loss of Y chromosome from human bone marrow cells with aging.', *Cancer*, 30(4), pp. 889–894.
299. Pohl, G. and Shih, I.-M. M. (2004) 'Principle and applications of digital PCR', *Expert Rev Mol Diagn*, 4(1), pp. 41–47. doi: 10.1586/14737159.4.1.41.
300. Pollard, K. M. *et al.* (1990) 'In vitro posttranslational modification of lamin B cloned from a human T-cell line.', *Molecular and cellular biology*, 10(5), pp. 2164–75. Available at: <http://www.ncbi.nlm.nih.gov/pubmed/2325650> (Accessed: 21 September 2017).
301. Prokocimer, M. *et al.* (2009) 'Nuclear lamins: key regulators of nuclear structure and activities', *Journal of Cellular and Molecular Medicine*, 13(6), pp. 1059–1085. doi: 10.1111/j.1582-4934.2008.00676.x.
302. Pugh, G. E. *et al.* (1997) 'Distinct nuclear assembly pathways for lamins A and C lead to their increase during quiescence in Swiss 3T3 cells.', *Journal of cell science*. The Company of Biologists Ltd, 110 (Pt 19)(19), pp. 2483–93. Available at: <http://www.ncbi.nlm.nih.gov/pubmed/9410886> (Accessed: 8 May 2018).
303. Quyn, A. J. *et al.* (2010) 'Spindle orientation bias in gut epithelial stem cell compartments is lost in precancerous tissue.', *Cell stem cell*, 6(2), pp. 175–81. doi: 10.1016/j.stem.2009.12.007.
304. Ram, G. and Chinen, J. (2011) 'Infections and immunodeficiency in Down syndrome', *Clinical & Experimental Immunology*, 164(1), pp. 9–16. doi: 10.1111/j.1365-2249.2011.04335.x.
305. Ranade, D. *et al.* (2017) 'Chromosomal aneuploidies induced upon Lamin B2 depletion are mislocalized in the interphase nucleus', *Chromosoma*. Springer Berlin Heidelberg, 126(2), pp. 223–244. doi: 10.1007/s00412-016-0580-y.
306. Reichart, B. *et al.* (2004) 'Expression and localization of nuclear proteins in autosomal-dominant Emery-Dreifuss muscular dystrophy with LMNA R377H mutation.', *BMC cell biology*. BioMed Central, 5, p. 12. doi: 10.1186/1471-2121-5-12.
307. Reid, A. L. *et al.* (2014) 'Detection of BRAF-V600E and V600K in melanoma circulating tumour cells by droplet digital PCR', *Clinical Biochemistry*. The Canadian Society of Clinical Chemists, pp. 10–13. doi: 10.1016/j.clinbiochem.2014.12.007.
308. Reubinoff, B. E. *et al.* (2000) 'Embryonic stem cell lines from human blastocysts: somatic differentiation in vitro', *Nature Biotechnology*, 18(4), pp. 399–404. doi: 10.1038/74447.
309. Reuter, V. E. (2005) 'Origins and molecular biology of testicular germ cell tumors.', *Modern pathology : an official journal of the United States and Canadian Academy of Pathology, Inc*, 18 Suppl 2, pp. S51–S60. doi: 10.1038/modpathol.3800309.
310. Richards, M. *et al.* (2002) 'Human feeders support prolonged undifferentiated growth of human inner cell masses and embryonic stem cells', *Nature Biotechnology*, 20(9), pp. 933–936. doi: 10.1038/nbt726.
311. Richards, M. *et al.* (2003) 'Comparative Evaluation of Various Human Feeders for Prolonged Undifferentiated Growth of Human Embryonic Stem Cells', *Stem Cells*. John Wiley & Sons, Ltd., 21(5), pp. 546–556. doi: 10.1634/stemcells.21-5-546.
312. Riemer, D. *et al.* (1995) 'Expression of Drosophila lamin C is developmentally regulated: analogies with vertebrate A-type lamins. - PubMed - NCBI', *J Cell Sci.*, 108(10), pp. 3189–98. Available at: <https://www.ncbi.nlm.nih.gov/m/pubmed/7593280/> (Accessed: 9 February 2018).

313. Rober, R. A. *et al.* (1989) 'No Title', 105(2), pp. 365–78. Available at: <http://www.ncbi.nlm.nih.gov/pubmed/2680424> (Accessed: 9 February 2018).
314. Rodriguez, S. *et al.* (2009) 'Increased expression of the Hutchinson-Gilford progeria syndrome truncated lamin A transcript during cell aging.', *European journal of human genetics : EJHG*. Nature Publishing Group, 17(7), pp. 928–37. doi: 10.1038/ejhg.2008.270.
315. Rönn, R. E. *et al.* (2017) 'Reactive Oxygen Species Impair the Function of CD90⁺ Hematopoietic Progenitors Generated from Human Pluripotent Stem Cells', *STEM CELLS*, 35(1), pp. 197–206. doi: 10.1002/stem.2503.
316. Ruf, W. (2016) 'Hemostasis keeps the stem cell niche in order.', *Blood*. American Society of Hematology, 128(8), pp. 1027–9. doi: 10.1182/blood-2016-07-722421.
317. Rugo, R. E. *et al.* (2005) 'A single acute exposure to a chemotherapeutic agent induces hyper-recombination in distantly descendant cells and in their neighbors', *Oncogene*. Nature Publishing Group, 24(32), pp. 5016–5025. doi: 10.1038/sj.onc.1208690.
318. Sakaki, M. *et al.* (2001) 'Interaction between emerin and nuclear lamins.', *Journal of biochemistry*, 129(2), pp. 321–7. Available at: <http://www.ncbi.nlm.nih.gov/pubmed/11173535> (Accessed: 22 May 2018).
319. Sanchez, A. M., Barrett, J. T. and Schoenlein, P. V. (1998) 'Fractionated Ionizing Radiation Accelerates Loss of Amplified MDR1 Genes Harbored by Extrachromosomal DNA in Tumor Cells', *Cancer Research*, 58(17). Available at: http://cancerres.aacrjournals.org/content/58/17/3845?ijkey=e99eff810d735d5d4ec2ff3cc7b5cba7726ed312&keytype=tf_ipsecsha (Accessed: 14 August 2017).
320. De Sandre-Giovannoli, A. *et al.* (2003) 'Lamin A Truncation in Hutchinson-Gilford Progeria', *Science*, 300(5628), pp. 2055–2055. doi: 10.1126/science.1084125.
321. Sartore, R. C. *et al.* (2011) 'Retinoic Acid-Treated Pluripotent Stem Cells Undergoing Neurogenesis Present Increased Aneuploidy and Micronuclei Formation', *PLoS ONE*. Edited by S. T. Ferreira. Public Library of Science, 6(6), p. e20667. doi: 10.1371/journal.pone.0020667.
322. Sawant, S. G. *et al.* (2001) 'The bystander effect in radiation oncogenesis: I. Transformation in C3H 10T1/2 cells in vitro can be initiated in the unirradiated neighbors of irradiated cells.', *Radiation research*, 155(3), pp. 397–401. Available at: <http://www.ncbi.nlm.nih.gov/pubmed/11182789> (Accessed: 8 April 2017).
323. Scaffidi, P. and Misteli, T. (2005) 'Reversal of the cellular phenotype in the premature aging disease Hutchinson-Gilford progeria syndrome', *Nature Medicine*, 11(4), pp. 440–445. doi: 10.1038/nm1204.
324. Scaffidi, P. and Misteli, T. (2008) 'Lamin A-dependent misregulation of adult stem cells associated with accelerated ageing', *Nature Cell Biology*, 10(4), pp. 452–459. doi: 10.1038/ncb1708.
325. Schatorjé, E. *et al.* (2016) 'Primary immunodeficiency associated with chromosomal aberration – an ESID survey', *Orphanet Journal of Rare Diseases*. BioMed Central, 11(1), p. 110. doi: 10.1186/s13023-016-0492-1.
326. Schatten, G. *et al.* (1985) 'Nuclear lamins and peripheral nuclear antigens during fertilization and embryogenesis in mice and sea urchins. - PubMed - NCBI', *Proc Natl Acad Sci U S A.*, 82(14), pp. 4727–31. Available at: <https://www.ncbi.nlm.nih.gov/m/pubmed/3860820/>.
327. Schirmer, E. C. *et al.* (2003) 'Nuclear Membrane Proteins with Potential Disease Links Found by Subtractive Proteomics', *Science*, 301(5638), pp. 1380–1382. doi: 10.1126/science.1088176.
328. Schoenlein, P. V *et al.* (2003) 'Radiation therapy depletes extrachromosomally amplified drug resistance genes and oncogenes from tumor cells via micronuclear capture of episomes and double minute chromosomes.', *International journal of radiation oncology, biology, physics*, 55(4), pp. 1051–65. Available at: <http://www.ncbi.nlm.nih.gov/pubmed/12605985> (Accessed: 14 August 2017).
329. Schwanitz, G. and Zerres, K. (1987) 'Partial monosomy 22 as result of an X/22 translocation in a newborn with DiGeorge syndrome.', *Annales de genetique*, 30(2), pp. 80–4. Available at:

- <http://www.ncbi.nlm.nih.gov/pubmed/3314667> (Accessed: 13 January 2018).
330. Schwartz, P. H. *et al.* (2011) 'Traditional human embryonic stem cell culture.', *Methods in molecular biology (Clifton, N.J.)*. NIH Public Access, 767, pp. 107–23. doi: 10.1007/978-1-61779-201-4_8.
 331. Seelye, K. Q. (2001) 'The New York Times', *The President's Decision: The Overview; Bush Give His Backing For Limited Research On Existing Stem Cells*. Available at: <https://www.nytimes.com/2001/08/10/us/president-s-decision-overview-bush-gives-his-backing-for-limited-research.html> (Accessed: 19 May 2018).
 332. Sellner, L. N. and Taylor, G. R. (2004) 'MLPA and MAPH: New techniques for detection of gene deletions', *Human Mutation*, 23(5), pp. 413–419. doi: 10.1002/humu.20035.
 333. Selvaraj, S. *et al.* (2013) 'Whole-genome haplotype reconstruction using proximity-ligation and shotgun sequencing', *Nature Biotechnology*, 31(12), pp. 1111–1118. doi: 10.1038/nbt.2728.
 334. Sengupta, K. *et al.* (2007) 'Artificially introduced aneuploid chromosomes assume a conserved position in colon cancer cells.', *PloS one*. Public Library of Science, 2(2), p. e199. doi: 10.1371/journal.pone.0000199.
 335. Servick, K. (2014) *Science, U.S. Federal Court Dismisses Challenge to Stem Cell Patent | Science | AAAS*. Available at: <http://www.sciencemag.org/news/2014/06/us-federal-court-dismisses-challenge-stem-cell-patent> (Accessed: 5 May 2018).
 336. Sfeir, A. *et al.* (2009) 'Mammalian Telomeres Resemble Fragile Sites and Require TRF1 for Efficient Replication', *Cell*, 138(1), pp. 90–103. doi: 10.1016/j.cell.2009.06.021.
 337. Shaffer, L. G. (2007) 'Molecular Cytogenetic and Rapid Aneuploidy Detection Methods in Prenatal Diagnosis', *American Journal of Medical Genetics Part C (Seminars in Medical Genetics)*, 145, pp. 87–98. doi: 10.1002/ajmg.c.30114.
 338. Shay, J. W. and Wright, W. E. (2010) 'Telomeres and telomerase in normal and cancer stem cells.', *FEBS letters*. NIH Public Access, 584(17), pp. 3819–25. doi: 10.1016/j.febslet.2010.05.026.
 339. Shehata, H. R. *et al.* (2017) 'Droplet digital polymerase chain reaction (ddPCR) assays integrated with an internal control for quantification of bovine, porcine, chicken and turkey species in food and feed.', *PloS one*. Public Library of Science, 12(8), p. e0182872. doi: 10.1371/journal.pone.0182872.
 340. Shete, A. *et al.* (2014) 'Spatial quantitation of FISH signals in diploid versus aneuploid nuclei.', *Cytometry. Part A : the journal of the International Society for Analytical Cytology*. NIH Public Access, 85(4), pp. 339–52. doi: 10.1002/cyto.a.22426.
 341. Shimi, T. *et al.* (2008) 'The A- and B-type nuclear lamin networks: microdomains involved in chromatin organization and transcription', *Genes & Development*, 22(24), pp. 3409–3421. doi: 10.1101/gad.1735208.
 342. Shimi, T. *et al.* (2011) 'The role of nuclear lamin B1 in cell proliferation and senescence', *Genes & Development*, 25(24), pp. 2579–2593. doi: 10.1101/gad.179515.111.
 343. Shirahashi, H. *et al.* (2004) 'Differentiation of Human and Mouse Embryonic Stem Cells Along a Hepatocyte Lineage', *Cell Transplantation*, 13, pp. 197–211. Available at: www.cognizantcommunication.com (Accessed: 18 February 2018).
 344. Shoeman, R. L. and Traub, P. (1990) 'The in vitro DNA-binding properties of purified nuclear lamin proteins and vimentin.', *The Journal of biological chemistry*, 265(16), pp. 9055–61. Available at: <http://www.ncbi.nlm.nih.gov/pubmed/2345165> (Accessed: 22 May 2018).
 345. Silva, M. M. *et al.* (2015) 'Robust Expansion of Human Pluripotent Stem Cells: Integration of Bioprocess Design With Transcriptomic and Metabolomic Characterization', *STEM CELLS Translational Medicine*, 4(7), pp. 731–742. doi: 10.5966/sctm.2014-0270.
 346. Simbolo, M. *et al.* (2013) 'DNA Qualification Workflow for Next Generation Sequencing of Histopathological Samples', *PLoS ONE*, 8(6). doi: 10.1371/journal.pone.0062692.
 347. Simon, D. N., Zastrow, M. S. and Wilson, K. L. (2010) 'Direct actin binding to A- and B-type lamin tails and actin filament bundling by the lamin A tail.', *Nucleus (Austin, Tex.)*. Taylor & Francis, 1(3), pp. 264–72. doi: 10.4161/nucl.1.3.11799.

348. Sinitsky, M. Y. and Druzhinin, V. G. (2014) 'The application of the cytokinesis-block micronucleus assay on peripheral blood lymphocytes for the assessment of genome damage in long-term residents of areas with high radon concentration.', *Journal of radiation research*. Oxford University Press, 55(1), pp. 61–6. doi: 10.1093/jrr/rrt091.
349. Sirard, M.-A. (2012) 'Factors Affecting Oocyte and Embryo Transcriptomes', *Reproduction in Domestic Animals*, 47, pp. 148–155. doi: 10.1111/j.1439-0531.2012.02069.x.
350. Sironen, A., Uimari, P. and Vilkki, J. (2011) 'Comparison of different DNA extraction methods from hair root follicles to genotype Finnish Landrace boars with the Illumina PorcineSNP60 beadchip', *Agricultural and Food Science*, 20(2), pp. 143–150.
351. Skalníková, M. *et al.* (2000) 'Spatial arrangement of genes, centromeres and chromosomes in human blood cell nuclei and its changes during the cell cycle, differentiation and after irradiation.', *Chromosome research : an international journal on the molecular, supramolecular and evolutionary aspects of chromosome biology*, 8(6), pp. 487–99. Available at: <http://www.ncbi.nlm.nih.gov/pubmed/11032319> (Accessed: 22 May 2018).
352. Skottman, H. and Hovatta, O. (2006) 'Culture conditions for human embryonic stem cells', *Reproduction*, 132(5), pp. 691–698. doi: 10.1530/rep.1.01079.
353. Snyder, T. M. *et al.* (2011) 'Universal noninvasive detection of solid organ transplant rejection.', *Proceedings of the National Academy of Sciences of the United States of America*, 108(15), pp. 6229–6234. doi: 10.1073/pnas.1013924108.
354. Solovei, I. *et al.* (2013) 'LBR and Lamin A/C Sequentially Tether Peripheral Heterochromatin and Inversely Regulate Differentiation', *Cell*, 152(3), pp. 584–598. doi: 10.1016/j.cell.2013.01.009.
355. Song, W. K. *et al.* (2015) 'Treatment of macular degeneration using embryonic stem cell-derived retinal pigment epithelium: preliminary results in Asian patients.', *Stem cell reports*. Elsevier, 4(5), pp. 860–72. doi: 10.1016/j.stemcr.2015.04.005.
356. Sperber, H. *et al.* (2015) 'The metabolome regulates the epigenetic landscape during naive-to-primed human embryonic stem cell transition.', *Nature cell biology*. NIH Public Access, 17(12), pp. 1523–35. doi: 10.1038/ncb3264.
357. Sperger, J. M. *et al.* (2003) 'Gene expression patterns in human embryonic stem cells and human pluripotent germ cell tumors.', *Proceedings of the National Academy of Sciences of the United States of America*, 100(23), pp. 13350–13355. doi: 10.1073/pnas.2235735100.
358. Stacey, G. N. *et al.* (2017) 'Preservation and stability of cell therapy products: recommendations from an expert workshop', *Regenerative Medicine*. Future Medicine Ltd London, UK , 12(5), pp. 553–564. doi: 10.2217/rme-2017-0073.
359. *STEMCELL TECHNOLOGIES* (2018) *hPSC Genetic Analysis Kit*.
360. Stephenson, E. L. and Braude, P. R. (2010) 'Derivation of the King's College London human embryonic stem cell lines', *In Vitro Cellular & Developmental Biology - Animal*, 46(3–4), pp. 178–185. doi: 10.1007/s11626-010-9276-4.
361. Stewart, C. and Burke, B. (1987) 'Teratocarcinoma stem cells and early mouse embryos contain only a single major lamin polypeptide closely resembling lamin B', *Cell*. Cell Press, 51(3), pp. 383–392. doi: 10.1016/0092-8674(87)90634-9.
362. Stopper, H. *et al.* (2003) 'Increased cell proliferation is associated with genomic instability: elevated micronuclei frequencies in estradiol-treated human ovarian cancer cells.', *Mutagenesis*, 18(3), pp. 243–7. Available at: <http://www.ncbi.nlm.nih.gov/pubmed/12714689> (Accessed: 14 August 2017).
363. Strain, M. C. *et al.* (2013) 'Highly Precise Measurement of HIV DNA by Droplet Digital PCR', *PLoS ONE*. Edited by Y. Wu. Public Library of Science, 8(4), pp. 2–9. doi: 10.1371/journal.pone.0055943.
364. Strelkov, S. V. *et al.* (2004) 'Crystal Structure of the Human Lamin A Coil 2B Dimer: Implications for the Head-to-tail Association of Nuclear Lamins', *Journal of Molecular Biology*, 343(4), pp. 1067–1080. doi: 10.1016/j.jmb.2004.08.093.
365. Stuurman, N., Sasse, B. and Fisher, P. A. (1996) 'Intermediate Filament Protein

- Polymerization: Molecular Analysis of *Drosophila* Nuclear Lamin Head-to-Tail Binding', *Journal of Structural Biology*, 117(1), pp. 1–15. doi: 10.1006/jsbi.1996.0064.
366. Sugamori, K. S., Brenneman, D. and Grant, D. M. (2011) 'Liver-Selective Expression of Human Arylamine N-Acetyltransferase NAT2 in Transgenic Mice', *Drug Metabolism and Disposition*, 39(5), pp. 882–890. doi: 10.1124/dmd.111.038216.
367. Suh, Y.-A. *et al.* (1999) 'Cell transformation by the superoxide-generating oxidase Mox1', *Nature*. Nature Publishing Group, 401(6748), pp. 79–82. doi: 10.1038/43459.
368. Summersgill, B. M. *et al.* (2001) 'Definition of chromosome aberrations in testicular germ cell tumor cell lines by 24-color karyotyping and complementary molecular cytogenetic analyses', *Cancer Genetics and Cytogenetics*, 128(2), pp. 120–129. doi: 10.1016/S0165-4608(01)00414-9.
369. Swift, J. and Discher, D. E. (2014) 'The nuclear lamina is mechano-responsive to ECM elasticity in mature tissue.', *Journal of cell science*. Company of Biologists, 127(Pt 14), pp. 3005–15. doi: 10.1242/jcs.149203.
370. Szczerbal, I., Foster, H. a. and Bridger, J. M. (2009) 'The spatial repositioning of adipogenesis genes is correlated with their expression status in a porcine mesenchymal stem cell adipogenesis model system', *Chromosoma*. Springer-Verlag, 118(5), pp. 647–663. doi: 10.1007/s00412-009-0225-5.
371. Taapken, S. M. *et al.* (2011) 'Karyotypic abnormalities in human induced pluripotent stem cells and embryonic stem cells.', *Nature biotechnology*. Nature Publishing Group, a division of Macmillan Publishers Limited. All Rights Reserved., 29(4), pp. 313–4. doi: 10.1038/nbt.1835.
372. Taimen, P. *et al.* (2009) 'A progeria mutation reveals functions for lamin A in nuclear assembly, architecture, and chromosome organization.', *Proceedings of the National Academy of Sciences of the United States of America*. National Academy of Sciences, 106(49), pp. 20788–93. doi: 10.1073/pnas.0911895106.
373. Takagi, Y. *et al.* (2005) 'Dopaminergic neurons generated from monkey embryonic stem cells function in a Parkinson primate model.', *The Journal of clinical investigation*. American Society for Clinical Investigation, 115(1), pp. 102–9. doi: 10.1172/JCI21137.
374. Takahashi, K. *et al.* (2007) 'Induction of Pluripotent Stem Cells from Adult Human Fibroblasts by Defined Factors', *Cell*. Cell Press, 131(5), pp. 861–872. doi: 10.1016/J.CELL.2007.11.019.
375. Takahashi, K. and Yamanaka, S. (2006) 'Induction of pluripotent stem cells from mouse embryonic and adult fibroblast cultures by defined factors', *Cell*. Department of Stem Cell Biology, Institute for Frontier Medical Sciences, Kyoto University, Kyoto 606-8507, Japan., 126(4), pp. 663–676. doi: S0092-8674(06)00976-7 [pii].
376. Takei, Y. *et al.* (2008) 'Overexpression of PTEN in ovarian cancer cells suppresses i.p. dissemination and extends survival in mice', *Molecular Cancer Therapeutics*, 7(3). Available at: <http://mct.aacrjournals.org/content/7/3/704.long> (Accessed: 15 August 2017).
377. Talbert, P. B. and Henikoff, S. (2006) 'Spreading of silent chromatin: inaction at a distance', *Nature Reviews Genetics*. Nature Publishing Group, 7(10), pp. 793–803. doi: 10.1038/nrg1920.
378. Tanabe, H. *et al.* (2002) 'Evolutionary conservation of chromosome territory arrangements in cell nuclei from higher primates.', *Proceedings of the National Academy of Sciences of the United States of America*, 99(7), pp. 4424–4429. doi: 10.1073/pnas.072618599.
379. Tanaka, T. and Shimizu, N. (2000) 'Induced detachment of acentric chromatin from mitotic chromosomes leads to their cytoplasmic localization at G(1) and the micronucleation by lamin reorganization at S phase', *Journal of Cell Science*, 113(4). Available at: http://jcs.biologists.org/content/113/4/697?ijkey=8fdd4c17279ac440d5b17d577c3b7ceda526f8d4&keytype2=tf_ipsecsha (Accessed: 14 August 2017).
380. Thomson, J. a *et al.* (1998) 'Embryonic stem cell lines derived from human blastocysts', *Science (New York, N.Y.)*. Wisconsin Regional Primate Research Center, University of Wisconsin, Madison, WI 53715, USA., 282(5391), pp. 1145–1147. doi: 10.1126/science.282.5391.1145.
381. Torres, E. M., Williams, B. R. and Amon, A. (2008) 'Aneuploidy: cells losing their balance.', *Genetics*. Genetics Society of America, 179(2), pp. 737–46. doi: 10.1534/genetics.108.090878.

382. Tosca, L. *et al.* (2015) 'Genomic instability of human embryonic stem cell lines using different passaging culture methods.', *Molecular cytogenetics*. BioMed Central, 8, p. 30. doi: 10.1186/s13039-015-0133-8.
383. Traverso, G. *et al.* (2002) 'Detection of proximal colorectal cancers through analysis of faecal DNA Mammographic screening : no reliable supporting evidence ? For personal use . Only reproduce with permission from The Lancet Publishing Group .', 359, pp. 403–404.
384. Tsai, M.-Y. *et al.* (2006) 'A Mitotic Lamin B Matrix Induced by RanGTP Required for Spindle Assembly', *Science*, 311(5769), pp. 1887–1893. doi: 10.1126/science.1122771.
385. Tusell, L. *et al.* (2010) 'Different outcomes of telomere-dependent anaphase bridges', *Biochemical Society Transactions*, 38(6). Available at: <http://www.biochemsoctrans.org/content/38/6/1698.long> (Accessed: 1 April 2017).
386. Uemura, T. *et al.* (1987) 'DNA topoisomerase II is required for condensation and separation of mitotic chromosomes in *S. pombe*.', *Cell*, 50(6), pp. 917–25. Available at: <http://www.ncbi.nlm.nih.gov/pubmed/3040264> (Accessed: 14 August 2017).
387. Unger, C. *et al.* (2008) 'Good manufacturing practice and clinical-grade human embryonic stem cell lines', *Human Molecular Genetics*, 17(R1), pp. R48–R53. doi: 10.1093/hmg/ddn079.
388. Unger, C. *et al.* (2009) 'Immortalized human skin fibroblast feeder cells support growth and maintenance of both human embryonic and induced pluripotent stem cells', *Human Reproduction*, 24(10), pp. 2567–2581. doi: 10.1093/humrep/dep232.
389. Uppender, M. B. *et al.* (2004) 'Chromosome transfer induced aneuploidy results in complex dysregulation of the cellular transcriptome in immortalized and cancer cells.', *Cancer research*. NIH Public Access, 64(19), pp. 6941–9. doi: 10.1158/0008-5472.CAN-04-0474.
390. Utani, K. *et al.* (2010) 'Emergence of Micronuclei and Their Effects on the Fate of Cells under Replication Stress', *PLoS ONE*. Edited by M. Freitag. Public Library of Science, 5(4), p. e10089. doi: 10.1371/journal.pone.0010089.
391. Utani, K., Kawamoto, J. and Shimizu, N. (2007) 'Micronuclei Bearing Acentric Extrachromosomal Chromatin Are Transcriptionally Competent and May Perturb the Cancer Cell Phenotype', *Molecular Cancer Research*, 5(7). Available at: <http://mcr.aacrjournals.org/content/5/7/695.long> (Accessed: 14 August 2017).
392. Vaughan, A. *et al.* (2001) 'Both emerlin and lamin C depend on lamin A for localization at the nuclear envelope.', *Journal of cell science*, 114(Pt 14), pp. 2577–90. Available at: <http://www.ncbi.nlm.nih.gov/pubmed/11683386> (Accessed: 8 May 2018).
393. Venables, R. S. *et al.* (2001) 'Expression of individual lamins in basal cell carcinomas of the skin', *British Journal of Cancer*, 84(4), pp. 512–519. doi: 10.1054/bjoc.2000.1632.
394. Vergnes, L. *et al.* (2004) 'Lamin B1 is required for mouse development and nuclear integrity', *Proceedings of the National Academy of Sciences*, 101(28), pp. 10428–10433. doi: 10.1073/pnas.0401424101.
395. Vernardis, S. I. *et al.* (2017) 'Human embryonic and induced pluripotent stem cells maintain phenotype but alter their metabolism after exposure to ROCK inhibitor.', *Scientific reports*. Nature Publishing Group, 7, p. 42138. doi: 10.1038/srep42138.
396. Vierbuchen, T. *et al.* (2010) 'Direct conversion of fibroblasts to functional neurons by defined factors', *Nature*. Nature Publishing Group, 463(7284), pp. 1035–1041. doi: 10.1038/nature08797.
397. Visser, a E. and Aten, J. a (1999) 'Chromosomes as well as chromosomal subdomains constitute distinct units in interphase nuclei.', *Journal of cell science*, 112 (Pt 1, pp. 3353–3360.
398. Vitomirov, A. *et al.* (2017) 'Random shearing as an alternative to digestion for mitochondrial DNA processing in droplet digital PCR.', *Mitochondrion*. NIH Public Access, 32, pp. 16–18. doi: 10.1016/j.mito.2016.11.005.
399. Vogelstein, B. and Kinzler, K. W. (1999) 'Digital PCR', *Proceedings of the National Academy of Sciences*. National Academy of Sciences, 96(16), pp. 9236–9241. doi: 10.1073/PNAS.96.16.9236.
400. Volpi, E. V *et al.* (2000) 'Large-scale chromatin organization of the major histocompatibility complex and other regions of human chromosome 6 and its response to interferon in interphase

- nuclei.', *Journal of cell science*, 113 (Pt 9, pp. 1565–76. Available at: <http://www.ncbi.nlm.nih.gov/pubmed/10751148> (Accessed: 1 May 2017).
401. Wang, A. *et al.* (2011) 'Induced pluripotent stem cells for neural tissue engineering', *Biomaterials*, 32(22), pp. 5023–5032. doi: 10.1016/j.biomaterials.2011.03.070.
402. Wang, J. *et al.* (2014) 'Chromosome boundary elements and regulation of heterochromatin spreading.', *Cellular and molecular life sciences : CMLS*. NIH Public Access, 71(24), pp. 4841–52. doi: 10.1007/s00018-014-1725-x.
403. Wang, L., McLeod, H. L. and Weinshilboum, R. M. (2011) 'Genomics and Drug Response', *N Engl J Med.*, 364(12), pp. 1144–1153. doi: 10.1056/NEJMra1010600.Genomics.
404. Wang, X. *et al.* (2008) 'Enterococcus faecalis induces aneuploidy and tetraploidy in colonic epithelial cells through a bystander effect.', *Cancer research*. NIH Public Access, 68(23), pp. 9909–17. doi: 10.1158/0008-5472.CAN-08-1551.
405. Wazir, U. *et al.* (2013) 'The clinicopathological significance of lamin A/C, lamin B1 and lamin B receptor mRNA expression in human breast cancer', *Cellular and Molecular Biology Letters*, 18(4), pp. 595–611. doi: 10.2478/s11658-013-0109-9.
406. Weimer, R. *et al.* (1992) 'Characterization of centromere arrangements and test for random distribution in Go, G1, S, G2, G1, and early S' phase in human lymphocytes', *Hum Genet*, 88, pp. 673–682. Available at: http://download.springer.com.ezproxy.brunel.ac.uk/static/pdf/766/art%253A10.1007%252FBF02265296.pdf?originUrl=http%3A%2F%2Flink.springer.com%2Farticle%2F10.1007%2FBF02265296&token2=exp=1493756963~acl=%2Fstatic%2Fpdf%2F766%2Fart%25253A10.1007%25252FBF02265296.pdf%3Dhttp%253A%252F%252Flink.springer.com%252Farticle%252F10.1007%252FBF02265296*~hmac=3f45a42b520c890b554f0d789472967ca8631e03250efc8c8d25d3c2fd7d5707 (Accessed: 2 May 2017).
407. Wernig, M. *et al.* (2008) 'A drug-inducible transgenic system for direct reprogramming of multiple somatic cell types', *Nature Biotechnology*, 26(8), pp. 916–924. doi: 10.1038/nbt1483.
408. White, J. and Dalton, S. (2005) 'Cell cycle control of embryonic stem cells.', *Stem cell reviews*, 1(2), pp. 131–138. doi: 10.1385/SCR:1:2:131.
409. Wiblin, A. E. *et al.* (2005) 'Distinctive nuclear organisation of centromeres and regions involved in pluripotency in human embryonic stem cells.', *Journal of cell science*, 118(Pt 17), pp. 3861–3868. doi: 10.1242/jcs.02500.
410. Willis, N. D. *et al.* (2008) 'Lamin A/C Is a Risk Biomarker in Colorectal Cancer', *PLoS ONE*. Edited by K. G. Hardwick, 3(8), p. e2988. doi: 10.1371/journal.pone.0002988.
411. Woodbine, L. *et al.* (2011) 'Endogenously induced DNA double strand breaks arise in heterochromatic DNA regions and require ataxia telangiectasia mutated and Artemis for their repair.', *Nucleic acids research*. Oxford University Press, 39(16), pp. 6986–97. doi: 10.1093/nar/gkr331.
412. Worman, H. J. *et al.* (1988) 'A lamin B receptor in the nuclear envelope.', *Proceedings of the National Academy of Sciences of the United States of America*, 85(22), pp. 8531–4. Available at: <http://www.ncbi.nlm.nih.gov/pubmed/2847165> (Accessed: 22 May 2018).
413. Yamamori, T. *et al.* (2012) 'Ionizing radiation induces mitochondrial reactive oxygen species production accompanied by upregulation of mitochondrial electron transport chain function and mitochondrial content under control of the cell cycle checkpoint', *Free Radical Biology and Medicine*, 53(2), pp. 260–270. doi: 10.1016/j.freeradbiomed.2012.04.033.
414. Yang, S. *et al.* (2008) 'Tumor progression of culture-adapted human embryonic stem cells during long-term culture', *Genes, Chromosomes and Cancer*, 47(8), pp. 665–679. doi: 10.1002/gcc.20574.
415. Yang, S. H. *et al.* (2011) 'Are B-type lamins essential in all mammalian cells?', *Nucleus (Austin, Tex.)*. Taylor & Francis, 2(6), pp. 562–9. doi: 10.4161/nucl.2.6.18085.
416. Yermilov, V. *et al.* (1996) 'Effects of carbon dioxide/bicarbonate on induction of DNA single-strand breaks and formation of 8-nitroguanine, 8-oxoguanine and base-propenal mediated by

- peroxynitrite.', *FEBS letters*, 399(1–2), pp. 67–70. Available at: <http://www.ncbi.nlm.nih.gov/pubmed/8980121> (Accessed: 29 August 2017).
417. Yoon, B. S. *et al.* (2010) 'Secretory Profiles and Wound Healing Effects of Human Amniotic Fluid-Derived Mesenchymal Stem Cells', *Stem Cells and Development*, 19(6), pp. 887–902. doi: 10.1089/scd.2009.0138.
418. Yukl, S. A. *et al.* (2014) 'Advantages of using the QIAshredder instead of restriction digestion to prepare DNA for droplet digital PCR', *BioTechniques*, 56(4), pp. 194–6. doi: 10.2144/000114159.
419. Zagaria, A. *et al.* (2015) 'BCR-ABL1 e6a2 transcript in chronic myeloid leukemia: biological features and molecular monitoring by droplet digital PCR', *Virchows Archiv*. Springer Berlin Heidelberg, 467(3), pp. 357–363. doi: 10.1007/s00428-015-1802-z.
420. Zastrow, M. S., Vlcek, S. and Wilson, K. L. (2004) 'Proteins that bind A-type lamins: integrating isolated clues', *Journal of Cell Science*, 117(7), pp. 979–987. doi: 10.1242/jcs.01102.
421. Zhang, X. *et al.* (2006) 'Derivation of Human Embryonic Stem Cells from Developing and Arrested Embryos', *Stem Cells*. John Wiley & Sons, Ltd., 24(12), pp. 2669–2676. doi: 10.1634/stemcells.2006-0377.
422. Zhao, R. *et al.* (2014) 'A nontranscriptional role for Oct4 in the regulation of mitotic entry.', *Proceedings of the National Academy of Sciences of the United States of America*. National Academy of Sciences, 111(44), pp. 15768–73. doi: 10.1073/pnas.1417518111.
423. Zhou, G. *et al.* (2016) 'Optimal ROS Signaling Is Critical for Nuclear Reprogramming.', *Cell reports*. NIH Public Access, 15(5), pp. 919–925. doi: 10.1016/j.celrep.2016.03.084.
424. Zhu, G. *et al.* (2015) 'Highly Sensitive Droplet Digital PCR Method for Detection of EGFR-Activating Mutations in Plasma Cell-Free DNA from Patients with Advanced Non-Small Cell Lung Cancer', *J Mol Diagn*, 17(3), pp. 265–72. Available at: <http://www.ncbi.nlm.nih.gov/pubmed/25769900>.
425. Zink, D., Fische, A. H. and Nickerson, J. A. (2004) 'Nuclear structure in cancer cells', *Nature Reviews Cancer*, 4(9), pp. 677–687. doi: 10.1038/nrc1430.

Appendix I

Appendix I: Karyology

FCWES01

Karyotype: 46,XX[8]/46,XXad(12)(q24.3)[2]

Anomaly: 46,XX,del(19)(p10)[1]



FCWES02

Karyotype: 46,XX [19]

Anomaly: 47,XX,+9,add(10)(p15)[1]



MCWES01

Karyotype: 46,XY,?inv(6)q25.2q25.3) [19]

Anomaly: 45,XY,?inv(6)(q25.2q25.3),-10 [1]



MCWES02

Karyotype: 46,XY [19]

Anomaly: 45,X,-Y [1] and 45,XY, -20 [1]



Appendix II

Appendix II: Data Analysis

Nuclear Area Analysis of H9 Cells Grown Under Different Conditions

Human embryonic stem cell line H9 was grown in different media and matrices and the nuclear area was compared across the different conditions using Tukey's Multiple Comparison Test. The table below summarises the results, significant different between samples are shown as asterisks (*) when $p < 0.05$, ** when $p < 0.001$ and *** when $p < 0.0001$.

Tukey's Multiple Comparison Test	Significant? P < 0.05?	Summary
TeSR2 matrigel P3PS vs TeSR2 521 P9PS	Yes	*
TeSR2 matrigel P3PS vs NutriStem matrigel P6PS	Yes	***
TeSR2 matrigel P3PS vs NutriStem 521 P6PS	No	ns
TeSR2 matrigel P3PS vs NutriStem 511 P10PS	No	ns
TeSR2 matrigel P3PS vs E8 matrigel P7PS	Yes	***
TeSR2 matrigel P3PS vs E8 521 P6PS	No	ns
TeSR2 matrigel P3PS vs E8 511 P7PS	Yes	***
TeSR2 matrigel P3PS vs E8 vitronectin P3PS	No	ns
TeSR2 521 P9PS vs NutriStem matrigel P6PS	Yes	***
TeSR2 521 P9PS vs NutriStem 521 P6PS	Yes	***
TeSR2 521 P9PS vs NutriStem 511 P10PS	No	ns
TeSR2 521 P9PS vs E8 matrigel P7PS	No	ns
TeSR2 521 P9PS vs E8 521 P6PS	Yes	***
TeSR2 521 P9PS vs E8 511 P7PS	Yes	***
TeSR2 521 P9PS vs E8 vitronectin P3PS	No	ns
NutriStem matrigel P6PS vs NutriStem 521 P6PS	Yes	**
NutriStem matrigel P6PS vs NutriStem 511 P10PS	Yes	***
NutriStem matrigel P6PS vs E8 matrigel P7PS	Yes	***
NutriStem matrigel P6PS vs E8 521 P6PS	Yes	***
NutriStem matrigel P6PS vs E8 511 P7PS	No	ns
NutriStem matrigel P6PS vs E8 vitronectin P3PS	Yes	***
NutriStem 521 P6PS vs NutriStem 511 P10PS	Yes	***
NutriStem 521 P6PS vs E8 matrigel P7PS	Yes	***
NutriStem 521 P6PS vs E8 521 P6PS	No	ns
NutriStem 521 P6PS vs E8 511 P7PS	Yes	***
NutriStem 521 P6PS vs E8 vitronectin P3PS	Yes	**
NutriStem 511 P10PS vs E8 matrigel P7PS	Yes	*
NutriStem 511 P10PS vs E8 521 P6PS	Yes	***
NutriStem 511 P10PS vs E8 511 P7PS	Yes	***
NutriStem 511 P10PS vs E8 vitronectin P3PS	No	ns
E8 matrigel P7PS vs E8 521 P6PS	Yes	***
E8 matrigel P7PS vs E8 511 P7PS	Yes	***
E8 matrigel P7PS vs E8 vitronectin P3PS	Yes	***
E8 521 P6PS vs E8 511 P7PS	Yes	***
E8 521 P6PS vs E8 vitronectin P3PS	Yes	*
E8 511 P7PS vs E8 vitronectin P3PS	Yes	***

Nuclear Circularity of H9 Cells Grown Under Different Conditions

Human embryonic stem cell line H9 was grown in different media and matrices and the nuclear circularity was compared across the different conditions using Tukey's Multiple Comparison Test. The table below summarises the results, significant different between samples are shown as asterisks (*) when $p < 0.05$, ** when $p < 0.001$ and *** when $p < 0.0001$.

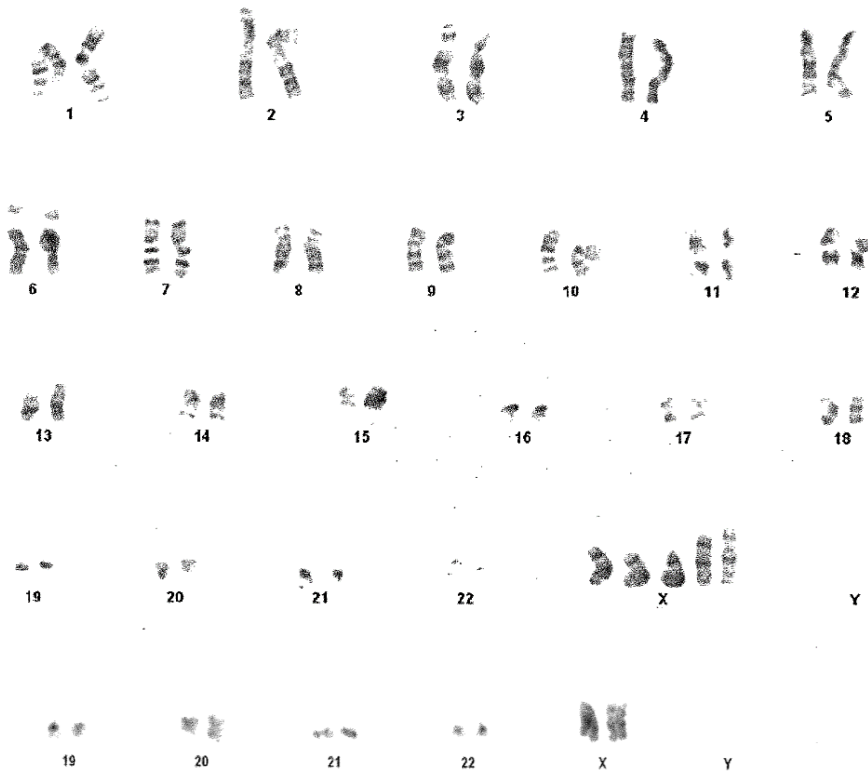
Tukey's Multiple Comparison Test	Significant? P < 0.05?	Summary
TeSR2 matrigel P3PS vs TeSR2 521 P9PS	Yes	***
TeSR2 matrigel P3PS vs NutriStem matrigel P6PS	No	ns
TeSR2 matrigel P3PS vs NutriStem 521 P6PS	No	ns
TeSR2 matrigel P3PS vs NutriStem 511 P10PS	No	ns
TeSR2 matrigel P3PS vs E8 matrigel P7PS	Yes	***
TeSR2 matrigel P3PS vs E8 521 P6PS	Yes	***
TeSR2 matrigel P3PS vs E8 511 P7PS	Yes	***
TeSR2 matrigel P3PS vs E8 vitronectin P3PS	No	ns
TeSR2 521 P9PS vs NutriStem matrigel P6PS	Yes	***
TeSR2 521 P9PS vs NutriStem 521 P6PS	Yes	***
TeSR2 521 P9PS vs NutriStem 511 P10PS	Yes	***
TeSR2 521 P9PS vs E8 matrigel P7PS	Yes	***
TeSR2 521 P9PS vs E8 521 P6PS	Yes	***
TeSR2 521 P9PS vs E8 511 P7PS	No	ns
TeSR2 521 P9PS vs E8 vitronectin P3PS	Yes	***
NutriStem matrigel P6PS vs NutriStem 521 P6PS	Yes	*
NutriStem matrigel P6PS vs NutriStem 511 P10PS	Yes	*
NutriStem matrigel P6PS vs E8 matrigel P7PS	Yes	***
NutriStem matrigel P6PS vs E8 521 P6PS	Yes	***
NutriStem matrigel P6PS vs E8 511 P7PS	Yes	***
NutriStem matrigel P6PS vs E8 vitronectin P3PS	Yes	***
NutriStem 521 P6PS vs NutriStem 511 P10PS	No	ns
NutriStem 521 P6PS vs E8 matrigel P7PS	Yes	**
NutriStem 521 P6PS vs E8 521 P6PS	Yes	***
NutriStem 521 P6PS vs E8 511 P7PS	Yes	***
NutriStem 521 P6PS vs E8 vitronectin P3PS	No	ns
NutriStem 511 P10PS vs E8 matrigel P7PS	Yes	**
NutriStem 511 P10PS vs E8 521 P6PS	Yes	***
NutriStem 511 P10PS vs E8 511 P7PS	Yes	***
NutriStem 511 P10PS vs E8 vitronectin P3PS	No	ns
E8 matrigel P7PS vs E8 521 P6PS	No	ns
E8 matrigel P7PS vs E8 511 P7PS	Yes	***
E8 matrigel P7PS vs E8 vitronectin P3PS	No	ns
E8 521 P6PS vs E8 511 P7PS	Yes	**
E8 521 P6PS vs E8 vitronectin P3PS	Yes	**
E8 511 P7PS vs E8 vitronectin P3PS	Yes	***

Appendix III

Appendix III: Karyology

NIBSC-5

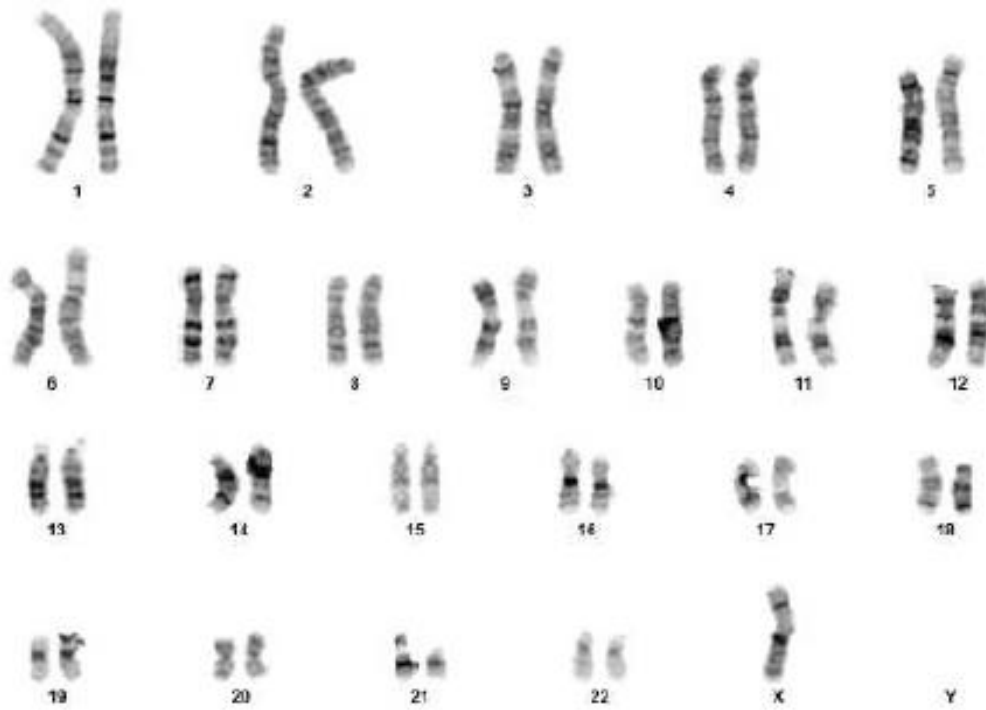
Karyotype: 49,XX, + X, + X, + X [15], 46, XX, [5]



mShef2 P28, 45,X,-X[26]/46,XX[4]



mShef2 P28, 45,X,-X[19]/46,XX[1]



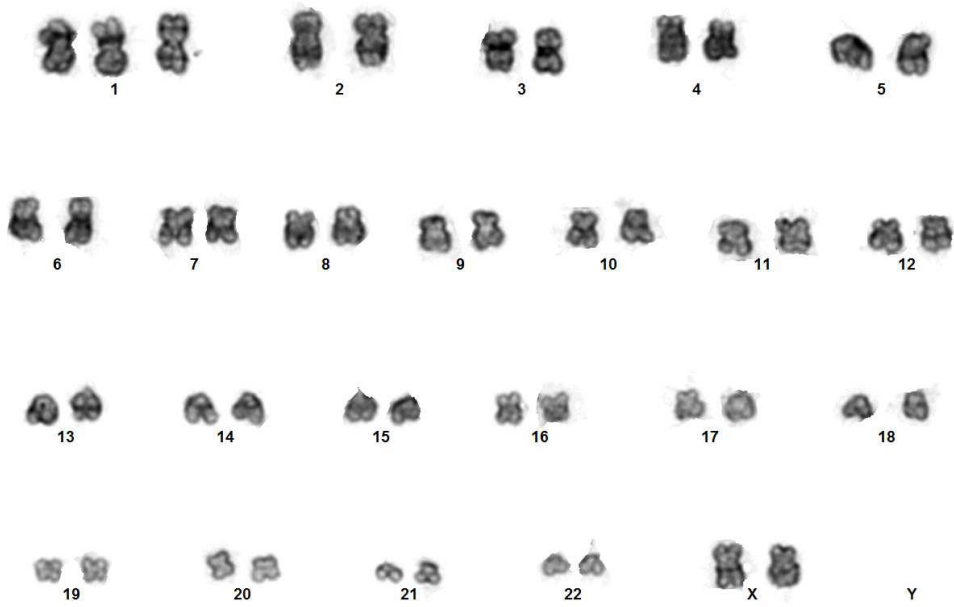
mShaf2 P28, 45,X-X[30]



masterShef2 P5PS, 46, XX [30]



mShef2 P5PS, 47,XX,i(1)(q10),+1[7]/46,XX[3]



Appendix IV

Appendix IV: Data Analysis

MasterShelf2 HDF Nuclear Area

One-way analysis of variance	
P value	< 0.0001
P value summary	***
Are means signif. different? (P < 0.05)	Yes
Number of groups	8
F	178.2
R square	0.4988

Tukey's Multiple Comparison Test	Mean Diff.	q	Significant? P < 0.05?	Summary
P3PS vs P4PS	-141.4	21.75	Yes	***
P3PS vs P5PS	-72.64	10.57	Yes	***
P3PS vs P6PS	-205.8	32.22	Yes	***
P3PS vs P7PS	-264.1	24.44	Yes	***
P3PS vs P8PS	-244.7	37.05	Yes	***
P3PS vs P9PS	-281.7	37.65	Yes	***
P3PS vs P10PS	-178.7	23.31	Yes	***
P4PS vs P5PS	68.78	9.965	Yes	***
P4PS vs P6PS	-64.40	10.03	Yes	***
P4PS vs P7PS	-122.6	11.33	Yes	***
P4PS vs P8PS	-103.3	15.57	Yes	***
P4PS vs P9PS	-140.3	18.68	Yes	***
P4PS vs P10PS	-37.26	4.844	Yes	*
P5PS vs P6PS	-133.2	19.60	Yes	***
P5PS vs P7PS	-191.4	17.32	Yes	***
P5PS vs P8PS	-172.1	24.59	Yes	***
P5PS vs P9PS	-209.1	26.69	Yes	***
P5PS vs P10PS	-106.0	13.24	Yes	***
P6PS vs P7PS	-58.25	5.415	Yes	**
P6PS vs P8PS	-38.92	5.966	Yes	***
P6PS vs P9PS	-75.87	10.24	Yes	***
P6PS vs P10PS	27.14	3.573	No	ns
P7PS vs P8PS	19.32	1.775	No	ns
P7PS vs P9PS	-17.62	1.540	No	ns
P7PS vs P10PS	85.39	7.386	Yes	***
P8PS vs P9PS	-36.95	4.862	Yes	*
P8PS vs P10PS	66.06	8.492	Yes	***
P9PS vs P10PS	103.0	12.07	Yes	***

masterShef2 HDF Nuclear Circularity

One-way analysis of variance	
P value	< 0.0001
P value summary	***
Are means signif. different? (P < 0.05)	Yes
Number of groups	8
F	48.88
R square	0.2273

Tukey's Multiple Comparison Test	Mean Diff.	q	Significant? P < 0.05?	Summary
P3PS vs P4PS	-0.04698	5.599	Yes	**
P3PS vs P5PS	0.05971	7.984	Yes	***
P3PS vs P6PS	0.07359	10.58	Yes	***
P3PS vs P7PS	-0.008717	0.7412	No	ns
P3PS vs P8PS	-0.04669	6.494	Yes	***
P3PS vs P9PS	-0.08080	9.921	Yes	***
P3PS vs P10PS	-0.04996	5.988	Yes	***
P4PS vs P5PS	0.1067	12.18	Yes	***
P4PS vs P6PS	0.1206	14.50	Yes	***
P4PS vs P7PS	0.03827	3.034	No	ns
P4PS vs P8PS	0.0002949	0.03464	No	ns
P4PS vs P9PS	-0.03381	3.622	No	ns
P4PS vs P10PS	-0.002975	0.3129	No	ns
P5PS vs P6PS	0.01388	1.877	No	ns
P5PS vs P7PS	-0.06843	5.689	Yes	**
P5PS vs P8PS	-0.1064	13.97	Yes	***
P5PS vs P9PS	-0.1405	16.48	Yes	***
P5PS vs P10PS	-0.1097	12.58	Yes	***
P6PS vs P7PS	-0.08231	7.031	Yes	***
P6PS vs P8PS	-0.1203	16.94	Yes	***
P6PS vs P9PS	-0.1544	19.14	Yes	***
P6PS vs P10PS	-0.1235	14.94	Yes	***
P7PS vs P8PS	-0.03797	3.205	No	ns
P7PS vs P9PS	-0.07208	5.789	Yes	**
P7PS vs P10PS	-0.04124	3.278	No	ns
P8PS vs P9PS	-0.03411	4.124	No	ns
P8PS vs P10PS	-0.003270	0.3862	No	ns
P9PS vs P10PS	0.03084	3.319	No	ns

masterShef2 Matrigel™ Nuclear Area

One-way analysis of variance	
P value	< 0.0001
P value summary	***
Are means signif. different? (P < 0.05)	Yes
Number of groups	6
F	77.54
R square	0.3039

Tukey's Multiple Comparison Test	Mean Diff.	q	Significant? P < 0.05?	Summary
P5PS vs P6PS	-147.9	21.06	Yes	***
P5PS vs P7PS	-23.29	1.987	No	ns
P5PS vs P8PS	-7.372	0.9653	No	ns
P5PS vs P9PS	-159.3	18.39	Yes	***
P5PS vs P10PS	-91.21	11.96	Yes	***
P6PS vs P7PS	124.7	10.84	Yes	***
P6PS vs P8PS	140.6	19.27	Yes	***
P6PS vs P9PS	-11.39	1.362	No	ns
P6PS vs P10PS	56.74	7.791	Yes	***
P7PS vs P8PS	15.92	1.340	No	ns
P7PS vs P9PS	-136.0	10.82	Yes	***
P7PS vs P10PS	-67.92	5.719	Yes	**
P8PS vs P9PS	-152.0	17.11	Yes	***
P8PS vs P10PS	-83.84	10.65	Yes	***
P9PS vs P10PS	68.13	7.679	Yes	***

masterShef2 Matrigel™ Nuclear Circularity

One-way analysis of variance	
P value	< 0.0001
P value summary	***
Are means signif. different? (P < 0.05)	Yes
Number of groups	6
F	120.6
R square	0.4044

Tukey's Multiple Comparison Test	Mean Diff.	q	Significant? P < 0.05?	Summary
P5PS vs P6PS	-0.03790	3.775	No	ns
P5PS vs P7PS	-0.2883	17.21	Yes	***
P5PS vs P8PS	-0.2655	24.33	Yes	***
P5PS vs P9PS	-0.2682	21.67	Yes	***
P5PS vs P10PS	-0.2237	20.53	Yes	***
P6PS vs P7PS	-0.2504	15.24	Yes	***
P6PS vs P8PS	-0.2276	21.84	Yes	***
P6PS vs P9PS	-0.2303	19.27	Yes	***
P6PS vs P10PS	-0.1858	17.86	Yes	***
P7PS vs P8PS	0.02278	1.341	No	ns
P7PS vs P9PS	0.02011	1.120	No	ns
P7PS vs P10PS	0.06458	3.806	No	ns
P8PS vs P9PS	-0.002672	0.2105	No	ns
P8PS vs P10PS	0.04180	3.716	No	ns
P9PS vs P10PS	0.04447	3.509	No	ns

mShef2 HDF Nuclear Area

One-way analysis of variance	
P value	< 0.0001
P value summary	***
Are means signif. different? (P < 0.05)	Yes
Number of groups	8
F	77.91
R square	0.3466

Tukey's Multiple Comparison Test	Mean Diff.	q	Significant? P < 0.05?	Summary
P3PS vs P4PS	-116.6	12.50	Yes	***
P3PS vs P5PS	-123.8	10.69	Yes	***
P3PS vs P6PS	-187.5	16.95	Yes	***
P3PS vs P7PS	-218.7	22.96	Yes	***
P3PS vs P8PS	-176.7	16.50	Yes	***
P3PS vs P9PS	-236.5	26.48	Yes	***
P3PS vs P10PS	-22.21	2.088	No	ns
P4PS vs P5PS	-7.196	0.5996	No	ns
P4PS vs P6PS	-70.93	6.170	Yes	***
P4PS vs P7PS	-102.1	10.18	Yes	***
P4PS vs P8PS	-60.07	5.384	Yes	**
P4PS vs P9PS	-119.9	12.67	Yes	***
P4PS vs P10PS	94.39	8.512	Yes	***
P5PS vs P6PS	-63.74	4.759	Yes	*
P5PS vs P7PS	-94.93	7.811	Yes	***
P5PS vs P8PS	-52.88	4.036	No	ns
P5PS vs P9PS	-112.8	9.641	Yes	***
P5PS vs P10PS	101.6	7.788	Yes	***
P6PS vs P7PS	-31.19	2.676	No	ns
P6PS vs P8PS	10.86	0.8592	No	ns
P6PS vs P9PS	-49.01	4.384	Yes	*
P6PS vs P10PS	165.3	13.14	Yes	***
P7PS vs P8PS	42.06	3.714	No	ns
P7PS vs P9PS	-17.82	1.844	No	ns
P7PS vs P10PS	196.5	17.46	Yes	***
P8PS vs P9PS	-59.87	5.529	Yes	**
P8PS vs P10PS	154.5	12.58	Yes	***
P9PS vs P10PS	214.3	19.92	Yes	***

mShef2 HDF Nuclear Circularity

One-way analysis of variance	
P value	< 0.0001
P value summary	***
Are means signif. different? (P < 0.05)	Yes
Number of groups	8
F	142.5
R square	0.4925

Tukey's Multiple Comparison Test	Mean Diff.	q	Significant? P < 0.05?	Summary
P3PS vs P4PS	0.3599	36.89	Yes	***
P3PS vs P5PS	0.09850	8.129	Yes	***
P3PS vs P6PS	0.05801	5.013	Yes	*
P3PS vs P7PS	0.005608	0.5628	No	ns
P3PS vs P8PS	0.06370	5.687	Yes	**
P3PS vs P9PS	0.02345	2.510	No	ns
P3PS vs P10PS	-0.04498	4.042	No	ns
P4PS vs P5PS	-0.2614	20.83	Yes	***
P4PS vs P6PS	-0.3019	25.11	Yes	***
P4PS vs P7PS	-0.3543	33.78	Yes	***
P4PS vs P8PS	-0.2962	25.38	Yes	***
P4PS vs P9PS	-0.3365	33.99	Yes	***
P4PS vs P10PS	-0.4049	34.91	Yes	***
P5PS vs P6PS	-0.04049	2.891	No	ns
P5PS vs P7PS	-0.09289	7.308	Yes	***
P5PS vs P8PS	-0.03480	2.540	No	ns
P5PS vs P9PS	-0.07505	6.136	Yes	***
P5PS vs P10PS	-0.1435	10.52	Yes	***
P6PS vs P7PS	-0.05240	4.298	No	ns
P6PS vs P8PS	0.005692	0.4305	No	ns
P6PS vs P9PS	-0.03455	2.955	No	ns
P6PS vs P10PS	-0.1030	7.826	Yes	***
P7PS vs P8PS	0.05809	4.905	Yes	*
P7PS vs P9PS	0.01785	1.766	No	ns
P7PS vs P10PS	-0.05059	4.297	No	ns
P8PS vs P9PS	-0.04024	3.553	No	ns
P8PS vs P10PS	-0.1087	8.466	Yes	***
P9PS vs P10PS	-0.06843	6.082	Yes	***

mShef2 Matrigel™ Nuclear Area

One-way analysis of variance	
P value	< 0.0001
P value summary	***
Are means signif. different? (P < 0.05)	Yes
Number of groups	6
F	219.3
R square	0.5243

Tukey's Multiple Comparison Test	Mean Diff.	q	Significant? P < 0.05?	Summary
P5PS vs P6PS	208.2	20.71	Yes	***
P5PS vs P7PS	124.6	15.77	Yes	***
P5PS vs P8PS	-128.7	15.32	Yes	***
P5PS vs P9PS	-112.4	14.44	Yes	***
P5PS vs P10PS	114.3	15.12	Yes	***
P6PS vs P7PS	-83.59	8.083	Yes	***
P6PS vs P8PS	-337.0	31.40	Yes	***
P6PS vs P9PS	-320.6	31.28	Yes	***
P6PS vs P10PS	-93.94	9.317	Yes	***
P7PS vs P8PS	-253.4	28.97	Yes	***
P7PS vs P9PS	-237.1	29.09	Yes	***
P7PS vs P10PS	-10.35	1.305	No	ns
P8PS vs P9PS	16.32	1.889	No	ns
P8PS vs P10PS	243.0	28.80	Yes	***
P9PS vs P10PS	226.7	29.00	Yes	***

mShef2 Matrigel™ Nuclear Circularity

One-way analysis of variance	
P value	< 0.0001
P value summary	***
Are means signif. different? (P < 0.05)	Yes
Number of groups	6
F	278.4
R square	0.5834

Tukey's Multiple Comparison Test	Mean Diff.	q	Significant? P < 0.05?	Summary
P5PS vs P6PS	-0.4903	36.90	Yes	***
P5PS vs P7PS	-0.3926	37.61	Yes	***
P5PS vs P8PS	-0.2315	20.80	Yes	***
P5PS vs P9PS	-0.3829	37.23	Yes	***
P5PS vs P10PS	-0.4325	43.30	Yes	***
P6PS vs P7PS	0.09770	7.150	Yes	***
P6PS vs P8PS	0.2589	18.23	Yes	***
P6PS vs P9PS	0.1074	7.928	Yes	***
P6PS vs P10PS	0.05779	4.337	Yes	*
P7PS vs P8PS	0.1612	13.92	Yes	***
P7PS vs P9PS	0.009695	0.9004	No	ns
P7PS vs P10PS	-0.03991	3.807	No	ns
P8PS vs P9PS	-0.1515	13.24	Yes	***
P8PS vs P10PS	-0.2011	18.00	Yes	***
P9PS vs P10PS	-0.04961	4.802	Yes	*

Appendix V

Appendix V: FASTQC Files

masterShef2 HDF P10 S1



masterShef2 HDF P10 S2



masterShef2 HDF P10 S3



masterShef2 HDF P11 S1



masterShef2 HDF P11 S2



masterShef2 HDF P11 S3



mShef2 HDF P9 S1



mShef2 HDF P9 S2



mShef2 HDF P9 S3



mShef2 HDF P11 S1



mShef2 HDF P11 S2



mShef2 HDF P11 S3



masterShef2 Matrigel™ P9 S1



masterShef2 Matrigel™ P11 S1



masterShef2 Matrigel™ P11 S2



masterShef2 Matrigel™ P11 S3



mShef2 Matrigel™ P10 S2



mShef2 Matrigel™ P10 S3



mShef2 Matrigel™ P11 S1

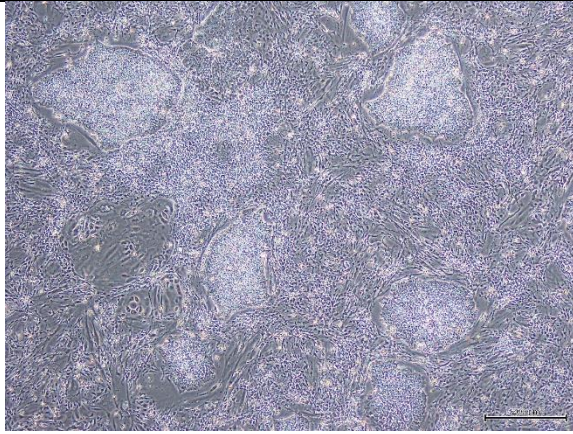
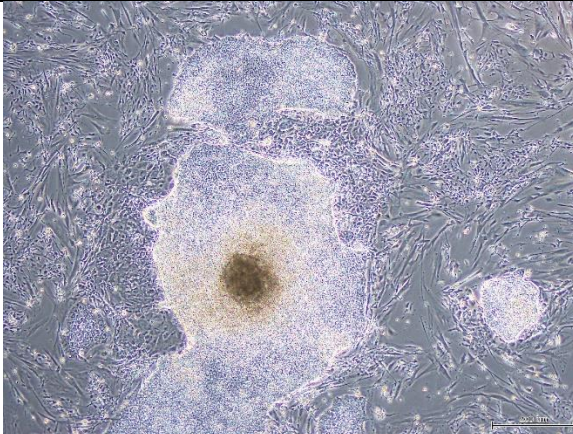
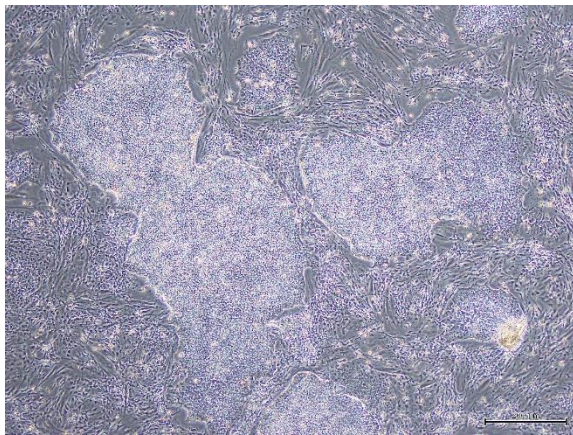
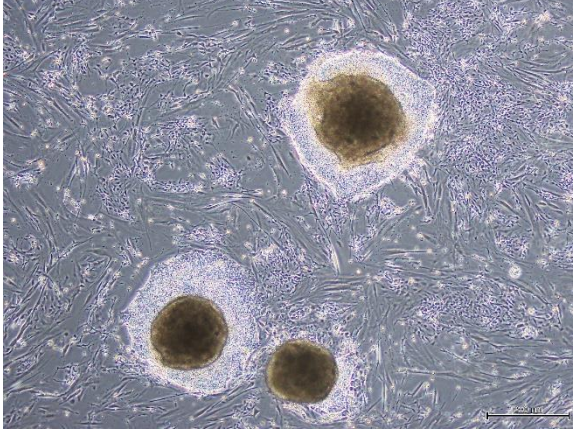
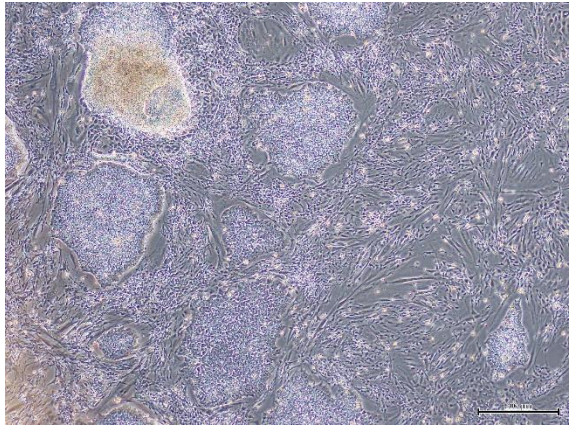
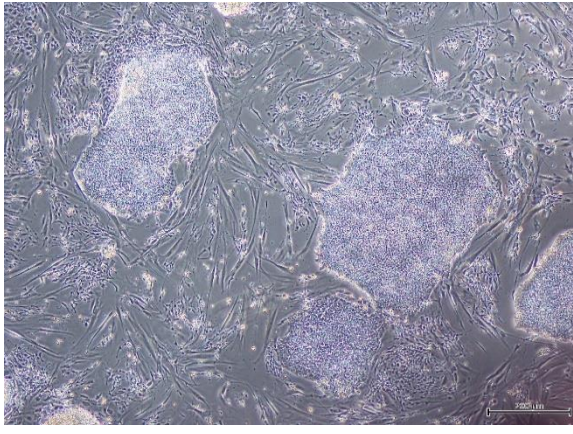


mShef2 Matrigel™ P11 S2



Appendix VI

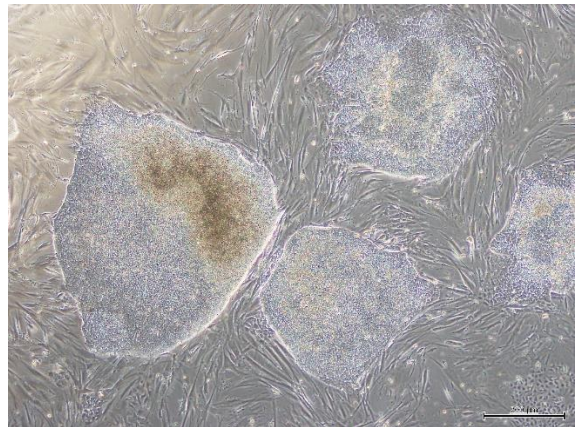
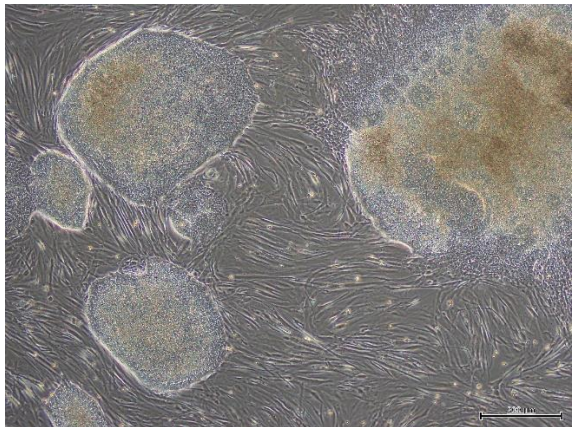
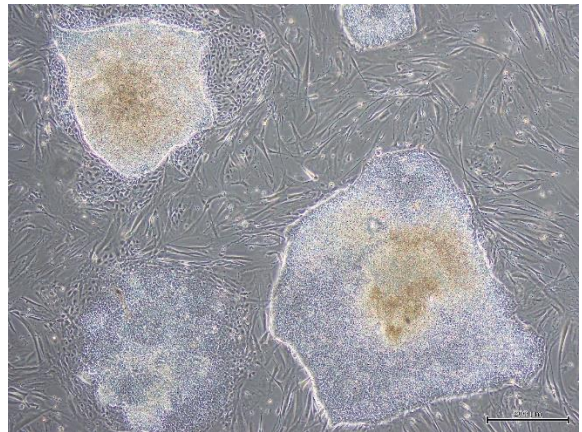
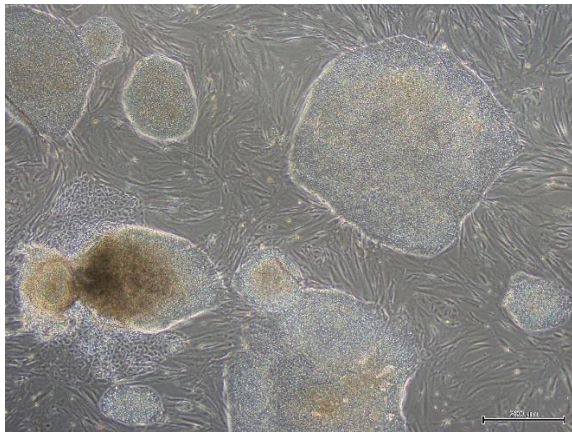
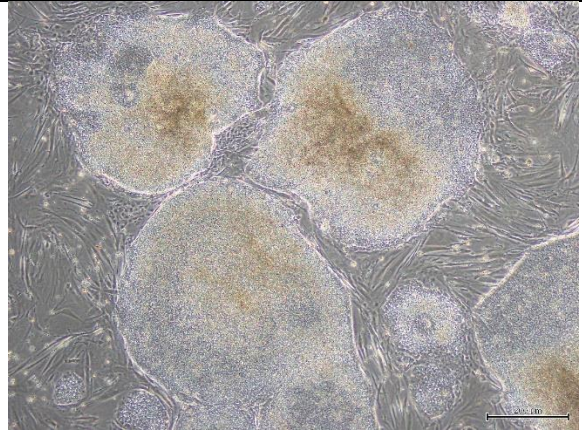
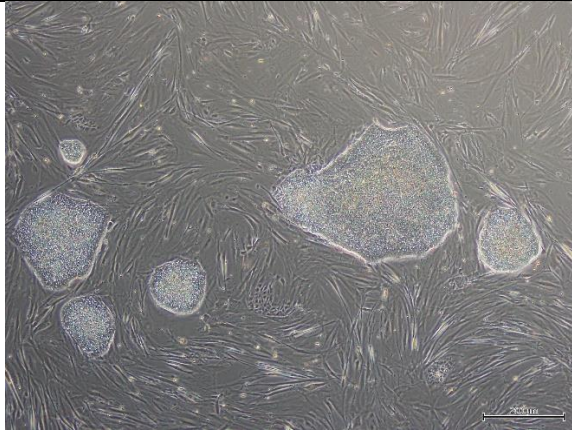
Appendix VI: Stem Cell Colony Images

P1PS	
Mastershef2	MShef2
 <p>Micrograph showing a dense, confluent layer of stem cell colonies on a Mastershef2 feeder layer. The colonies are irregularly shaped and densely packed. A scale bar in the bottom right corner indicates 200 μm.</p>	 <p>Micrograph showing a stem cell colony on an MShef2 feeder layer. The colony is large and irregularly shaped, with a prominent dark brown pigmented center. A scale bar in the bottom right corner indicates 200 μm.</p>
 <p>Micrograph showing a stem cell colony on a Mastershef2 feeder layer. The colony is large and irregularly shaped. A scale bar in the bottom right corner indicates 200 μm.</p>	 <p>Micrograph showing three distinct stem cell colonies on an MShef2 feeder layer. Each colony has a dark brown pigmented center. A scale bar in the bottom right corner indicates 200 μm.</p>
 <p>Micrograph showing a stem cell colony on a Mastershef2 feeder layer. The colony is large and irregularly shaped. A scale bar in the bottom right corner indicates 200 μm.</p>	 <p>Micrograph showing a stem cell colony on an MShef2 feeder layer. The colony is large and irregularly shaped. A scale bar in the bottom right corner indicates 200 μm.</p>

P2PS

Mastershef2

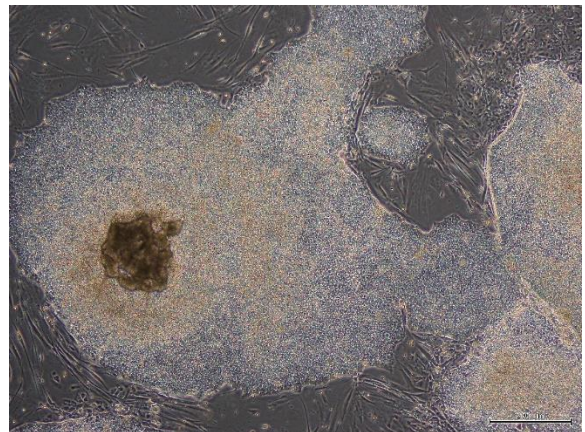
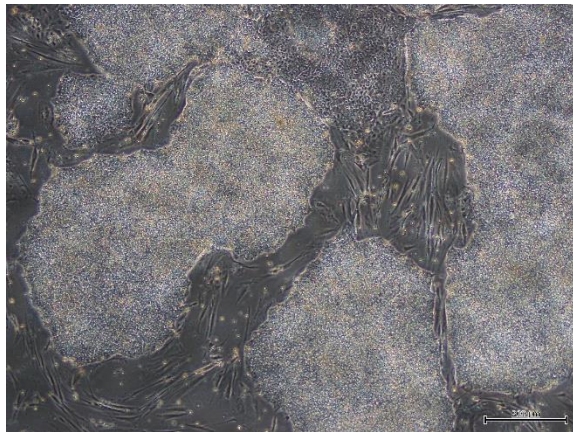
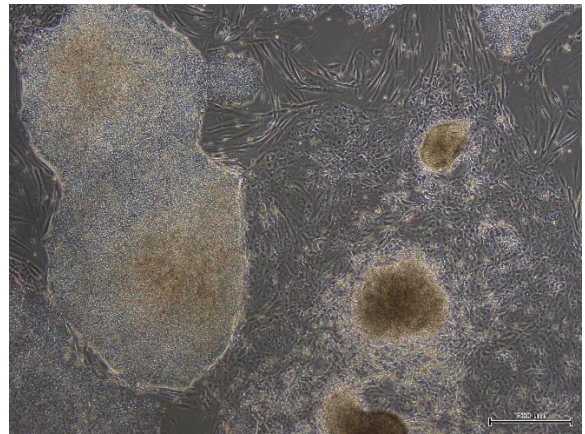
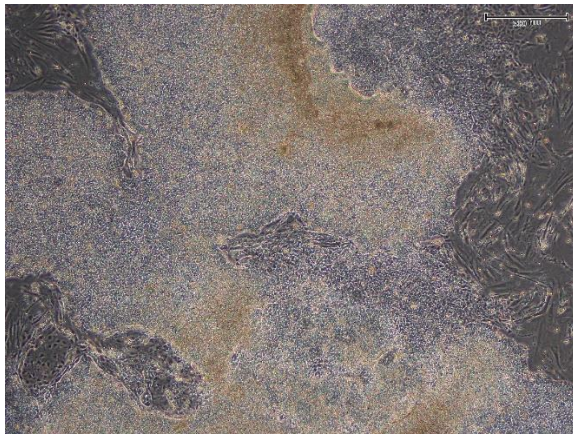
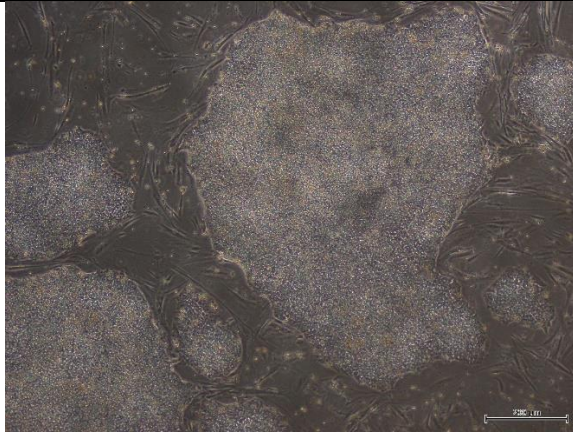
MShef2



P3PS

Mastershef2

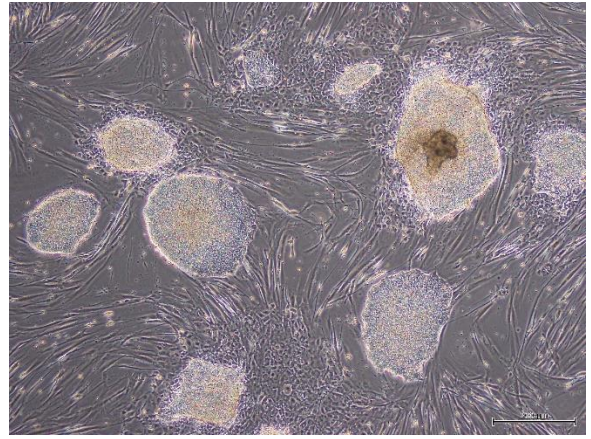
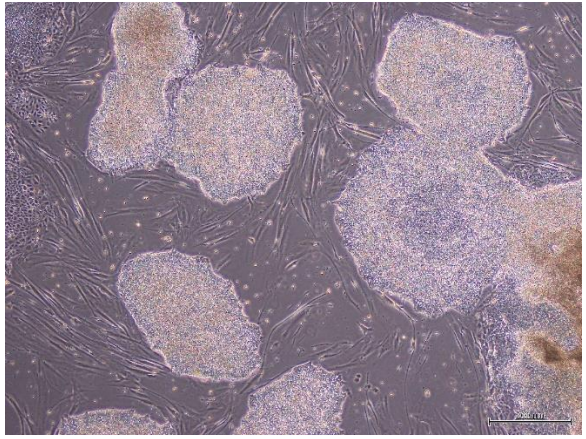
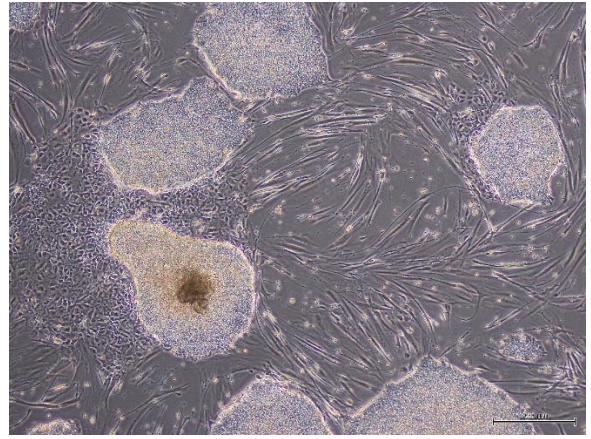
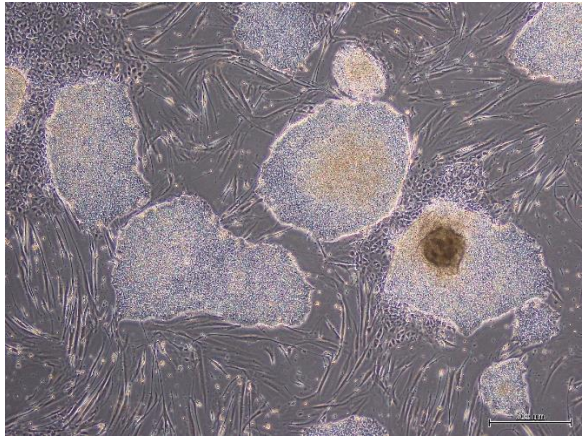
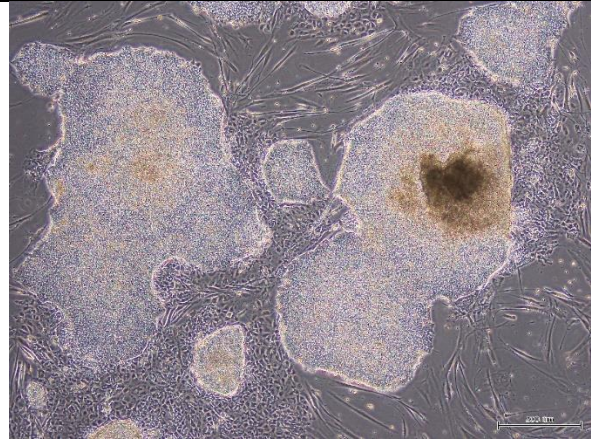
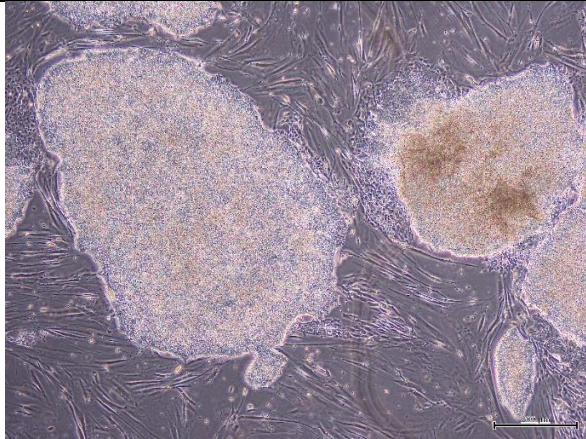
MShef2



P4PS

Mastershef2

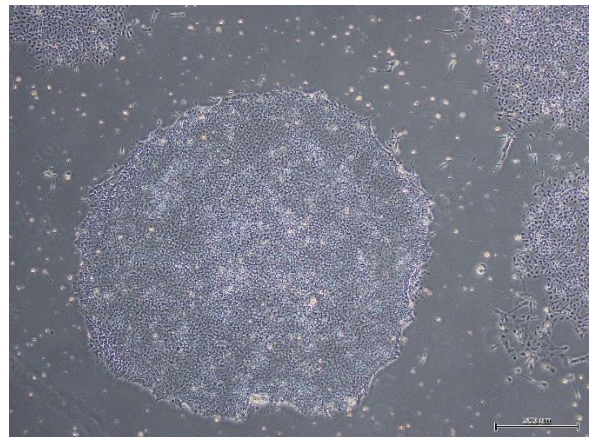
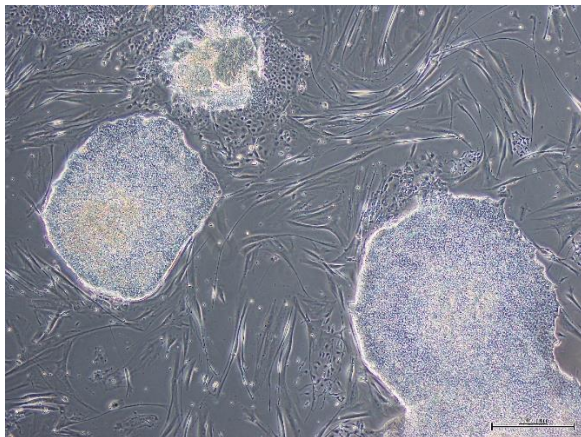
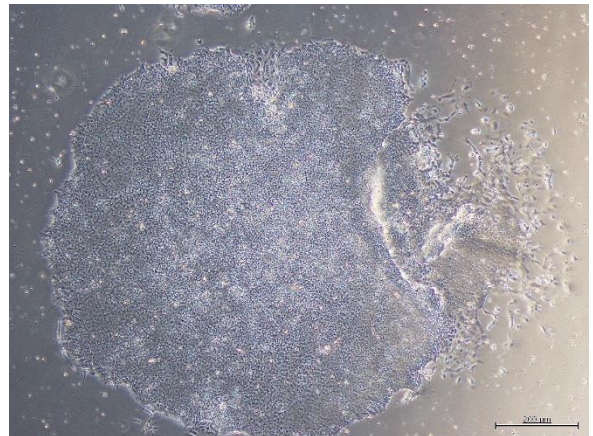
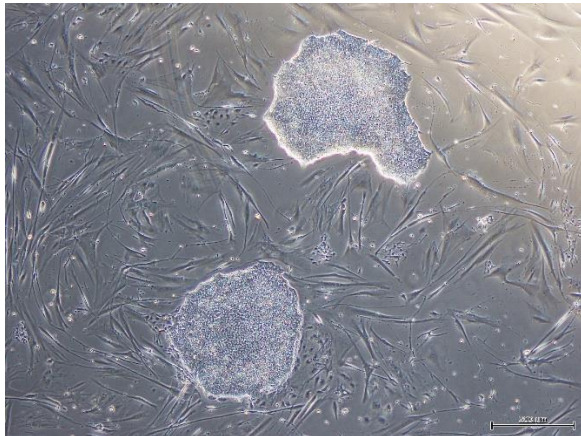
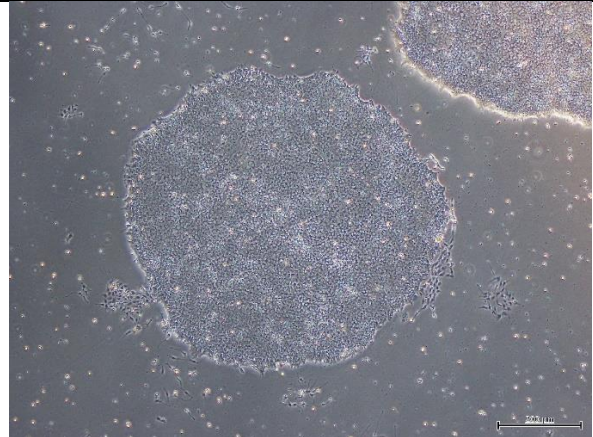
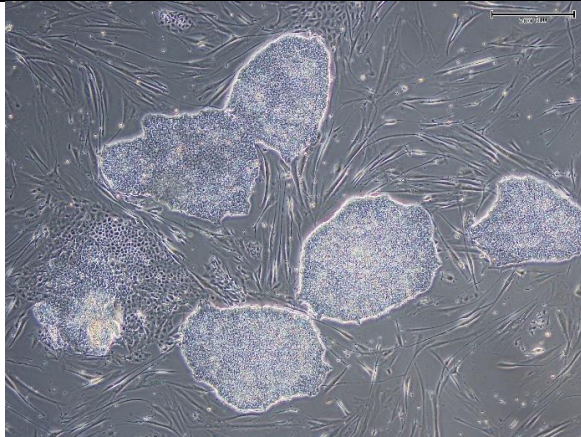
MShef2



P5PS

Mastershef2 HDF

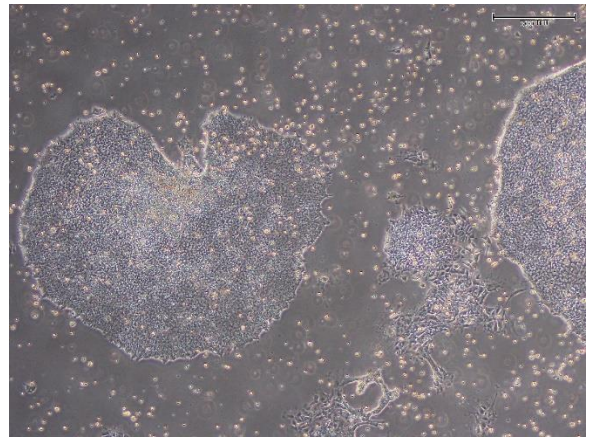
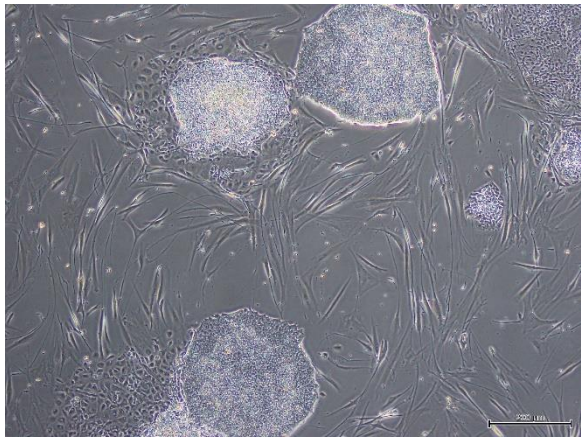
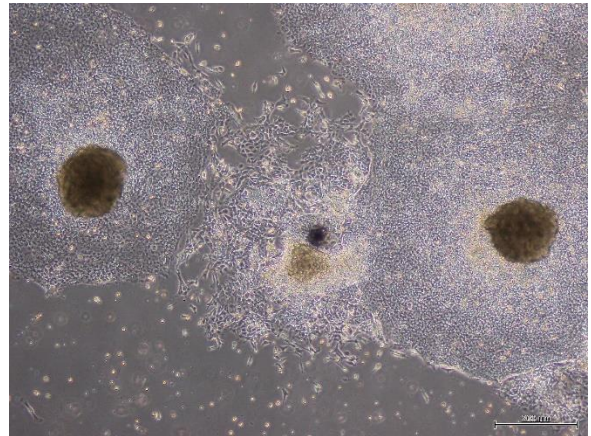
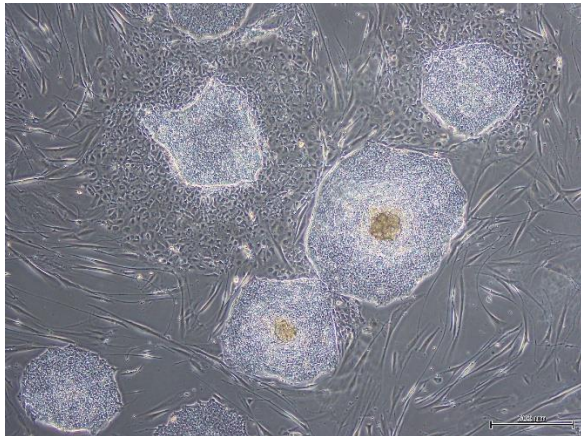
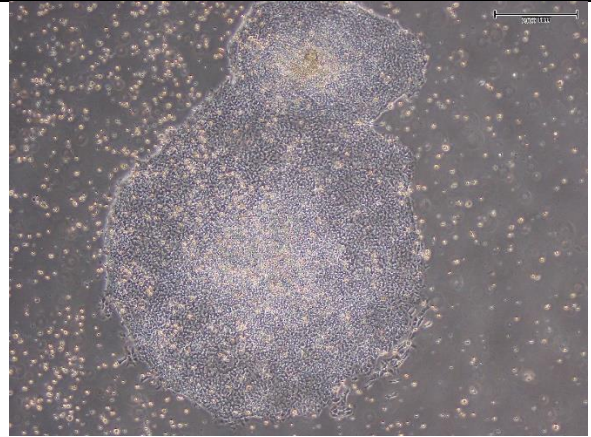
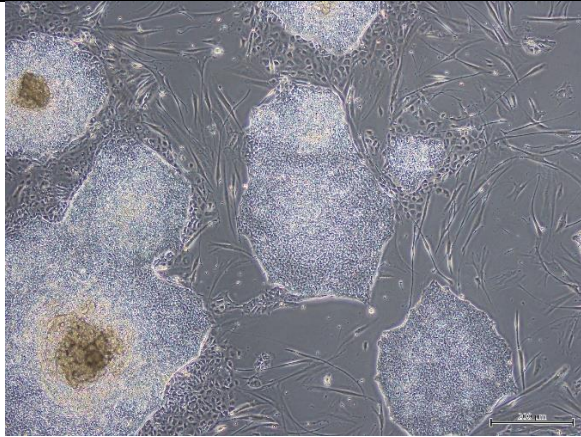
Mastershef2 Matrigel



P5PS

MShef2 HDF

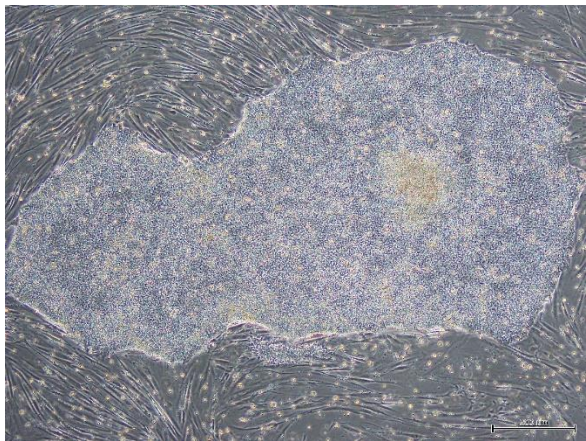
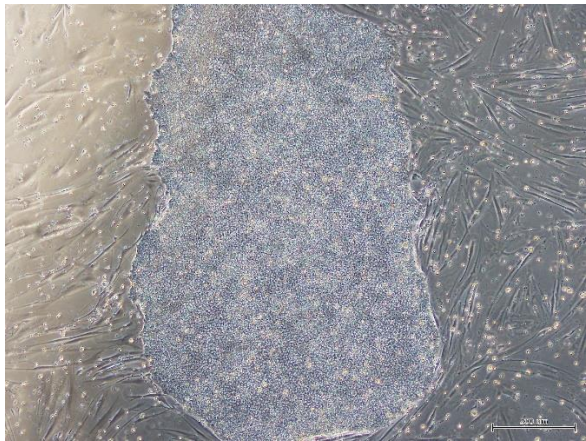
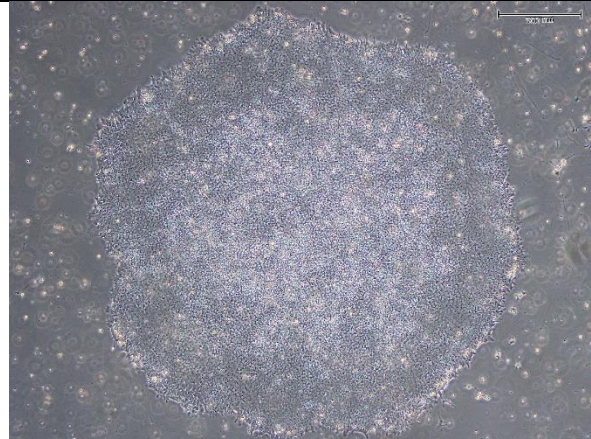
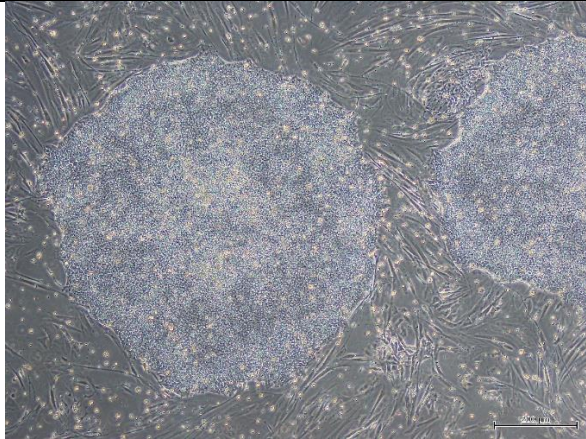
MShef2 Matrigel



P6PS

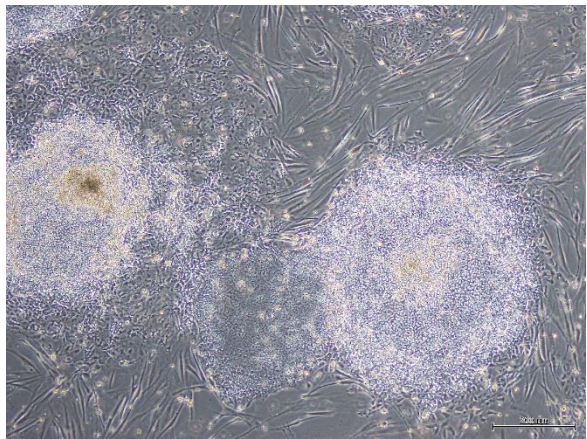
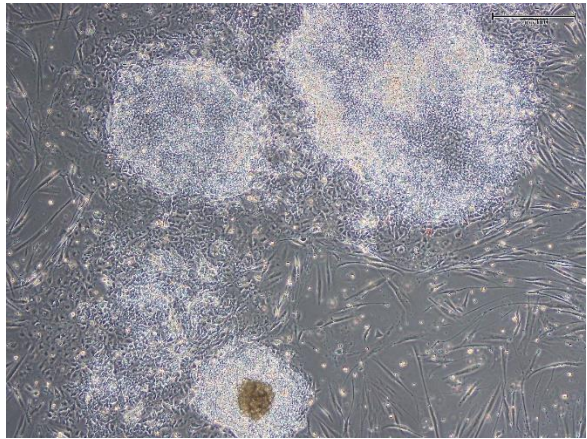
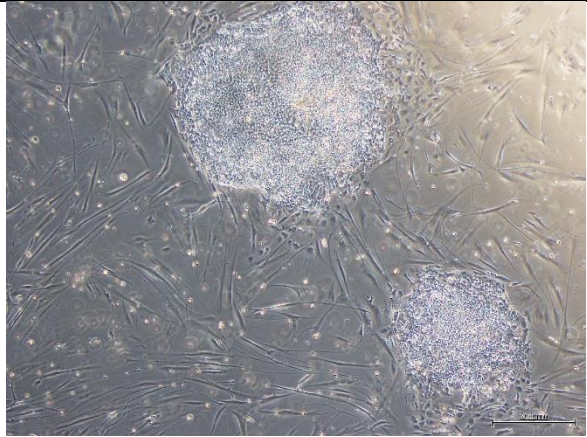
Mastershef2 HDF

Mastershef2 Matrigel



P6PS

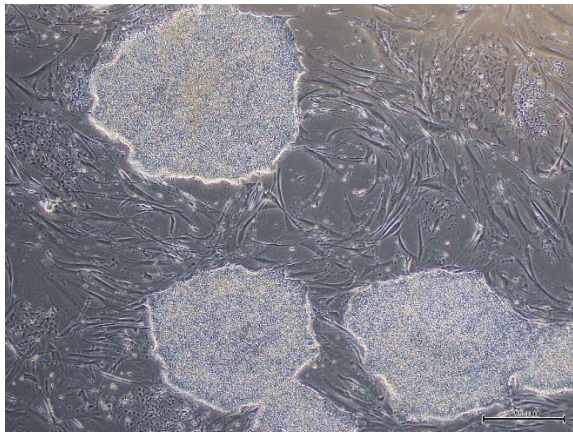
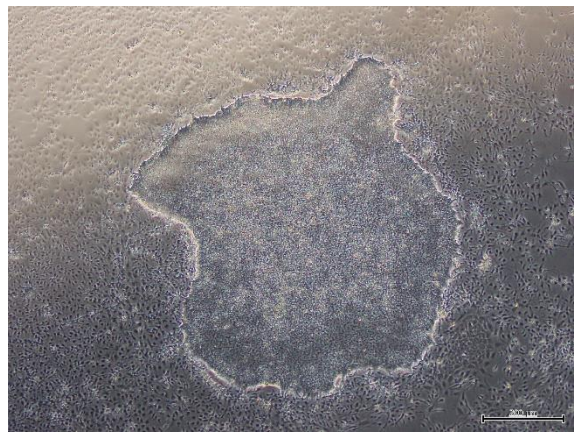
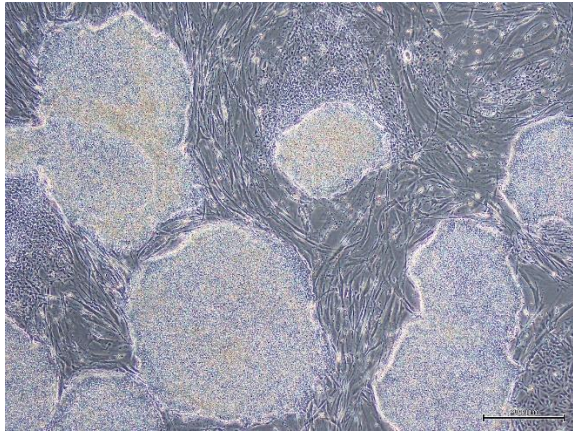
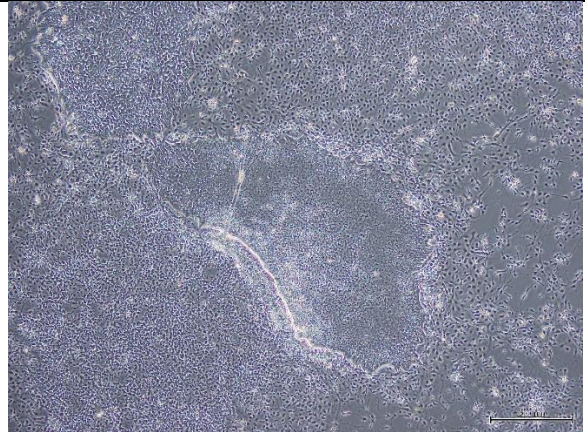
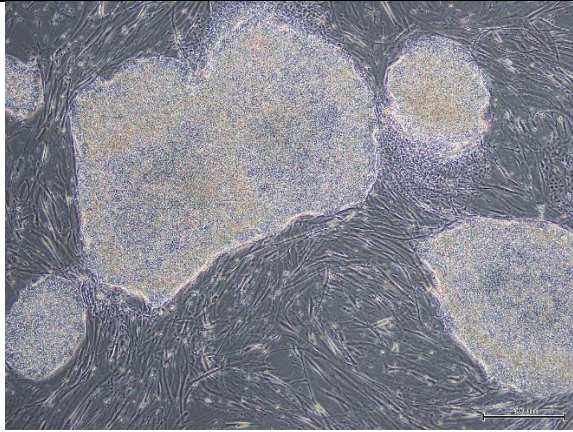
MShef2 Matrigel



P7PS

Mastershef2 HDF

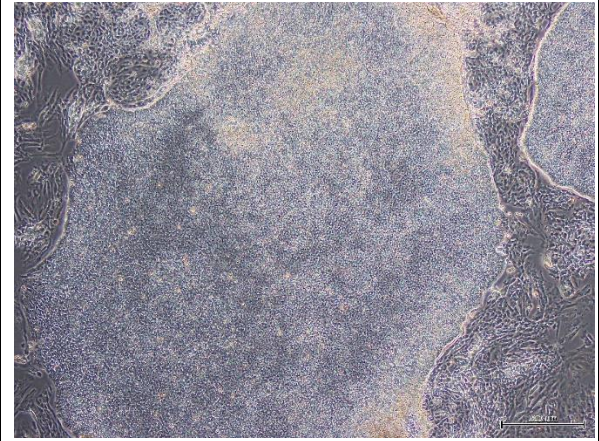
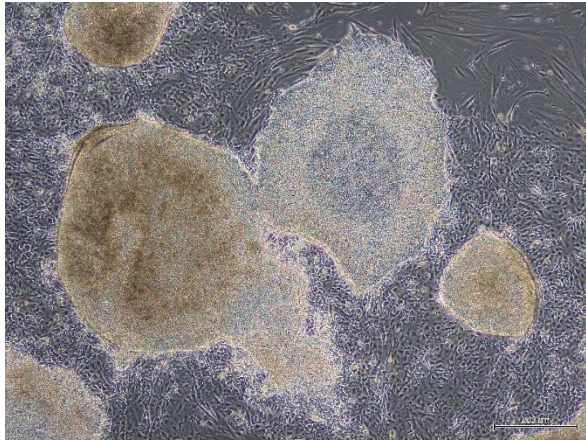
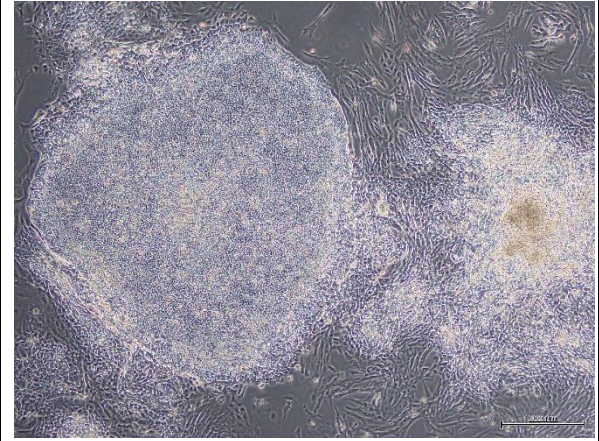
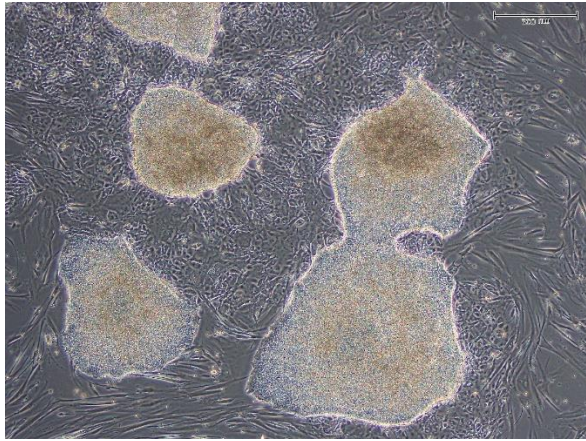
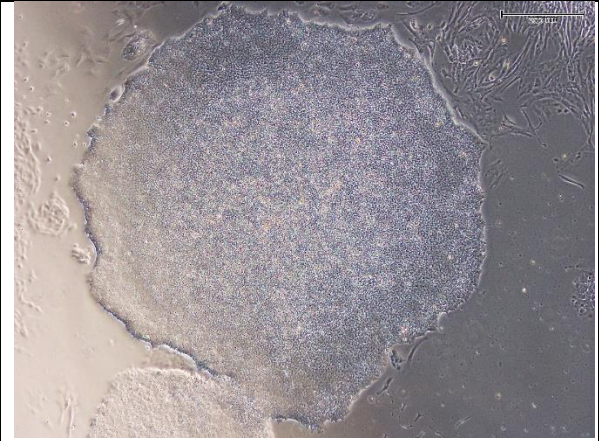
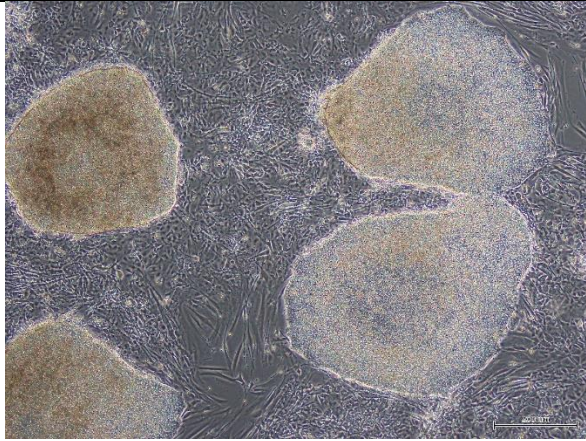
Mastershef2 Matrigel



P7PS

MShef2 HDF

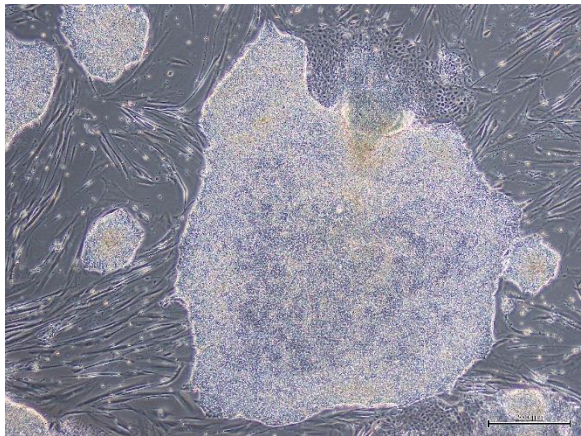
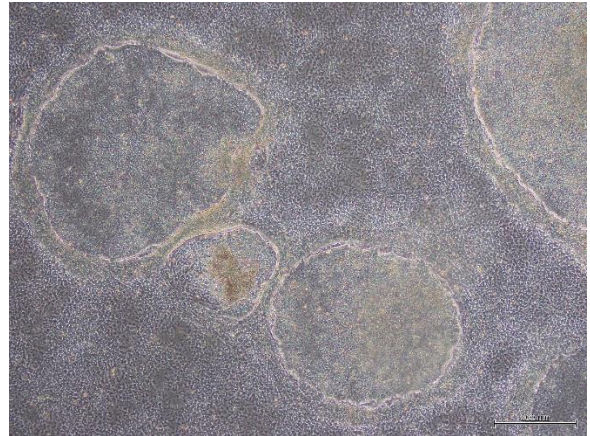
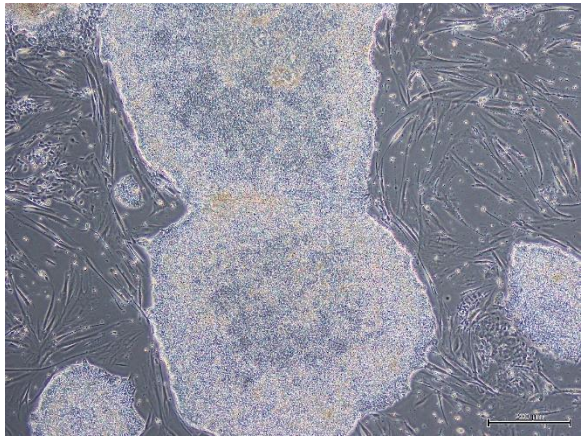
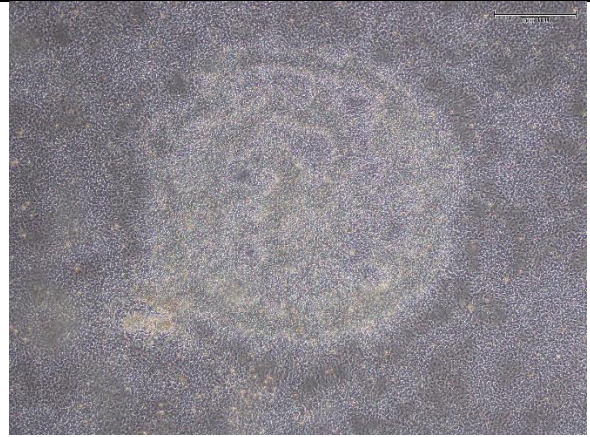
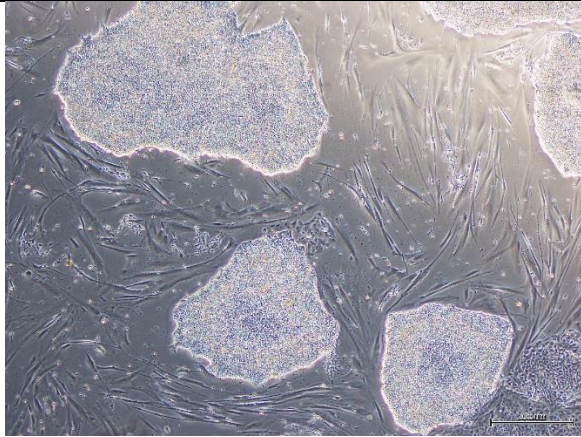
MShef2 Matrigel



P8PS

Mastershef2 HDF

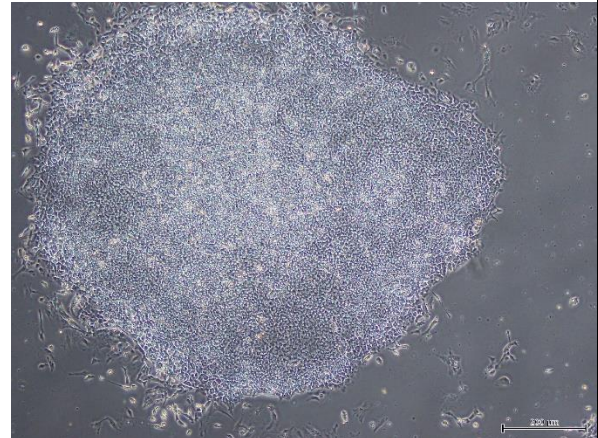
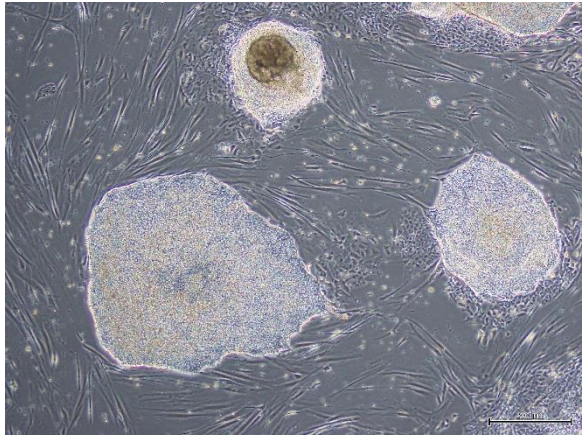
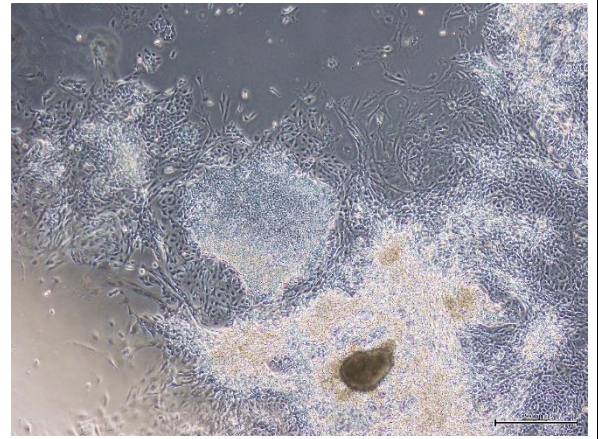
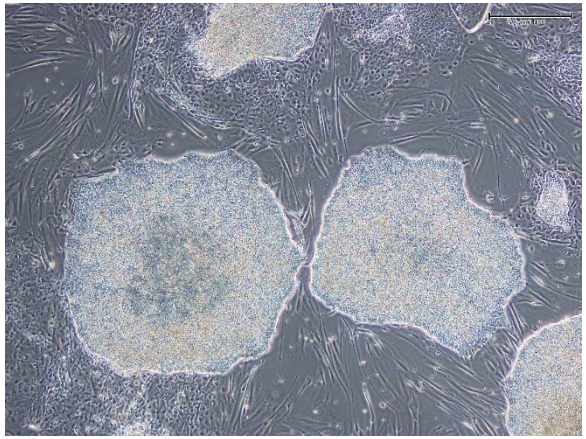
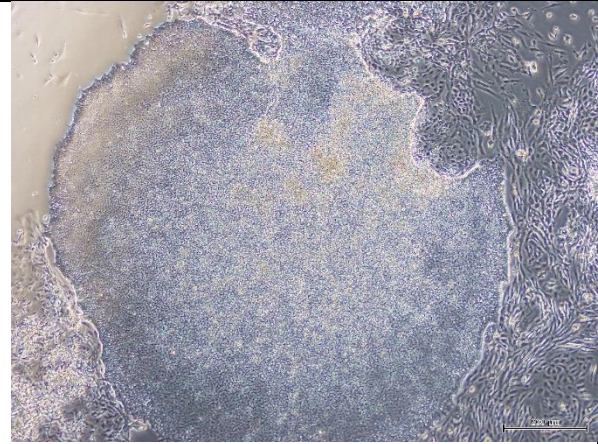
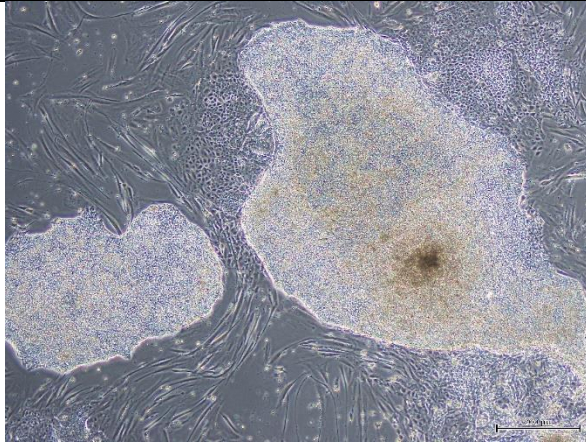
Mastershef2 Matrigel



P8PS

MShef2 HDF

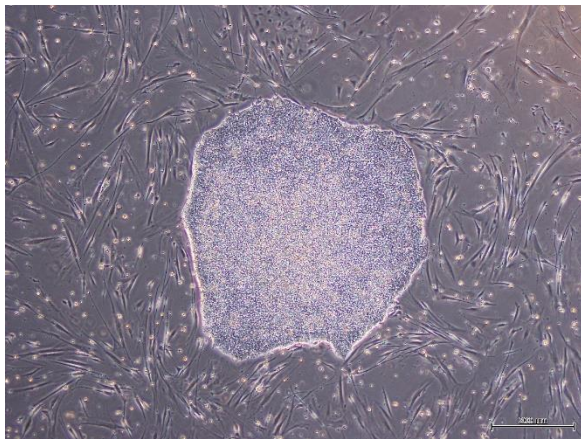
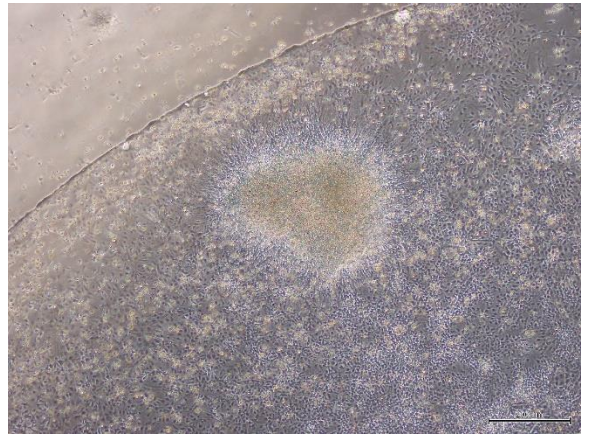
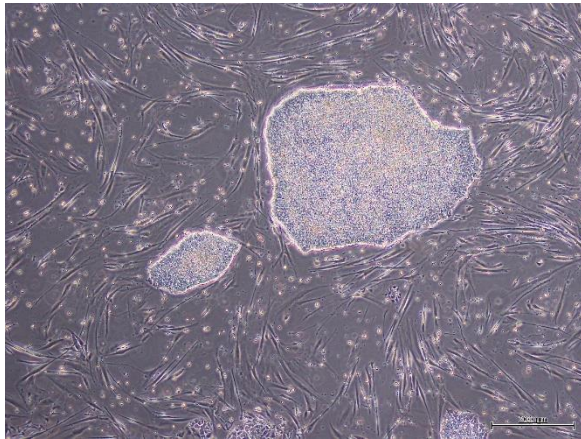
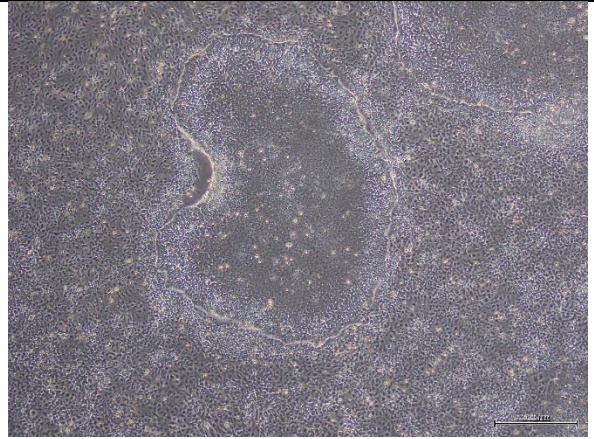
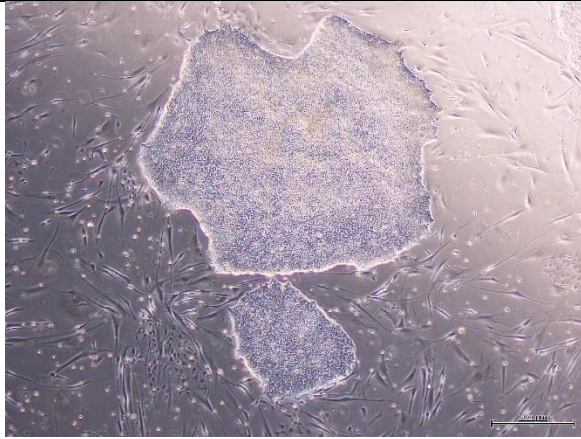
MShef2 Matrigel



P9PS

Mastershef2 HDF

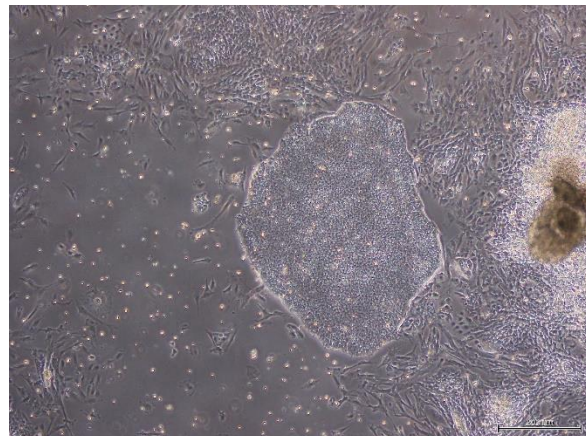
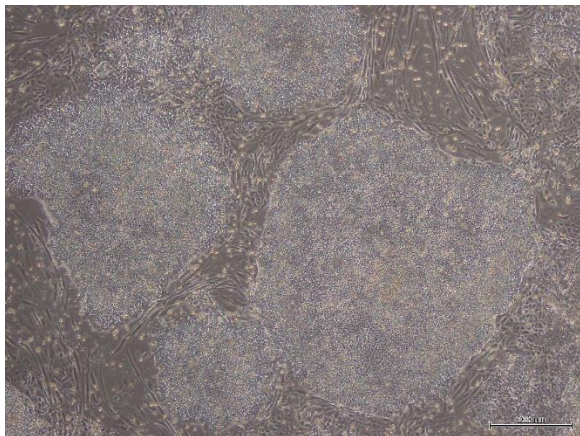
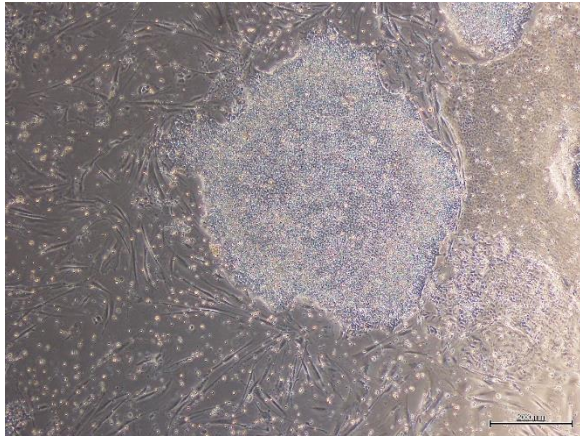
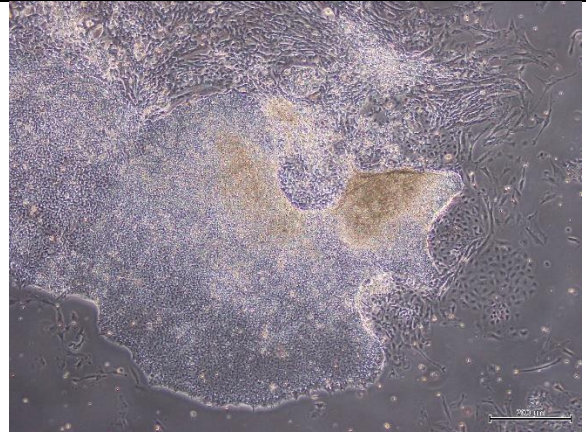
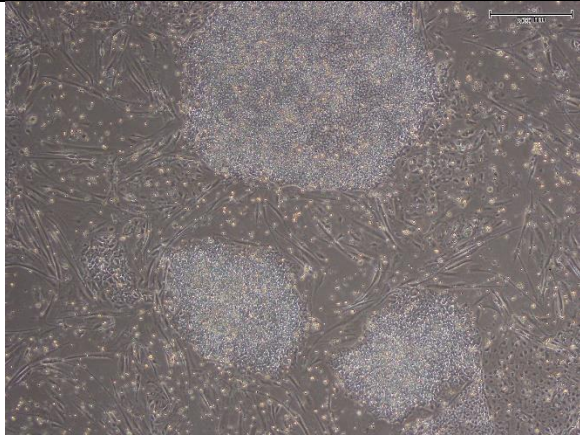
Mastershef2 Matrigel



P9PS

MShef2 HDF

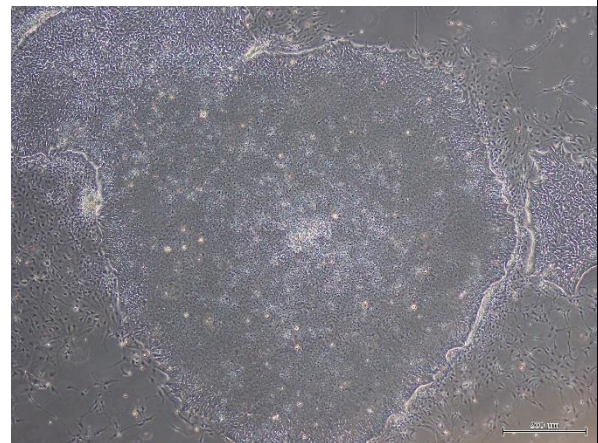
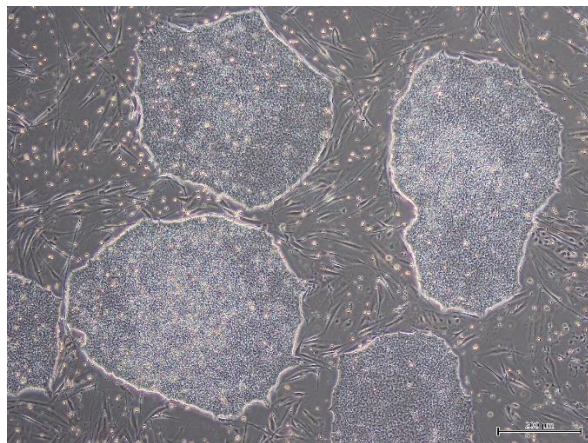
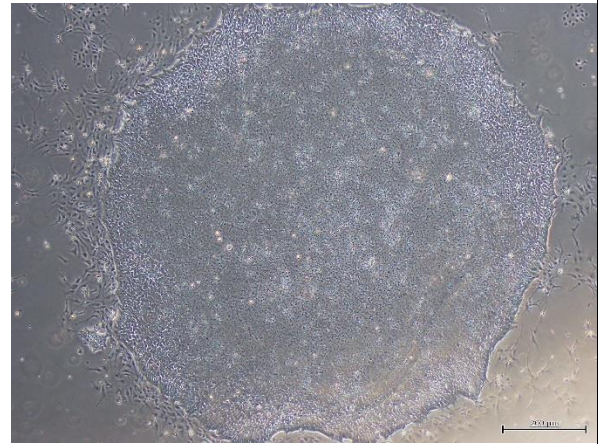
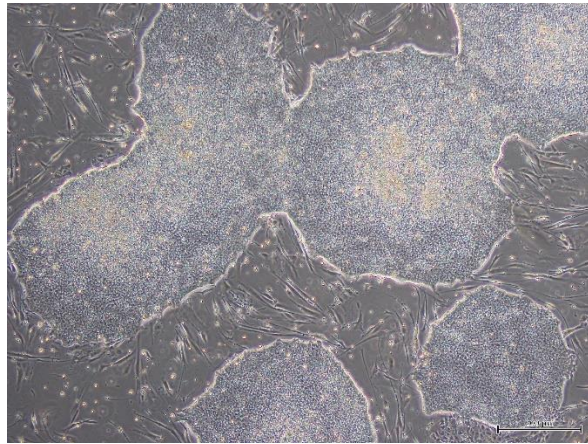
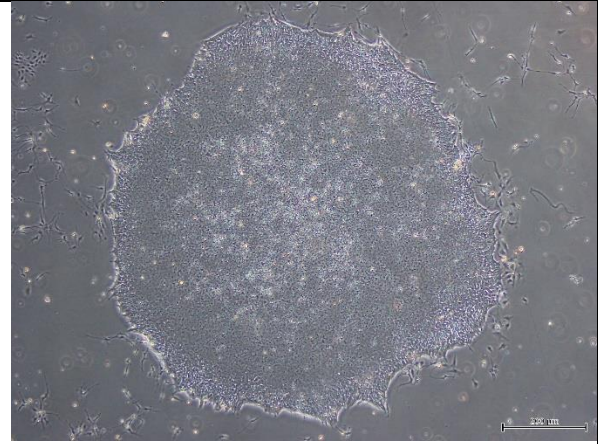
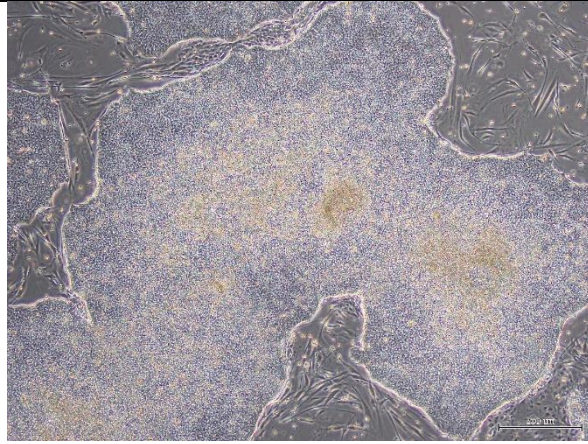
MShef2 Matrigel



P10PS

Mastershef2 HDF

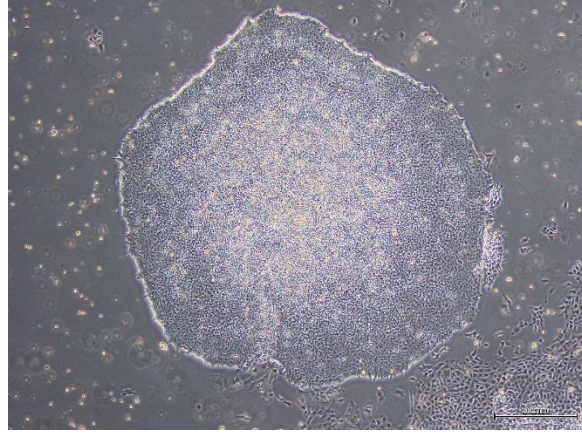
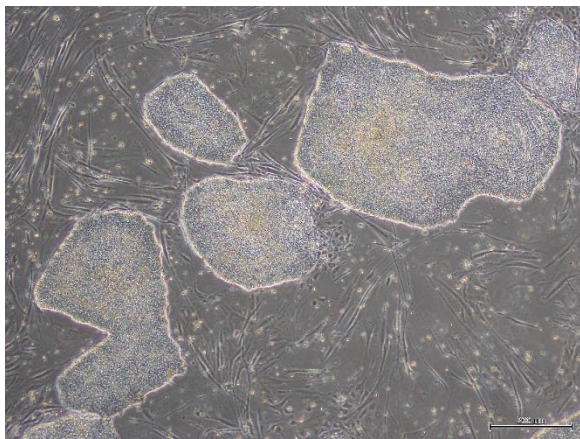
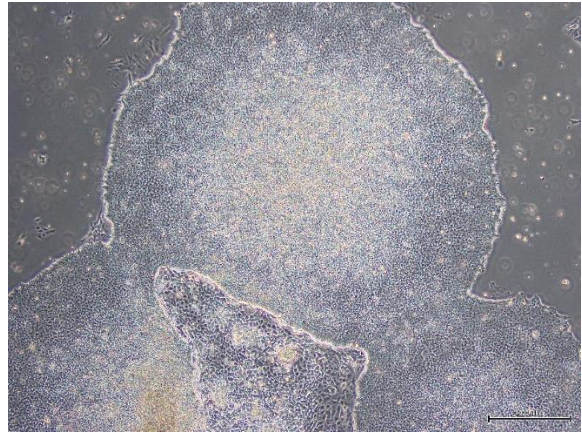
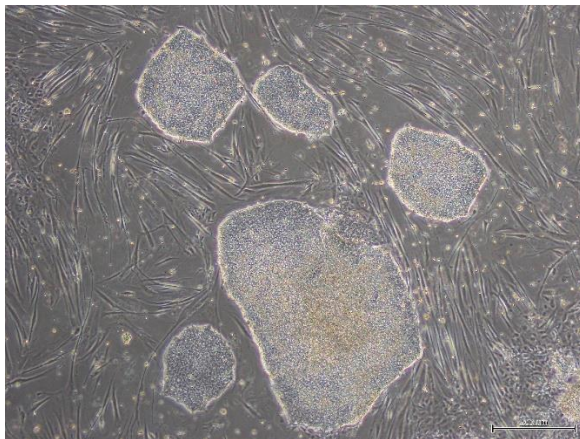
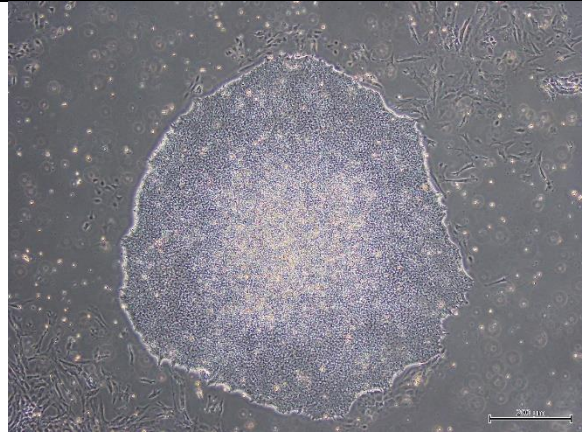
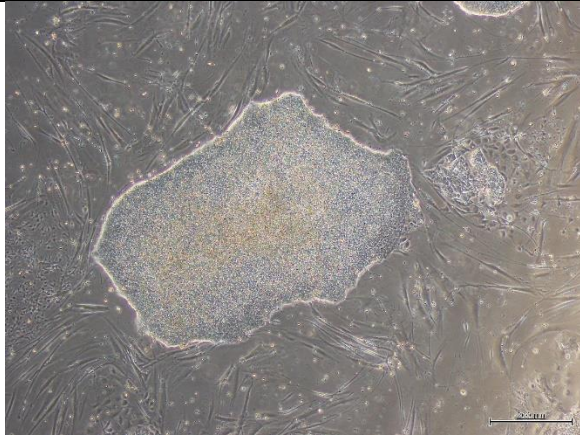
Mastershef2 Matrigel



P10PS

MShef2 HDF

MShef Matrigel



Appendix VII

Appendix VII: List of Genes Generated from the RNA-Seq Analysis

Upregulated genes in hESCs cultured on HDFs:

masterShef2 and mShef2 (31 genes)

<i>FGA</i>
<i>FGG</i>
<i>PLVAP</i>
<i>HOXD9</i>
<i>LCN1</i>
<i>IGF2, INS, INS-IGF2</i>
<i>MMP28</i>
<i>HOXB8</i>
<i>CRHBP</i>
<i>SLN</i>
<i>ABO</i>
<i>ART4</i>
<i>HOXB9</i>
<i>FGB</i>
<i>ENTPD3</i>
<i>HAND2</i>
<i>AKAP4</i>
<i>H19, MIR675</i>
<i>WISP1</i>
<i>AHSG</i>
<i>APOC3</i>
<i>AFP</i>
<i>RGS1</i>
<i>HOXC4, HOXC5, HOXC6</i>
<i>REN</i>
<i>SLC39A2</i>
<i>RSPO2</i>
<i>HOXC8</i>
<i>HOXB-AS3</i>
<i>AQP1</i>
<i>HAND1</i>

masterShef2 (125 genes)

<i>IFI44L</i>	<i>RAMP1</i>	<i>SAMD5</i>
<i>MLC1</i>	<i>WNT11</i>	<i>APOA2</i>
<i>OSR1</i>	<i>TBX4</i>	<i>P2RY6</i>
<i>RALYL</i>	<i>SH3TC1</i>	<i>COLEC11</i>
<i>FIBIN</i>	<i>LINC00645</i>	<i>CLEC14A</i>
<i>CD34</i>	<i>HOXB3</i>	<i>C1orf61</i>
<i>FLI1</i>	<i>PI15</i>	<i>LRRN4</i>
<i>SCN3A</i>	<i>MEP1A</i>	<i>PGM5</i>
<i>ALB</i>	<i>FMO1</i>	<i>CPED1</i>
<i>PLG</i>	<i>APOC2, APOC4</i>	<i>HPX</i>
<i>DIO3</i>	<i>SMLR1</i>	<i>EGFLAM</i>
<i>SERPINC1</i>	<i>DIO1</i>	<i>GRIA2</i>
<i>COL3A1</i>	<i>APOB</i>	<i>TBX20</i>
<i>FSTL5</i>	<i>C7</i>	<i>SULT2A1</i>
<i>FAM163A</i>	<i>HAVCR1</i>	<i>CLEC1B</i>
<i>CXCL14</i>	<i>ITIH2</i>	<i>MIR143, MIR143HG</i>
<i>EPAS1</i>	<i>TTR</i>	<i>SYT10</i>
<i>ASGR2</i>	<i>ANXA8</i>	<i>PRDM6</i>
<i>GSTA1</i>	<i>ALX4</i>	<i>ANXA8L1</i>
<i>CNTN5</i>	<i>RGS13</i>	<i>FSHR</i>
<i>CDH10</i>	<i>FOXF1</i>	<i>GATA6-AS1</i>
<i>HSD17B2</i>	<i>ESAM</i>	<i>VTN</i>
<i>PITX2</i>	<i>PLA2G12B</i>	<i>NPY</i>
<i>SLC40A1</i>	<i>AGT</i>	<i>PDE7B</i>
<i>HOXC10</i>	<i>LINC00461, MIR9-2</i>	<i>GSTA2</i>
<i>APOA1</i>	<i>RBP4</i>	<i>HAPLN1</i>
<i>MEOX2</i>	<i>FENDRR</i>	<i>COL15A1</i>
<i>LUM</i>	<i>HOXB6</i>	<i>CD93</i>
<i>HOXA10, HOXA9</i>	<i>PDZRN4</i>	<i>HOPX</i>
<i>HMGCS2</i>	<i>SLC17A8</i>	<i>SOAT2</i>
<i>ACSL5</i>	<i>KYNU</i>	<i>APOA4</i>
<i>CTSE</i>	<i>ADRB3</i>	<i>THBD</i>
<i>GUCY1A3</i>	<i>SLCO2B1</i>	<i>FOXA1</i>
<i>HKDC1</i>	<i>CDH5</i>	<i>CSGALNACT1</i>
<i>KISS1</i>	<i>ATP10B</i>	<i>MGP</i>
<i>GOS2</i>	<i>LRP1B</i>	<i>GFAP</i>
<i>C2orf80</i>	<i>GBP4</i>	<i>GJB1</i>
<i>TF</i>	<i>CREB3L3</i>	
<i>HOXD11</i>	<i>ITGA8</i>	
<i>LINC01158</i>	<i>F2</i>	
<i>GABRP</i>	<i>KCNQ5</i>	
<i>PECAM1</i>	<i>HGF</i>	
<i>ADAMTS9</i>	<i>FEZF2</i>	
<i>TCF21</i>	<i>SERPINA1</i>	

mShef2 (23 genes)

<i>IGF1</i>
<i>CDKN2B-AS1</i>
<i>HOXB7</i>
<i>LOC101927901</i>
<i>PENK</i>
<i>HOXA13</i>
<i>HTR1E</i>
<i>RHAG</i>
<i>UGT2B11</i>
<i>TYRP1</i>
<i>PRR9</i>
<i>HOXC11</i>
<i>CBLN2</i>
<i>KCNE4</i>
<i>HOXD13</i>
<i>ALDH1A2</i>
<i>HOTTIP</i>
<i>HOXB4</i>
<i>C4BPB</i>
<i>TECRL</i>
<i>GAPT</i>
<i>COLEC10</i>
<i>ARHGDIB</i>

Downregulated genes in hESCs cultured on HDFs:

masterShef2 and mShef2 (4 genes)

<i>APOD</i>
<i>ITGBL1</i>
<i>COMP</i>
<i>MMP1</i>

masterShef2 (7 genes)

<i>EREG</i>
<i>DMRTA2</i>
<i>TIMP3</i>
<i>SERPINE1</i>
<i>SOX6</i>
<i>PLEKHD1</i>
<i>HP</i>

mShef2 (26 genes)

<i>SAMD9L</i>
<i>EMX2</i>
<i>IFI44L</i>
<i>WNT8B</i>
<i>ZIC1</i>
<i>IFI44</i>
<i>PAX5</i>
<i>NPTX1</i>
<i>LINC00925</i>
<i>OASL</i>
<i>NT5E</i>
<i>PAX8</i>
<i>SERPINB2</i>
<i>MAGEA4</i>
<i>LINC-PINT</i>
<i>IFIT2</i>
<i>CFH</i>
<i>POU3F2</i>
<i>OAS2</i>
<i>ABCC3</i>
<i>RSAD2</i>
<i>TBX5</i>
<i>WNT7B</i>
<i>PSG4</i>
<i>SAMD9</i>
<i>CILP</i>

Upregulated genes in the different cell lines masterShef2 and mShef2:

HDFs and Matrigel™ (4 genes)

<i>POU3F4</i>
<i>ZNF572</i>
<i>ZNF560</i>
<i>D21S2088E</i>

HDFs (12 genes)

<i>KHDC3L</i>
<i>RMRP</i>
<i>CST1</i>
<i>ZNF300P1</i>
<i>LOC401010</i>
<i>CXCL8</i>
<i>DEFA6</i>
<i>ZNF208</i>
<i>TRPM2</i>
<i>CST2</i>
<i>ZNF728</i>
<i>RBM46</i>

Matrigel™ (81 genes)

<i>FGA</i>	<i>TMEM132C</i>	<i>LINC00925</i>	<i>COL19A1</i>	<i>POU3F3</i>
<i>IFI44L</i>	<i>CILP</i>	<i>SERPINC1</i>	<i>LPL</i>	<i>NFIX</i>
<i>CYP26B1</i>	<i>FABP1</i>	<i>SLC17A8</i>	<i>MEP1A</i>	<i>CFI</i>
<i>LINC00461, MIR9-2</i>	<i>MAP6</i>	<i>TFAP2B</i>	<i>FMO1</i>	<i>C1orf61</i>
<i>AGT</i>	<i>EMX2</i>	<i>FSTL5</i>	<i>SFTA1P</i>	<i>AHSG</i>
<i>SFRP4</i>	<i>C2orf80</i>	<i>ATP10B</i>	<i>APOC2, APOC4</i>	<i>KISS1</i>
<i>MLC1</i>	<i>HTR1A</i>	<i>SERPINA7</i>	<i>SMLR1</i>	<i>DCN</i>
<i>OLIG3</i>	<i>WNT8B</i>	<i>GPM6A</i>	<i>LIPC</i>	<i>TECRL</i>
<i>LOC440896</i>	<i>ZIC1</i>	<i>CNTN5</i>	<i>DIO1</i>	<i>SLC18A3</i>
<i>ZNF732</i>	<i>ITGBL1</i>	<i>PAX8</i>	<i>POU3F2</i>	
<i>PXDNL</i>	<i>GRIA2</i>	<i>CDH10</i>	<i>S100B</i>	
<i>RBP4</i>	<i>ELMOD1</i>	<i>NPAS3</i>	<i>TTR</i>	
<i>SCN4B</i>	<i>OTX1</i>	<i>HOXC10</i>	<i>MGP</i>	
<i>FGG</i>	<i>MIR143, MIR143HG</i>	<i>LOC145845</i>	<i>FGB</i>	
<i>SCN3A</i>	<i>DMRTA2</i>	<i>POSTN</i>	<i>SPARCL1</i>	
<i>NPTX1</i>	<i>APOC3</i>	<i>PTX3</i>	<i>WNT7B</i>	
<i>PLG</i>	<i>AFP</i>	<i>SERPINA1</i>	<i>SCN1A</i>	
<i>A2M</i>	<i>COMP</i>	<i>DPYSL5</i>	<i>GFAP</i>	

Downregulated genes in the different cell lines masterShef2 and mShef2:

HDFs and Matrigel™ (5 genes)

<i>APOA2</i>
<i>MMP28</i>
<i>REN</i>
<i>TTR</i>
<i>HP</i>

HDFs (7 genes)

<i>NPTX1</i>
<i>CTSE</i>
<i>TMEM132C</i>
<i>MYBPC1</i>
<i>DMRTA2</i>
<i>NPPB</i>
<i>SOX6</i>

Matrigel™ (109 genes)

<i>FOXF1</i>	<i>SLC6A19</i>	<i>PITX2</i>	<i>LCN15</i>	<i>HOXA11-AS</i>	<i>HAPLN1</i>	<i>ARHGDI B</i>
<i>SYTL5</i>	<i>GYPE</i>	<i>SLC40A1</i>	<i>WISP1</i>	<i>CDKN2B-AS1</i>	<i>MAGEA4</i>	<i>ZNF662</i>
<i>FGA</i>	<i>NLRP7</i>	<i>H19, MIR675</i>	<i>AHSG</i>	<i>AADACL3</i>	<i>LINC01559</i>	<i>HOXB5</i>
<i>RHAG</i>	<i>MYCT1</i>	<i>APOA1</i>	<i>LRRN4</i>	<i>AFP</i>	<i>LINC00607</i>	<i>LINC01139</i>
<i>XCL1</i>	<i>COL3A1</i>	<i>SAMSN1</i>	<i>HOXD11</i>	<i>MYL3</i>	<i>LOC101927901</i>	<i>PKP1</i>
<i>ZNF596</i>	<i>PLVAP</i>	<i>OIT3</i>	<i>TF</i>	<i>PRDM6</i>	<i>COLEC10</i>	<i>GSTA2</i>
<i>TLR4</i>	<i>HOXD9</i>	<i>NPNT</i>	<i>CRHBP</i>	<i>RGS1</i>	<i>HOPX</i>	<i>HAND1</i>
<i>DPPA5</i>	<i>RNASE1</i>	<i>HGF</i>	<i>EGFLAM</i>	<i>ADGRF4</i>	<i>TRPM2</i>	<i>PRR9</i>
<i>CPA2</i>	<i>FAM163A</i>	<i>LINC01108</i>	<i>MEPE</i>	<i>DNMT3L</i>	<i>TFF1</i>	<i>TNNT2</i>
<i>FIBIN</i>	<i>CBLN2</i>	<i>ABHD12B</i>	<i>TBX20</i>	<i>FSHR</i>	<i>ACTC1</i>	<i>SLC28A3</i>
<i>RBP4</i>	<i>MYL4</i>	<i>SERPINA1</i>	<i>GATA4</i>	<i>TBX4</i>	<i>APOA4</i>	<i>DNM3OS</i>
<i>ZAP70</i>	<i>SYNPO</i>	<i>GGT5</i>	<i>FRMPD4</i>	<i>HOXB7</i>	<i>DUSP27</i>	<i>HOXD10</i>
<i>PTPN20</i>	<i>GBP4</i>	<i>IGF2, INS, INS-IGF2</i>	<i>ITGA11</i>	<i>GPAT2</i>	<i>ANXA8</i>	<i>AQP1</i>
<i>FMOD</i>	<i>TCHH</i>	<i>KCTD16</i>	<i>SLN</i>	<i>GATA6-AS1</i>	<i>LOC101927915</i>	
<i>ENTPD3</i>	<i>IGF1</i>	<i>P2RY6</i>	<i>TCF21</i>	<i>VTN</i>	<i>FGB</i>	
<i>HAND2</i>	<i>KLHL41</i>	<i>KCNE4</i>	<i>DEFA6</i>	<i>NPY</i>	<i>RBM46</i>	

Passage Affected Genes:

masterShef2 HDF and Matrigel™ (1 gene)

<i>TTR</i>

masterShef2 HDFs (3 genes)

<i>CST1</i>
<i>SOX6</i>
<i>HP</i>

masterShef2 Matrigel™ (9 genes)

<i>ATP10B</i>
<i>IFI44L</i>
<i>MLC1</i>
<i>SERPINA1</i>
<i>AFP</i>
<i>FGB</i>
<i>HAND1</i>
<i>FSTL5</i>
<i>GFAP</i>

mShef2 HDFs (2 genes)

<i>RMRP</i>
<i>NPTX1</i>

mShef2 Matrigel™ (5 genes)

<i>PENK</i>
<i>PRR9</i>
<i>HOXC11</i>
<i>HTR1E</i>
<i>TECRL</i>

